CO_2 Savings from Micro-CHP: Influence of Operating Regimes, Demand Variations and Energy Storage

David Kane BSc (Hons)

Doctor of Philosophy

Heriot-Watt University

Department of Mechanical Engineering

June 2012

Abstract

A high temporal precision model was developed to assess the performance of thermal load following micro-CHP system design variants in detail for a number of design days. Carbon savings (relative to a base-case energy system) and prime mover lifetime drivers (thermal cycling and operating duration) were quantified. Novel performance metrics were defined, including Potential Thermal Supply Demand Ratio, and Effective Carbon Intensity of μCHP-Generated Electricity. Significant relative carbon savings were found for design variants with a PTSDR between 0.1-1.5, suggesting that it is a design selection parameter for thermal supply/demand matching. Alternative μCHP operating regimes, restricted seasonal operation, changing thermal demand, fuel and electricity grid carbon intensities, and energy storage (using batteries and hydrogen) were studied. It was found that annual relative carbon savings in excess of 23% were achievable for appropriately-sized design variants, with relatively high electrical efficiency, once a complex control strategy is applied. The control strategy also reduces thermal cycling for the μCHP design variant (versus the Thermal Load Following operating regime), hence increasing prime mover lifetime.

Dedication

This thesis is dedicated to my family; Tom, Liz, Gillian and Emma.

Thank you for everything.

Acknowledgements

I am especially grateful to Marcus Newborough, for his support as supervisor over many years, especially after leaving for pastures new. I am glad you took a chance on the young guy brazen enough to ask for a job.

I would like to thank those within Heriot-Watt University that helped, inspired and cajoled me toward completion, including Phil, Wolf and Dave.

I am grateful to EPSRC for a studentship awarded as part of the TARBASE project, and for the opportunities that it offered as part of a major research consortium within the Carbon Vision Buildings programme, as jointly funded by EPSRC and the Carbon Trust.

Finally, thank you to my friends, family and colleagues who encouraged me to start my studies, and to never give up!

Table of Contents

A high temporal precision model was developed to assess the performance of thermal load following micro-CHP system design variants in detail for a number of design days. Carbon savings (relative to a base-case energy system) and prime mover lifetime drivers (thermal cycling and operating duration) were quantified. Novel performance metrics were defined, including Potential Thermal Supply Demand Ratio, and Effective Carbon Intensity of μCHP-Generated Electricity. Significant relative carbon savings were found for design variants with a PTSDR between 0.1-1.5, suggesting that it is a design selection parameter for thermal supply/demand matching. Alternative μCHP operating regimes, restricted seasonal operation, changing thermal demand, fuel and electricity grid carbon intensities, and energy storage (using batteries and hydrogen) were studied. It was found that annual relative carbon savings in excess of 23% were achievable for appropriately-sized design variants, with relatively high electrical efficiency, once a complex control strategy is applied. The control strategy also reduces thermal cycling for the μCHP design variant (versus the Thermal Load Following operating regime), hence increasing prime mover lifetime. 2

Table of Tables

Table of Figures

Glossary

1-D	1-Dimensional
2-D	2-Dimensional
3-D	3-Dimensional
λ_{Layer}	Thermal Conductivity of layer within construction element [$Wm^{-1}K^{-1}$]
ΔQ_{aux}	Reduction in auxiliary thermal generation between μCHP and base-case scenarios
ΔT_m	Minimum temperature differential used in boiler exponential cooling equation [K]
η_{alt}	Efficiency of Alternator [%]
η_{burner}	Efficiency of Burner [%]
η_{carnot}	Carnot Efficiency [%]
η_{eg}	Gross Electrical Efficiency [%]
η_{e}	Net Electrical Efficiency [%]
η_{FOC}	Efficiency penalty of Stirling Engine due to fraction of Carnot Efficiency achieved by its design [%]
η_{hr}	Heat Recovery Efficiency [%]
$\eta_{parasitic}$	Efficiency penalty of prime mover net electricity efficiency due to electric generation required for system parasitic loads [%]
η_{tot}	Total Efficiency (thermal and electrical) of CHP prime mover [%]
η_{th}	Thermal Efficiency [%]
η_{th-aux}	Thermal Efficiency of auxiliary boiler [%]
η_{th100}	Thermal Efficiency at full load when not condensing [%]
η_{th100c}	Thermal Efficiency at full Load when condensing [%]
ρ_{Water}	Density of water [kgm^{-3}]
τ	Exponential time constant
$\tau_{Shutdown}$	Shutdown time constant [s]
$\tau_{Start-up}$	Start-up time constant [s]
μCHP	Micro-Combined Heat and Power
A_{Door}	Area of doors in wall construction element [m^2]
A_{Floor}	Area (internal or external) of floor construction element [m^2]
$A_{Glazing}$	Area (internal or external) of glazing construction element [m^2]

$A_{NetWall}$	Net area of wall construction element once doors and glazing are removed [m^2]
A_{Roof}	Area (internal or external) of roof construction element [m^2]
A_{Store}	External Surface area of Thermal Store [m^2]
A_{Wall}	Area (internal or external) of wall construction element [m^2]
ab_{Wall}	Absorptivity of external surface of wall construction element
ACH	Air Changes per Hour
AFC	Alkaline Fuel Cell
ASHRAE	The American Society of Heating, Refrigerating and Air-Conditioning Engineers
BC	Base-case
BETTA	British Electricity Trading and Transmission Arrangements
BIM-G	Building Integrated Micro-Generation Model
BRE	Building Research Establishment
BREDEM	Building Research Establishment Domestic Energy Model
c_{Air}	Specific Heat Capacity of air [$Jkg^{-1}K^{-1}$]
c_{Wall}	Specific Heat Capacity of wall construction element [$Jkg^{-1}K^{-1}$]
c_{Water}	Specific Heat Capacity of water [$Jkg^{-1}K^{-1}$]
CCGT	Combined Cycle Gas Turbine
CCT	Colour Temperature (of light source) [K]
CFL	Compact Fluorescent Lamps
CI	Carbon Intensity [$kgCO_2/kWh$]
$CI_{en\text{-}eff}$	Effective carbon intensity of µCHP generated electricity (on net basis) [$kgCO_2/kWh$]
$CI_{en\text{-}eff\text{-}op}$	Effective operational carbon intensity of µCHP generated electricity (on net basis) [$kgCO_2/kWh$]
CI_{fuel}	Carbon Intensity of fuel (for prime mover & boiler) [$kgCO_2/kWh$]
CI_{gen}	Carbon Intensity of electricity generated (on net basis) by µCHP prime mover [$kgCO_2/kWh$]
CI_{grid}	Carbon Intensity of National Electricity Grid [$kgCO_2/kWh$]
CI_{ne}	Carbon Intensity of net generated electricity of the prime mover where the thermal output of the prime mover is not used [$kgCO_2/kWh$]

CI_{system}	Carbon Intensity of µCHP system (prime mover & aux) [$kgCO_2/kWh$]
CRI	Colour Rendering Index
CHP	Combined Heat and Power
CO_2	Carbon Dioxide
C_p	Specific Heat Capacity [$Jkg^{-1}K^{-1}$]
CsO-24hr	Continuous Output over 24 hours operating regime
CsO-DDP	Continuous Output over Daily Demand Periods operating regime
CsO-TDP	Continuous Output over Thermal Demand Periods operating regime
CtO	Constant Operation operating regime
dBA	Decibel Acoustic
DEM	Domestic Energy Model (as published by TASRBASE project)
DHW	Domestic Hot Water
d_{Layer}	Thickness of layer within construction element [m]
DOE-2	An energy modelling tool
DNO	Distributed Network Operator
DTI	Department of Trade and Industry
e_{Wall}	Emissivity of external surface of wall construction element
E_{Annual}	Estimated annual energy consumption of appliance [kWh]
EEC	Electrical Export Credit
E_{HG}	Thermal Energy Input of Heat Generator to Thermal Store [kWh]
EID	Electrical Import Displacement
ESP-r	A building energy simulation tool
$E_{Weekday}$	Estimated daily energy consumption of appliance during weekday occupancy pattern [kWh]
$E_{Weekend}$	Estimated daily energy consumption of appliance during weekend occupancy pattern [kWh]
F_{100}	CHP Prime Mover Fuel Input at full load (kW)
F_{aux100}	Boiler Fuel Input at full load when not condensing [kW]
F_{auxBC}	Fuel consumption of boiler in base-case energy system [kWh]
F_{auxCHP}	Fuel consumption of µCHP auxiliary boiler [kWh]
$f_{ExponEndAux}$	Exponential Cut-Off Factor [% of Target Value]
FC	Fuel Cell

F_{CHP}	CHP Prime Mover Fuel Input (kW) or Consumption [kWh]
FIT	Feed-In-Tariff
FPSE	Free-Piston Stirling Engine
F_{System}	µCHP System (Prime Mover & Aux) Fuel Consumption [kWh]
GLS	General Lighting Service, i.e. incandescent tungsten filament light bulb
h_{Store}	Heat Transfer Co-efficient (to air) of Thermal Store [$Wm^{-2}K^{-1}$]
$h_{Wall-Ext}$	Heat Transfer Co-efficient of external surface of wall construction element [$Wm^{-2}K^{-1}$]
$h_{Wall-In}$	Heat Transfer Co-efficient of internal surface of wall construction element [$Wm^{-2}K^{-1}$]
h_{W-EXT}	Convection co-efficient for convective heat transfer between the wall surface and the external air at the dry bulb air temperature
H_2	Hydrogen Molecule
HGCP	Heat Generator Circulation Pump
H_{NRTB}	Total heat loss co-efficient from all non-repeating thermal bridges in the wall construction element [WK^{-1}]
HVCA	Heating and Ventilation Contractors' Association
HX	Heat Exchanger
ICE	Internal Combustion Engine
IEA	International Energy Agency
$kgCO_2$	Kilogram of Carbon Dioxide
$KM_{Radiator}$	Characteristic Heat Output of radiators [$WK-^{1}$]
KM_{Pipe}	Characteristic Heat Output of pipework [$WK-^{1}$]
kW_e	Kilowatt of electrical power
kW_{th}	Kilowatt of thermal power
LPG	Liquefied Petroleum Gas
LW	Long Wave
m_{Air}	Mass of air within building envelope [kg]
m_{Wall}	Mass of wall construction element [kg]
MCFC	Molten Carbonate Fuel Cell
Micro-CHP	Micro-Combined Heat and Power
MTP	Market Transformation Programme

MR	Maximum Rectangle
$m_{SHWFlow}$	Mass of water flowing around SHDS during one simulation timestep [kg]
MW	Megawatt of power, $1x10^6$Watts
MWh	Megawatt-hour, i.e. energy consumed over 1 hour at rate of 1MW
NEG	National Electricity Grid
NG	Natural Gas
n_{Pipe}	Pipe Constant, as used in the Characteristic Equation of the flow and return pipe sections
$n_{Radiator}$	Radiator Constant, as used in the Characteristic Equation of the radiator
$n_{WeeksHoliday}$	Number of weeks building vacant due to occupant holidays [weeks]
NO_x	Nitrous Oxide
O_2	Oxygen molecule
ORC	Organic Rankine Cycle
PDS	Primary Demand Scenario
P_e	Net Electrical Output of CHP Prime Mover [kW]
P_{e100}	Net Electrical Output of CHP Prime Mover at Full Load [kW]
P_{eg}	Gross Electrical Output of CHP Prime Mover [kW]
PAFC	Phosphoric Acid Fuel Cell
PEM	Proton Exchange Membrane (Fuel Cell)
$P_{ParasiticCHP}$	Parasitic Electrical Load of CHP prime mover [kW]
$P_{pFiring}$	Parasitic Electrical Load during Firing [kW]
$P_{pStandby}$	Parasitic Electrical Load during Standby [kW]
P_{th}	Thermal Output of CHP Prime Mover [kW]
P_{th100}	Thermal Output of CHP Prime Mover at Full Load [kW]
ppm	Parts per million
PTSDR	Potential Thermal Supply:Demand Ratio
PV	Photovoltaic (i.e. Solar PV)
Q_{100}	Thermal Output @ 100% Load [kW]
$Q_{A\&L}$	Casual Thermal Gains from Appliances & Lighting [kW]
Q_{Casual}	Total Casual Thermal Gains [kW]
Q_{CHP}	Thermal Output Energy from prime mover [kWh]
Q_e	Generated Electrical Energy (on a net basis) of prime mover [kWh]

$Q_{eeg\text{-}CHP}$	Gross Electrical Energy exported from household to NEG [kWh]
$Q_{eig\text{-}BC}$	Gross Electrical Energy imported during base-case scenario [kWh]
$Q_{eig\text{-}CHP}$	Gross Electrical Energy imported during µCHP scenario [kWh]
Q_{Floor}	Heat loss from building through floor construction element [kW]
$Q_{Glazing}$	Heat loss from building through glazing construction element [kW]
$Q_{Metabolic}$	Metabolic Casual Thermal Gain [kW]
$Q_{Pipe\text{-}Flow}$	Heat loss from the flow pipework section of the SHDS [kW]
$Q_{Pipe\text{-}Return}$	Heat loss from the return pipework section of the SHDS [kW]
$Q_{Radiator}$	Heat loss from radiator to building airspace [kW]
Q_{Roof}	Heat loss from building through roof construction element [kW]
Q_{SHd}	Simulated Daily Space Heating Demand, as used in climate derivation correlations [kWh]
Q_{SHDS}	Heat Output from SHDS to building airspace [kW]
Q_{SHDSIn}	Heat Input to SHDS from Heat Source (Generator or Store) [kW]
$Q_{StoreLoss}$	Heat loss form thermal store or DHW Tank [kW]
Q_{th}	Thermal Output Energy [kWh]
$Q_{th\text{-}aux}$	Boiler (auxiliary or main) thermal output energy [kWh]
$Q_{th\text{-}system}$	µCHP system (prime mover & aux) thermal output energy [kWh]
$Q_{thDemand\text{-}BC}$	Heat demand for a scenario with base-case energy system [kWh]
Q_{Vent}	Heat loss from building due to ventilation & Infiltration [kW]
Q_{Wall}	Heat loss from building through wall construction element [kW]
RCS	Relative Carbon Saving (versus base0case energy system)
R_{si}	Thermal resistance of internal surface of wall construction
R_{se}	Thermal resistance of external surface of wall construction
RSO	Restricted Seasonal Operation
RSO-NoHSum	Restricted Seasonal Operation without High Summer PDS
RSO-NoSummer	Restricted Seasonal Operation without High Summer or Summer PDS
$r_{turn\text{-}down}$	Turndown Ratio [%]
S	Daily Total Orientation Averaged Solar Irradiance [$kWhm^{-2}$]
SAP	Standard Assessment Procedure
S_{da}	Daily Average of Solar Irradiance [$kWhm^{-2}$]
SBC	Stefan Boltzmann Constant, $5.6697x10^{-8}$

SE	Stirling Engine
SH	Space Heating
SHCP	Space Heating Circulation Pump
SHDS	Space Heating Distribution System
SHGC	Solar Heat Gain Co-efficient
SHW	Space Heating Water
SOFC	Solid Oxide Fuel Cell
SW	Short Wave
t	Timestep (in 5-second increments)
T_{GRD}	Ground temperature used for calculation of long wave radiative exchange with wall construction element [°K]
T_{SKY}	Sky temperature used for calculation of long wave radiative exchange with wall construction element [°K]
T_{WALL}	Wall temperature used for calculation of long wave radiative exchange with wall construction element [°K]
T_C	Operating temperature of cold end (or cold space) of Stirling Engine [°C]
TDP	Thermal Demand Period
T_{eda}	Daily Average External Dry Bulb Air Temperature [°C]
TGD	Thermal Generation Displacement
T_H	Operating temperature of hot end (or hot space) of Stirling Engine [°C]
TLF	Thermal Load Following operating regime
tm	Time since start-up or shutdown of energy generation device [s]
$T_{Pipe-Flow}$	Temperature of water within flow pipe section of SHDS [°C]
$T_{Pipe-Return}$	Temperature of water within return pipe section of SHDS [°C]
$t_{Shutdown}$	Time elapsed since generation device was shutdown [s]
t_{Start}	Time elapsed since generation device was started [s]
t_{TDP}	Cumulative Duration of Thermal Demand Periods [hours]
T_{Ext}	Temperature of thermal store water [°C]
$T_{Ext-d-Ave}$	Daily Average External Dry Bulb Air Temperature [°C]
T_{Grd}	Temperature of exposed ground, for radiation calculations [°K]
T_{Ground}	Annual Average Ground Temperature under dwelling [°C]
T_{In}	Temperature of internal air volume [°C]

T_{PipeF}	Temperature of water in SH flow pipe [°C]
T_{PipeR}	Temperature of water in SH return pipe [°C]
$T_{Radiator}$	Temperature of water in radiator [°C]
T_{Sky}	Temperature of sky, for radiation calculations [°K]
T_{Store}	Temperature of thermal store water [°C]
T_{Wall}	Temperature of external surface of wall element [°K]
T_{Wall_Ext}	Temperature of external surface of wall element [°C]
T_{Wall_In}	Temperature of internal surface of wall element [°C]
ΔT_{Store}	Change in thermal store water temperature [°C]
TARBASE	Technology Assessment for Radically Improving the Built Asset Base (A collaborative academic research project under the carbon vision buildings program co funded by the Carbon Trust and the Engineering and Physical Sciences Research Council)
ThT_{Wall}	Thermal Transmittance of wall construction element [$Wm^{-2}K^{-1}$]
TRNSYS	Transient System Simulation Tool (simulation software)
TSW	Thermal Store Water
U_{Door}	U-Value of doors, as factored into wall construction [$Wm^{-2}K^{-1}$]
U_{Floor}	U-Value of floor construction element [$Wm^{-2}K^{-1}$]
$U_{Glazing}$	U-Value of glazing construction element [$Wm^{-2}K^{-1}$]
U_{NRTBAF}	U-value adjustment factor for non-repeating thermal bridges [$Wm^{-2}K^{-1}$]
U_{Roof}	U-Value of roof construction element [$Wm^{-2}K^{-1}$]
U-Value	Heat loss per unit area, per degree Kelvin of temperature differential, of a building element [$Wm^{-2}K^{-1}$]
U_{wall}	U-Value of wall construction element [$Wm^{-2}K^{-1}$]
$U_{wallRTB}$	U-value of wall incorporating a repeating thermal bridge [$Wm^{-2}K^{-1}$]
V_{Air}	Volume of air within building envelope [m^3]
V_{Store}	Volume of water within Thermal Store [m^3]
$V_{Infiltration}$	Infiltration Rate [Air Changes/Hours]
$V_{Ventilation}$	Ventilation Rate [Air Changes/Hours]

List of Publications

1. Kane D. and Newborough M., Estimating carbon savings for domestic base-load micro-CHP systems, Proceedings World Renewable Energy Congress (WREC-IX); Florence; 19-25 August 2006
2. Kane D & Newborough M, Scenarios for Carbon Abatement in Dwellings by Implementation of Stirling Engine Micro-CHP Systems; The Fourth International Conference on Energy Efficiency in Domestic Appliances and Lighting (EEDAL); London; June 2006
3. Jenkins D, Fletcher J and Kane D, A model for evaluating the impact of battery storage on microgeneration systems in dwellings, Energy Conversion and Management 49, 2413-2424, 2008
4. Jenkins D.P., Fletcher J. and Kane D., Lifetime prediction and sizing of lead-acid batteries for microgeneration and storage applications, IET Renewable Power Generation, 49, 2413-2424, 2008
5. A.D. Peacock, D.P. Jenkins, D. Kane, Investigating the potential of overheating in UK dwellings as a consequence of extant climate change, Energy Policy, Volume 38, Issue 7, Large-scale wind power in electricity markets with Regular Papers, July 2010, Pages 3277-3288
6. Peacock A.D., Banfill P.F., Newborough M., Kane D., Turan S., Jenkins D., Ahadzi M., Bowles G., Eames P.C., Singh H., Jackson T., Berry A; Reducing CO_2 Emissions through Refurbishment of UK Housing; European Council for an Energy Efficient Economy (eceee) 2007 Summer Study, Côte d'Azur, France 4-9 June, 2007
7. A.D. Peacock, D.P. Jenkins, D. Kane, M. Newborough, and P.F.G. Banfill; Micro-generation in the UK - potential effect on electricity, household and transport sectors; UKERC Meeting Place; Sustainable Energy UK: Meeting the science and engineering challenge; Oxford; May 2008
8. Peacock, A Banfill, P F Turan, S Jenkins, D Ahadzi, M Bowles, G Kane, D Newborough, M Eames, P C Singh, H Jackson, T, A Berry; Reducing CO_2 emissions through refurbishment of non-domestic UK buildings; Improving Energy Efficiency in Commercial Buildings (IEECB) Conference; 10 - 11 April 2008

9. Peacock A.D., Jenkins D. P. & Kane D.; Appendix C: UK Government Department for Communities and Local Government/UK Green Building Council, Report on carbon reductions in new non-domestic buildings, December 2007
10. TARBASE Domestic Sector Dissemination Event – CO_2 emissions reduction for domestic buildings (CIRIA Event), Inmarsat, London, 11th November 2006
11. D.P. Jenkins et al, Non-domestic conclusions of the TARBASE project – Reducing CO_2 emissions of existing buildings, 2010, Urban Energy Research Group, School of Built Environment, Heriot-Watt University, Edinburgh
12. Peacock A.D., Jenkins D.P., Kane D., Investigating the potential of overheating in UK dwellings as a consequence of extant climate change, Energy Policy, Volume 38, Issue 7, Pages 3277-3288, July 2010
13. Jenkins D.P., Peacock A.D., Banfill P.F.G., Kane D., Ingram V., Kilpatrick R., Modelling carbon emissions of UK dwellings – The TARBASE Domestic Model, Applied Energy, Volume 93, May 2012, Pages 596–605

1 Introduction

1.1 Overview of Research Topic

The exclusive electricity supply of virtually all UK domestic buildings is the National Grid, with an electrical efficiency and carbon intensity (calculated as primary fuel input to electricity delivered to dwelling) that varies throughout the day and year. This variation is in response to the mixture of generation on-line at any point, including fossil fuel generators, nuclear power stations, renewable power sources, and storage (such as pumped hydro). In 2009, thermal efficiency (i.e. electricity generated over average energy content of fuel input) was 36.4% for coal-fired generation and 46.7% for combined cycle gas turbines (CCGT) [1]. This low electrical efficiency is inherent to centralised electricity generation, where heat from the energy conversion process is ejected to the atmosphere, and electrical losses occur over the transmission and distribution network. In the current climate of energy awareness, where concerns over carbon emissions, energy costs and security of energy supply have prompted drives to reduce both carbon emissions and primary energy consumption, there is an impetus to maximise electrical efficiency.

In the last decade, energy studies in the UK have typically considered the long term marginal carbon intensity (CI) of grid electricity as 0.43kgCO_2/kWh [2], as introduced by DEFRA. The approximate carbon intensity of electricity generated by coal-fired stations and CCGT plant has been quoted as 0.96kgCO_2/kWh and 0.44kgCO_2/kWh respectively [3]. Investigations of electrical micro-generation technologies, that is power sources with electrical capacities typically below 50kW_e (or in some definitions below 5kW_e), typically use the marginal carbon intensity when calculating the relative carbon savings between electricity generated by the micro-generator and the National Electricity Grid (NEG).

Climate change research is a complex topic, out with the domain of this project; however, atmospheric carbon dioxide (CO_2) concentration has been identified as a major contributor to global warming. International and UK studies [4][5][6][7] have called for large changes in the rate of CO_2 emissions associated with energy use, e.g.

reductions of 60% between 2000 and 2050, in order to stabilise atmospheric carbon dioxide concentrations within levels predicted to limit the effects of global warming on the global climate.

The UK government has set ambitious greenhouse gas emission reduction targets of 80% (of 1990 emissions) by 2050, with an interim target of 34% by 2020 [8]. The European Union (EU) set wide ranging targets to integrate emissions reductions, supply of energy from renewable sources, and energy efficiency improvements, with "20-20-20" calling for 20% improvements (versus 1990 levels) in each of these areas [9][10]. Within the context of these targets, the UK government has made specific commitments to reduce the carbon footprint of dwellings [11][12].

The interest in renewable technologies, which in some definitions includes low-carbon technologies such as micro-Combined Heat and Power (micro-CHP or μCHP), is driven by the issues of climate change, security of supply, and affordable energy. Renewable or low-carbon micro-generation technologies include μCHP, solar photovoltaic (PV), solar thermal, heat pumps, biogas- and biomass-fired boilers, and wind turbines. To secure investment and drive adoption of renewable technologies, the European Union agreed to the Renewable Energy Directive 2009 (2009/28/EC), which requires 20% of energy (from electricity, heat, and transport) consumed by member states to come from renewable sources by 2020. Within this framework, the UK government has agreed to a 15% target for energy (for the purposes of transport, heat and electricity) to be supplied by renewable sources by 2020 [13][14]. The devolved administrations in the UK (Scotland, Northern Ireland and Wales) have produced targets for renewable energy production in support of central government [15][16][17]. The Scottish government has targeted 100% of electricity to be generated from renewable sources by 2020 [15].

Energy policies and technology uptake are not only driven by climate change concerns, economic factors or security of supply concerns (due to resource scarcity and geopolitical circumstances). Recent market research [67] on μCHP systems discusses the impact of Japanese and German energy policy changes on μCHP uptake since the

Fukushima-Daiichi nuclear power station disaster. With Japanese energy policy priorities shifting to incorporate distributed generation as a means of meeting peak electrical demands on the national grid, annual sales of $1kW_e$ μCHP systems have more than doubled to 18,000 units. In Germany, the disaster prompted a rethink of the national energy strategy, with a planned end to nuclear electrical generation by 2022. This so called "Energie U-turn" presents an opportunity for distributed generation, supported by the re-introduction of the German μCHP purchase subsidy [67].

In this thesis, an alternative approach to domestic energy supply is considered at a discrete dwelling level, where a building-integrated micro-generation system provides electricity in combination with the NEG. Micro-Combined Heat and Power (μCHP) systems are one form of building-integrated micro-generation, and will be the primary focus of this thesis. In contrast to centralised electrical generation systems, the investigated μCHP systems utilize a much higher proportion of primary input energy, through the recovery of heat from an electrical generation process, and the avoidance of transmission and distribution losses [20]. These μCHP systems can also be referred to as co-generation systems, and in a domestic context they predominately have a rated electrical output (P_e) of $5kW_e$ or less. This fits within the UK government's definition of micro-generation, as defined in recent strategy documents [21]. In support of the policies discussed previously, the UK government has supported [18] combined heat and power research, development and deployment (for μCHP and larger systems), including domestic field trials of μCHP systems [19].

There is a distinction between micro-generation technologies that generate electricity only, and μCHP systems. To understand the economic and carbon reduction potential of an electricity-only generator, the demand profile and potential for generation need to be understood for a single fuel. Where storage is employed to maximise on-site utilisation of generated electricity, the behaviour of the storage device needs to be understood. μCHP adds several layers of additional complexity; the need to understand the demand profiles and supply potential for two types of end use energy demands (under varying load conditions), the co-incidence of both demands, the storage of heat and/or electricity, and the responsiveness of demand to supply. This

final point does not apply to electrical systems (with the exception of changing efficiencies of storage technologies over the range of state-of-charge levels), but it is a significant matter for thermal systems. The thermal mass within thermal stores and space heating distribution systems introduces the dynamic response of thermal demand profiles to the profile of thermal generation. The distinction between static and dynamic demand profiles is drawn in Section 1.6.3, and it is argued that this distinction is often overlooked in the investigation of μCHP performance, where many studies are confined to the response of supply to demand.

The issues co-incidence of thermal and electrical demand and dynamic response of demand to supply, especially within the operating constraints of different μCHP technologies, is the core of the research issue investigated in this project. In order to conceive, model and analyse any energy supply approach, the transient nature of demand must be characterised and understood, in both daily and annual contexts. To this end, this research project was undertaken to explore and build an understanding of the relationships between transient demand and supply. Part of this research exercise is to understand the technological constraints placed on μCHP systems, and their resultant ability to follow variable thermal and electrical demand. With this understanding, operating and control practices can be defined and investigated to maximise μCHP system performance.

1.2 Introduction to Domestic Energy Demand

In 2010, domestic demand accounted for 32% of the UK's final energy consumption [22] or 564TWh [22] per annum, and as such, contributes approximately 17% to the UK's total CO_2 emissions [23]. It was estimated that in 2009, Space Heating (SH) accounted for 61% of total energy consumption in dwellings, Domestic Hot Water (DHW) for 18%, lights and appliances (in the form of electricity) accounted for 18%, and cooking for 3% [24].

At a discrete household level, the demand for electricity and SH/DHW can vary drastically, where the majority of dwellings have annual electrical and thermal

demands of 2-15MWh and 5-25MWh respectively [25]. The variation in demand is influenced by human behavioural factors, building performance, appliance and energy system efficiency, and local climate factors. This energy consumption is not spread evenly across a year – demand curves display seasonal, daily and continuous variations. As a rough guide, it can be presumed that whilst the annual energy consumption differs between domestic buildings due to both static factors (i.e. building fabric, appliance ownership, number of occupants and location) and dynamic factors (climate variations, occupancy patterns, space heating system inertia, energy storage capacity), temporal variations are driven by dynamic factors alone. Understanding these factors is an essential part of the system analysis process for alternative energy supply options. Occupant behaviour and the resultant appliance, DHW and ventilation utilisation practices can be considered both a static and dynamic factor. The "typical" behaviour of a particular group of occupants results in an average level of energy consumption over time, typically located within the ranges discussed previously. However, the variation in user behaviour introduces temporal variations throughout the day, between individual days, between weekdays and weekends, and across the seasons.

Domestic energy consumption is projected to grow due to a number of factors including: increasing population [26] and a decreasing average size of households [26] resulting in more dwellings; and increased ownership and usage of a number of existing and emerging appliances. However, it should be noted that making such predictions is extremely difficult, as there are a number of factors that will reduce energy consumption per household, and factors where the future effects are not readily discernible, such as climate.

Building regulations, for new builds and extensive refurbishments, are forcing reductions in space heating energy consumption through improved building fabric, and in electrical consumption by mandating energy efficient lighting [27]. A minority of new homes exceed the minimum efficiency standards, instead voluntarily following eco-home standards such as PassivHaus, which introduce primary energy demand and specific heating demand requirements of <120kWh/m^2/year and <15kWh/m^2/year

respectively [28]. However, 80% of the UK housing stock that will be present in 2030 will have been constructed before 2005 [29]. Consequently, technologies and legislation that affect existing housing will play a significant role in domestic energy consumption and carbon emissions. Various European standards have mandated efficiency improvements in new heating equipment, appliances and lighting, with newer standards [30] covering an increasing number of traditional domestic appliances and consumer electronics. The intent of this legislation is to decrease energy consumption per dwelling.

It is postulated that accurate predictions of energy consumption and/or carbon emission reductions can only be made by considering an energy system with high temporal precision. This supported by research undertaken by Hawkes and Leach [31], who reported overestimation of carbon savings by up to 40% using hourly as opposed to 5-minute μCHP analysis. As such, detailed models have been created to estimate energy demand with a sub-minute time-base, then subsequently analyse the performance of micro-generation systems under those temporally precise demand conditions.

A very limited number of domestic energy monitoring projects, reporting on the variation of energy consumption throughout the day or year, have been conducted (and published) in the UK. Certainly, there are insufficient numbers of samples in any datasets to consider any energy consumption profiles representative of particular dwelling and household types.

In this project, a bottom-up approach to domestic demand modelling was taken, in order to synthesis time-varying demand profiles, as discussed in Chapters 2 and 3. This is similar in approach to other projects that estimated demand in a bottom-up manner, such as TARBASE [32][33] and 40% House [34]. However this project strove to identify rational demand profiles with a high level of temporal precision throughout a day for a particular dwelling and household, instead of annual demand for a stock of buildings.

Bottom-up definition of demand was a challenge, however, as there are limited sources of detailed data on energy consumption of specific appliances, lighting and DHW within a domestic context. Much of the existing data is based upon projects involving some combination of household size and economic status, product sales data and average energy consumptions from small-scale monitoring projects or appliance certification tests. With this scarcity of data, a limited appliance monitoring programme was undertaken, as discussed in Section 3.6, which in itself was not representative of any appliance stock.

1.3 Introduction to Current Domestic Energy Supply

There were around 25 million dwellings in the UK as of 2006 [35], where approximately 91% of these have a central heating system [36]. Gas-fired boilers provided the heat generation for 87% of these centrally-heated homes [37], with oil-fired boilers accounting for 4% of such dwellings [37]. The BRE Domestic Energy Fact File reports that the proportion of gas and oil boilers that are condensing has grown rapidly since 2000, standing at approximately 15% by 2006, with increasing growth projected through to 2020 [38]. The maturity of domestic gas boiler technology has resulted in seasonal efficiencies of up to 93%, leaving minimal opportunities for carbon savings through further improvements of domestic condensing boiler technology. It is important to consider seasonal efficiencies, which account for the variation in efficiency due to operation at part load and non-condensing operation, as discussed in Section 2.4.5. All efficiencies discussed in this thesis are Higher Heating Value (HHV).

The limited penetration of condensing boilers into the dwelling stock has resulted in a stock-level average efficiency of domestic central heating boilers of around 76% [39]. The minimum boiler seasonal efficiency permitted under the current UK building regulations is 88% [40]. With mean life expectancies of domestic boilers, by boiler type, of between 15-30 years for boilers installed from 1980 onwards [41], an opportunity exists to replace the existing boiler fleet within the next few decades. Although the average efficiency of installed domestic boilers can be increased by around 17% merely by applying current technologies, there is little scope for

subsequent improvement. Therefore, research into carbon abatement has pursued other avenues, one of which is co-generation of heat and electricity, using a μCHP system.

In the UK, the majority of natural gas-fired dwellings are connected to the national gas grid, with the minority using propane or liquefied petroleum gas (LPG), delivered in bulk or in bottles. From the statistics quoted previously, dwellings with gas-fired central heating accounted for 79% of the UK domestic building stock in 2006. As such, it was decided to consider dwellings attached to the national gas grid in this project, with the associated fuel carbon intensity of 0.19kgCO_2/kWh [42]. However, the model and accompanying methodology developed in this project can be applied to μCHP (and other energy systems) using alternative fuel types, including those generated on-site as an energy storage medium (e.g. hydrogen).

The National Grid Company operates the electrical transmission systems of England and Wales, and of Scotland, since April 2005, at which point they were integrated under the British Electricity Trading and Transmission Arrangements (BETTA), introduced in the Energy Act 2004 [43]. The transmission system in Northern Ireland, whose demand is reported within UK-wide energy figures, is linked to both Scotland and the Republic of Ireland through interconnectors. A number of Distributed Network Operators (DNOs) operate the electrical distribution systems throughout the UK, linking transmission systems with points of demand (i.e. buildings and industry). Central and distributed electrical generating stations (including pumped hydro, which stores electrical energy during periods of low demand to provide peak load output during high demand, and renewables such as wind farms) are operated by a vast number of companies. Through a complex balancing mechanism, electricity generation is managed to meet demand. In recent years, government subsidies such as the Feed-In Tariffs (FITs) have encouraged the deployment of distributed generation, from renewable and low-carbon sources [21].

However, μCHP technologies have been awarded minimal support compared to other technologies such as solar photovoltaic [21], where the FITs generation rate (paid for

each kWh of generated electricity) is 11p/kWh for micro-CHP (with a proposed rise to 12.5p/kWh), compared with 16.8-21p/kWh for domestic-scale Solar PV systems [21]. This is primarily due to a lack of widespread commercial availability of μCHP systems and uncertainty regarding the potential of μCHP to deliver CO_2 and cost savings. A Carbon Trust field trial programme [19] identified carbon savings of -5% to 5% for domestic-scale μCHP systems, which suggest that the technology may increase the carbon footprint of dwellings if improperly implemented. This is in contrast to many demand-side energy efficiency measures, such as improvement of building fabric, where there is confidence in the energy saving potential of many technologies, even if this does not always directly translate into CO_2 savings when a proportion of heat loss reduction is used to increase thermal comfort. This uncertainty in μCHP performance is an issue for policymakers (i.e. will subsidies result in CO_2 savings), μCHP owners (i.e. will the system provide cost benefits to justify the installed cost) and for those involved in the development and sale of μCHP systems (i.e. will performance drive sufficient sales to justify the investment). Addressing this uncertainty by determining potential CO_2 savings and predicting effects on system lifetime (and hence the economic case for implementation) for μCHP systems, as undertaken in this doctoral project, is a worthwhile endeavour.

Hawkes [44] identified that the Large Combustion Plant Directive legislation will force approximately 12 GW of oil-fired and coal-fired generating plants to close before 2016. Peacock & Newborough [45] discussed the required replacement, within the next few decades, of much of the UK's existing centralised electricity generating plant as an opportunity for the deployment of distributed generation. This distributed generation could entail renewable or fossil-fuelled technologies; either integrated to buildings or operated stand-alone [7][46]. Crozier-Cole & Jones [63] estimated that the UK market potential for gas-fired μCHP systems based on Stirling Engine (SE) technology was 13.5 million units, with a potential for a further 1.7 million systems suitable for low-demand homes, and the potential for approximately 800,000 oil-fired μCHP systems. An opportunity exists for μCHP to provide dispatchable generation capacity to the NEG. A dispatchable generator can be switched on and off, or modulated, with minimal notice,

in contrast to non-dispatchable generators, such as nuclear reactors, that take a significant period of time to respond to any signal to change output level.

The advantage of supply-side interventions like µCHP is that a system (of suitable design) may provide a CO_2 saving comparable with a demand-side measure, whilst having the ability to be dispatched to satisfy a proportion of the building's electrical demand, reducing the load on the NEG. The demand on the NEG varies throughout the day, between days of the week, and across the year [47]. With the varying energy demand on the NEG, and technical restrictions on the operation of particular generators (such as start-up times, ramp rates and poor part-load efficiencies), demand-side management becomes more important in balancing supply and demand [48]. As the domestic sector accounted for 36% of UK primary electrical consumption in 2010 [49], it introduces a significant proportion of the load variations on the NEG. Others have reported options [50][51][52] to modulate demand in dwellings, by changing user interaction with appliances or directly changing appliances.

Assuming that the 13.5 million potential systems identified by Crozier-Cole & Jones [63] were deployed, with an average net electrical output of $1kW_e$, this represents 13.5GW of installed capacity, or approximately 22% of the 2009-2010 maximum demand [1]. Such implementation would make a significant contribution to the government's 2020 renewables generation targets, as discussed in the UK Energy White Paper [46]. Others have studied the effects of such penetration levels of µCHP on the supply-demand balance of the national grid and the distribution infrastructure [45][53][54][55]. The scope of this project, however, is limited to the performance of µCHP systems within the dwelling, where it is assumed that any electrical exports to the NEG are welcomed, displacing electrical generation and the associated carbon emissions elsewhere on the grid.

1.4 Introduction to Micro-CHP

The performance of µCHP systems will be the prime focus of the doctorate project, due to the interest by the UK Government and utilities in its implementation for

reduction of carbon emissions from the domestic sector. µCHP systems can de-carbonise the co-provision of heat and electricity, and if suitably configured, could provide electricity to a building independently of the NEG on a permanent or temporary basis. As a distributed form of electricity generation, µCHP systems could, due to the export of electricity not utilised on-site, displace centralised electrical generation required for other consumers on the national grid.

This research project does not attempt to undertake an economic analysis of µCHP systems, nor does it address the issues of ownership and deployment, or the policies supporting uptake of µCHP. Examples of such economic analysis include Hawkes & Leach [58][73], Hawkes et al [75][114], Sigma Elektroteknisk [85], and Allen et al [105]. Allen et al [105] reports that by late 2007, approximately 1,000 µCHP systems were installed in the UK, where modelling results indicated that financial paybacks in the range of 3-5 years were feasible. This payback was calculated based on annual domestic energy demand of 15-18MWh of natural gas and 2.5MWh of electricity, and installed system costs of approximately £3,000 (which related to a $1kW_e$ Whispergen SE unit) [105]. In the evaluation of their field trial [19], the Carbon Trust estimate µCHP payback as 20 years, based on the poor performance reported, and marginal costs (versus a condensing boiler) of £1,500.

Other investigations have tackled current or proposed policies supporting µCHP, including Hawkes & Leach [60], Allen et al [105], Saunders et al [119], Watson et al [121], Watson [122] and Williams [123]. A variety of µCHP system deployment routes, to the domestic market, have been discussed by Crozier-Cole and Jones [63] and Watson [122]. In future investigations, it may be important to investigate policy & legislation changes required to support the new paradigm of energy provision by distribution combined heat and power generation. Harrison [97] notes that as certain SE µCHP system designs, as discussed in Section 1.4.2, may require extended pre-heat periods (before electrical generation commences), the duration to which a home is heated above ambient temperature may increase. This could be especially relevant for fuel cell systems, variants of which (particularly SOFC) may be technically limited to operating continuously throughout the day, with recovered heat used to maintain the

home at a higher set-back temperature. As this increases the mean internal temperature of the dwelling, it will adversely affect the Standard Assessment Procedure (SAP) rating, which is used to underpin policy measures and building regulations. However, Harrison [97] argues that as the increase in setback temperature enhances thermal comfort of the occupants, this is a positive effect, presumably if the μCHP system offers a carbon saving versus a traditional boiler system. Harrison concludes that UK homes may very well follow European practices of using heating controls with setback rather than regular periods where space heating is off.

A μCHP system typically incorporates a prime mover to generate electricity, from which useful heat is recovered, and an auxiliary thermal generator, which can operate in parallel or independently of the prime mover. When the μCHP is attached to a space heating network, a thermal store is commonly installed [131], and may even be integrated with the μCHP product [134]. In contrast, electrical storage is a niche feature of μCHP systems, which tends to be investigated or integrated for off-grid solutions or where utilisation of on-site renewable generation is an imperative, regardless of economic cost or other factors affecting feasibility [106][112]. In situations where the fuel needs to be processed before input to the prime mover, for instance reformation of natural gas to hydrogen for a Proton Exchange Membrane[1] (PEM) fuel cell, a fuel sub-system is required. Such systems are also required where fuel needs to be stored, such as for off-grid systems, or when hydrogen is created using on-site electrolysis. A control system is required to manage the operation of all μCHP system components defined above. Aspects of this control may be delegated to discrete equipment, such as the charge controller for battery-based electrical storage, and the control system will interface with the building's space heating and DHW controls.

μCHP units are commercially available, or in field trial stage, with electrical capacities up to 50kW$_e$. However, domestic-scale systems tend to be <5kW$_e$, whilst larger units are aimed at small non-domestic applications, a definition supported in literature [87]. It is prudent to note that current regulations limit the net electrical output of electrical

[1] Also referred to as Polymer Electrolyte Membrane

generating equipment to 16A per phase [65], which is approximately 3.7kW$_e$ on a single-phase domestic supply, above which a 3-phase electrical supply to the dwelling would be required, at additional cost. As pointed out by Hawkes et al [163], at the start of their Micro-CHP Accelerator Program, the Carbon Trust defined µCHP as <3kW$_e$, but later added the prefix 'domestic', in order to conform with an applicable EU directive [19].

Several candidate technologies for µCHP prime movers are under development, primarily for natural gas-fired systems, although oil, LPG, biomass and solar-heat-driven prime movers have been investigated. The generic families of prime mover are internal combustion engines, external combustion engines, fuel cells and micro-turbines.

Internal combustion engines, which are usually derived from automotive or industrial designs, are fuelled by petrol, diesel, natural gas or LPG.

External combustion engine technologies include Stirling cycle and Organic Rankine cycle designs, with prototypes and commercial offerings of each type available. However, the majority of prime mover development has focussed on Stirling Engines.

There are several fuel cell (FC) technologies, with associated variants and sub-types, but Proton Exchange Membrane (PEM), Solid Oxide Fuel Cell (SOFC), Molten Carbonate Fuel Cells (MCFC), Phosphoric Acid Fuel Cell (PAFC) and Alkaline Fuel Cell (AFC) have all been the focus of development for stationary power generation [66]. For µCHP prime movers, PEM- and SOFC-based systems have seen field trials and commercial availability.

Current micro-turbine technology has typically been restricted to co-generation systems between 25-80kW$_e$ [64]. More recently, the transition of a prototype 3kW$_e$ micro-turbine based µCHP system from lab testing to field trials has been announced [67]. However, micro-turbines have not been as popular as other prime movers in publically-disclosed µCHP designs.

The prime mover technologies mentioned above are discussed in Sections 1.4.1 to 1.4.5, with details of efficiencies, operational constraints, and the challenges reported in the development of μCHP systems based on each technology. These prime movers can achieve full load electrical efficiencies of approximately 10-35% for Stirling Engines, to 45%-55% for SOFC-based μCHP systems. However, performance in real-life operation will depend largely on the design aspects of the μCHP system, such as prime mover technology and capacity, energy storage configurations, and the operating regime applied. The real-life performance will also drive the lifetime and servicing requirements of μCHP systems, potentially deviating from the average values discussed in Sections 1.4.1 to 1.4.5. An overview of the operating regimes, and associated control methodologies, is presented in Section 1.5, with discussion of the major operational factors expected to affect lifetime.

A range of research and development (R&D) projects, focussing on prime movers, storage and control equipment for μCHP, are underway with various commercial, academic and government bodies. Several domestic μCHP units have been sold or are in field trials in the UK, EU (especially Germany), Japan, South Korea, Australia and North America [67]. A number of μCHP systems with Stirling Engine, internal combustion engine, PEM or SOFC prime movers have entered the market [64]. A trade press article [153] in mid-2009 claimed that 22,700 μCHP systems were sold worldwide during 2008, with cumulative sales exceeding 100,000. Indeed, 30,000 fuel cell μCHP systems were sold in Japan over 18 months following the Fukushima-Daiichi disaster. In Sections 1.4.1 to 1.4.5, a summary of field trial activities and commercial availability of μCHP systems is presented for the associated technology.

1.4.1 Internal Combustion Engine

Internal combustion engines (ICEs) have been adopted for a wide range of transport, stationary power generation and motive load applications (such as agricultural machinery). In an ICE, a mixture of fuel and air is ignited within a combustion chamber, and the expansion of the combustion gases exerts force on a piston, converting chemical energy to mechanical. Knight and Ugursal [130] discuss the classification of

small automotive and industrial engines as Otto cycle, where the fuel/air mixture is ignited by a spark, or diesel cycle, where the fuel/air mixture is ignited by heating due to compression. Knight and Ugursal [130] point out that ICEs with a resultant electrical output (from an attached alternator) of less than 30kW$_e$, within which domestic-scale μCHP systems exist, are frequently spark ignition. Onovwiona & Ugursal [64] discuss that natural gas-fired spark ignition engines are usually derived from diesel engines, and achieve fast start-up with significant heat recovery potential.

ICEs can achieve a net electrical efficiency (η_e) between 21-30%, with Knight & Ugursal [130] quoting 25-35% for natural-gas fired ICEs, and Dentice d'Accadia et al [87] presenting manufacturers' data quoting 21-30% for μCHP systems with net electrical outputs between 1-15kW$_e$. The latter quotes total system efficiencies (i.e. net electrical output plus useful thermal output) from 70% to over 90% [87]. Knight & Ugursal [130] discuss the altitude degradation of engine efficiency, roughly 4% reduction (versus efficiency at sea level) per 300 meters of altitude. Part load electrical efficiency is understood to remain within 85-95% of full-load efficiency until electrical output drops below 75%, at which point electrical efficiency reduces dramatically whilst thermal efficiency (in terms of useful heat output) increases.

Heat recovery from an ICE, for co-generation purposes, is typically achieved by heat exchangers coupled to the exhaust, engine oil and engine cooling water. Kelly et al [129] presented simulation results, validated by experimental data, demonstrating that heat recovery temperature (and hence useful heat output) is a function of the ICE's transient behaviour. The longer that an engine has stopped and allowed to cool before it is restarted, the lower the heat recovery temperature, and the longer it will take to return to steady state operation under constant engine operation. Onovwiona et al [117] expand this to electrical output, where they reference experimental data published by Voorspools and D'haeseleer [72] that indicates that transient operation has a negligible effect on electrical output, even after a cold start (i.e. an extended period has elapsed since the engine was last in operation).

ICEs require regular maintenance and servicing, where automotive engines can achieve 20,000 hours of operation before replacement, and the more expensive industrial engines are more reliable, with maximum lifetimes up to 20 years (which based on annual runtime of 1,500-4,000 hours would equal 30,000-80,000 hours) [130]. Dentice d'Accadia et al [87] consider the typical operating duration lifetime of automotive engines to be unfeasibly short for application as a μCHP prime mover. A report by Sigma Elektroteknisk [85] considers the 10-15 year lifetime of a prime mover to be equal to 50,000 hours, and compares this to typical automotive ICE lifetimes of 4,000 hours, and service intervals of 200 hours. Harrison [86] claims that existing ICE-based μCHP systems can achieve service intervals of 3,500 hours. However, there is a lack of data in the public domain regarding maintenance requirements and lifetime of currently installed μCHP systems, whether based on ICE's or other technologies. As such, any lifetime estimates should be treated with scepticism.

Dentice d'Accadia et al [87] discussed several design issues for ICE prime movers. They discuss the lack of a low-displacement engine with water cooling system, a significant source of useful heat recovery, which makes it difficult to build a domestic-scale μCHP system with high total system efficiency. They also consider that the weight of a typical ICE, with associated balance-of-plant, is too high for a domestic μCHP system that may be expected to be wall-hung. A 2010 market research report highlighted this as an issue in some countries, especially where the traditional heating appliance location is the attic, but not in others where the basement is the preferred location [88]. Volkswagen and the German utility Lichtblick have developed an ICE-based natural gas-fired μCHP unit, with an electrical output of 20kW_e [89], targeted at German householders for installation in their basements, which is similar in size to a large domestic fridge.

A report by the MicroMap project [84] points out the challenges faced by developers of ICE-based μCHP systems, notably the need to control noise and emissions. Harrison [86] claims that the inherent difficulty in controlling the internal combustion process, an issue not found with other prime movers, presents challenges with noise and emissions. Acoustic attenuation is required to control noise, and MicroMap concludes

that noise levels from μCHP systems installed in habitable areas of the home should not be louder than domestic appliances that operate continuously, e.g. freezers, which have a noise level 35-40dBA. Both MicroMap and Sigma Elektroteknisk [85] point out that internal combustion engines need costly, and potentially bulky, flue cleaners such as catalytic convertors to achieve suitable emissions control.

Several manufacturers have brought ICE-based μCHP products to the market, including Senertec and Valiant of Germany [90], and Honda of Japan. Market research by Delta [67] shows that ICE-based systems have dominated μCHP sales during 2005-2011, with the majority of sales in Germany and Japan.

The Honda Motor Company has sold several versions of its ECOWILL ICE μCHP system in Japan since launch in 2003 [91]. Since March 2007, Honda and Climate Energy LLC began retail sales of the ECOWILL unit in the US under the brand name freewatt[1] [91]. The 2007 version of the natural gas-fired μCHP unit produced by the Honda Motor Company generates 1.0kW_e (net) of electricity at a peak efficiency of 22.5%, with a total system efficiency of 85.5% [92]. An optional thermal store can be installed to supply SH and DHW systems [134]. The μCHP system is designed to be installed either outside, in a basement or utility room. Honda have achieved low noise levels (only 47 dBA at 1 meter), and low pollutant emissions by passing the engine exhaust through a catalytic converter.

The German boiler manufacturer Valliant currently market 1.0kW_e, 3.0kW_e and 4.3kW_e natural gas-fired μCHP systems under the ecoPOWER brand [93], where the larger systems were originally developed by Marathon Engine Systems of the US [94]. The 1kW_e natural gas-fired ecoPOWER unit was developed with Honda [95][96], and generates electricity at a peak efficiency of 26.3%, with a total system efficiency of 92% [91]. Senertec produce natural gas-fired ICE-based μCHP systems with electrical outputs between 5kW_e and 5.5kW_e.

[1] http://www.freewatt.com/power_gen.asp

1.4.2 Stirling Engine

A Stirling Engine (SE) is a closed-cycle regenerative heat engine, where a working fluid enclosed within the engine is heated by an external source [133]. As heat is added externally, there is no need for combustion within the engine itself, so an SE is referred to as an external combustion engine. The heat source does not have to employ combustion of a fuel as Stirling Engines can be supplied with heat from a range of sources including solar thermal, nuclear, geothermal, or other waste heat sources [108]. Bio-gas, LPG, and oil-fired versions of SE µCHP systems are expected to follow the natural gas-fired systems that have been developed to date [85].

An SE operates on the thermodynamic Stirling cycle, which is represented in Figure 1.1 with the corresponding stages quoted in the accompanying text.

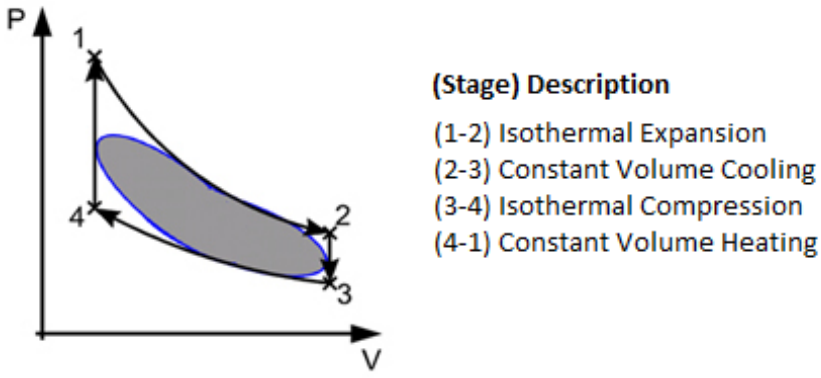

Figure 1.1: Pressure-Volume plot of Stirling cycle, where the theoretical cycle is indicated by the lines, and the ellipse represents the cycle of a practical engine (due to smooth continuous motion) – adapted from http://sunpower.com/services/technology/stirling.php

In a SE, one area of the engine (sometimes referred to as the hot end or hot space) is maintained at a high temperature (T_H) and another area of engine (sometimes referred to as the cold end or cold space) is maintained at a much lower temperature (T_C). The working fluid, which always remains in the gaseous state, is moved between areas by a displacer. A regenerator is used to capture a significant proportion of the heat lost as the working gas is cooled in transit from the hot space to cold space. The regenerator then relinquishes this thermal energy to the working gas as it transits from the cold space to the hot space, increasing the thermal efficiency (power out to thermal energy

in) of the engine [133]. There are multiple configurations of Stirling Engine, classified by the arrangement of their main components (primarily Alpha, Beta & Gamma), with distinction drawn between the drive methods (Kinematic and Free-Piston) [64].

In Beta and Gamma engine configurations, a displacer is used to displace the working gas between hot and cold spaces, causing heating (Stage 4-1) and cooling (Stage 2-3), whilst maintaining a constant volume of gas. The movement of a piston causes the compression (Stage 3-4) and expansion (Stage 1-2) of the working gas, during which the temperature remains constant due to heat rejection and addition respectively, hence those stages are isothermal [133]. In a Beta engine the piston and displacer are in the same cylinder, whilst in a Gamma engine the piston is in a separate cylinder [86].

In Alpha engine configurations, the hot and cold spaces are in two separate cylinders, each with a piston, where the working gas is driven between the spaces through the regenerator. The movement of the piston in the cold space cylinder causes compression, and the movement of the piston in the hot space cylinder causes expansion. Unlike the displacer in Beta and Gamma engine configurations, both pistons do work on the gas [86].

In a Kinematic Stirling Engine, the reciprocating motions of the piston(s) are converted to rotational motion by a crank, coupled to the displacer by a mechanical linkage. This rotational motion is used to drive a generator to produce electricity. In a Free-Piston Stirling Engine (FPSE), there is no crank (and hence no rotating components). Instead, the linear motion of the piston typically drives a linear alternator, and the displacer is driven by a pressure variation in the space between the piston and cylinder head [64].

Kinematic SEs require sealing to prevent leakage of the working gas (which is at high pressure) from the cylinder(s) and ingress of lubricating oil into the cylinder(s) [130]. The FPSE concept was introduced to avoid such sealing problems, where the entire engine and alternator casing is hermetically sealed, effectively eliminating leaks. The only potential leak path is the cable glands for the electrical conductors [130]. In a FPSE, the working gas should act as a lubricant, which is designed to eliminate friction

and wear due to mechanical contact, increasing efficiency and lifetime respectively [130]. In a Kinematic SE, any mechanical friction within the cylinders or the mechanical coupling will introduce inefficiencies to the engine's design.

Senft [132] discusses the "internal thermal loss"; that is the thermal transfer between the hot end and cold spaces of the SE. The mechanical output and efficiency of the SE is directly related to the magnitude of temperature difference between these spaces. Heat transfer between the spaces would reduce hot end temperature and increase cold end temperature, reducing the differential, hence decreasing power output and efficiency. Conduction is the major heat transfer mechanism, both through the engine structure and the working fluid. Senft also notes that SE efficiency is also limited by the efficiency of transferring thermal energy from the heat source to the working gas in the hot space, and from the working gas in the cold end to the thermal sink.

The internal thermal loss, heat transfer efficiency and friction discussed previously introduce inefficiencies in a practical engine, reducing the engine performance from that of the theoretical Stirling cycle to that of a practical SE, as illustrated in Figure 1.1. Other assumptions [133] of the theoretical Stirling cycle contribute to this performance gap: the regenerator is not 100% efficient in practice; there is fluid friction between the working gas and internal components; the smooth reciprocating motion of the piston does not achieve the same distribution of working fluid as discontinuous motion; and some of the compression and expansion takes place in dead space, i.e. not volume swept by the piston(s). The fraction of Carnot (η_{foc}) is sometimes called the relative efficiency, and is the ratio of actual thermal efficiency to Carnot efficiency [83][133].

The net electrical efficiency of a SE μCHP prime mover, η_e, can be calculated using equation (1.1). The Carnot efficiency (η_{carnot}) is the theoretical limit of efficiency, as driven by the hot and cold space temperatures (in degrees Kelvin), as calculated using equation (1.2) [133]. The burner efficiency (η_{burner}) is the combustion efficiency of fuel, and the alternator efficiency (η_{alt}) is the efficiency of conversion from mechanical work to electrical power in the linear alternator (for FPSE) or generator (for Kinematic SE).

The parasitic efficiency ($\eta_{parasitic}$) accounts for the proportion of gross electrical output consumed by balance-of-plant within the μCHP system.

$$\eta_e = \eta_{carnot} * \eta_{foc} * \eta_{burner} * \eta_{alt} * \eta_{parasitic} \quad (1.1)$$

$$\eta_{carnot} = 1 - \left(\frac{T_C}{T_H} \right) \quad (1.2)$$

The Carnot efficiency introduces two major design challenges for a SE-based μCHP system. There are two main heat recovery mechanisms in a SE prime mover: transfer of heat from the cold space heat exchanger and exhaust heat recovery from the external combustion system [98]. Some systems may also recover heat lost through the cylinder walls. It is important to balance lower cold space temperatures (which will increase electrical efficiency) with the need for high enough temperatures at the cold heat exchanger (HX) to transfer sufficient quantities of heat to the heat recovery medium.

Increasing the hot space temperature will increase efficiency; however it will increase the time required to pre-heat the engine before electrical generation commences (and thereafter reaches rated output). In addition, the effect of high temperatures on materials (for both metallic components and seals) is a major factor in system cost and lifetime. Corria et al [108] points out that a temperature rise from 360°C to 700°C resulted in a 25% (of original efficiency) rise in electrical efficiency for the commercially available Solo Stirling Engine. Van der Woude et al [102] reported net electrical efficiency increase from 10% to 11% by increasing hot space temperature of a Stirling Technology Company (STC) 1kW_e FPSE. Beale [101] discusses ceramics and alternatives to austenitic stainless steels that can permit higher temperatures, without lifetime issues, which will increase engine efficiency above 30%.

However, there are a wide spread of assumed efficiency values in the academic literature. Dentice d'Accadia et al [87] understood net electrical and total efficiencies of SE-based μCHP systems to be in the ranges of 10-33% and 70-90%, respectively, for engines between 0.8 kW_e and 11.4kW_e. This is likely due to the number of different

lab concepts, field trial designs and commercial products reported for SE μCHP. The MicroMap project [84] examined several μCHP systems expected to market early to mid-2000's; the 0.75kW$_e$ Whispertech beta-type Kinematic SE, which achieves 12% η_e using novel wobble-yoke coupling between engine and generator; BG Group's 0.75kW$_e$ FPSE with linear alternator, achieving 16% η_e; and Sigma Elektroteknisk's 3.2kW$_e$ Beta-type Kinematic SE, achieving 25% η_e. Crozier-Cole and Jones [63] understand that the Sigma system achieves a total efficiency of 96%. Sigma [85] also presented manufacturer's quoted electrical efficiencies for Kawasaki's 1.2kW$_e$ FPSE (27% η_e), Toshiba's 4.1kW$_e$ engine (34% η_e), and Mitsubishi's 3.8kW$_e$ engine (36% η_e).

Moriarty states that current efficiencies of 9-15% for domestic-scale Kinematic SEs could be significantly improved upon if manufacturing quantities justified the additional costs [158]. Keller [104] compares the operating η_e of the Whispergen Kinematic SE-based μCHP system, reported from field trials as 7.5-14%, with laboratory tests reporting 21%. This suggests that the control of the SE plays an important part in the operational efficiency of a μCHP system.

It is clear that there is scope for further development of SE prime mover technology. Harrison [86] discussed development by Sigma Elektroteknisk on a Beta-type engine, where it was believed that modification could raise the existing η_e of 20% to over 30%. Analysis of Stirling cycle, electrical conversion and burner efficiencies by Thombare and Verma [83] suggested that a maximum η_e of 40% should be achievable. Kaarsberg et al [128] claimed that current designs are simple and cheap, and that high value SE systems can achieve a η_e above 40%.

Part-load efficiency of FPSEs coupled with linear alternators units were discussed by Lane [127], who claimed that electrical efficiency remained within the 30-33% band with load variations of 35%-100%. Knight & Ugursal [130] expect electrical efficiencies at 50% load, for systems with rated efficiencies of 35-50%, to be in the 34-49% range.

FPSE development at Sunpower Inc., as reported by Lane and Beale [99], estimated greater than 40,000 hours heater head lifetime, ultimately limited by creep, at 650°C.

They later reported [126] on higher creep-limited lifetimes of 60,000 hours for FPSE units with electrical efficiencies between 30-35%. Wood [100] summarised later development at Sunpower Inc., where FPSEs achieving electrical efficiencies between 25-35% has already accumulated 70,000 operating hours. Onovwiona & Ugursal [64] expect FPSE technologies to achieve operating lifetimes of 10 years. The µCHP manufacturer Solo Kleinmotoren [161] estimates engine lifetime of 20,000-40,000 hours. Mayer & Cie [162] reported on the design and test of a $3kW_e$ SE µCHP system with a 30,000 hour design lifetime. According to Kaarsberg et al [128], one brand of FPSE has demonstrated greater than 50,000 hours continuous operation on single engine/alternator, and greater than 150,000 hours on composite machines. However, their lifetime expectation is closer to 30,000 hours.

Service requirements for FPSE are expected to eliminate mechanical maintenance [64], limiting maintenance to the burner and balance-of-plant, which should be similar to those of a condensing boiler. Ribberink et al [98] agreed that the Enatec consortium's $1kW_e$ FPSE should deliver high reliability and long life with no required maintenance due to the lack of sealing or lubrication problems inherent in their design. Onovwiona & Ugursal [64] expect SE service intervals, presumably for Kinematic variants, to be in the range of 5,000-8,000 hours. Kaarsberg et al's [128] expectations are more conservative, with service intervals between 3,500-5,000 hours, which they understand to be greater than 1 year of "economic" operation. Solo Kleinmotoren [161] quote service intervals of 6,000-8,000 hours for their SE µCHP system.

Harrison [86] points out that µCHP operation is normally heat-led, due to its high heat-to-power ratio (on current systems). However, such heat-led operation can introduce excessive thermal cycling if not properly controlled. A thermal cycle occurs when the prime mover is switched on and off again. Houwing & Bouwmans [81] defined operating constraints for their modelling exercise upon the field trial experience with SE µCHP systems at Gasunie, the Dutch utility. They utilised a 30-minute minimum runtime for the SE prime mover that was designed to limit thermal cycling, which was understood to damage the engine. Whispergen incorporate a 30-minute minimum run-time to prevent frequent thermal cycling in their Whispergen Model PPS24-ACLG

SE-based μCHP system [71]. Solo Kleinmotoren [161] notes that more than one thermal cycle per day would unacceptably limit the lifetime (and efficiency) of their μCHP system's prime mover. Kelly et al [129] believed that minimising thermal cycling of SEs was beneficial to their longevity and maintenance requirements. It is generally understood that both cumulative operating duration and thermal cycling limit the life expectancy of the prime mover [56] [69].

Lane and Beale [126] discuss the fast response and high part-load efficiency characteristics of FPSE designs. However, thermal cycling also introduces operational inefficiencies, as energy is expended to attain the required hot space temperature by heating a section of the engine. When the engine is switched off the hot space cools, releasing thermal energy to the environment where it cannot be recovered. Houwing & Bouwmans [81] quote SE prime mover start-up and cool-down durations of approximately 3 minutes, from communication with Gasunie regarding their μCHP field trials. In contrast, Entchev et al [160] discussed the challenges for start-up and shut down in early development models, with start-up periods lasting 10-30 minutes, depending on the time elapsed since the engine was switched off. They related this to a requirement to cool SE for a 30-65 minute period after shut down. The difference in start-up periods may be related to both the engine design and whether the auxiliary burner (used as an auxiliary boiler) contributes thermal input to warm-up the hot space.

Van der Woude et al [102] report on trial results for nine FPSE-based μCHP systems developed by STC; 3 operated in the lab and 6 in field trials. They witnessed a drop of η_e from 10% (in the lab) to 8% (in the field) due to an average of 13 thermal cycles per day, with systems with a 60l DHW tank. A Canadian study of the Whispergen systems by Entchev et al [110], with heat-led operation in test houses with simulated occupancy, incorporated a thermal store in addition to DHW tank, to reduce thermal cycling.

In contrast to the other prime movers discussed in Section 1.4, SEs are relatively simplistic, with no requisite for fuel processing, no strict requirements on moisture and

air handling, and external combustion of fuel. The latter characteristic predicates the use of combustion sub-systems that are comparable to the established gas-fired boilers, the dominant micro-generation technology in domestic space heating provision.

For a μCHP system aimed at mass market deployment, there are numerous practical and cost benefits associated with using established burner technology. Many aspects of a μCHP system may require costly and time consuming R&D before a commercially-viable product is available; utilising existing designs where possible (i.e. for a gas combustion sub-system) will reduce R&D activities and hence development costs. Many existing designs will have a proven operating record, with readily-available (to the manufacturer) information on failure mechanisms, expected lifetimes and projected service intervals, limiting technical and commercial risk. Installers and service technicians are already familiar with such technology, limiting additional training requirements for μCHP. Existing supply chains are in place for the manufacture of such burners, and the provision of spare parts, which should limit the parts costs.

Lane and Beale [126] claim that SEs are quieter than ICEs due to the controlled nature of external combustion versus internal combustion. Onovwiona & Ugursal [64] agree with this assessment, and point out that the lower frequency of power pulse per revolution compared with ICEs will limit vibration, another source of acoustic emission. Ribberink et al [98] claims that FPSEs operate silently, although it should be noted that the burner, flue fans and circulation pumps will introduce noise. Development of the Whispergen μCHP system has improved acoustic designs to enable installation in kitchens, with noise levels similar to domestic freezers [159].

In 2010, Delta [88] reported that several hundred SE-based μCHP systems were currently under test in Germany, The Netherlands and UK. It is worth noting that interpreting market statistics is complicated by varying definitions of μCHP (typically up to either $5kW_e$ or $50kW_e$) and manufacturers who define their product as either domestic or small commercial systems. Delta claimed that Whispertech, Remeha and Baxi (where the latter two companies had recently merged) had more than 1,000 units that were currently participating, or had previously participated, in field trials. Delta

summarised field trial results reported in 2010 for SEs, where the average η_e (across the trial period) ranged between 5-15%. Running hours of 1,500-4,000 per annum were recorded, depending on the dwelling's thermal demand and whether a thermal store was installed. The μCHP systems exported between 15-70% of generated electricity, where systems with a thermal store exported the highest proportions.

Market research released by Delta [67] in May 2012 claimed that BDR Thermea is the only manufacturer offering 1kW$_e$ μCHP systems, with less than 1,000 units installed. In addition, they discuss the launch of 1kW$_e$ μCHP systems by German manufacturers Viessmann and BDR Thermea (under the Senertec brand). Both systems utilise Microgen Engine Corporation's FPSE. The Microgen unit was originally developed by BG Group using a linear FPSE design from Sunpower of the US, but has since been sold to a consortium of boiler developers.

1.4.3 Fuel Cells

As discussed in Section 1.4, there are a large number of fuel cell technologies, with associated variants and sub-types, including Proton Exchange Membrane (PEM), Solid Oxide Fuel Cell (SOFC), Molten Carbonate Fuel Cells (MCFC), Phosphoric Acid Fuel Cell (PAFC) and Alkaline Fuel Cell (AFC) [66].

In a fuel cell, hydrogen and oxygen (the reactants) are combined to create water, by the electrochemical processes of oxidation of hydrogen and reduction of oxygen. An electrolyte is sandwiched between two electrodes (anode and cathode), where the electrodes are accompanied by a catalyst. Hydrogen (as the H_2 molecule) is fed into the anode, and oxygen (O_2), from either air or a concentrated source, is passed over the cathode.

In PAFC and PEM fuel cells [157], the catalyst at the anode encourages the hydrogen molecule to split into positively-charged ions (protons in this case) and negatively-charged electrons. The electrolyte only allows ions to pass through to the cathode, so the electrons are forced to flow around an electrical circuit to reach the cathode, hence creating an electrical current. At the cathode, the oxygen molecules combine

with the protons and electrons, in the presence of a catalyst, to produce water and heat. In SOFC, MCFC, and AFC [157], the catalyst at the cathode encourages the oxygen molecule to “reduce”, acquiring electrons to create a negatively-charged oxygen ion. Again, the electrolyte only allows ions to pass through to the anode. At the anode, the oxygen ions combine with the fuel (containing hydrogen and oxygen), in the presence of a catalyst, to produce water, heat, carbon dioxide and electrons. These electrons flow through the anode, around an electrical circuit to the cathode (where they reduce oxygen atoms), hence creating an electrical current.

As a single fuel cell generates a relatively low current at low voltage, cells are physically and electrically stacked to produce electrical power at suitable current and voltage levels to allow efficient conversion into a.c. or d.c. electricity at the required voltage. These stacks are also designed to facilitate the transport of reactants and reaction products to and from each cell, including thermal management.

Each of the fuel cell technologies operate at a different temperature, and with different requirements for fuel purity and water management. In all FCs, a proportion of the hydrogen fuel does not react and leaves the FC as off-gas. PEM FCs operate at relatively low temperatures, between 50°C-100°C, and SOFC operate at relatively high temperatures, between 700°C-1,000°C, depending on design [66]. The low operating temperature of PEM, typically 80°C, can provide challenges in recovering useful heat at an adequate temperature. Heat recovery from a FC prime mover may include thermal losses from the stack, heat from the produced water and off-gas, and heat recovery from an external reformer.

The high temperature of SOFC and MCFC allow them to internally reform hydrocarbon fuels, such as natural gas, so that free hydrogen molecules are available at the anode [157]. Low temperature fuel cells (including PEM) require, if a source of pure hydrogen is not available, an external reformer to strip the hydrogen molecules from hydrocarbon fuel, producing a gas called reformate. A PEM FC also requires that the fuel processing system include a shift catalyser to reduce carbon monoxide concentration in the reformate before it enters the FC. The off-gas is typically

combusted to provide process heat for the external reformer. As the reformation process is endothermic with an efficiency of approximately 70%, it significantly reduces the η_e of a PEM μCHP system compared with the electrical efficiency of a PEM stack.

The net electrical efficiency of PEM and SOFC μCHP systems were broadly characterised by Dentice d'Accadia et al [87] as 30-40% and 40%, respectively, where PEM μCHP systems have a total efficiency of 90%. Entchev [111] compared FC efficiency with engine-based prime movers (which are limited by Carnot cycle efficiency), where he claimed that an electrical efficiency of 50% is potentially achievable with a realistic total efficiency of 75-85%. Comparing electrical efficiencies between FC types is difficult, as efficiencies may be quoted at a stack-level or system-level (i.e. including fuel sub-system and balance-of-plant inefficiencies).

As relatively immature technologies, many FCs under investigation may not reach the expected efficiency targets. Lab tests by Gigliucci et al [112] on a $4kW_e$ PEM initially identified net electrical and total efficiencies of 18% and 50%, respectively. They reported that "obvious" improvements to their experimental system increased these efficiencies to 28% and 68%. Hamada et al [113] reported net electrical and total efficiencies of 43% and 78%, respectively, for a $1kW_e$ PEM system under lab tests. Goto et al's laboratory investigation [103] of a $0.75kW_e$ PEM found net electrical and total efficiencies of 35% and 85%.

Industry research by Delta [88] in 2010 on commercial field trial results states that German and Japanese developers reported average η_e of 30% and 33%, respectively, for their $1kW_e$ PEM μCHP systems. They relay the experience of Japanese developers, where total efficiencies were limited to 80-85% due to the costs involved in overcoming the challenge of recovering low-grade heat. Kyocera's $0.7kW_e$ SOFC-based μCHP system (designed specifically for Japan's restriction on electricity export) has had mixed results, with average electrical efficiencies between 28-48%, depending on thermal and electrical load profiles [88]. Delta [88] claim that a SOFC μCHP developer has achieved average total efficiencies of 92% during their latest field trails, due to a design focus on thermal integration within the stack.

In contrast to other technologies, FCs can deliver higher gross electrical efficiencies at part-load than at full load, due to increased electrical efficiency at stack-level. Whether this translates to higher η_e at part-load depends on the design of the balance-of-plant within the system. Experimental results by Hamada et al [113] show that net efficiency can closely follow the relationship of gross efficiency with load. Onovwiona & Ugursal [64] agree that net electrical efficiency can remain relatively similar to that at rated output down to load levels between 25-33%.

Experimental investigation of a PEM FC by Hubert et al [116] identified part-load performance results of 38% gross electrical efficiency, and 69% heat recovery efficiency, at 75% load. This compares favourably with full load (5.2kW$_e$ gross) values of 36% gross electrical efficiency, and 72% heat recovery efficiency. Lab test results by Gigliucci et al [112] on a 4kW$_e$ PEM system demonstrates that despite reduced fuel processing efficiency and reduced fuel utilisation at part load, the increase in stack efficiency leads to an increase in electrical efficiency between 100% and 80% of load, and a corresponding decrease in thermal efficiency. This is supported by results published by Hamada et al [113]. Hawkes & Leach [73] discuss the high part-load electrical efficiency of SOFC, which may exceed the full load efficiency.

When considering the reported efficiencies of PEM μCHP systems from experimental studies, it is important to understand the effect of fuel processing sub-system efficiency on the system's η_e. This not usually an issue for SOFC-based systems, as they reform natural gas internally. Walmark et al [120] reported that their PEM setup had a fuel processing sub-system efficiency of 62%, which is similar to the range of PEM efficiency (48-62%), dependent on load condition, reported by Gigliucci et al [112]. However, fuel processing is an aspect of fuel cell μCHP development where potential for efficiency improvements may exist for many prototype systems, as is clear by comparing the previous results with those of Hubert et al [116]. They state that the fuel reforming efficiency drops from 76.6% at full load to 69.5% at 75% load condition.

Walmark et al [120] discussed the challenges of achieving load variations with natural gas-fired PEMs due to the fuel processing sub-system. The experimental system studied took approximately 10 minutes to fully respond to a requested change in load, primarily driven by the response of the reformer. Goto et al [103] related the start-up time of a PEM to the reformer temperature, which in turn is a function of the time elapsed since it ceased operation. They found that electrical output commences once the reformer reaches operating temperature (55 minutes from ambient temperature), from which point it takes roughly 40 minutes to reach full load, for a 0.75kW_e net rated output PEM, with a ramp rate of 0.25W_e/s. Reformer temperature falls to approximately 240°C in 70 minutes, which would result in a 35-minute reformer re-heat period, and to 120°C after 12 hours (45 minutes to re-heat), within which the idle periods of a domestic µCHP systems in daily usage would likely fall. Hamada et al [113] report similar temporal behaviours during start-up for a 1kW_e PEM system.

The concept of fuel cell output degradation over time is complex, and is a function of various operating conditions, including cumulative operating hours or output, load changes, and thermal cycles [156]. Indeed, Hawkes, Brett & Brandon [114] investigated the impact of cumulative output and thermal cycling degradation mechanisms on the carbon savings and economic case for PEM and SOFC-based µCHP systems. Dorer & Webber [109] understood that the adverse effects (including material deterioration, lifespan reduction and increased maintenance cost) of thermal cycling on current SOFC systems, continuous operating regimes were envisaged for SOFC µCHP. Hawkes & Leach [73] identified thermal stresses within cells during start-up and across cells during full or part load operation as a cause of mechanical failure. They claim that SOFCs have a lifetime of roughly 5 years (or 40,000 hours) at full load, although they believe that 70,000 hours is possible with further development.

De Bruijn et al [156] states that a stationary PEM FC may see electrical power output and efficiency degradation of approximately 10% over a 40,000 hour lifetime if operated at constant output. However, if load changes and thermal cycling is introduced due to the demand profile, and allowed by the operating regime and control algorithms of a µCHP system, then degradation rates can increase by several

orders of magnitude. In the context of μCHP system research in the public domain, degradation effects have not been the focus of widespread testing, however they do receive some attention. Hamada et al [113] reports that after 600 hours of cumulative operation and multiple thermal cycles, η_e had decreased to 95% of the efficiency when laboratory testing of their PEM commenced. Gigliucci et al [112], however, report no noticeable decays in system performance after 550 cumulative operating hours.

Knight and Ugursal [130] pointed out that maintenance requirements vary with type of FC, where the major overhaul of a FC involves replacement of the shift catalyser, reformer catalyser and FC stack. They claim that replacement of the stack is likely required every 4-8 years, the reformer catalyst every 5 years, and the shift catalyst every 3-5 years. Routine maintenance incorporates FC stack, reformer and balance-of-plant, where fuel filter changes typically occur every 2,000-4,000 hours [130]. To put this in context, Delta [88] report on field trial results within Europe and Japan for both PEM and SOFC μCHP systems. The typical cumulative annual operation of FC-based μCHP systems are 4000-7000 hours, with European runtime closer to the lower end of the scale. It is prudent to note that SOFC μCHP results from Japan were quoted as having the longest runtimes.

Knight and Ugursal [130] discuss field trial results for ten 5kW_e PEM FCs that achieved average availability (for an individual system) of 95.8% over approximately 52,000hours of combined runtime. As with other μCHP prime mover technology, however, more practical experience is needed before full confidence can be placed in maintenance, servicing and reliability estimates.

Fuel is not combusted in a fuel cell; however the anode off-gas, which comprises about 8-15% hydrogen [130], is burned in a lean combustion process in the reformer. Controlling the temperature of this lean combustion process limits NO_x emissions, although it should be noted that a main product of the natural gas reforming process is CO_2. This is supported by experimental results discussed by Hamada et al [113], where they analysed the exhaust gas from a 1kW_e PEM system, and found NO_x to be at a low level of 4.8ppm. Knight and Ugursal [130] note that FC technology has the potential (if

systems are properly designed) to limit emissions versus internal combustion technologies.

Field trials for FC systems have been underway since the mid-2000's, with approximately 3,000 PEM μCHP systems trialled in Japan before the commercial launch of those systems [88]. Kyocera have also executed field trials with their SOFC system [88]. In Europe, the Callux project supported the majority of FC μCHP field trial activity by Hexis, for roughly 50 units of their SOFC-based system, and Baxi Innotech, for 93 units of their PEM-based system [88].

Kiwa Gas Technology revealed in early 2011 [150] that, after a series of laboratory simulations in their Dutch laboratories on 4 systems from different international manufacturers, with some adaptions made for the typical Dutch dwelling, two FC μCHP systems were selected for field trials. These $1kW_e$ systems are being demonstrated, in a joint project between Kiwa, GasTerra and the Dutch government, to assess the potential for economic and CO_2 savings.

Recent market research by Delta [67] reports on exception sales of Panasonic's ENE-FARM FC-based $1kW_e$ μCHP system in Japan, with 2011-12 financial year sales of almost 18,000, vastly in excess of the target of 8,000, and 2009's sales figures of under 5,000. These sales are due to a policy shift in response to the shutdown of significant nuclear electrical generating capacity after the Fukushima-Daiichi disaster, and have spurred development by other manufacturers such as Toshiba, Toyota and JX. They claim that JX launched the world's first SOFC μCHP system in late 2011, whilst Japanese sales of PEM μCHP systems have reached the sales level of ICE-based systems. Delta [67] reports on government subsidies in South Korea, of up to 80% of capital cost, which has seen in excess of 400 FC-based μCHP installations during 2011, attracting development from major manufacturers such as Samsung. In the US, ClearEdge Power[1] has installed a hundred $5kW_e$ FC μCHP systems, and has signed a deal with an Austrian energy developer [67] to sell the $5kW_e$ units to homes and commercial properties.

[1] http://www.clearedgepower.com/residential/fuel-cell-power-generator

Delta [67] reports on the launch of the BlueGen SOFC-based μCHP systems by Ceramic Fuel Cell Ltd (CFCL) of Australia. With a η_e of 60% and limited thermal output resulting in a total efficiency of 85%, it is not being marketed as a replacement for traditional condensing boiler, although development is underway in the UK and Germany for such a product based on CFCL's Gennex fuel cell module [151]. The prime mover is designed to operate at a steady output level of 1.5kW_e for peak efficiency, or at steady output level between 0.5kW_e to 2.0kW_e with efficiencies of 36% and 57% respectively [152]. CFCL have a mixture of sales, field trial and development activities underway in a number of countries, including Australia, US, Japan, Germany, The Netherlands and the UK [151].

Ceres Power of the UK are developing a SOFC-based μCHP system, collaborating with Itho-Daalderop Group for field trials in The Netherlands, Belgium and Luxemburg in 2014/15, and a commercial launch in 2016 [153]. This follows a field trial programme with British Gas in the UK, where 5 units were deployed in dwellings in early 2011, with a second wave scheduled to follow in late-2011, and a third wave of at least 150 installations in 2012 [154].

A range of additional development and field trial activity is believed to be underway [155] with Topsoe, Acumentrics and Ceres Power all developing SOFC-based μCHP systems, and Ebara-Ballard and Eneos Celltech developing PEM-based μCHP.

1.4.4 Organic Rankine Cycle Engine

The Rankine cycle is a heat-engine operating cycle, commonly used in conventional fossil fuel and nuclear generation plants. A working fluid is pumped from a condenser, then heated in an evaporator by an external heat source. The working fluid expands as it passes through a turbine (which generates electricity), and the fluid is then condensed in a condenser, where it begins the cycle again. In a μCHP unit, useful heat is recovered from the condenser, and potentially from the flue gases from the external heat source [135]. In an organic Rankine cycle (ORC), the working fluid is an organic compound with a boiling point lower than that of water, which enables the Rankine cycle to operate with a relatively low grade heat source [136].

Harrison [97] discusses the 1kW$_e$ Inergen μCHP system, based on an ORC prime mover, under development by Baxi in the UK. He claims that the system exhibits good service life, relatively low manufacturing costs, but relatively low electrical efficiency. Energetix, under the Kingston brand name, expect to introduce [137] a 1.1kW$_e$ ORC-based μCHP system to the UK market in 2012, following the results of field trials in 2011/12 [138], which can operate from natural gas or LPG. Industry press reports that the Kingston system has an electrical efficiency of approximately 10% [139]. In Germany, Lion Energy has developed the lion-Powerblock μCHP system, which used an ORC prime mover to generate 2kW$_e$ of electricity [140].

μCHP systems with ORC prime movers that use renewable fuels have been investigated. Quoilin et al [146] reported on simulation results for a biomass-fired μCHP system, where the performance of selected working fluids was validated.

Cogen Microsystems in Australia have developed a μCHP system based on a Rankine engine, where the external heat source is hot water circulated from solar thermal panels [141]. Their system generates 1kW$_e$ of electricity and 8.8kW$_{th}$ of useful thermal output. They have undertaken a field trail in Australia [142], and continue to develop their product. It is prudent to note that a significantly greater area of solar thermal panels would be required to capture the same amount of input energy in the UK than in Australia, especially during winter months, increasing the capital cost and system footprint. The basic principle was previously investigated by Best & Riffat [106], who concluded that a home in South-east England, consuming 4,000kWh of electricity per annum, would require 66m^2 of evacuated tube solar thermal collectors.

1.4.5 Micro-Turbine

A micro-turbine consists of several main components, as depicted in Figure 1.2; the compressor, turbine, recuperator, combustor, generator and heat recovery system. The compressor pressurises input air, which is then pre-heated within a recuperator, and fed to a combustor. In the combustor, the hot air and fuel are ignited, and the expansion of the resulting combustion gases drives the turbine. The turbine shares a

shaft with the compressor, and as such the rotation of the turbine drives the compressor. In single shaft designs, the generator is on the same shaft, and high frequency electronics is used to generate electricity at the required frequency (i.e. 50Hz in the UK). In two shaft designs, the turbine also rotates a second shaft connected to a gearbox, to reduce the speed of rotation, which in turn interfaces with an electrical generator. The hot exhaust gas from the turbine is fed to the recuperator, where it pre-heats the compressed air before it enters the combustor [64]. In a µCHP system, this cooled exhaust is passed through a heat recovery system to transfer heat to a heat recovery circuit, providing useful heat output from the system.

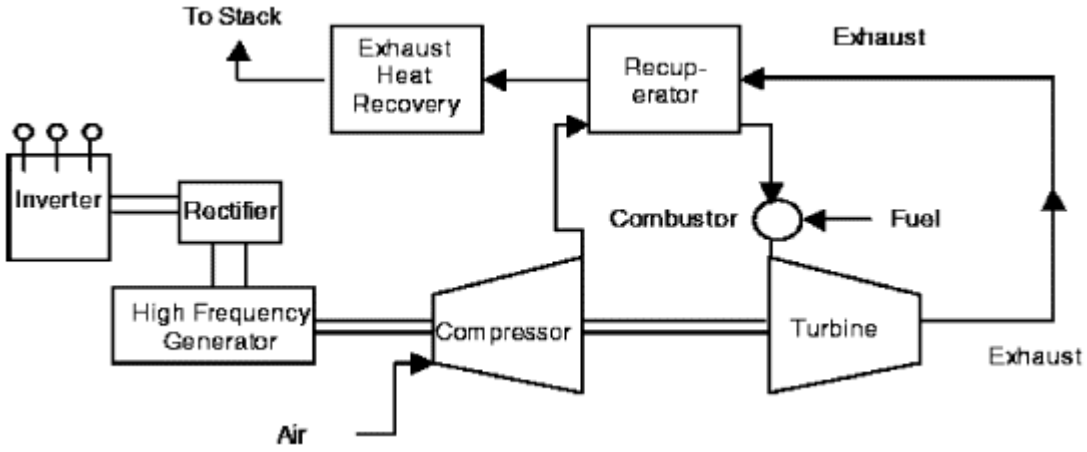

Figure 1.2: Schematic of Micro-Turbine components and operation. Source: Onovwiona & Ugursal [64], Figure 5

Onovwiona and Ugursal stated that current micro-turbine technology has typically been restricted to co-generation systems between 25-80kW$_e$ [64]. Their comparative review of micro-turbines versus other prime mover technologies suggests that the technology has advantages that may justify further development. The emissions from micro-turbines are typically lower than ICEs, primarily due to the continuous combustion of the former, similar to Stirling Engines. They claim that micro-turbines will exhibit lower noise and vibration than ICEs. They point out that whilst micro-turbines have the potential for lower maintenance than ICEs due to simplicity of design and fewer moving parts, the longevity of main components has yet to be fully proven. However, maintenance costs are currently expected to be similar to ICEs, in part due to

the requirement for specialist skilled maintenance personnel. A major overhaul would be required every 20,000-40,000 hours.

Onovwiona and Ugursal [64] discuss the part-load performance of micro-turbines, with η_e remaining at rated levels until electrical output falls to 80% of rated output, after which η_e reduces to 85% of rated efficiency at 50% of rated load. They discuss rated η_e values of 25-30% for prime movers with capacities of 30kW_e or higher, where smaller units are likely to have a lower electrical efficiency. This is supported by the Dutch manufacturer MTT [143], who claims that their 3kW_e (rated output) natural gas-fired micro-turbine μCHP prototype has achieved electrical efficiencies of 16% in lab tests. Delta [67] reported that MTT intend to start field trials late 2012 or early 2013 [144]. In addition, MTT have announced a co-operative research project, under the EU EUREKA framework, to develop a variant of their μCHP system fuelled by heating oil [145].

1.5 Micro-CHP Control & Operating Regimes

In addition to technological development (of prime movers, storage and balance-of-plant), consideration must be given to operational control of these μCHP systems. Control systems incorporate both equipment (such as sensors and interfaces with critical components such as fuel valves and pumps) and some form of logic (likely deployed as a software algorithm). The aim of the control system is to maximise the performance of the μCHP system as a whole, i.e. prime mover, auxiliary thermal generation, fuel sub-systems and storage sub-systems. Depending on the complexity of the control system, it may attempt to maximise one or more performance metrics, including carbon emission savings, economic cost saving and system lifetime. A well-designed control system will consider the operating constraints of each μCHP system component, incorporating the appropriate logic to maximise performance in light of such constraints. The effectiveness of control systems within the context of the variability of demand profiles is an important consideration for μCHP performance assessment.

In the context of micro-generation system operation and control, it is important to discriminate between operating regimes, control strategies, control signals and control drivers.

Operating Regimes dictate the manner in which the system operates, and what the system is designed to achieve. Common operating regimes, as discussed by Newborough [61], are summarised below, although a myriad of alternative or hybrid regimes could be conceived:

- "Thermal Load Following", where the system attempts to match thermal demand on a temporal basis
- "Electrical Load Following", where a similar approach is taken to electrical demand
- "Continuous-Output Operation", where the system is operated continuously for sustained periods of time, e.g. annual heating seasons
- "Constant-Output Operation", where the system is operated at constant load for one or more periods per day
- "Autonomous Operation", where the system satisfies all onsite energy demands without electrical grid support

Control Strategies are the methods by which the concept system responds to changes in demand. Multiple control strategies can be combined within the control algorithms of a μCHP system. Examples of control strategies include:

- "Output Modulation", usually of an electrical prime mover or thermal auxiliary, where the generator's part load operation is constrained within certain energetic or temporal limits
- "Thermal Store Temperature Control", where the temperature of the storage medium drives operational state of a heat generating device
- "Electrical Peak Shaving", where electrical generation and storage operation is controlled to limit the electrical import power level
- "Thermal Dumping", in the context of thermal output from the prime mover that is purposely ejected to the external environment in order to allow the prime mover to continue generation of electricity. It is prudent to note that

micro-CHP systems deployed in the UK cannot, under the current regulatory framework, be designed to dump thermal output during normal operation

- "Economic Optimisation", where output is dispatched (i.e. directed or curtailed) based on some economic signal, for instance real-time electricity and/or fuel prices

Control Signals are derived from observation of a physical, or virtual, parameter that is used by the control algorithm to trigger a change in operating state. These parameters include:

- Temperature of the internal air within the dwelling
- State of charge of electrical storage
- Temperature of thermal storage medium
- Electrical demand
- Energy output of non-dispatchable generation
- Grid electrical import/export prices
- Other network-derived generation/storage/export incentives

Control Drivers are the reason behind the control strategies implemented by a system operating under a specific operating regime. These drivers can be time-dependent or independent, and the Control Driver of a discrete dwelling may be considered as the satisfaction of a Control Signal from an external network, i.e. electrical grid or natural gas network. They include minimisation of fuel consumption and carbon footprint, maximisation of utilisation of on-site generation.

Harrison [86] argues that μCHP system operation is heat-led, as the prime mover attempts to satisfy some or all of the thermal demand, where electricity is generated as a by-product. This is contrary to the technical principles of prime mover operation, where otherwise wasted heat is recovered at a temperature useful for the building's SH and/or DHW systems. Electricity is typically considered the premium output, as the carbon intensity of grid electricity is several times larger than the carbon intensity of thermal energy generated by a natural gas-fired boiler. However, the electrical efficiencies achieved by the majority of prime mover technologies discussed in Section

1.4 are too low to generate electricity with a carbon intensity less than or equal to that of the NEG, hence use of the recovered heat to displace boiler fuel is required in order for μCHP systems to reduce CO_2 emissions. This concept is explored in Section 5.2.2.

Hawkes & Leach [58] state that heat-led control (i.e. thermal load following operating regime) has been the standard assumption of the μCHP industry. Simple thermal or electrical load following operating regimes assumes that the prime mover, and associated balance-of-plant, is capable of undergoing frequent thermal cycles. However, as discussed in Sections 1.4.2 and 1.4.3, μCHP systems based on certain prime movers suffer significant efficiency and lifetime penalties due to thermal cycling, and may have transient performance characteristics that vastly restrict output for long periods since start-up. To avoid these issues, it is important to develop more complex control systems, incorporating operating regimes and control algorithms to reduce the impact of such characteristics, and to achieve a good match between supply and demand. The latter entails an understanding of the thermal and electrical load profiles (and cumulative totals), and their levels of co-incidence, over the course of the day and year. Selecting a μCHP system design whose output can match the demand profile of a particular dwelling is essential in maximising performance and lifetime.

Various operating and control systems have been applied to modelled systems in the published literature, including thermal load following [61][3][81][77][76]; electrical load following [62][53][80][57][76]; continuous operation [62]; and least-cost control [58][81]. A previous study [45] explored the concept of centralised control of aggregated load from multiple μCHP systems, and such an approach has been brought to market by the German utility Lichtblick, using the ICE-based system discussed in Section 1.4.1. A number of investigations, both practical and modelling-based, that have considered various approaches to the control and operation of μCHP systems are discussed in Section 1.6.

1.6 Review of Micro-CHP Modelling

The academic literature includes many examples of μCHP modelling, using a variety of approaches, with a number of key aims that include the assessment of environmental and economic performance. As a broad overview, there are a few major distinguishing features of published technical (as opposed to studies predominately focused on economic, policy or mass penetration issues) investigations of μCHP, as summarised below:

- Type of modelling and the aim of the investigation; some have undertaken simulation to support practical measurements, with a focus on accurately predicting the performance of a type of μCHP system under discrete conditions, and potentially projecting performance over a longer timeframe or under different demand scenarios. A significant bulk of research has focussed on optimisation of one or more μCHP system characteristics, to maximise economic and/or environmental performance. The remaining investigations tend to use simulation to estimate the performance of particular μCHP systems, under a range of demand scenarios, to report on economic and/or environmental performance
- Temporal precision of modelling, where iteration intervals (i.e. timesteps) have varied from minutes to months
- Temporal extent of modelling exercises, which have either encompassed an entire year, or discrete “design days” or “design weeks” that typically represent high, medium and low points on an annual distribution of daily energy demand
- Source of energy demand data; some studies utilise recorded demand profiles, some estimate demand profiles before modelling, and others generate load profiles as part of the μCHP performance simulation
- Response of thermal demand to supply; in some investigations, the thermal demand profile is static, in that the over- or under-supply (due to operating restrictions) of thermal energy from the μCHP system can have no effect on the demand profile used for subsequent iterations. Whilst some investigators have matched supply and demand via a thermal store to introduce some responsiveness of demand to supply, others integrate a μCHP model with thermal building simulation to dynamically calculate demand each iteration

- Integration of operating restrictions of µCHP systems, particular those of prime mover, fuel sub-systems and auxiliary thermal generation; Many studies disregard start-up performance characteristics, part-load characteristics, modulation limitations and State-of-Charge-related performance of electrical storage
- The addition of storage sub-systems to a µCHP system to circumvent operating restrictions, or lessen their impact on performance
- Operating Regimes and control approaches adopted by models, where thermal load following and electrical load following regimes are common, whilst hybridised operating practices to minimise operating cost, usually referred to as "least-cost", have been investigated
- Breadth of modelling exercise; some studies have investigated multiple discrete building variants, or the same building variant with differing characteristics, in an attempt to understand the impact of demand scenarios on µCHP performance. Others have investigated the impact of µCHP penetration on the NEG by simultaneously modelling multiple buildings, usually with a range of demand scenarios, optionally applying centralised control signals to manage aggregated demand and export profiles

1.6.1 Overview of µCHP Modelling Approaches

µCHP modelling has been applied to support experimental investigations, with a focus on accurately predicting the performance of a type of µCHP system under discrete conditions in order to identify design or control improvements. Gigliucci et al [112] simulated a 4kW$_e$ PEM-based µCHP system with battery storage, using models of FC stack, balance-of-plant and batteries based on FORTRAN and Aspen Plus. During their investigation, modelling results were used to identify obvious improvements to increase η_e from 18% to 28%. Boait et al [147] developed a model of SE µCHP, coupled with an existing stochastic model of domestic energy demand. They correlated model predictions of electrical generation and export with field trial results of a 1kW$_e$ system, in order to predict electrical import displacement and export for six household scenarios comprising three different dwelling variants and two patterns of occupation and appliance use.

Hawkes et al [163] compare optimisation-based and simulation-based modelling techniques for the assessment of μCHP economic and/or environmental performance. Much of the published μCHP research has focussed on optimisation of one or more μCHP system characteristics, including prime mover capacity, auxiliary boiler capacity and operational control strategies. One of the key aspects of optimisation is to avoid over-sizing (which can decrease the operational performance of a μCHP system) or under-sizing (which decreases environmental and economic benefits). Shaneb et al [80] discuss the techniques that can be used for optimisation, including the maximum rectangle method, linear programming, non-linear programming (e.g. quadratic), mixed-integer nonlinear programming, fuzzy logic and genetic algorithms. They compare the maximum rectangle (MR) method for thermal and electrical sizing of prime movers with simulation results for PEM μCHP system design variants between 0.5-4kW_e, operating under both heat-led and electric-led regimes. Interestingly, the MR method to size a prime mover versus thermal demand, as applied to heat-led operation, suggests a prime mover capacity slightly lower than that for optimum carbon saving, but with a higher annual cost. An optimisation routine using linear programming is used to select a prime mover rated electrical output (for PEM, SOFC, ICE & SE variants) and auxiliary boiler thermal capacity with minimum annual cost. They found that much lower electrical capacities were derived from optimisation, unless export electricity was rewarded at a suitably high cost. Such low prime mover capacities were shown to drastically limit CO_2 reductions. In subsequent research, Shaneb et al [79] used a linear programming optimisation technique to optimise operating strategies of μCHP systems under various economic scenarios. They compared the modelling results for 1kW_e and 2kW_e PEM μCHP systems operating under heat-led, electric-led and optimised operating regimes.

Hawkes et al [163] used a unit commitment optimisation approach to select the rated electrical output (over the range 0.75-4kW_e) which maximised economic returns for μCHP systems based on ICE, SE, PEM and SOFC technologies. They continued to investigate the optimal system within each technology over a range of annual thermal

demand scenarios, and concluded that there may be an optimum value of thermal demand that corresponds to maximum carbon saving for each technology.

Hawkes & Leach [73] used a sparse quadratic programming optimisation technique to identify the optimum electrical output and auxiliary boiler capacity of a SOFC μCHP system, for a given energy demand, under technical operating constraints.

Hawkes, Brett & Brandon [115] used a mixed integer linear programming approach to optimise SFOC μCHP designs, under a number of operating constraints. These were the energy penalty during start-up and shut down, 60-minute minimum up-time, restricted minimum down-time, maximum output ramp rate and limited turn-down ratio. They identified reductions in generated electricity due to start-up and minimum up-time (8%) and maximum ramp rate and no turn-down (9%). They later extended [114] the optimisation exercise to investigate the impact of cumulative output and thermal cycling degradation mechanisms on the carbon savings and economic case for PEM and SOFC μCHP systems.

Optimisation-based investigations typically fix demand profiles due to the computational requirements that tend to restrict the number of variables that can be changed, hence making the demand non-responsive to supply, as discussed later in this section. An alternative approach to understanding suitable designs and operating regimes of μCHP systems is to run separate simulations for a range of design variants, with differing values of capacity and efficiency, and compare performance results. This "design variant" approach was adopted by Peacock & Newborough [3], who investigated a number of variants with a range of η_e (10/15/20/25/30%) and P_e (1/1.5/2/2.5/3kW$_e$).

The remaining investigations simulate μCHP systems with defined characteristics and control regimes, in order to estimate the technical, economic and/or environmental performance of μCHP systems, under a range of demand scenarios. Dorer & Webber [109] simulated μCHP systems with SE, ICE, PEM and SOFC prime movers using TRNSYS 16.1 transient building and systems simulation code. Kelly et al [129] created a generic

CHP model that uses a performance map that links electrical and thermal efficiency with electrical output at part-load. They investigated thermal cycling and duration at load conditions for a 0.75kW$_e$ SE µCHP system, as they believed that minimising thermal cycling is beneficial for longevity and essential for low maintenance. Onovwiona et al [117] investigated three capacities of ICE-based µCHP system, using code that they developed as an add-on the ESP-r building simulation tool. Their aim was to understand and compare electrical and total efficiencies under electrical load following and constant output operating regimes, utilising both thermal and electrical storage.

1.6.2 Temporal Precision & Temporal Extent of Modelling

The importance of temporal precision in µCHP modelling was originally discussed by Hawkes & Leach [31], who compare 60, 30, 10, 5-minute demand profiles aggregated from 5-minute demand profiles. Their investigation incorporates SE- and SOFC-based µCHP systems, with electrical efficiencies of 15% and 35-45% (part-load dependent) respectively, in three houses of differing demand without thermal storage. They undertook two cost optimisation exercises to minimise whole life cost of the µCHP system. In the system design optimisation exercise, they found that optimum rated electrical output, using 5-minute profiles, can be 22-66% smaller than the optimum values based on hourly profiles. Their dispatch optimisation results, for a fixed system size, showed that CO_2 savings can be overestimated by up to 40% using hourly versus 5-minute profiles. They attribute this to extended CHP operating hours when using an hourly modelling timestep.

The literature contains examples of a wide range of temporal precision in use for µCHP, or larger CHP, modelling exercises. Cockroft and Kelly [107] used hourly heat and electrical demand profiles with their parametric model of µCHP operation. Shaneb et al [80] used hourly thermal and electrical demand data to perform optimisation of µCHP design parameters. Halliday et al [148] use hourly thermal loads and half-hourly electrical loads to investigate CHP economic and environmental performance of FC-based CHP systems using two published CHP screening tools. Hinojosa et al [76]

reviewed several commercial and public domain CHP feasibility tools[1] that use demand profiles with temporal precision between 30-minute and monthly. The bottom-up demand simulations and CHP analysis, undertaken by Dorer & Webber [109] and Onovwiona et al [117] used 15-minute timesteps. Modelling exercises were undertaken by Boait et al [147] and Kelly et al [129] using 5-minute temporal precision. Newborough [61], Agar & Newborough [62], and Peacock & Newborough [3][45][53][57] used 1-minute demand profiles in their studies.

As an alternative to modelling of μCHP performance over a full year, "design days" can be used to investigate discrete 24-hour periods [61][73]. Typically, multiple "design days" are defined to represent the various seasons and major differences in occupancy (i.e. weekday vs. weekend). Whilst Houwing & Bouwmans [81] do not attempt to estimate annual carbon savings, instead quoting daily emission reductions, modelling results from these design days can be weighted by frequency to create an annual estimate of results [31][85]. Sigma [85] refer to this as a "bin day" method. Alternatively, "design days" can be chosen from sequential annual modelling results in order to analyse or illustrate typical behaviours during particular seasons or load conditions without losing temporal definition due to the effect of averaging 365 days of results [3]. As they retain the peaks and high rate of change of demand, these design days can be a useful tool to investigate transient performance issues or control strategies [61][62], where "design weeks" [129] can be useful in the investigation of intra-day storage. Aside from the temporal definition, there are other benefits for implementing a design day approach: it is much less computationally intensive, allowing relatively complex simulations, with high temporal precision, to be undertaken without specialist hardware, software or programming skills; and where source data is not available to reflect the diversity of demand over a full year, it circumvents the requirement to define temporally-precision demand or demand-driver profiles for a full year. The "design day" approach also allows a comparison between μCHP performance and thermal or electrical demand, although in order to derive a statistically valid relationship from this comparison of performance versus demand, a significant numbers of design days would be required.

[1] SEA/RENUE, CHP Sizer 2, Ready Reckoner, EnergyPro 3

1.6.3 Demand Models & µCHP Modelling

Newborough [61], Agar & Newborough [62], and Peacock & Newborough [3][45][53] [57] draw upon a demand dataset, recorded by an energy utility in 1996, with annual thermal and electrical demand data for approximately 30 UK dwellings. This data had a temporal resolution of 1 minute, where the thermal demand recorded was boiler gas consumption, for SH and DHW. A sub-set of the nine most commonly used dwellings had annual thermal demand values ranging from 9.3-27.2MWh, electrical demands values ranging from 3.5-7.5MWh, and annual heat-to-power ratios of 1.5-5.7. After correction for boiler efficiency, it was assumed that gas demand equalled thermal demand from the µCHP system or an intermediary thermal store.

Gas and electrical consumption data recorded by BRE, on an hourly basis, for 130 houses in the Milton Keynes Energy Park during 1988-91 was used by Staffell et al [149] in their simulations to investigate the economics of FC µCHP.

Some investigations have used demand profiles with reduced temporal resolution versus original measurement. In their economic comparison of µCHP, Solar PV and micro-wind, under various regulatory and policy issues, Watson et al [121] used electrical profiles averaged out to 30-minute resolution from data measured with 5-minute precision. Houwing & Bouwmans [81] modelled a SE-based µCHP system using the sample winter, shoulder (i.e. spring and autumn) and summer heat and power demand profiles published by Peacock & Newborough [57], where daily simulation is undertaken for heat-led, electric-led, and various least cost operating regimes, with a temporal precision of 15 minutes. From a modelling simplicity standpoint, they justified ignoring the transient behaviour of the prime mover and boiler, as they understood the start-up period of an SE to be 3 minutes, much smaller than their selected timestep.

In an optimisation exercise for SOFC µCHP, Hawkes & Leach [73] sampled six design days each from three properties in a BRE dataset of electrical demand profiles with a temporal resolution of 5 minutes. However, in the absence of thermal demand data,

they used a top-down load modelling approach, synthesising thermal demand profiles using assumed space heating profiles to correspond with gas consumption statistics. This is similar to the approach used by Sigma [85] to estimate electrical profiles using seasonal averages, corresponding to their three design days representative of summer, shoulder and winter. For an earlier comparison of prime mover technologies, Hawkes & Leach [82] used 5-minute electrical demand profiles derived from the DTI Domestic Photovoltaic Field Trial. Although not explicitly discussed, it appears that they used a similar process as above to create a number of 5-minute thermal demand profiles to investigate the effect of future demand scenarios on μCHP economics.

Halliday et al [148] generated hourly and 30-minute thermal demand profiles from building simulation, and used the 30-minute annual electrical demand profiles, averaged across the domestic stock, from the Electricity Association. This is an example of pre-defining thermal demand profiles by building simulation, upon which CHP performance is modelled retrospectively. Cockroft and Kelly [107] adopted a similar approach, where their space heating demand profile was defined using ESP-r (the building simulation tool), they synthesised hot water profiles, and they modified grid-level aggregated average domestic demand profiles to reflect a 30% increase. They then applied a parametric model of CHP to these static hourly loads to estimate performance.

The tendency to use static demand profiles in optimisation modelling, due to computational requirements, was discussed earlier in this section. A static demand profile is one which has been defined prior to consideration of the actual thermal output of a heat generator and/or thermal storage device, i.e. the ability for thermal energy supply to follow thermal demand. In modelling exercises that use a static thermal demand profile, over-supply of thermal energy during any timestep is typically disregarded, and under-supply is assumed to have been met from an auxiliary heat generator, typically without constraint. Papufragkou et al [68] modelled a small CHP system supplying a group of eight dwellings. They assumed that the CHP system, presumably the prime mover alone, responds to satisfy the entirety of thermal demand profile of the building. This approach does not account for the operating

restrictions faced by prime mover technology, such as start-up conditions and maximum turn-down ratios (i.e. part-load limitations), nor does the demand profile dynamically respond to the temporal profile of energy supply.

Where an investigation uses demand profiles from a measurement dataset, or derived from another estimated technique, demand profiles will be static. A degree of response has been introduced by some, notably Peacock & Newborough [3][45][53][57], and also Houwing & Bouwmans [81], where both groups matched thermal supply with a static demand profile via a thermal store, which buffers the output of the µCHP system. Not all thermal store approaches introduce response with the same level of temporal precision as Peacock & Newborough. Monthly consumption estimates for gas and electricity generated by Hot2000 simulation tool are converted to hourly estimates using degree-hours (the difference between external temperature and a base temperature, from which it is assumed that internal gains and solar gain will maintain the required internal air temperature) by Alanne et al [105]. These static loads are then interfaces with an excel-based SOFC µCHP model with a 1,000l seasonal thermal store.

1.6.4 Thermal Supply:Demand Matching & µCHP Operating Constraints

In simulation (and potentially optimisation) based modelling, the demand for thermal energy is calculated using the balance of energy demand and supply in the previous iteration, accounting for thermal inertia due to storage within building fabric or heat distribution systems. In responsive (dynamic) thermal demand modelling, an over- or under-supply of thermal energy from the µCHP system during any iteration will result in a different demand profile than one simulated for an energy system that perfectly follows demand. This is especially important when investigating operating regimes and control methodologies in light of the operating restrictions inherent to prime mover, auxiliary boiler and energy storage technologies. An example of this may be a µCHP system with a control algorithm that restricts thermal cycling and modulation. The control system may allow a thermal store or the room air temperature to exceed nominal set points, in lieu of dumping thermal energy outside the dwelling. This would ultimately reduce thermal demand during subsequent iterations, although a

sufficiently sophisticated simulation routine would account for the increased rate of heat loss due to an increased temperature differential (e.g. between the dwelling airspace and exterior).

Many investigations have coupled μCHP models with building simulation tools or thermal simulation algorithms, including EnergyPlus, ESP-r [117][129], TAS [74], DOE-2[1] [77][128], and TRNSYS [68][109]. Electrical demand profiles may be synthesised from bottom-up models, such as Boait et al [147], who applied the electrical load model developed by Stokes [164][165], or adapted from existing electrical demand datasets. It is unclear whether many of these approaches integrate the electrical demand due to the auxiliary boiler and space heating distribution system (i.e. pumps and controls).

Kaarsberg et al [128] simulated a representative home in DOE-2 to generate hourly thermal and electrical demand profiles. They used a cost model to optimise prime mover capacity, before undertaking FC μCHP simulation (without transient or part-load consideration) based on the static demand profiles. De Paepe et al [77] also used the DOE-2 simulation tool to generate thermal and electrical load profiles, and simulate operation of five μCHP systems, on an hourly basis for two dwellings for a full year. These systems include 1kW_e and 9.5kW_e SE-based units (with net electrical efficiencies of 12% and 24% respectively), 4.kW_e and 5.5kW_e ICE-based units, and a 4kW_e FC (with electrical and total efficiencies of 25% and 55% respectively). They implemented a bottom-up approach to demand modelling, as lists of installed equipment and usage profiles (presumably of lights, appliances, DHW, and heating system) were collected by questioning the households.

Dorer & Webber [109] used the TRNSYS transient building and systems simulation code, which accounted for the transient interaction of μCHP systems with building heat demand and heat distribution systems. They used existing DHW, internal heat gain and electric load profiles, where the heating controls were configured to correspond with the occupancy patterns of those load profiles. Even though their approach incorporated part-load and transient characteristics of various prime mover

[1] http://apps1.eere.energy.gov/buildings/tools_directory/software.cfm/ID=34/pagename=alpha_list

technologies (SE, ICE, PEM, and SOFC), and their dependency on distribution system flow and return temperatures, the 5-minute temporal resolution is too low to capture much of the detail for SE-based systems. The response of space heating and DHW tank temperature control is in the order of seconds. If a modelling approach considers prime mover response to thermal demand on a 5-minute basis then it would disregard the difference in transient thermal response between boilers and prime movers, as can be understood with reference to Section 2.4. With a sub-minute temporal precision, the potential of prime movers to displace auxiliary boiler generation can be investigated, as the duration of transient response for those generators is on the order of seconds to several minutes. This would be especially important on days with limited to modest thermal demand where the space heating distribution system and the DHW tank do not require continuous thermal energy input.

Kelly et al [129] created a generic CHP model, which integrates with the ESP-r thermal simulation tool, based upon a performance map that links electrical and thermal efficiency with electrical output at part load. The model couples the flow and return temperatures of space heating distribution system with the thermal mass of the prime mover in order to simulate transient performance during start-up. Another ESP-r linked µCHP model was developed by Onovwiona et al [117], specifically for ICE prime movers, although simulation timesteps are limited to 15 minutes.

In published µCHP modelling exercises, operating restrictions of µCHP systems - particularly those of the prime mover, fuel sub-systems and auxiliary thermal generation – have been disregarded or included with varying degrees of simplification. The benefits of high temporal precision in µCHP modelling were discussed earlier in this section, but it is asserted that increased temporal precision is pointless unless some operating restrictions are applied to the µCHP system. Operating restrictions can be broadly characterised as physical and elective, where the former restrictions are unavoidable due to physical processes within the system, and the latter are voluntarily enforced by a control system. Physical restrictions include transient start-up performance characteristics, part-load characteristics, maximum ramp rates and state-of-charge-related performance of electrical storage. Elective restrictions include

minimum run-time, modulation limitations, restricted thermal dumping and maximum ramp rates. These voluntary restrictions are typically imposed to avoid excessive inefficiencies, such as where gross electrical generation does not exceed parasitic loads at low part-load, or to limit lifetime or degradation effects, such as by limiting thermal cycling or ramp rates.

Papufragkou et al's [68] modelling approach does not account for the operating restrictions faced by prime mover technology, such as start-up conditions and maximum turn-down ratios (i.e. part-load limitations). In their earlier SE modelling, Peacock & Newborough [53] do not incorporate transient effects, modulation or the dependence of heat recovery efficiency (and hence thermal efficiency of prime mover) on the return temperature from the space heating distribution system (or more accurately, thermal store temperature), due to a lack of relevant data. However, they do incorporate [57] modulation of prime mover output, and eventually part-load efficiencies and transient start-up limitations on output.

Hawkes & Leach [73] incorporated a maximum ramp rate, minimum part-load and thermal dumping limit of $0.5kW_{th}$ in their optimisation modelling of SOFC μCHP. Their approach enabled them to calculate electrical efficiency based on load factor during every 5-minute timestep within each design day. Hawkes et al [75] continued to refine SOFC optimisation by applying a bottom-up approach to part-load efficiency calculation using stack modelling and power systems design limitations on ramp rates.

Houwing & Bouwmans [81] modelled a SE-based μCHP system with electrical and total efficiencies of 15% and 90% respectively, and a thermal store. They account for part-load operation at a fixed output level, $0.55kW_e$ compared with $1.1kW_e$ at full load, but do not reduce efficiency at part-load. Using the sample winter, shoulder and summer heat and power demand profiles from Peacock & Newborough [57], daily simulation is undertaken for heat-led, electric-led and various least-cost operating regimes, with a temporal precision of 15 minutes. Transient behaviour of the prime mover and boiler is ignored, as they understand SE start-up period to be 3 minutes, much smaller than

their selected timestep. They do not consider the effect of thermal store temperature on condensing operation of the boiler.

Thermal storage has been proposed as a means of alleviating the impact of operating constraints of prime movers on µCHP performance and lifetime. Hawkes et al [74] investigated thermal storage to improve overall economics of SOFC µCHP, under a range of thermal profiles, although the round trip efficiency of 81% was fairly low. However, their optimisation technique, for auxiliary boiler capacity and electrical output, does not introduce responsiveness between demand and supply. Other optimisation exercises utilise thermal storage; Shaneb et al [79] compares the economic impact of heat-led, electric-led and cost-optimised operating regimes on a PEM µCHP system with a thermal store without the ability to thermal dump. Ferguson & Ugursal [78] model the thermal and electrical output of a PEM-based µCHP system, with thermal store, using ESP-r to generate thermal loads with 5-minute precision. Their investigation of thermal load following operation finds a maximum prime mover thermal capacity to satisfy all thermal demand without use of the auxiliary burner. It is worth noting, however, that the temporal precision may be low enough to mask high peak demand due to DHW consumption with high draw-off rates. The thermal store temperature is the control signal for generation, where they maintain a 10°C band between auxiliary (60°C) and prime mover (70°C) cut-off, and a low auxiliary trigger temperature (55°C), to provide sufficient storage capacity.

Houwing & Bouwmans [81] model a SE-based µCHP system with a 100l thermal store that supplies the SH network directly, and DHW via a heat exchanger. A staggered temperature control approach switches on prime mover (60°C), and then auxiliary boiler (58°C), maintaining stored water temperature above 60°C (for the vast majority of the time) to avoid legionella bacteria growth and its associated health risks. The prime mover switches off at 75°C, and the auxiliary at 68°C, and as the control system does not allow thermal dumping, this limits the prime mover runtime. A weakness of their approach is that they do not consider heat losses from the thermal store, which would shorten time periods between thermal generation, and extend thermal generation (prime mover and auxiliary) runtimes.

Electrical storage has been investigated as a means of minimising primary energy consumption or achieving autonomous operation, for example Best & Riffat [106]. In their investigation of ICE-based μCHP, Onovwiona et al [117] assumed that transient behaviour of electrical output (during start-up or load change) was negligible. However, they utilised the relationships between thermal efficiency and time elapsed since engine start, as derived by Voorspools & D'haeseleer [72] for distinct time bands since previous engine operation. Modelling electrical load following operation, they incorporate part-load thermal and electrical efficiencies of prime mover, whilst for constant output operation, they derive battery charge and discharge efficiencies from state of charge. In either operating regime, unrestricted thermal dumping is permitted.

1.6.5 Electrical Storage & Grid Interaction

The integration of electrical storage within a μCHP system has not been investigated to the same extent as thermal storage because the prevalent CO_2 accounting method for grid-connected micro-generation systems assumes that all of the electricity which is generated, but not used instantaneously on-site, will be exported and used elsewhere, displacing the equivalent quantity of electricity from central generation [118]. In calculating the reduction in CO_2 emissions footprint for a dwelling with μCHP, versus a base-case scenario without on-site generation, the change in net electrical import is typically considered. In the base-case scenario, net electrical import is equal to the total consumption of electricity within the dwelling. With a μCHP system, net import is the difference between total electrical demand and the total μCHP generated electricity. Net import can also be calculated as the arithmetic difference between actual electrical imports and electrical exports; both methods will produce the same value. Difference in net import can be used in a carbon footprint reduction calculation if exported electricity is assigned the same carbon intensity of grid electricity assigned to import electricity. This approach has been used by the majority of the research in the field, with the exception of those studying time-varying carbon intensities of grid electricity due to the daily and seasonal mixtures between fossil fuel, renewable and nuclear generation. Pout and Hitchin [118] point out that the UK building regulations and Standard Assessment Procedure (SAP), used to assess the energy efficiency of new

domestic properties in the UK for compliance purposes, both use this CO_2 accounting convention. However, economic evaluations of μCHP commonly apply a reduced price to export compared with import, which is reflective of market conditions (unless influenced by regulation or subsidy).

In an earlier paper, Hitchin & Pout [124] argue that the carbon intensity used for both displaced electrical import (between scenarios with and without μCHP) and electrical export should use the incremental carbon intensity. They argue that incremental CI should include both direct and indirect effects, i.e. CI of marginal plant whose generation would be displaced by generation from CHP, and avoided new generation that would not be installed and operated due to the deployment of a fleet of μCHP. Hawkes & Leach [59] considered the ability for mass penetration of μCHP to displace central generation by modelling the availability of prime movers using a heat-led operating regime. Their investigation included SE, ICE and generic FC-based systems, where the reported capacity credit increased from 48% for SE to 75% for ICE and 92% for FC, due to decreasing heat-to-power ratio.

Others have investigated the impact of μCHP penetration on the NEG by simultaneously modelling multiple buildings, usually with a range of demand scenarios, applying centralised control signals to manage aggregated demand and export profiles. Investigations by Peacock & Newborough [57] and Boait et al [147] found that, for particular electrical demand profiles, up to 40-50% of electrical generation can be exported from a dwelling, depending on prime mover technology, capacity and operating regime.

Peacock & Newborough [45] aggregated the μCHP modelling results of 50 dwellings, using a demand profile dataset, to investigate resultant electrical peak load, load factor and energy flows due to mass penetration of μCHP at a local level. They investigated SE prime movers, with 15% η_e, incorporating transient output and efficiency characteristics during start-up. Comparing thermal load following with an aggregated control operating regime (to smooth the electrical load profile for the group of dwellings), they concluded that aggregated control methodologies can

significantly increase capacity factors versus heat-led operation. This addressed the issue of low capacity factor raised by their earlier research [53], where they compared capacity factors for penetration levels across several prime mover technologies and capacities.

The majority of μCHP modelling has focused mainly on dwelling-centric operating regimes, such as thermal load following, electrical load following and hybridised operating practices to minimise operating cost, usually referred to as "least-cost". Newborough [61] broadly characterises μCHP systems as either network-connected, where power can flow to and from the national grid, or autonomous systems that have little or no interaction with the grid. He defines several operating regimes where the prime mover operates at constant output either continuously, or for distinct pre-configured time periods defined by household occupancy. He discussed the potential for utilising such operating regimes for a system incorporating electrical storage. Agar & Newborough [62] discuss the challenge in identifying a prime mover technology that could operate under such regimes without some drawback.

Peacock & Newborough [57] investigated both thermal and electrical load following, and explored the concept of restricted and unrestricted thermal dumping (or thermal surplus). They assessed the environmental and economic impact of thermal dumping for 1kW$_e$ 15% η_e SE-based and 1kW$_e$ and 3kW$_e$ 50% η_e FC-based μCHP systems. They found that switching from restricted to unrestricted thermal dumping reduced thermal cycling (from 1,898 to 1,182 for SE) whilst penalising CO_2 savings and cost; relative CO_2 savings of 10% were reduced to a carbon penalty of 3%.

In their investigation of SE-, ICE- and FC-based μCHP, De Paepe et al [77] implemented a thermal load following operating regime with a seasonal operating restriction, in that the space heating was switched off during the 4 summer months. The value of seasonal restriction was recognised by Peacock & Newborough [57], who reported significantly reduced prime mover run-times during summer months, due to limited thermal demand (for heat-led), and the need to restrict thermal dumping (electric-led) to maximise CO_2 savings. Seasonal restriction has been applied in economic modelling,

where Hawkes & Leach [58] switch operating regimes and control strategies between seasons to limit running costs, based on seasonal electricity export prices.

Many studies have investigated multiple discrete building variants, or the same building variant with differing characteristics, in an attempt to understand the impact of demand scenarios on μCHP performance. Future scenarios with reduced building heat loss were investigated by Hawkes & Leach [125], who concluded that SOFC-based μCHP systems maintain carbon savings as thermal demand reduces, whilst ICE- and SE-based systems do not. Hawkes & Leach [60] compared the economic and carbon reduction cases for application of FC-, ICE- and SE-based μCHP in existing, refurbished and newly-built homes. They conclude that government policy supporting both energy efficiency measures (to reduce thermal demand) and μCHP (to satisfy thermal demand) can be justified. However, they warn that high heat-to-power ratio technologies in dwellings with low or inconsistent heat demand, which could correspond with new-build or smaller refurbished homes, should not be granted policy support. It is prudent to note that whilst heat-to-power ratio is a function of the prime mover technology, it is also a function of design of particular systems; hence advances in SE technology could dramatically decrease its heat-to-power ratio.

To understand the relationship between thermal demand and relative carbon savings (RCS), Peacock & Newborough [3] used full factorial design to create, by multiple linear regression, a relationship between carbon emissions from a μCHP system and the thermal demand of the dwelling, rated thermal and electrical outputs of the CHP system (for a particular set of operating constraints and control methodology). Again using a matrix of prime mover design variants, they concluded that RCS (as a percentage of carbon footprint of the conventional boiler system) increased with increasing thermal demand of the building.

Operating regime has a significant impact on the relationship between relative CO_2 savings and thermal demand, as supported by Shaneb et al [80]. In their optimisation sizing exercise, they conclude that μCHP systems with higher electrical capacities save more CO_2 when heat-led, and less when electric-led.

1.6.6 Reported CO2 Savings

Published investigations of μCHP, as discussed in this section and otherwise, have applied an assortment of modelling approaches to determine μCHP performance, in terms of carbon reduction potential and/or economic viability. There has been a significant variation in the predicted relative CO_2 savings potential reported for μCHP systems. Hamada et al [113] have estimated the carbon abatement potential of a PEM μCHP system as 20%. Hawkes & Leach [58] compared SE-, ICE- and SOFC-based systems, under thermal and electrical load following regimes, and RCS between 10% and 19%. Peacock & Newborough [57] reported carbon savings between 40% and -3% for 3kW_e FC-based and 1kW_e SE-based μCHP systems, respectively.

The effect of changing grid intensity was investigated by De Paepe et al [77], for a range of SE-, ICE- and FC-based μCHP, where they assumed that exported electricity was assigned a CI equal to that of grid imports. With a Belgium average grid intensity of 0.272kgCO_2/kWh, they reported RCS of between -6% and 12%, rising to 17%-48% when compared with a grid intensity of 0.617kgCO_2/kWh. Due to the capacities of modelled systems (1-9.5kW_e), they note that 85-90% of generated electricity is exported, which underlines the sensitivity of CO_2 savings to the CI assigned to export electricity. Peacock & Newborough agree, stating that due to the high proportion of electrical export (44–74%) from systems with relatively high P_e, the CO_2 savings attributable to such systems largely depend on the assumption of equal carbon intensities of electricity import and export carbon.

Prior research [3] agrees that the variation in reported CO_2 savings can be attributed to variation in prime mover technology, system design (whose aspects include the integration of storage technologies, operating regimes and control algorithms), externalities (carbon intensities and prices of fuel, import and export electricity), and the magnitude and shape of the dwelling's demand profile. It is pointed out that, between the investigations reported in this chapter, an array of electrical and thermal efficiencies have been used to represent each prime mover technology. In addition, various modelling approaches have been applied which implement or disregard, to varying degrees, transient performance, part-load performance and other operating

restrictions of μCHP systems. The limitations or economic emphasis of the modelling approaches, as discussed in this section, that were adopted by published investigations cast some doubt on the validity of predicted CO_2 savings attributed to μCHP systems. As the range of CO_2 savings reported can be very low, or even negative, especially for low-η_e prime mover designs, it is conceivable that many μCHP systems may not provide significant carbon savings. This is supported by field trial results from the Carbon Trust's Micro-CHP Accelerator programme [19], which reported relative carbon savings (versus a condensing boiler) of -5% to 5% for domestic μCHP (<5kW_e), and 6% to 11% for commercial μCHP (5-10kW_e).

Therefore, the Building Integrated Micro-Generation (BIM-G) model was conceived to facilitate the investigation of μCHP systems. The originality of the BIM-G modelling and analysis methodology is the transient, bottom-up approach to demand definition, coupled with micro-generation and storage performance modelling. A major point of novelty of the BIM-G model is that a dynamic link exists, integrating supply calculations and demand estimation. This permits the supply:demand matching algorithms to account for the effect of previous energy generation, at whatever output level, on the energy demand during the preceding iteration. This is a departure from other modelling approaches discussed previously, which were constrained by static relationships between demand and supply profiles, based on historic measurements of demand. The approach taken by BIM-G allows transient performance, part-load performance and other operating restrictions to be modelled with high temporal precision. This is a departure from other modelling approaches, such as Peacock & Newborough [3], or Hawkes & Leach [58], which were constrained by static relationships between demand and supply profiles, based on historic measurements of demand.

As discussed by Ferguson & Ugursal [78], there exists a need for a modelling tool that can not only estimate performance of μCHP systems, but evaluate different system designs and control strategies, and determine the optimum sizing of systems based on particular technologies under different demand conditions. The application of the BIM-G model in this project will investigate the relationship between performance and

thermal demand, in order to inform the design and specification processes for μCHP systems.

Regardless of the magnitude of RCS identified in this project, it should be acknowledged that μCHP systems have yet to prove themselves on a commercial basis. Only once μCHP, of whichever prime mover technologies, proves itself to be reliable, cost effective and environmentally friendly in operation, will mass deployment be a possibility. As discussed in Section 1.1, governments are offering financial support to encourage consumer uptake, however to achieve widespread adoption, μCHP systems must offer an affordable solutions for homeowners, landlords and builders.

The focus of this research is carbon abatement potential of μCHP, as calculated relative to a base-case energy system using a condensing boiler, hence it is considered the most important performance metric. Whilst this project does not provide an economic analysis of μCHP performance, it is prudent to acknowledge that the operational lifetime of the μCHP system will have a major impact on the financial feasibility of such systems. Therefore, the investigation presented in Chapter 4 onwards includes analysis of cumulative annual operating hours and thermal cycling (i.e. start-stop cycles) of the prime mover, both of which are understood to limit life expectancy [56] [69]. This issue of thermal cycling is significant enough to spur developers to include minimum run time conditions within the control logic of their μCHP systems [70][71].

1.7 Research Outline & Aims

A core component of the author's work is the BIM-G Model, which the author has developed to assess the implementation of building integrated micro-generation technologies. This model is a combination of software procedures and methodologies that can be used to generate electrical and thermal load profiles for buildings, and assess the energy and carbon performance of micro-generation and storage technologies. The unique aspects of the BIM-G modelling and analysis methodology are: the transient, bottom-up approach to both thermal and electrical demand profile

definition; and the subsequent application of μCHP modelling with transient performance and operating constraints, in order to perform supply:demand matching with a high degree of temporal precision.

The aims of this project are:

- Identify the relationship between relative carbon savings, thermal demand and design parameters of μCHP system design variants operating under thermal load following operation regime
- Determine the impact of operating regimes on prime mover lifetime, and operating regimes and energy storage on relative carbon savings
- Define alternative operation regimes to maximise RCS and prime mover lifetime, determining their feasibility for application to various prime mover technologies

In the pursuit of the aforementioned aims, the main objectives of the project are:

- Develop a model and accompanying methodology to synthesis thermal and electrical load profiles, with a temporal precision of 5 seconds, for a dwelling with suitably large, yet plausible and relatively common, thermal demand profile
- Record electrical profiles for selected domestic appliances, along with temperature data to estimate the distribution of heat emission that causes an appliance casual thermal gains profile
- Design and apply a supply:demand matching methodology that integrates transient performance characteristics, part-load characteristics and other operating restrictions for micro-generation and energy storage technologies
- Research conceptual μCHP system "design variants", within discrete daily demand scenarios relating to UK dwellings, with a series of "design days", and estimate the relative change (versus a base-case scenario) in carbon emissions, fuel consumption and grid electricity imports and exports
- Determine the impact of rated electrical efficiency and rated electrical output of design variants on RCS, in the context of current and potential development

of prime mover technologies, identifying the design variants with maximum RCS

- Identify the relationship between thermal demand and μCHP performance metrics, and the effects of design variant characteristics and operating regimes
- Relate RCS and lifetime-drivers from design days to annual values, and investigate operating strategies to maximise annual carbons savings and prime mover lifetime
- Estimate the effect of changing thermal demand profiles on annual RCS and prime mover lifetime
- Understand the impact of carbon intensities (of fuel and NEG) on RCS, and the resultant effect on the selection of operating regimes
- Explore the potential for electrical storage to achieve autonomous operation, whilst quantify the impact on carbon savings and prime mover lifetime
- Derive relationships to assist in the μCHP systems design and specification processes, in which a rated electrical output and operating regime are selected to maximise the environmental performance and lifetime of a μCHP system of fixed electrical efficiency to be installed in a dwelling of defined thermal demand

This research project involves software development, data gathering and interpretation, simulation exercises and analysis of simulation results. This is visualised in Figure 2.1 in the context of the BIM-G Model.

1.7.1 Thesis Structure

In Chapter 2, the technical underpinnings of the BIM-G model are presented, along with the performance characteristics and operating restrictions of μCHP and condensing boilers.

The methodology for defining demand profiles is discussed in Chapter 3, where the Primary Demand Scenarios are defined. Additionally, Chapter 3 features the results of appliance electrical and temperature monitoring, and a regression analysis to quantify the effect of external temperature and solar irradiation on thermal demand of the

building variant. This analysis was used to define climate profiles for the Primary Demand Scenarios.

The methodology, results, analysis and conclusions of thermal load following SE µCHP modelling are presented in Chapter 4. In this chapter, several novel performance analysis methodologies are defined during the analysis of µCHP systems.

Drawing upon these novel methodologies, alternative operating regimes are defined in Chapter 5. These operating regimes are dynamically combined on a seasonal basis in order to maximise carbon savings and prime mover lifetime.

Alternative scenarios are explored in Chapter 6, where the impact of changing annual thermal demand on carbon savings and lifetime is presented, alongside a study of changing carbon intensities of fuel and grid electricity.

The concept of integrating electrical storage technologies, and potentially solar PV systems, with µCHP systems is investigated in Chapter 7, The concepts of battery storage and energy storage as hydrogen (by electrolysis) are explored, in the context of an autonomous energy system.

Chapter 8 summarises the main conclusions from the project, and presents themes for further research, as identified during the study.

1.8 References

[1] Department of Energy & Climate Change and Office National Statistics; Digest of United Kingdom Energy Statistics 2010; London; 2010; Table 5.10

[2] M. Batey and C. Pout; Delivered Energy Emission Factors for 2003; Online at http ://projects.bre.co.uk/emissionfactors/2003EmissionFactorUpdate.pdf; Dec. 2005

[3] A.D. Peacock and M. Newborough; Effect of heat-saving measures on the CO_2 savings attributable to micro-combined heat and power (mCHP) systems in UK dwellings; Energy; 33; 2008; pp601–612

[4] Intergovernmental Panel on Climate Change (IPCC);2002; http://www.ipcc.ch/

[5] Department of Trade and Industry; Inter-Departmental Analysts Group Report: Long Term Reductions in Greenhouse Gas Emissions in the UK; February 2002; http://www.dti.gov.uk/energy/greenhousegas

[6] The Cabinet Office; Performance and Innovation Unit (PIU) Report; The Energy Review; February 2002; http://www.piu.gov.uk/2002/energy/report/

[7] Royal Commission on Environmental Pollution; 22nd Report; June 2000; http://www.rcep.org.uk

[8] UK climate change act (2008); Access online March 2012 at http://www.decc.gov.uk/en/content/cms/legislation/cc_act_08/cc_act_08.aspx

[9] EU 2050 ROADMAP; Access online March 2012 at http://eur-lex.europa.eu/LexUriServ/LexUriServ.do?uri=CELEX:52011DC0112:EN:NOT

[10] Europa, n.d.20-20-20 Goal [online]. Accessed online March 2012 at http:// europa.eu/legislation_summaries/energy/energy_efficiency/en0002_en.htm

[11] Department of Trade and Industry; The energy challenge, energy review; 2006

[12] Department of Environment, Food & Rural Affairs; Climate change, the UK programme 2006—tomorrow's climate, today's challenge; 2006

[13] DECC; The UK National Renewable Energy Action Plan (NREAP); 2009; accessed online February 2012 at http://www.decc.gov.uk/en/content/cms/ meeting_energy/renewable_ener/uk_action_plan/uk_action_plan.aspx

[14] DECC; The UK Renewable Energy Strategy; 2009; Accessed online February 2012 http://www.decc.gov.uk/assets/decc/what%20we%20do/uk%20energy%20supply/energy%20mix/renewable%20energy/renewable%20energy%20strategy/1_20090717120647_e_@@_theukrenewableenergystrategy2009.pdf

[15] Scottish Government; 2020 Route Map; 2011; accessed online February 2012 at http://www.scotland.gov.uk/Publications/2011/08/04110353/0

[16] Welsh Assembly; Renewable Energy Route Map; 2008; accessed online Feb. 2012 at http://wales.gov.uk/about/cabinet/cabinetstatements/2008/routemap/

[17] DETINI; Energy -Strategic Framework for NI; 2010; accessed online Feb. 2012 at http://www.detini.gov.uk/deti-energy-index/deti-energy-strategic-energy-framework.htm

[18] Department of Environment, Food & Rural Affairs; The Government's Strategy for Combined Heat and Power to 2010, Sustainable Energy Policy; April 2004

[19] Carbon Trust; Micro-CHP Accelerator Interim Report; CTC726; November 2007

[20] M Pehnt; Micro Cogeneration Towards Decentralized Energy Systems; Chapter 1: Micro Cogeneration Technology; ISBN 3-450-25582-6; 2006

[21] Department of Energy & Climate Change; The Microgeneration Strategy; Accessed online February 2012 at http://www.decc.gov.uk/en/content/cms/meeting_energy/microgen/strategy/strategy.aspx

[22] Department of Energy & Climate Change and Office National Statistics; Energy consumption in the United Kingdom: 2011; Published online July 2011 at http://www.decc.gov.uk/en/content/cms/statistics/publications/ecuk/ecuk.aspx ; Table 1.4

[23] Department of Energy & Climate Change and Office National Statistics; 2011 UK greenhouse gas emissions, provisional figures and 2010 UK greenhouse gas emissions, final figures by fuel type and end-user; Published online March 2012 at http://www.decc.gov.uk/assets/decc/11/stats/climate-change/4817-2011-uk-greenhouse-gas-emissions-provisional-figur.pdf; Table 2

[24] Department of Energy & Climate Change and Office National Statistics; Energy consumption in the United Kingdom: 2011; Published online July 2011 at http://www.decc.gov.uk/en/content/cms/statistics/publications/ecuk/ecuk.aspx ; Table 3.6

[25] Shorrock L D and Utley J I, Domestic Energy Fact File 2003. Garston, Watford, UK: Building Research Establishment, 2003

[26] Market Transformation Programme; Briefing Note BNXS25; UK Household and Population Figures 1970 - 2020; pp1; 12/01/07; v2.1

[27] Scottish Executive, Building Standards Division; May 2011; Technical Handbooks 2011 Domestic Energy; Section 6: Energy; Accessed online My 2012 at http://www.scotland.gov.uk/Resource/Doc/217736/0120386.pdf

[28] http://www.passivhaus.org.uk/standard.jsp?id=18; Accessed online May 2012

[29] Peacock et al; Reducing CO_2 Emissions through Refurbishment of UK Housing; European Council for an Energy Efficient Economy (eceee) 2007 Summer Study; Côte d'Azur; France; 4-9 June 2007

[30] European Union; Ecodesign for energy-using appliances; Accessed online Apr 2012 via "Summaries of EU legislation" website http://europa.eu/legislation_summaries/other/l32037_en.htm; Last Updated 13th October 2008

[31] A. Hawkes and M. Leach, Impacts of temporal precision in optimisation modelling of micro-Combined Heat and Power, Energy, Volume 30, Issue 10, July 2005, Pages 1759-1779

[32] D.P. Jenkins, A.D. Peacock, P.F.G. Banfill, D. Kane, V. Ingram, R. Kilpatrick, Modelling carbon emissions of UK dwellings – The Tarbase Domestic Model, Applied Energy, Volume 93, May 2012, Pages 596-605.

[33] Peacock A, Newborough M. and Banfill P, Technology assessment for radically improving the built asset base (TARBASE), WREC 2005, Aberdeen, 22-27 May 2005

[34] Boardman B, et al., 40% House. Oxford, UK: Environmental Change Institute, 2005

[35] J I Utley & L D Shorrock; Domestic Energy Fact File 2008; Building Research Establishment; 2008; Table 6

[36] J I Utley & L D Shorrock; Domestic Energy Fact File 2008; Building Research Establishment; 2008; Table 20

[37] J I Utley & L D Shorrock; Domestic Energy Fact File 2008; Building Research Establishment; 2008; Table 21

[38] J I Utley & L D Shorrock; Domestic Energy Fact File 2008; Building Research Establishment; 2008; Table 23

[39] J I Utley & L D Shorrock; Domestic Energy Fact File 2008; Building Research Establishment; 2008; Table 24

[40] J I Utley & L D Shorrock; Domestic Energy Fact File 2008; Building Research Establishment; Section 6.6

[41] Market Transformation Programme; Briefing Note BNDH11; The Domestic Heating Boiler Energy Model: Methods and Assumptions; Table 2

[42] DECC, Digest of UK Energy Statistics:2009, Department of Energy and Climate Change, London, UK

[43] Department of Energy & Climate Change and Office National Statistics; Digest of United Kingdom Energy Statistics 2010; London; 2010; Section 5.48

[44] A.D. Hawkes; Estimating marginal CO_2 emissions rates for national electricity systems; Energy Policy; 38; 2010; pp5977–5987

[45] A.D. Peacock, M. Newborough, Controlling micro-CHP systems to modulate electrical load profiles, Energy, Volume 32, Issue 7, July 2007, Pages 1093-1103

[46] Department of Trade and Industry; Energy White Paper, Our energy future—creating a low carbon economy; The Stationery Office; February 2003

[47] DECC; Energy Trends Special feature – GB electricity demand variation; Published online Sept 2010 at http://www.decc.gov.uk/assets/decc/Statistics/publications/trends/articles_issue/560-trendssep10-electricity-demand-article.pdf

[48] Jeston S; Selecting a dynamic load management solution to meet the challenges facing the electricity industry; Load management and demand response; London; 2nd-3rd February 2006

[49] Department of Energy & Climate Change and Office National Statistics; Energy consumption in the United Kingdom: 2011; Published online July 2011 at http://www.decc.gov.uk/en/content/cms/statistics/publications/ecuk/ecuk.aspx ; Table 1.7

[50] M. Newborough and P. Augood; Demand-side management opportunities for the UK domestic sector; IEE Proc., Gener. Transm. Distrib. 146, 283 (1999); DOI:10.1049/ip-gtd:19990318

[51] S. Deering, M. Newborough, S.D. Probert, Rescheduling electricity demands in domestic buildings, Applied Energy, Volume 44, Issue 1, 1993, Pages 1-62

[52] M. Newborough, S.D. Probert, Intelligent automatic electrical-load management for networks of major domestic appliances, Applied Energy, Volume 37, Issue 2, 1990, Pages 151-168

[53] A.D. Peacock, M. Newborough, Impact of micro-combined heat-and-power systems on energy flows in the UK electricity supply industry, Energy, Volume 31, Issue 12, September 2006, Pages 1804-1818

[54] Mott MacDonald, DGCG & DTI; System integration of additional micro-generation (SIAM); September 2004

[55] Ingram S, et al. The impact of small scale embedded generation on the operating parameters of distribution networks, DTI. Report No K/EL/00303/04/01, 2003

[56] M. Newborough, Demand modulation for micro-CHP systems, EPSRC Final Report GR/J8130, 1997

[57] A.D. Peacock, M. Newborough, Impact of micro-CHP systems on domestic sector CO_2 emissions, Applied Thermal Engineering, Volume 25, Issues 17–18, December 2005, Pages 2653-2676

[58] A.D. Hawkes and M.A. Leach, Cost-effective operating strategy for residential micro-combined heat and power, Energy, Vol. 32, Issue 5, May 2007, pp 711-723

[59] A.D. Hawkes, M.A. Leach, The capacity credit of micro-combined heat and power, Energy Policy, Volume 36, Issue 4, April 2008, Pages 1457-1469

[60] A.D. Hawkes, M.A. Leach, On policy instruments for support of micro combined heat and power, Energy Policy, Volume 36, Issue 8, August 2008, pp 2973-2982

[61] M. Newborough; Assessing the benefits of implementing micro-CHP systems in the UK; Proceedings of the Institution Mechanical Engineers; Vol. 218; Part A: J; Power and Energy; 2004

[62] Agar, W. R., & Newborough, M.; Implementing micro-CHP systems in the UK residential sector; Journal Of The Institute Of Energy; 1998; 71(489); pp178-189

[63] Crozier-Cole T. and Jones G.; The potential market for micro-CHP in the UK; Report P00548; Energy Saving Trust; London; 2002

[64] Onovwiona H.I. and Ugursal V.I; Residential cogeneration systems: review of the current technology; Renewable and Sustainable Energy Reviews; Volume 10; Issue 5; October 2006; pp. 389-431

[65] The Energy Networks Association; Engineering Recommendation G83/1: Recommendations For The Connection Of Small-scale Embedded Generators (Up to 16A per Phase) in Parallel with Public Low-Voltage Distribution Networks”; 2008; http://www.energynetworks.org

[66] EERE Information Center, US Department of Energy; February 2011; Accessed online February 2012 at http://www1.eere.energy.gov/hydrogenandfuelcells/fuelcells/pdfs/fc_comparison_chart.pdf

[67] Scott Dwyer, Delta Energy & Environment; Micro-CHP; Cogeneration & On-Site Power Production Magazine; Volume 13; Issue 2; pp53-59; 1st May 2012; Access online at http://www.cospp.com

[68] Papafragkou A., Bahaj A.S., James P.A.B. and Jentsch M.F.; Energy flows in domestic buildings: residential combined heat and power (CHP) microgrids; Proceedings World Renewable Energy Congress (WREC-IX); Florence; 19-25 August 2006

[69] Roger Dettmer; Home Station; IEE Review January 1998; pp11-13

[70] Winkler W, editor; FC TEST NET fuel cell survey; ENG-2-CT-2002-20657; 2006

[71] AC Whispergen system—product specification; 11 June 2003; Accessed online Feb 2006 at www.whispergen.com

[72] K.R. Voorspools, W.D. D'haeseleer; The evaluation of small scale cogeneration for residential heating; Int. J. Energy Res.; 26; 2002; 1175–1190

[73] Adam Hawkes, Matthew Leach, Solid oxide fuel cell systems for residential micro-combined heat and power in the UK: Key economic drivers, Journal of Power Sources, Volume 149, 26 September 2005, Pages 72-83

[74] A.D. Hawkes, P. Aguiar, B. Croxford, M.A. Leach, C.S. Adjiman, N.P. Brandon, Solid oxide fuel cell micro combined heat and power system operating strategy: Options for provision of residential space and water heating, Journal of Power Sources, Volume 164, Issue 1, 10 January 2007, Pages 260-271

[75] A.D. Hawkes, P. Aguiar, C.A. Hernandez-Aramburo, M.A. Leach, N.P. Brandon, T.C. Green, C.S. Adjiman, Techno-economic modelling of a solid oxide fuel cell stack for micro combined heat and power, Journal of Power Sources, Volume 156, Issue 2, 1 June 2006, Pages 321-333

[76] L.R. Hinojosa, A.R. Day, G.G. Maidment, C. Dunham, P. Kirk, A comparison of combined heat and power feasibility models, Applied Thermal Engineering, Volume 27, Issue 13, September 2007, Pages 2166-2172

[77] Michel De Paepe, Peter D'Herdt, David Mertens, Micro-CHP systems for residential applications, Energy Conversion and Management, Volume 47, Issues 18 & 19, November 2006, Pages 3435-3446

[78] Alex Ferguson, V. Ismet Ugursal, Fuel cell modelling for building cogeneration applications, Journal of Power Sources, Volume 137, Issue 1, 5 October 2004, Pages 30-42

[79] O.A. Shaneb, P.C. Taylor, G. Coates, Optimal online operation of residential µCHP systems using linear programming, Energy and Buildings, Volume 44, January 2012, Pages 17-25

[80] O.A. Shaneb, G. Coates, P.C. Taylor, Sizing of residential µCHP systems, Energy and Buildings, Volume 43, Issue 8, August 2011, Pages 1991-2001

[81] M. Houwing and I. Bouwmans, "Agent-Based Modeling of Residential Energy Generation with Micro-CHP," Proceedings of the 2nd International Conference on Integration of Renewable and Distributed Energy Resources, Napa, CA, USA, 2006

[82] A.D. Hawkes and M.A. Leach, Comparison of Fuel Cell and Combustion Micro-CHP under Future Residential Energy Demand Scenarios, Centre for Energy Policy and Technology, Imperial College London, June 2007

[83] D.G. Thombare, S.K. Verma, Technological development in the Stirling cycle engines, Renewable and Sustainable Energy Reviews, Volume 12, Issue 1, January 2008, Pages 1-38

[84] MICRO-MAP Project; Mini And Micro ChP – Market Assessment And Development Plan; Summary Report; accessed online at http://www.microchap.info/MICROMAP%20publishable%20Report.pdf

[85] Sigma Elektroteknisk AS; Micro Chp Technology & Economic Review; Report For Future Cogen Project; June 2003; accessed online at http://www.microchap.info/Future%20Cogen%20Micro%20CHP.pdf

[86] J. Harrison; Micro combined heat and power; EA Technology; 2004; accessed online at http://www.microchap.info/Micro%20CHP%20I%20Mech%20E.pdf

[87] M. Dentice d'Accadia, M. Sasso, S. Sibilio, L. Vanoli, Micro-combined heat and power in residential and light commercial applications, Applied Thermal Engineering, Volume 23, Issue 10, July 2003, Pages 1247-1259

[88] Delta Energy & Environment; Micro-CHP Performance: Experience from Installations and Demonstrations; Ref: M-CHP-F-21; January 2010; http://www.delta-ee.com

[89] http://www.lichtblick.de/h/english_information_395.php; Accessed May 2012

[90] http://www.vaillant.de/Presse/Press-Releases/article/Vaillant_Group_takes_over_combined_heat_and_power_systems_manufacturer_Cogenon.html; Accessed May 2012

[91] http://world.honda.com/cogenerator/index.html; Accessed May 2012

[92] http://world.honda.com/news/2007/c070717Compact-Household-Cogeneration-Unit/; Accessed May 2012

[93] http://www.vaillant-group.com/media-services/press-archive/2012/datednews/Vaillant_Group_uebernimmt_Blockheizkraftwerk-Hersteller_Cogenon.html; Accessed May 2012

[94] Marathon Engine Company; Datasheet; Accessed online May 2012 at http://www.marathonengine.com/downloads/Ecopower%20Brochure_031811.pdf

[95] http://www.vaillant.de/Presse/Press-Releases/article/Vaillant_and_Honda_install_micro-CHP_systems_throughout_Germany.html; Accessed May 2012

[96] http://newsroom.honda.co.uk/News/vaillant-and-honda-present-micro-combined-heat-and-power-system-for-domestic-use-730.aspx; Accessed May 2012

[97] Harrison, J., 2004. Micro combined heat & power for housing. In: Proceedings of 3rd International Conference on Sustainable Energy Technologies, Nottingham, UK, June 2004

[98] Ribberink, J.S. et al., 2000. Stirling based micro co-generation system for single households. In International Stirling Forum 2000. p. 10.

[99] N.W. Lane & W.T. Beale; A 5kW Electric Free-Piston Stirling Engine; Sunpower Inc.; USA; 1995; accessed online at http://www.sunpower.com/library/pdf/publications/Doc0062.pdf

[100] J.G. Wood; Status of Free Piston Stirling Technology at Sunpower, Inc.; Sunpower Inc.; USA; 2003; accessed online at http://www.sunpower.com/library/pdf/publications/Doc0085.pdf

[101] W.T. Beale; Applications of Simple Stirling Engines; Third International Stirling Engine Conference; Rome, Italy; 23-26 June 1986; accessed online at http://www.sunpower.com/library/pdf/publications/Doc0001.pdf

[102] R. van der Woude, E. ten Haaken, S. Zutt, B. Vriesema & G. Beckers; Intermediate Results Of The Enatec Micro Cogeneration System Field Trials;

International Stirling Forum 2004; Osnabrück, Germany; 5-7 May 2004; Accessed online at ftp://kerntechniek.nl/pub/www/library/report/2004/rx04011.pdf

[103] Ryuichiro Goto, Yasuhiro Hamada and Hideki Kubota; Study on residential cogeneration systems in cold regions Power generation and exhaust heat recovery of a polymer electrolyte fuel cell; Proceedings of the World Renewable Energy Congress IX; Florence, Italy; 2006

[104] H. W. Keller; WhisperGen und SEM – Testbetrieb von stromerzeugenden Heizungen; Presentation 7th Sept. 2006; Leipzig, Germany; Accessed online http://stromerzeugende-heizung.de/download/vortrag_08_prof_keller_09_06.pdf

[105] Kari Alanne, Arto Saari, V. Ismet Ugursal, Joel Good, The financial viability of an SOFC cogeneration system in single-family dwellings, Journal of Power Sources, Volume 158, Issue 1, 14 July 2006, Pages 403-416

[106] F.G. Best, S.B. Riffat, Miniature combined heat and power system, Renewable Energy, Volume 6, Issue 1, February 1995, Pages 49-51

[107] Jeremy Cockroft, Nick Kelly, A comparative assessment of future heat and power sources for the UK domestic sector, Energy Conversion and Management, Volume 47, Issues 15–16, September 2006, Pages 2349-2360

[108] Maria Eugenia Corria, Vladimir Melian Cobas, Electo Silva Lora, Perspectives of Stirling Engines use for distributed generation in Brazil, Energy Policy, Volume 34, Issue 18, December 2006, Pages 3402-3408

[109] Viktor Dorer, Andreas Weber, Energy and CO_2 emissions performance assessment of residential micro-cogeneration systems with dynamic whole-building simulation programs, Energy Conversion and Management, Volume 50, Issue 3, March 2009, Pages 648-657

[110] Evgueniy Entchev, John Gusdorf, Mike Swinton, Mike Bell, Frank Szadkowski, Walter Kalbfleisch, Roger Marchand, Micro-generation technology assessment for housing technology, Energy and Buildings, Volume 36, Issue 9, September 2004, Pages 925-931

[111] Evgueniy Entchev, Residential fuel cell energy systems performance optimization using “soft computing” techniques, Journal of Power Sources, Volume 118, Issues 1–2, 25 May 2003, Pages 212-217

[112] G. Gigliucci, L. Petruzzi, E. Cerelli, A. Garzisi, A. La Mendola, Demonstration of a residential CHP system based on PEM fuel cells, Journal of Power Sources, Volume 131, Issues 1–2, 14 May 2004, Pages 62-68

[113] Yasuhiro Hamada, Makoto Nakamura, Hideki Kubota, Kiyoshi Ochifuji, Mitsunori Murase, Ryuichiro Goto, Field performance of a polymer electrolyte fuel cell for a residential energy system, Renewable and Sustainable Energy Reviews, Volume 9, Issue 4, August 2005, Pages 345-362

[114] A.D. Hawkes, D.J.L. Brett, N.P. Brandon, Fuel cell micro-CHP techno-economics: Part 2 – Model application to consider the economic and environmental impact of stack degradation, International Journal of Hydrogen Energy, Volume 34, Issue 23, December 2009, Pages 9558-9569

[115] A.D. Hawkes, D.J.L. Brett, N.P. Brandon, Fuel cell micro-CHP techno-economics: Part 1 – model concept and formulation, International Journal of Hydrogen Energy, Volume 34, Issue 23, December 2009, Pages 9545-9557

[116] Charles-Emile Hubert, Patrick Achard, Rudolf Metkemeijer, Study of a small heat and power PEM fuel cell system generator, Journal of Power Sources, Volume 156, Issue 1, 19 May 2006, Pages 64-70

[117] Hycienth I. Onovwiona, V. Ismet Ugursal, Alan S. Fung, Modeling of internal combustion engine based cogeneration systems for residential applications, Applied Thermal Engineering, Volume 27, Issues 5–6, April 2007, Pages 848-861

[118] Christine Pout, Roger Hitchin, Apportioning carbon emissions from CHP systems, Energy Conversion and Management, Volume 46, Issues 18–19, November 2005, Pages 2980-2995

[119] R.W. Saunders, R.J.K. Gross, J. Wade, Can premium tariffs for micro-generation and small scale renewable heat help the fuel poor, and if so, how? Case studies of innovative finance for community energy schemes in the UK, Energy Policy, Volume 42, March 2012, Pages 78-88

[120] Cecilia Wallmark, Sofia Enbäck, Markku Rissanen, Per Alvfors, Göran Lindbergh, Integration of the components in a small-scale stationary research PEFC system, Journal of Power Sources, Volume 159, Issue 1, 13 September 2006, pp 613-625

[121] Jim Watson, Raphael Sauter, Bakr Bahaj, Patrick James, Luke Myers, Robert Wing, Domestic micro-generation: Economic, regulatory and policy issues for the UK, Energy Policy, Volume 36, Issue 8, August 2008, Pages 3095-3106

[122] Jim Watson, Co-provision in sustainable energy systems: the case of micro-generation, Energy Policy, Volume 32, Issue 17, November 2004, pp 1981-1990

[123] Jo Williams, The deployment of decentralised energy systems as part of the housing growth programme in the UK, Energy Policy, Volume 38, Issue 12, December 2010, Pages 7604-7613

[124] Hitchin, E & Pout C; 2002; The carbon intensity of electricity: how many kgC per kWh_e?'; *Building Services Engineering Research & Technology*; 23; 4; pp. 215-222

[125] A.D. Hawkes & M. Leach; Future scenarios for micro-CHP in the UK as residential building insulation improves; eceee 2007 Summer Study Proceedings; 2007

[126] Lane, N, & Beale, W 1997, 'Stirling Engines for Gas-Fired Micro-Cogen and Cooling', *Cogeneration And Competitive Power Journal*, 12, 1, pp. 62-78, British Library Document Supply Centre Inside Serials & Conference Proceedings

[127] Lane, NW 2005, 'Commercialization Status Of Free-Piston Stirling Machines', *International Stirling Engine Conference*, pp. 30-37, British Library Document Supply Centre Inside Serials & Conference Proceedings

[128] Kaarsberg, Tina; Fiskum, Ronald; Deppe, Andreas; Kumar, Satish; Rosenfeld, Arthur; Romm, Joseph; et al.(2000). Combined Heat and Power for Saving Energy and Carbon in Residential Buildings. Lawrence Berkeley National Laboratory: Lawrence Berkeley National Laboratory. Retrieved from: http://www.escholarship.org/uc/item/6kc9t47g

[129] Kelly, N, Clarke, J, Ferguson, A, & Burt, G 2008, 'Developing and testing a generic micro-combined heat and power model for simulations of dwellings and highly distributed power systems', Proceedings Of The Institution Of Mechanical Engineers - Part A - Power & Energy, 222, 7, p. 685

[130] Knight, Ian Paul and Ugursal, Ismet; 2005; Residential Cogeneration Systems: A Review of The Current Technologies. A report of Subtask A of FC+COGEN-SIM The Simulation of Building-Integrated Fuel Cell and Other Cogeneration Systems;

IEA/ECBCS; Accessed online at http://www.ecbcs.org/docs /annex_42_Review_Residential_Cogen_Technologies.pdf

[131] Dries Haeseldonckx, Leen Peeters, Lieve Helsen, William D'haeseleer, The impact of thermal storage on the operational behaviour of residential CHP facilities and the overall CO_2 emissions, Renewable and Sustainable Energy Reviews, Volume 11, Issue 6, August 2007, Pages 1227-1243

[132] Senft, J. R. (1998), Theoretical limits on the performance of Stirling Engines. Int. J. Energy Res., Vol. 22: pp 991–1000

[133] Walker 1973, *Stirling Cycle Machines / By G. Walker*, Clarendon, 1973

[134] http://www.freewatt.com/products.asp?id=194&name=HydronicPlus; Accessed May 2012

[135] http://www.distributedenergy.com/DE/Articles/Better_Cogeneration_through_Chemistry_The_Organic_1864.aspx; Accessed May 2012

[136] Palmer, D.A.; Handbook of applied thermodynamics; 1987; ISBN 9780849332715

[137] Energetix; Datasheet: Kingston Micro-CHP system; Accessed May 2012 at http://www.genlec.com/files/10133%20Genlec%20A4%20Kingston%20insert%20-210911.pdf

[138] http://www.genlec.com/homeowner/faq.html#faq8; Accessed May 2010

[139] http://greentech.co.uk/energetix-launch-micro-chp-boiler-for-uk-homes-341; Accessed May 2012

[140] http://www.powerblock.eu/de/lion-powerblock/konkurrenzstark.php; Accessed May 2012

[141] http://www.cogenmicro.com/index.php?select=79; Accessed May 2012

[142] http://www.cogenmicro.com/index.php?select=144; Accessed May 2012

[143] http://www.mtt-eu.com/en/technology; Accessed May 2012

[144] http://www.mtt-eu.com/en/applications/micro-chp; May 2012

[145] http://www.mtt-eu.com/en/news; Accessed May 2012

[146] Quoilin, S., Lemort, V., & Lebrun, J. (2008, April); Study of an Organic Rankine Cycle Associated to a Biomass-Fuelled Boiler for Cogeneration Application; http://hdl.handle.net/2268/1288

[147] P.J. Boait, R.M. Rylatt, M. Stokes, Optimisation of consumer benefits from microCombined Heat and Power, Energy and Buildings, Volume 38, Issue 8, August 2006, Pages 981-987

[148] Halliday et al Fuel cells providing heat and power in the urban environment August 2005 Tyndall Centre for Climate Change Research Technical Report 32

[149] I. Staffell, R. Green, K. Kendall, Cost targets for domestic fuel cell CHP, Journal of Power Sources, Volume 181, Issue 2, 1 July 2008, Pages 339-349

[150] http://www.kiwagastechnology.com/gastechnology/news.aspx?id=11900; Accessed online May 2012

[151] Brendan Dow, Ceramic Fuel Cells Limited; Investor Update Half Year to December 2011; February 2012; Accessed online May 2012 at http://www.cfcl.com.au/Assets/Files/20120229_Investor_Update-_Feb%202012.pdf

[152] Ceramic Fuel Cells Limited; Gennex Fuel Cell Module Datasheet; Accessed online May 2012 at http://www.cfcl.com.au/Assets/Files/Gennex_Brochure_(EN)_Apr-2010.pdf

[153] Ceres Power Holdings plc; Press Release 25th April 2012; New Strategic Partnership to Access Benelux Market; Accessed online May 2012

[154] Ceres Power Holdings plc; Press Release 1st February 2011; Ceres Power commences residential CHP field trials in consumers' homes; Accessed online May 2012

[155] Sytze Dijkstra, Delta Energy and Environment; Micro-CHP edging towards the mass market; Cogeneration and On-Site Power Production; july–august 2009; pp59-63; Accessed online at http://www.cogeneurope.eu/medialibrary/2011/06/14/c68cb18d/COSPP-article-Micro-CHP-edging-towards-the-mass-market.pdf

[156] De Bruijn F A, Dam V A T and Janssen G J M; Review: durability and degradation issues of PEM fuel cell components; Fuel Cells; 8; 2008; pp 3–22

[157] http://www1.eere.energy.gov/hydrogenandfuelcells/fuelcells/current_technology.html; Accessed online May 2012

[158] Moriarty D. Keynote Address, 12th International Stirling Engine conference. Durham: September 6–9, 2005.

[159] http://www.microchap.nl/stirling_engine.htm; Accessed May 2012

[160] Entchev et al; Micro-CHP technologies for distributed generation in Canada workshop; NREL; Canada; 2003

[161] A. Baumuller & E. Schmieder; Field-Test and Market Introduction of a 10 kW Stirling Engine as CHP- and Solar- Module; Proceedings of 10th International Stirling Engine Conference 2001 (10th ISEC); 24-26 September 2001; Osnabruck; Germany; pp106-113

[162] Mayer & Cie. GmbH & Co.; Stirling Power Station Mini CHP with longlife Stirling Engine; Project Report for EU-LIFE program LIFE99 ENV/D/000.452

[163] A. Hawkes, I. Staffell, D. Brett, N. Brandon; 2009; Fuel cells for micro-combined heat and power generation. ENERG ENVIRON SCI , 2 (7) 729 – 744

[164] M. Stokes, Removing barriers to embedded generation: a fine-grained load model to support low voltage network performance analysis, Ph.D. Thesis, De Montfort University, Leicester, UK, 2005

[165] M. Stokes, M. Rylatt, K. Lomas, A simple model of domestic lighting demand, Energy and Buildings 36 (2004) 103–116.

2 Modelling & Analysis Methodology

2.1 Introduction to BIM-G Model

Research tools to undertake the modelling and analysis tasks required to investigate micro-generation systems and building demand, with such a high degree of integration and temporal precision, were not available at the outset of this doctoral project. Therefore, a methodology was developed to generate demand profiles, simulate micro-generation systems and analyse their performance. This methodology was designated the Building Integrated Micro-Generation (BIM-G) Model, which incorporates software routines, derived demand data and analysis techniques. The BIM-G model was written in Visual Basic for Application (VBA), where functions are executed via spreadsheet user interfaces, where the simulation timestep is 5 seconds.

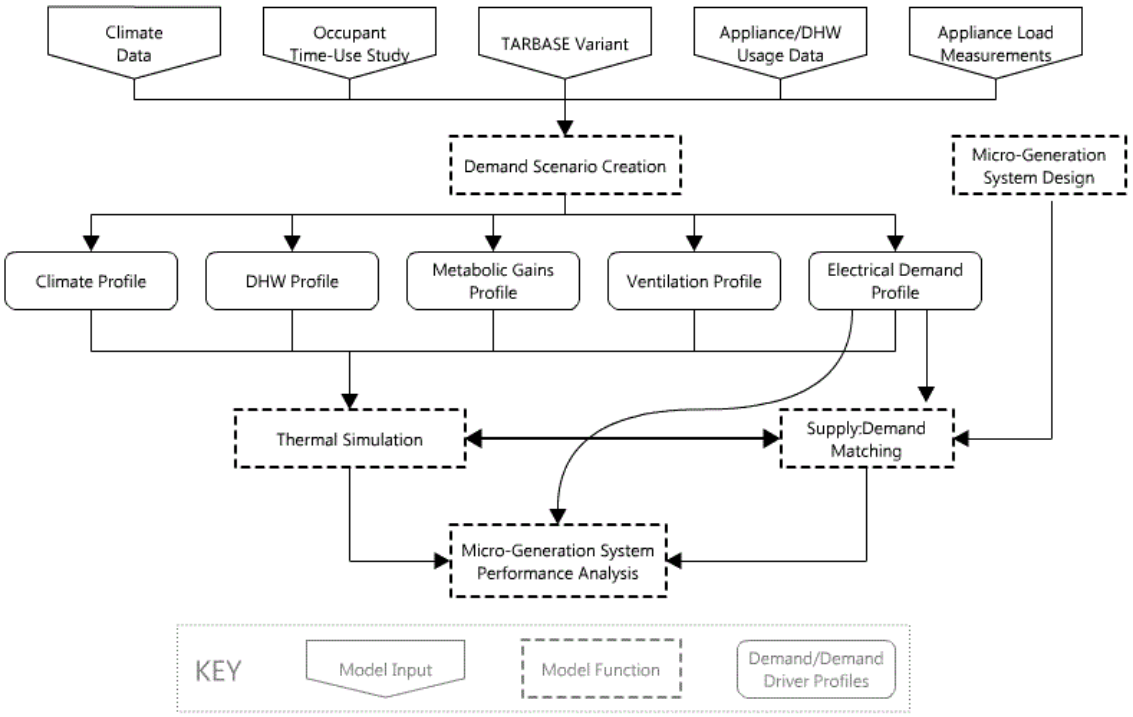

Figure 2.1: BIM-G Model Methodology; Sequence of execution for constituent routines

The sequence in which the BIM-G model methodology is applied to the investigation of a concept micro-generation system is shown in Figure 2.1. Each model function is discussed in its entirety in the upcoming sections of this chapter, with the exception of Demand Scenario Creation. Due to the scope and complexity of the methodology and

data sources underpinning the creation of a demand scenario, Chapter 3 is dedicated to the topic. However, a brief discussion on the demand profiles generated by this function is provided in Section 2.2, in order to aid the reader's understanding of intervening discussions. Similarly, whilst specific details of micro-generation system designs are given in the chapters corresponding to particular systems, the concepts underpinning system performance modelling are explored in Section 2.4.

2.2 Demand Scenario Creation

The originality of the BIM-G modelling and analysis methodology is the transient, bottom-up approach to demand definition. The behaviour of the occupants (both in terms of their interaction with appliances, lighting and DHW outlets, and the temporal configuration of space heating controls) is a major driver of thermal and electrical demand. In order to create demand scenarios, user behaviour must be considered alongside other drivers of domestic energy demand, i.e. the physical dwelling characteristics, representative climate data, occupancy patterns, appliance and lighting ownership, and environmental comfort requirements (for air temperature and ventilation).

The purpose of the Demand Scenario Creation model function is to generate a set of daily demand profiles, which will be used as input data to the Thermal Simulation, Supply:Demand Matching and Micro-Generation System Performance Analysis functions. These daily profiles can represent either direct demand, i.e. consumption of DHW or electricity, or a demand driver, e.g. incidental thermal gain or external temperature. The profiles describe the temporal variation of the direct demand or demand driver.

A set of profiles, as shown in Table 2.1, is generated for each Primary Demand Scenario. To create the Primary Demand Scenarios, as defined in Section 3.9, a climate demand profile is generated for each climate scenario (see Section 3.8), and two versions of the remaining demand profiles are created to represent each occupancy pattern (see Section 3.3.1).

Profile	Description
Metabolic Gains	Demand Driver Profile – 24 hours @ 5 seconds Thermal gain to dwelling from occupants (kW_{th}) Driven by occupancy pattern and appliance/DHW usage events
DHW	Demand Profile – 24 hours @ 5 seconds DHW draw-off profile (litres)
Ventilation	Demand Driver Profile – 24 hours @ 5 seconds Total ventilation rate (Air Changes per Hour, ACH) Includes infiltration and ventilation due to mechanical extractor fans in kitchen and bathroom, driven by DHW and hob/oven usage
Electrical Demand	Demand & Demand Driver Profile – 24 hours @ 5 seconds Electrical usage by appliances & lighting (kW_e) Thermal gain to dwelling from appliances & lighting (kW_{th}) [Does not include boiler and Space Heating Distribution System electrical demand]
Climate	Demand Driver Profile – 24 hours @ 1 hour External Air Temperature (°C) Solar Irradiance from North, South, East & West (kWh/m^2)

Table 2.1: Demand Profiles, as generated for each Demand Scenario

As demand is driven by actions of occupants within a physical building, the definition of the dwelling is the first step in creating a demand scenario, as illustrated in Figure 2.2. It is beyond the scope of this project to consider a wide range of scenarios that cover every conceivable household and dwelling, or indeed to exploit a stock model approach, with large numbers of scenarios designed to cumulatively represent a large proportion of the dwelling and household stocks. Therefore, as discussed in Section 3.2.1, a domestic building variant was selected from those defined for the TARBASE project [1][2]. The composition of the occupying household was defined using a study[1] undertaken by the author for the TARBASE project [3]. In this study, the UK General Household Study [4] was analysed to identify common household compositions, in terms of age (adult or child) and employment status (full-time, part-time or none). Occupancy patterns were defined for the dwelling by assigning each occupant a time period in which to sleep and a period in which to vacate the dwelling. In order to define the lengths of these periods, the UK Time Use Survey [5] was analysed to produce distributions of sleep and vacancy duration by type of occupant (i.e. age and employment status). These occupancy patterns are used to provide a temporal framework for sequencing appliance, lighting, DHW and ventilation usage events, ensuring that mutually exclusive conditions do not occur, i.e. use of a DHW outlet

[1] See Appendix A

when the dwelling in unoccupied. Please refer to Section 3.3 for further details of household composition and occupancy patterns.

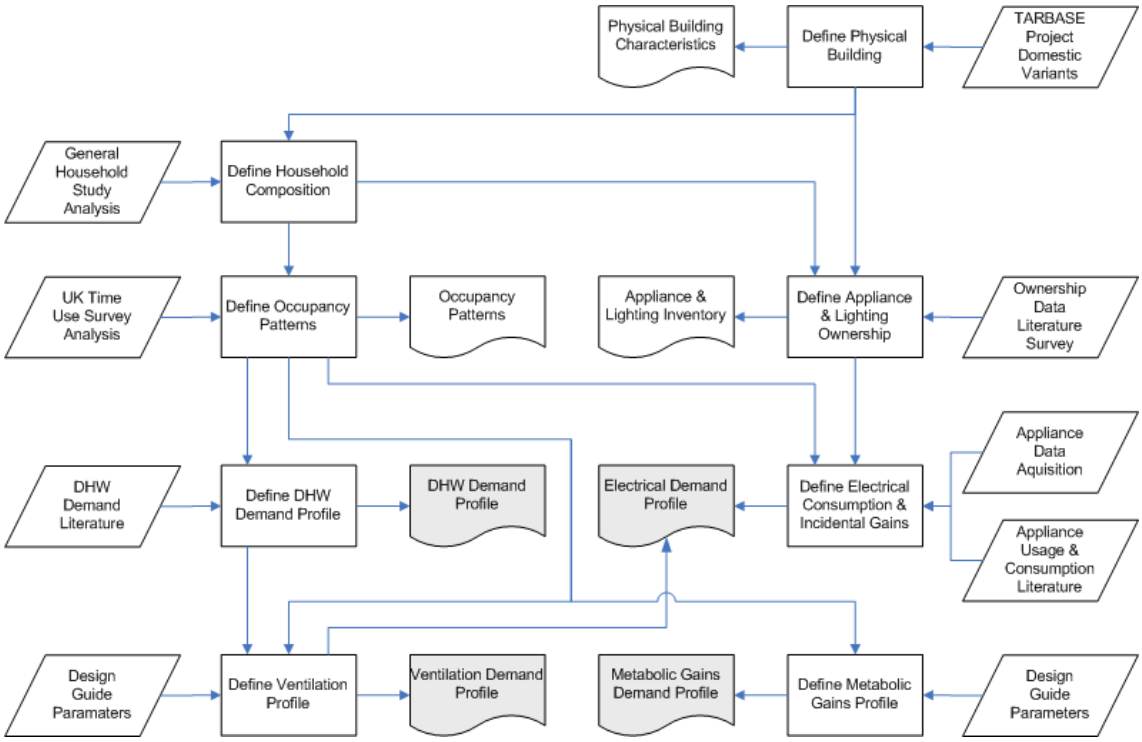

Figure 2.2: Sequence of investigation required to create demand scenario profiles for BIM-G model (excluding climate profile)

Electrical demand profiles include the electricity consumption from lights and appliances, and the incidental thermal gains to the dwellings corresponding to the operation of these devices. It should be noted that the final dwelling electricity consumption profile will include the consumption of Space Heating Distribution System pumps and controls, and boiler parasitic loads (see Sections 2.3.4 and 2.4.3 for details). The bottom-up approach to synthesising electrical demand profiles relies on the definition of an inventory of appliance and lighting ownership, and a sequence of usage events. Such inventories were created, by the author and others, during the TARBASE project to represent discreet households in building variants. A suitable inventory was selected for use with the Primary Demand Scenarios, and is presented in Sections 3.6 and 3.7. The annual usage data and assumptions accompanying this inventory were augmented by further review of the literature and available data, in order specify usage events for each occupancy pattern. With a scarcity of available data on real-time appliance consumption, an exercise was undertaken (see Section 3.6

and Appendix D) to acquire electrical load signatures from selected appliances, along with temperature measurements, to be used in the estimation of incidental thermal gains. The electrical demand profiles for the Primary Demand Scenarios are presented in Section 3.6, along with details of appliance usage and casual thermal gains assumptions.

As discussed by Newborough & Probert [6], DHW consumption data with sufficient temporal precision to simulate a sub-hourly demand response is scarce. Therefore, DHW consumption profiles composed by Jordan & Vajen [7], for solar water heating simulation, were examined to identify daily, weekly and annual consumption levels representative of the defined household. A sequence of DHW events was then created to coincide with appliance and lighting usage events, and occupancy patterns. The DHW demand profiles, generated from this sequence and event consumption data from Jordan & Vajen, for the Primary Demand Scenarios are presented in Section 3.4.

Once the occupancy patterns were defined, and sequences of usage events created for appliances, lighting and DHW, categorisations of occupant behaviour can be made. Using design guide values for metabolic emissions from occupants undertaking a range of activities, metabolic gains demand profiles can be created. Full details can be found in Section 3.3.2, along with metabolic gains profiles for the Primary Demand Scenarios.

The Ventilation Demand Profile is similarly generated from occupancy patterns and specific appliance and DHW events, coupled with design guide values for intentional ventilation rates, and the rate of air infiltration. Further details are given in Section 3.5.

2.3 Thermal Simulation

2.3.1 Building Heat Balance

The Thermal Simulation function of the BIM-G Model is a set of algorithms to simulate the heat balance of the building airspace, space heat distribution system (SHDS) and thermal storage. Thermal simulation is performed concurrently with the Supply:Demand Matching routine, with calculations performed for 5-second timesteps.

This is essential to allow the Supply:Demand matching routine to respond dynamically to changes in thermal demand, and indeed thermal storage capacity, due to the thermal energy transfers associated with the previous timesteps.

The basis of the Thermal Simulation function is the transient simulation of the dwelling's internal air temperature, achieved using a simplified version of the Heat Balance method described by ASHRAE [8] shown in Figure 2.3. This internal air temperature is then used to control the operation of heat generation equipment, and any circulation pumps, within the dwelling.

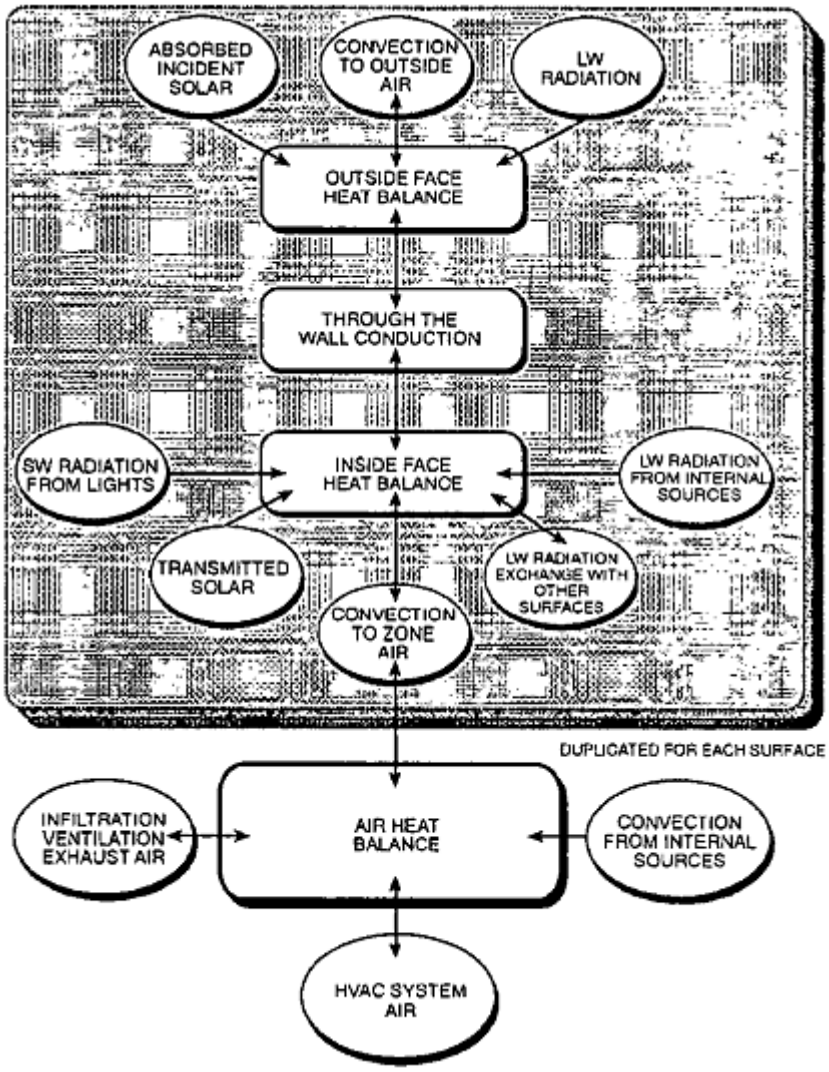

Figure 2.3: Schematic of Building Heat Balance method, as defined by ASHRAE [8], where the shaded area represents the heat balance for a surface of the external building fabric. A simplified version of this heat balance model is used within Thermal Simulation function of the BIM-G Model.

The dwelling under investigation is conceptualised as a collection of construction elements that represent the thermal resistance and capacity of the building fabric components that separate the dwelling's internal airspace from the external environment. These construction elements are analogous to the building surfaces discussed by ASHRAE [8]. The various 1-dimensional heat transfer paths and mechanisms included in the heat balance are displayed diagrammatically in Figure 2.4. By comparison of Figure 2.3 and Figure 2.4, the simplifications of the ASHRAE heat balance method can be identified.

The complex radiative transfer computations between internal dwelling surfaces, passive building contents (such as furniture), and the internal airspace were not undertaken in the BIM-G model. Instead, it considers the dwelling as 1-dimensional construction elements of defined areas (unlike the 2-D or 3-D representations used in dedicated building thermal simulation packages[1,2,3]).

The wall construction is represented using an external and internal surface, with an associated thermal mass. However, due to the complexity of simulating heat transfer through the roof, glazing and ceiling, heat loss through these construction elements was calculated using a U-value approach. Because of this, the thermal mass effects due to the roof, glazing and ceiling construction elements was not considered in the BIM-G model. This U-value approach does not account for short-wave radiation transfer at their external surfaces, and it uses static combined convective and long-wave radiative heat transfer co-efficients for heat transfer calculations between the external environment, construction elements and internal airspace. Although this removes the temperature dependence of the heat transfer co-efficient from the heat loss calculation, this was considered acceptable due to the relatively low temperature difference between the construction elements and the external and internal environments.

[1] ESP-r; Strathclyde University; www.esru.strath.ac.uk

[2] TAS; Environmental Design Solutions Limited; www.edsl.net

[3] IES; Integrated Environmental Solutions (IES) Ltd; www.iesve.com

The heat transfer calculation between the internal wall surface and the internal airspace also uses a static (i.e. does not vary with temperature differential) convective heat transfer co-efficient. Again, this was considered acceptable due to the relatively low temperature difference between the construction elements and the internal airspace.

For simplicity, the effects of humidity on the heat balance were not considered. As the concept energy systems did not include air-conditioning or dehumidification units, which alters the relative humidity of the internal air, it was considered acceptable to omit the calculation of humidity from the BIM-G model. Therefore, the latent fraction of casual thermal gains, from appliances and occupants, is disregarded.

The decision to use a single-zone, 1-D thermal model, without humidity calculations, was taken because of the complexity involved in designing, developing, testing (with various building types), validating, and defining input data for, a multi-zone 3-dimensional simulation tool [9]. Using 1-D finite difference analysis method for heat conduction through the wall elements, and 1-D U-value calculation for each transfer through the other construction elements, vastly shortened software development time, which was vital, as the focus of the doctoral project is µCHP system analysis, and not thermal simulation tool design.

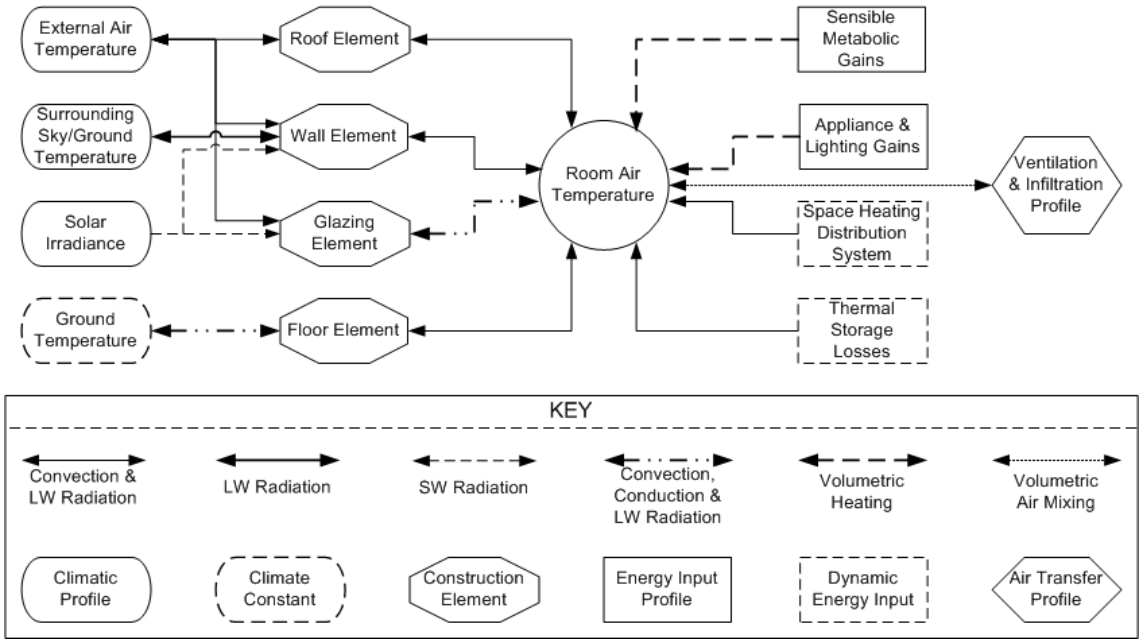

Figure 2.4: Heat transfer mechanisms and paths simulated within the BIM-G Model's Thermal Demand Estimation routine

The simplified heat balance method is ultimately used to calculate the building's internal air temperature, T_{in}, using equation (2.1), for an airspace of predefined mass, m_{Air}. The remaining terms are defined in the remainder of this section.

$$T_{in}(t) = T_{in}(t-1) - \frac{\left(Q_{Floor}(t) + Q_{Wall}(t) + Q_{Roof}(t) + Q_{Glazing}(t) + Q_{Vent}(t) - Q_{Casual}(t) - Q_{StoreLoss}(t) - Q_{SHDS}(t)\right)}{\left(m_{Air} * c_{Air}\right)} \quad (2.1)$$

2.3.2 Construction Elements

The wall construction element can be considered to have three distinct components; an external surface, internal surface and bulk material. Using finite difference analysis, the resultant heat flow between the internal and external environments is simulated, with due consideration for the thermal capacity of the building fabric.

The heat loss from the airspace through wall construction element is calculated using equation (2.2), which accounts for combined convective and radiative heat transfer using the combined heat transfer co-efficient, $h_{Wall\text{-}In}$. This transfer is driven by the temperature differential between internal air and the internal surface of the wall element, T_{Wall_In}, across the surface area of the wall, A_{Wall}.

$$Q_{Wall}(t) = h_{Wall\_In} * A_{Wall} * \left[T_{In}(t-1) - T_{Wall\_In}(t)\right] \quad (2.2)$$

The internal wall surface temperature is in turn calculated using equation (2.3), which accounts for the conduction of heat through the wall element to its external surface. The conductive heat transfer is calculated using the temperature differential between the internal and external (T_{Wall_Ext}) surfaces, and the thermal transmittance of the wall construction, ThT_{Wall}. The thermal capacity of the wall element is represented by its mass, m_{Wall}, and the average specific heat capacity of its constituent layers, c_{Wall}.

$$T_{Wall\_In}(t) = T_{Wall\_In}(t-1) + \left(\frac{A_{Wall}}{m_{Wall} * c_{Wall}}\right) * \left[\begin{array}{l}\left(h_{Wall\_In} * \left(T_{In}(t-1) - T_{Wall\_In}(t)\right)\right) - \\ \left(ThT_{Wall} * \left(T_{Wall\_In}(t-1) - T_{Wall\_Ext}(t)\right)\right)\end{array}\right] \quad (2.3)$$

The thermal transmittance of the wall construction is calculated using equation (2.4), from the sum of the wall element's constituent layers, by considering the thermal conductivity of the layer (λ_{Layer}) and the layer thickness (d_{Layer}) as demonstrated in BS EN ISO 6946 [10]. This thermal transmittance is related to the planar sections of the wall only, i.e. it does not account for thermal bridging or external doors.

$$ThT_{Wall} = \frac{1}{\sum_{Layer=1,2,3,etc} \left(\frac{d_{Layer}}{\lambda_{Layer}}\right)} \quad (2.4)$$

A planar U-value of 0.49 was then calculated using the thermal transmittance and the horizontal internal and external surface resistances, R_{si} & R_{se}, using equation (2.5). The standard values of internal and external surface resistances quoted in BS EN ISO 6946 [10] were used in all calculations.

$$U_{Wall} = \frac{1}{\left(R_{si} + \frac{1}{ThT_{Wall}} + R_{se}\right)} \quad (2.5)$$

Both linear and repeating thermal bridges were considered in the calculation of thermal transmittance values for the wall construction. For timber fame constructions, as selected for the building variant during the TARBASE project, Table 3.13 of CIBSE

Guide A [11] provides a cross reference between planar U-values, and U-values incorporating a repeating thermal bridge for typical timber frame constructions, which is referred to as $U_{WallRTB}$.

This average U-value for the wall element was then adjusted to account for non-repeating thermal bridges, as defined by BRE IP1/06 [14]. A heat loss co-efficient was calculated for each type of non-repeating thermal bridge, as shown in Table 2.2, using values of linear thermal transmittance from Table 3 of BRE IP1/06 [14].

Non-Repeating Thermal Bridges	Bridge Length (m) or Qty. of Corners	Linear Thermal Transmittance (W/mK)	Heat Loss Co-Efficient (W/K)
Glazing Sills	5.884	0.04	0.24
Glazing Lintels	5.884	0.3	1.77
Door Jamb	8.4	0.05	0.42
Door Lintel	1.8	0.3	0.54
Intermediate Floor	34	0.07	2.38
Ground Floor (incorporated in Ground Floor U-value)	34	0.16	0.00
Eaves	16	0.06	0.96
Gable	18	0.24	4.32
Corners (Normal)	8	0.09	0.72
Total			**11.34**

Table 2.2: Heat loss co-efficient calculated for each type of non-repeating thermal bridge, along with length of bridge (or quantity of corners) and linear thermal transmittance, for each non-repeating thermal bridge type

A U-value adjustment factor for non-repeating thermal bridges (U_{NRTBAF}) was calculated using equation (2.6), by dividing the total heat loss co-efficient from all non-repeating thermal bridges (H_{NRTB}) by the wall element surface area.

$$U_{NRTBAF} = \frac{H_{NRTB}}{A_{Wall}} \tag{2.6}$$

To account for the increased heat loss through solid external doors, due to the increased U-value of external doors (U_{Door}), the repeating thermal bridge-corrected wall U-value is averaged with U_{Door} by surface area. The final U-Value of the wall, as used in BIM-G simulations, is calculated using equation (2.7).

$$U_{Wall} = \left(\frac{\left[A_{NetWall} * U_{WallRTB}\right] + \left[A_{Doors} * U_{Door}\right]}{A_{NetWall} + A_{Doors}} \right) + U_{NRTBAF} \quad (2.7)$$

The thermal transmittance of the wall construction element, as used in BIM-G simulations, was calculated using equation (2.8), where the U-value (U_{Wall}) was calculated using equation (2.7). This thermal transmittance is corrected for repeating & non-repeating thermal bridges, and the presence of external doors.

$$ThT_{Wall} = \frac{1}{\left(R_{si} + \frac{1}{U_{Wall}} + R_{se} \right)} \quad (2.8)$$

To calculate the external surface temperature, various heat transfer processes are simulated using equation (2.9). The convection co-efficient ($h_{W\text{-}Ext}$) is used to calculate convective heat transfer between the wall surface and the external air at the dry bulb air temperature, T_{Ext}. Long-wave radiative exchange between the wall (with an emissivity, e_{Wall}) and surrounding ground and sky is calculated using the associated temperatures in degrees Kelvin, T_{Wall}, T_{Ground} and T_{Sky}.

$$T_{Wall\_Ext}(t) = T_{Wall\_Ext}(t-1) + \left(\frac{A_{Wall}}{m_{Wall} * c_{Wall}}\right) * \left[\begin{array}{l} \left(ThT_{Wall} * \left(T_{W\_In}(t-1) - T_{W\_Ext}(t-1)\right)\right) - \\ \left(h_{W\text{-}Ext} * \left(T_{Wall\_Ext}(t-1) - T_{Ext}(t)\right)\right) + \\ \left(\frac{ab_{Wall}}{A_{Wall}} * \sum^{N,E,S,W} \left[A_{Wall} * S(t)\right]\right) + \\ \left(e_{Wall} * SBC * 0.5 * \left[\left(T_{Sky}^4 - T_{Wall}^4\right) + \left(T_{Grd}^4 - T_{Wall}^4\right)\right]\right) \end{array}\right] \quad (2.9)$$

Energy transfer from short-wave solar radiation incident on the external surface of the wall element is calculated for each primary direction in equation (2.9). This short-wave energy exchange is dependent on the diffuse and direct normal solar radiation on the simulation day, the latitude of the site, the time of year (for sun angles), orientation of the building and the absorptivity of the external wall surface, ab_{Wall}. A solar irradiance model was developed (see Section 3.8) to calculate the total incident solar irradiation, per unit area (S), on a vertical surface facing in each primary direction. This model is executed, on the chosen climate data, during the Demand Scenarios Conception phase of the methodology.

Heat loss through the glazing construction element, calculated using equation (2.10), incorporates the heat transfer through the bulk material of the glazing, and a solar gain (due to long-wave radiation) to the internal airspace calculated using an ASHRAE approximation method [12]. This ASHRAE method uses a solar heat gain co-efficient (SHGC) to estimate the proportion of incident solar irradiance (S, as discussed above) that is transmitted into the dwelling.

$$Q_{Glazing}(t) = \left(U_{Glazing} * A_{Glazing} * \left[T_{In}(t-1) - T_{Ext}(t)\right]\right) + \left(SHGC * \sum^{N,E,S,W}\left[A_{Glazing} * S(t)\right]\right) \quad (2.10)$$

Heat transfer through the material of the frame and glass pane is called using the glazing element's U-value ($U_{Glazing}$). This U-value, as defined in BS EN ISO 6946:1997 [10], incorporates the thermal resistance of each layer (in this case averaged between frame and glazing areas) and the internal and external surface resistance to convective and long-wave radiative exchange. This external surface resistance ignores the effects of incident short-wave radiation [10], which is simulated using the ASHRAE method discussed above.

The roof element is a representation of the constructions and materials of the external roof and internal ceiling, with the resultant mass, thickness, thermal resistance, and specific heat capacity. The wall element is the area weighted total representation of wall, doors and glazing units, with similar physical parameters. Equation (2.11) is used to calculate the heat loss from the building through the roof construction element.

$$Q_{Roof}(t) = U_{Roof} * A_{Roof} * \left[T_{In}(t-1) - T_{Ext}(t)\right] \quad (2.11)$$

The floor element represents the ground-floor construction, where the floor U-value (U_{Floor}) was calculated from a planar U-value (of the constituent layers), then applying corrections factors to account for the exposed perimeter [13] and linear thermal bridging [14] between the floor and wall elements. The surrounding ground temperature (T_{Ground}) is assumed to equal the annual average air temperature, as set out in BSEN12831:2003 [15], and suggested by CIBSE [16]. The heat loss through the floor construction element was calculated using equation (2.12).

$$Q_{Floor}(t) = U_{Floor} * A_{Floor} * [T_{In}(t-1) - T_{Ground}] \quad (2.12)$$

The heat loss due to ventilation and infiltration is calculated using equation (2.13). The infiltration rate ($V_{Infiltration}$) is a constant value specified alongside the building construction, whilst the varying ventilation rate ($V_{Ventilation}$) is imported from the ventilation demand driver profile.

$$Q_{Vent}(t) = [V_{Infiltration} + V_{Ventilation}(t)] * V_{Air} * \left[\frac{T_{In}(t-1) - T_{Ext}(t)}{3}\right] \quad (2.13)$$

2.3.3 Casual Thermal Gains

The BIM-G Model considers the two forms of "casual" or incidental thermal gains to the building, as calculated in equation (2.14); Metabolic Gains ($Q_{Metabolic}$) and Appliance & Lighting Gains ($Q_{A\&L}$).

$$Q_{Casual}(t) = Q_{A\&L}(t) + Q_{Metabolic}(t) \quad (2.14)$$

Although uncontrollable in a conventional sense, casual thermal gains are commonly considered in the design of building energy services. As discussed in Section 2.2, appliance and lighting gain is included in the electrical demand profile, and a discrete metabolic gain profile is produced for each demand scenario. Further details on the creation of these casual thermal gain profiles are given in Sections 3.3.2 and 3.6. As discussed in Section 2.3.1, the latent fraction of casual thermal gains is disregarded, as the BIM-G model does not include simulation of humidity levels.

2.3.4 Space Heating Distribution System

Within a dwelling, a space heating distribution system (SHDS) is utilised to distribute thermal energy from a central heat generator, to the individual rooms. In the UK, the dominant SHDS is a wet central heating system [39], in which a volume of water is pumped through pipework to a series of heat emitters (typically radiators).

The effect of using a SHDS is to introduce thermal lag between heat generation and heat delivery to the dwelling airspace. Initial development work on the BIM-G model omitted a SHDS. When BIM-G results were compared against internal air measurements recorded by the author in several dwellings, several features of the resulting temperature profiles were skewed. Without a SHDS, the internal air temperature fell sharply on cessation of heat generation, which in practice does not occur due to residual thermal energy stored in the volume of space heating water (SHW) and metal of the radiators and pipework, which gradually transfers to the air mass over time. Similarly, internal air temperature rose sharply when the heat generator was activated, whilst in practice the increase is much more gradual, as the SHW acts as a buffer.

In order to increase the accuracy of thermal simulation, a simplified space heating distribution system was devised. To work within the limits of a single zone, 1-D model, simplifications were necessary, yet worthwhile, as they would serve to introduce an indicative thermal lag term to the thermal demand estimation routine. The SHDS has four sections; a heat emitter (i.e. radiator), a heat exchanger (HX) within the heat generator, a flow pipe (from heat generator HX to emitter), and a return pipe (from emitter to heat generator HX). This arrangement is displayed in Figure 2.5. Each section contains a volume of SHW, where flow between the sections is simulated every time-step by calculating the average temperature for each element based on a single flow volume (at the previous temperature of that element) being replaced with a flow volume of the preceding element (at the previous temperature of that element). The emitter and pipes are defined with a surface area, for which the heat transfer to the internal air volume is calculated based on temperature differential. The energy transfer into the heat generator's HX is determined by the heat output of the heat generators under simulation. If a thermal store is specified for a particular demand scenario, then the HX volume considered is that of HX within the thermal store, and not of the heat generator.

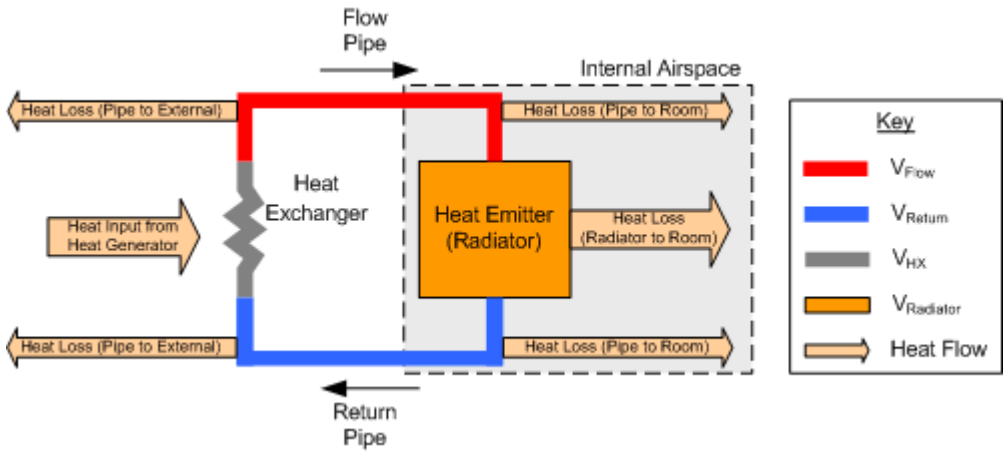

Figure 2.5: Schematic of Space Heating Distribution System (SHDS) concept used in BIM-G model, where each section of the SHDS relates to a volume of water whose temperature is calculated each time-step based on flow between each section and indicated heat flows

It may be argued that a full heat and mass flow model of the SHDS for a given dwelling should have been implemented. This would have involved further division of the SHW into smaller elements, and a heat transfer characteristic dictated by the position of the element within the SHDS and the temperature of surrounding elements. The increase in simulation accuracy that this approach would have offered would have been attained if the exact geometry of the SHDS was known. To have done so would have required specifying a discrete system for each dwelling considered, which was considered beyond the scope of this investigation. The major drawback of the simplified approach is that the temperature within each section is representative of the average across the section, and hence the extremes of temperatures entering and leaving the sections are not calculated.

In the end, the complex approach was considered impractical within the constraints of the BIM-G Model, as it would require full geometric and technical specification of the SHW distribution system, including pumps, pipework, heat emitters and expansion vessels. The resources required for such development, as well as the intrinsic binding of any results to that particular system design, were deemed inappropriate, especially as the rationale of the BIM-G model was to remain generic.

The design of the SHDS was undertaken using a domestic wet central heating design guide [17], published by an industry body, the Heating and Ventilation Contractors' Association (HVCA). Using the SHDS design methodology described in the guide [17], the rated emitter thermal output was derived, and from numerical analysis of typical emitter characteristics, the associated SHW volume and emitter surface area was calculated. From pipework layout estimations, undertaken using a floor plan of the dwelling, and numerical analysis of typical pipework lengths per radiator from the HVCA guide, the surface areas and volumes of both pipes were calculated. If the SHDS is specified with a thermal store, the HX volume is calculated from a relationship with store volume, as derived from the HVCA guide [17]. If the SHDS is specified with no thermal store, the heat generator HX volume is taken as the HVCA guide's typical value.

When the SHDS circulation pump is activated, the BIM-G model simulates the flow of SHW by volume-averaged recalculation of SHW temperatures in each section of the SHDS. The rate at which the SHW circulates was chosen using the HVCA design guide [17], with supporting information from the relevant British Standard [18].

In the HX section of the heat generator, any temperature rise is calculated from heat generator output acting on the volume of water in the section. If a thermal store is specified, the input energy flow to the SHDS (Q_{SHDSIn}) from the thermal store to the HX section (of the SHDS) is calculated from the temperature difference between the SHW in the thermal store HX and water in the thermal store itself, using equation (2.15).

$$Q_{SHDSIn} = m_{SHWFlow} * c_{Water} * \left[T_{Store}(t) - T_{PipeF}(t)\right] \quad (2.15)$$

Heat transfer between the heat emitter and internal air was calculated using the "characteristic equation" of a typical radiator, as defined by the relevant British Standard [19] and the HVCA guide [17]. This "characteristic equation" quantifies the heat transfer due to convection and radiation, for radiators of an assumed height, in relation to the temperature difference between the SHW in the emitter and internal air. The characteristic equation is applied in the BIM-G model using equation (2.16),

where $KM_{Radiator}$ is the characteristic heat output, and $n_{Radiator}$ the radiator constant. These values were derived by performing a power-type regression on data from the HVCA guide [17], which related the temperature difference between the radiator water and surrounding air to radiator thermal output.

$$Q_{Radiator} = KM_{Radiator} * \left[T_{Radiator}(t) - T_{In}(t)\right]^{n_{Radiator}} \quad (2.16)$$

Equation (2.16) is also used to calculate the heat loss from the flow ($Q_{Pipe\text{-}Flow}$) and return ($Q_{Pipe\text{-}Return}$) pipework sections of the SHDS, using values for KM_{Pipe} and n_{Pipe} again derived by regression from data in the HVCA guide [17], and the pipe water temperatures, $T_{Pipe\text{-}Flow}$ & $T_{Pipe\text{-}Return}$. The water temperature in the return pipe is used as a control signal for the SHDS circulation pump, as discussed in Section 2.3.6. The heat loss from the pipework is assumed to split between heated and unheated portions of the dwelling, i.e. some of the heat of the heat quantified by $Q_{Pipe\text{-}Flow}$ & $Q_{Pipe\text{-}Return}$ enters the dwelling's heated airspace, and the remainder is immediately lost to the environment under suspended floors and in unheated loft spaces. The BIM-G model uses a 50:50 split, as no definitive information was available to the contrary. The heat loss is based on heat transfer from the exterior surface of the pipes, using the minimum pipe insulation standard quoted by industry guidance material [17].

The final heat input to the dwelling's internal airspace, Q_{SHDS}, is calculated using equation (2.17).

$$\begin{aligned} Q_{SHDS}(t) = &\left(KM_{Radiator} * \left[T_{Radiator}(t-1) - T_{In}(t-1)\right]^{n_{Radiator}}\right) + \\ &\left(0.5 * KM_{Pipe} * \left(\left[T_{Pipe\text{-}Flow}(t-1) - T_{In}(t-1)\right]^{n_{Pipe}} + \left[T_{Pipe\text{-}Return}(t-1) - T_{In}(t-1)\right]^{n_{Pipe}}\right)\right) \end{aligned} \quad (2.17)$$

2.3.5 Thermal Storage Configurations

In theory, many configurations of thermal storage, for space heating, DHW or both are possible, and like SHDSs, many designs are used in practice. The purpose of this research is not to predict the performance of specific thermal storage system designs, but to compare the performance of concept micro-generation systems, within the boundaries of realistic dwelling energy systems. In this chapter, the simulation

methodology for both thermal storage arrangements used within this research is detailed. As discussed in Chapter 1, a thermal store is typically specified alongside μCHP systems to aid the matching of supply and demand, increasing prime mover run-times.

In order to simulate thermal energy transfer within the BIM-G model, without resorting to computational fluid dynamics and 3-dimensional heat transfer equations, a simplified power balance approach has been adopted, as in equation (2.18). If we assume that the heating loop instantaneously transfers thermal energy from the heat generator to the heat exchanger within the store, which in turn transfers all thermal energy instantaneously (within the bounds of a 5-second timestep) to the thermal store's water, then any thermal generation from the heat generator (within the limits of its output) results in an increase in thermal store water temperature, ΔT_{Store}. This temperature rise is calculated by re-arranging equation (2.18).

$$E_{HG} = t_{Iteration} * c_{water} * \rho_{water} * V_{Store} * \Delta T_{Store} \quad (2.18)$$

The basic thermal storage configuration considered in this project is an indirectly heated DHW tank, see Figure 2.6, where the input heat exchanger is connected to the primary circulation loop of the heat generator, and the output heat exchanger is used to supply DHW. In this setup, the control strategy uses a temperature sensor within the tank to maintain the water temperature within the tank between a target and a trigger temperature.

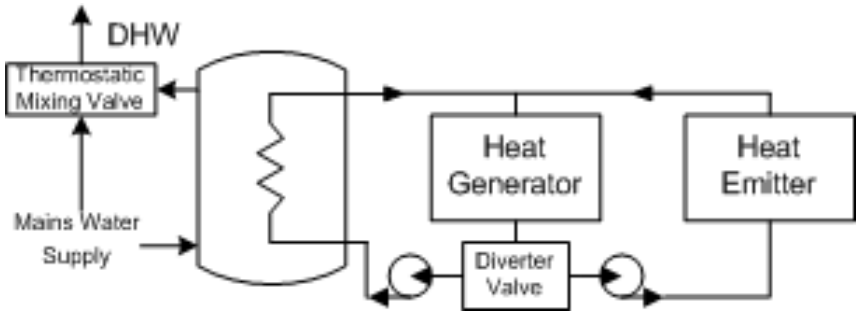

Figure 2.6: Diagram of Thermal Storage with DHW Tank, as simulated within BIM-G model

When the tank water temperature drops below the trigger temperature, the operation of the heat generator is triggered, within the constraint of an active signal from the DHW/SH timer control. If a freely modulating heat generator is present, then the heat generator output is calculated as the difference between the current DHW tank temperature, and the target DHW tank temperature. If a restricted modulation heat generator is used, then the closest modulation level is used, as dictated by that heat generators control strategy.

With a thermal store in situ, see Figure 2.7, a complex control strategy is implemented to control the operation of the heat generator and associated heating loop pump, with respect to thermal output modulation and pump status. The control logic is primarily driven by input from a temperature sensor within the thermal store, with adjustable temperature overrides, which are tailored to increase heat generator runtimes, or reduce on/off cycles, as deemed appropriate by design. Control temperatures are presented in Table 2.3

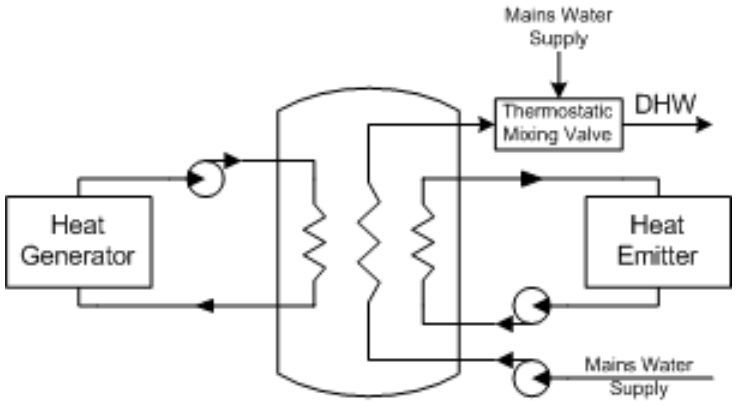

Figure 2.7: Diagram of Thermal Store, as simulated within BIM-G model, showing heat exchangers for heat generator (i.e. heat input), space heating distribution system (heat output via heat emitter), and domestic hot water supply

Thermal energy for the SHDS is withdrawn from the thermal store via an immersed heat exchanger, which itself is a section of the SHDS, as discussed in Section 2.3.4, and displayed in Figure 2.5.

The simulation of draw-off of hot water from the thermal store for DHW purposes relies on three assumptions. Firstly, delivery of 50°C tap water requires 60°C extracted water (to account for pipework cooling). Secondly, a thermostatic mixer valve will add cold water to keep the DHW within safety tolerances at the tap. The flow rates of DHW draw-off assumptions discussed in Section 3.4 are assumed to equal the water flow rate from the DHW tank, or through the DHW heat exchanger in the thermal store. In reality, the occupant may receive a slightly higher flow rate, as the thermostatic mixing valve introduces additional cold water to ensure that water temperatures at the tap are within safe limits. Finally, studies by Jordan & Furbo [20] show that a stratified tank will draw-off temperatures of within 10% of original top-of-tank temperatures until around 70% of the tank is discharged. It was therefore assumed that a thermal store usually maintained between 75°C and 85°C will be capable of supplying DHW at a temperature of at least 60°C.

Heat loss from the heating loops which supply the thermal store and DHW tank (from the heat generator) to the environment is ignored, as the loss is assumed to be small, due to the shot length of the loop, insulation of the loop, and the possibility of its placement within the same enclosure as the heat generator. Thermal lags due to the circulation of the heat transfer fluid (with its associated volume) within the heating loop are not considered due to the 5-second iteration timestep used in the BIM-G model. The relatively small volume of fluid coupled with a relatively high circulation rate, and the effects of heat conducting throughout the relatively short length of heating loop and fluid, should mean that such thermal lags are minor in the context of 5 seconds.

The thermal loss from the thermal store or DHW tank is calculated each iteration using equation (2.19), using typical values of heat–loss co-efficient (h_{Store}), as specified in British Standards publication [21], manufacturer's association standards [22], and an academic research publication [23] incorporating well-insulated thermal storage. The surface area of the DHW tank or Thermal Store, A_{Store}, is calculated using the dimensional requirements detailed in Table 1 of BS1566-1 [21].

$$Q_{StoreLoss}(t) = A_{Store} * h_{Store} * [T_{Store}(t) - T_{In}(t)] \quad (2.19)$$

It is worth noting that the introduction of a thermal store will increase the thermal demand on the heat generator. If the storage capacity, and hence surface area, increases between the DHW tank and thermal store then the standing heat loss will increase, assuming that the heat-loss co-efficient (due to insulation) of the storage vessels are the same. In addition, the increased thermal throughput for the storage vessel, as both space heating and DHW demands are supplied via the thermal store, will increase distribution losses (from heat generator to the thermal store).

2.3.6 Space Heating Circulation Pump Control

The provision of space heating is governed by control of the space heating circulation pump (SHCP), which drives SHW around the SHDS. The status of the pump is controlled by reference to an internal air temperature sensor. The control routine associated with the internal air temperature uses a hysteresis range around the target internal air temperature. This range was chosen after consultation with thermal comfort research, which suggested a range of tolerance around a target temperature, and typical hysteresis values quoted in room thermostat manufacturer's literature. The typical values for target temperature, trigger temperature, i.e. lower limit of hysteresis, and limit temperature, i.e. upper limit of hysteresis, are displayed in Figure 2.8. These values could be varied to produce alternative demand scenarios, to alter thermal comfort requirements, as discussed in Chapter 6.

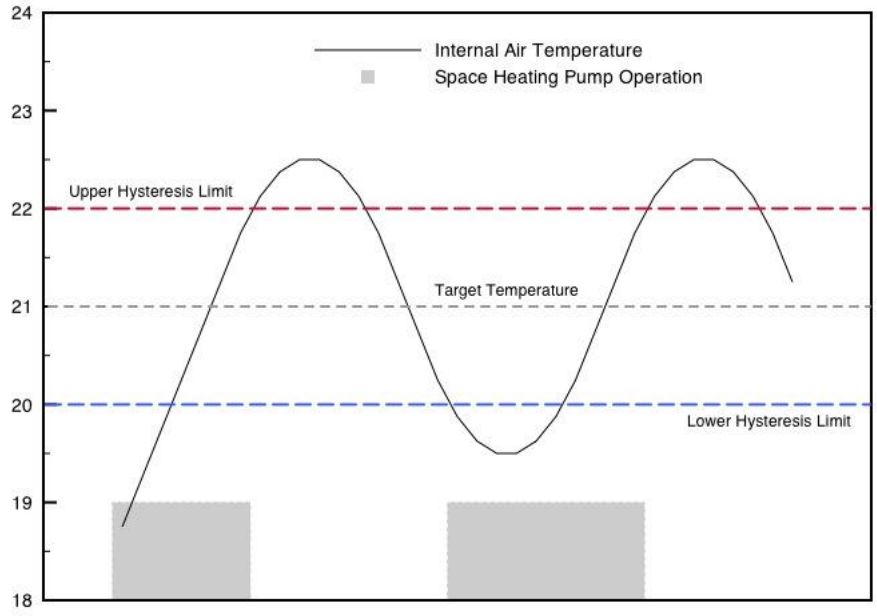

Figure 2.8: Internal air temperature control strategy adopted in BIM-G model

The operation of the space heating circulation pump, as represented in Figure 2.8 by the shaded area, is in effect the control signal, from the control strategy monitoring internal air temperature, for space heating thermal input to the internal air volume. This control signal triggers a series of control decisions, the nature and extent of which depend on the presence, or otherwise, of a thermal store connected to the SHDS.

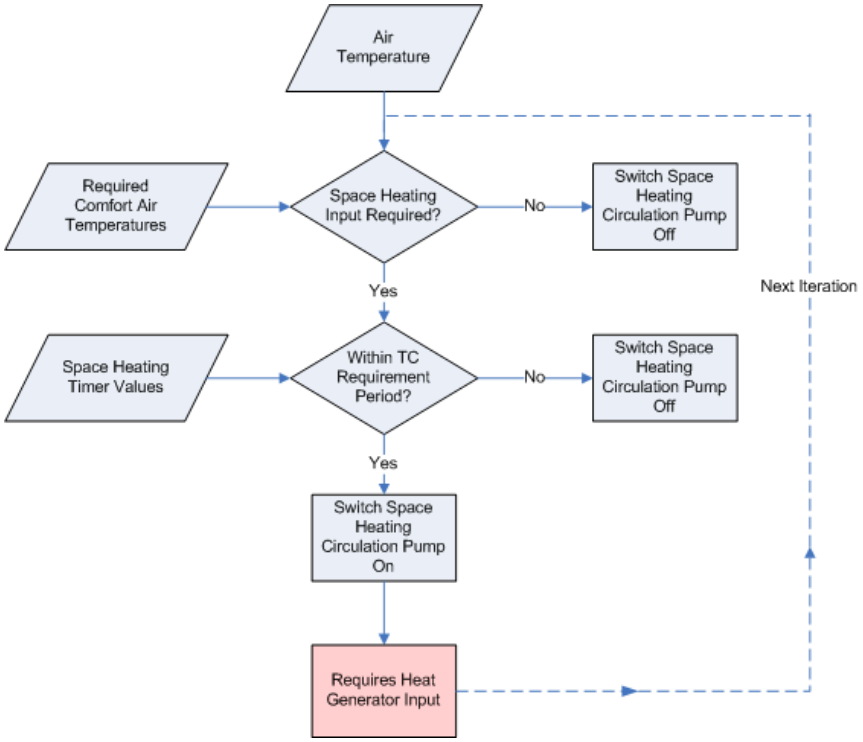

Figure 2.9: Decision Tree for Space Heating Control, for concept systems without a Thermal Store, to decide whether heat generator input to SHDS is required, along with operation of the Space Heating Circulation Pump

In Figure 2.9, the procedure for space heating control is described using a flow diagram, for SHDSs without a thermal store. This procedure for SHDSs with a thermal store is presented in Figure 2.10. It is prudent to note that the operation of heat generators, as prime mover heat recovery systems, primary boilers or auxiliary boilers, are constrained in a manner alluded to, but not detailed in, these flow diagrams, by the individual operating regime of a concept system, and the control strategy implemented within that regime. The operation of the heat generator within a SHDS with a dedicated DHW tank is controlled by signals from the SHDS and DHW tank, and as such the thermal input available to raise the temperature of SHW is dependent on the thermal demand from the DHW tank at that time. Alternatively, the maximum thermal extraction from the space heating heat exchanger of the thermal store is indirectly dependent on thermal extraction through the DHW heat exchanger, as DHW-driven extraction will lower thermal store water temperature, hence reducing thermal extraction potential.

Concept systems that incorporate a thermal store are designed with a Heat Generator Circulation Pump (HGCP), which circulates the heating medium, i.e. water, between the heat generator's heat exchanger, and the input heat exchanger in the thermal Store.

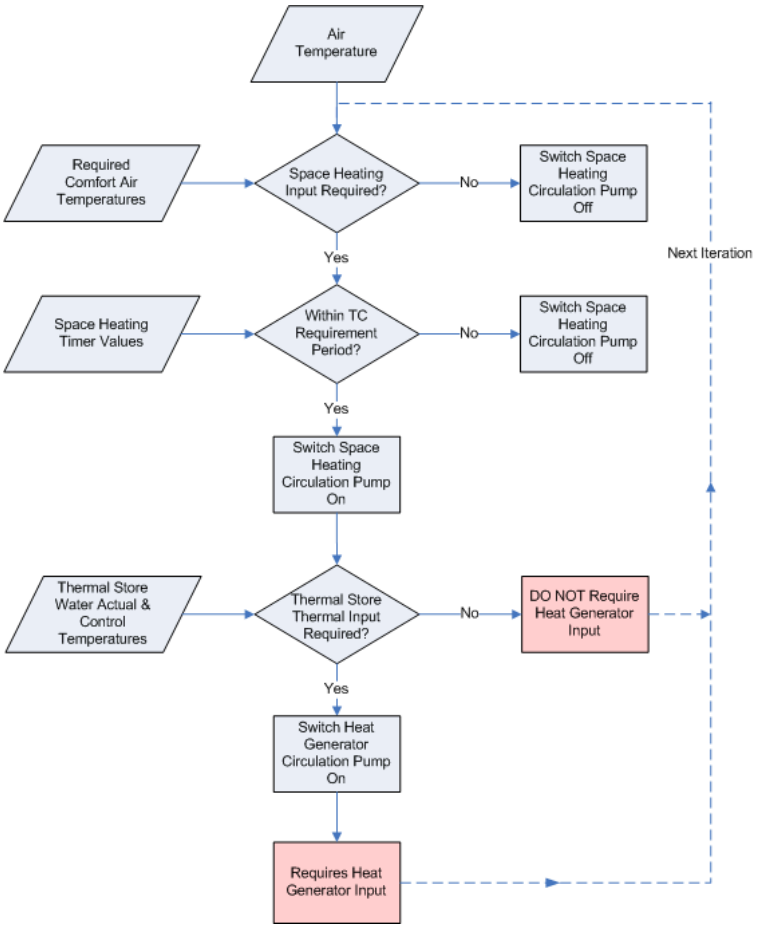

Figure 2.10: Decision Tree for Space Heating Control, for concept systems with a Thermal Store, to decide whether thermal input from thermal store to SHDS is required, along with operation of the SHCP and whether heat generator input to thermal store is required to maintain thermal store water temperatures

The default values of air, DHW Tank control temperatures, as used with the base-case (i.e. condensing boiler only) concept system with BIM-G, are detailed in Table 2.3. This internal air temperature is consistent with World Health Organisation air temperatures established comfort and health of (18-24°C), as quoted by Agar & Newborough [24].

Temperature	Value
Dwelling Comfort Air Target (°C)	21
Dwelling Air Upper Limit – switches off SHDS pump (°C)	21
Dwelling Air Trigger – switches on SHDS pump (°C)	20
DHW Tank Target (°C)	65
DHW Tank Upper Limit for thermal input (°C)	65
DHW Tank Trigger for thermal input (°C)	59

Table 2.3: Control temperatures used in control of space heating, DHW Tank & Thermal Store

For µCHP concept systems, there is a more complex set of control temperatures, to control modulation of the prime mover, as discussed in Section 2.4.4, and its interoperability with the auxiliary boiler. These temperatures, as detailed in Table 2.4, are used to modulate the prime mover, and switch off auxiliary boiler, to lower output as the thermal store approaches the target temperature.

Temperature	Value
Thermal Store Target (°C)	85
Thermal Store CHP@40% Modulation Trigger Temp (°C)	84
Thermal Store CHP@70% Modulation Trigger Temp (°C)	82
Thermal Store CHP@100% Modulation Trigger Temp (°C)	80
Thermal Store Aux Limit Temp (°C)	81
Thermal Store Trigger for thermal input (°C)	85

Table 2.4: Control temperatures used in control of thermal store in Thermal Load Following µCHP concept systems

2.3.7 BIM-G Model Validation

A model was created of the building variant described in Section 3.2.2, using the ESP-r building simulation tool [9]. The simulation was populated with a profile of casual thermal gains due to occupants, appliances and lighting, which was generated as discussed in Sections 3.3.2, 3.6 & 3.7. A ventilation profile, as discussed in Section 3.5, was specified, alongside the thermal demand periods (for space heating control) defined in Table 3.24. This simulation exercise was used to investigate the effects of changing casual thermal gains from appliance and lighting on domestic overheating and potential space cooling requirements [3].

The aforementioned simulation results were also used to provide a degree of validation for the BIM-G model. Similarly, estimated annual results for the BIM-G

model, using the Primary Demand Scenarios defined in Section 3.9, were compared with results from version 4 of the TARBASE Domestic Energy Model (DEM) [40]. The results of this validation exercise, in terms of required input to SHDS, are presented in Table 2.5.

	BIM-G	TARBASE	TARBASE: No Solar	ESP-r
Space Heating Requirements (kWh)	18,137	15,240	20,064	17,658
Difference vs. BIM-G (kWh)	-	-2,897	1,927	-479
Difference vs. BIM-G (%)	-	-16%	11%	-3%

Table 2.5: Space Heating Requirements (as input to space heating distribution system) results from BIM-G thermal model validation exercise

Due to the differences between the BIM-G model, ESP-r, and the TARBASE model, as summarised in Table 2.6, a significant difference in reported thermal requirements was expected. In reality, the difference between BIM-G and ESP-r was minimal, although it should be noted that some functions like latent heat transfer and thermal bridging were not configured in ESP-r. When comparing with the steady state TARBASE DEM, it is important to bear in mind the co-incidence of thermal gains (from appliances and solar radiation via glazing) and Thermal Demand Periods (TDPs). On a sunny winter's day, for instance, much of the heat derived from solar gain to the building during the day, when the dwelling is unoccupied, will have been lost before the next TDP. To understand the range of potential impacts this effect could have on a steady state model, TARBASE space heating requirements were calculated with and without solar gains, as presented in Table 2.5. These results are distributed around the BIM-G result, providing some confidence that the BIM-G model is generally agreeable with other validated models.

BIM-G	Tarbase	ESP-r
Dynamic, 5-second	Steady State	Dynamic, used 15-minute
Discrete climate days	Annual Average Temperature	Continuous annual hourly temps
Discrete 5-second thermal gains & ventilation profiles	Annual averages (over TDPs) for gains & ventilation value	Estimated hourly gains & ventilation profiles
Solar gain profile calculated from hourly data	Solar gain assumed to occur during TDP	Solar gain profile calculated from hourly data
Simple dimensions required	Simple dimensions required	Needs full definition of building geometry
1D	1D	3D
No Latent heat transfer	No latent heat transfer	Can do latent heat transfer, if configured
Part Radiation	No Radiation, except surface heat transfer co-efficient in U-Value	Full Radiation
Pre-Simulation building	No requirement, as steady state	Pre-Simulation building
During TDPs, comfort temp not always maintained, due to restricted output of SHDS and heat generators	Thermal comfort always met during TDPs	Thermal comfort always met during TDPs
Thermal Bridges using U-value adjustments	Thermal Bridges using U-value adjustments	Thermal Bridges could not be successfully implemented in version of the software used
Simplified thermal mass: accounts for wall construction (with doors) only	Does not account for thermal mass	Considers thermal mass of all building elements

Table 2.6: Comparison of thermal modelling features (BIM-G, TARBASE DEM & ESP-r)

It is argued that simulating annual thermal demand without a high level of accuracy is not an issue, so long as the annual thermal demand is not an outlier on the thermal demand distribution presented in Figure 3.5. However, the daily profile of space heating, and the response of internal air temperature (which is the control driver for space heating control) to SHDS input is important. This forms the basis of the temporal response of thermal demand to supply, which is argued in Chapter 1 to be important in the modelling of μCHP system transient performance. In Figure 2.11, the space heating demand as calculated in ESP-r, to balance heat loss during the 15-minute timestep, is compared with the thermal output from the SHDS, as calculated by the BIM-G model, averaged to 15-minute temporal precision. There are two distinct differences; at the start and then the end of each TDP. Without full definition of a SHDS, ESP-r does not consider the thermal lag introduced by the thermal mass of the water in the SHDS. This can be observed within BIM-G by comparing the SHDS thermal input with thermal output in Figure 2.11. In addition, BIM-G includes the transient performance curve of the condensing boiler, where output is limited as the boiler reaches nominal operating

temperature. Once a TDP ends, some of the stored heat within the boiler is transferred to the SHDS, maintaining its temperature for longer, prolonging SHDS thermal output.

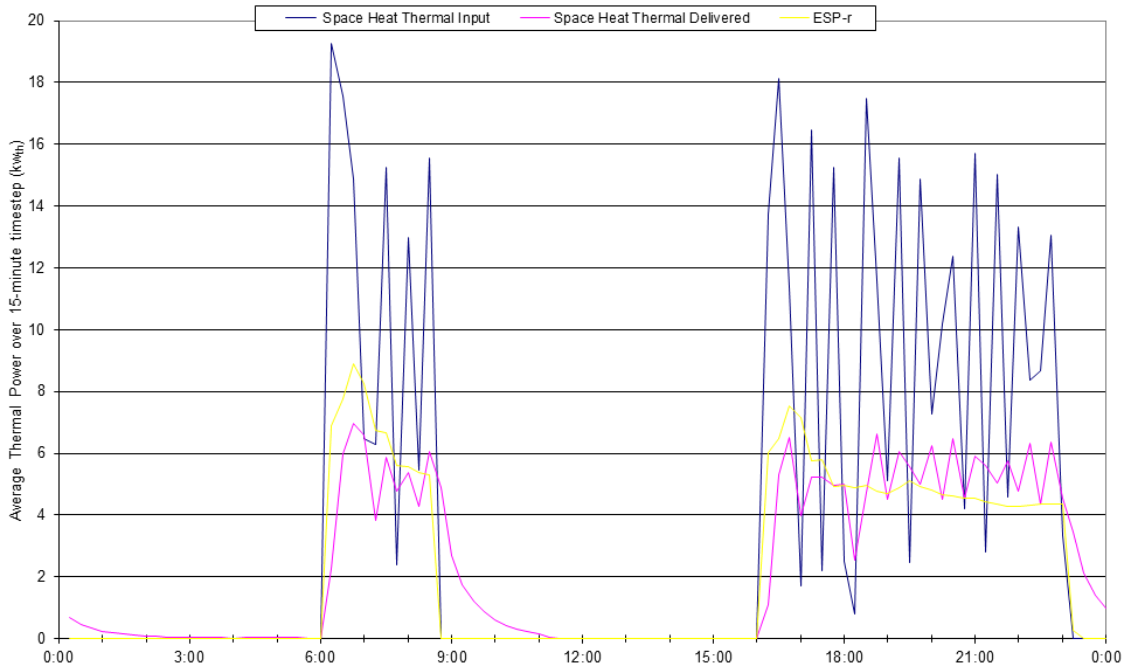

Figure 2.11: Comparison of SHDS thermal input and SHDS output from BIM-G model with ESP-r space heating demand, on 15-minute timebase, for Weekday operating pattern and Shoulder climate demand scenario

Figure 2.12 presents the internal air temperature simulated by BIM-G and ESP-r, where the difference at the start and end of the TDPs has been explained previously in the context of SHDS thermal output. During the TDPs, the temperature fluctuations are expected due to control hysteresis (as presented in Figure 2.8) and the thermal lag introduced by the thermal mass of the SHDS. The general agreement between the temperature plots adds confidence to the validity of the BIM-G thermal model as a tool to estimate the approximate transient response of a space heating distribution system within a dwelling.

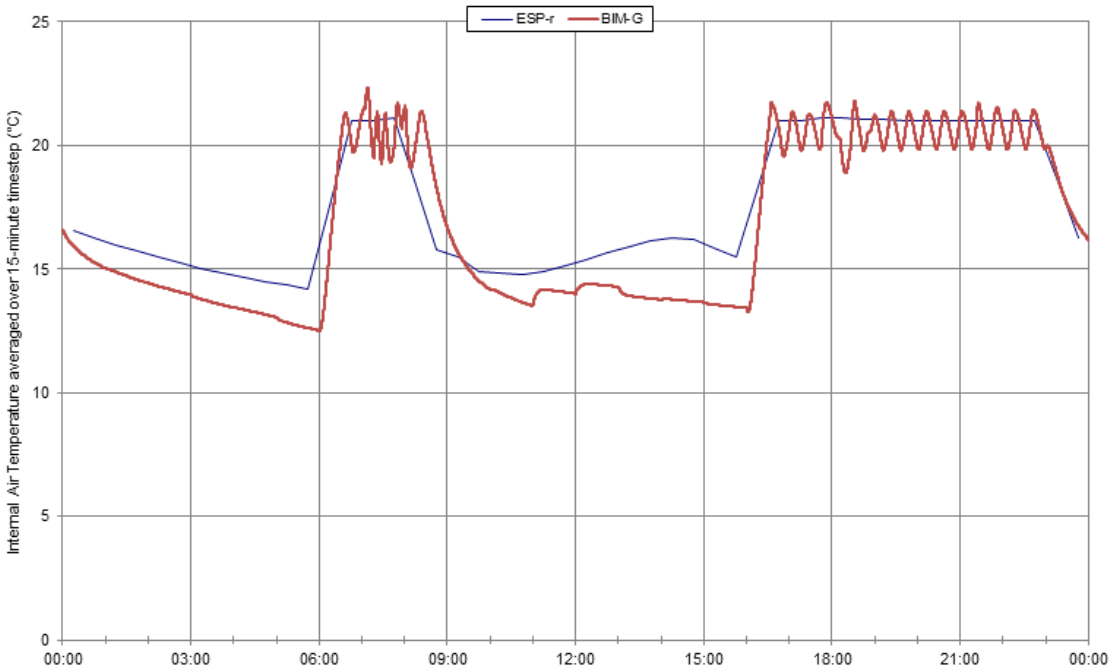

Figure 2.12: Comparison of Internal Air Temperature between BIM-G model and ESP-r, on 15-minute timebase, for Weekday operating pattern and Winter climate demand scenario

2.4 Concept System Design

2.4.1 Overview of Concept System Design

The design and specification of concept µCHP systems is an essential step in the modelling methodology. A concept system incorporates a prime mover, energy storage devices, auxiliary generation and a control sub-system. A fuel sub-system is required for particular prime mover technologies (e.g. PEM) and/or fuel supply options (e.g. an engine-based µCHP system that operates from stored hydrogen only). From this definition, a separate concept system will be defined, for otherwise identical systems, operating under each operating regime. In the context of modelling methodology though, this information must be simplified into a selection of simulation parameters. These parameters, summarised in Table 2.7, dictate the operational abilities of electrical prime movers, thermal generation equipment, thermal and electrical storage, fuel sub-systems and control sub-systems. During this study, performance results from the Supply:Demand Matching routine have been used to inform subsequent Concept System design, guiding the selection of parameters for further investigation.

System Component	Simulation Parameters
Prime Mover	Electrical Rated Output & Modulation Steps
	Full & Part Load Efficiencies (Electrical & Heat Recovery)
	Start-up & Shutdown Transient Performance Curves
Thermal Generation	Thermal Rated Output & Modulation Details
	Full & Part Load Thermal Efficiency
	Start-up & Shutdown Transient Performance Curves
Thermal Storage	Volume & Surface Area
	Heat–loss Co-efficient
	Target & Hysteresis Temperatures
	SHDS Thermal Store HX Volume
Electrical Storage	Electrical Capacity
	Maximum Charge & Discharge Currents
Fuel Sub-System	Full & Part Load Power Requirements
	Start-up & Shutdown Transient Performance Curves
Control Sub-System	Operating Regime & SH Timers
	Prime Mover Modulation Control Temperatures
	Network Derived Generation Signals

Table 2.7: Simulation Parameters by Concept System Component

The basis of this research project is an investigation into the carbon abatement opportunity of µCHP systems within a dwelling. To this end, a comparative assessment of µCHP is required versus one or more established building integrated micro-generation technologies. From the discussion in Section 1.3, there is a clear case for adopting a condensing gas boiler as the base-case energy system for building integrated thermal generation within dwellings, with exclusive reliance on national grid electrical imports for electrical energy provision.

For each concept system, a range of design variants will be specified and investigated. These design variants represent changes in the values of numerical parameters, as opposed to technology types or operating regimes, of a concept system as outlined in Table 2.7. As will be discussed in Section 2.4.6, the default set of design variants relate to variations in net electrical output and net electrical efficiency. The simulation parameters used for the base-case energy system (referred to as concept system BC) and thermal load following SE-based µCHP system (concept system SE-TLF) are detailed in the following sub-sections of Section 2.4. They were specified on the basis of literature review, and limited temperature monitoring on a domestic boiler. The simulation parameters for the concept systems defined in Chapters 5, 6 and 7 are defined in the corresponding sections of those chapters.

Before defining parameters, the basic premise of several shared performance characteristics are explained in Sections 2.4.2 to 2.4.4.

2.4.2 Start-up & Shutdown Performance Curves

The performance of energy conversion technologies is usually discussed and calculated on a steady state basis. The assumption made for thermal processes, such as the combustion or reformation of fuel, is that all involved materials are at their designed operating conditions (temperature and pressure). In reality, micro-generation energy conversion is a dynamic process, which follows electrical and thermal demand, and other control signals. Energy flows into the materials of the energy conversion device (e.g. prime mover or boiler), or fuel processor, until a "steady state" condition is reached. Whilst the device operates at rated output, temperatures within the device will typically remain (approximately) static. Depending on the technology, the temperature of the device may decrease at part-load, or remain at the same temperature as rated output. Once the device switches off, the temperature will eventually return to the ambient temperature of its surroundings. The time required to reach the steady state condition varies with operating conditions (i.e. fuel input, ambient temperature), the thermal mass of the device, and time elapsed since the device last operated. The time to reach ambient conditions is a function of thermal mass, temperature difference between the device and ambient, plus any intentional method of increased heat loss (e.g. a circulation pump continuing to force heat transfer medium through the device's heat exchanger to recover more useful heat).

If the effects of increased heat loss are ignored, the solution to Newton's law of cooling could be applied to estimate cooling of the energy conversion device. The solution shown, equation (2.20), calculates the temperature difference between the device and ambient conditions, ΔT, after the time elapsed since shutdown, t_e. In order to solve the equation, the exponential time constant, τ, must be derived. The mathematical behaviour described by equation (2.20) would generally be called a decaying exponential function.

$$\Delta T(t_e) = \Delta T_o e^{-t_e/\tau} \tag{2.20}$$

$$\tau = \frac{\rho c_p V}{h A_s} \tag{2.21}$$

In order to derive the exponential time constant using equation (2.21), detailed information would be required about the energy conversion devices (prime mover and boiler). This information would have been used to quantify the heat capacity (c_p), density (ρ), volume (V), surface area (A_s), and heat transfer co-efficient (h). However, this was outside of the focus of this project; instead an estimate was made on the basis of temperature monitoring of a domestic boiler, and a literature review of experimental experience with SE prime movers, as presented in Section 1.4.2.

The monitoring exercise consisted of thermocouples installed at the following locations on or near a domestic combination condensing boiler:

- Exterior of Pipe exiting Main HX
- Exterior of Space Heating Flow Pipe
- Exterior of Space Heating Flow Pipe
- Other side of room containing boiler, out of direct sunlight

These temperatures were monitored in order to identify a relation between temperature and time elapsed after boiler shutdown that could be expressed using decaying exponential function. The time profile of temperature increase after the boiler's initial ignition was also expressed using a decaying exponential function applied in a different manner, as shown in equation (2.22), where the temperate difference approaches a maximum value, ΔT_m.

$$\Delta T(t_e) = \Delta T_m \left(1 - e^{-t_e/\tau}\right) \tag{2.22}$$

Before the monitoring exercise, the internal air temperature was approximately 19°C, which rose to approximately 21°C by the time the boiler ceased operation. Whilst the

boiler cooled down, room air temperature remained relatively steady at 20±1°C. The boiler was started late afternoon in early April, 8 hours since its previous firing cycle.

The monitoring results in Figure 2.13 show that the boiler was initially ignited at 16:50:44, after which it cycled for over 90 minutes, in response to SHDS flow and return temperatures. At 18:30:29, the boiler was switched off, and monitoring ceased 3 hours and 45 minutes later. From an analysis of the cooling curve, an exponential time constant for shutdown, $\tau_{Shutdown}$, was derived for the condensing boiler.

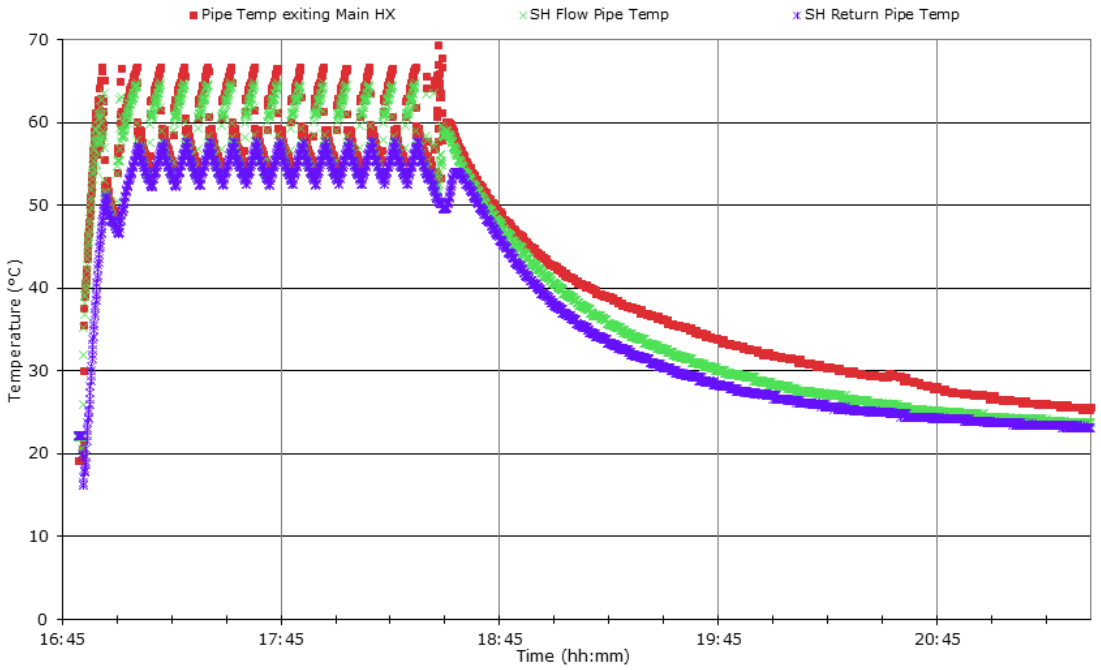

Figure 2.13: Temperatures recorded during boiler monitoring exercise

Considering the time period when the boiler initially fired, as shown in Figure 2.14, approximately 4 minutes elapse since boiler ignition at 16:50:44 until the HX temperature reaches a steady value. The exponential relationship of boiler temperature to time is skewed due to the circulation of SHW around the SHDS as the boiler warms up. A relationship of the form in equation (2.23) was derived, with an exponential time constant for start-up, $\tau_{Start\text{-}Up}$, of 40 seconds for the condensing boiler.

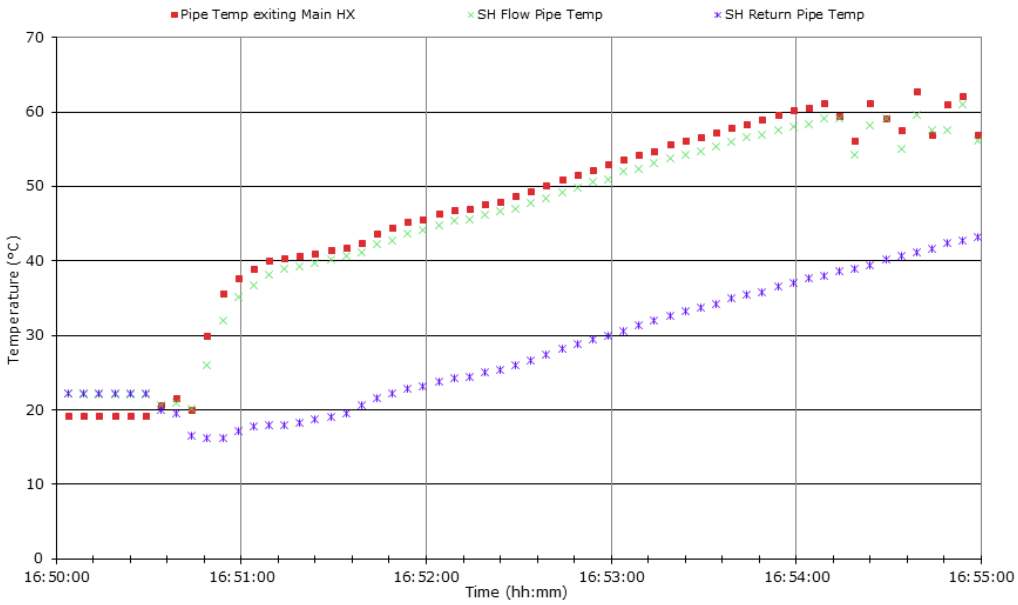

Figure 2.14: Temperatures recorded during first 5 minutes of boiler monitoring exercise

For the purposes of simulation within the BIM-G model, the transient performance of each generator within each concept system is required. The simulations undertaken in the current investigation are limited to a condensing boiler and a Stirling Engine prime mover. The Supply:Demand matching procedure of the BIM-G model does not implement a thermal model of boiler or prime mover, as others have applied (see Section 1.6). Instead, transient performance is modelled by considering the thermal efficiency as a function of temperature during start-up, referred to as the dynamic thermal efficiency, η_{th}. This is achieved using equation (2.23), as adapted from the generic equation (2.22), where t_{start} is time elapsed since generation device (i.e. boiler or prime mover) was started, and η_{th100} is the thermal efficiency at rated output.

$$\eta_{th}(t) = \eta_{th100} * \left(1 - e^{\left(\frac{-t_{start}}{\tau_{Start-Up}}\right)}\right) \qquad (2.23)$$

Due to the continuous mathematical nature of exponential decay (i.e. it does not reach zero), and technical limitations within the programming language, a cut-off factor is applied to the exponential relationship in equation (2.23). Once the thermal efficiency is sufficiently close (within 1%) to η_{th100}, the simulation assumes it has reached η_{th100} on

the next iteration. The thermal efficiency is then calculated based on the modulation condition of the device, as discussed in Section 2.4.4, until the device is switched off.

Whenever generation is started, the thermal readiness of the generation device is calculated using equation (2.24), where the effective time elapsed since start-up (t_{start}) is then used with equation (2.23). The value thermal efficiency, η_{th}, will depend upon the temperature of the device, which is already understood to be a function of the time elapsed since shutdown, $t_{shutdown}$.

$$t_{start} = \tau_{Start-Up} * \ln\left(1 - \frac{\eta_{th}}{\eta_{th100}}\right) \quad (2.24)$$

Once the generation device has been shut down, the thermal efficiency is calculated using equation (2.25), using the exponential time constant for shutdown, $\tau_{Shutdown}$. As with start-up, a cut-off factor is used to set η_{th}=0 once the value of η_{th} is sufficiently close to zero (within 1%), to avoid calculation issues with the simulation code.

$$\eta_{\text{th}}(\text{t}) = \eta_{\text{th100}} * \text{e}^{\left(\frac{-\text{t}_{\text{shutdown}}}{\tau_{Shutdown}}\right)} \quad (2.25)$$

If the generation device is switched off before the generation device completes a start-up cycle, then equation (2.26) is used to calculate the effective time elapsed since shutdown, $t_{shutdown}$, which is then used with equation (2.25).

$$t_{shutdown} = -\tau_{Shutdown} * \ln\left(\frac{\eta_{th}}{\eta_{th100}}\right) \quad (2.26)$$

During a boiler start-up cycle, the Supply:Demand Matching routine calculates the thermal output of the boiler, $Q_{th\text{-}aux}$, using the dynamic thermal efficiency of the boiler, $\eta_{th\text{-}aux}$, and fixed 100% fuel input, F_{aux100}, as per equation (2.27).

$$Q_{\text{th-aux}}(\text{t}) = \eta_{\text{th}}(\text{t}) * F_{\text{aux100}} \quad (2.27)$$

During a prime mover start-up cycle, the Supply:Demand Matching routine calculates the thermal output of the prime mover, Q_{th}, using the dynamic thermal efficiency, η_{th}, and fixed 100% fuel input, F_{100}, as per equation (2.28).

$$P_{\text{th}}(\text{t}) = \eta_{\text{th}}(\text{t}) * F_{100} \tag{2.28}$$

The net electrical output of the prime mover, P_e, is calculated using the dynamic thermal efficiency, as shown in equation (2.29). The routine assumes that no electrical output occurs during start-up until the value of gross and net output is greater than or equal to the minimum modulation step, e.g. 40% of rated output. Once that lower limit has been exceeded, net electrical efficiency is calculated using equation (2.30) until the exponential cut-off factor discussed previously forces P_e equal to P_{e100}, unless the prime mover is switched off before that point is reached.

$$P_e(\text{t}) = \frac{\eta_{th}(t)}{\eta_{\text{th}100}} * P_{\text{e}100} \tag{2.29}$$

Start-up and shutdown performance curves for the SE prime mover were derived from the operational temperature plot created by vom Schloss et al [32]. The derived values of the time constants, $\tau_{\text{Start-Up}}$ and τ_{Shutdown}, are 300 seconds and 900 seconds respectively. These assumptions compare with 3 minutes for both start and stop by Houwing et al [33], and 11 minutes by Peacock & Newborough [34]. This includes the time for electrical synchronisation between the generator and the NEG, as discussed by Peacock & Newborough [34]. During SE prime mover start-up, the fuel input to the auxiliary boiler is assumed to be 100%, as it contributes to the warm-up of the SE hot space, as discussed in Section 1.4.2.

2.4.3 Parasitic Electrical Loads

The electrical parasitic loads of each concept system were derived from the individual loads of the prime mover, condensing boiler, space heating distribution system circulation pump, domestic hot water circulation pump, and system standby and controls.

In most discussions, the electrical efficiency and electrical output of prime movers are quoted in this thesis as net values, where any parasitic balance-of-plant loads specific to the prime mover (and fuel-processing sub-system if discussing alternative fuels or fuel cell prime movers) have been accounted for. In the case of a SE prime mover, an internal parasitic load of 100W is applied, regardless of rated electrical output or load condition. This results in a varying ratio between net and gross electrical efficiency between electrical capacities and load conditions. The value of 100W was selected after reviewing the datasheets of a number of μCHP products on the market. As the parasitic loads internal to the μCHP system are met from the prime mover, the parasitic loads that remain for μCHP concept systems are identical to those of the boiler, SHDS and thermal storage. These are the parasitic loads associated with the base-case energy systems, and are defined below.

A breakdown of condensing boiler (whether as primary or auxiliary generator) parasitic loads by source [35] is presented in Table 2.8, where the pump drives the fluid circuit that transfers thermal energy to the thermal store or DHW tank. The values for pump and fan loads were chosen to match the best practice recommendations, where the use of variable speed, electronic components is claimed to save around 50% [36] compared to traditional energy consumption. The electrical parasitic loads for space heating distribution system and domestic hot water circulation pumps are 25W each, as best practice recommendations [36] are assumed. The control of these pumps was discussed in detail in sections 2.3.5 and 2.3.6.

Source	Load (W)
Pump	25
Boiler Fans	40
Gas Valves	7
Total Parasitic Load	**72**

Table 2.8: Electrical Parasitic Load (Watts) for Condensing Boiler: Breakdown by Source

The parasitic load for system standby and control is continuous across the simulation period, and applies to all condensing boiler-only and μCHP concept systems. The sources of electrical parasitic load, as detailed in Table 2.9, were derived from literature review [35].

Source	Load (W)
Boiler Standby	8
Programmers	2
Total Parasitic Load	**10**

Table 2.9: Electrical Parasitic Load during standby for condensing boiler, as specified in all Concept Micro-Generation Systems: Breakdown by Source

2.4.4 Modulation

The review of Stirling Engine prime mover technology in Section 1.4.2 discussed the variation of efficiency with load condition. For µCHP systems using a thermal load following operating regime, modulation is an alternative to thermal cycling or thermal dumping. Lane [37] claimed that electrical efficiency remained within the 30-33% band, under load conditions between 35% and 100%, for FPSEs coupled with linear alternators. Indeed, Peacock & Newborough [38] identified the modulation settings of the commercially available Whispergen SE-based µCHP system as 33%, 71% and 100%. Peacock and Newborough adopted the approach of fixed modulation steps in their modelling exercise [38], using 45% and 75%. Houwing & Bouwmans [81], however, modelled µCHP with a single 50% modulation step. During the TARBASE project, a review of modulating capabilities of early field trial units was undertaken [1], and fixed modulation steps of 40% and 70% were identified, and thereafter adopted by Peacock & Newborough [41].

These modulation steps (40% and 70%) have been adopted for SE-based µCHP systems in the BIM-G model. As the prime mover modulates, both the electrical and thermal net output reduce to these load conditions. With the fixed internal parasitic load of the SE prime mover, as discussed in Section 2.4.3, and a fixed gross electrical efficiency, the net electrical efficiency therefore reduces at part load. This reduction is 1% and 3% (of net electrical efficiency at rated output) for the 70% and 40% modulation steps respectively. This agrees with the expectations of Knight & Ugursal [42] that electrical efficiencies would reduce by approximately 1% (versus rated electrical efficiency) at 50% load.

The modulation of the condensing boiler is discussed in Section 2.4.5.

2.4.5 Condensing Boiler Specifications

The specifications for the condensing boiler were assumed by collation of "typical" boiler operation information from a variety of sources. The selection of each specification value is described in the paragraphs below.

The rated thermal load of the boiler was selected after calculation of required boiler capacity for the dwelling variant described in Chapter 3. The boiler sizing method employed was from the relevant British Standard [25], with reference to guides published by the Energy Saving Trust [26] and the Heating and Ventilation Contractors' Association [27]. The modulation characteristics of the boiler are similar to typical modern condensing boilers, with unrestricted modulation between rated output and a minimum output, defined by a turn down ratio. Values of this ratio depend on specific boiler manufacturers, but a figure of 20% was chosen to correspond with data [28][29] suggesting that the efficiency of modulating boilers remain within a few percent over the range of 20-100%, during non-condensing operation.

As mentioned previously, within the operating range within which the boiler is modulated, thermal efficiency is assumed constant. A thermal efficiency of 88%, at rated output during non-condensing operation, was assumed, which corresponds to an efficiency of 93% during condensing when space heating distribution system return water temperatures of around 54°C, as supported by Building Research Establishment data [30] on condensing boiler operation.

The transient performance of the condensing boiler is simulated using start-up and shutdown performance curves, as discussed in Section 2.4.2. Table 2.10 summarises the simulation parameters defined for the condensing boiler, whether as the sole heat generator in the base-case energy system, or as an auxiliary boiler in a μCHP concept system.

Parameter	Notation	Value	Reference
Thermal Output @ 100% Load (kW_{th})	$\mathbf{Q_{100}}$	$20kW_{th}$	[25][26][27]
Turndown Ratio (%)	$\mathbf{r_{turn-down}}$	20%	[28][29]
Thermal Efficiency @ 100% Load [Non-Condensing] (%)	$\mathbf{n_{th100}}$	88.0%	[30]
Thermal Efficiency @ 100% Load [Condensing] (%)	$\mathbf{n_{th100c}}$	93.0%	[30]
Fuel Input @ 100% Load [Non-Condensing] (kW)	$\mathbf{F_{aux100}}$	22.727kW	Calculation
Start-up Time Constant (seconds)	$\mathbf{\tau_{Start-up}}$	40s	Fig 2.14
Shutdown Time Constant (seconds)	$\mathbf{\tau_{Shutdown}}$	3600s	Fig 2.13
Exponential Cut-Off Factor (% of Target Value)	$\mathbf{f_{ExponEndAux}}$	99%	Sec 2.4.2
Parasitic Electrical Load [Standby & Control] (kW_e)	$\mathbf{P_{pStandby}}$	$0.01kW_e$	[35]
Parasitic Electrical Load [Firing] (kW_e)	$\mathbf{P_{pFiring}}$	$0.072kW_e$	[36]

Table 2.10: Summary of parameters used to simulate Condensing Boiler, for Basecase concept system and auxiliary boiler

The base-case energy system incorporates an indirect DHW tank, whose operation is explained in Section 2.3.5, as such devices are typically specified alongside a condensing boiler in domestic installations [27]. The capacity of the DHW tank was selected as 150l, using design sizing guidance from the HVCA guide [17], based on the building characteristics and occupancy scenario defined in Chapter 3. As expected, initial simulations with the BIM-G model reported DHW tank standing heat losses that increase with capacity.

2.4.6 Micro-CHP System Sizing & Efficiency

A matrix of design values were specified for net electrical output (P_e) and net electrical efficiency (η_e) of a SE µCHP system at full load. For most concept systems, simulations were performed using all matrix entries to understand the variation in operational performance and lifetime-drivers with rated electrical output and electrical efficiency. Later simulations were undertaken for selected design variants, typically because a particular operating regime was suited to only very high efficiency units. The values of P_e were selected to coincide with domestic-scale systems, as defined in Section 1.4, whilst the electrical efficiencies were selected to reflect the range of efficiencies identified in Section 1.4.2 from field trail systems, lab development activities, and technological potential.

Net electrical efficiency is calculated using equation (2.30), using the net electrical output from the CHP system, and the fuel input to the prime mover (i.e. not the auxiliary boiler fuel input), F_{CHP}.

$$\eta_e = \frac{P_e}{F_{CHP}} \tag{2.30}$$

Gross electrical efficiency, η_{eg}, is calculated using equation (2.31), where the gross electrical output from the CHP system, P_{eg}, includes the parasitic electricity consumption of the system, $P_{ParasiticCHP}$. The internal parasitic load of a SE-based μCHP system was defined as 100W in Section 2.4.3.

$$\eta_{eg} = \frac{P_{eg}}{F_{CHP}} = \frac{\left(P_e + P_{ParasiticCHP}\right)}{F_{CHP}} \tag{2.31}$$

Thermal efficiency, η_{th}, is calculated using equation (2.32), where the useful thermal output from the prime mover, Q_{CHP}, varies with modulation condition and start-up status.

$$\eta_{th} = \frac{P_{th}}{F_{CHP}} \tag{2.32}$$

The thermal efficiency can also be considered in terms of gross electrical efficiency and heat recovery efficiency of the prime mover, η_{hr}, and calculated using equation (2.33).

$$\eta_{th} = \eta_{hr} * (1 - \eta_{eg}) \tag{2.33}$$

Heat recovery efficiency, η_{hr}, of the prime mover is calculated from the thermal efficiency and the gross electrical efficiency using equation (2.34). The heat recovery efficiency was assumed to be constant during operation, regardless of modulation condition, except during prime mover start-up, where the heat recovery efficiency is determined by start-up performance curves (refer to section 2.4.2 for details). In their modelling exercises [38][41], Peacock and Newborough assumed that heat recovery

efficiency did not vary with modulation. Experimental results published by Entchev et al [31] suggest that SE prime movers can achieve heat recovery efficiencies between 89-95% during test runs.

$$\eta_{hr} = \frac{\eta_{th}}{\left(1 - \eta_{eg}\right)} \tag{2.34}$$

The heat recovery efficiency was defined as 88%, as reported from SE μCHP lab tests [31], which as discussed in Section 2.4.6 is assumed to remain constant outside of start-up conditions. During start-up conditions, as discussed in Section 2.4.2, the performance characteristics of the prime mover differ from those during steady state operation, as the heat recovery efficiency changes accordingly.

The rated thermal output of each design variant discussed previously can be calculated using the corresponding net electrical efficiency and output, and the heat recovery efficiency. These thermal outputs are presented in Table 2.11, along with the total system efficiency, η_{tot} (i.e. total prime mover thermal and electrical output over fuel input), and prime mover fuel consumption.

Net Electrical Output, P_e (kW_e)	Net Electrical Efficiency, η_e (%)	Thermal Output, P_{th} (kW_{th})	Thermal Efficiency, η_{th} (%)	Total Prime Mover Efficiency, η_{tot} (%)	Prime Mover Fuel Input, F_{CHP} (kW)
0.5	15	2.41	72.2	87.2	3.33
1	15	4.90	73.5	88.5	6.67
2	15	9.89	74.1	89.1	13.33
3	15	14.87	74.4	89.4	20.00
4	15	19.86	74.5	89.5	26.67
5	15	24.85	74.5	89.5	33.33
0.5	20	1.67	66.9	86.9	2.50
1	20	3.43	68.6	88.6	5.00
2	20	6.95	69.5	89.5	10.00
3	20	10.47	69.8	89.8	15.00
4	20	13.99	70.0	90.0	20.00
5	20	17.51	70.0	90.0	25.00
0.5	25	1.23	61.6	86.6	2.00
1	25	2.55	63.8	88.8	4.00
2	25	5.19	64.9	89.9	8.00
3	25	7.83	65.3	90.3	12.00
4	25	10.47	65.5	90.5	16.00
5	25	13.11	65.6	90.6	20.00
0.5	30	0.94	56.3	86.3	1.67
1	30	1.97	59.0	89.0	3.33
2	30	4.02	60.3	90.3	6.67
3	30	6.07	60.7	90.7	10.00
4	30	8.13	60.9	90.9	13.33
5	30	10.18	61.1	91.1	16.67
0.5	35	0.73	51.0	86.0	1.43
1	35	1.55	54.1	89.1	2.86
2	35	3.18	55.7	90.7	5.71
3	35	4.81	56.2	91.2	8.57
4	35	6.45	56.4	91.4	11.43
5	35	8.08	56.6	91.6	14.29

Table 2.11: Net Electrical, Thermal and Total Prime Mover Efficiencies, and Net electrical Output and Thermal Output (rated values) of µCHP Prime Mover design variants

2.5 Supply:Demand Matching

As discussed in Section 1.6, the matching of energy supply systems (i.e. µCHP), with their associated transient performance characteristics and operating restrictions, to demand on a temporal basis is important for µCHP analysis. A major point of novelty of the BIM-G model is that a dynamic link exists, integrating supply calculations and demand estimation. This permits the supply:demand matching algorithms to account for the effect of previous energy generation, at whatever output level, on the energy demand during the preceding iteration.

The Supply:Demand matching software routine is central to the modelling and analysis methodology, in that it ties together demand modelling, in terms of responsive simulation and profile definition, with concept system operation and control. The algorithms developed for the Supply:Demand Matching routine approximate the performance (in terms of thermal and electrical output, fuel input, interchange with storage device and parasitic energy loads) of concept micro-generation systems, on a transient basis, in response to signals from control algorithms. As discussed in Section 1.7, the iterative specification of novel control algorithms in response to performance metrics generated during the simulation of previous concept systems is a key objective of this research project.

The control algorithms within the Supply:Demand matching procedures dispatch the various micro-generation and storage sub-systems, in accordance with the specified control strategies, to satisfy the dwelling's energy demand. These control algorithms are specific to the operating regime specified for an individual concept system, but a common concept exists between all variations of the control algorithms, in that control decisions are made on the bases of sub-system dispatchability and priority.

A dispatchable sub-system is a micro-generation or storage device that can be modulated, to increase or decrease output, or even start and stop operation, in response to a control signal. Examples of dispatchable micro-generation devices are μCHP prime movers (i.e. Stirling Engines, fuel cells, internal combustion engines), primary or auxiliary gas boilers, and electrical generators without heat recovery. Storage sub-systems, such as thermal storage hot water tank and lead-acid batteries, are dispatchable, in that they can be controlled, but are usually constrained to a greater extent than micro-generation devices, as they have a finite energy storage capacity.

A non-dispatchable sub-system is a micro-generation device that cannot be modulated on demand, for technological or operating regime reasons. Examples of technologically constrained micro-generation systems are renewable generators, such as solar PV,

solar thermal and micro-wind, which rely on the co-incidence of suitable climatic conditions to generate specific quantities of electricity or heat.

However, as Voorspools and D'haeseleer [43] argued, the dispatchability of a μCHP prime mover will depend on its operating regime and the context of its control system. They reason that grid-connected μCHP systems that are controlled solely in the context of the dwelling's load, without control signals from the NEG, will appear as non-dispatchable generation to the central controller of the NEG. Furthermore, where an operating regime required a prime mover to operate continuously for a pre-determined time period, or interdict operation for during a time period, the prime mover is effectively non-dispatchable during those periods.

The priority of these sub-systems in respect to the control algorithms is dictated by the operating regime of a concept system. In the majority of operating regimes, a measure of thermal control is implemented, where thermal demand–related control signals are used to call on thermal generation, when the output available thermal energy from non-dispatchable thermal generation, and thermal storage devices, is insufficient. When an operating regime is directed by electrical control signals, then dispatchable electrical generation is called upon when renewable electrical generation, and electrical storage capacity, is insufficient. In these cases, non-dispatchable generation devices have priority by default, as they cannot be "turned off", although their output could technically be diverted to an energy sink and "dumped". Extractions from storage devices are next in the priority list, with dispatchable generation having the lowest priority. Energy delivery to the sources of local building demand is prioritised, with excess energy delivered to energy stores, exported to the NEG, or dumped to the environment, as is appropriate for the form of energy and as dictated by the specific operating regime.

Alternative operating regimes prioritise the continuous or constant operation of μCHP prime movers, and as such output from non-dispatchable generation is utilised at time of supply shortfall, and stored, exported or dumped at times of excess.

As alluded to above, the specific operation of the supply:demand matching procedures are dependent on the concept system under operation. Therefore, the details of the control algorithms that govern supply:demand matching are given in the appropriate chapters or sections describing each concept system.

2.6 System Performance Analysis

The final step in the BIM-G modelling and analysis methodology is to quantify the performance of concept systems. Therefore a series of Performance Metrics have been specified, which are used to compare simulation results for µCHP concept systems with the base-case energy system. These performance metrics are presented in Table 2.12, with associated descriptions and units of measure or merit. Some of these metrics are absolute values, which can be compared with the base-case energy systems or other concept system. Relative Carbon Savings (RCS), however, are defined as the reduction in CO_2 emissions for the concept systems relative to the base-case energy system. In the investigation of µCHP systems, lifetime-related performance metrics are discussed in Section 4.2.2. The metrics are typically presented as either daily values (for a particular demand scenario) or annual values (by weighting the results of the Primary Demand Scenarios defined in Chapter 3).

Performance Metric	Simulation Parameters	Units of Measure
Fuel Consumption	Consumption of Natural Gas, which fuel µCHP systems and auxiliary boilers	kWh
Gross Electrical Import	Electrical Import to dwelling from national grid, as gross total of electricity imports	kWh
Gross Electrical Export	Electrical Export from dwelling to national grid, as gross total of electricity exports	kWh
Net Electrical Import	Electrical Import to dwelling from national grid, as total of electricity imports net of electrical exports (negative indicates net export)	kWh
Net Carbon Emissions	Calculated from Natural Gas Consumption & Net Electrical Import, where electrical export receives full carbon credit	$kgCO_2$
Relative Carbon Savings	Calculated as difference between base-case and concept system Net Carbon Emissions, presented as absolute value or percentage of base-case net carbon emissions	$kgCO_2$ or % of base-case $kgCO_2$
Average Net Electrical Efficiency	Average Electrical Efficiency of µCHP prime mover, net of µCHP & auxiliary parasitic loads	% (kWh Electrical / kWh Fuel)
Average Net Thermal Efficiency	Average Thermal Efficiency of µCHP prime mover and auxiliary boiler, as delivered to Thermal Store	% (kWh Thermal / kWh Fuel)
Average Electrical Storage Round-trip Efficiency	Average Round-trip efficiency of input-storage-extraction cycle of electrical storage sub-system	% (kWh Input / kWh Extracted)
Prime Mover Operating Hours	The duration of prime mover operation, usually quantified on daily basis for design days, and on an annual basis	Hours/Day or Hours/Year
Prime Mover Thermal Cycles	The quantity of thermal cycles experienced by the prime mover, usually quantified on daily basis for design days, and on an annual basis	Thermal Cycles/Day or Thermal Cycles/Year

Table 2.12: Performance Metrics for µCHP systems adopted in BIM-G model

2.7 References

[1] Peacock A, Newborough M. and Banfill P, Technology assessment for radically improving the built asset base (TARBASE), WREC 2005, Aberdeen, 22-27 May 2005

[2] Peacock et al; Reducing CO_2 Emissions through Refurbishment of UK Housing; European Council for an Energy Efficient Economy (eceee) 2007 Summer Study, Côte d'Azur, France 4-9 June 2007

[3] A.D. Peacock, D.P. Jenkins, D. Kane, Investigating the potential of overheating in UK dwellings as a consequence of extant climate change, Energy Policy, Volume 38, Issue 7, Pages 3277-3288, July 2010

[4] Office of National Statistics; General Household Survey 2002-2003; London; [Computer File]; 1st edition; UK Data Archive [distributor]; July 2004; SN4981

[5] Office of National Statistics; United Kingdom Time Use Survey 2000 (TUS); London; [Computer File]; 3rd ed.; UK Data Archive [distributor]; Sept 2003; SN4504

[6] Newborough & Probert; Intelligent rapid-response water heater for supplementing outputs from a domestic hot water store; Building Services Engineering Research and Technology, Vol. 15, No. 3, 141-148 (1994); pp144

[7] Jordan & Vajen; Realistic Domestic Hot-Water Profiles in Different Time Scales; V2.0; Universität Marburg; May 2001

[8] American Society of Heating, Refrigerating and Air-Conditioning Engineers; ASHRAE Fundamentals Handbook; 2001; Ch29; Non-Residential Cooling And Heating Load Calculations

[9] Clarke J A 1996. "The ESP-r System: Advances in Simulation Modeling" Building Services Journal pp27–9, May 1996

[10] British Standards Institution; BS EN ISO 6946:1997; Building components and building elements— Thermal resistance and thermal transmittance— Calculation method

[11] Chartered Institute of Building Services Engineers; Guide A Environmental Design; 7th Edition; Issue 2; January 2007; Section 3.3.11.5

[12] American Society of Heating, Refrigerating and Air-Conditioning Engineers; ASHRAE Fundamentals Handbook; 2005; Ch31; Fenestration; pp36

[13] Chartered Institute of Building Services Engineers; Guide A Environmental Design; 7th Edition; Issue 2; January 2007; Section 3.5.2

[14] Ward, TI; BRE Scotland; Assessing the effects of thermal bridging at junctions and around openings; IP1/06; February 2006

[15] British Standards Institution; BS EN 12831:2003; Heating systems in buildings— Method for calculation of the design heat load; Section 6.1; pp14

[16] Chartered Institute of Building Services Engineers; Guide A; Section 3.A4; pp3-29

[17] Heating and Ventilating Contractors Association (HVCA); HH_DHS1; Guide to Good Practice - Domestic Heating Specification

[18] British Standards Institution; BS EN 12828:2003; Heating systems in buildings - Design for water-based heating systems

[19] British Standards Institution; BS EN 442-2:1997; Specification for radiators and convectors - Part 1: Test methods and rating

[20] Jordan & Furbo; Solar Energy 78 (2005) 291–300; Thermal stratification in small solar domestic storage tanks caused by draw-offs

[21] British Standards Institution; BS 1566-1:2002; Copper Cylinders for Domestic Purposes

[22] Waterheater Manufacturers Association; Performance Specifications for Thermal Stores

[23] K. Ellehauge; Report on Solar combisystems modelled in Task 26 – Appendix 1 – Generic System #2: A Solar Combisystem based on a heat exchanger between the collector loop and space-heating loop; December 2002; pp8

[24] Agar, W. R., & Newborough, M.; Implementing micro-CHP systems in the UK residential sector; Journal Of The Institute Of Energy; 1998; 71(489); pp178-189

[25] British Standards Institute; BS EN 12828:2003; Heating systems in buildings - Design for water-based heating systems; 2003

[26] Energy Saving Trust; CE54; Whole House Boiler Sizing Method for Houses and Flats; December 2003

[27] Heating and Ventilating Contractors Association (HVCA); HH_DHS1; Guide to Good Practice - Domestic Heating Specification

[28] Efficient Domestic Heating and Hot Water Systems in Northern Ireland; EST Workshop

[29] Residential Equipment Part Load Curves for Use in DOE-2; Hugh Henderson (CDH Energy Corporation) & Yu Joe Huang (LBNL) & Danny Parker (Florida Solar Energy Center); Feb 1999; Doc No. LBNL-42175

[30] Building Research Energy Conservation Support Unit; Building Research Establishment; “High Efficiency Condensing Boilers (Domestic Applications) For Installers In The United Kingdom”; General Information Report GIR 16; Feb. 1994

[31] E. Entchev, J. Gusdorf, M. Swinton, M. Bell, F. Szadkowski, W. Kalbfleisch, R. Marchand, Micro-generation technology assessment for housing technology, Energy and Buildings, Volume 36, Issue 9, September 2004, Pages 925-931

[32] J. vom Schloss et al; Development of a Multi-Fuel Burner for a Small Scale Stirling Engine; Proceedings of INFUB 2006; Porto, Portugal; April 2006

[33] M. Houwing, R.R. Negenborn, P.W. Heijnen, B. De Schutter, and H. Hellendoorn; Least-cost model predictive control of residential energy resources when applying µCHP; Technical report 07-007; Delft University of Technology; The Netherlands; July 2007; http://pub.deschutter.info/abs/07 007.html

[34] A.D. Peacock, M. Newborough, Controlling micro-CHP systems to modulate electrical load profiles, Energy, Volume 32, Issue 7, July 2007, Pages 1093-1103

[35] Market Transformation Programme; Briefing Note BNDH20; Use of Electricity in Non-Electric Heating Systems; 01/12/06; pp3

[36] Market Transformation Programme; Briefing Note BNDH20; Use of Electricity in Non-Electric Heating Systems; 01/12/06; pp5-6

[37] Lane, NW 2005, 'Commercialization Status Of Free-Piston Stirling Machines', International Stirling Engine Conference, pp. 30-37, British Library Document Supply Centre Inside Serials & Conference Proceedings

[38] Peacock & Newborough; Impact of micro-CHP systems on domestic sector CO_2 emissions; Applied Thermal Engineering 25 (2005); 2653–2676

[39] Market Transformation Programme; Policy Brief > Domestic Heating > UK Energy Consumption: Domestic Heating: Heat Generation; pp1; 10/11/06; Downloaded from www.mtprog.com;18/01/07

[40] Jenkins et al, Modelling carbon emissions of UK dwellings – The TARBASE Domestic Model, Applied Energy, Volume 93, May 2012, Pages 596–605

[41] A.D. Peacock and M. Newborough; Effect of heat-saving measures on the CO_2 savings attributable to micro-combined heat and power (mCHP) systems in UK dwellings; Energy; 33; 2008; pp601–612

[42] I.P. Knight and I. Ugursal; 2005; Residential Cogeneration Systems: A Review of The Current Technologies. A report of Subtask A of FC+COGEN-SIM The Simulation of Building-Integrated Fuel Cell and Other Cogeneration Systems; IEA/ECBCS; Accessed online at http://www.ecbcs.org/docs /annex_42_Review_Residential_Cogen_Technologies.pdf

[43] K.R. Voorspools, W.D. D'haeseleer, Reinventing hot water?: Towards optimal sizing and management of cogeneration: A case study for Belgium, Applied Thermal Engineering, Volume 26, Issue 16, November 2006, Pages 1972-1981

3 Defining Primary Demand Scenarios

3.1 Demand Scenario Generation Methodology

The initial stage of the Modelling and Analysis Methodology, as described in Chapter 2, was the Demand Scenario Generation procedure, during which parameters were defined to inform the subsequent stages of the methodology. In this chapter, the methodology and assumptions underlying this procedure are defined, and the derived Demand Scenarios are presented.

As discussed in Chapter 1, existing demand data is scarce, which limits the number of μCHP investigations based on demand datasets with a high temporal precision. As discussed in Sections 1.2 and 1.6, some investigators have attempted to create bottom-up demand models as an alternative to top-down demand models. In a bottom-up demand model, demand profiles are created by considering the energy consumption during operation of each appliance, light and other energy consuming device, and the factors that drive operation. In order to produce an accurate energy demand profile, information on the time-varying load of the device must be available and coupled with an in-depth understanding of the frequency, duration, and typical timings of usage, across a day, week and year.

The relationship between μCHP system performance and thermal demand, especially with regards to thermally constrained operation, has been the topic of many investigations, as has been discussed in depth in Section 1.6. In this context, it is essential to analyse μCHP systems under various thermal load conditions. Therefore, it was crucial to define a set of demand scenarios with a spread of associated daily thermal demand profiles. Preliminary research undertaken by the author [1][2] highlighted the importance of electrical interchange with the NEG to environmental performance results; hence the demand scenarios include variations in daily electrical demand profiles. These demand scenarios enable the performance of concept micro-generation systems to be analysed across daily and temporal variations in thermal and electrical demand, collectively or independently.

Previous studies have estimated annual performance of micro-generation systems from a series of “design days”, as discussed in Section 1.6. A similar approach is taken during this investigation, with the results of the eight primary demand scenarios accumulated in a specific ratio to estimate annual performance. This ratio weights the likelihood of occurrence of each climatic variation in demand scenario, using a statistical representation of daily average space heating demand derived from the climate dataset, and the expected occurrence of weekday and weekend occupancy patterns.

Within the remit discussed above, a Demand Scenario Conception Methodology was developed (see Figure 3.1) to produce transient electrical demand profiles, and transient thermal demand driver profiles. The casual thermal gains profiles due to occupants, appliances and lighting, generated by BIM-G as discussed in Sections 3.3.2, 3.6, & 3.7, was used in a published investigation into the effects of changing casual thermal gains from appliances and lighting on domestic overheating and potential space cooling requirements [3]. The measured electrical profiles of appliances (presented in Section 3.6), as generated during a data acquisition exercise discussed in Section 3.6 and Appendix D, were subsequently used by Kilpatrick et al [4] in their development of a separation filter designed to disaggregate whole-dwelling electrical load profiles into different appliance categories. A simplified version of the methodology was applied within the TARBASE project [5], to estimate electrical demand values, and synthesise occupancy patterns and casual gain values for use in annual steady state thermal demand calculations.

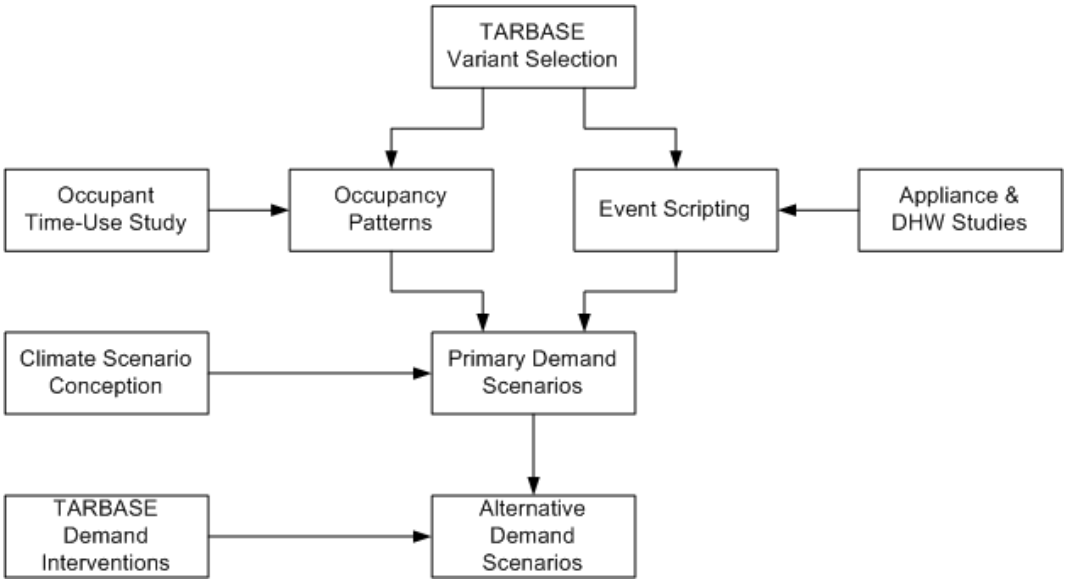

Figure 3.1: Demand Scenarios Conception Methodology

A demand profile quantifies time-varying energy demand, with a particular temporal precision, over a 24 hour time period. Demand profiles are driven by numerous user decisions to operate equipment or services in the dwelling. A narrative is defined for each occupancy pattern, describing the actions of the household as a whole (i.e. common meal times) and each occupant individually. This narrative describes when the occupants undertake the activities broadly defined in Section 3.3.2. A script defines when user decisions, within the context of the narrative, trigger events and the nature of each event. An event can be the operation of a light, appliance or extractor fan; the usage of DHW; or the introduction of additional ventilation to the dwelling (e.g. by operating trickle vents). Standby and continuous appliance loads are also represented in a script by an associated event.

Events are the basis of the bottom-up approach to demand estimation employed within the modelling and analysis methodology. These events describe three discrete types of interaction between an occupant and energy consuming device: appliance operation, DHW utilisation and controlled ventilation. The nature of individual event types are described in the associated sub-sections in this chapter, but the overarching concept is that multiple events are arranged to create daily event scripts for each dwelling activity. The scripts are translated, with the assistance of supporting data, into daily profiles of electrical demand and thermal demand drivers (i.e. ventilation rate,

DHW utilisation and casual thermal appliance gains). Throughout the process of event scripting, two primary objectives exist. Firstly, incompatible events must not occur simultaneously, such as a single-user appliance in use by two occupants at the same time, or an occupant performing two exclusive tasks concurrently. Secondly, the final profiles must produce demand scenarios which exhibit plausible demand characteristics.

When creating scripts, a plausible and logical order of events was defined, in order to describe realistic prerequisites for an occupant activity (i.e. need to turn on a light in bathroom or kitchen before they use an appliance when there is insufficient daylight, or fill and activate the dishwasher after the evening meals have been prepared and eaten). As presented in Section 3.10.5, in the synthesized demand profiles, much of the electrical and thermal demand is co-incident. This is expected, as space heating is required when the building is occupied, and DHW is consumed by occupants only when they are in the home. Since the scripts are written to reflect a plausible pattern of behaviour arbitrarily defined for the occupants, the majority of appliances, and all lights, are used only when the dwelling is occupied.

The aim of demand scenario conception is to compose a series of scripts, define a number of simulation parameters for the BIM-G model, and synthesis demand and demand driver profiles for design days (as defined in Section 1.6). Demand driver profiles are metabolic gains, ventilation rates, DHW usage, external air temperature and incident solar radiation. Simulation parameters, such as dwelling size and construction, space heating timer, and target thermal comfort temperatures, are collated at this point for use in subsequent procedures. In addition, electrical load profiles of selected appliances had to be measured, in a very limited sample, due to the scarcity of appliance load data. The appliances measured were typically event-driven, i.e. the user manually switches them on, as opposed to continuous or standby loads. However, where insufficient data was available in the literature to estimate standby or continuous loads, a sample appliance was measured. A limited temperature measurement exercise was undertaken to derive estimated thermal gains profiles from appliances. With the exception of “wet” appliances (where a proportion of their

electrical energy consumption will exit the dwelling as warm water), most appliances were assumed to convert electrical energy to thermal energy entering the dwelling at their average rate of electrical consumption. Following the principle of heat rejection from boilers and prime movers, as discussed in Section 2.4.2, exponential heating and cooling curves were defined to describe the casual heat gain from appliances and lighting at the start and end of a usage event.

The conception of demand scenarios was undertaken in two stages. The initial stage identified Primary Demand Scenarios (PDS), as presented in Section 3.9, which were designed for use with performance analysis of all concept micro-generation systems. Within the domain bounded by these scenarios, a large spread of total thermal demand is present, whilst both the distribution of electrical energy requirement throughout the day, and the daily total of electrical demand, vary between some of these primary scenarios. An approach is defined in Section 3.8 to create annual estimates of demand from the Primary Demand Scenarios using weighting factors applied to each PDS design day.

Alternative Demand Scenarios were subsequently conceived to investigate the effects of demand-side interventions, both positive and negative, on the performance of concept micro-generation systems. Whilst these were not applied directly to the studies presented in this thesis, the approximate annual differences were used to inform the study on the impact of changing annual thermal demand on μCHP, as presented in Chapter 6.2. The thermal gain and selected demand driver profiles generated for the Alternative Demand Scenarios were used in other studies published in the academic literature [3].

In the upcoming sections, the various data sources and selection processes are described, and final results of these selections are presented. The assumptions underlying demand scenario conception are discussed in Sections 3.2 to 3.7, and the derivation of climate scenarios for design days is presented in Section 3.8. Supporting data for the assumed appliance and lighting demand assumptions are discussed in Sections 3.6 and 3.7, and appliance load measurements are presented in 3.6. Finally,

definitions and comparative assessment of the primary demand scenarios are presented in Sections 3.9 and 3.10.

3.2 Building Construction

3.2.1 TARBASE Variant & UK Domestic Sector Energy Demands

The early stages of the TARBASE project called for the bottom-up definition of building energy demand drivers [6]; and quantification of annual energy demand, using steady state calculation methods [5]. Analysis of UK domestic sector building stock models [7] was undertaken, to understand the distributions of annual thermal and electrical demand across dwellings, as plotted in Figure 3.3 and Figure 3.5, and the contribution of various construction types to the carbon emissions of the domestic building stock, presented in Figure 3.2. Domestic Building Variants were defined using each of the four major construction types; detached, semi-detached, terraced and flat; including the specification of building fabric elements.

Within the scope of this doctoral project, one of the TARBASE Domestic Building Variants was selected as the basis of the demand scenario. The decision to select a detached dwelling was two-fold; detached dwellings are the largest contributors to UK domestic carbon emissions, as shown in Figure 3.2; and detached buildings are more likely to have greater floor areas than other dwelling construction types. With such a large dwelling, it is reasonable to assume that the occupying household may be economically prosperous [8], and that suitable space is available to house a micro-generation system. A large building will exhibit a higher thermal demand than a similarly constructed and occupied smaller building. Furthermore, an economically prosperous household in a large dwelling can be assumed to have a greater likelihood of owning and operating more electrical appliances and lighting; hence increasing the electrical demand of the dwelling. Mansouri et al [49] agree that increased household income can be an indicator of elevated appliance ownership levels.

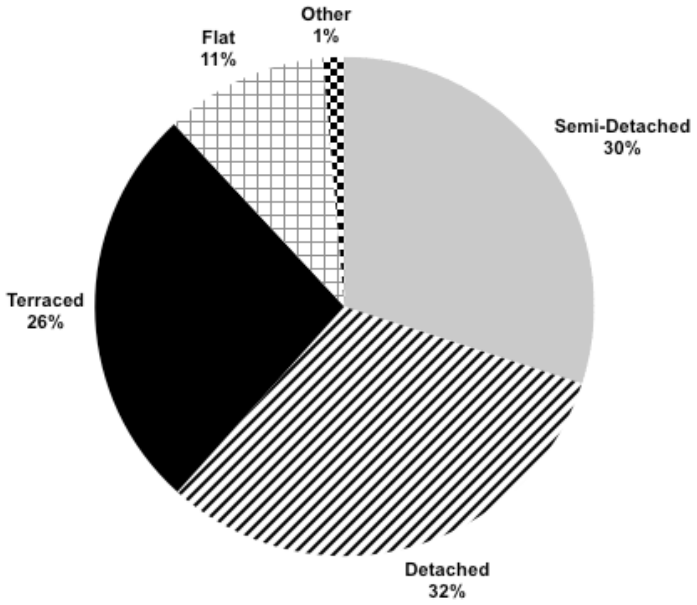

Figure 3.2: Distribution of Domestic Carbon Emissions by Construction Type

Using data derived by the TARBASE project, distributions of UK domestic sector electrical consumption (Figure 3.3) and space heating thermal demand (Figure 3.5) were created. The estimated annual energy demands for the selected TARBASE building variant, calculated using a selection of steady-state methods, are summarised in Table 3.1 and indicated on the aforementioned distributions. The space heating demand differs from the values (15,240-20,064kWh) presented in Table 2.5 for the thermal model validation exercise in Section 2.3.7. The value in Table 3.1 was derived from an earlier version of the TARBASE domestic model, where the treatment of solar gains differed from version 4, as used in Section 2.3.7. As discussed in Section 2.3.7, it is reasonable to expect the BIM-G model and TARBASE model to produce different thermal demand results on the basis of differing thermal modelling techniques.

Annual Energy Demand Type	**Approximate Annual Values (kWh)**
Space Heating Thermal Demand	18,000
Domestic Hot Water Thermal Demand	3,400
Total Thermal Demand	**21,400**
Electrical Consumption	**4,400**

Table 3.1: Annual Energy Figures from TARBASE Steady State Modelling for Selected Building Variant

Analysis of Figure 3.3 demonstrated that the electrical consumption of the chosen TARBASE building variant is representative of the annual consumption of around 30% of dwellings, and exhibits above average consumption, as supported by Figure 3.4, taken from Hawkes and Leach [9].

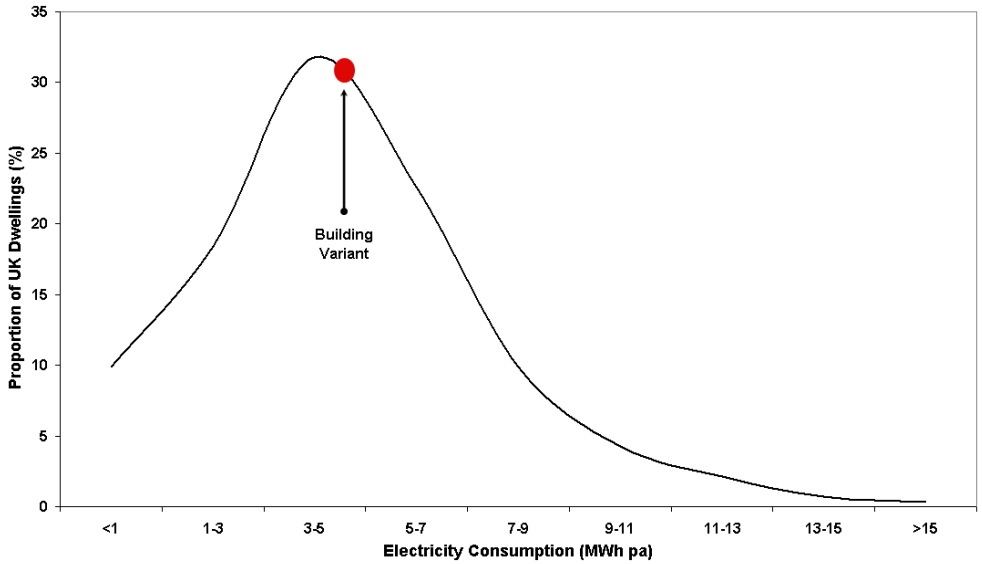

Figure 3.3: Distribution of Annual Electrical Consumption in UK Domestic Sector, indicating consumption of selected Building Variant, as derived by TARBASE project

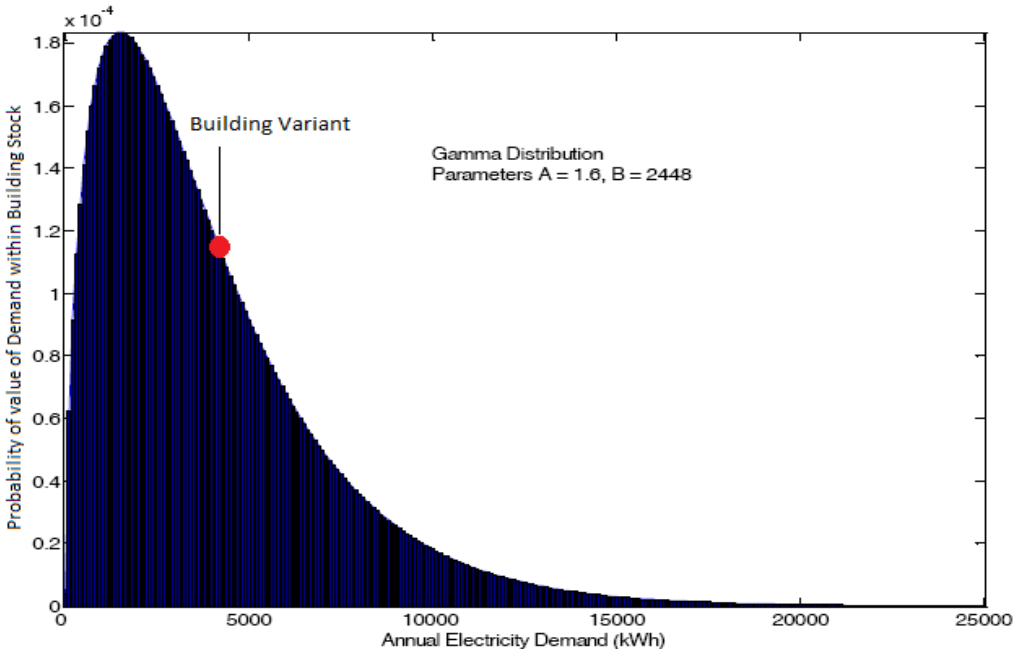

Figure 3.4: Probability Distribution of Annual Electrical Demand in UK Domestic Sector, based on a gamma distribution of electrical demand across the building stock, as defined by the parameters indicated. The location of the building variant on the distribution is indicated. Distribution adapted from Hawkes & Leach [9]

With reference to Figure 3.5, the space heating demand of the building variant is situated in the upper end of the distribution, and is representative of between 15-20% of UK dwellings. When the distribution of total heat demand (i.e. space heating and domestic hot water) for the UK domestic sector (as presented by Mariyappan [10] and shown in Figure 3.6) is considered, it is clear that the selected dwelling exhibits higher-than-average thermal demand, without lying in the tail of the distribution.

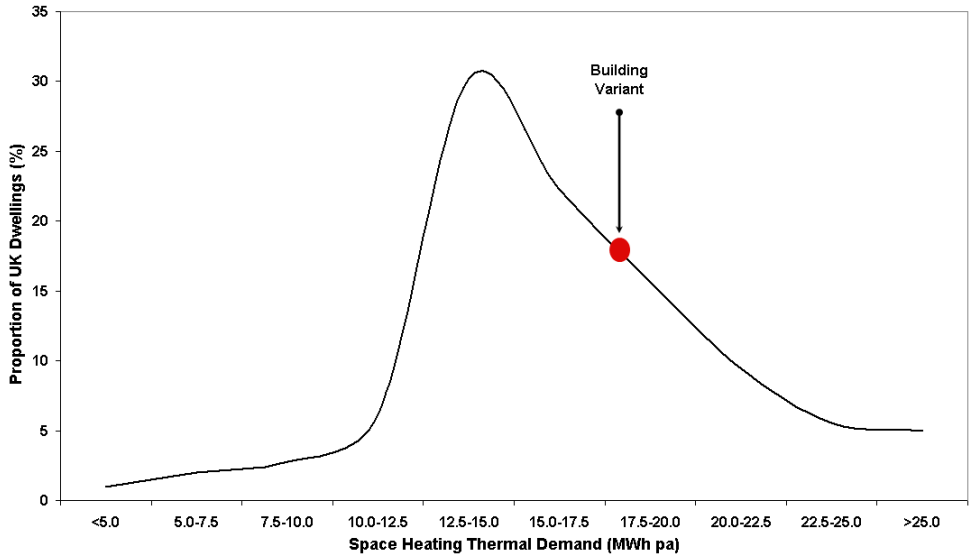

Figure 3.5: Distribution of Annual Space Heating Thermal Demand in UK Domestic Sector, indicating demand of selected Building Variant, as derived by TARBASE project

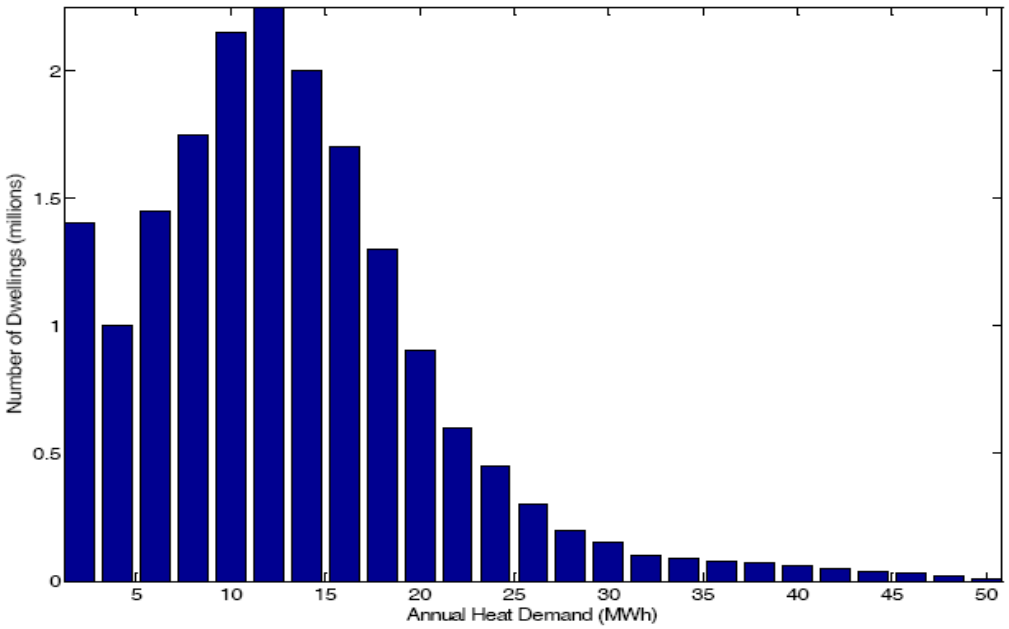

Figure 3.6: Distribution of Annual Heat Demand (Space Heating plus Domestic Hot Water) in UK Domestic Sector. Figure taken from Mariyappan [10]

In accordance with the arguments presented above, this building has greater-than-average thermal and electrical demands, which would increase the carbon abatement potential of a μCHP system [11] implemented within the dwelling, as compared to dwellings with the UK average energy demands.

3.2.2 Physical Building Characteristics

The definition of the building variant's physical characteristics, i.e. physical dimensions, age and building fabric elements, was undertaken, in collaboration with industry partners [4], using building specifications from an established house builder [4], and data derived from the Scottish House Condition Survey [12] and English House Condition Survey [13]. The physical attributes of the building variant are presented in Table 3.2, from which simulation parameters were derived for the Thermal Demand Estimation routine. As discussed in Section 2.3.2, these U-values were corrected to account for thermal bridging effects before being used as simulation inputs for the BIM-G model.

Physical Attribute	Value
Length	8 m
Width	9 m
Height to Soffit	6 m
Total Floor Area	144 m^2
Wall Type	Timber Frame, Clad with Brick, with 50mm Mineral Fibre Insulation
Wall Planar U-Value	0.49 W/m^2K
Wall Construction Element U-Value (corrected for Doors and Repeating & Non-Repeating Thermal Bridges)	0.682 W/m^2K
External Door type	Solid Wooden Door
External Door U-Value	3.23 W/m^2K
Roof Type	Pitched with Tiles, 100mm Glass wool Loft Insulation
Roof U-Value	0.40 W/m^2K
Floor Type	Chipboard, with 40mm Mineral Fibre Insulation
Floor U-Value	0.45 W/m^2K
Glazing Type	Double Glazed, uPVC
Glazing Area	43.3 m^2
Ratio of Glazing by Orientation	N:0%, E:43%, S:23%, W:34%
Glazing U-Value	2.75 W/m^2K
Background Infiltration Rate	0.395 ACH

Table 3.2: Physical Attributes of Building Variant

The layout of the building is illustrated in Figure 3.2, which was used in the ESP-r simulation of the building in the BIM-G thermal model validation exercise discussed in Section 2.3.7.

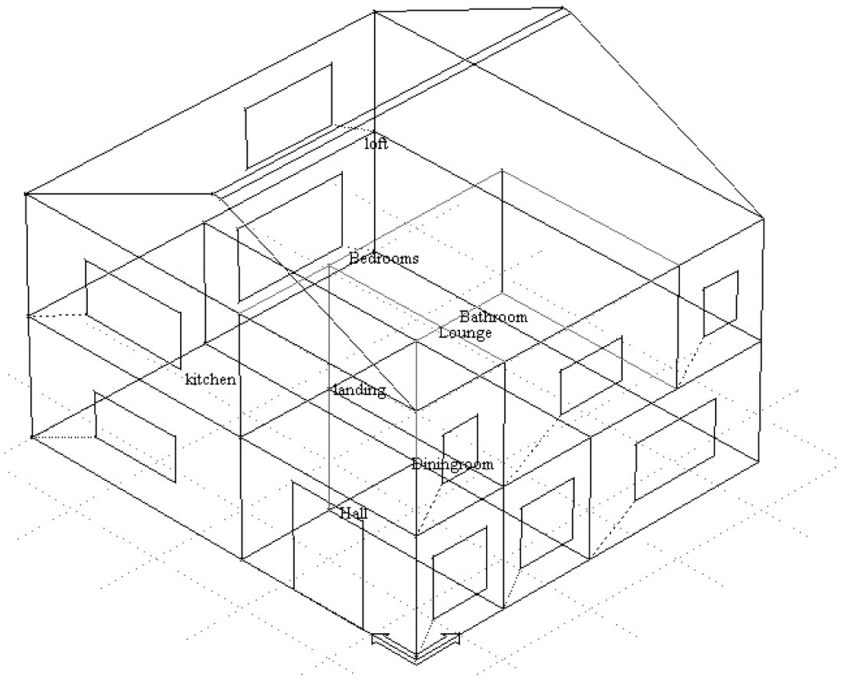

Figure 3.7: Wireframe representation of Physical Building Variant

3.3 Occupancy Patterns and Metabolic Gains

3.3.1 Occupancy Patterns

The behaviour of the occupants (both in terms of their interaction with appliances, lighting and DHW outlets, and the temporal configuration of space heating controls) is a major driver of thermal and electrical demand. Profiles were created which described the occupancy status of each occupant: absent from dwelling; “active” in dwelling; asleep in dwelling. In Sections 3.4 to 3.7, the relevance of each occupancy status to the associated event scripting is discussed at length, including the reliance of certain appliance usage events on active occupancy. By superimposition of all four profiles, a dwelling occupancy profile was created that identified periods of “active occupancy”, “inactive occupancy” and “absence”. These periods were used to dimension the space heating thermal demand periods, as defined in Section 3.9, and are used to constrain micro-generation systems functioning within certain operating regimes.

The definition of a household to occupy the building variant was undertaken with three goals in mind; firstly, to represent, in terms of numbers, and preferably composition, a significant portion of UK households; secondly, to suit the building variant and greater-than-average demands wanted from the building variant; and finally, to produce plausible demand profiles. Analysis of the UK General Household Survey 2002/03 [14], as presented in Appendix A, suggested that four-person households account for around 13%[1] of UK households, whilst larger households account for less than 6%[2] cumulatively. Hence, a household with four members, as defined in Table 3.3, was chosen as a compromise between a large household with associated demand, and the remit to maximise representation of household stock. The decision to specify the household composition of three working adults and one school-attending child was made in light of research undertaken on the UK Time Use Survey 2000 [15] that suggested a range of occupancy, and vacancy, durations from both schoolchildren and adults. The particular household represents almost 18% of four-person households, and could be expected to represent a family with a grown-up offspring who has remained within the family home.

Occupant	Description
1	Working Adult Male
2	Working Adult Female
3	Working Adult Male (Offspring)
4	School-attending Child

Table 3.3: Definition of Occupants as used in BIM-G model

Occupancy profiles were created after analysis of the UK Time Use Survey 2000 [15], in conjunction with the UK General Household Survey [14], from which distributions (see Figure 3.8) of occupant vacancy due to employment (or full-time education) were derived. Further analysis of this data showed that the peak of the distribution was much greater during weekdays, than weekend days. Two occupancy patterns were then defined for each, one that represents weekdays, and another for weekend days, where the vacancy durations have been selected from the upper and lower end,

[1] Appendix A, Table B.3

[2] Appendix A, Table B.3

respectively, of the distribution in Figure 3.8. The assumption of two discrete occupancy patterns and approximate duration of weekday vacancy is supported [16] by similar assumptions within the established BRE Domestic Energy Model (BREDEM).

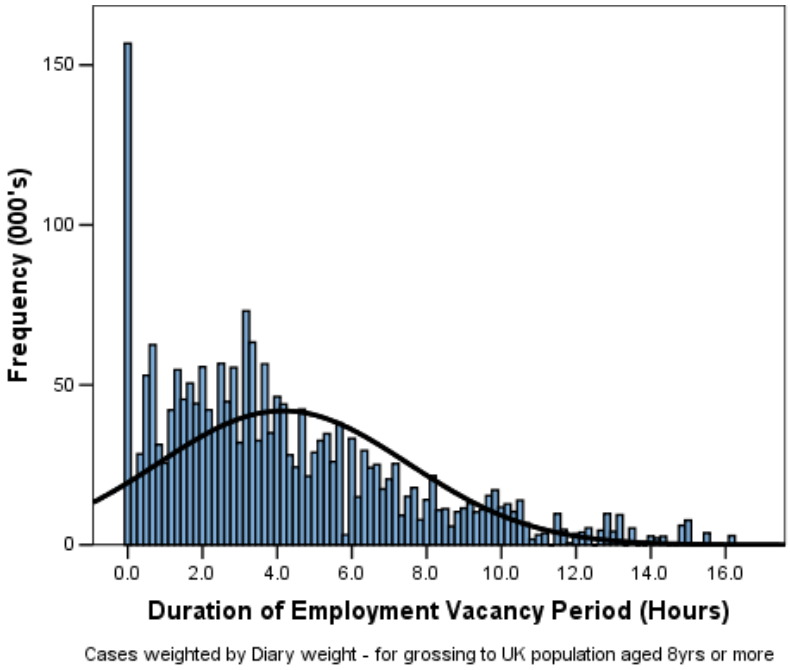

Figure 3.8: Distribution of Occupant Vacancy Periods, generated from analysis of the UK Time Use Survey 2000 [15]

The duration of sleeping periods were selected using the distribution in Figure 3.9, where longer periods were selected for the child than the adults. As before, the period of dwelling nocturnal inactivity was selected with the assumptions of the BREDEM model [16] in mind. The particulars of each occupant's occupancy pattern are given in Table 3.4.

Activity	Occupant	Weekday Start Time	Weekday Stop Time	Weekend Start Time	Weekend Stop Time
Sleeping	1	23:00	07:00	23:00	07:00
	2	23:00	07:00	23:00	07:30
	3	23:00	07:00	23:00	08:00
	4	22:00	07:30	22:30	08:00
Vacant	1	08:15	17:45	10:00	11:30
	2	08:30	16:30	13:30	15:30
	3	07:30	17:15	18:30	21:30
	4	08:30	16:30	13:30	15:30

Table 3.4: Occupancy Patterns of Individual Occupants

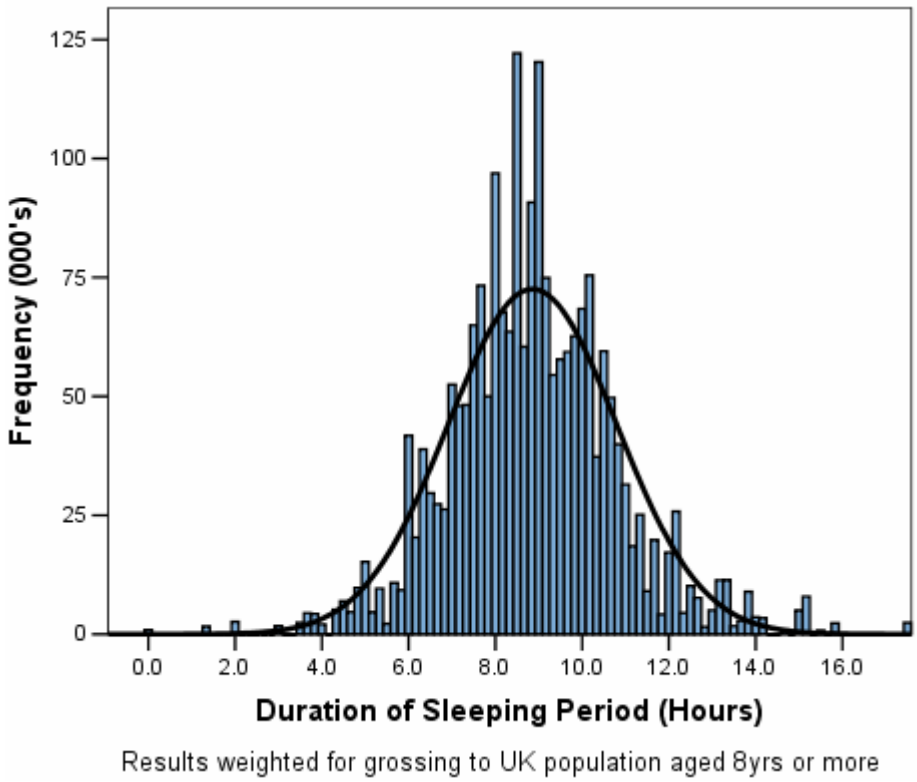

Figure 3.9: Distribution of Occupant Sleeping Periods, generated from analysis of the UK Time Use Survey 2000 [15]

The occupancy patterns defined in this section are consistent with the analysis undertaken by Agar & Newborough [17] upon a demand dataset, recorded by an energy utility in 1996, with annual thermal and electrical demand data for approximately 30 UK dwellings. This data had a temporal resolution of 1-minute, where the thermal demand recorded was boiler gas consumption, for space heating and DHW. They concluded that daily thermal and electrical demand profiles were functions of occupancy characteristics, and identified 2 basic types of profile, occurring in any home in any season; Type A on a weekday and Type B on a weekend. Despite the association with weekday and weekend, they conclude that relative proportions of Type A and B profiles are a function of the household's lifestyle. Type A was characterised as unoccupied for several hours per day. Type B was characterised as one or more members in residence for 24 hours.

In their µCHP modelling exercise, Hawkes et al [18] used similar operating patterns, both in terms of vacancy and sleep durations, and in the split between weekday and weekend operating patterns.

3.3.2 Metabolic Gains

Design guide-derived assumptions [19] on task-dependant metabolic heat emission were correlated with ASHRAE [20] design estimates on gender and age specific emissions to produce specific values of metabolic gains for each occupant whilst undertaking a defined type of activity. A range of occupant activities are defined within the UK Time Use Survey [15], including "Watching TV", "Cooking", "Laundry", "Washing and Dressing", "Ironing" and "House Cleaning". Whilst these discrete activities were considered when composing a narrative for the occupants, a simplified approach was applied to the consideration of metabolic gains. The increased metabolic rate of "Active" was used whenever an occupant uses, or interacts with, a domestic cleaning appliance (i.e. washing machine, dishwasher or vacuum cleaner), or cooks a meal involving the hob or oven. All other activities are classed as sedentary.

Since the BIM-G model does not simulate humidity levels and moisture transfer, for reasons discussed in Section 2.3.1, and a disparity of up to 64% exists between total and sensible metabolic gains, it was deemed necessary to segregate the sensible and latent fractions of the metabolic gain. To this end, activity specific sensible-latent metabolic gain ratios were derived from ASHRAE design guide data [20], and applied to the calculated metabolic gains.

The metabolic gains to the dwelling, as calculated using the above methodology, are detailed in Table 3.5. The metabolic gain corresponding to the "Active" state was calculated as the average of the range of metabolic gains for housework.

Activity	Adult Male	Adult Female	Child
Sleeping	55.4	47.0	41.5
Sedentary	71.4	60.7	53.6
Active (Housework, Cooking)	96.2	81.8	72.2
Vacant	0.0	0.0	0.0

Table 3.5: Sensible Metabolic Gains (W) by Gender, Age and Activity

Using the occupancy patterns discussed in the previous sub-section, and the values for metabolic gains, a metabolic casual thermal gains profile was produced, as visualised in

Figure 3.10. It is prudent to note that “active occupancy”, as described in the previous sub-section, is distinct from the “active” activity type, as “active occupancy” is a dwelling circumstance where at least one occupant is in the “active” or “sedentary” state. The time periods with active occupancy are tabulated for weekday and weekend occupancy patterns in Appendix B.2.1 and Appendix B.2.2.

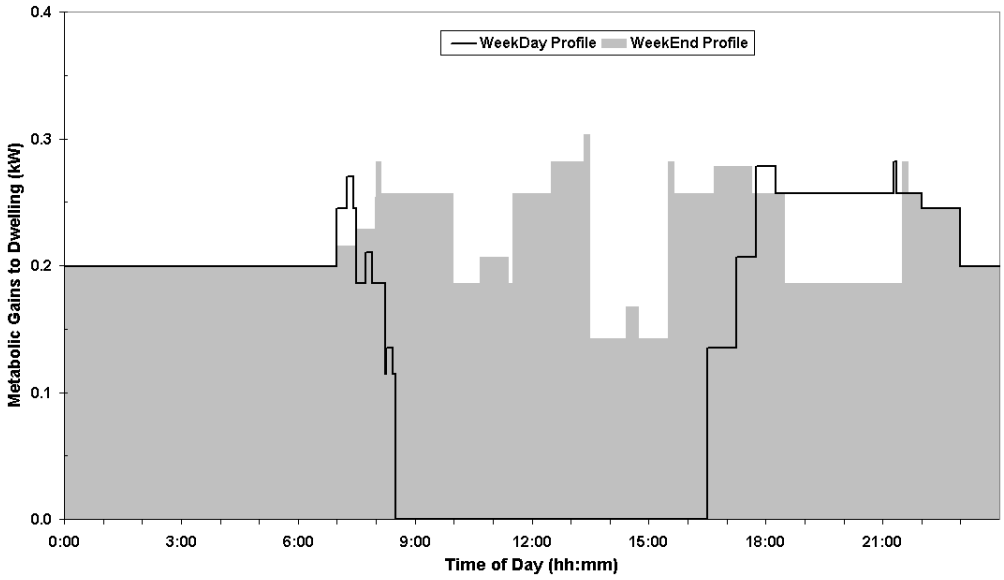

Figure 3.10: Metabolic Gain Profiles, for entire household, produced for Weekday & Weekend Occupancy Patterns

3.4 Domestic Hot Water Utilisation

The use of domestic hot water (DHW) can account for significant proportions of domestic energy demand; annually around 22% [21] on average over the domestic building stock. It can be difficult to quantify energy use relating to domestic hot water, due to heat losses from thermal storage infrastructure shared with space heating systems, and electrical balance-of-plant consumption shared with space heating systems. This issue complicates the comparative assessments of DHW energy consumption between demand scenarios defined in this project. Identifying DHW usage is further complicated by the displacement of DHW demand by the inclusion of cold-fill washing machines, electric showers or cold-fill dishwashers. This makes it difficult to compare synthesis DHW usage profiles with empirical datasets where the components of DHW demand have not been defined.

The variation of DHW throughout the day, across the week and between seasons is difficult to predict because of the quantity of occupant- and building-specific factors that drive the magnitude and pattern of consumption. Building factors include draw-off lengths (i.e. the volume of water in the hot water pipe between the DHW tank or combination boiler and the particular DHW outlet in use, the number of type of outlets (individual or mixer taps for sinks or showers, bath taps, supplies to dishwashers and washing machines). Occupant factors include the number of occupants, typical occupancy patterns, effects of their lifestyle, their age, bathing habits, and social or cultural expectations.

In the context of μCHP systems, where a thermal demand is required during any generation period to maximise carbon abatement potential, DHW utilisation is a source of thermal demand which, in the absence of available and robust empirical data to the contrary, is assumed to be mostly independent of climatic conditions - as opposed to space heating demand. As a thermal store has been specified for the μCHP simulations in this project, the sensitivity of μCHP system performance to modest changes in the daily distribution of DHW consumption is minimised. DHW still accounts for the base-load of thermal demand, with sustained requirements for heat outside of the heating season, which halts space heating requirements.

Jordan & Vajen [76] created DHW draw-off profiles to support IEA Task 26 simulation studies of solar thermal systems. These profiles were synthesised with 1-minute, 6-minute and hourly temporal precision, for a period of a year, using probability distributions. They defined four categories of DHW load; short (e.g. hand washing), medium (e.g. dish washing), bath and shower. For each category, a mean flow rate, duration, daily frequency and statistical distribution of flow rates. The first three of these variables have been presented in Table 3.6, along with the assumed usage within both occupancy scenarios within the BIM-G Model. Jordan & Vajen [76] used an assumed daily average consumption of 200 litres, coupled with the distribution of flow rates, and a sinusoidal function with an amplitude of ±10 % (of average daily consumption), to generate distributions of flow rates over the day and year. The

values used in their DHW load synthesis were drawn from a range of DHW monitoring studies in Germany and Switzerland.

Draw-Off Type	Bathroom Hand Wash	Kitchen Hand Wash	Kitchen Dishes	DHW Shower	Bath	Total DHW
Duration (mins)	1	1	1	5	10	
Rate (l/min)	1	1	6	8	14	
Volume (l)	1	1	6	40	140	
No. of Events (Weekday)	11	11	3	4	0	29
No. of Events (Weekend)	16	14	4	4	0	38
Daily Consumption (Weekday) (l)	11	11	18	160	0	200
Daily Consumption (Weekend) (l)	16	14	24	160	0	214
Annual Consumption (l)	**4998**	**4067**	**1127**	**1372**	**0**	**11564**

Table 3.6: Domestic Hot Water consumption, including duration, volume and number of draw-off events, and daily and annual consumption volume, as assumed in demand profiles

As Newborough & Probert [48] discussed, DHW consumption data is scarce. The profiles synthesised by Jordan & Vajen [76] were used by R. Spur et al [79] and later Knight & Ribberink [81] when defining load profiles for IEA Annex 42. The review of available DHW measurements by Knight & Ribberink [81] indicated that the majority of studies utilised a temporal precision of 60-minute, which is not particularly useful in the definition of DHW events in the order of 1-10 minutes.

The DHW profiles for both occupancy patterns are presented in Figure 3.11, based on the script of DHW events tabulated in Appendix B.2.3. The load profiles generated for use with the BIM-G model assumed that an electric shower was in use instead of a shower fed from the DHW system. However, the consumption information in Table 3.6 is used in the definition of the electrical shower appliance event, as discussed in Section 3.6.3. The general theme of increased consumption during early mornings and evenings is replicated in the annual accumulation, by hour of day, of DHW consumption data recorded in US homes, as used by the NAHB in a DHW heater performance study [80].

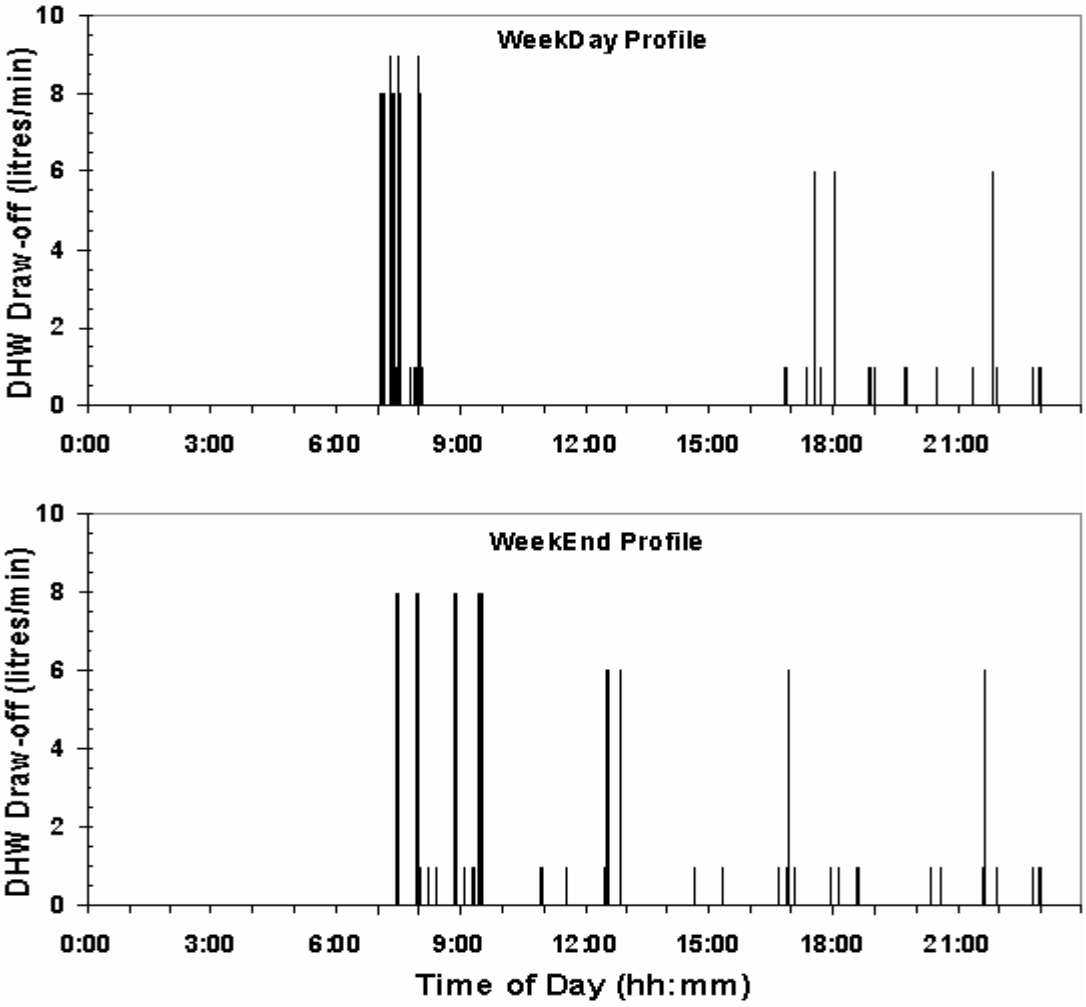

Figure 3.11: DHW Draw-off Profiles for Weekday & Weekend Occupancy Patterns

3.5 Ventilation

In order to account for ventilation due to opened windows and doors, and trickle ventilation devices (such as window vents), the TARBASE project utilises an occupancy driven ventilation rate. This ventilation rate, of 0.31 ACH [3], occurs only when the dwelling is actively occupied, i.e. some of the occupants are awake. This ventilation is in addition to infiltration through (and between) the construction elements of the building. Unlike a dynamic model of occupant-controlled ventilation, this approach assumes minimal interaction of the occupants with windows and trickle vents. The TARBASE approach has been adopted for the BIM-G model, as the production of a dynamic-method ventilation profile would require an in-depth understanding of the drivers behind occupant-controlled ventilation (for instance moisture control, indoor

air quality and thermal comfort) and the development of a suitably complex, multi-zone air transfer model. It is therefore prudent to note that the ventilation profile is the same across the design days for different seasons. It was concluded that, within the bounds of a 1-D, single-zone thermal model, the constant air change assumption would produce plausible simulation results.

Within the dwelling, the occupants trigger intentional (or scheduled) ventilation, corresponding to an activity that produces large volumes of water vapour, for instance cooking, showering and bathing. This intentional ventilation is provided through extractor fans, where the dwelling variant has been defined to incorporate extractor fans in the kitchen and bathroom.

The bathroom extractor fans are triggered by shower or bath usage, where the extractor is turned on simultaneously with the shower, and turned off 5 minutes after the shower finishes, as per industry-body installer guidance [22]. The kitchen extractor fans are triggered by hob or oven usage, where the extractor is turned on simultaneously with the first cooking appliance, and turned off 5 minutes after the last appliance finishes. The energy loads, consumptions, and usage durations for both extractor fans are detailed in Table 3.7.

Appliance Signature ID	**EF1A**	**EF2A**
Description	Bathroom Extractor	Kitchen Extractor
Steady Electric Load (kW_e)	0.0140	0.0300
Steady Heat Emission (kW_{th})	0.0140	0.0300
Weekday Usage Duration (h:mm)	0:40	1:00
Weekday Energy Consumption (kWh)	0.0093	0.0300
Weekend Usage Duration (h:mm)	0:40	1:40
Weekend Energy Consumption (kWh)	0.0093	0.0500
Annual Energy Consumption (kWh)	**2.2**	**12.3**

Table 3.7: Extractor Fan consumption, including daily and annual duration and consumption volume, as assumed in demand profiles

The ventilation profiles for both occupancy patterns are compared in Figure 3.12, based on the script of ventilation events tabulated in Appendix B.2.6.

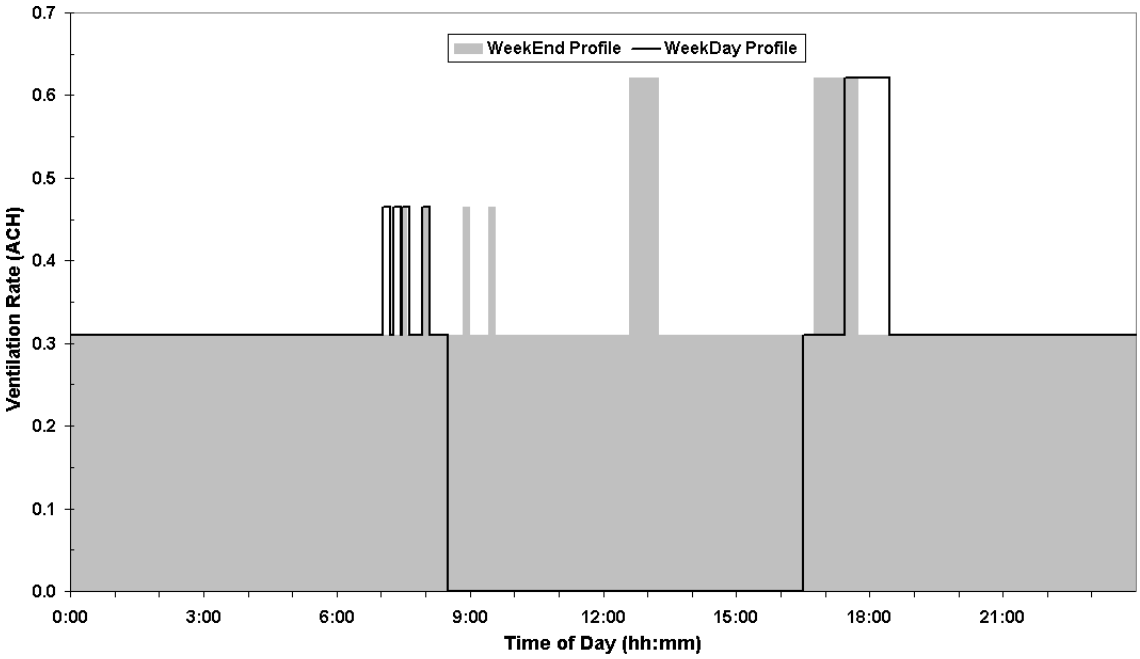

Figure 3.12: Ventilation Profiles generated for Weekday & Weekend Occupancy Patterns, combining occupancy-related background ventilation and extractor fan usage

3.6 Appliances

The nature of electrical demand due to appliances, and indeed artificial lighting, within the home is driven by a number of factors, which can be considered as household factors or behavioural factors. Household factors tend to influence the cumulative appliance consumption of the dwelling, encompassing the ownership of appliances, energy efficiency of owned appliances, composition of a household (i.e. quantity of occupants at each age, gender and employment status), and socio-economic grouping of the occupants (which affects their frugality when using appliances). It is easy to comprehend that many of these factors are inter-related, which makes it difficult to derive simple relationships between these factors and domestic energy use. The relationship between these factors and energy consumption has been investigated extensively by others, such as Mansouri et al [58], 40% House [8] and DECADE [60]. Multiple studies have been conducted by the Market Transformation Programme (a UK government-funded research group to support implementation of energy efficiency legislations), and within academia [49][52][58][59], on appliance ownership and energy consumption. Analysis by DECC [23], as presented in Table 3.8, estimates the contribution of categories of appliances and lighting to a typical dwelling's appliance

and lighting electrical load. It should be acknowledged that these estimates do not incorporate personal care appliances and other miscellaneous electric loads (e.g. burglar and fire alarms).

Category	Contribution to dwelling A&L consumption
Light	17%
Refrigeration	17%
Wet Appliances	17%
Consumer Electronics & ICT	33%
Cooking	16%
Total	**100%**

Table 3.8: Contribution of appliance and lighting types to the average UK domestic electricity consumption for appliances and lighting, as taken from DECC [23]

The frequency of appliance usage is driven by flexible decisions, made on hourly, daily and weekly bases [24], hence introducing significant variations in demand throughout the day and week, and between seasons. Capasso et al [25] identified a number of behavioural functions that drive energy consumption on a time-varying basis. These include the availability of an occupant to interact with appliances and lighting, due to their presence in the dwelling and whether they are awake, and the ability of occupants to interact with various appliances simultaneously, which he termed their "human resources". This concurs with load data analysis by Wright and Firth [26] to understand how occupancy contributed to patterns in domestic electrical load profiles, and the assumption of Yao & Steemers [24] that most appliances operate when occupants are at home and awake. Capasso et al [25] also use Walker's [27] definition of "proclivity" of an occupant to partake in certain activities, such as cooking, personal hygiene or entertainment, at any particular time. Research undertaken as part of the UK Time Use Survey [15] provides statistical analysis of occupant surveys with profiles describing the probability that an occupant will be undertaking a range of activities at any particular time of the day. Other behaviour aspects to energy consumption include habitual patterns of behaviour and response to external factors such as energy prices [47]. An example UK domestic load profile from a measured demand dataset [46] is presented in Figure 3.13.

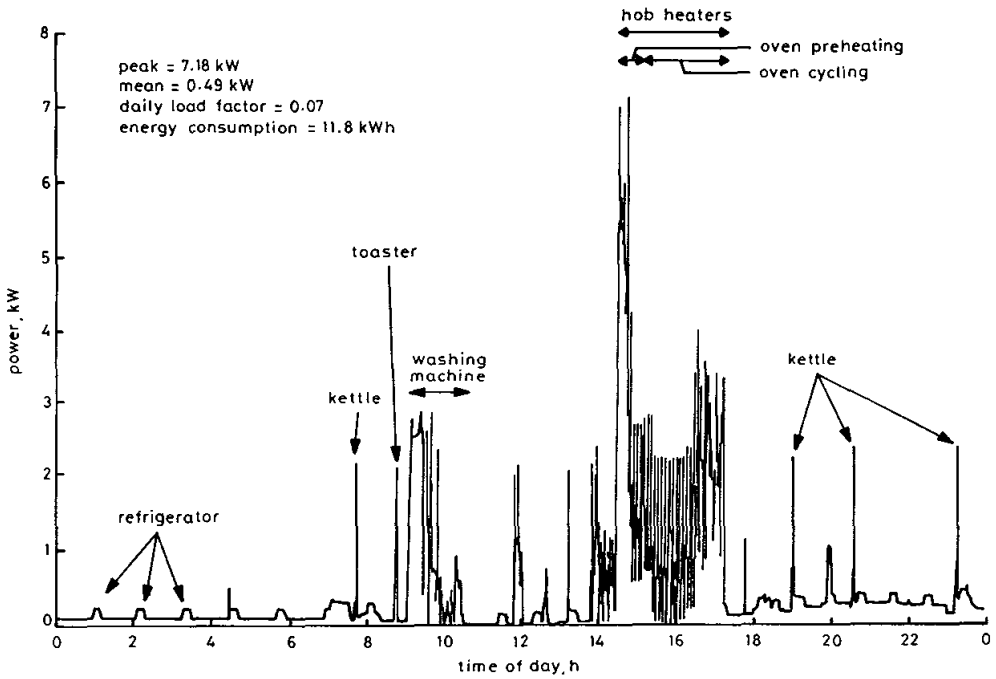

Fig.7 *Example of a Sunday electricity demand profile from an individual household (employing a gas-fired central heating system) with an electric cooker and kettle*

Figure 3.13: Example of a domestic electrical load profile for a Sunday, as extracted from the a demand measurement dataset, and annotated by Newborough & Augood [46]

As discussed in Chapter 1, detailed demand data is scarce, whether that data is consumption patterns with high temporal precision or appliance usage information. Even where data exists, new data is required, as it can be very limited (in terms of appliance and household samples & technologies) and out of date [36]. A number of studies have attempted to draw conclusions from existing datasets to inform consumption models, including Paatero & Lund [28], Wright & Firth [26] and others [24][28][29][30][31]. Appliance data on ownership, usage and loads, coupled with occupancy data and assumptions, have been used to populate various bottom-up domestic load models [28][25][24][32][33][34][35]. The majority of domestic energy models are stochastic, using a type of probabilistic approach [24][25][28][33][34][35], although neural network approaches have been applied [29], and also regression analysis of measured demand versus energy drivers [30][32].

The synthesis of domestic load profiles is a highly complex task, especially since energy consumption is linked with a range of subjective lifestyle-driven factors which cannot be easily defined with a high level of precision [25]. Stokes et al [33] argues that simulated demand profiles are required for renewable energy technology models, due

to the limited availability of electrical demand data, and the time and costs involved in collecting new data. Expected patterns in consumption have been identified by the data analysis studies discussed earlier, and discussed at length by Wood & Newborough [47]. They classify components of domestic electricity consumption as ‘‘predictable’’, ‘‘moderately predictable’’ and ‘‘unpredictable’’. “Predictable” loads are typically cyclic loads (such as refrigeration), relatively continuous loads (such as broadband routers and alarms) and standby loads. ‘Moderately predictable’’ consumption is driven by the habits of occupants, such as typical times when they eat, attend to their personal hygiene, undertake housework tasks and relax. Stokes et al [33] agree that occupants tend to patterns day-to-day, going to bed and rising at similar times across weekdays. “Unpredictable” consumption patterns are driven by climatic factors, random variations in occupancy patterns, and other unpredictable factors within a simplified load model.

An appliance list was defined similar to that in TARBASE research [5], on the basis of appliances typically found in UK dwellings, as shown in Table 3.13. Average annual energy consumption figures, by dwelling, were identified from a range of sources as discussed in the following sections, and where available, typical usage frequency data. As mentioned, all energy consumption data is typically averaged across the UK domestic sector, so it is not unreasonable to expect a particular dwelling and household to exhibit consumption significantly different from the average.

In order to evaluate micro-generation systems, it is assumed that there is a general need to convey information on an annual basis. In addition, the information supporting the domestic demand drivers, such as Market Transformation Programme studies, is quoted on an annual basis. A design day approach to demand modelling has been adopted in the BIM-G model, with a single occupancy pattern used to represent all 5 weekdays, and a single pattern to represent both weekend days. The extrapolation from daily to annual profiles is desired, therefore, in order to ascribe annual demand drivers to individual daily demand scenarios, and to estimate annual results of concept system performance from an array of daily performance profiles. This extrapolation would have two basic dimensions – occupancy pattern and climate - added to which

are considerations of annual holidays and intra-daily, i.e. within a discrete 24-hour period, storage implications. When considering non-climate dictated usage of appliances, lighting or DHW, equation (3.1) is used to calculate annual energy consumption of a particular appliance, or indeed the dwelling as a whole. The energy consumption of each appliance during each occupancy pattern is calculated as the sum of the energy consumption of that appliance during each usage event. The occupants of the dwelling are assumed to take annual holidays together, resulting in a number of weeks per year where the dwelling is completely unoccupied 24 hours per day. These annual holidays are assumed to have reduced energy consumption, where standby-enabled appliances are turned off, but essential continuous constant operation appliances, such as refrigeration equipment, remain active. The duration of the annual holiday is assumed as 2 weeks, spread across weekday and weekend days with the conventional 5:2 ratio.

$$E_{annual} = \left[\left(E_{weekday} * 5\right) + \left(E_{weekend} * 2\right)\right] * \left(52 - n_{WeeksHoliday}\right) \quad (3.1)$$

As a consequence of representing 5 days (i.e. during the week) using a single script, the BIM-G model does not account for varying appliance use between days within the week. This may result in annual consumptions for particular appliances that exceed an expected annual total, as it is scripted for 5 days per week instead of the average weekly usage frequency of 3 or 4 times per week. With the exception of lighting using during daylight hours, the two occupancy patterns do not incorporate seasonal variations in appliance usage. Yao & Steemers [24] recognised that some appliance usage is linked to season (e.g. slightly increased cooking and indoor entertainment activities in winter versus summer months), as supported by analysis of load profiles by Wright & Firth [26]. Whilst Hart & Dear [37] identified the response of domestic refrigeration consumption to external climate in Australia, a complex methodology would have been applied to separate the effect if temperature differential (fridge to room) from the other factors that affect consumption, such as door opening, addition of warm food, etc.

As discussed in Section 3.1, narratives were defined for each occupancy pattern to describe sequences of "typical" or "reasonable" behaviour within the home, for individuals or groups of occupants. These narratives are used to define appliance, lighting, DHW and ventilation usage scripts in the BIM-G model. The narratives are based around the periods of active occupancy within the dwelling, as defined earlier in this chapter, as presented in Table 3.9 and Table 3.10 .

Sig ID	Type	Weekday – Occupant			
		1	2	3	4
Active (1)	*Start*	07:44:00	08:16:00	07:16:00	~
	Stop	07:54:00	08:26:00	07:26:00	~
	Duration	00:10:00	00:10:00	00:10:00	~
Active (2)	*Start*	21:17:00	16:30:00	~	~
	Stop	21:22:00	18:15:00	~	~
	Duration	00:05:00	01:45:00	~	~

Table 3.9: Active Occupancy periods by occupant for weekday occupancy pattern

Sig ID	Type	Weekend – Occupant			
		1	2	3	4
Active (1)	*Start*	07:59:00	13:20:00	15:30:00	~
	Stop	08:09:00	13:30:00	15:40:00	~
	Duration	00:10:00	00:10:00	00:10:00	~
Active (2)	*Start*	12:30:00	16:40:00	21:30:00	~
	Stop	13:30:00	17:40:00	21:40:00	~
	Duration	01:00:00	01:00:00	00:10:00	~
Active (3)	*Start*	14:25:00	10:40:00	~	~
	Stop	14:45:00	11:25:00	~	~
	Duration	00:20:00	00:45:00	~	~

Table 3.10: Active Occupancy periods by occupant for weekend occupancy pattern

The scripting of appliances events depends on the type of appliance load, namely:

- Appliances that are always "on", or are "on" whenever the appliance is not otherwise used for a discretionary event, such as:
    - Continuous (HVAC controls, routers, cordless phones)
    - Standby (of discretionary loads)
    - Cyclic loads (i.e. refrigeration) with limited response to user activity
- Discretionary loads, triggered by activity, with either:
    - Varying load profiles of set duration (washing machine, dishwasher, tumble dryer)

- Varying load profiles of user defined duration (hair dryer, electric iron)
- Steady loads of user defined duration (consumer electronics, lighting, extractor fans)

The author measured the load signatures of a number of domestic appliances, with high temporal precision, using data acquisition equipment, in order to represent the "shape" of the electrical demand profiles resulting from variations in electrical load during appliance operation. Surface temperature measurements were also taken of some appliances, which were used in conjunction with external studies on casual thermal gains from appliances, to produce a transient profile of appliance casual gain. This is related to the technique of inferring energy use and duration during usage events of industrial plant, as reported by Brown and Wright [38]. The event details for appliances with a time carrying load profile are summarised in Table 3.11 and Table 3.12, and events for appliances with steady loads in Table 3.13

Appliance	Event Description	Event Duration (h:mm:ss)	Event Cons. (kWh)	Casual Gain Description	Event Casual Gain (kWh)
Electric Oven	200°C	0:46:45	1.117	τ= 2mins	1.117
Electric Toaster	2 Slices @ Medium	0:02:30	0.060	τ= 30s	0.060
Microwave oven	Full Power - 7mins	00:07:00	0.113	τ= 2mins	0.113
Fridge Freezer	24hour Cycling	24:00:00	0.719	Steady @ average load	0.719
Vertical Freezer	24hour Cycling	24:00:00	1.226	Steady @ average load	1.226
Electric Kettle	1.5l of water (>2 hours since last use)	0:05:05	0.158	τ= 1min	0.158
	0.75l of water (>1/2 hour since last use)	0:02:30	0.080	τ= 30s	0.080
Electric Shower	8kW Shower	0:05:00	0.667	τ= 5 mins, 25% of input	0.167
Hair Straighteners		0:15:30	0.045	τ= 30s	0.045
Hair Dryer		0:09:55	0.031	τ= 30s	0.031
Dishwasher	Standard Wash (55°C)	1:30:00	0.855	τ= 5 mins, 5% of input	0.043
Washing Machine	40°C degree Wash	1:01:55	0.549	τ= 2mins, 5% of input	0.027
Tumble Dryer	Full Power	1:26:15	0.929	τ= 2mins, 5% of input	0.046
Electric Iron	Full Power	0:36:10	0.306	τ= 2mins	0.306

Table 3.11 Appliances with usage events where the electric load varies - event duration, energy consumption during event, description of casual gain estimation, and energy released as casual gain during and after appliance usage event

Appliance	Weekday Events		Weekend Events		Annual Energy Consumption (kWh)	Annual Casual Gain (kWh)
	Qty	Cumulative Consumption (kWh)	Qty	Cumulative Consumption (kWh)		
Electric Oven	1	1.117	1	1.117	383.2	383.2
Electric Toaster	2	0.121	2	0.121	41.4	41.4
Microwave oven	1	0.113	1	0.113	38.6	38.6
Fridge Freezer	1	0.719	1	0.719	246.8	246.8
Vertical Freezer	1	1.226	1	1.226	420.6	420.6
Electric Kettle	2	0.317	3	0.475	124.2	124.2
	2	0.159	3	0.239	62.3	62.3
Electric Shower	4	2.667	4	2.667	914.7	228.7
Hair Straighteners	2	0.089	2	0.089	30.6	30.6
Hair Dryer	2	0.061	2	0.061	20.9	20.9
Dishwasher	1	0.855	1	0.855	293.4	14.7
Washing Machine	1	0.549	1	0.549	188.4	9.4
Tumble Dryer	1	0.929	1	0.929	318.6	15.9
Electric Iron	1	0.306	0	0.000	74.8	74.8

Table 3.12: Overview of usage events where the electric load varies as applied to occupancy patterns and annual cumulative figures for electrical consumption and thermal casual gains

Appliance	Event Description	Cont. Load (kW_e)	Weekday Events		Weekend Events		Annual Energy Cons. (kWh)	Annual Casual Gain (kWh)
			Duration (hh:mm)	Cons. (kWh)	Duration (hh:mm)	Cons. (kWh)		
Audio Device (3-off with identical usage)	FM Tuner	0.026	1:00	0.026	2:00	0.052	11.5	11.5
	CD Player	0.028	0:30	0.014	0:30	0.014	4.8	4.8
	Standby	0.009	22:30	0.203	21:30	0.194	68.6	68.6
Burglar & Smoke Alarms	Continuous	0.0024	24:00	0.058	24:00	0.058	19.8	19.8
Cordless Telephone	Continuous	0.004	24:00	0.096	24:00	0.096	32.9	32.9
Mobile Telephone Charger (4 devices with identical usage)	Charging	0.004	8:00	0.032	8:00	0.032	11.0	11.0
	Standby	0.001	16:00	0.016	16:00	0.016	5.5	5.5
Broadband Access Device	Continuous	0.0035	24:00	0.084	24:00	0.084	28.8	28.8
Digital Decoder	Continuous	0.0109	24:00	0.262	24:00	0.262	89.7	89.7
DVD Player	Standby	0.0017	24:00	0.041	24:00	0.041	14.0	14.0
VCR	Standby	0.0096	24:00	0.230	24:00	0.230	79.0	79.0
Microwave oven	Standby	0.005	23:53	0.119	23:53	0.119	41.0	41.0
Laptop (2 devices with identical usage)	Trickle Charge	0.004	24:00	0.096	24:00	0.096	32.9	32.9
Games Console	On Mode	0.03	1:30	0.045	2:00	0.060	16.9	16.9
	Standby	0.005	22:30	0.113	22:00	0.110	38.3	38.3
Clock Radio	Continuous	0.0023	24:00	0.055	24:00	0.055	18.9	18.9
Television in Lounge 26" LCD	On Mode	0.08	6:30	0.520	6:30	0.520	178.4	178.4
	Standby	0.001	17:30	0.018	17:30	0.018	6.0	6.0

Television in Bedroom 20" CRT (2 devices with identical usage)	On Mode	0.09	2:30	0.225	2:30	0.225	77.2	77.2
	Standby	0.003	21:30	0.065	21:30	0.065	22.1	22.1
Extractor Fan in Bathroom	On Mode	0.014	0:40	0.009	0:40	0.009	3.2	3.2
Extractor Fan in Kitchen	On Mode	0.03	1:00	0.030	1:40	0.050	12.3	12.3
Washing Machine	Standby	0.0024	22:58	0.055	22:58	0.055	18.9	18.9
Vacuum Cleaner	On Mode	1.6	0:12	0.320	0:00	0.000	78.4	78.4

Table 3.13: Appliances with steady load events - value of steady load, cumulative duration and consumption during weekday operating pattern, weekend operating pattern, and annually

The load profiles described in Table 3.11 and Table 3.13 combined, along with lighting loads discussed in 3.7, to prepare appliance electrical loads profiles for weekday and weekend occupancy patterns, as presented in Figure 3.14. A comparison of appliance and lighting casual thermal gains, as driven by climate dependency of lighting discussed in Section 3.7.2, are presented in Figure 3.15.

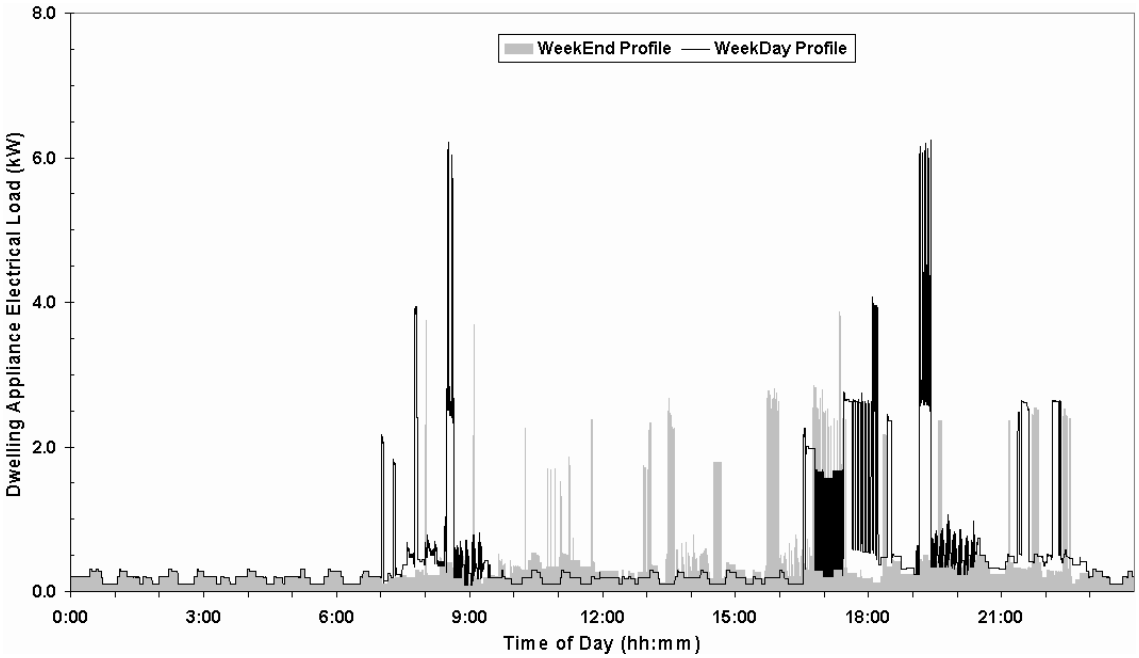

Figure 3.14: Dwelling Appliance Electrical Load Profiles for each occupancy pattern

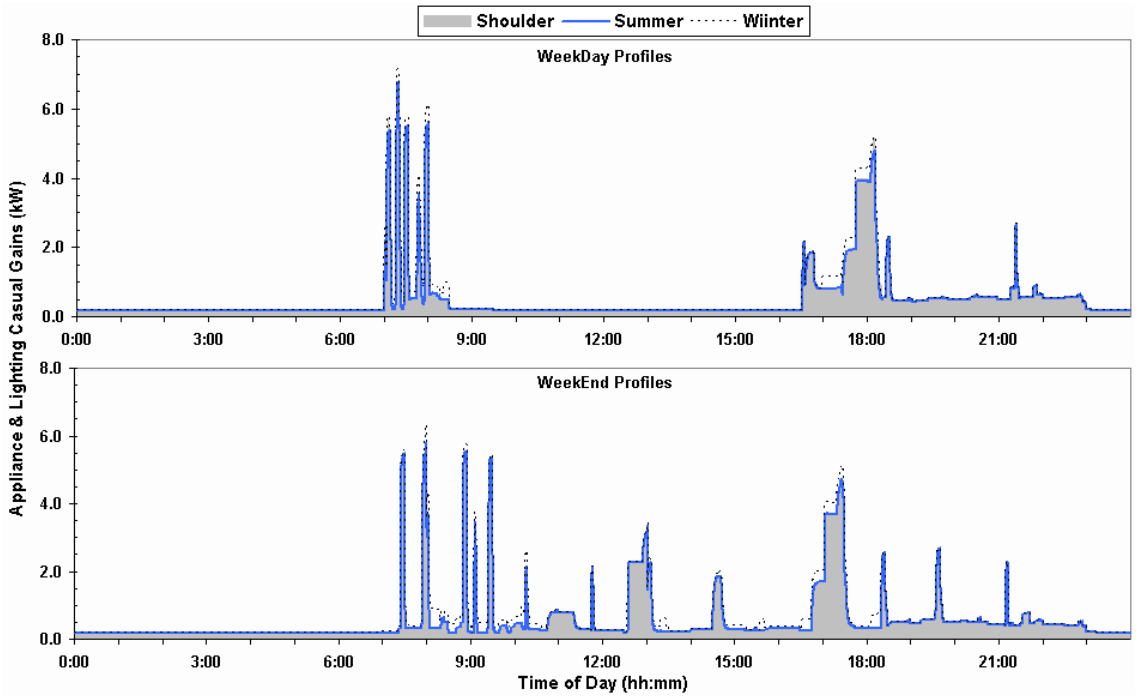

Figure 3.15: Comparison of Thermal Casual Gains from Appliances & Lighting, for Weekday and Weekend occupancy patterns

3.6.1 Burglar & Smoke Alarms

The MTP [56] reports that electrical loads range from 1-22W, operating continuously throughout the year, are typical for a home security system incorporating both burglar and smoke alarm features. It is prudent to note that MTP state that data for these appliances have large uncertainties on usage, and hence such a large range of consumption. Discussions with a home security installer [55] identified average load of approximately 2.4 watts for a modem system, which was used as the assumed consumption figure in the BIM-G model.

3.6.2 Catering

The catering appliances specified included an electric oven, gas hob, microwave oven, electric toaster and electric kettle. An electric oven was selected over a gas oven, as over 60% of households owned an electric oven by 2006 [53]. Similarly, the MTP claims that consumer preference is for gas hobs, rather than electric alternatives, with approximately 54% of households owning a gas hob by 2006 [53]. A grill for cooking was not specified, a viewpoint supported by the MTP modelling [54], where grill use is excluded due to lack of data on the utilisation of that appliance.

Mansouri & Newborough [52] identified annual electrical consumption for electric ovens (not including microwave ovens) in UK households between 130-800 kWh, with an average of approximately 400kWh. A report by the MTP [53] states that the average energy consumption per utilisation event is 1.16kWh for an energy class B rated appliance (B-rated ovens hold 76% of the 2005 market [54]). During the measurement exercise, the oven usage event consumed roughly 1.12kWh, where the oven measured did not use a standby mode. With an assumed frequency of 1 event per day, every day (except for 2 weeks holidays), the annual consumption of the electric oven in the dwelling is calculated as approximately 383kWh. This consumption is within the range identified by Mansouri & Newborough, and near the average consumption quoted by the MTP. The duration of the measured electrical load profile presented in Figure 3.16 is 46 minutes and 15 seconds. Utilisation 7 days per week results in a cumulative weekly usage of 5.4 hours, which is supported by the majority of respondents in the study by Mansouri et al [58]. The total energy consumed during operation was assumed to be released as a casual thermal gain using a decaying exponential function, as displayed in Figure 3.16.

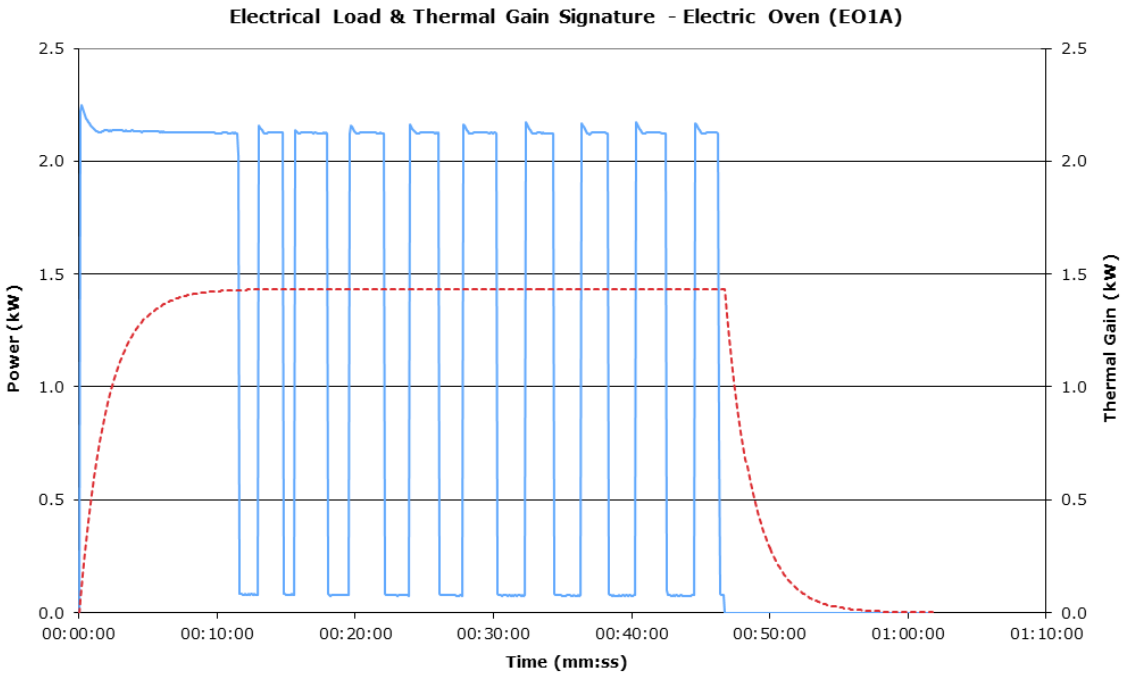

Figure 3.16: Electrical Load Profile (as measured) and Thermal Gain Profile (as estimated) of Electric Oven

The MTP [53] quote results for gas hobs from the DECADE model, produced as part of the EU SAVE project, where the average energy consumption per use as 0.9kWh. They also assume that the average number of uses per year is 424, resulting in annual energy consumption of 381.6kWh. By assuming that the hob was used once per weekday (for evening meals) and twice per day at the weekend (for lunch and evening meal), the BIM-G model incorporates 441 uses. Applying the average consumption-per-use value of 0.9kWh from MTP, the annual gas consumption calculated for the gas hob is 396.9kWh of natural gas, with zero electrical consumption (as it was assumed to have no standby load). An assumed steady output of $2kW_e$ is taken from Mansouri et al's study [58] on domestic cooking, which was used to calculate the event duration in Table 3.14. At 27 minutes, it is within the range of typical usage times (15 to 45 minutes) between "large" ($1.6\text{-}3kW_e$) and small ($1\text{-}1.5kW_e$) hobs quoted by Wood & Newborough [47]. As the gas hob operates by combusting gas in the open, the thermal gain to the dwelling airspace, as presented in Figure 3.17, was assumed to follow the start and stop pattern of the hob's gas consumption. It is acknowledged that some energy may be stored in the material of the hob itself, and released slowly over time, however this is assumed to be minimal compared to the energy released by the combustion products.

Gas Usage & Casual Thermal Gains Signatures	
Description	$2kW_e$ Steady Load – same values for casual thermal gain
Event Duration (hrs)	0:27:00
Event Energy (kWh)	0.9000
Qty of Events in WD Scenario	1
WD Scenario Energy (kWh)	0.9000
Qty of Events on WE Scenario	2
WE Scenario Energy (kWh)	1.8000
Annual Energy (kWh)	**396.9**

Table 3.14: Appliance Event Energy Consumption (Natural Gas), Event Duration and Event Thermal Gain, with cumulative values calculated for each occupancy pattern and annually

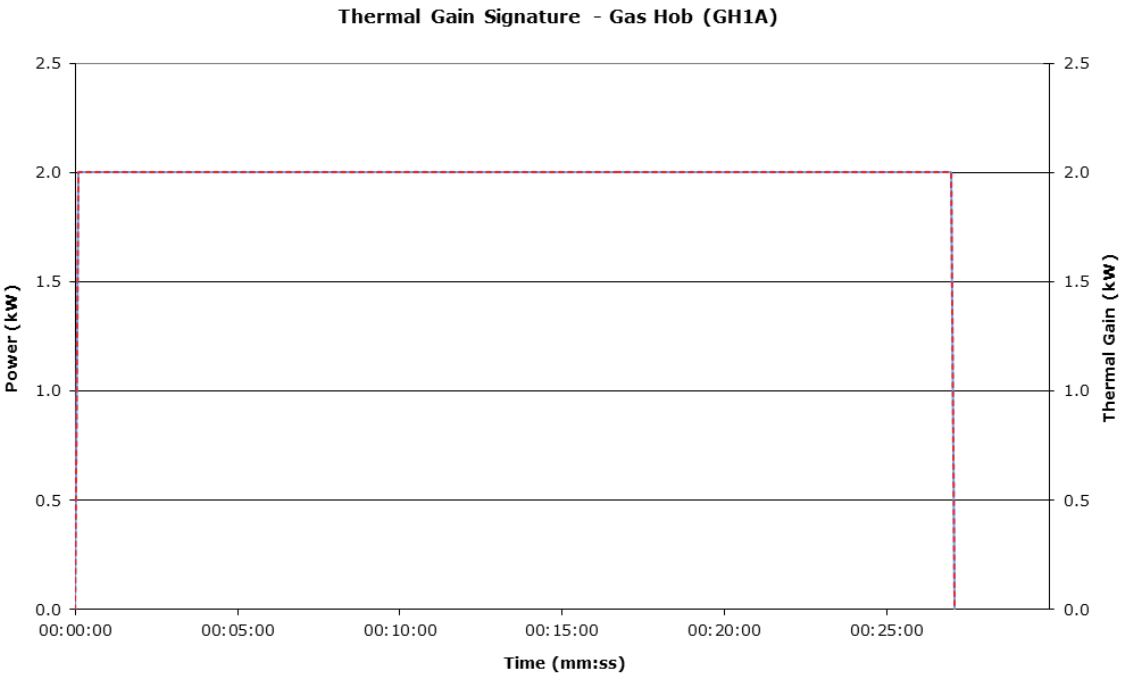

Figure 3.17: Thermal Gains Profile estimated for Gas Hob

In 1995, Herring [59] discussed the average annual energy consumption of electric toasters, quoting a figure of 12kWh. However, the DECADE model [60] reported the steadily increasing energy consumption of electric toasters from 1970 to 1992. It was unclear whether this was due to increasing penetration (EST [61] claim that 80% of household own toasters by the mid-2000s), increasing load of typical toasters, or increased usage. It was assumed that the toaster was used twice, every day, at breakfast time. A toaster was monitored during operation at the mid-point setting, with a load as presented in Figure 3.18. The event duration of 2.5 minutes was consistent with typical usage of 2-10 minutes quoted by Wood and Newborough [47]. The total energy consumed during operation was assumed to be released as a casual thermal gain using a decaying exponential function, as displayed in Figure 3.19.

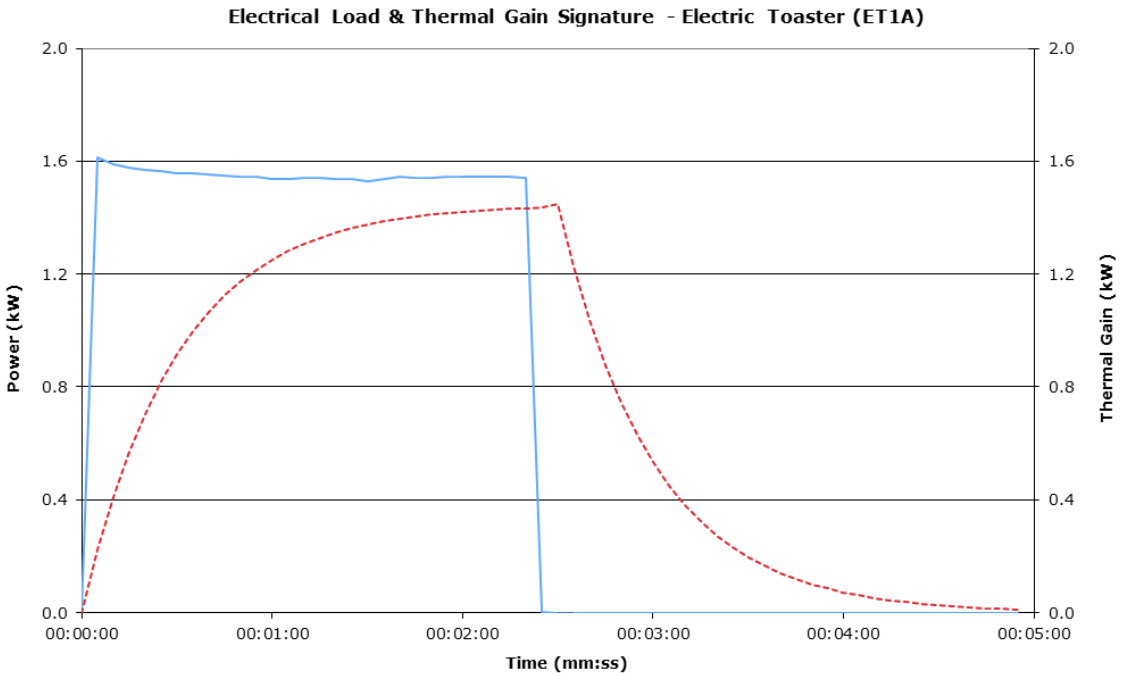

Figure 3.18: Electrical Load Profile (as measured) and Thermal Gain Profile (as estimated) of Electric Toaster

Mansouri & Newborough [49] estimated the average annual electricity consumption of microwave ovens as 75 kWh per household, whilst MTP report [51] that the DECADE model uses 87kWh and the MTP model uses 91kWh. Data from MTP [53] suggests that standby consumptions range from 2W to 6W, whereas the MTP model [53] uses a standby figure of 2.6W. This compared with a 5W standby load measured for a sample appliance. A 7 minute event duration was selected to agree with data collected by Mansouri et al [58], where the majority of usage for the main meal was in the range of 5 to 10 minutes, and other categories, such as “cooking vegetables”, “warming up” and “defrosting”, were dominated by responses in the <5 minutes and 5-10 minutes ranges. Using the measured appliance electrical load profile for a 7 minute event, as shown in Figure 3.19, the casual thermal gain was estimated by assuming that the total electrical energy consumed during the event was released in a manner characterised by a decaying exponential function. Assuming the microwave oven is used once per day, and that it remains on standby for the remaining time, annual consumption of the microwave oven in the dwelling was calculated as 80kWh.

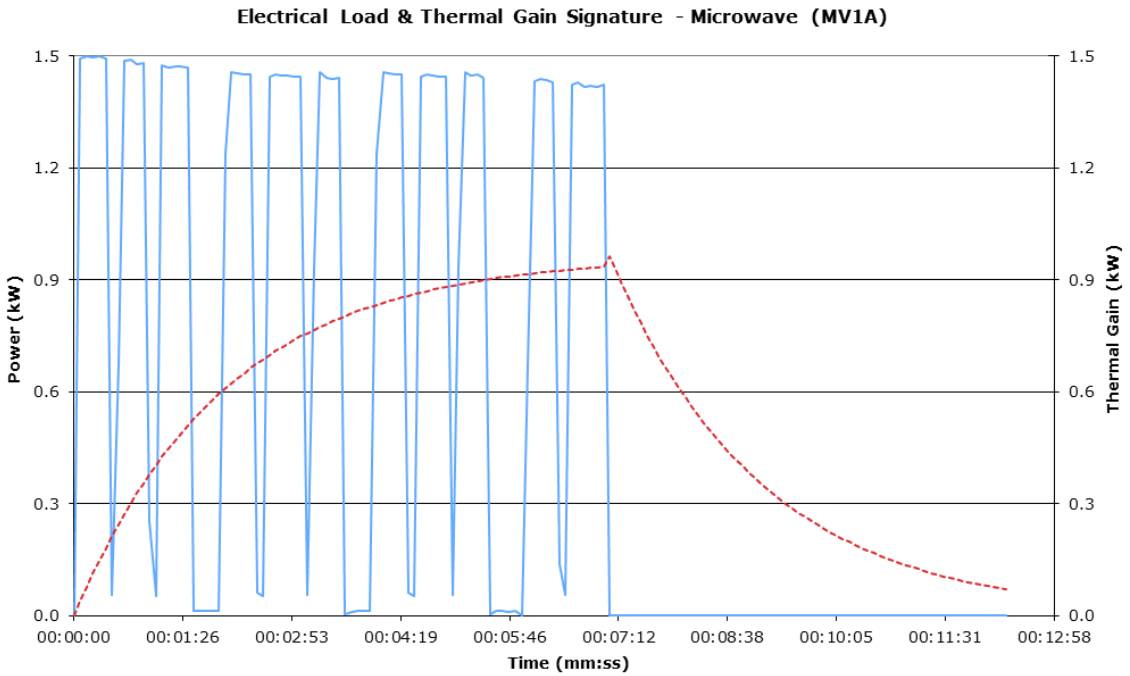

Figure 3.19: Electrical Load Profile (as measured) and Thermal Gain Profile (as estimated) of Microwave oven during a usage event (i.e. not during standby)

A 1994 study by Mansouri et al [58] found that the average annual consumption of electric kettles has remained steady at 250kWh per household since 1987, whilst the MTP estimate of 169.6kWh [50]. Wood & Newborough [47] quote kettle usage event durations in the range of 2-5 minutes. Load profiles were measured for a cold kettle (i.e. several hours since it was last used), filled from the kitchen tap with cold water to both full (Figure 3.20) and half capacity (Figure 3.21). The duration of these events was 2.5 and 5 minutes respectively. A narrative was defined that incorporated an even split between event types (half and full capacity), with 4 during a weekday and 6 at the weekend. This resulted in 1,568 events per annum, which was consistent with the MTP's assumption of 1,542 events per year [50]. The annual consumption of the electrical kettle in the dwelling was calculated as 186.5kWh, between the two estimates discussed above. As before, a decaying exponential function as used to estimate dissipation of input energy as thermal gain. This assumption does not account for the proportion of thermal energy that is contained within the liquid ingested the occupants, and then later dissipated in the dwelling and elsewhere.

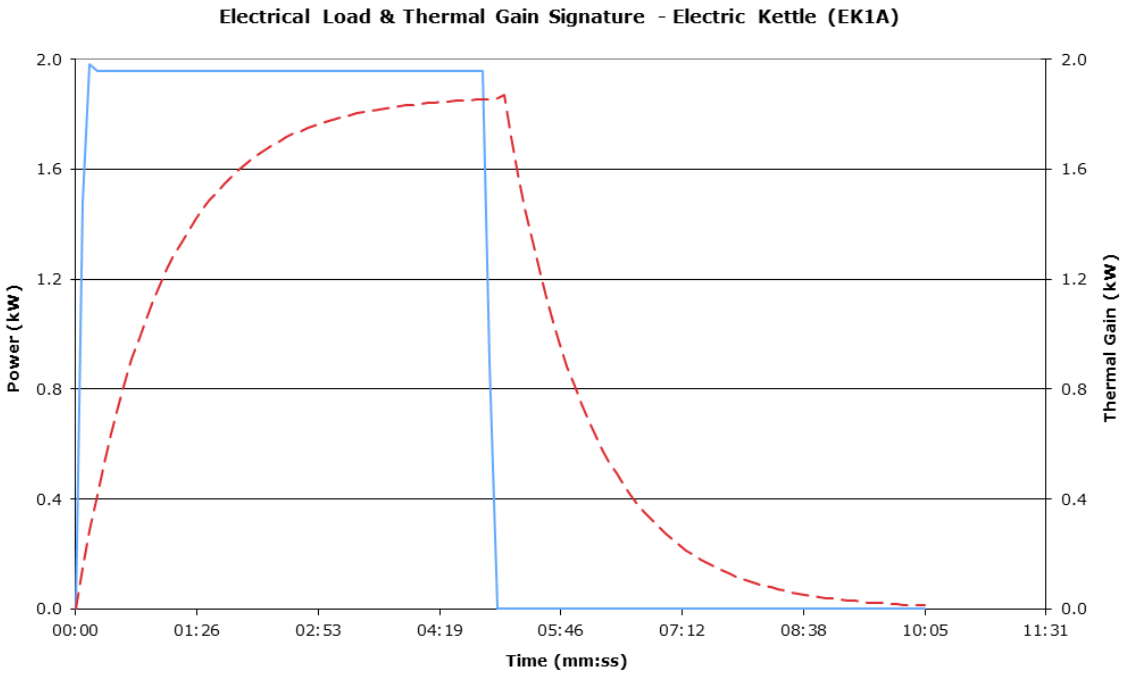

Figure 3.20: Electrical Load Profile (as measured) and Thermal Gain Profile (as estimated) of Electric Kettle filled to full capacity

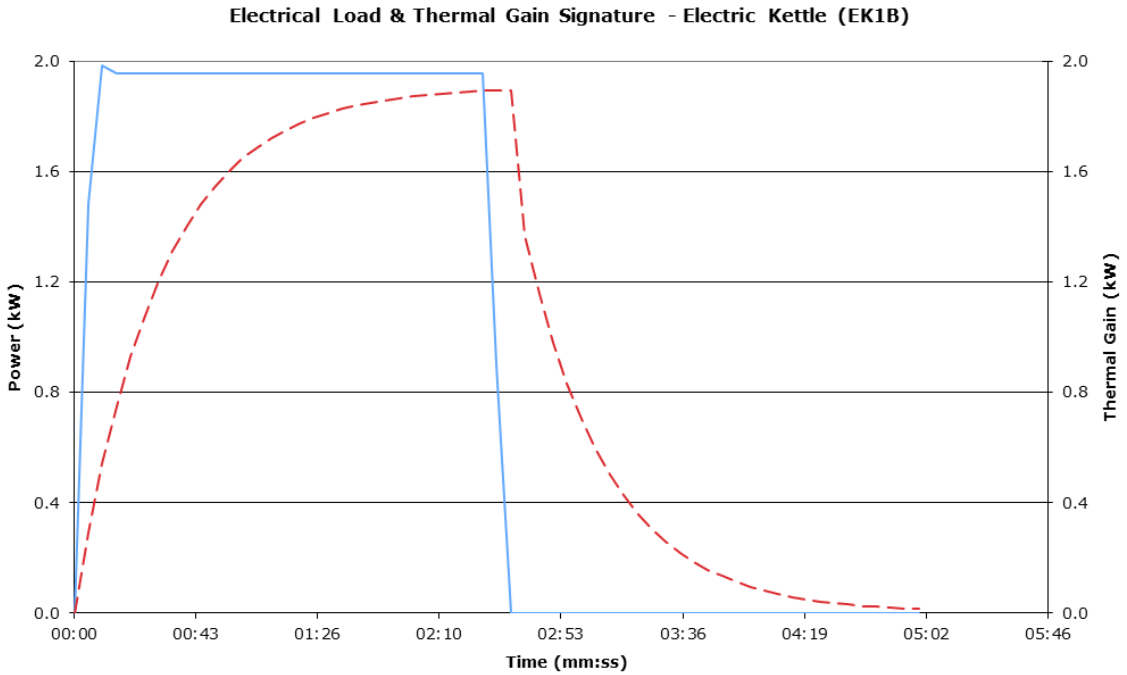

Figure 3.21: Electrical Load Profile (as measured) and Thermal Gain Profile (as estimated) of Electric Kettle filled to half capacity

3.6.3 Electric Shower

For the primary demand scenarios, an electric shower was selected for use within the dwelling, as an MTP policy brief [77] quoted that around 50% of UK dwellings have electric showers. It is assumed that each occupant takes a 5 minute shower, once per day, every day of the week. This usage pattern agrees with shower utilisation profiles created by Jordan & Vajen [76], which were based upon consumption studies carried out in Switzerland and Germany. It is assumed that 25% of electrical energy input is realised as a casual thermal gain to the dwelling, as estimated within the BREDEM model [74], where again a decaying exponential function has been used to characterise casual gain. The exponential time constant was derived using temperature logging data for an electric shower, as presented in Figure 3.23, where the exterior of the shower device's casing was monitored before, during and after a 5 minute shower usage event.

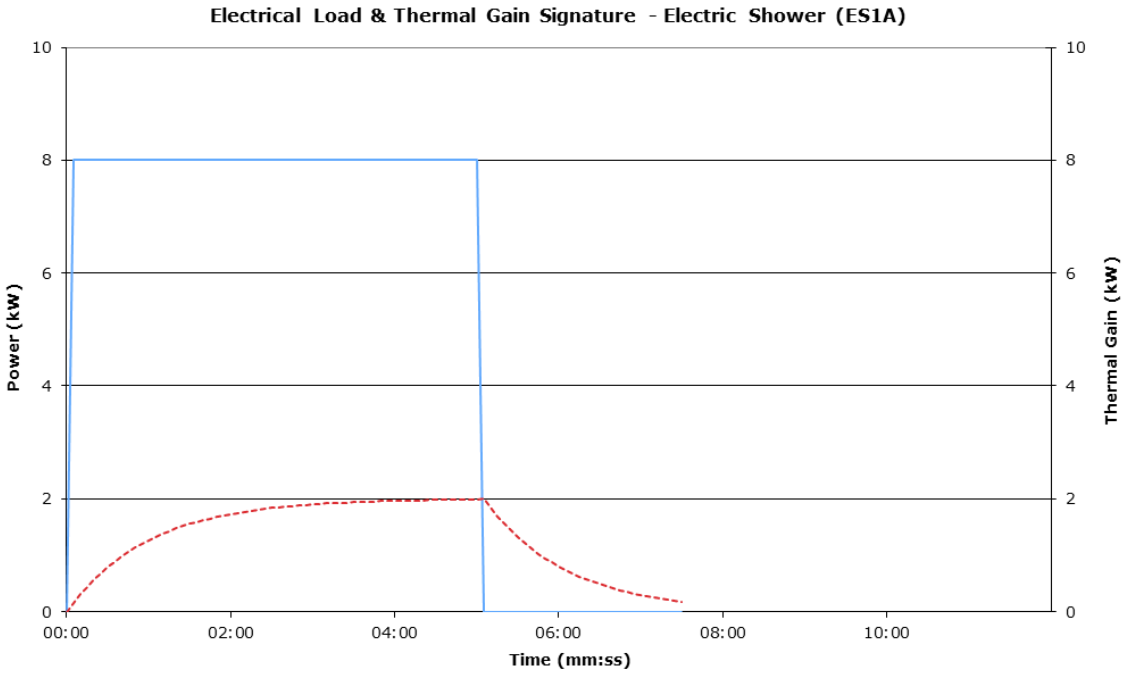

Figure 3.22: Electrical Load Profile (as measured) and Thermal Gain Profile (as estimated) of Electric Shower

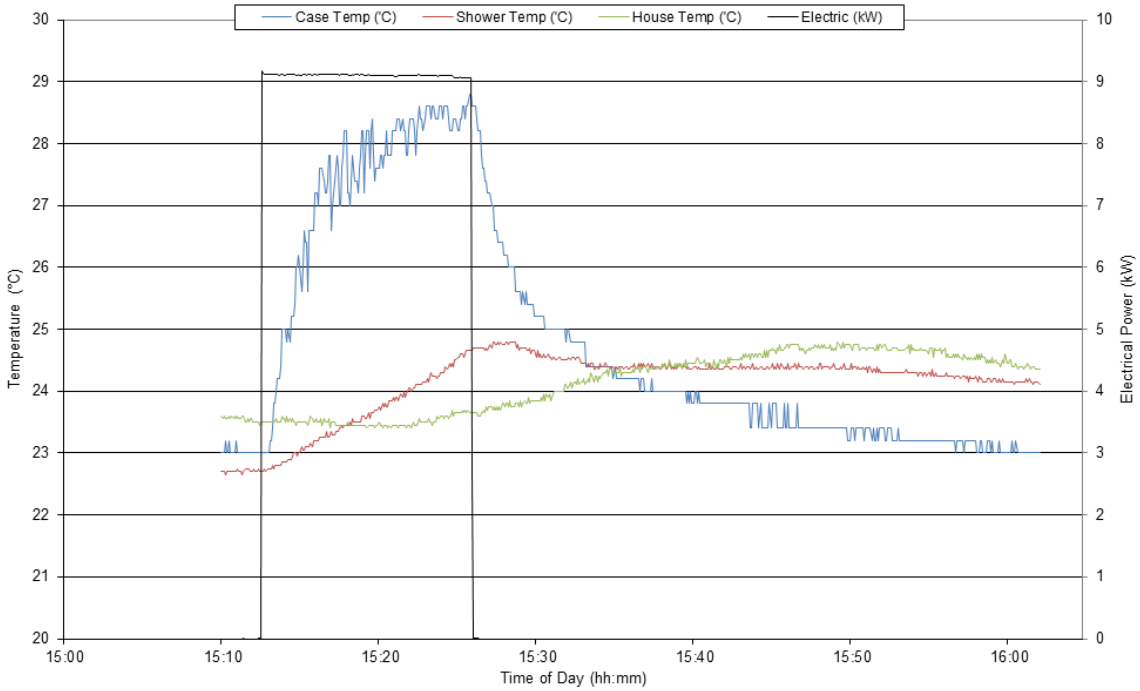

Figure 3.23: Temperature monitoring results for electric shower

3.6.4 Hair Care

Electrical load profiles for a hair dryer and a set of hair straighteners were measured, as presented in Figure 3.24 and Figure 3.25. Research undertaken on hair dryers and hair straighteners for the TARBASE project [5] suggested that average annual energy consumption of each appliance was 36kWh. It is assumed that this consumption is split evenly between each working day, for each appliance. From the event consumptions calculated in the monitoring exercise, the annual consumption of the hair dryer and hair straighteners is calculated as 21kWh and 31kWh respectively. Usage patterns of twice per day (corresponding to two occupants) for both appliances were assumed, where hair drier use precedes hair straightener use. There is no issue with timing between events of the same appliance, as it is assumed that the dwelling contains two of each hair care appliance.

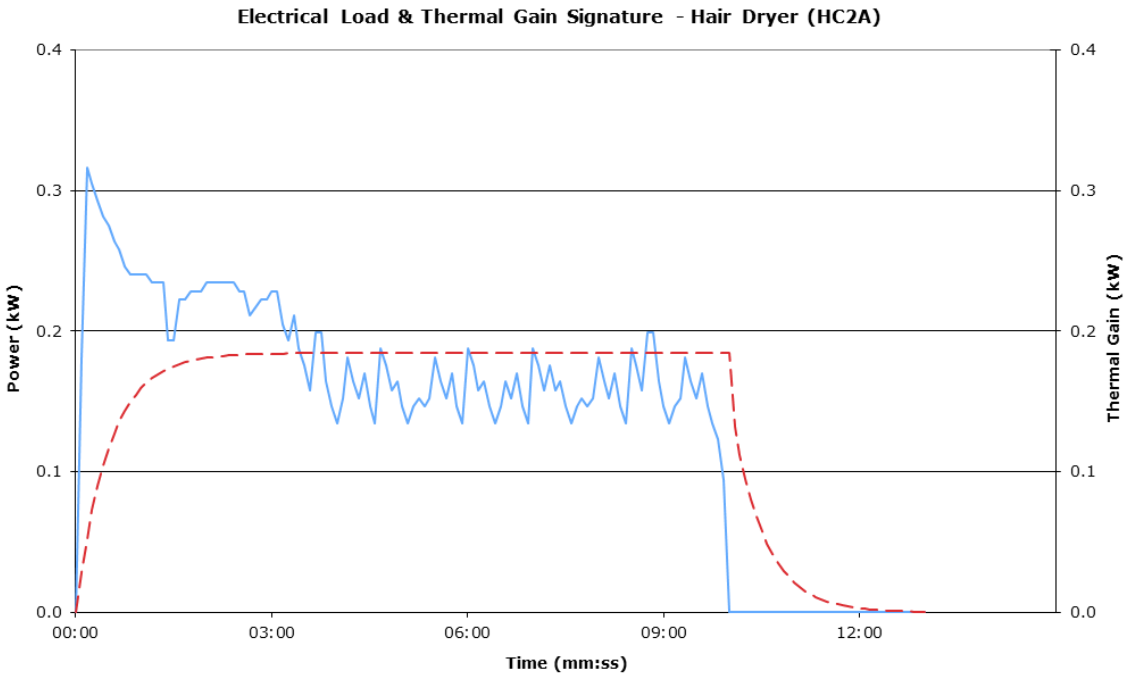

Figure 3.24: Electrical Load Profile (as measured) and Thermal Gain Profile (as estimated) of Hair Dryer

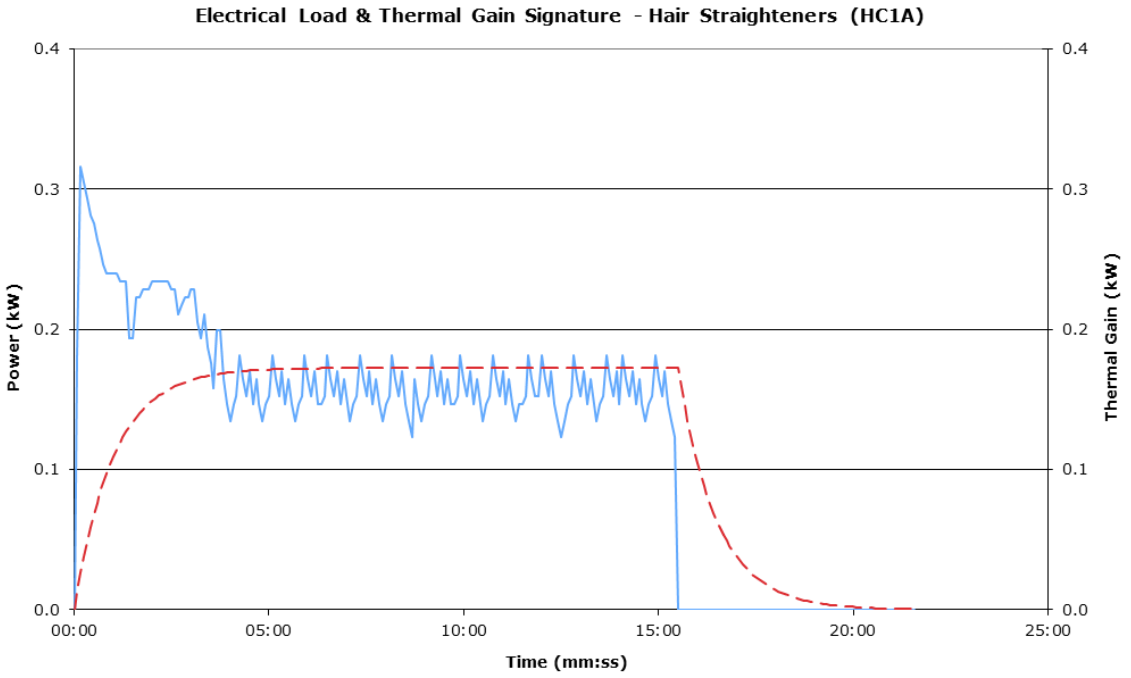

Figure 3.25: Electrical Load Profile (as measured) and Thermal Gain Profile (as estimated) of Hair Straighteners

3.6.5 Home Care & Laundry

Data extracted from a MTP report [65] indicates average annual consumption of 284.5kWh for a dishwasher. The annual consumption calculated from a measured appliance electrical load signature (Figure 3.26 as 292.4kWh, assuming 1 wash cycle per day. The assumed wash cycle frequency is supported by the study by Mansouri et al [58], which suggests that over 50% of household utilise their dishwasher in that manner. It is assumed that the dishwasher has no standby loads, as it is several years old, and the MTP report [65] suggests that only newer dishwashers exhibit standby loads. An MTP study on casual thermal gains from appliances [78] concluded that wet appliances, including dishwashers, dispose of 95% of electrical energy consumed through the wastewater outlet. Using surface temperature measurements of a dishwasher in-situ, decaying exponential equations were derived to characterise the heating and cooling of the dishwasher's external casing, and estimate the thermal gain profile based on 5% of electrical consumption, as presented in Figure 3.26.

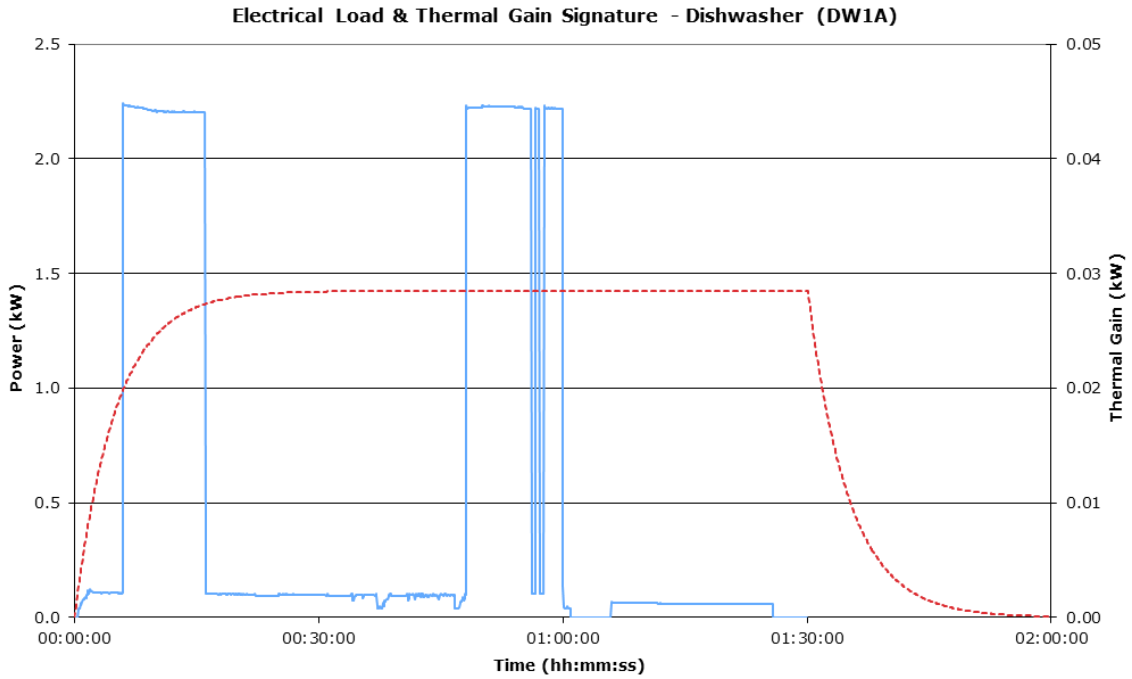

Figure 3.26: Electrical Load Profile (as measured) and Thermal Gain Profile (as estimated) of Dishwasher

The MTP [66] indicate that the annual electrical consumption of washing machines is 192kWh or higher, depending on energy rating of appliance. They also claim that

washing machines have an average standby load of 2.1W. The annual consumption of the washing machine in BIM-G is calculated as 209kWh, using the measured electrical load profile presented in Figure 3.27, and assuming 1 wash cycle per day. This usage assumption is within the distribution of wash cycles per household presented by Mansouri et al [58]. The 5% useful thermal gain to the dwelling was taken from an MTP study on casual appliance gains [78].

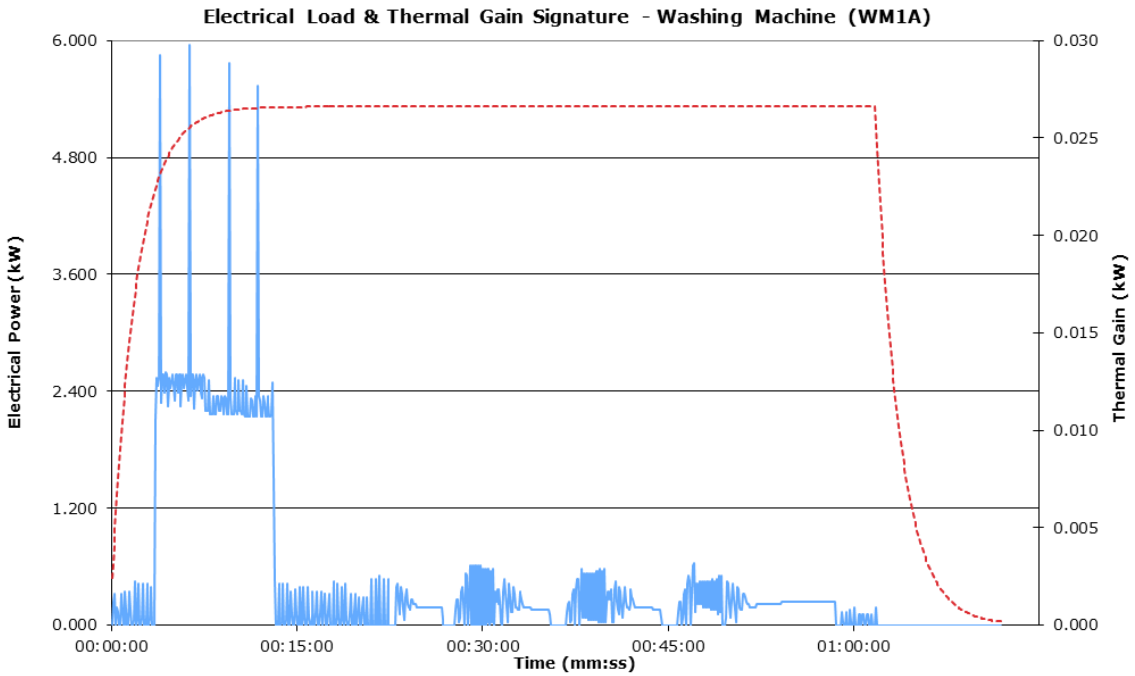

Figure 3.27: Electrical Load Profile (as measured) and Thermal Gain Profile (as estimated) of Washing Machine

The MTP [67] indicates that the average annual consumption of Tumble Dryers is 318kWh, with no standby loads on older appliances. The annual consumption of the tumble dryer in the dwelling is calculated as 318.6kWh, based on the measured load profile presented in Figure 3.28, and 1 event per day. The usage pattern was assumed to match with the washing machine's cycles, as limited data exists to quantify number of cycles [67]. The 5% useful thermal gain to the dwelling was taken from an MTP study on casual appliance gains [78].

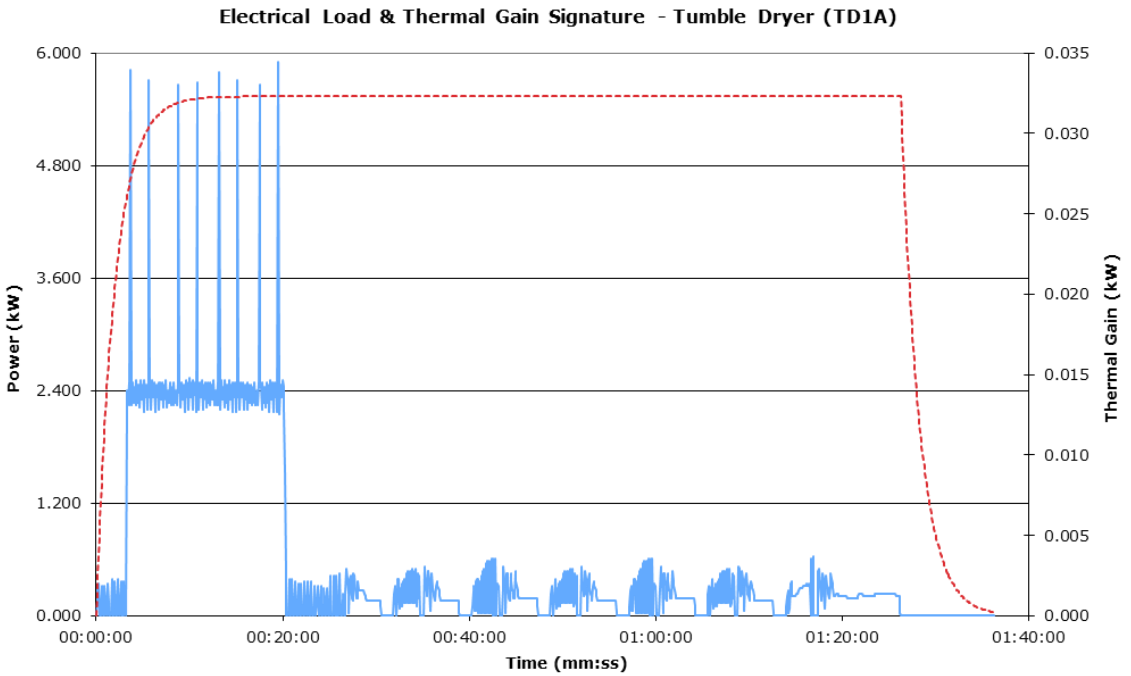

Figure 3.28: Electrical Load Profile (as measured) and Thermal Gain Profile (as estimated) of Tumble Dryer

The MTP [62] report that vacuum cleaners are used approximately 1 hour per week, with an average load of 1.6kW during operation. Within the MTP report, no holiday allowance has been used, resulting in a calculated annual consumption of 83kWh. The annual consumption of the vacuum cleaner in BIM-G is calculated as 78.4kWh, based on 2 weeks of annual holiday for the occupants. The estimated weekly usage from the MTP report [62] was divided equally between the working days, to provide 12 minutes of continuous usage per day. An argument could be made to split this usage, as the vacuum cleaner is moved around the home, but similarly, it could be argued that a different area of the dwelling is vacuumed each day. A continuous electrical load profile of 1.6kW$_e$ is used to represent this appliance's electrical load signature, as spot appliance measurements have demonstrated this to be the case.

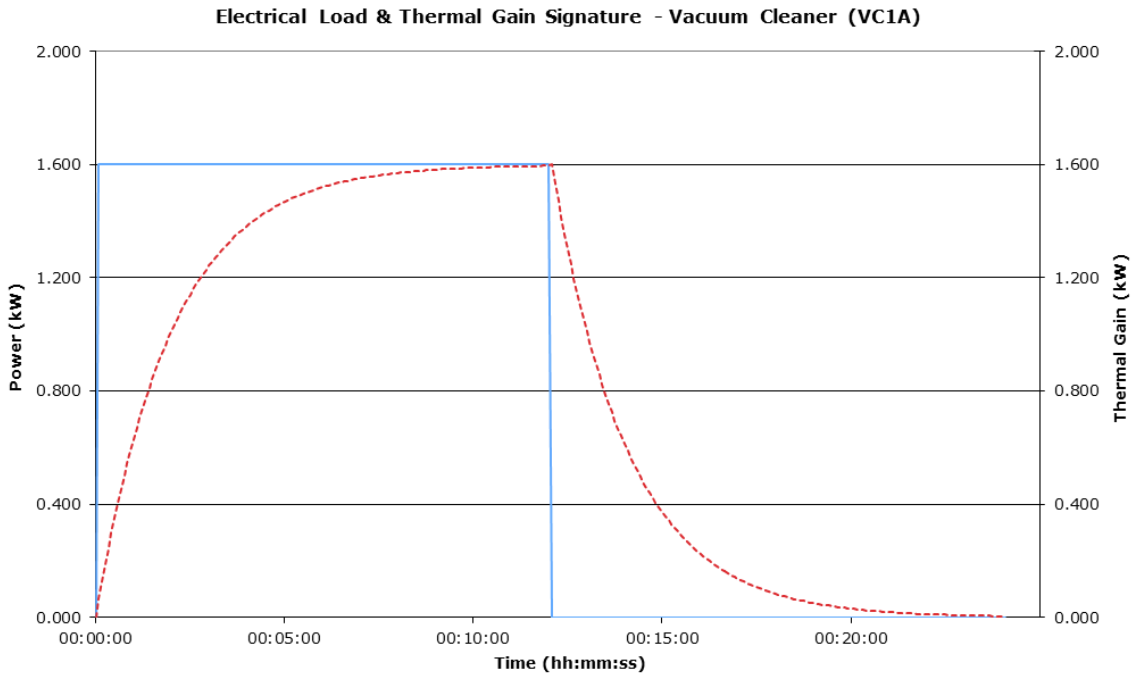

Figure 3.29: Electrical Load Profile (as estimated) and Thermal Gain Profile (as estimated) of Vacuum Cleaner

Herring [59] reports that the average annual energy consumption of electric irons is 75kWh. The energy consumption of a measured appliance usage event, as presented in Figure 3.30, is 0.31kWh. Assuming that this consumption is split evenly between each working day, with consideration for 2 weeks annual holiday, the annual consumption within the BIM-G model is 76kWh. As with the dishwasher, surface temperature measurements were used to derive exponential time constants for decaying exponential function to represent heating and cooling curves of the appliance. Assuming that all of the electrical consumption is dissipated as heat, the thermal gain profile for this appliance was estimated as presented in Figure 3.30.

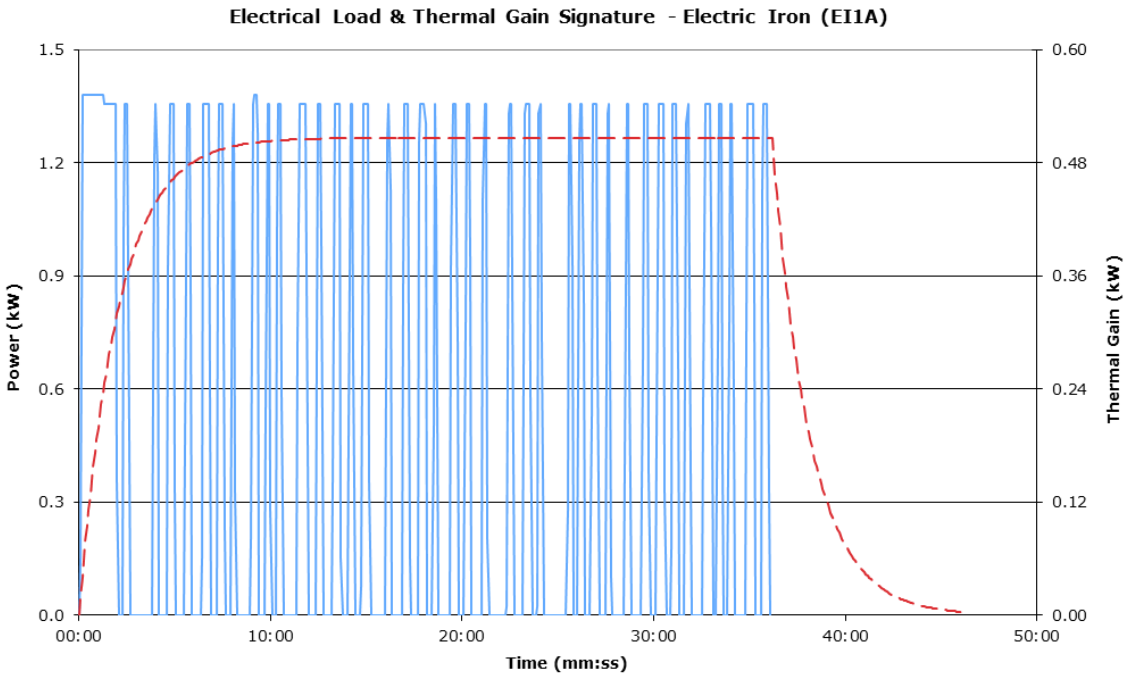

Figure 3.30: Electrical Load Profile (as measured) and Thermal Gain Profile (as estimated) of Electric Iron

3.6.6 Home Electronics & ICT

Several MTP reports [68][69] present results of various studies on television numbers and energy consumption by technology type. The 3 televisions were selected for the dwelling, as supported by [68], which quotes TV ownership of 2.4 to 2.9 per home. As the dwelling is heavily occupied and houses a fairly prosperous household, the selection of 3 TVs is not unreasonable, and is applied to other research [3]. Furthermore, the report [68] states that there is typically a primary TV, with a screen size greater than 24" (LCD appliance in this demand profile), and secondary TVs, with screen sizes below 24". The usage figures of 6.5 hours per day for primary televisions, and 2.5 hours per day for secondary televisions, were extracted from the MTP report [68] discussed previously. The energy consumptions in standby and operating modes were taken from an MTP report [69] that covered televisions on a technology-by-technology basis.

MTP reports [63] that digital decoders are commonly left turn on 24 hours per day, all year, with an average electrical load of 8.56W. Electrical load measurements of a sample device confirmed that the load remained fairly steady of 10.6W, which was

applied in the BIM-G model. Information on the annual energy consumption of DVD Players was very scarce in 2006. A load monitoring exercise showed that a sample DVD player consumes 1.7W in standby. The annual consumption of the DVD player in the BIM-G model was calculated using this measurement, assuming 24-hour constant standby operation. Research undertaken on VCRs for the TARBASE project found that annual energy consumption is 84kWh [5]. A continuous electrical load profile is used to represent this appliance's electrical load signature, as measurements of this appliance suggest a standby load equal to the annual energy consumption.

Research undertaken on powered audio for the TARBASE project suggested standby loads of 10W, and average daily usage from around 1 hour. Using electrical load monitoring equipment, several powered audio systems were logged in FM Tuner, CD Player and Standby modes. A MTP report [56] supports the standby loads measured within this exercise. Three powered audio appliances were chosen: a communal device and two assigned to individual occupants (the child and young adult). The electrical load signatures used to represent these appliances were continuous loads, with associated continuous thermal gains profiles.

The MTP [56] report that the average (over 24 hours) energy consumption of a clock radio is 1.5W, resulting in annual consumption of 12.1kWh, assuming that the appliance is operated all year round, with no holiday interruption. The annual consumption of the alarm clock in the BIM-G model is assumed to equal that quoted by MTP. A continuous profile has been selected; even though MTP states that electrical load can rise to 4W (from the continuous 2.3W), as the difference is insignificant compared to electrical demands totalling several kW_e in the dwelling.

Research undertaken on games consoles chargers by TARBASE [5] found that they consume 105kWh annually. MTP report [56] on standby consumption states that standby loads are between 0 and 12.5W. Load measurements were undertaken on a sample games console, as presented in Figure 3.31. Annual consumption of the games console in the dwelling is calculated as 65.5kWh, with consideration of reliance of television operation. Although significantly less than the TARBASE figure, a range of

consumptions are assumed due to the spread of utilisation and unit energy consumption of such a device.

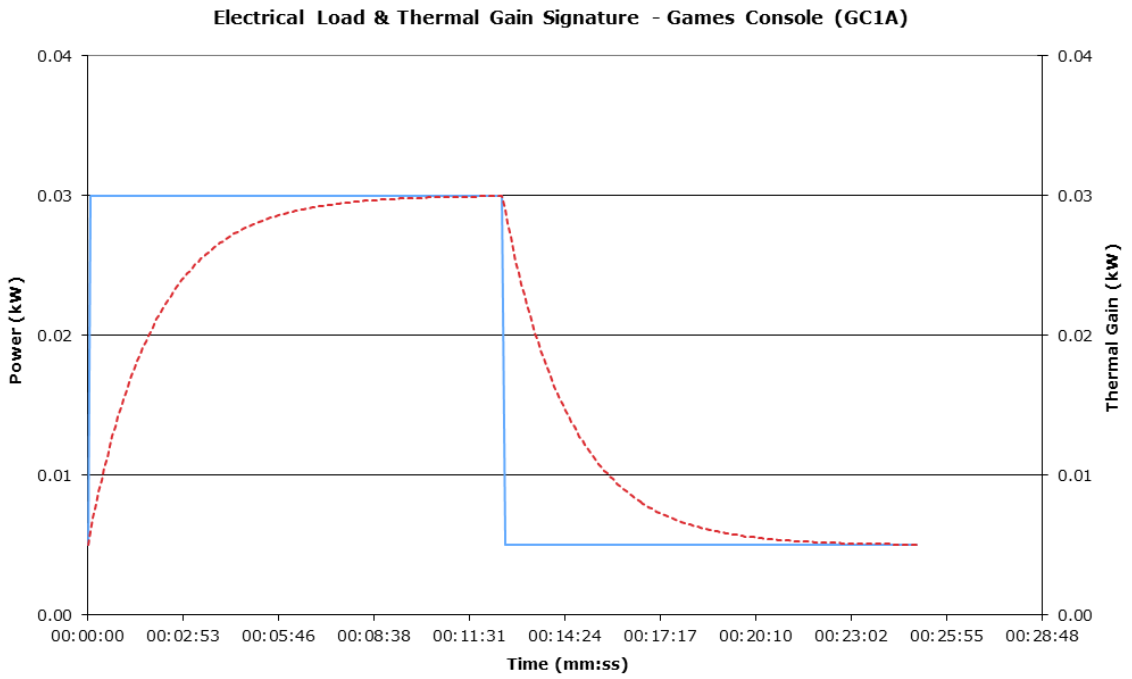

Figure 3.31: Electrical Load Profile (as measured) and Thermal Gain Profile (as estimated) of Games Console

There were two laptops defined for the dwelling variant. The EU Energy Star website's energy calculator for PC equipment quotes an annual energy consumption of 33kWh for a laptop. This annual consumption figure was used in the BIM-G, assuming 24 hour continuous operation for the charger.

Research undertaken on broadband access devices for the TARBASE project quotes an MTP report [64], specifying 31kWh. This was used as the annual consumption of the broadband access device in the dwelling, where a continuous, constant electrical load profile is used to represent this appliance's electrical load signature.

The MTP [56] report that mobile phone chargers have a standby load of 1W. This was verified by appliance monitoring, and electrical loads during charging were measured as 4W. The annual consumption of the household's stock of 4 mobile telephone chargers, used for an average of 8 hours every night, is calculated as 65.9kWh.

Research undertaken by the TARBASE project estimated the annual energy consumption of cordless telephones as 35kWh [5]. The annual consumption of the telephone in the BIM-G model was calculated using the TARBASE figure, and assuming 24-hour continuous operation.

3.6.7 Refrigeration

The MTP [57] presented sales-weighted average energy consumptions, by energy efficiency rating, for fridge-freezers and freezers in 2006, based from energy label daily consumption figures (i.e. lab testing not actual consumption in use). They report that fridge-freezer energy consumption varies between 206kWh (A++ rating) and 278.9kWh (A rating). The electrical load profile of a sample fridge-freezer was measured for 24 hours, hence incorporating the standby loads. From the measured load profile in Figure 3.32, the annual consumption of the fridge freezer was calculated as 247kWh.

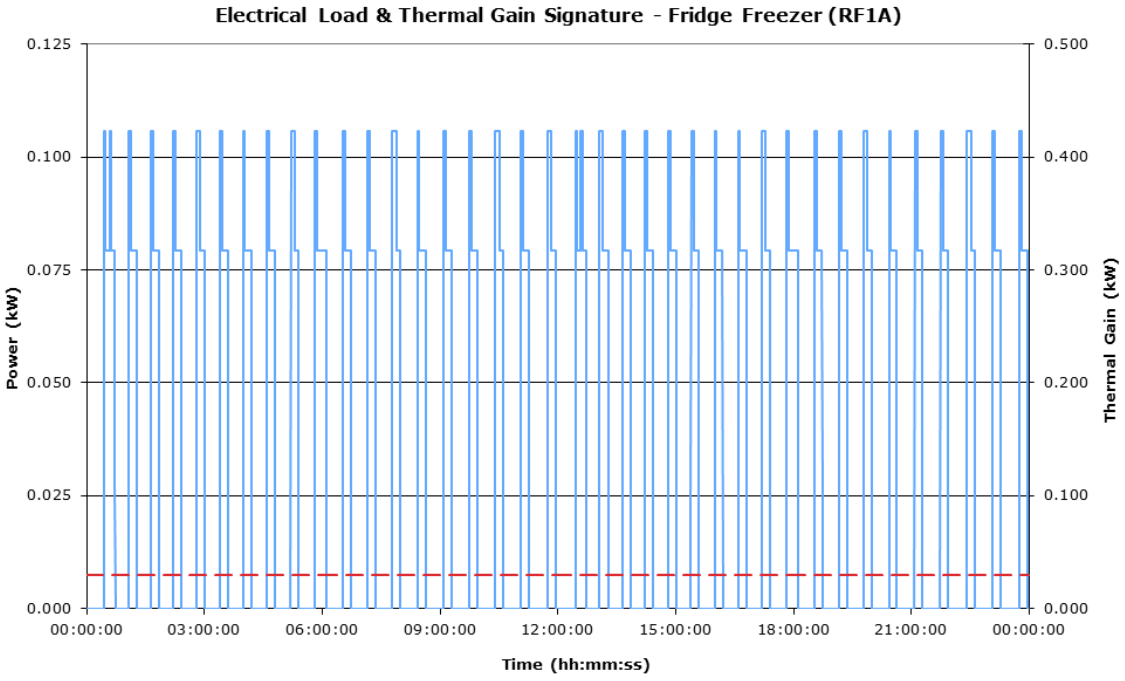

Figure 3.32: Electrical Load Profile (as measured) and Thermal Gain Profile (as estimated) of Fridge Freezer

The MTP reported 2006 sales-weighted average energy consumption of freezers in the UK was 299kWh, with average consumption, per energy rating, ranging from 153-612kWh [57]. The standby loads are incorporated into the measured electrical load

signature (see Figure 3.33), as a 24-hour measurement was logged continuously, resulting in an annual consumption of 446kWh.

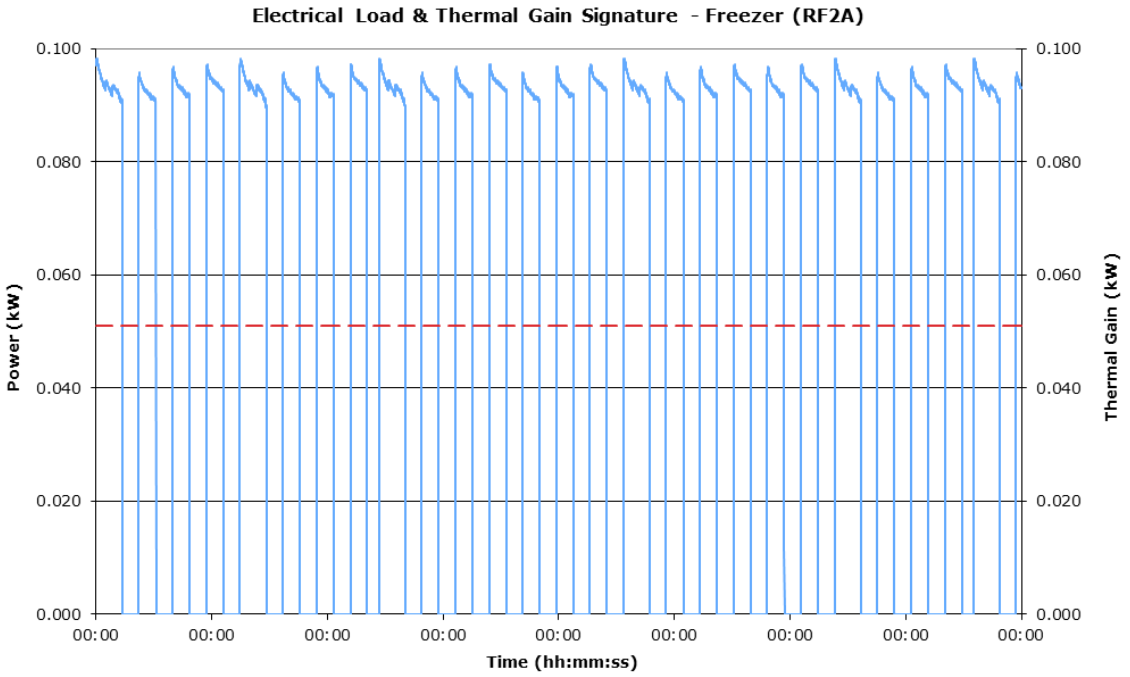

Figure 3.33: Electrical Load Profile (as measured) and Thermal Gain Profile (as estimated) of Freezer

3.7 Lighting

Lighting is estimated to account for 17% of UK domestic electricity consumption, as estimated at a national level by DECC [23]. Despite the concerns regarding the accuracy of this figure in Section 3.6, lighting is still expected to be a major contributor to electrical demand. The derivation of lighting demand as discussed in this section was undertaken for the TARBASE project [5][6], and used in other published studies [3]. Domestic electrical load modelling was discussed in Section 3.6, in all of which the timings of individual lighting loads are derived from some form of probability distribution. As a narrative of occupant activities is defined within the BIM-G methodology to script events for discrete design days, the probabilistic approach used by other studies [33][35] would be unsuitable.

Stokes et al [33] discuss the relationship between lighting demand and time of day on a typical weekday, which is characterised by a peak on the morning and evening, corresponding with peak activities within the home. They conclude that no linear relationship existing between lighting demand and time of day because of the influence of daylight and the behaviour of the occupants, however behaviour of a set of occupants tends to follow a regular pattern day-to-day. As discussed in Section 3.6, occupancy drives energy consumption patterns, which Richardson et al [35] acknowledge as essential for lighting, as they tend not to be operated independently of occupants (like a washing machine on timer, for instance). In their stochastic lighting load model, Richardson et al [35] weight the frequency of use towards rooms most frequently in use at certain times (i.e. kitchen and ding room at meal time or bedrooms in the late evening). This is discussed further in Section 3.7.2.

Stokes et al [33] consider annual distribution of lighting demand to have a stronger link with climate profiles, and link lighting usage to sunrise and sunset in their load model. Richardson et al [35] agree that human perception of natural light level in a building is a key factor in the usage of electric lighting, as supported by Yao & Steemers [24]. This discussed in the context of seasonally-dependant lighting in Section 3.7.2.

Although there is data available on the distribution of lighting technologies in use in the domestic sector, major studies such as those used by the MTP [70] are pre-year 2000. Attempts to project from MTP using Mintel sales data [72] were unsatisfactory, as they do not account for lamp replacement rates or increased lamp numbers per dwelling. The assumptions for lighting fixtures present in each variant were made, not in an attempt to represent an average home, but to replicate a plausible dwelling. This approach was necessary to avoid the distortion of results that is systematic of “averaged” data, gleaned from stock models and the like, and to avoid dependence on outdated data. A similar approach was taken by Richardson et al [35], where they randomly selected a representative set of lighting units of different technologies from trade association statistics. On a basis of assumed income and occupant stereotype, the building variant was arbitrarily chosen to have implemented the energy efficient lighting technologies (i.e. compact fluorescent lamps and low voltage halogen

spotlights) to a different extent. It is worth noting that the lighting demand profile assumptions were made in 2004/05, before energy efficient lighting technologies were as prevalent as today, partially because of legislation banning certain General Lighting Service (GLS) lamps from sale in the UK [71].

3.7.1 Lighting Requirements & Technologies

There are three main requirements for lighting provision in a dwelling; minimum illuminance levels, minimum colour rendering index (CRI) and colour temperature (CCT). Light is not only a requirement for safety and use of household amenities, but for the perceived comfort of the occupants. The accepted measure of light provision is the average light delivered (lumens) per unit area of the dwelling (m^2), which is typically referred to as the lux level (1 lux = 1 lumen/m^2). The distribution and control of light are important factors in comfort.

The required lighting provision in each zone of the dwelling is quoted in industry design guides [73], along with daily average hours of lighting expected in that dwelling zone, and these are presented in Table 3.15. The light intensity required from the light source in each zone was calculated using the floor area of each zone multiplied by the minimum required illuminance.

Dwelling zones	Minimum Illuminance (lux)	Zone Floor Area (m^2)	Light Intensity (Lumens)	Light Usage (hrs/day)	Minimum CRI	Suitable CCT
Hall	150	8	1,200	4	>80 (Allows accurate colour judgements to be made)	"Warm" light preferable (Ideally around 3,000K)
Lounge	150	36	5,400	3.9		
Landing	150	8	1,200	3.5		
Dining	100	8	800	1.9		
Kitchen	300	20	6,000	1.5		
Bedrooms	50	48	2,400	0.9		
Bathrooms	150	16	2,400	0.5		

Table 3.15: Light requirements of each dwelling zone, as derived from CIBSE design guide [73] and calculation of required light intensity from minimum illuminance level and floor are of each zone

The lighting technologies considered when defining a lighting demand profile are presented in Table 3.16. It was assumed that the vast majority of light, as of 2005, was

supplied by GLS incandescent bulbs, due to their overwhelming market share [70]. In an attempt to limit the myriad of lamp options for the simple lighting model, GLS lighting was represented solely by a 60W lamp, as it was the predominate GLS lamp [70]. The circuit efficacy (lumens per total watt input), light point power (lamp + ballast), light output, CRI and CCT assumed for all 2005 lighting technologies are shown in Table 3.16

Lighting Technology	Circuit Efficacy (lm/W)	Circuit Power (W)	Lamp Output (Lumens)	Colour Rendering Index	Colour Temperature (K)
GLS	13	60	780	90-100	2800
Low Voltage Halogen	20	25	500	90-100	3000
CFL	55	18	1098	80-100	~3000

Table 3.16: Lighting technologies considered in the definition of the lighting demand profile

Several energy efficient technologies, that were still fairly niche in 2005, were defined, namely Low Voltage Halogen and Compact Fluorescent Lamps (CFL). The performance of these technologies was chosen to reflect average values [70]. The resultant requirement for light was calculated using utilisation factor, as defined in the design guides [73] as the amount of light from lamp directed towards useful illumination of room & occupant's activities. The resultant lighting loads, lamp rating and annual energy consumption is presented in Table 3.17

Dwelling Area	Floor Area (m^2)	CIBSE Illum. (lux)	Light Intensity (Lumens)	Use per Day (Hrs)	Bulb Type	Util. factor	Lamp Load (W)	Daily Energy Consumption (Wh)	Annual Energy Cons. (kWh)
Hall	8	150	1200	4	CFL	0.7	40	87.3	48
Lounge	36	150	5400	3.9	CFL	0.7	100	382.9	208
Landing	8	150	1200	3.5	CFL	0.7	40	76.4	42
Dining	8	100	800	1.9	GLS	0.7	60	116.9	64
Kitchen	20	300	6000	1.5	Halogen	0.7	300	450.0	245
Bedrooms	48	50	2400	0.9	GLS	0.7	180	166.2	90
Bathroom	16	150	2400	0.5	GLS	0.7	180	92.3	50

Table 3.17: Lighting requirement, and resultant loads and energy consumption for dwelling

3.7.2 Scheduling & Climate Dependency of Lighting Demand

The lighting script was written to reflect the activities of the occupants, as described by the occupancy patterns described in Section 3.3.1, specifically the periods of active

occupancy by each occupant as tabulated in Appendices B.2.1 and B.2.2. The lighting electrical load profiles for the weekday and weekend occupancy patterns, during the Winter or Extreme Winter climate scenarios, are presented in Figure 3.34 and Figure 3.35 respectively, based on the script of lighting events tabulated in Appendix B.2.5. The adopted spread of lighting usage is consistent with that reported by Hawkes et al [18] in their µCHP modelling exercise. On weekdays, the majority of lighting usage is for bathroom, kitchen and bedrooms in the morning. In the late afternoon and evening, lighting use is expected to transition from the kitchen (to prepare evening meal), to the dining room (to eat), and then to the living room and bedrooms (for leisure time and bedtime routines).

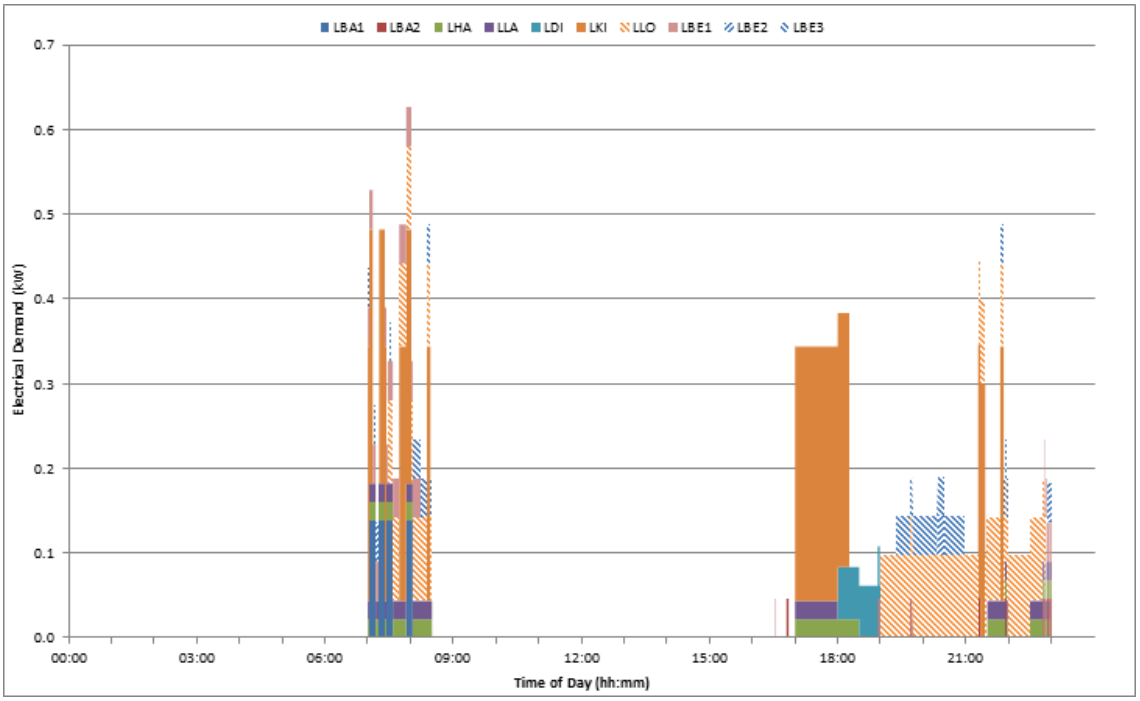

Figure 3.34: Lighting electrical demand profile for primary demand scenarios using weekday occupancy pattern and winter or extreme winter climate scenarios

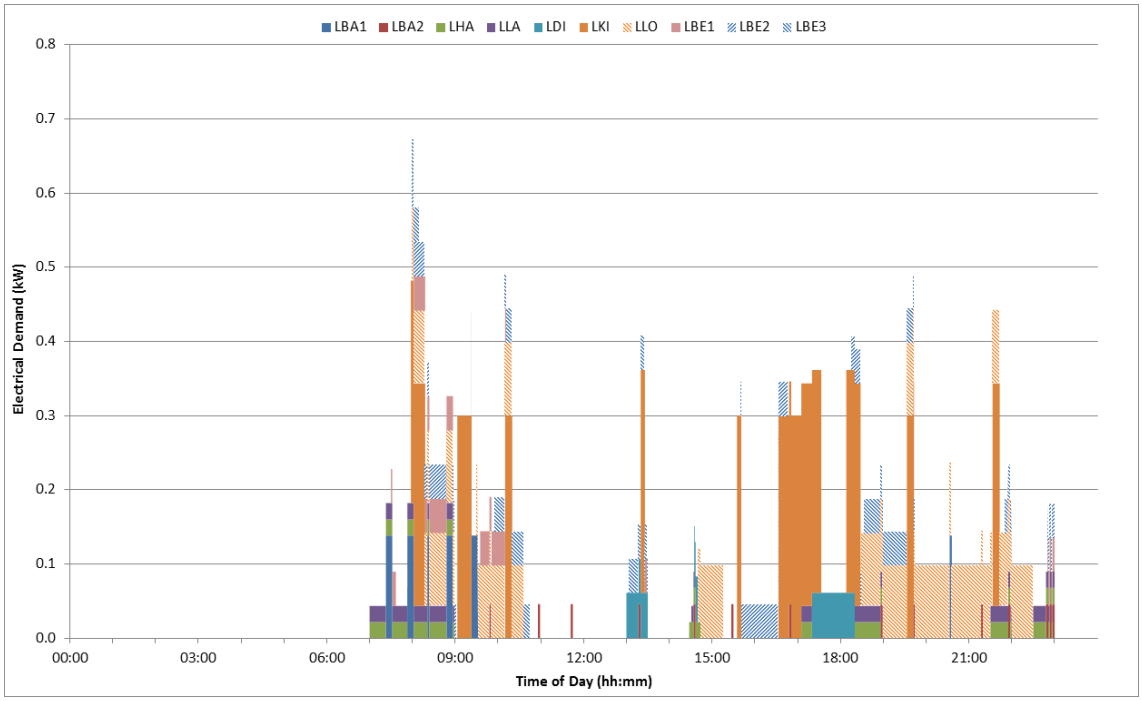

Figure 3.35: Lighting electrical demand profile for primary demand scenarios using weekend occupancy pattern and winter or extreme winter climate scenarios

A climate dependency was introduced within the lighting demand profiles, as it was understood that lighting demand is a function of daylight [33][35]. It should be noted that lighting usage is also a strong function of occupant behaviour, i.e. despite sufficient daylight an occupant may leave a light on or turn it on out of habit. However, seasonal dependence of lighting demand was a simple method to introduce a limited degree of variation in electrical demand profiles between seasons, due to the scarcity of data to support seasonal dependence assumptions for the appliances discussed in Section 3.6.

Climate	Daylight Start Time	Daylight End Time	Hours of Daylight	Reduction vs. Summer	Impact on Weekday (hh:mm:ss)	Impact on Weekend (hh:mm:ss)
Summer & High Summer	05:56:18	17:55:22	11:59:04	-	-	-
Shoulder	06:22:22	17:46:49	11:24:27	00:34:37	00:08:33	00:08:33
Extreme Winter & Winter	09:05:32	14:52:22	05:46:50	06:12:14	02:55:22	05:08:32

Table 3.18: Times of sufficient daylight levels to forego artificial lighting, for each climate scenario, with relative durations compared to summer scenarios for each occupancy pattern

On the basis that the occupants will forego the use of artificial lighting when sufficient daylight is available, the lighting electrical demand profiles for both weekday and weekend profiles were adjusted using the daylight times in Table 3.18. These profiles are plotted for both occupancy patterns in Figure 3.36, comparing the climate scenarios.

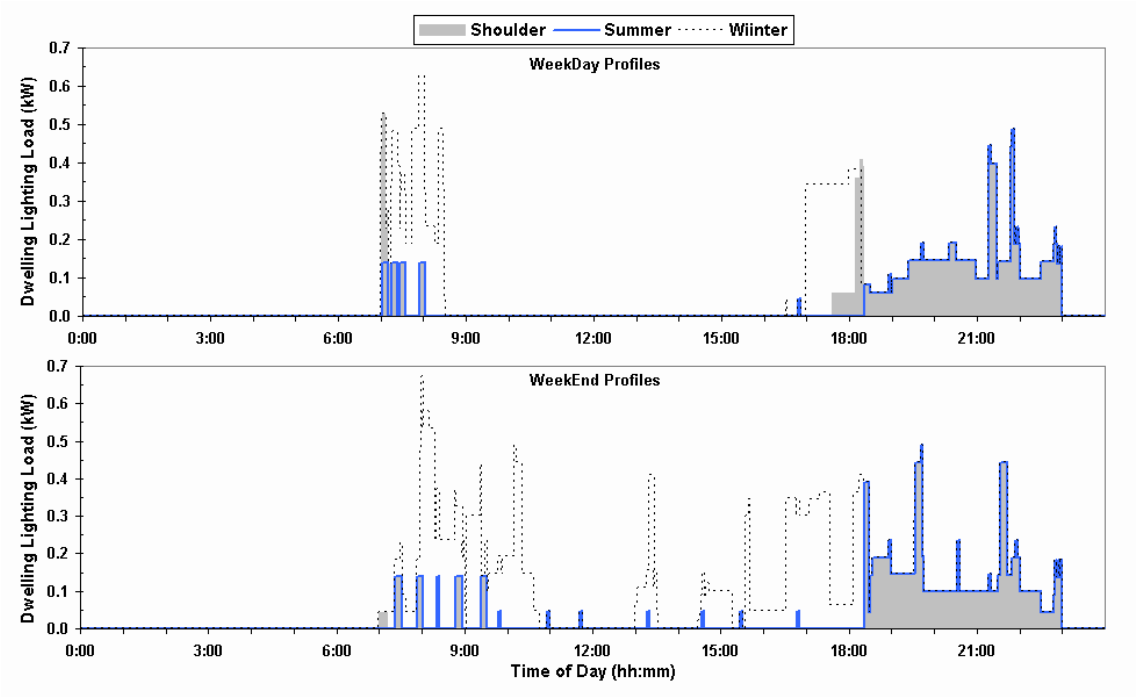

Figure 3.36: Comparison of Seasonal Lighting Profiles, for Weekday and Weekend occupancy patterns

3.8 Climate Scenarios

The climate data was derived from CIBSE Test Reference Year 2005 for Edinburgh, which is a composite of typical months of climate data from the period 1983 to 2004 [39]. These CIBSE Test Reference Year data files have been used on the TARBASE project for 14 locations around the UK. The climate dataset includes hourly values for external dry bulb air temperature, and both global and diffuse solar irradiance on a horizontal surface. The former variable is used directly by the BIM-G model's Thermal Demand Estimation routine, whilst a solar irradiance model was developed, based on CIBSE [40] and ASHRAE [41] methodologies, to utilise the latter variables. This model

estimates solar irradiance on the vertical surfaces of the dwelling, in each of the primary compass directions, from the CIBSE climate dataset's solar variables.

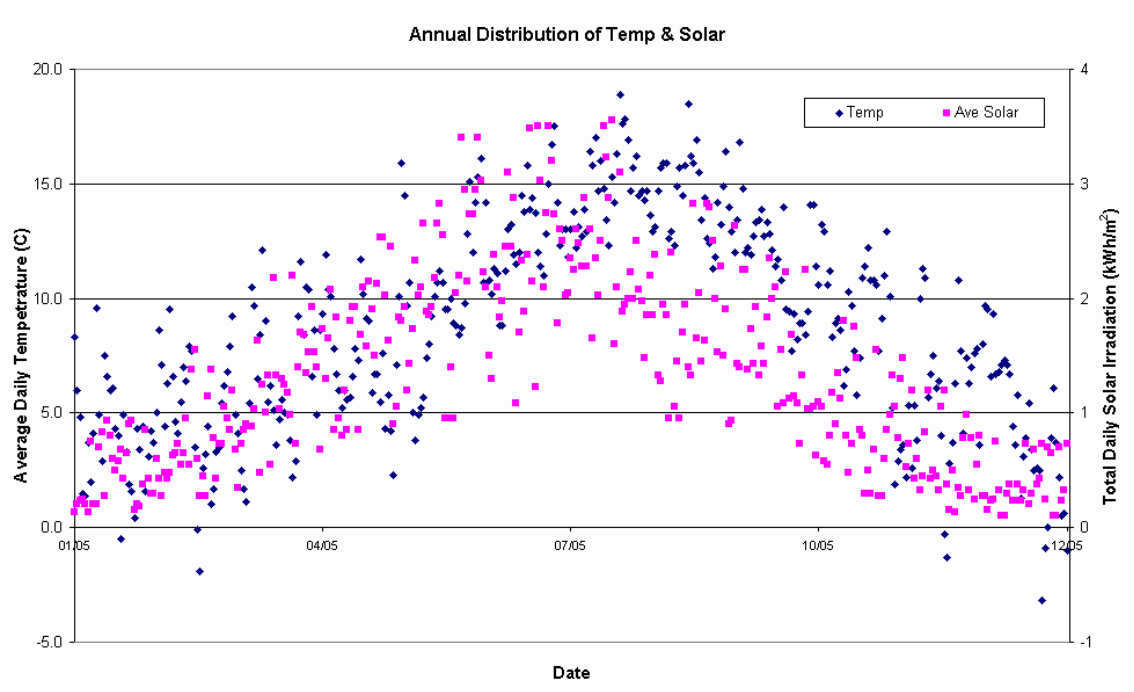

Figure 3.37: Distribution of Climatic Variables, Daily Averaged External Dry Bulb Air Temperature and Daily Total Orientation Averaged Solar Irradiance, for CIBSE Test Reference Year 2005, Edinburgh

If the daily average of the external dry bulb air temperature is calculated, and plotted alongside the total orientation-averaged Solar Irradiance values for the selected annual climate dataset, a distinct distribution of each variable is seen (Figure 3.37). In order to understand the relationship resulting from the interaction of these climatic variables, on the daily space heating demand of the dwelling, a relationship was derived, using results (Table 3.19) from BIM-G simulations undertaken using a range of synthetic daily climate profiles. These synthetic profiles were constructed from 7 daily solar profiles, and 7 daily external temperature profiles, all of which are evenly distributed across the appropriate range of climatic variable values.

	Daily Total Solar Irradiance (kWh/m^2)						
Daily Averaged External Air Temperature (°C)	**0.5**	**1**	**1.5**	**2**	**2.5**	**3.0**	**3.5**
-3.2	109.0	102.6	96.2	90.3	84.3	78.5	70.6
-0.9	97.7	92.5	86.8	80.8	76.2	68.6	60.6
3.1	78.8	73.7	67.7	61.6	56.0	49.6	41.7
6.9	61.1	56.1	49.3	43.7	36.5	30.9	22.9
10.9	41.7	37.9	29.3	23.8	17.2	11.6	5.9
14.8	20.7	14.0	12.4	8.0	7.1	0.0	1.9
18.8	8.7	5.7	2.6	2.0	0.0	0.0	0.0

Table 3.19: Daily Space Heating Thermal Demand (kWh), as simulated by BIM-G model, for each Synthetic Climate Profile described by a value of both Daily Total Solar Irradiance and Daily Average External Air Temperature, investigated for the Weekday Occupancy Pattern

Using a multiple linear regression technique and the solver function in MS Excel, equation (3.2) was derived to characterise the aforementioned relationship. The Simulated Daily Space Heating Thermal Demand (kWh), Q_{SHd}, is a function of Daily Average External Dry Bulb Air Temperature (°C), T_{eda}, and Daily Total Orientation Averaged Solar Irradiance (kWh/m^2), S_{da}.

$$Q_{SHd} = -0.02T_{eda}^{\ 2} - 0.597S_{da}^{\ 2} - 4.584T_{eda} - 10.09S_{da} - 0.01\left(S_{da} \times T_{eda}\right) + 98.951 \qquad (3.2)$$

When quantifying the statistical robustness of this equation in comparison to the matrix of simulated data in Table 3.19, it is important to consider the significance of those matrix values equal to zero. The detailed simulation results for these synthetic climate profiles show that average internal temperatures during TDPs can exceed the comfort and space heating set-point temperatures. In effect, the occupants may wish the dwelling to be cooled during these days, i.e. the space heating thermal demand may be negative. In reality, this cooling may be achieved by increasing the ventilation rate of the building, for instance by opening windows. As the simulations results presented in Table 3.19 quantify the gross demand for space heating only, and not a net thermal heating and cooling demand, they are limited to a minimum value of zero. The derived relationship, however, is not limited in kind, so statistical analysis should be confined to results greater than zero, in order to gain an accurate measure of statistical robustness. With such an argument in mind, Figure 3.38 shows the coefficient of determination (R^2) correlation between simulated and calculated results,

using equation (3.2), is 99.85%, in comparison to 96.58% if such reasoning is overlooked.

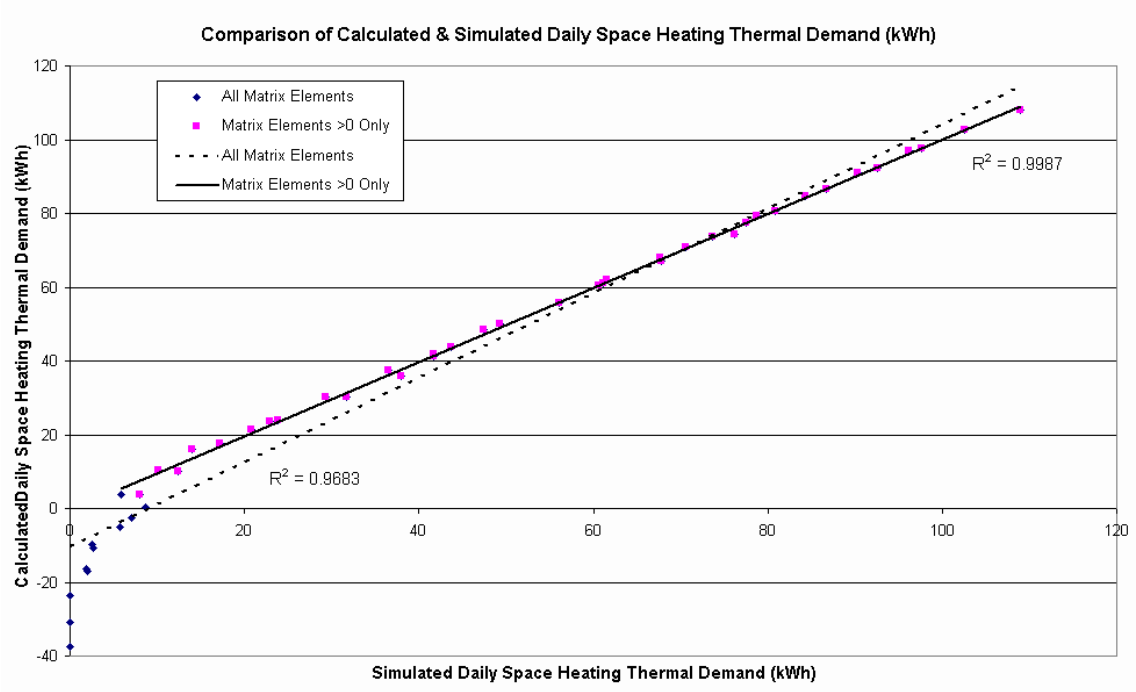

Figure 3.38: Comparison of Calculated and Simulated Daily Space Heating Thermal Demand (kWh), plotted for all synthetic climate profiles described by the values of Daily Total Solar Irradiance and Daily Average External Air Temperature in Table 3.19 (referred to as matrix values), with trend lines for all matrix values and for matrix values that are greater than zero

Equation (3.2) was then applied to the daily-averages for the climate dataset to produce an annual distribution of space heating thermal demand, see Figure 3.39, as simulated using the weekday occupancy pattern only. It should be noted that for approximately 10% of the year, or around 36 days, the building exhibits zero space heating demand or less, if the space heating system attempts to achieve 21°C throughout the TDPs. If this period was to be taken as the length of this non-heating season, it would be in disagreement with Dickson et al [42] who assumes heating season lengths of 3-4 months, depending on climate, and both Hawkes et al [18] and De Paepe [45] who assume 3 months in their modelling exercises. It is assumed, after analysis of average dwelling temperatures in BRE's Domestic Energy Fact File [43], that during the summer months, people may tolerate internal temperatures below the nominal comfort temperature for portions of the TDPs, as a result of disabling their

space heating system, and allowing the dwelling internal temperature to free-float. Without adequate data to quantify the tolerance of occupants to free-floating, a study was undertaken to ascertain the sensitivity of heating season length to changes in the minimum tolerable daily average internal air temperature, calculated across the TDPs of a simulation profile.

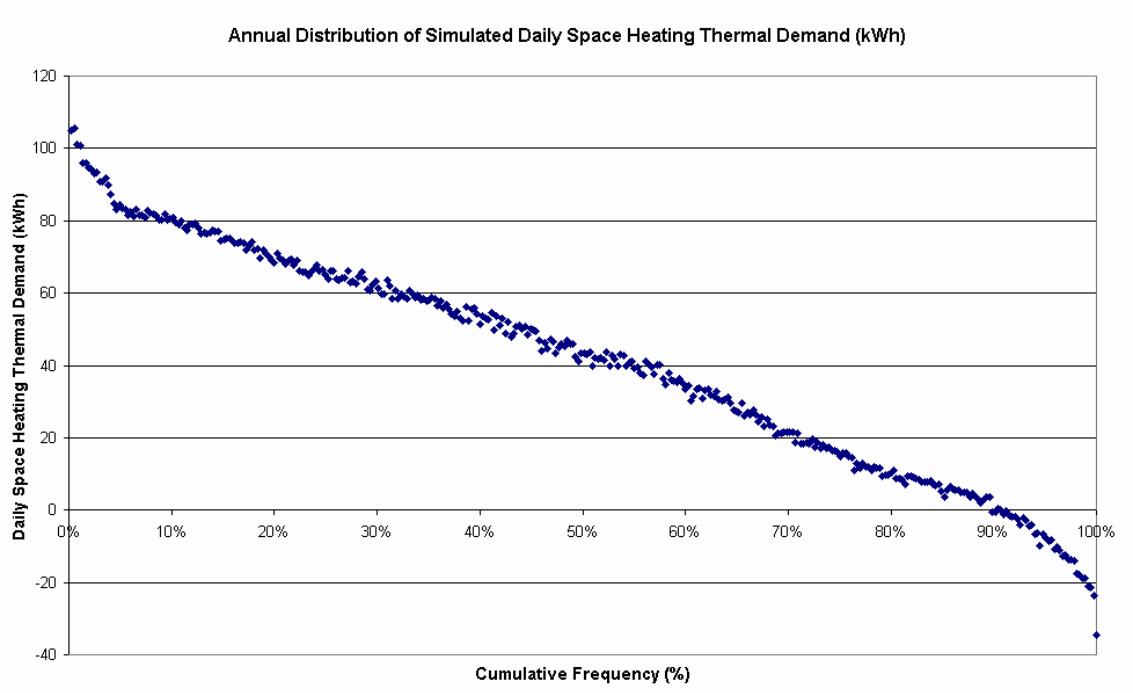

Figure 3.39: Annual Distribution of Calculated Daily Space Heating Thermal Demand (kWh), for the Weekday Occupancy Pattern, using the relationship defined in equation (3.2)

The aforementioned study entailed re-simulation of the synthetic climate profiles tabulated in Table 3.19, with the space heating systems operating regime suitably altered, such that no space heating was delivered to the dwelling. The ensuing temporal simulation results depicted the free-floating internal temperature – the averages of which, as calculated across each profile's TDPs, are presented in Table 3.20.

Daily Averaged External Air Temperature (°C)	Daily Total Solar Irradiance (kWh/m²)						
	0.5	**1**	**1.5**	**2**	**2.5**	**3.0**	**3.5**
-3.2	0.9	1.8	3.0	4.9	5.8	7.0	8.1
-0.9	2.7	3.7	4.9	6.8	7.7	8.9	10.0
3.1	6.3	7.3	8.5	9.5	11.2	12.5	13.5
6.9	9.8	10.8	12.0	13.9	14.7	16.0	17.0
10.9	13.3	14.2	15.4	17.3	18.2	19.4	20.5
14.8	16.9	17.8	19.0	20.9	21.8	23.0	24.1
18.8	20.2	21.2	22.3	24.2	25.1	26.4	27.4

Table 3.20: Simulated Average Free-Floating Internal Air Temperature during TDPs, for each Synthetic Climate Profile, tabulated per Daily Total Irradiance and Daily Average External Air Temperature, for the Weekday Occupancy Pattern

Multiple linear regression analysis was performed on this data, to create a relationship between climate variables and average free-floating internal air temperature during TDPs. Using this relationship, the length of the heating season can be calculated, see Table 3.21, under the assumption that it is driven by the occupant's tolerance of average free-floating internal air temperatures. The length of the heating season is a function of the local climate, and hence location. As this investigation uses a climate file for Edinburgh, the length of heating season would be longer than averages for the UK or England.

Minimum Average Temperature (°C)	Heating Season (days)	Non- Heating Season (days)	Heating Season Length (% of year)
21	331	34	10%
20.5	327	38	12%
20	313	52	17%
19.5	299	66	22%
19	287	78	27%
18.5	276	89	32%
18	268	97	36%
17.5	262	103	39%
17	251	114	45%

Table 3.21: Heating Season Length vs. Minimum Average Free-Floating Internal Air Temperature

After a brief review of the available literature, no specific data on the tolerable non-heated temperatures during the UK summer climate was found. However, studies by Summerfield et al [44], and Shorrock and Utley [43], both concluded that average internal occupied temperatures were in the range of approximately 19-20°C.

Therefore, the heating season length for the simulated dwelling, within the climate dataset described previously, was assumed as 313 days, corresponding to that calculated from the minimum average free-floating temperature of 20°C. That is, the heating season length has been determined on the basis that the occupant will tolerate an internal temperature (during periods where the building is normally heated, i.e. the TDPs) as low as 20°C before switching the space heating system on.

Applying the heating season length assumption discussed previously to the annual distribution of calculated space heating demand in Figure 3.39, where the space heating demand of those days exhibiting average free-floating temperatures of 20°C or above was assumed to be zero, a distribution of heating-only space heating demand was generated, see Figure 3.40. With the goal of selecting representative Climate Scenarios, five "typical" climate days were selected from the previous set of synthetic daily climate profiles, which were representative of particular regions of the distribution, as marked on Figure 3.40.

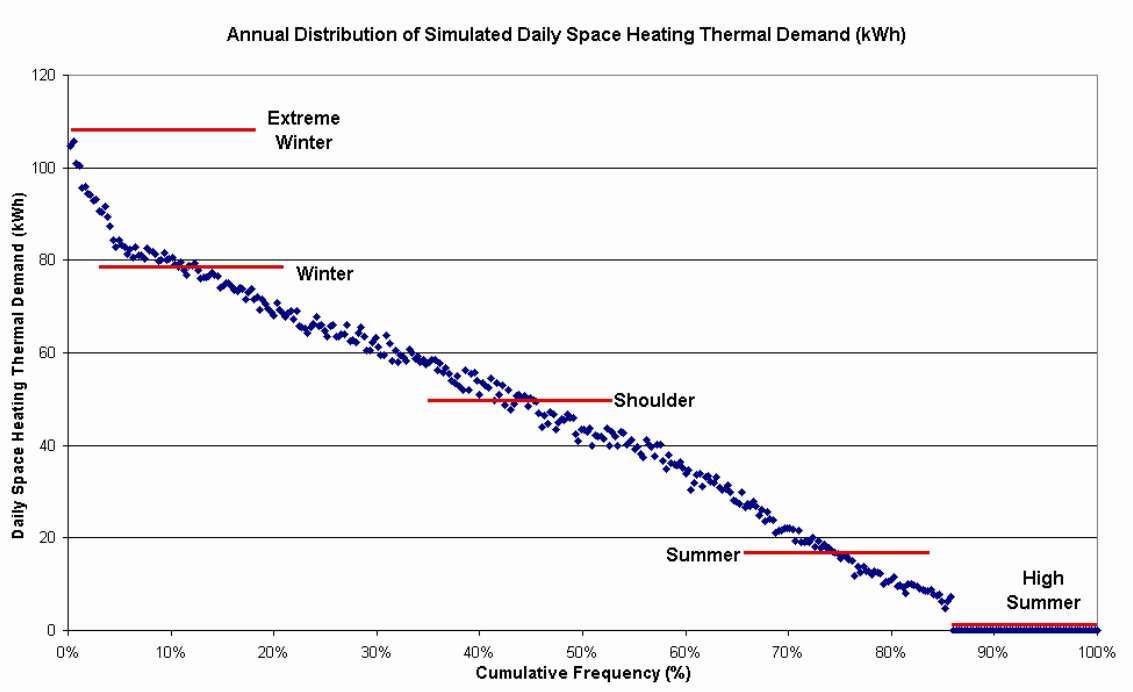

Figure 3.40: Annual Distribution of Calculated Daily Space Heating Thermal Demand (kWh), for the Weekday Occupancy Pattern, adjusted for Heat Generation only during Heating Season, where the red lines indicate the Daily Space Heating Thermal Demand (kWh) – i.e. the value on the y-axis – as simulated for Design Days using the indicated climate scenario

Using Microsoft Excel's Solver feature, the frequency (i.e. number of days per year) of each Climate Scenario (except for those corresponding to zero Space Heating Demand, whose frequency is explicitly specified by the heating season length discussed previously) required to synthesise an Annual Thermal Demand for Space Heating equal to that calculated by summation of the distribution in Figure 3.40, was estimated (Table 3.22).

Climate Scenario	Daily Solar Irradiance (kWh)	Daily Average Temp (°C)	SH Demand (kWh)	Frequency (Days)	Weight	Total SH Demand of Scenario (kWh)
Extreme Winter (**EWin**)	0.511	-3.2	109.0	1	0.0027	109
Winter (**Win**)	0.511	3.1	78.8	69.3	0.1900	5461
Shoulder (**Sh**)	1.489	6.9	49.3	177.9	0.4875	8767
Summer (**Sum**)	2.488	10.9	17.2	64.7	0.1774	1110
High Summer (**HSum**)	2.488	16.8	0	52	0.1425	0

Table 3.22: Climate Scenarios, and associated Daily Solar Irradiance, Daily Average External Temperature, Space Heating Demand (kWh), Frequency, and Weighting Factor, with Total Space Heating Demand Attributed to each Climate Scenario

The hourly values of external air temperature and solar irradiance are plotted for each climate scenario in Figure 3.41 to Figure 3.45.

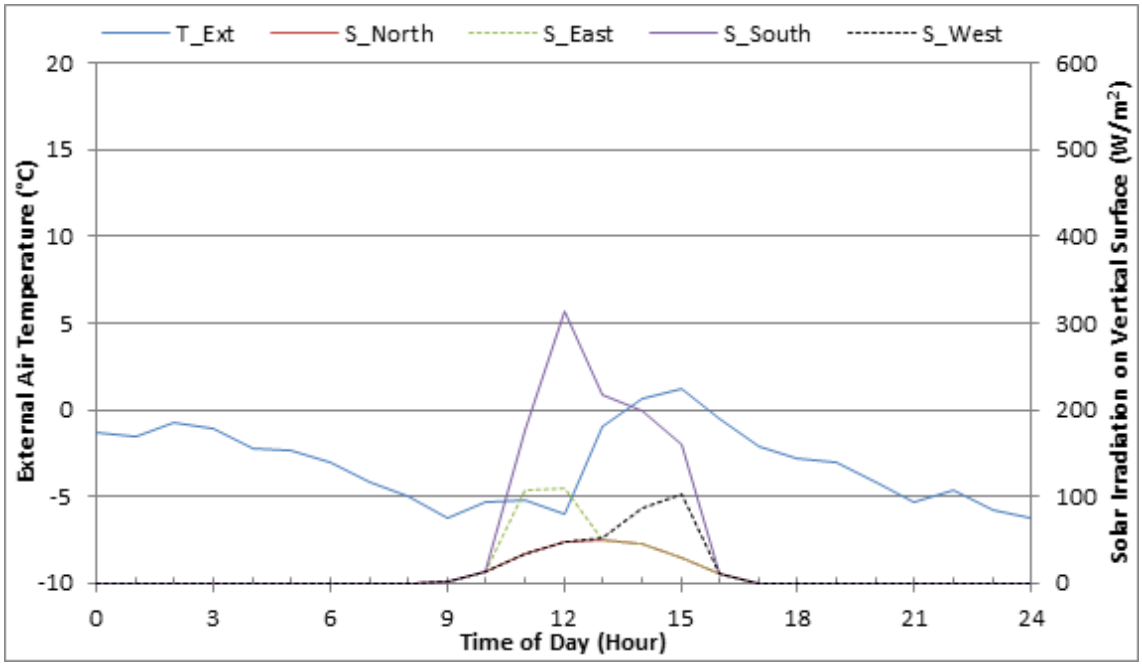

Figure 3.41: Hourly climate values used for Extreme Winter climate scenario with External Air Temperature (T_Ext) and Solar Irradiation on Vertical Surface from North, South, East & West facing surface (S_South, S_North, S_East, S_West)

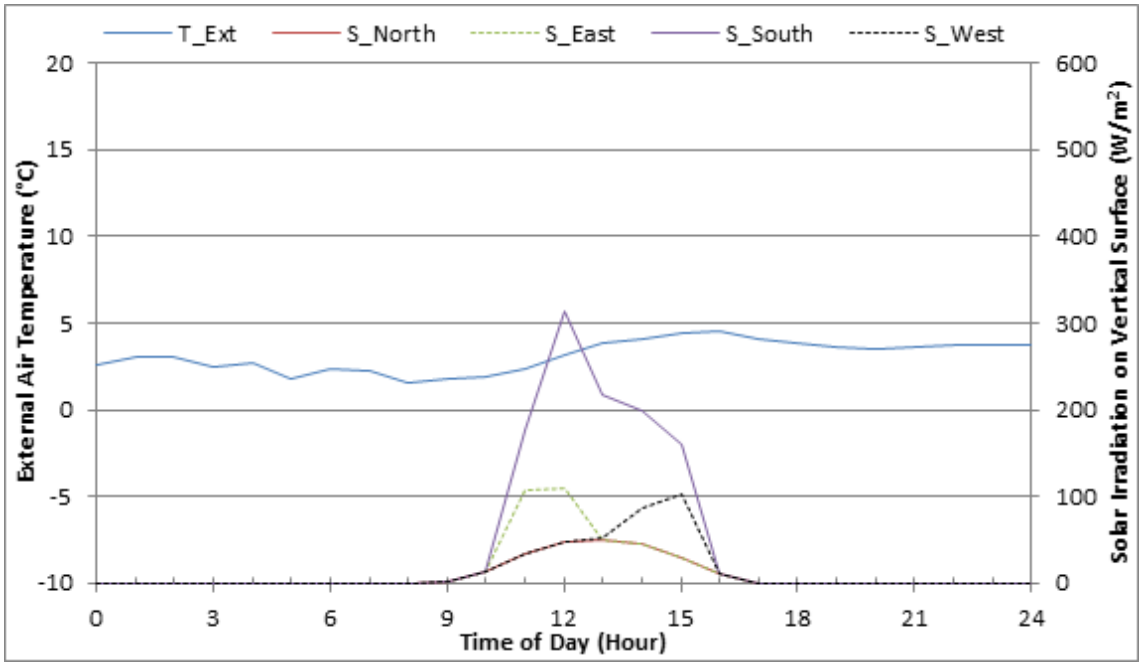

Figure 3.42: Hourly climate values used for Winter climate scenario with External Air Temperature (T_Ext) and Solar Irradiation on Vertical Surface from North, South, East & West facing surface (S_South, S_North, S_East, S_West)

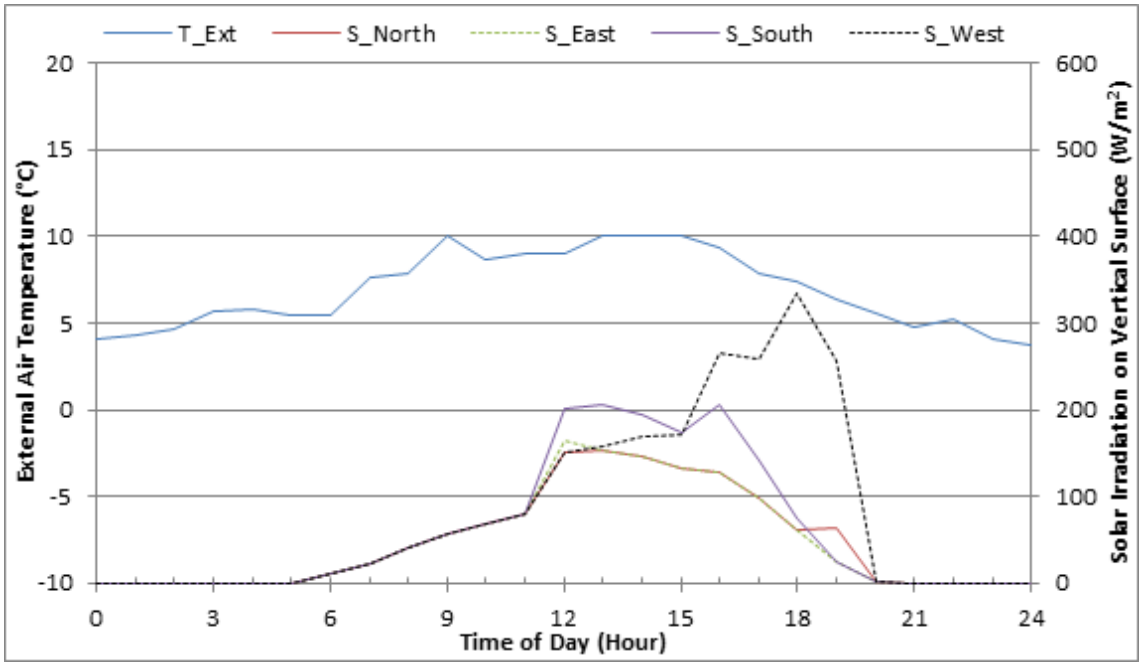

Figure 3.43: Hourly climate values used for Shoulder climate scenario with External Air Temperature (T_Ext) and Solar Irradiation on Vertical Surface from North, South, East & West facing surface (S_South, S_North, S_East, S_West)

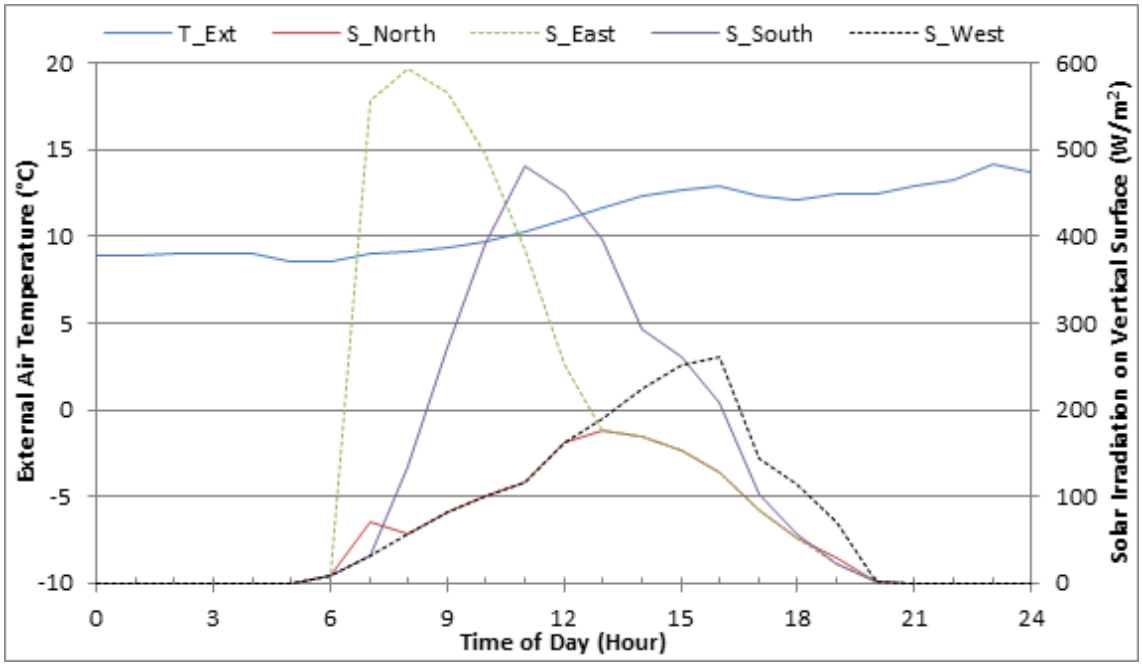

Figure 3.44: Hourly climate values used for Summer climate scenario with External Air Temperature (T_Ext) and Solar Irradiation on Vertical Surface from North, South, East & West facing surface (S_South, S_North, S_East, S_West)

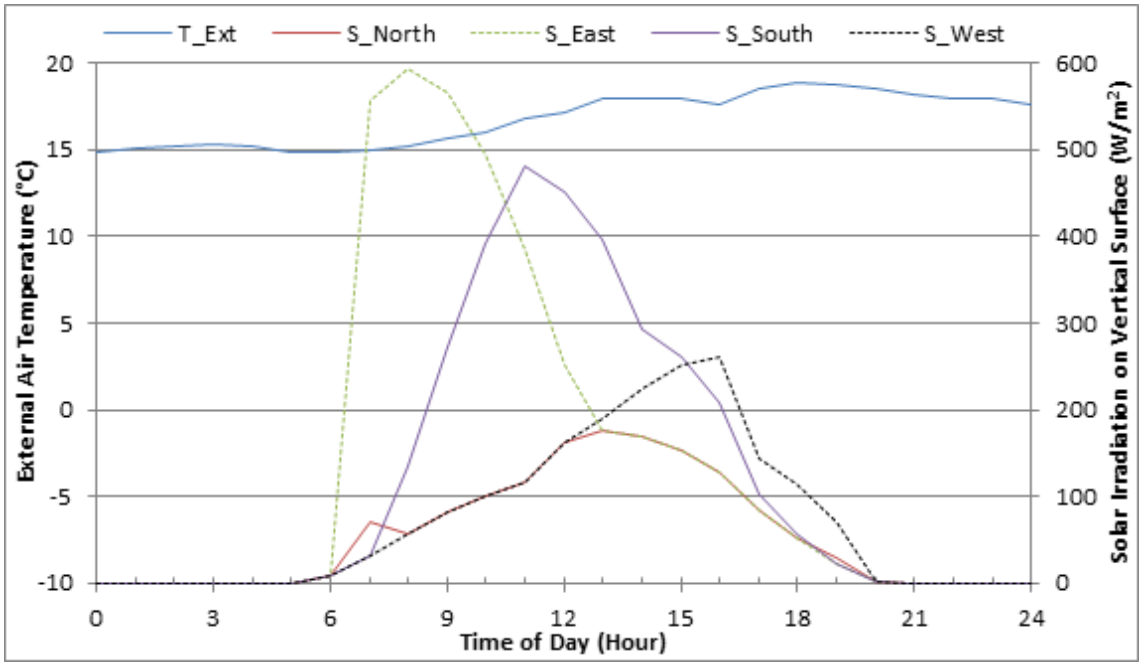

Figure 3.45: Hourly climate values used for High Summer climate scenario with External Air Temperature (T_Ext) and Solar Irradiation on Vertical Surface from North, South, East & West facing surface (S_South, S_North, S_East, S_West)

The climate scenario selection methodology described in this section evolved from the simple selection of daily-averaged External Air Temperature and total orientation-averaged Solar Irradiance values typical of Winter, Shoulder and Summer seasons, as used in preliminary investigations [1][2]. It was deemed necessary to define additional climate scenarios in order to investigate µCHP performance when thermal demand is limited to DHW provision, and to provide a design day with very high thermal demand, in order to facilitate analysis of µCHP performance versus thermal demand.

3.9 Primary Demand Scenarios

The conception of a demand scenario relies upon an understanding of the demand drivers acting upon the dwelling. The majority of these demand drivers are related to the behaviour or decisions of the occupants; whilst the rest are uncontrollable, such as building construction and climate. For reasons explained in the previous sections, the composition of the household and the construction of the dwelling were selected prior to demand scenario conception, and held constant throughout. As a method of representing the effects of the remaining occupant-related demand drivers, two

occupancy patterns have been specified; identified by the “type” of day they may typically represent for the chosen household; Weekday and Weekend. The features of these occupancy patterns, and data analysis undertaken to derive them, are discussed in Section 3.3, but in essence they represent a day with and day without a significant period of dwelling vacancy.

Each member of the household was assigned an occupancy pattern, relative to the appropriate demand scenario. These occupancy patterns have been segregated on the assumption that during a weekday, all occupants vacate the dwelling to attend places of employment or education, on a largely concurrent basis. In contrast, the occupancy profile of the dwelling during a weekend day comprises short vacancy periods, where the dwelling is partially or fully occupied at any point in time. The duration of these vacancy periods was informed by analysis of the UK Time Use Survey 2000 [15], where distributions of vacancy periods for members of households with a similar composition were produced.

There are two daily script types selected to represent the dwelling variant: Weekday and Weekend. The former represents a “standard” working day, where all occupants are absent from the dwelling, attending their place of work or educational institution. The duration of these absences are selected using data derived from the UK General Household Survey and the UK Time Use Survey 2000, from which ranges of vacancy durations were extracted. The latter represents a “standard” weekend day, where the dwelling is occupied by at least one person at all times, although individual occupancy is intermittent.

Finally, the variation in the remaining demand driver, climate, is represented by five daily climate scenarios, as derived using the methodology presented in Section 3.8.

Through combination of these occupancy patterns and climate scenarios the Primary Demand Scenarios, as presented in Table 3.23, are constructed.

Primary Demand Scenario	Climate Scenario	Occupancy Pattern	Frequency (Days/yr)	Annual Weighting Factor
WD-EWin	Extreme Winter	Weekday	0.7	0.0020
WE-EWin	Extreme Winter	Weekend	0.3	0.0008
WD-Win	Winter	Weekday	49.5	0.1357
WE-Win	Winter	Weekend	19.8	0.0543
WD-Sh	Shoulder	Weekday	127.1	0.3482
WE-Sh	Shoulder	Weekend	50.8	0.1393
WD-Sum	Summer	Weekday	46.2	0.1267
WE-Sum	Summer	Weekend	18.5	0.0507
WD-HSum	High Summer	Weekday	37.1	0.1018
WE-HSum	High Summer	Weekend	14.9	0.0407

Table 3.23: Occupancy Pattern, Climate Scenario, and Annual Weighting Factor of Primary Demand Scenarios

The resultant Thermal Demand Periods, for timing of space heating and DHW service requirements, are presented in Table 3.24 for each occupancy pattern of primary demand scenario. They are fairly consistent with the assumptions of both De Paepe et al [45] and Hawkes et al [18] in their µCHP modelling exercises. De Paepe et al defined TDPs of 6am-8am and 5pm-10pm on weekdays, and 7am-10pm on weekends. Hawkes et al defined TDPs of 6am-9am and 6pm-11pm on weekdays, and 8am-11pm on weekends.

Occupancy Pattern	Period A Start Time	Period A Stop Time	Period B Start Time	Period B Stop Time
Weekday	06:00	08:30	16:00	23:00
Weekend	06:00	23:00	~	~

Table 3.24: Thermal Demand Periods used for Space Heating Timer, by Occupancy Pattern

3.10 Base-Case Demand and CO_2 Emissions

3.10.1 Specifications of Base-Case Energy System

The specification of the base-case energy system, including transient performance characteristics, is discussed in Section 2.4.

3.10.2 Simulation Methodology for Primary Demand Scenarios

The Supply:Demand Matching procedure of the BIM-G model was tailored to the operation of the base-case energy system, and simulations were performed for each of the primary demand scenarios. In order to retain a measure of comparability between the results of each scenario, normalisation of initial values of simulation variables was required. For each climate scenario, the 10 daily pre-simulation loops were performed, as discussed in Section 4.2.4, which allowed the fabric and space heating distribution system values to reach an approximate equilibrium, which would reflect their values in real-life. These values were subsequently applied as start-up values for both occupancy patterns, such that the primary demand scenarios that share a climate scenario also share the aforementioned start-up values.

Perhaps more significantly, variations in DHW tank temperatures, as found after the aforementioned pre-simulation loops, if applied to other demand scenarios, could alter values of daily demand by several percent. Since the pre-simulation loops are necessary for realistic simulation, yet the consecutive occurrence of identical climate and occupancy demand drivers is not, it was decided to normalise the initial DHW tank temperature across all primary demand scenarios.

3.10.3 Thermal Demand Profiles

The building's thermal demand at every time-step is calculated by the supply:demand matching and building heat balance algorithms discussed in Section 2.3. The thermal demand profile is specific to not only the demand scenario, building construction, and space heating distribution system, but to the thermal energy system (e.g. boiler and thermal storage) and control & operating regimes in use. The thermal energy system responds to control signals (from air and water temperature sensors and timers) which decide if thermal output from the heat generator and/or thermal storage is required. This response is governed by the thermal output capacity of the generator or thermal storage, start-up profile of the generator, and other control restrictions (such as part-load levels and minimum run-times).

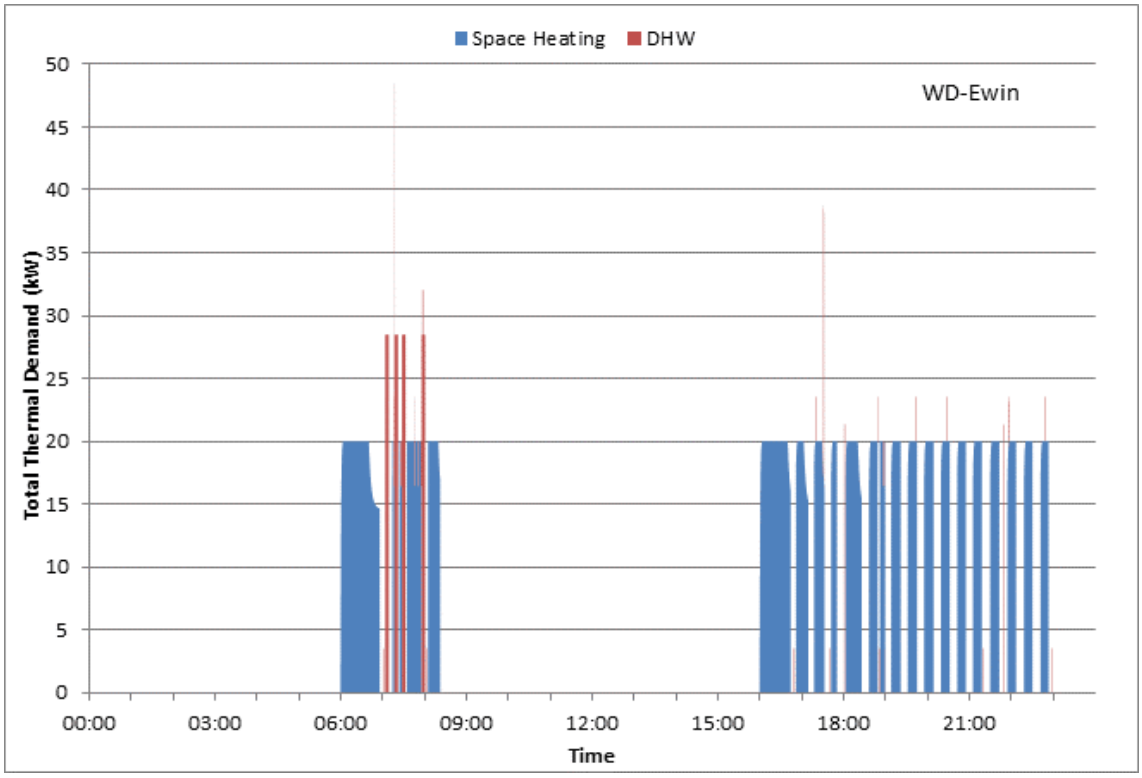

Figure 3.46: Thermal Demand profile for Weekday-Extreme Winter (WD-EWin), disaggregated by Space Heating & DHW

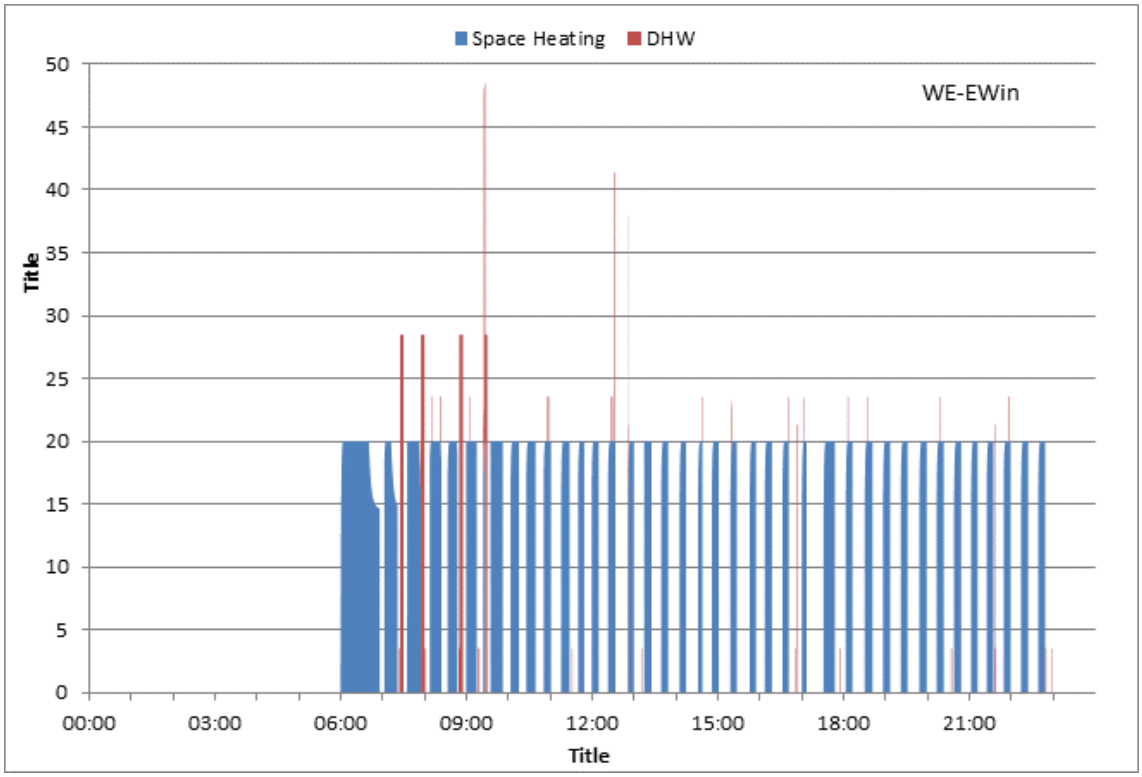

Figure 3.47: Thermal Demand profile for Weekend-Extreme Winter (WE-EWin), disaggregated by Space Heating & DHW

The simulation results presented in Table 3.25 detail the thermal demands for each primary demand scenario, along with the contribution of each scenario's thermal demand to the annual total.

	Daily Scenario Results				*Annual Impact of Demand Scenario*			
Demand Scenario	**Space Heating Demand (kWh)**	**DHW Demand (kWh)**	**Total Thermal Demand (kWh)**	**Fuel Used (kWh)**	**Space Heating Demand (kWh)**	**DHW Demand (kWh)**	**Total Thermal Demand (kWh)**	**Fuel Used (kWh)**
HSum-WD	0.0	12.1	12.1	14.3	0	448	448	530
Sum-WD	19.9	12.0	31.9	36.4	922	553	1,475	1,683
Sh-WD	53.6	12.1	65.7	74.1	6,811	1,536	8,347	9,420
Win-WD	85.1	12.1	97.2	110.4	4,213	599	4,812	5,470
EWin-WD	114.9	12.1	127.1	144.4	82	9	91	103
HSum-WE	0.0	13.6	13.6	16.4	0	202	202	244
Sum-WE	20.9	13.5	34.4	39.7	387	249	636	734
Sh-WE	67.7	13.6	81.3	91.9	3,442	690	4,132	4,673
Win-WE	112.9	13.5	126.4	143.4	2,236	268	2,504	2,841
EWin-WE	153.6	13.5	167.1	190.4	44	4	48	54
Annual	**N/A**	**N/A**	**N/A**	**N/A**	**18,137**	**4,557**	**22,694**	**25,752**

Table 3.25: Thermal Demand (kWh) and Boiler Fuel Consumption (kWh) for the Simulation results for Base-case Energy System, operating under all Primary Demand Scenarios, with annual contribution to annual results, where demand is disaggregated by space heating (input to radiator network) & DHW (input to tank)

Between all 10 primary demand scenarios, the total thermal demand varies between 12.1 to 167.1 kWh. This provides a number of thermal demand scenarios with which to assess µCHP performance. As illustrated in Figure 3.5, the annual space heating demand calculated for the building variant is larger than the peak value in the national distribution of annual demand, whilst remaining close enough to the maxima so as not to be considered an outlier.

3.10.4 Electrical Demand Profiles

The building's electrical profile is synthesised from static and dynamic elements. The electrical loads for ventilation and appliance loads, as described in Sections 3.5 and 3.6 respectively, are particular to an occupancy pattern, i.e. weekday or weekend. Lighting loads were specified based on occupancy pattern and climate scenario, as discussed in Section 3.7. When the supply:demand matching function of the BIM-G model is

executed, electrical loads, both standby & control and operating, for the boiler and space heating pumps, are dynamically added to the pre-defined demand profile, to generate the building's electrical demand profile.

The electrical demand profiles for Extreme Winter and High Summer climate scenarios, for Weekday and Weekend occupancy profiles respectively, are plotted in Figure 3.48 and Figure 3.49. Within the TDPs (i.e. when the space heating system is controlled to satisfy demand), the electrical load is higher during the Extreme Winter climate scenario ,as the boiler fires and space heating pumps are active in order to satisfy thermal demand. As the space heating system is switched off during the High Summer climate scenario, the heating systems electrical load is limited to boiler standby & control loads, and short periods of boiler operation to satisfy provision.

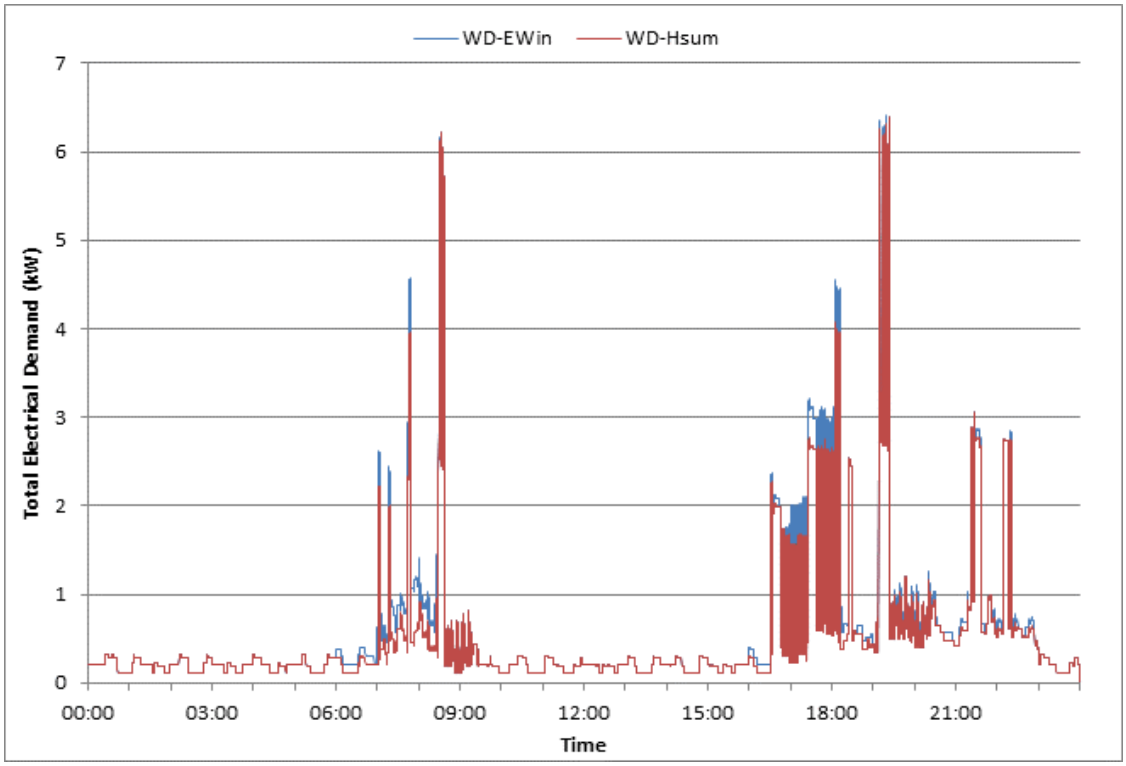

Figure 3.48: Electrical Demand Profile for WD-EWin (Weekday-Extreme Winter) and WD-HSum (Weekday-High Summer) Primary Demand Scenarios

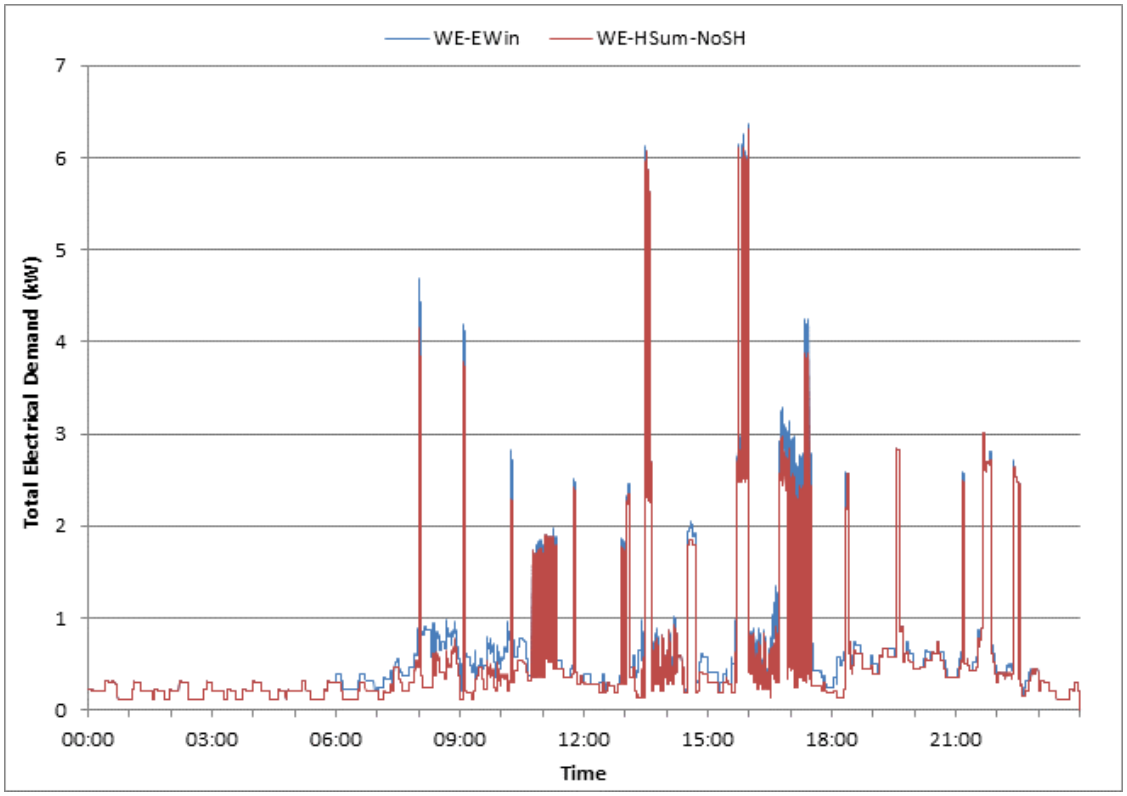

Figure 3.49: Electrical Demand Profile for WE-EWin (Weekend-Extreme Winter) and WE-HSum (Weekend-High Summer) Primary Demand Scenarios

The electrical demand profile for a different energy system will differ from those of the base-case energy system, due to different standby & control and operating loads, and a different profile of generator operation due to different thermal output capacity, thermal storage, control restrictions and start-up behaviour. However, the distribution of electrical consumption within and without TDPs is summarised in Table 3.26. Without the integration of electrical storage, any thermal load following µCHP system will be limited to displacing electrical demand within the TDPs.

Demand Scenario	Electrical Consumption in TDP				Electrical Consumption Outwith TDP			
	SHDS & Boiler	Other	Total		SHDS & Boiler	Other	Total	
	(kWh)	(kWh)	(kWh)	(%)	(kWh)	(kWh)	(kWh)	(%)
HSum-WD	0.16	8.36	8.52	72%	0.14	3.19	3.34	22%
Sum-WD	0.26	8.36	8.62	72%	0.14	3.19	3.34	22%
Sh-WD	0.43	8.54	8.97	73%	0.14	3.19	3.34	21%
Win-WD	0.59	9.26	9.85	75%	0.15	3.19	3.34	20%
EWin-WD	0.75	9.26	10.01	75%	0.14	3.19	3.34	20%
HSum-WE	0.24	10.85	11.09	89%	0.07	1.36	1.43	10%
Sum-WE	0.35	10.85	11.19	89%	0.07	1.36	1.43	10%
Sh-WE	0.57	10.86	11.43	89%	0.07	1.36	1.43	10%
Win-WE	0.80	12.24	13.03	90%	0.07	1.36	1.43	9%
EWin-WE	1.02	12.24	13.26	90%	0.07	1.36	1.43	9%

Table 3.26: Electrical Demand (kWh) for each Primary Demand Scenario, disaggregated between dynamic demand (from heating system) and pre-defined demand (form lights, appliances & ventilation), and split by period consumed (within & without TDP)

The cumulative electrical consumption towards annual demand, from each Primary Demand Scenario, is presented in Table 3.27. As illustrated in Figure 3.3, the annual electrical demand calculated for the building variant corresponds with a value slightly greater than the maxima of the national electrical demand distribution.

	Daily Scenario Results			*Annual Impact of Demand Scenario*		
Demand Scenario	**Heating System Electrical Demand (kWh)**	**Other Electrical Demand (kWh)**	**Total Electrical Demand (kWh)**	**Heating System Electrical Demand (kWh)**	**Other Electrical Demand (kWh)**	**Total Electrical Demand (kWh)**
HSum-WD	0.30	11.55	11.86	11	429	440
Sum-WD	0.40	11.55	11.96	19	534	553
Sh-WD	0.57	11.73	12.30	73	1,491	1,564
Win-WD	0.74	12.45	13.18	36	617	653
EWin-WD	0.90	12.45	13.34	1	9	10
HSum-WE	0.31	12.21	12.52	5	181	186
Sum-WE	0.42	12.21	12.62	8	226	233
Sh-WE	0.64	12.22	12.86	33	621	654
Win-WE	0.87	13.60	14.46	17	269	287
EWin-WE	1.09	13.60	14.69	0	4	4
Annual	N/A	N/A	N/A	**202**	**4,381**	**4,583**

Table 3.27: Electrical Demand (kWh) for the Simulation results for Base-case Energy System, operating under all Primary Demand Scenarios, with annual contribution to annual results, disaggregated by heating system (boiler operating, pump, and standby & control loads) and other loads (lights, appliances & ventilation fans)

3.10.5 Co-incidence of Thermal & Electrical Demand

The co-incidence of thermal and electrical demand was plotted for the climate scenario with highest thermal demand (Extreme Winter). Referring to both occupancy profiles, Figure 3.50 (weekday) and Figure 3.51 (weekend), it is important to note that whilst thermal demand and high (i.e. non-base-load) electrical demand is typically linked to the same TDPs, this does not guarantee co-incidence of demand. The cyclic nature of thermal input demand from water-based heating systems drives boilers to cycle during a TDP. It is also important to remember that occupants may trigger high magnitude, long duration electrical loads before leaving the building, or even by timer. This is demonstrated in Figure 3.50, where a washing machine started several minutes before the end of the TDP, therefore the majority of electrical consumption for that appliance occurs when thermal demand is zero.

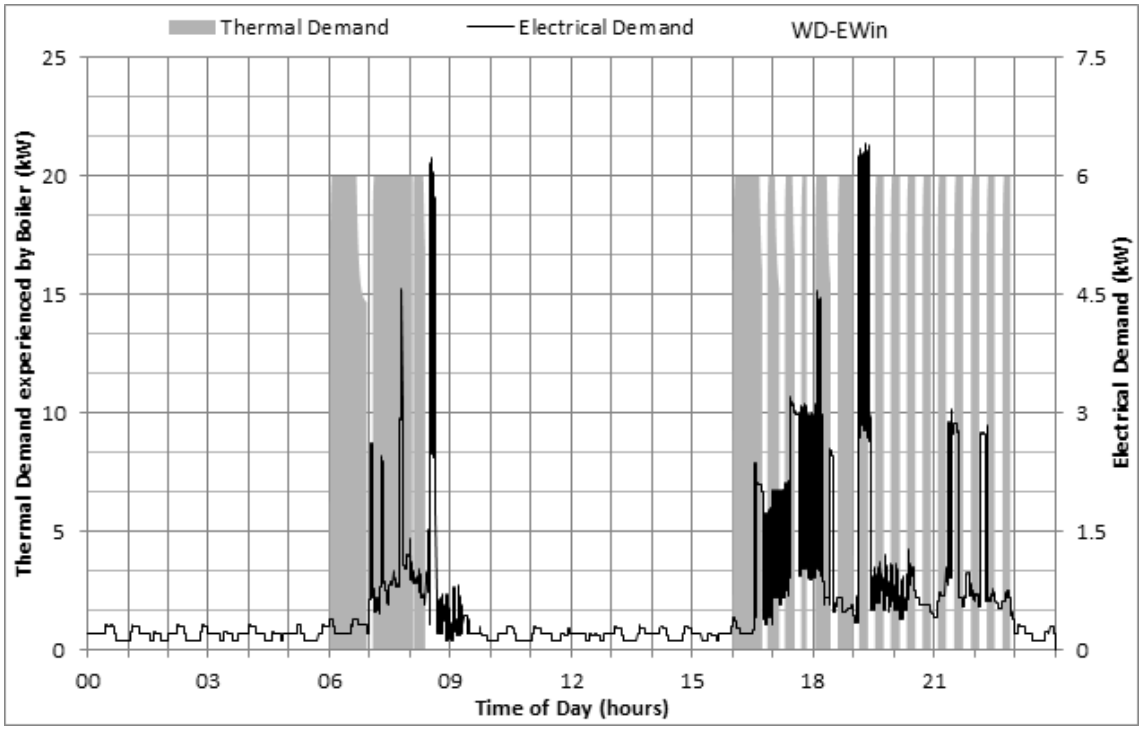

Figure 3.50: Thermal and Electrical demand profiles for base-case energy system operating under Extreme Winter - Weekday primary demand scenario

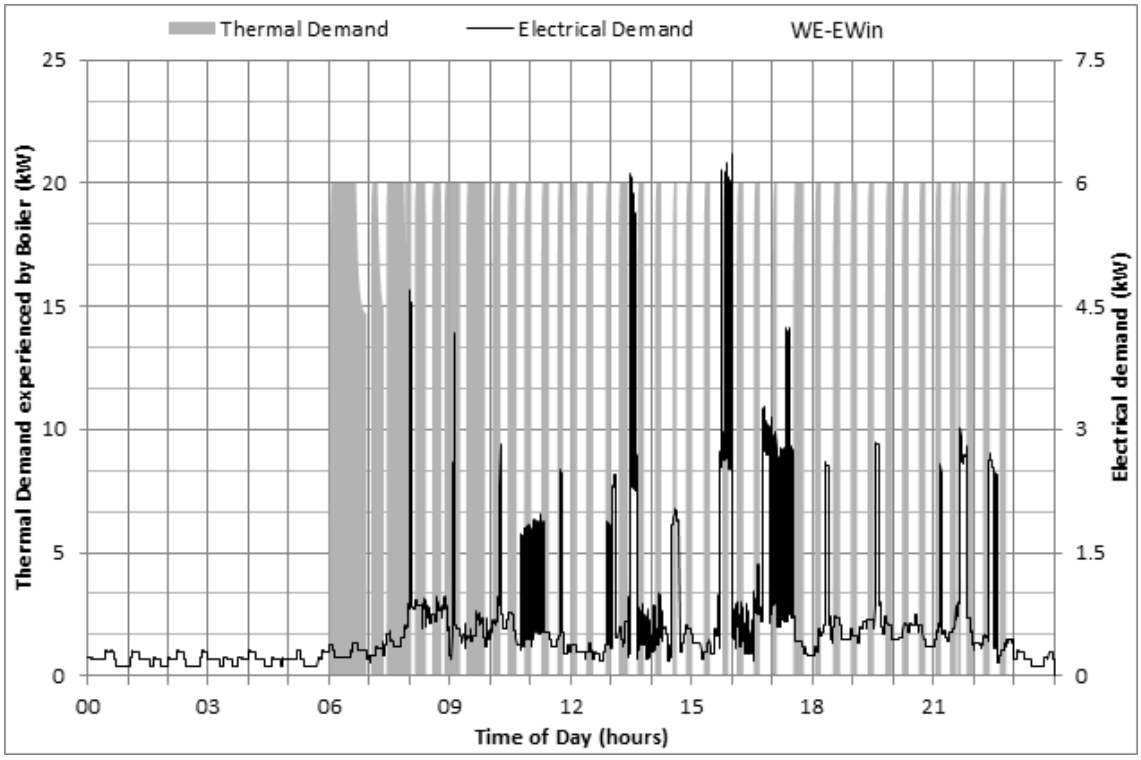

Figure 3.51: Thermal and Electrical demand profiles for base-case energy system operating under Extreme Winter - Weekend primary demand scenario

The thermal and electrical demand profiles for both High Summer climate demand scenarios, where thermal demand is due to domestic hot water only, is presented in Figure 3.52 and Figure 3.53. Due to the limited thermal demand, co-incidence of thermal and electrical demand is dramatically reduced in comparison to the Extreme Winter demand scenarios.

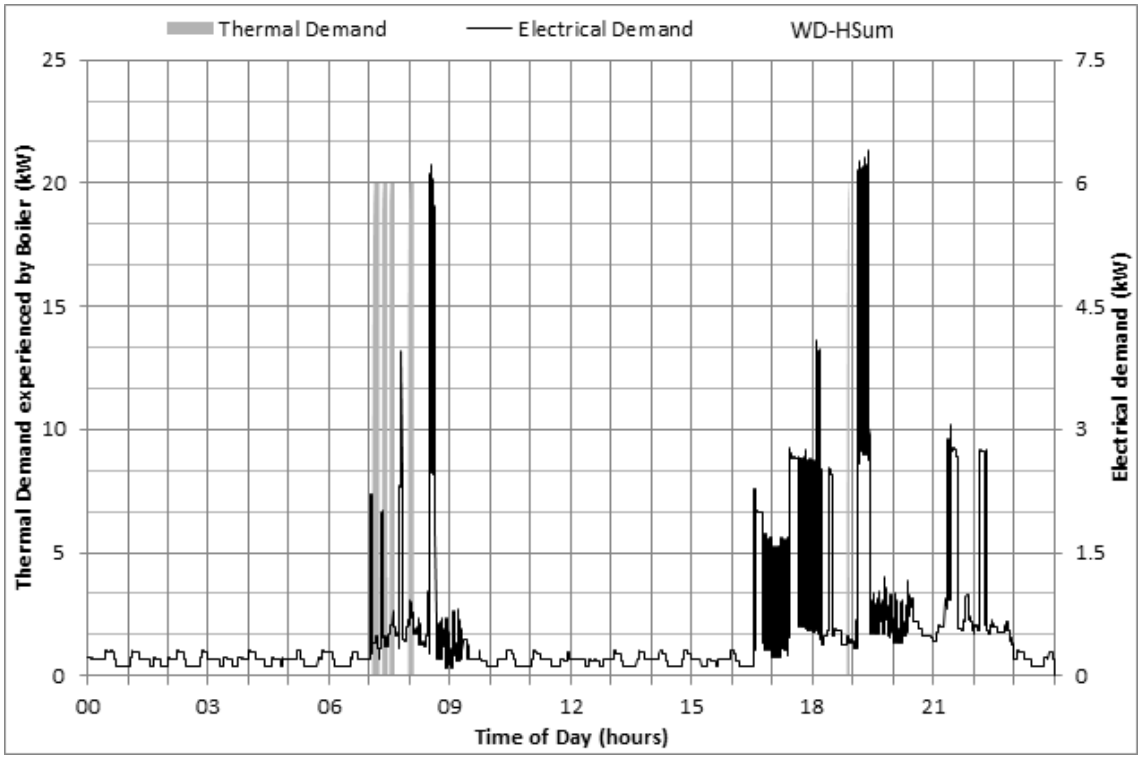

Figure 3.52: Thermal and Electrical demand profiles for base-case energy system operating under High Summer - Weekday primary demand scenario

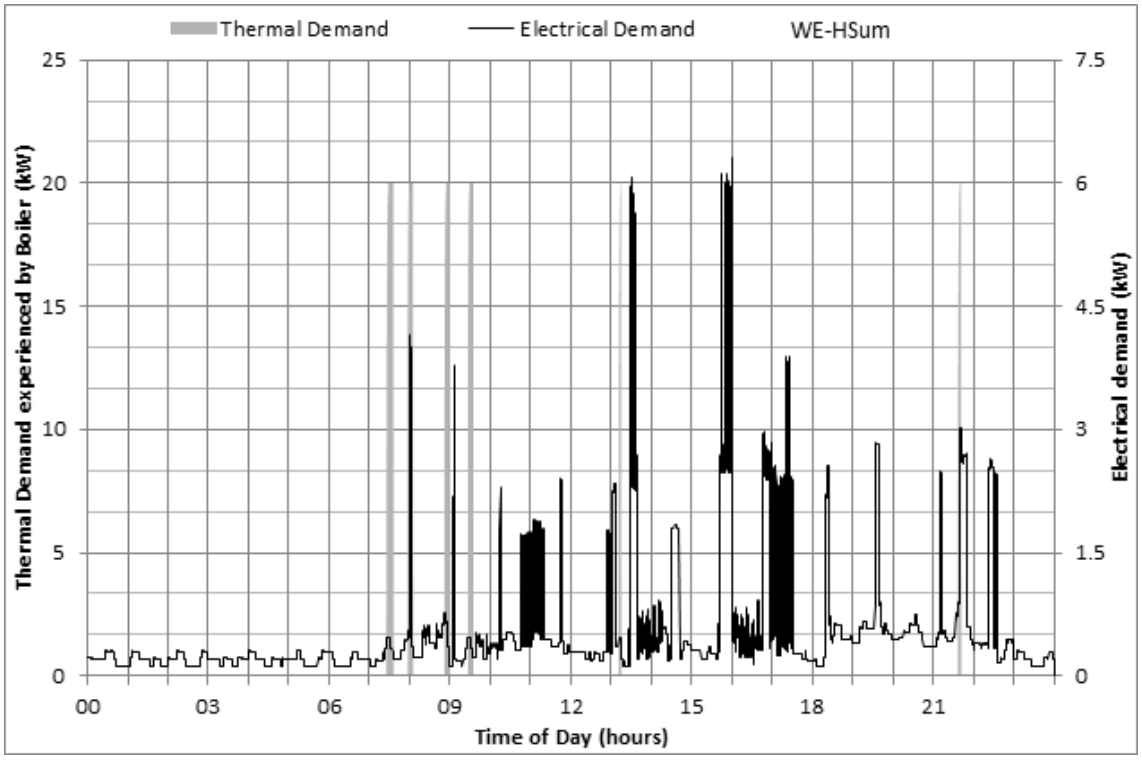

Figure 3.53: Thermal and Electrical demand profiles for base-case energy system operating under High Summer - Weekend primary demand scenario

The heat-to-power ratio for the Extreme Winter, Shoulder, and High Summer primary demand scenarios are plotted in Figure 3.54, Figure 3.55 and Figure 3.56 respectively. The effect of frequent cycling apparent in the Extreme Winter plot is due to the space heating temperature control, as it responds to both internal air temperature and SHDS return temperature. This cycling reduces in frequency for the shoulder PDS, as the milder climate reduces heat loss, therefore increasing the time taken for the internal air temperature to decay from the space heating cut-off temperature to the trigger temperature. The cycling that remains in the High Summer PDS is due to the DHW Tank, as it call for heat input due to DHW consumption and standing heat losses.

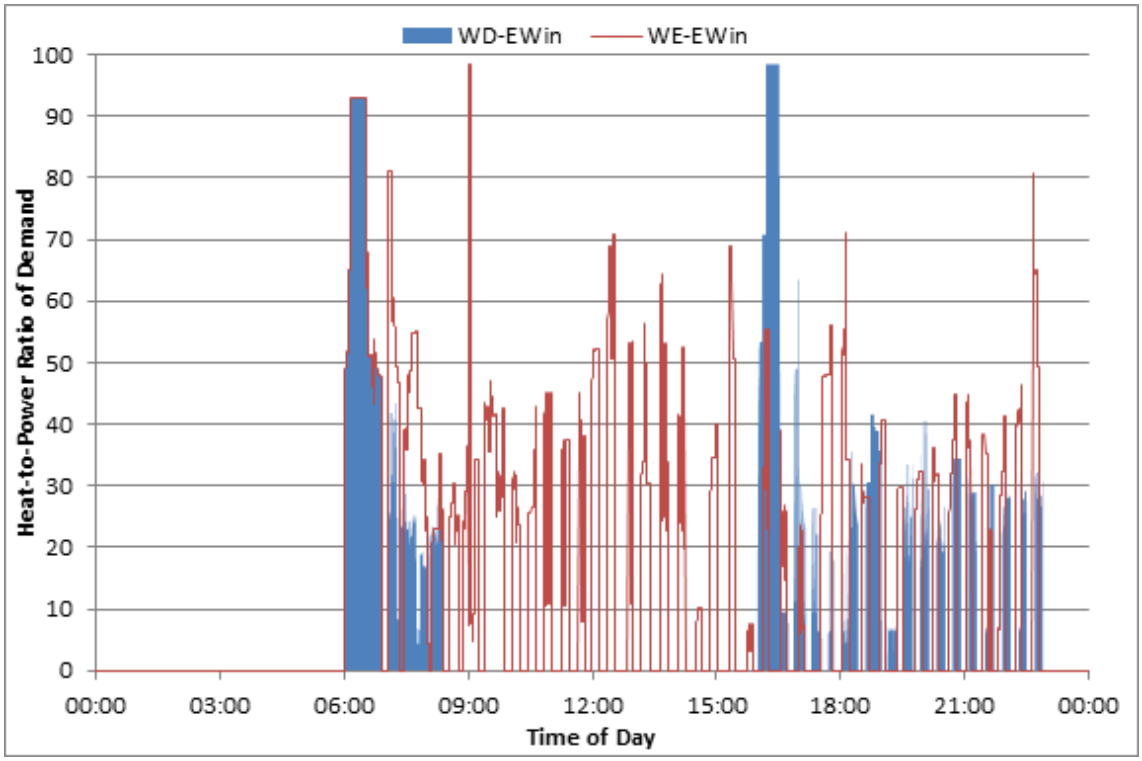

Figure 3.54: Heat-to-Power Ratio of Demand for Weekday-Extreme Winter and Weekend-Extreme Winter Primary Demand Scenarios

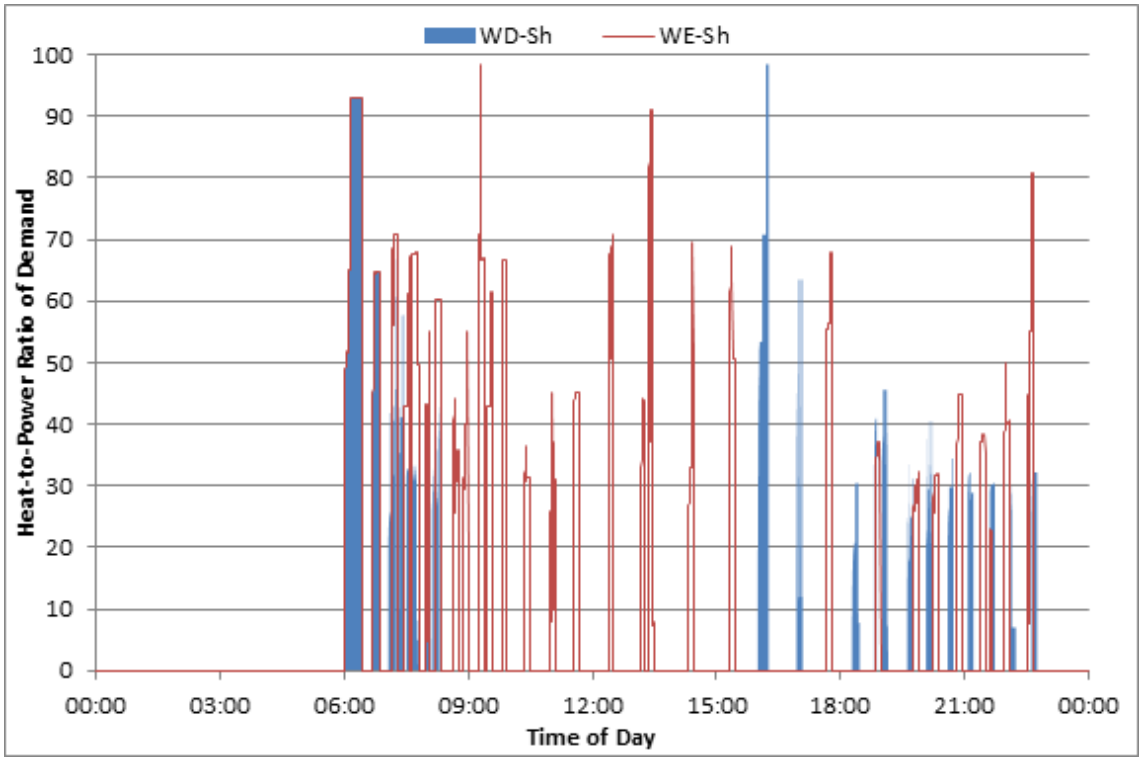

Figure 3.55: Heat-to-Power Ratio of Demand for Weekday-Shoulder and Weekend-Shoulder Primary Demand Scenarios

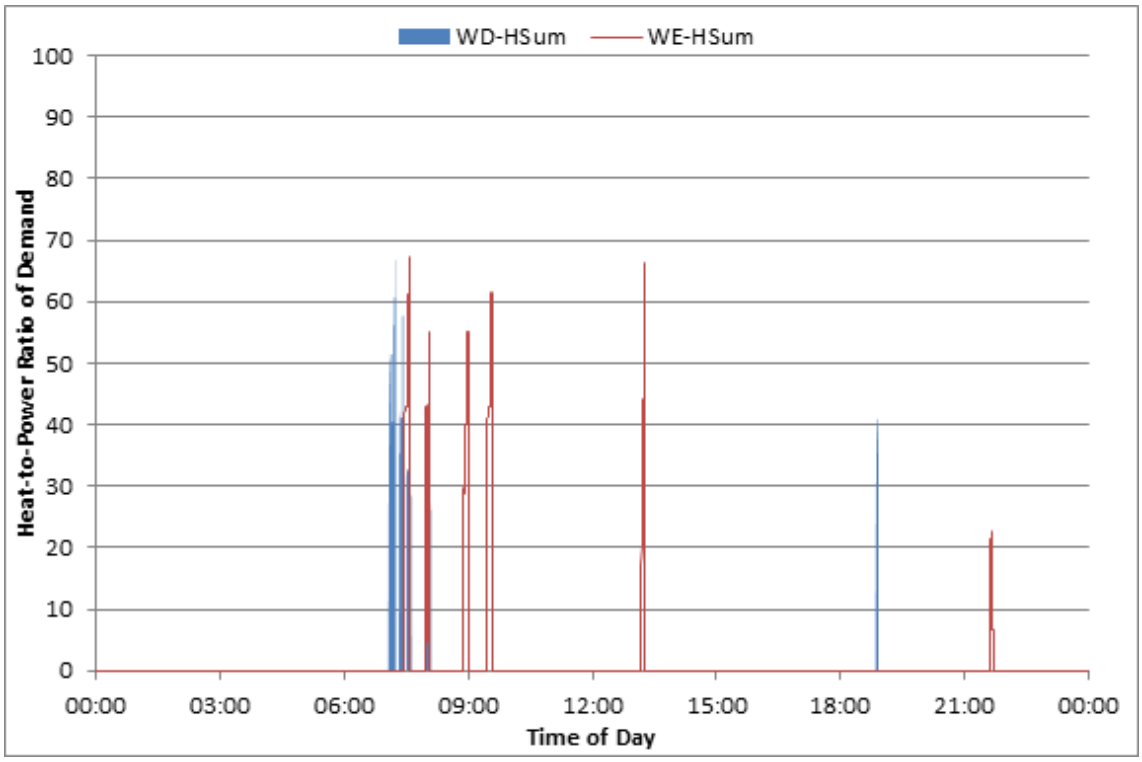

Figure 3.56: Heat-to-Power Ratio of Demand for Weekday-High Summer and Weekend-High Summer Primary Demand Scenarios

A μCHP operating regime could potentially use the instantaneous heat-to-power ratio as a control signal, to decide whether the prime mover or auxiliary boiler should be started to satisfy demand. An advanced variant of such an operating regime could feature an intelligent control system that has been pre-trained with a relationship linking the typical durations of high heat-to-power ratio to external temperature. Such a feature could be used to reduce the frequency of thermal cycling of a prime mover, by ensuring that it starts only when a particular range of heat-to-power ratio is likely to be maintained.

3.10.6 Carbon Footprint

In Table 4.5, carbon performance figures are presented for the base-case energy system operating under each primary demand scenario, along with the contribution to the annual carbon footprint from each scenario.

		Daily Scenario Results			***Annual Impact of Demand Scenario***		
Demand Scenario	**Frequency (Days per Annum)**	**Natural Gas Carbon Emissions ($kgCO_2$)**	**Electrical Import Carbon Emissions ($kgCO_2$)**	**Total Carbon Emissions ($kgCO_2$)**	**Natural Gas Carbon Emissions ($kgCO_2$)**	**Electrical Import Carbon Emissions ($kgCO_2$)**	**Total Carbon Emissions ($kgCO_2$)**
HSum-WD	37.1	2.7	5.1	7.8	101	189	290
Sum-WD	46.2	6.9	5.1	12.1	312	238	558
Sh-WD	127.1	14.1	5.3	19.4	1,790	672	2,462
Win-WD	49.5	21.0	5.7	26.7	1,039	281	1,320
EWin-WD	0.7	27.4	5.7	33.2	20	4	24
HSum-WE	14.9	3.1	5.4	8.5	46	80	126
Sum-WE	18.5	7.5	5.4	13.0	140	100	240
Sh-WE	50.8	17.5	5.5	23.0	888	281	1,169
Win-WE	19.8	27.2	6.2	33.5	540	123	663
EWin-WE	0.5	36.2	6.3	42.5	10	2	12
Annual	365	N/A	N/A	N/A	**4,893**	**1,971**	**6,864**

Table 3.28: Carbon Emissions (kg CO_2) for the Simulation results for Base-case Energy System, operating under all Primary Demand Scenarios, with annual contribution to annual results

3.11 References

[1] D. Kane and M. Newborough; Scenarios for Carbon Abatement in Dwellings by Implementation of Stirling Engine Micro-CHP Systems; Energy efficiency in domestic appliances and lighting: proceedings of the 4th international conference EEDAL ´06; 21-23 June 2006, London, United Kingdom; volume 3. - Luxembourg: Office for Official Publications of the European Communities, 2006

[2] D. Kane and M Newborough; Estimating carbon savings for domestic base-load micro-CHP systems; World Renewable Energy Congress IX: Proceedings of WREC '06; 2006

[3] A.D. Peacock, D.P. Jenkins, D. Kane, Investigating the potential of overheating in UK dwellings as a consequence of extant climate change, Energy Policy, Volume 38, Issue 7, Pages 3277-3288, July 2010

[4] R.A.R. Kilpatrick, P.F.G. Banfill, D.P. Jenkins, Methodology for characterising domestic electrical demand by usage categories, Applied Energy, Volume 88, Issue 3, March 2011, Pages 612-621

[5] Jenkins et al, Modelling carbon emissions of UK dwellings – The TARBASE Domestic Model, Applied Energy, Volume 93, May 2012, Pages 596–605

[6] P.F. Banfill et al; Reducing CO_2 emissions through refurbishment of UK housing; eceee 2007 Summer Study Proceedings; 2007

[7] Shorrock L D and Utley J I, Domestic Energy Fact File 2003. Garston, Watford, UK: Building Research Establishment, 2003

[8] Boardman B, et al., 40% House. Oxford, UK: Environmental Change Institute, 2005; pp29

[9] A.D. Hawkes and M.A. Leach, Comparison of Fuel Cell and Combustion Micro-CHP under Future Residential Energy Demand Scenarios, Centre for Energy Policy and Technology, Imperial College London, June 2007

[10] Mariyappan J, The Adoption of Distributed Generation: Scenarios, Drivers, Constraints and Impacts for the UK, in DEST. Imperial College London: London, UK, 2003

[11] A.D. Peacock and M. Newborough, Impact of micro-CHP systems on domestic sector CO_2 emissions, Applied Thermal Engineering, Volume 25, Issues 17-18, December 2005, Pages 2653-2676

[12] Scottish Executive National Statistics, Scottish House Condition Survey 2002, Edinburgh, 2002, Accessed online at http://www.esds.ac.uk/findingData/snDescription.asp?sn=4977

[13] Office of the Deputy Prime Minister (ODPM), English House Condition Survey 2001. Building the Picture, ODPM, London (2003)

[14] Office of National Statistics; General Household Survey 2002-2003; London; [Computer File]; 1st edition; UK Data Archive [distributor]; July 2004; SN4981

[15] Office of National Statistics; United Kingdom Time Use Survey 2000 (TUS); London; [Computer File]; 3rd edition; UK Data Archive [distributor]; September 2003; SN4504

[16] Anderson et al; Building Research Establishment; 2002; BREDEM-12 Model description 2001 update; pp8

[17] Agar, W. R., & Newborough, M.; Implementing micro-CHP systems in the UK residential sector; Journal Of The Institute Of Energy; 1998; 71(489); pp178-189

[18] A.D. Hawkes, P. Aguiar, B. Croxford, M.A. Leach, C.S. Adjiman, N.P. Brandon, Solid oxide fuel cell micro combined heat and power system operating strategy: Options for provision of residential space and water heating, Journal of Power Sources, Volume 164, Issue 1, 10 January 2007, Pages 260-271

[19] CIBSE Guide A - Environmental Design; 7th Edition; Issue 2; pp1-6; Table 1.4; 2006

[20] American Society of Heating, Refrigerating and Air-Conditioning Engineers; ASHRAE Fundamentals Handbook; 2001; Ch29: Non-Residential Cooling And Heating Load Calculations; pp. 29.4; Table 1

[21] Market Transformation Programme; v1.2; www.mtprog.com; Sept 2006; BNWAT18: Accounting for the trade-off between energy and water use - Innovation Briefing Note

[22] Heating and Ventilating Contractors Association (HVCA); HH_DHS1; Guide to Good Practice - Domestic Heating Specification

[23] DECC; Energy Consumption in the UK Domestic data tables 2011 Update; Table 3.10

[24] R. Yao, K. Steemers; A method of formulating energy load profile for domestic building in the UK; Energy and Buildings, 37 (2005), pp. 663–671

[25] A. Capasso, W. Grattieri, R. Lamedica, A. Prudenzi; A bottom-up approach to residential load modelling; IEEE Transactions on Power Systems, 9 (2) (1994), pp. 957–964

[26] Andrew Wright, Steven Firth, The nature of domestic electricity-loads and effects of time averaging on statistics and on-site generation calculations, Applied Energy, Volume 84, Issue 4, April 2007, Pages 389-403

[27] C. Walker, A residential electrical load model, Ph.D. thesis, University of New Hampshire, 1982

[28] J.V. Paatero, P.D. Lund. A model for generating electricity load profiles. International Journal of Energy Research Vol. 30:5, p. 273-290. 2006

[29] M. Aydinalp, V.I. Ugursal, A.S. Fung, Modelling of the appliance, lighting, and space-cooling energy consumptions in the residential sector using neural networks, Applied Energy, Volume 71, Issue 2, February 2002, Pages 87-110

[30] Keith J. Baker, R. Mark Rylatt, Improving the prediction of UK domestic energy-demand using annual consumption-data, Applied Energy, Volume 85, Issue 6, June 2008, Pages 475-482.

[31] S. Firth, K. Lomas, A. Wright, R. Wall, Identifying trends in the use of domestic appliances from household electricity consumption measurements, Energy and Buildings, Volume 40, Issue 5, 2008, Pages 926-936.

[32] Lane, A. Modelling domestic electricity consumption, John Rylands Library P5844, Manchester University; 1998.

[33] M. Stokes, M. Rylatt, K. Lomas, A simple model of domestic lighting demand, Energy and Buildings, Volume 36, Issue 2, February 2004, Pages 103-116

[34] M. Stokes, M. Rylatt, J. Mardaljevic, K. Lomas, M. Thomson, D. Infield, Solar city: managing the uptake of solar energy technologies from an electrical supply network perspective, in: Proceedings of the 5th Symposium of International Urban Planning and Environment Association, Oxford, UK, September 2002.

[35] I. Richardson, M. Thomson, D. Infield, A. Delahunt, Domestic lighting: A high-resolution energy demand model, Energy and Buildings, Vol. 41, Issue 7, July 2009, Pages 781-789

[36] Energy Saving Trust, The rise of the machines. A review of energy using products in the home from the 1970s to today, June2006, Accessed online December 2006 at www.est.org.uk/uploads/documents/aboutest/Riseofthemachines.pdf

[37] M. Hart, R. de Dear, Weather sensitivity in household appliance energy end-use, Energy and Buildings, Volume 36, Issue 2, February 2004, Pages 161-174

[38] Brown & Wright, Non0invasive and cost effective monitoring of energy consumption

[39] G.J. Levermore and J.B. Parkinson; Analyses and algorithms for new Test Reference Years and Design Summer Years for the UK; Building Service Engineering 2006; 27; 311

[40] Chartered Institute of Building Services Engineers Guide J; Section 5

[41] American Society of Heating, Refrigerating and Air-Conditioning Engineers; ASHRAE Fundamentals Handbook; 2005; Ch31; Fenestration

[42] C.M. Dickson, J.E. Dunster, S.Z. Lafferty, L.D. Shorrock; BREDEM: Testing monthly and seasonal versions against measurements and against detailed simulation models; Building Services Engineering Research and Technology; August 1996; 17; 135-140

[43] L D Shorrock and J I Utley; Domestic energy fact file 2003; pp. 77; BR 457; Building Research Establishment; 2003

[44] A.J. Summerfield, R.J. Lowe, H.R. Bruhns, J.A. Caeiro, J.P. Steadman, T. Oreszczyn; Milton Keynes Energy Park revisited: Changes in internal temperatures and energy usage; Energy and Buildings; 39; 2007; pp. 783–791

[45] Michel De Paepe, Peter D'Herdt, David Mertens, Micro-CHP systems for residential applications, Energy Conversion and Management, Volume 47, Issues 18 & 19, November 2006, Pages 3435-3446

[46] M. Newborough and P. Augood; Demand-side management opportunities for the UK domestic sector; IEE Proc., Gener. Transm. Distrib. 146, 283 (1999)

[47] G. Wood, M. Newborough, Dynamic energy-consumption indicators for domestic appliances: environment, behaviour and design, Energy and Buildings, Volume 35, Issue 8, September 2003, Pages 821-841

[48] M. Newborough, S.D. Probert, Intelligent automatic electrical-load management for networks of major domestic appliances, Applied Energy, Volume 37, Issue 2, 1990, Pages 151-168

[49] Iman Mansouri, Marcus Newborough, Douglas Probert, Energy consumption in UK households: Impact of domestic electrical appliances, Applied Energy, Volume 54, Issue 3, July 1996, Pages 211-285

[50] Market Transformation Programme; v1.3; www.mtprog.com; Oct 2006; BNCK06: Trends in kettle type and usage and possible impact on energy consumption

[51] Market Transformation Programme; v1.2; www.mtprog.com; Oct 2006; BNCK05: Historical microwave oven use and options to increase usage in the future

[52] I. Mansouri, M. Newborough, Dynamic energy consumption indicators for appliances, Report to ETSU, Report No. E/CG/00145/00/00/4255, February 1999

[53] Market Transformation Programme; v2.1; www.mtprog.com; Aug 2006; BNCK01: Assumptions underlying the energy projections of cooking appliances

[54] Market Transformation Programme; www.mtprog.com; Nov 2006; Policy Brief: UK Energy Consumption of Domestic Cooking Appliances

[55] Personal Communication with David McKay, AFA Fire & Security, September 2007

[56] Market Transformation Programme; v1.1; www.mtprog.com; Nov 2006; BNXS36: Estimated UK Standby Electricity Consumption in 2004

[57] Market Transformation Programme; v2.1; www.mtprog.com; Sept 2006; BNC08: Assumptions underlying the energy projections for domestic cold appliances

[58] I. Mansouri, M. Newborough, D. Probert, Energy consumption in UK households: Impact of domestic electrical appliances, Applied Energy, Volume 54, Issue 3, July 1996, Pages 211-285

[59] Herring, H., Electricity use in minor appliances in the UK, Energy, Vol20, No7, pp705-710, 1995

[60] DE B. Boardman, D. Favis-Mortlock, M. Hinells, K. Lane, G. Milne, E. Small, V. Strang, J. Wade, DECADE, First year report, Energy and Environment Programme, Environment Change Unit, University of Oxford, 1994

[61] Energy Saving Trust; The rise of the machines; Publication Reference CO126; June 2006; London; Accessed online October 2006 at

http://www.energysavingtrust.org.uk/content/download/28169/337639/version/3/file/Riseofthemachines.pdf

[62] Market Transformation Programme; v1.3; www.mtprog.com; Oct 2006; BNXS30: Vacuum cleaners – UK market, technologies, energy use, test methods and waste

[63] Market Transformation Programme; v1.1; www.mtprog.com; Aug 2006; BNDA03: Digital TV Adapters in the UK – Rationale for Projecting Future Energy Consumption

[64] Market Transformation Programme; www.mtprog.com; 2003; BNBROAD1: Energy requirement implications of broadband communication technology 2003–2010

[65] Market Transformation Programme; v2.1; www.mtprog.com; Sept 2006; BNW07: Assumptions underlying the energy projections for domestic dishwashers

[66] Market Transformation Programme; v2.0; www.mtprog.com; Jul 2006; BNW05: Assumptions underlying the energy projections for domestic washing machines

[67] Market Transformation Programme; v2.1; www.mtprog.com; Sept 2006; BNW06: Assumptions underlying the energy projections for domestic tumble dryers

[68] Market Transformation Programme; v2.0; www.mtprog.com; Aug 2006; BNTV01: Televisions: Future Stock and Energy Trends

[69] Market Transformation Programme; www.mtprog.com; 2005; BNCE1: List of Assumptions for MTP Consumer Electronics Sector

[70] Market Transformation Programme; www.mtprog.com; March 2008; BNDL01: Assumptions for energy scenarios in the domestic lighting sector; Version 4.0

[71] The Lighting Association; European EUP Legislation vs. UK Voluntary Agreement; Accessed online May 2012 at http://www.lightingassociation.com/files/downloads/427/Lamp_Phase_Out_Chart.pdf

[72] MINTEL Market Intelligence; Domestic Lighting; UK; May 2006

[73] Chartered Institute of Building Services Engineers; Guide A Environmental Design; 7th Edition; Issue 2; January 2007; Section 1.8

[74] Anderson et al; BREDEM-12 Model Description - 2001 Update; 2001; Building Research Establishment (BRE); Garston, UK

[75] CIBSE Guide A - Environmental Design; 7th Edition; Issue 2; pp1-6; Table 1.4; 2006

[76] Jordan & Vajen; Solar Energy; Vol. 69; Nos. 1-6; pp. 197-208; 2000; Influence of the DHW Load Profile on the Fractional Energy Savings: A Case Study of a Solar Combi-System with TRNSYS Simulations

[77] Market Transformation Programme; www.mtprog.com; Jun 2006; Policy Brief: UK Water Consumption of Domestic Showers

[78] Market Transformation Programme; v8.2; www.mtprog.com; Jan 2007; BNXS05: The Heat Replacement Effect

[79] Roman Spur, Dusan Fiala, Dusan Nevrala, Doug Probert, Influence of the domestic hot-water daily draw-off profile on the performance of a hot-water store, Applied Energy, Volume 83, Issue 7, July 2006, Pages 749-773

[80] NAHB Research Center, Inc.; domestic hot water system modeling for the design of energy efficient systems; Report prepared for NREL; April 2002

[81] Knight & Ribberink; European and Canadian non-HVAC Electric and DHW Load Profiles for Use in Simulating the Performance of Residential Cogeneration Systems; IEA Annex 42; May 2007

4 Thermal Load Following Micro-CHP Systems

4.1 Introduction

The development of micro-CHP systems has encompassed several prime mover technologies, as discussed in Section 1.4, where ICE-based systems have accounted for most sales to date, whilst SE, PEM and SOFC prime movers account for the majority of development activities. When selecting a prime mover for a μCHP system, operational performance, system lifetime and flexibility of application are important alongside the issues of practicality and cost, as discussed in Section 1.4.

The current norm for domestic μCHP systems (in many countries) is some form of heat-led control, typically achieved by applying thermal load following operating regimes, as justified in Section 1.5. To effectively load follow, a prime mover must be capable of relatively quick start-up, fast load changes and relatively high efficiency across a wide range of part-load conditions. Fuel cell technologies, whilst having high part-load efficiencies, may take a long time to start-up due to the time for the fuel processing subsystem to reach operating temperature or restrictions on stack temperature ramp rates to prevent damage. The thermal cycling of fuel cells, to follow minimal load conditions, is understood to have prohibitive lifetime restrictions and significant efficiency penalties. Furthermore, there may be challenges in recovering heat at a useful temperature (i.e. higher than the thermal storage temperature) for PEM-based systems, especially at part-load or during start-up. The electrical output of ICEs respond quickly to changes in load, however their thermal output typically lags behind any increases in electrical load. The feasible part-load range of ICE-based μCHP is understood to be limited to 50-100%. Both of these factors may limit the proportion of thermal demand met from the prime mover versus an auxiliary boiler. Thermal cycling has not been identified as a major restriction to operating lifetimes of ICE-based μCHP systems.

There are a number of SE-based μCHP systems on the market, within utility and manufacturer field trials, or in laboratory testing and development. Whilst the expected electrical efficiencies of SE-based systems will not exceed those of FCs, they

have the potential to compete with current and proposed ICE-based designs. Unlike FCs, SEs can be thermally cycled, with a modest transient performance penalty during start-up. However, whilst thermal cycling has been identified as a driver of SE lifetime, SEs are understood to be capable of achieving 6,000 thermal cycles or more, an order of magnitude higher than many FC technologies. Once a SE (of appropriate design) has reached operating temperature, it can be modulated to load conditions over a wide range, with a response rate quicker than FC-based μCHP systems.

It is argued that SE-based μCHP systems are well-placed to operate under a thermal load following regime, although the effects of system design (i.e. rated output capacities and efficiencies) on performance and lifetime need to be understood.

In scoping the investigation of thermal load following SE μCHP, desirable outcomes of an SE μCHP control strategy were identified as critical to the goal of creating a low-carbon energy system, namely:

- Maximise average net electrical and thermal efficiencies during operation (as calculated on a daily or annual basis) to increase CO_2 emission reductions
- Minimise thermal cycling in order to increase prime mover operating lifetime, and to reduce the impact of transient performance penalties during start-up on average efficiencies
- Minimise auxiliary thermal generation and maximise use of prime mover thermal output, which would increase the run-time and electrical generation of a thermally-constrained μCHP system
- Balance the maximisation of operating duration of prime movers with cumulative operating hours lifetime constraint, particularly in periods where increased runtime provides minimal CO_2 reductions due to thermal dumping and/or low electrical efficiency
- Minimise thermal dumping, where excess thermal generation from the prime mover is dumped to atmosphere, as it cannot be utilised or stored at that time
- Maximise electrical output to provide a system with increased electrical export (at the expense of increase thermal dumping and increased fuel consumption) for systems with a suitable net electrical efficiency

The seasonal and occupancy dependence of any identified relationships was identified as an important part of the investigation, as it may lead to the combination of operating regimes during different seasons or occupancy patterns, in order to maximise performance and lifetime.

In this chapter, methodology and results are presented for an investigation of various design variants of a SE-based μCHP system controlled using the thermal load following operating regime. The total carbon footprint of the system, incorporating fuel consumption of the prime mover and auxiliary boiler, and import and export of electricity from/to the NEG is quantified for each design variant. The carbon footprints of the μCHP systems were compared with the base-case energy system (as discussed in Section 4.3), and relative carbon savings (versus the base-case) were calculated. The major factors affecting prime mover lifetime, namely thermal cycling and cumulative operating duration, are investigated for each design variant. In the investigation of μCHP system performance and lifetime, various control methods are identified to improve performance and lifetime, which are explored in this and following chapters. Finally, novel performance analysis methodologies are devised and applied to simulation results, in order to understand the sizing of μCHP systems versus thermal demand scenarios.

4.2 Stirling Engine Micro-CHP Simulation Methodology

4.2.1 System Design

The μCHP concept systems investigated in this chapter integrated a Stirling Engine prime mover with an auxiliary boiler, with the same performance and operating constraints as the condensing boiler defined for the base-case energy system (see Section 2.4.5), and a thermal store, as defined in Section 2.3.5.

As discussed in Section 2.4.6, a number of design variants were specified with values of net electrical output (P_e) and net electrical efficiency (η_e) between 0.5kW$_e$ to 5kW$_e$ (in 0.5kW$_e$ steps) and 15% to 35% (in 5% steps), respectively.

4.2.2 System Lifetime

As discussed in Section 1.4, there are two major factors understood to affect SE lifetime, namely thermal cycling and cumulative operating duration, both of which could constrain the real-life operation of µCHP systems [1][2]. These factors were discussed for SEs in Section 1.4.2, and for other prime mover technologies in the remaining sub-sections of Section 1.4. The relationship between Relative Carbon Savings (RCS) and these lifetime issues is vitally important, and is used to limit studies, in this and following chapters, to prime mover design variants with suitably low thermal cycling.

Defining a lifetime limit for thermal cycling is very difficult, primarily because of a scarcity of data. Sunpower [3] report a SE design life in excess of 40,000 hours, with systems under test having completed over 2,000 thermal cycles, but do not define an expected limit for thermal cycling. Solo Kleinmotoren [4] notes that more than one thermal cycle per day would unacceptably limit the lifetime (and efficiency) of their µCHP system's prime mover. With expected lifetimes of at least 10 years [5][6], and assumed operation 365 days per year, one cycle per day would result in lifetime of circa 3,650 cycles. Private communications [7] with an energy utility engineer trialling µCHP suggests that Stirling Engines can tolerate approximately 6,000 thermal cycles, for a variety of materials and bonding issues.

The lifetime estimates discussed in Section 1.4.2 are typically between 20,000 to 40,000 hours, although prototype lifetimes of 50,000 hours, 70,000 hours and 150,000 were reported. Lifetime is a function of cumulative operating hours, thermal cycling, and other real-life operating conditions. It is therefore reasonable to assume that systems operating outside of controlled laboratory conditions may experience shorter lifetimes than selected prototypes that are reported on in the public domain. With Onovwiona & Ugursal [6] expecting FPSE technologies to achieve operating lifetimes of 10 years, and Sunpower [5] expecting to exceed that figure, a cumulative operating duration lifetime of 20,000-40,000 hours fits with the annual duration results reported in Section 4.3.7 (2,000-3,500 hours). This is in line with Kaarsberg et al's [8]

expectations that service intervals of 3,500-5,000 hours are to be greater than 1 year of “economic” operation.

4.2.3 Demand Scenarios

Primary Demand Scenarios (as defined in Section 3.9) combine 5 seasonal climate profiles with 2 occupancy profiles to create 10 daily demand scenarios (for space heating, DHW & electricity). For the majority of μCHP system concepts, simulations were undertaken for all Primary Demand Scenarios.

Considering the Heating Season (as defined in Section 3.8), it was prudent to perform simulations for the demand profiles incorporating “Summer” and “High Summer” climate profiles without the provision of space heating. This reflects the expected behaviour of many occupants wherein space heating controls are switched off for many months over summer, regardless of occasional periods of low temperature that would normally result in a demand for space heating [9]. In their investigation of thermal load following SE-, ICE- and FC-based μCHP, De Paepe et al [10] incorporated a non-heating season in their control regime, in that the space heating was switched off for 4 months over the summer season.

4.2.4 Pre-simulation Start-up Procedure

A pre-simulation start-up procedure is required in order to produce realistic initial values of simulation variables used in the finite element analysis algorithms. These values include internal air temperature, thermal store water temperature, wall element surface temperatures, SHDS temperatures, and time elapsed since shutdown of prime mover and auxiliary boiler. The procedure involves the execution of a daily simulation for 10 consecutive days, using the same Primary Demand Scenario and system design. The values of the aforementioned variables at the end of this 10-day period are used as the initial values for subsequent simulations.

As the temperatures will be affected by the climatic conditions, the pre-simulation procedure is performed for each seasonal climate profile of a given system concept.

The initial values are then used for all designs variants, and both occupancy profiles for that seasonal climate profile.

4.2.5 Significance of Simulation Results

There are challenges inherent in comparing carbon savings results produced from discrete simulation runs. The actual thermal demand of the building depends on the temperature at which the internal air volume is maintained. The temperature profile is dependent on the supply:demand matching performed by the simulation algorithms every time step. Differences between temperature profiles generated by different simulations will result in variations in thermal demand, even if the temperatures experience by the synthetic occupants are within the defined control and acceptability boundaries.

The energy system does not satisfy building demand directly, but via a thermal store and SHDS. Any difference in temperature, between the start and end of the simulation period, of the thermal store and SHDS elements, represents energy stored within these simulated elements. Indeed, thermal energy can also be stored within the simulated wall element (as discussed in Section 2.3.2). A similar issue was tackled by Hawkes et al [11] in their µCHP optimisation modelling exercise, where they used a number of design days, as adopted in this investigation. Their optimisation constraints required that stored energy in the thermal store was zero at midnight, i.e. it had a state-of-charge of zero, to avoid transfer between days (and hence seasons). This was easily implemented as they did not consider the temperature of the thermal store, instead implementing a simple state-of-charge energy balance, nor did they consider the response of demand to supply, as they used fixed hourly demand profiles pre-defined by simulation. Like Hawkes et al, it is assumed that any additional energy in the thermal store at the end of the simulated design day, calculated using the difference in thermal store temperature pre- and post-simulation, is discarded. However, any shortfall in thermal store energy, i.e. thermal store temperature is lower post-simulation than pre-simulation, is ignored in the quantification of performance metrics. Analysis of the simulation results shows that any shortfalls are typically less than 1% of thermal demand on the simulation day.

A number of simulations were undertaken, using a range of daily demand scenarios, CHP prime mover design variants, operating regimes and control variations. Any of these factors could result in a difference in stored thermal energy, or temperature profile, as discussed above. If this is coupled with the inherent uncertainty in simulated thermal demand and energy system performance, as discussed in Section 2.3.7, then it is appropriate to define a confidence limit for any simulation results. To this end, it was assumed that RCS of at least 10% can be treated as significant, i.e. little confidence can be placed in the benefit of systems with positive savings below 10%, or the dis-benefit of systems with savings between 0 and -10% (i.e. carbon penalties).

4.2.6 Operating Regimes

As the investigation progressed, a number of operating regimes were defined to address the operational aspects discussed in Section 4.1. These operating regimes, as discussed in the relevant sections of Chapters 4 and 5, are:

- Thermal Load Following (TLF)
- Continuous Operation over Thermal Demand Periods (CsO-TDP)
- Continuous Operation over Daily Demand Periods (CsO-DDP)
- Continuous Operation over 24 hours (CsO-24hr)
- Constant Operation (CtO)

The results of the investigation of the Thermal Load Following operating regime are presented in this chapter, as this is reflective of the rationale applied to many previous µCHP studies, as discussed in Sections 1.5 and 1.6.

4.2.7 Seasonal Control Variations

Under all operating regimes, the µCHP system will attempt to supply thermal energy for all space heating and DHW loads throughout the heating season, and all DHW loads throughout the non-heating season (as represented by the High Summer climate profile; refer to Section 3.8 for details). Several control variations were considered for all operating regimes, in an attempt to maximise efficiency during operation, collectively referred to as Restriction Seasonal Operation (RSO). The control variations considered are:

- Prime mover operates during heating season only; auxiliary boiler provides DHW during non-heating season – referred to as Restricted Seasonal Operation – No High Summer (RSO-NoHSum)
- Prime mover does not operate during the Summer or High Summer climate profiles; auxiliary boiler provides DHW at those times - Restricted Seasonal Operation – No Summer (RSO-NoSummer)

In Section 5.3, the concept of dynamically varying operating regime by season is addressed, as an alternative to RSO, hence creating an annual control scheme.

4.3 Thermal Load Following Stirling Engine Micro-CHP Results

4.3.1 Concept System Attributes

The first operating regime investigated was Thermal Load Following (TLF). In this regime, the μCHP prime mover is switched on and off in response to the temperature of the thermal store, which in turn is driven by the demand of the SHDS and DHW usage. The μCHP system is controlled to allow operation only during the thermal demand periods, as defined in Table 3.24. Operation of the prime mover and auxiliary boiler are triggered, and the prime mover modulated in the steps pre-defined in Section 2.4.4, using the thermal store control temperatures in Table 2.4.

4.3.2 Carbon Saving Results for Primary Demand Scenarios

The basis of this thesis is that the most important performance metric for a μCHP system is carbon reduction versus the base-case domestic energy system. Simulations were undertaken for each of the 10 primary demand scenarios (PDSs), as defined in Section 3.9, for all the design variants discussed in Section 2.4.6. The RCS for the scenarios with weekday and weekend occupancy patterns are presented in Figure 4.1 and Figure 4.2 respectively. The values plotted are tabulated in Appendix E.1.

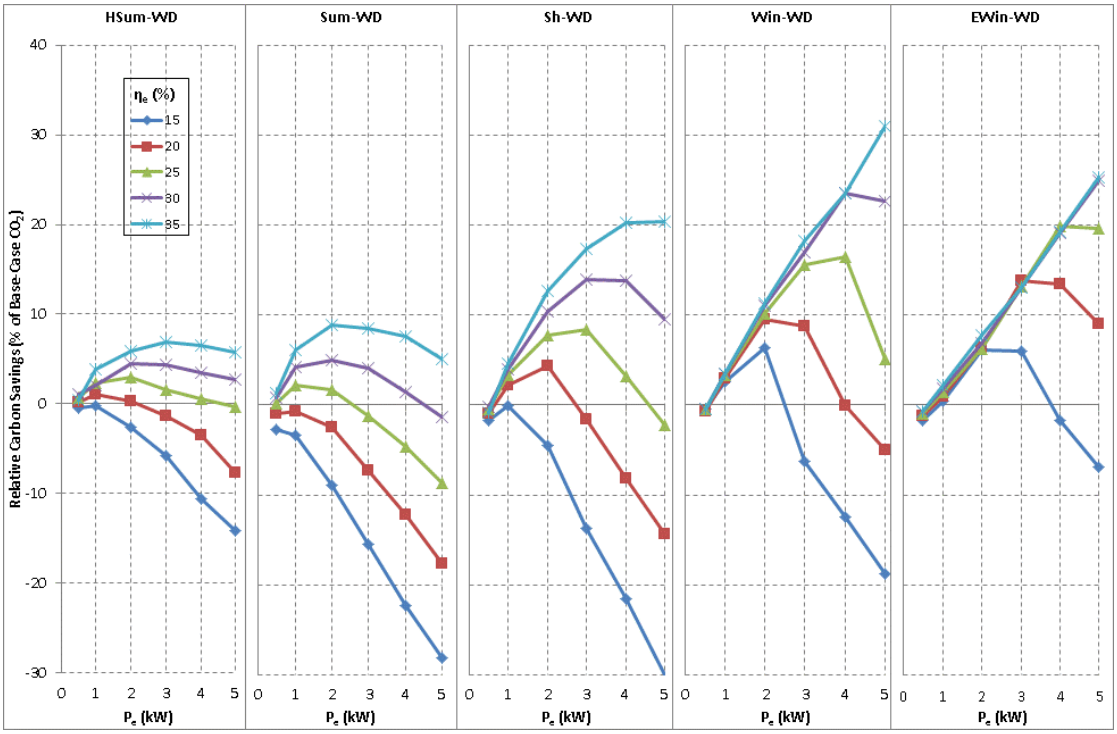

Figure 4.1: Relative Carbon Saving vs. Base-case energy system (%) for each design variant, for each Weekday PDS, for SE-TLF concept system

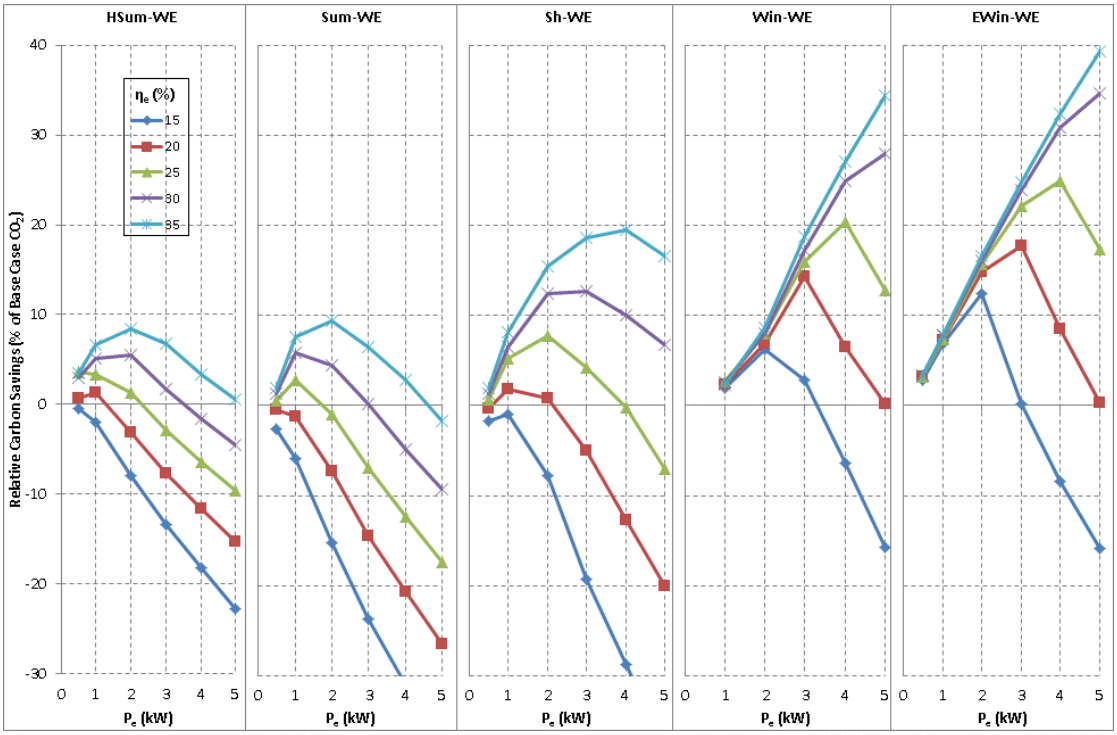

Figure 4.2: Relative Carbon Saving vs. Base-case energy system (%) for each design variant, for each Weekend PDS, for SE-TLF concept system

There are several comparisons that can be drawn between the results of each Primary Demand Scenario. There appears to be relationships between: prime mover rated electrical output (and hence rated thermal output) and RCS; thermal demand and relative carbon saving; prime mover η_e and RCS. The RCS are either insignificant, or represent carbon penalties, for all design variants during PDSs with low thermal demand. Systems with rated electrical output below $2kW_e$ exhibit similar carbon saving performance, as do systems with η_e below 30% for all but the Winter and Extreme Winters PDSs (with their high thermal demand).

The first and seconds relationships are both easy understood. Under thermal load following operation, greater cumulative thermal demand will require the prime mover to operate either longer or closer to full load, hence increasing electrical output and increasing efficiencies. As the thermal capacity of the prime mover increases with P_e (assuming that the electrical and heat recovery efficiencies remain the same), a prime mover under TLF operation would either operate for a shorter period or at lower load, hence decreasing electrical output and efficiencies.

The second relationship is influenced by electrical efficiency; presumably for two reasons. First, the thermal capacity of a prime mover will decrease with increasing electrical efficiency (assuming the heat recovery efficiency remains constant, as it does in this investigation), which should allow thermally-constrained μCHP systems to operate for longer. Secondly, increased electrical efficiency will reduce the fuel consumption of the prime mover.

Furthering the understanding of these relationships would support some form of design optimisation. Referring to each PDS in Figure 4.1 and Figure 4.2, the maximum RCS, within each PDS, for a μCHP system with a given net electrical efficiency occurs at a specific net electrical output. This electrical output increases independently with net electrical efficiency and thermal demand (i.e. between each PDS). However, this relationship is not consistent between the High Summer (HSum) and Summer (Sum) primary demand scenarios, for all but the 35% η_e design variants, as can be seen by referring to Table 4.1.

Design Variant	Relative Carbon Savings (% of Base-Case CO_2)					
P_e-η_e	HSum-WD	Sum-WD	WD Difference	HSum-WE	Sum-WE	WE Difference
0.5kW-15%	-0.5	-2.8	-2.3	-0.4	-2.6	-2.2
1kW-15%	-0.2	-3.3	-3.1	-1.9	-5.8	-3.9
2kW-15%	-2.7	-8.9	-6.3	-7.9	-15.2	-7.3
3kW-15%	-5.8	-15.5	-9.7	-13.3	-23.6	-10.3
4kW-15%	-10.6	-22.3	-11.7	-18.1	-31.0	-12.8
5kW-15%	-14.1	-28.2	-14.1	-22.7	-37.7	-15.0
0.5kW-20%	0.1	-1.0	-1.1	0.7	-0.4	-1.1
1kW-20%	1.1	-0.8	-1.8	1.3	-1.2	-2.4
2kW-20%	0.3	-2.5	-2.8	-3.1	-7.3	-4.3
3kW-20%	-1.3	-7.3	-6.0	-7.6	-14.5	-6.9
4kW-20%	-3.5	-12.3	-8.8	-11.6	-20.6	-9.0
5kW-20%	-7.6	-17.6	-10.0	-15.3	-26.4	-11.2
0.5kW-25%	0.7	0.2	-0.5	3.6	0.6	-3.1
1kW-25%	2.3	2.1	-0.2	3.3	2.9	-0.4
2kW-25%	3.0	1.7	-1.2	1.4	-1.0	-2.4
3kW-25%	1.6	-1.2	-2.8	-2.8	-7.0	-4.1
4kW-25%	0.5	-4.6	-5.1	-6.4	-12.4	-6.0
5kW-25%	-0.3	-8.7	-8.4	-9.5	-17.4	-7.9
0.5kW-30%	1.0	0.7	-0.3	3.0	1.2	-1.7
1kW-30%	2.1	4.2	2.1	5.1	5.8	0.7
2kW-30%	4.5	4.9	0.5	5.6	4.5	-1.1
3kW-30%	4.3	4.1	-0.2	1.8	0.2	-1.6
4kW-30%	3.4	1.5	-2.0	-1.6	-4.9	-3.3
5kW-30%	2.7	-1.3	-4.0	-4.5	-9.3	-4.9
0.5kW-35%	0.4	1.3	0.9	3.5	1.9	-1.6
1kW-35%	3.8	6.1	2.3	6.6	7.7	1.1
2kW-35%	5.9	8.9	3.1	8.4	9.4	1.0
3kW-35%	6.9	8.5	1.6	6.8	6.5	-0.3
4kW-35%	6.5	7.6	1.1	3.4	2.8	-0.6
5kW-35%	5.8	5.1	-0.7	0.5	-1.7	-2.2

Table 4.1: Comparison of RCS between HSum-WD & Sum-WD and HSum-WE & Sum-WE, for all design variants

As discussed in Section 4.2.7, the CHP system does not have a space heating load to satisfy during HSum, whilst it does during Sum, even if it is very low; 20kWh (WD) and 21kWh (WE). Further investigation identified that the low space heating demand, as satisfied from the thermal store, resulted in increased thermal cycling of prime mover and longer operation at part-load when operating under the Summer PDS, as opposed to High Summer. The reduction of useful energy output during warm-up periods (as driven by thermal cycling) and reduced thermal and electrical efficiencies during part-load operation resulted in decreased RCS (during Sum versus HSum) for many system design variants. This also explains the wider distribution between RCS values in Sum-WD than HSum-WD; the trend is that distribution narrows with increasing demand. With the significantly larger space heating demand associated with the Shoulder PDS,

the prime mover can operate for long enough to provide larger RCS for specific system design variants.

The interaction between thermal demand and the potential thermal supply of a μCHP prime mover is important in understanding the relationship between P_e, RCS and thermal demand, as previously discussed in this section. The position and magnitude of the RCS maxima (for any combination of η_e and thermal demand) previously discussed is affected by this interaction, as is the magnitude of RCS (either positive or negative) for system design variants diverging from these maxima. This will be explored in further detail in Section 4.3.9.

Finally, by comparing the RCS results presented in Figure 4.1 and Figure 4.2, the effect of the occupancy pattern (i.e. Weekday vs. Weekend) is apparently limited to the difference in thermal demand (as a daily total), as no major differences are apparent because of the temporal basis (i.e. shape) of the demand. However, further investigation identified that WE PDSs resulted in increased thermal cycling of prime mover and longer operation at part-load compared to WD PDSs. These effects were especially prevalent at low η_e, and at high electrical output. The resultant reduction in prime mover efficiencies limited the increase in RCS due to increased thermal demand between WD and WE PDSs.

4.3.3 Annual Carbon Savings Results & Seasonal Operation

In the previous section, simulation results for µCHP systems operating within discrete 24-hour demand scenarios were presented. In practice, the important performance metrics for end-users must be calculated for annual operation. Estimated annual results were calculated by amalgamating results from each primary demand scenario using the weighting factors in Table 3.23, and are presented in Figure 4.3.

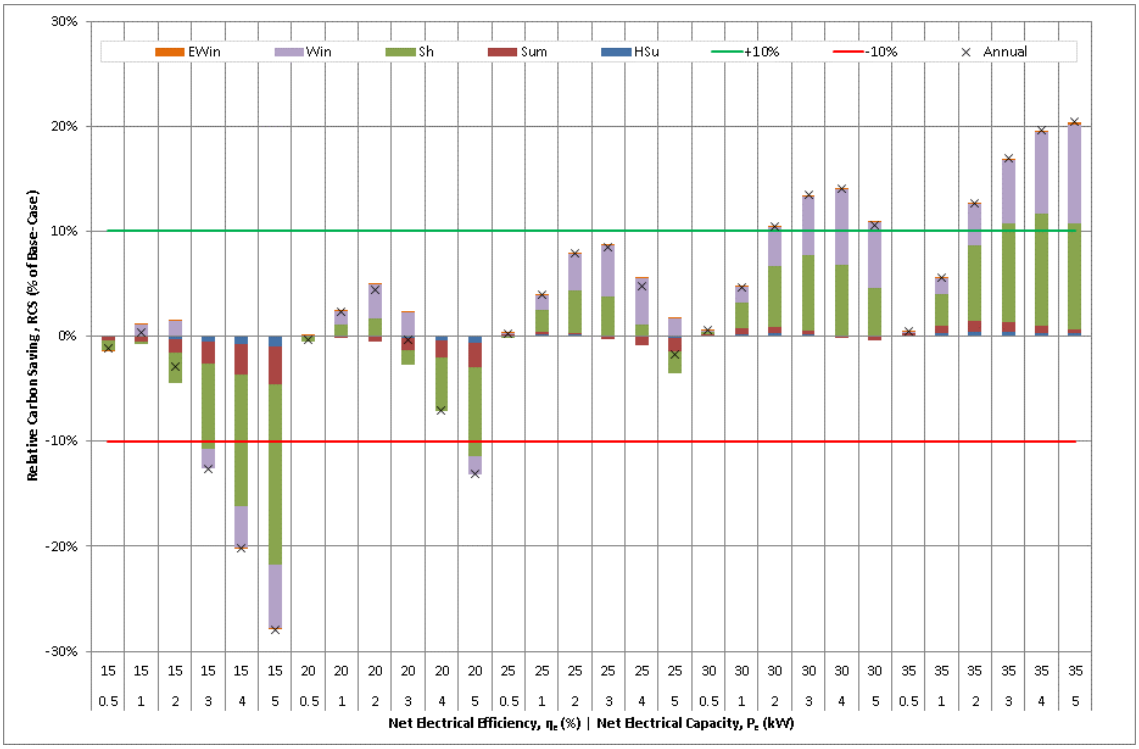

Figure 4.3: Annual RCS for SE TLF µCHP system, with the indicated contribution from each climate and assumed significance limits

The results presented in Figure 4.3 illustrate that significant carbon saving is possible within the design boundaries. It is prudent to note that design variants with η_e below 30% demonstrated insignificant relative carbon savings, and indeed significant relative carbon penalties in some cases, whilst carbon savings for design variants with rated net electrical output below 2kW$_e$ also showed insignificant results.

It is also apparent that the primary demand scenarios for the Winter and Shoulder climate make the largest contribution to carbons savings (or penalties). In some cases, operation during the High Summer and Summer climate scenarios may incur a carbon

penalty for a design variant with significant carbon savings due to performance during the remaining climate scenarios. This prompted an investigation of Restricted Seasonal Operation (RSO) applied to the TLF operating regime, where the prime mover is restricted during High Summer (and optionally Summer) climate scenarios. Thermal demand would therefore be met by the auxiliary boiler, with performance characteristics identical to the base-case energy system (hence providing neither carbon saving or penalty). The results of this investigation are presented in Figure 4.4.

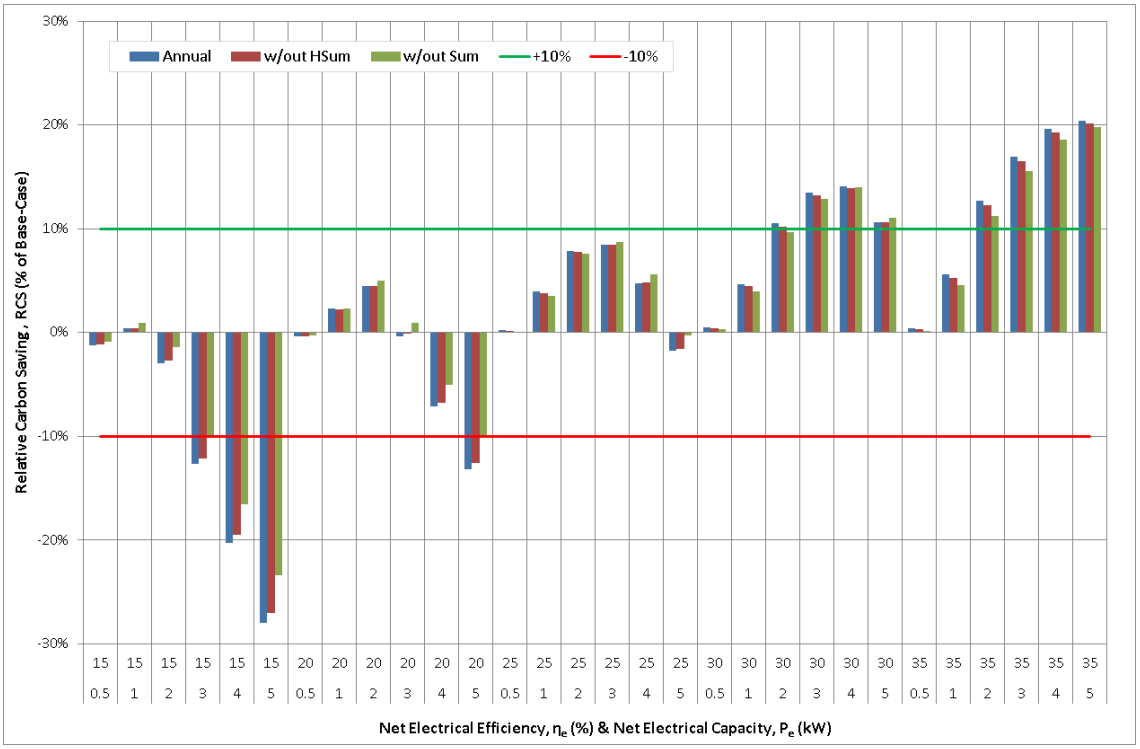

Figure 4.4: Annual RCS, for SE TLF µCHP system, where the prime mover operation has been completely restricted during the indicated climate scenarios (High Summer & Summer), along with assumed significance limits

Admittedly, the RSO of prime mover operation increases significant relative carbon savings for the 5kW$_e$-30% design variant only, and in fact decreases significant RCS for other design variants with η_e equal to 30% and 35%. However, the magnitude of these RCS decreases (several percentage points) is particularly interesting, as it suggests that (in the case of the climate data used in these simulations) reduction of prime mover operation from 365 to 248 days per year has a minimal effect on annual RCS for desirable design variants. This is discussed further in the context of prime mover lifetime in Section 4.3.8.

4.3.4 Carbon Saving Attribution

The concept of carbon abatement due to μCHP system operation is reliant on the utilisation of both heat and power production; hence requiring thermal and electrical generation levels with a magnitude equal to, or less than, the local thermal and electrical demands, and temporal co-incidence of supply and demand. With the addition of a thermal store, the need for co-incident utilisation of heat and power is diminished, although an efficiency penalty is accrued in relation to the temporal separation of thermal generation and thermal utilisation. The prevailing logic in the field of micro-generation in general has been to utilise the NEG as an unlimited source and sink of electricity, with the assumption that electrical export directly replaces an equal amount of centralised generation at the grid's average carbon intensity; hence decoupling on-site electrical generation from electrical demand. This presumption holds as long as no constraints exist on electrical imports and exports to and from the grid; either in terms of technological barriers, technologically-demanded legislative measures, economic incentives to reduce import, or economic penalties to dissuade export.

The common theme of carbon accounting approaches relating to μCHP systems in particular, and indeed micro-generation in general, is that carbon saving calculations are made with a base-case which describes the status quo currently in effect in relation to energy supply provision. In the case of domestic buildings, and this research project, the base-case is commonly quoted as a gas-fired boiler for thermal provision, with a connection to the NEG for electrical provision. The associated carbon footprint of the base-case is therefore the sum of the simple products of thermal and electrical demands with their associated carbon intensities.

Calculation of the carbon footprint of a μCHP system is slightly more complex, as it constitutes the carbon attributed to prime mover fuel consumption, auxiliary boiler fuel consumption, displacement of electrical import from NEG, and the carbon credit associated with electrical export to the NEG. This export carbon credit accounts for the displacement of central generation elsewhere on the NEG, with the aforementioned assumption of average NEG carbon intensity. The carbon saving, or indeed penalty,

associated with a μCHP system is then calculated as the difference in carbon footprints.

When analysing the operational results of μCHP systems, it is usually desired to quantify the proportion of carbon footprint, and savings, resulting from the mechanisms of electrical import displacement, electrical export carbon credit, and displacement of thermal-only generation. The ambiguity of carbon accounting methods in relation to μCHP systems is the attribution of carbon emissions from prime mover and auxiliary fuel consumption against each of the aforementioned mechanisms. A variety of attribution methods could be conceived, primarily motivated by the manner in which combined heat and power generation is perceived; i.e. as thermal generation with electricity as an incidental by-product, as electrical generation with useful thermal energy as a by-product, or as intentional production of both energy forms with some other proportional split of generation significance.

In the analysis presented below, the carbon footprint of the μCHP system is disaggregated by the three mechanisms discussed above, and presented as proportions of the base-case carbon footprint. The attribution of carbon to each mechanism can be summarised as:

- Thermal Generation Displacement (TGD), calculated using equation (4.1), is the difference between boiler fuel consumption in the base-case (F_{auxBC}) and auxiliary fuel consumption of the μCHP system (F_{auxCHP}), multiplied by the carbon intensity of the fuel (CI_{fuel})
- Electrical Import Displacement (EID), calculated using equation (4.2), is the reduction of gross electrical import (as opposed to net import defined in Section 1.6) to the dwelling from the NEG, between the base-case ($Q_{eig\text{-}BC}$) and concept system ($Q_{eig\text{-}CHP}$), multiplied by the carbon intensity of the NEG (CI_{grid})
- Electrical Export Credit (EEC), calculated using equation (4.3), is the gross electrical export of the dwelling to the NEG ($Q_{eeg\text{-}CHP}$), multiplied by the carbon intensity of the NEG (CI_{grid})

- Additional Fuel Consumption (ACF), calculated using equation (4.4), is the prime mover fuel consumption (F_{CHP}), multiplied by the carbon intensity of the fuel (CI_{fuel})

$$TGD = \left(F_{auxBC} - F_{auxCHP}\right) * CI_{fuel} \quad (4.1)$$

$$EID = \left\lfloor (Q_{eig-BC} - Q_{eig-CHP}) * CI_{grid} \right\rfloor \quad (4.2)$$

$$EEC = \left\lfloor Q_{eig-CHP} * CI_{grid} \right\rfloor \quad (4.3)$$

$$ACF = F_{CHP} * CI_{fuel} \quad (4.4)$$

Figure 4.5 shows that the cumulative effect of the Electrical Import Displacement and Electrical Export Credit mechanisms with the additional fuel required for the µCHP system result in carbon penalties. Only once the Thermal Generation Displacement mechanism is considered, for the design variants under investigation, can the net footprint of the system µCHP provide a relative carbon saving.

This behaviour is expected, as the carbon intensity of generated electricity (CI_{gen}), in the case of the particular µCHP design variants under investigation, is greater than that of the NEG. This stems from the underlying relationship between carbon intensity and η_e, where the former is equal to the carbon intensity of the fuel multiplied by the η_e of the generator for the form of energy in question. Mathematical analysis of this relationship, using the established carbon intensities of the natural gas fuel (CI_{fuel}=0.19kgCO_2/kWh) and NEG (CI_{grid}=0.44kgCO_2/kWh), stipulate that η_e below 44.2% will result in generated electrical carbon intensities exceeding that of the NEG.

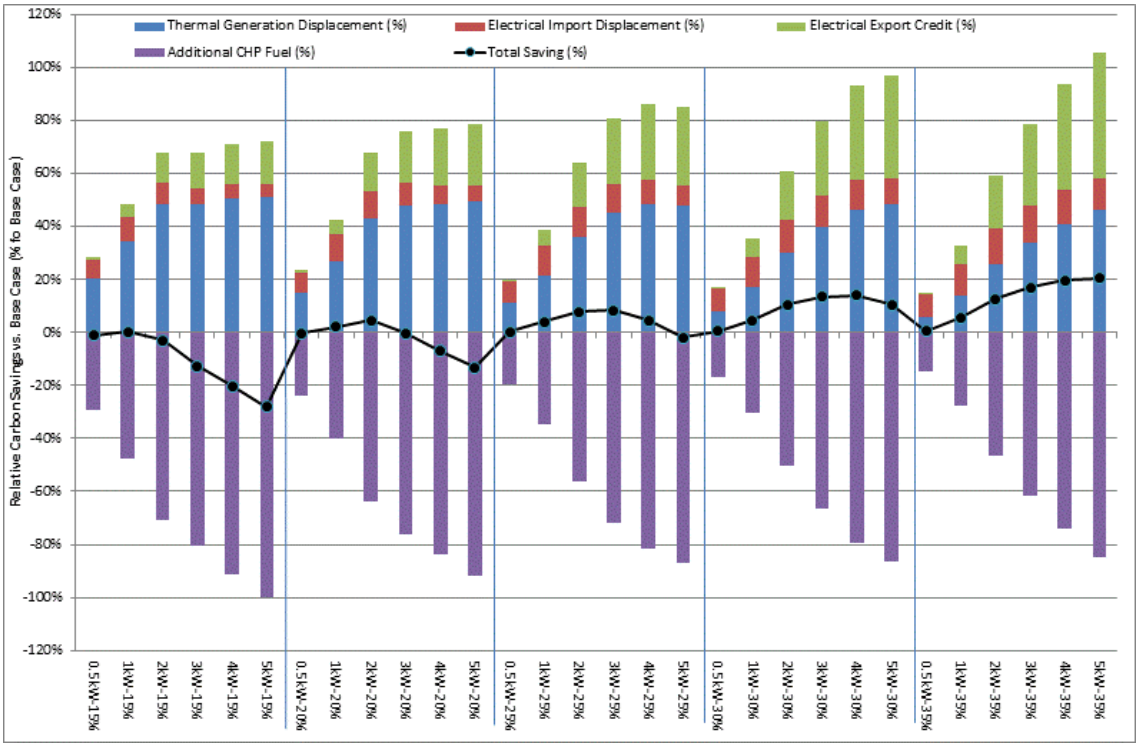

Figure 4.5: Annual Amalgamation of Relative Carbon Savings and constituents mechanisms, disaggregated by η_e

4.3.5 Thermal Generation Displacement

The relationship between Thermal Generation Displacement (TGD) and Rated Net Electrical Output (P_e), see Figure 4.6, is indicative of several constraints on the carbon saving potential of a concept µCHP system. Within the boundaries of the design options investigated, the RCS due to TGD appears to saturate for each η_e design option at a value between 45%-51%.

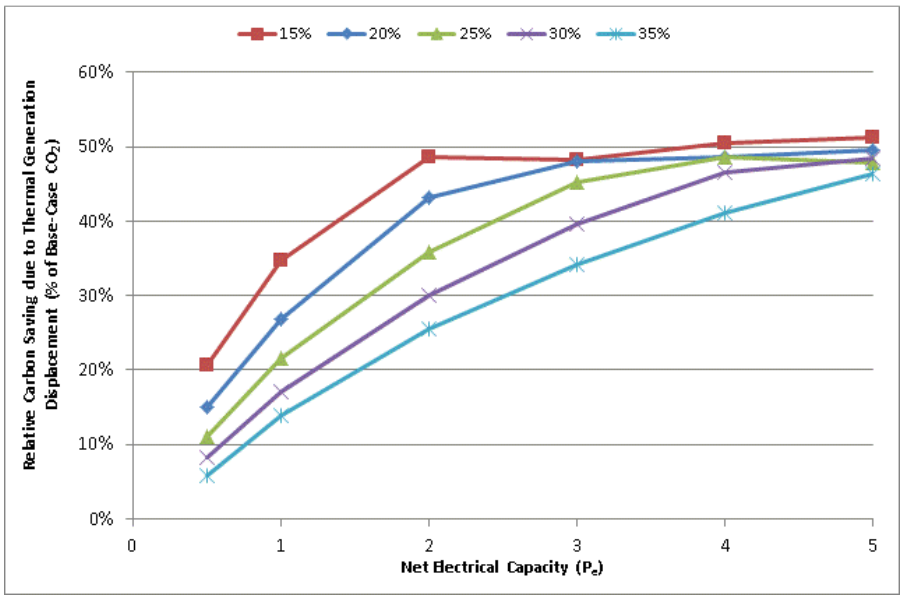

Figure 4.6: Relative Carbon Saving due to Thermal Generation Displacement vs. Net Electrical Capcity of Prime Mover for all design variants, disaggreagted by η_e

Plotting TGD versus the Thermal Output Capacity (P_{th}) of each design variant, as shown in Figure 4.7, suggests that the saturation previously identified is due to the relationship between TGD and P_{th}. Further analysis identified that 71% of the base-case carbon footprint was due to gas consumption to satisfy thermal demand. In the context of Figure 4.7, RCS due to TGD appears to saturate at approximately 72% of the thermally-derived carbon footprint of the base-case energy system.

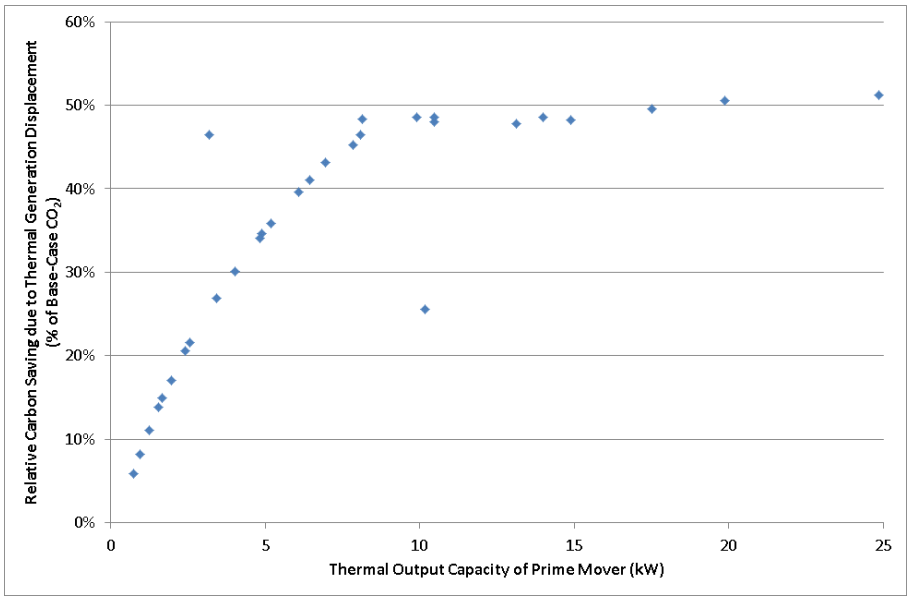

Figure 4.7: Relative Carbon Saving due to Thermal Generation Displacement vs. Thermal Output Capacity of Prime Mover for all design variants

In order to understand if this is related to thermal demand, the results for each design variant simulation, under Summer, Shoulder, Winter and Extreme Winter demand scenarios were analysed. As illustrated in Figure 4.8, the saturation level for Relative Carbon Saving due to Thermal Generation Displacement appears to increase with thermal demand.

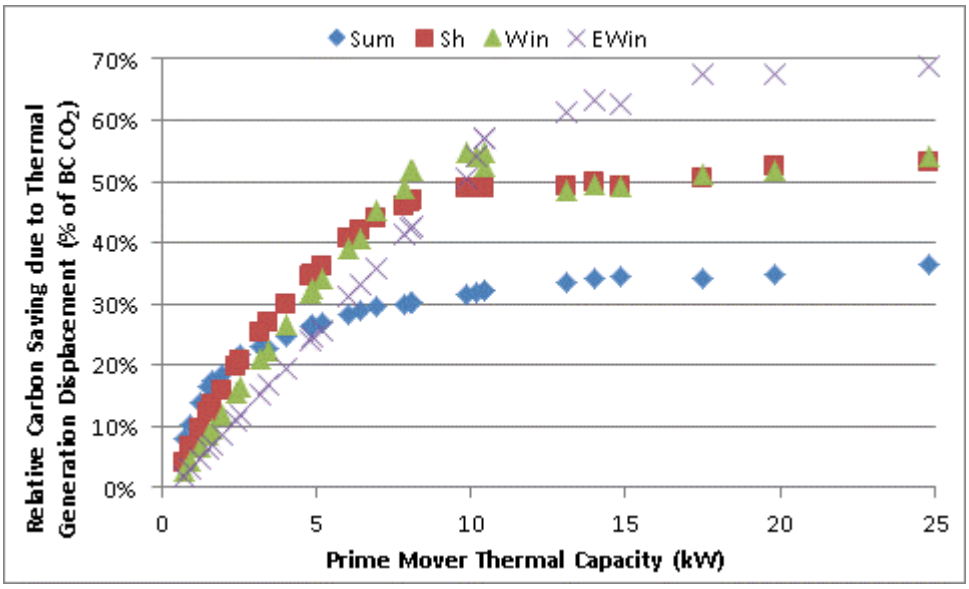

Figure 4.8: RCS due to Thermal Generation Displacement vs. Rated Thermal Output of Prime Mover, plotted for Weekday primary demand scenarios (except High Summer)

In Figure 4.9, the RCS is plotted versus the ratio between potential daily thermal supply and base-case thermal demand ($Q_{thDemand\text{-}BC}$). This novel metric, referred to a Potential Thermal Supply:Demand Ratio (PTSDR), is calculated using equation (4.5), where the prime mover's rated thermal capacity (P_{th}) is multiplied by the cumulative duration of the thermal demand periods (t_{TDP}), and divided by the thermal demand experienced by the same scenario using the base-case energy system.

$$PTSDR = \frac{(P_{th} * t_{TDP})}{Q_{thDemand-BC}} \qquad (4.5)$$

For simulations where PTSDR is greater than unity, the Relative Carbon Saving due to Thermal Generation Displacement begins to approach a maximum, after a dip. This maximum increases with thermal demand.

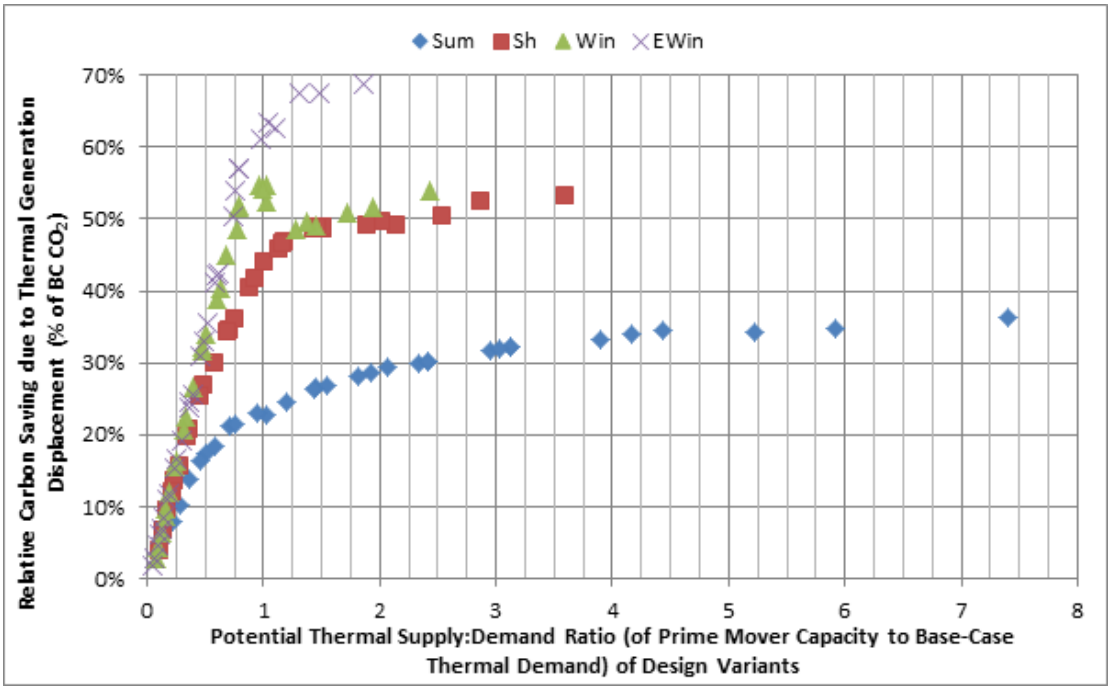

Figure 4.9: RCS due to Thermal Generation Displacement vs. PTSDR (Potential Thermal Supply:Demand Ratio), plotted for Weekday Primary Demand Scenarios (except H. Summer)

Further analysis identified that the design variants with the largest offset of auxiliary fuel consumption do not always have a large RCS. Indeed, as Figure 4.10 shows, the design variants with significant carbon penalties have the highest RCS due to Thermal Generation Displacement. Therefore, whilst Thermal Generation Displacement is a significant factor in overall RCS, it does not dominate other components of RCS.

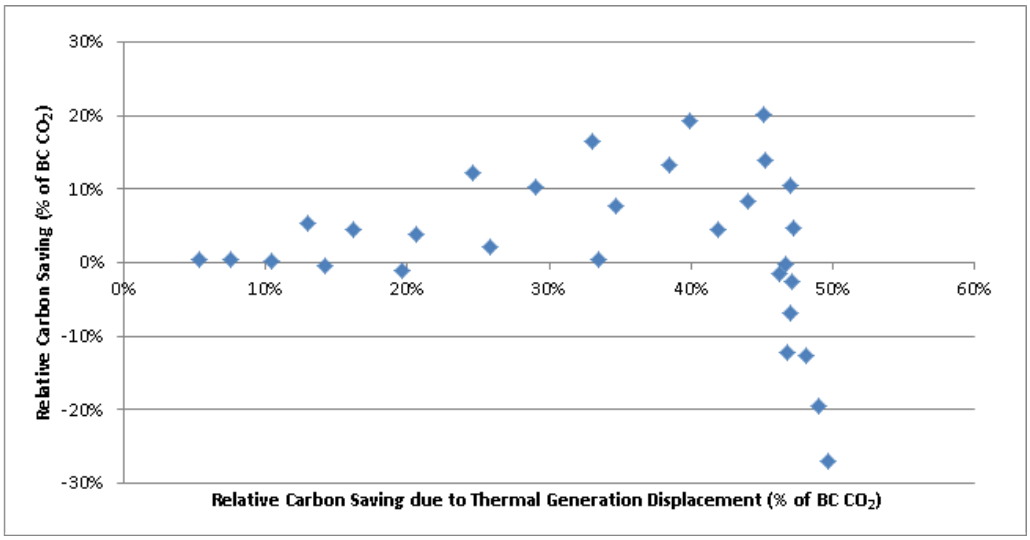

Figure 4.10: Relative Carbon Saving of each design variant, operating on an annual basis, vs. RCS due to Thermal Generation Displacement

As the relationship between Relative Carbon Savings and design variants is complex, as is the relationship between Relative Carbon Savings and RCS due to Thermal Generation Displacement, it was prudent to investigate further. The aforementioned carbon savings were plotted versus the PTSDR, as a measure of design variant, in Figure 4.11. It is now clear to see that attempting to increase the RCS due to displacement of thermal generation by increasing the thermal output of the prime mover does not result in increased RCS, once the ratio of potential thermal supply:demand increases much past unity.

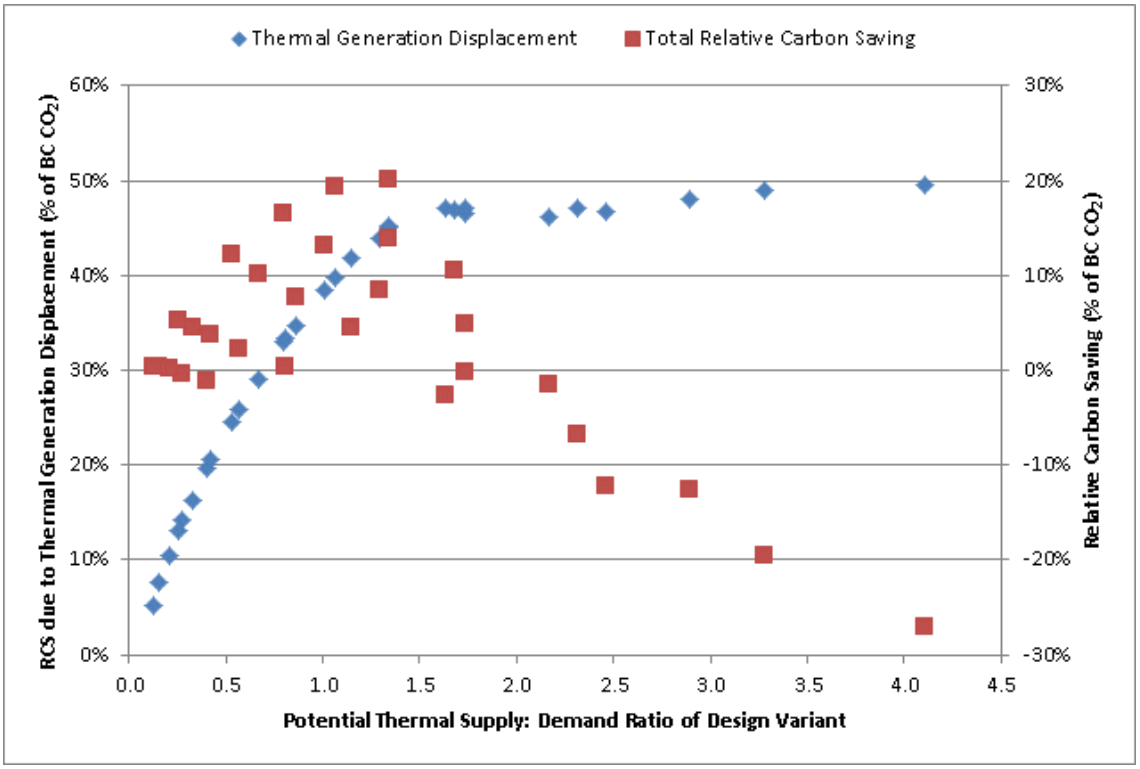

Figure 4.11: Relative Carbon Saving (RCS) of each design variant, operating on an annual basis, and RCS due to Thermal Generation Displacement, vs. PTSDR

It was already understood that design variants with large rated thermal outputs would be required to modulate or thermally cycle more frequently than lower capacity prime movers (under the same thermal demand conditions). This can be confirmed by considering Figure 4.12.

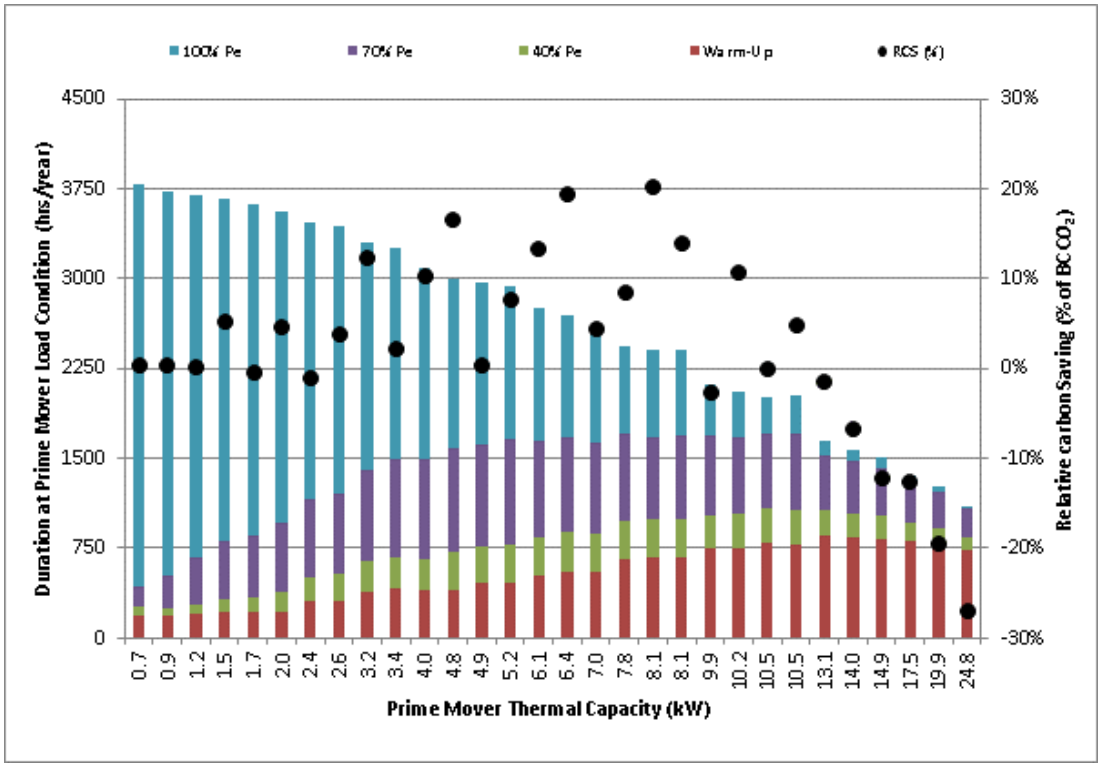

Figure 4.12: Prime Mover Duration at Load Conditions (hours annually) and RCS vs. Prime Mover Thermal Capacity (kW_{th})

When Figure 4.12 is re-plotted using PTSDR instead of thermal capacity, as in Figure 4.13, then distribution of significant and non-significant RCS results around a ratio of 0.5 to 1.5 is easily comprehended. From examination of Figure 4.13, it is clear that RCS are influenced by at least two factors. At a macro-scale, RCS is a function of PTSDR, where no significant RCS are found for design variants with a PTSDR below 0.5 or above 1.5. For design variants with similar PTSDR, there is a spread of RCS, which is due to differences in η_e, where higher η_e results in increased RCS.

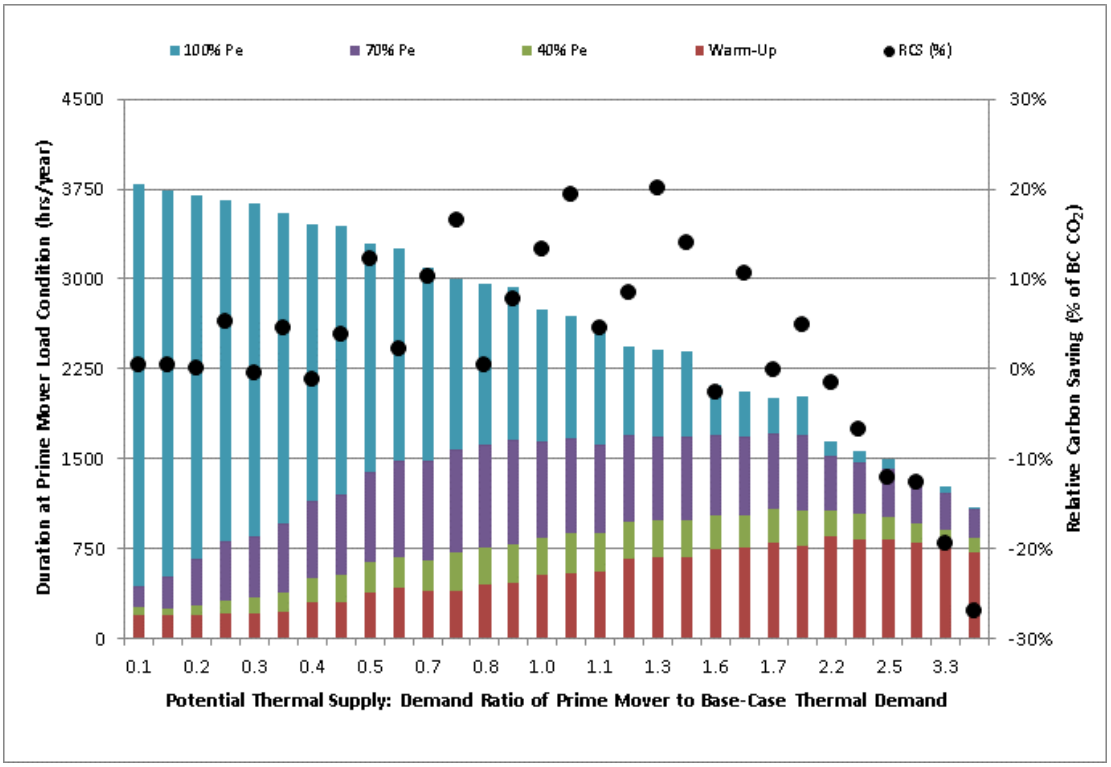

Figure 4.13: Prime Mover Duration at Load Conditions (hours annually) and RCS vs. PTSDR (prime mover to base-case thermal demand)

For design variants with apparently significant carbon savings, it is still relevant to understand the proportion of thermal output satisfied by the auxiliary boiler. In Figure 4.14, the remaining auxiliary fuel consumption that remains to be displaced is plotted for the 8 design variants with significant RCS over an annual period. The spread of total annual runtimes (across all load conditions) suggests that some design variants could perhaps displace additional auxiliary thermal generation by increasing run-times.

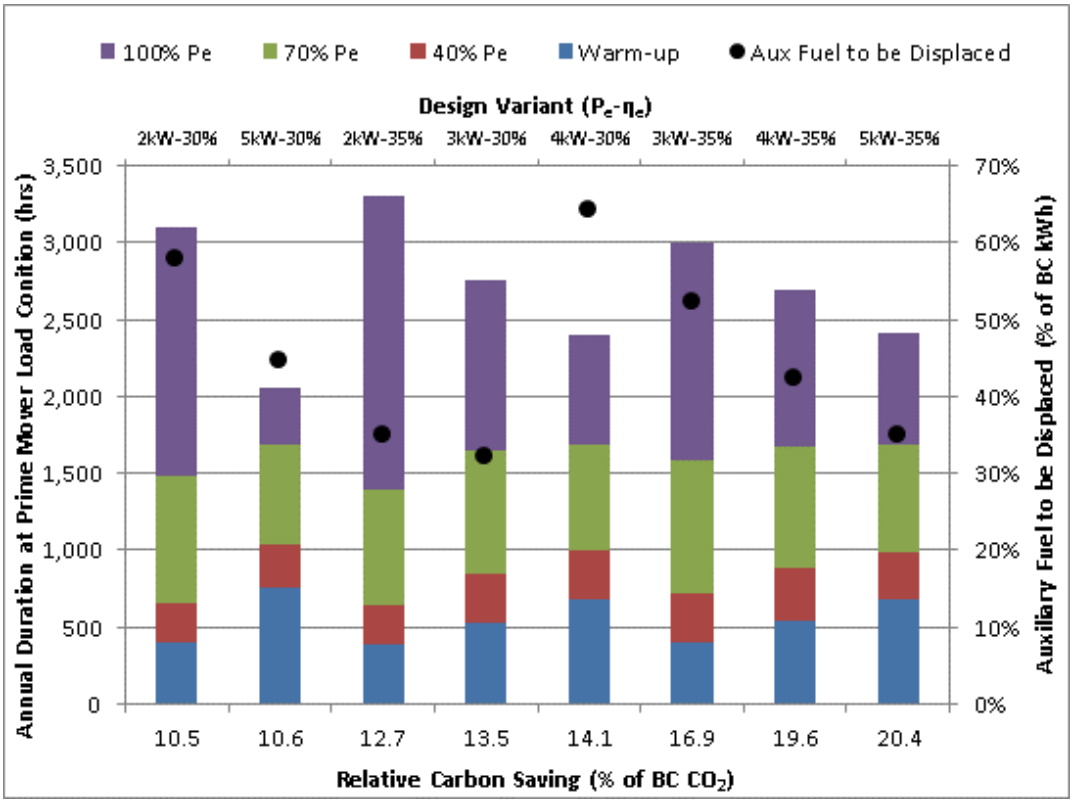

Figure 4.14: Duration of Prime Mover at Load Conditions (hours annually) and Auxiliary thermal generation remaining to be displaced versus RCS for 8 design variants

If the prime mover can satisfy a larger proportion of thermal demand than observed in the simulations discussed above, then RCS should increase, so long as the decreased reliance on axillary generation do not decrease system efficiency. Alternative operating regimes investigated in the remainder of this chapter aim to decrease reliance on auxiliary generation.

To conclude, within the control limitations provided by the TLF operating regime, it is impossible to displace all of the thermal generation from the gas boiler (71% of the base-case carbon footprint in this investigation). It is postulated that 100% of potential thermal carbon footprint displacement is, in practice, impossible in the concept systems discussed, due to several factors: the constraints on the thermal capacity of μCHP prime mover, as opposed to the base-case thermal generator, especially for prime movers with high rated η_e or low P_e; the differing start-up conditions of prime movers and thermal-only generators; and the occurrence of instantaneous thermal demands of sufficient magnitude to trigger auxiliary thermal generation in addition to the prime mover.

4.3.6 Electrical Import Displacement & Electrical Export Credit

As discussed in Section 4.3.5, a µCHP system without electrical storage, operating under a thermal load following regime, can only attempt to satisfy some of the electrical demand during the TDP. The electrical demand within the TDPs, for the demand profiles generated for the base-case energy system, was between 72-90%, as shown in Table 3.26. This equated to an average load throughout the TDPs of the primary demand scenarios of 0.7-1.1kW$_e$. On an annual basis, 78% of electrical demand was consumed during the TDPs, with an average load during TDPs of 0.8kW$_e$.

Investigation of displacement of electrical import across all simulated design variants, as presented in Figure 4.15, revealed that less than 50% of import was displaced, even when the rated electrical output of the prime mover was significantly larger than the average demand. The design variants with higher η_e consistently displaced more import, regardless of rated electrical output. The proportion of displacement peaks at a particular value of rated electrical output for each η_e family. The value of P_e where this maxima occurs increases with electrical efficiency. By scrutinising Figure 4.16, this maxima appears to correspond to a particular prime mover thermal capacity.

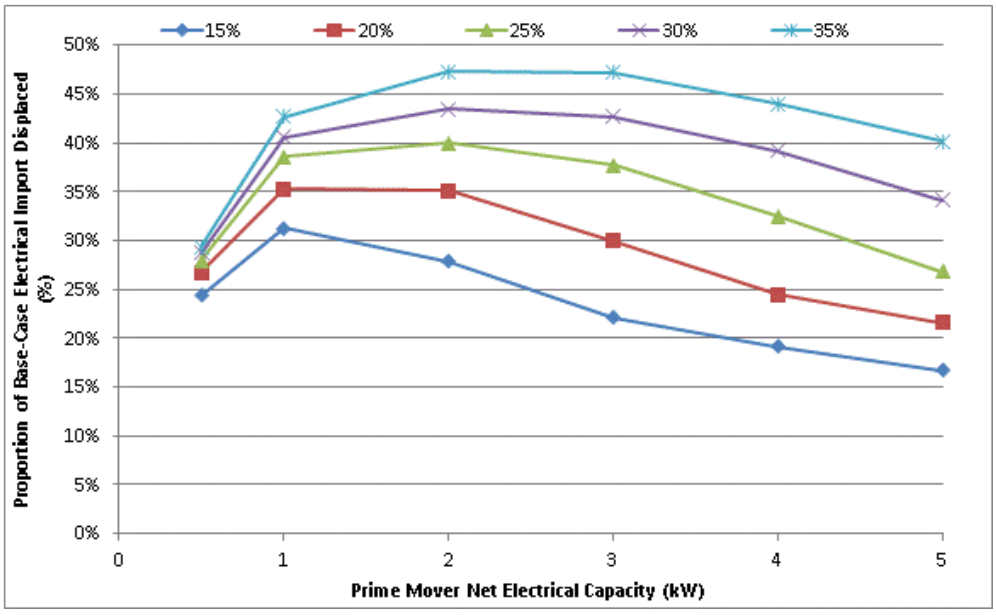

Figure 4.15: Proportion of base-case electrical Import displaced by each design variant of SE µCHP system operating annually in Thermal Load Following regime, disaggregated by η_e

Since electrical imports account for 29% of the base-case annual carbon footprint, RCS due to Electrical Import Displacement are less than 14%, as shown in Figure 4.16.

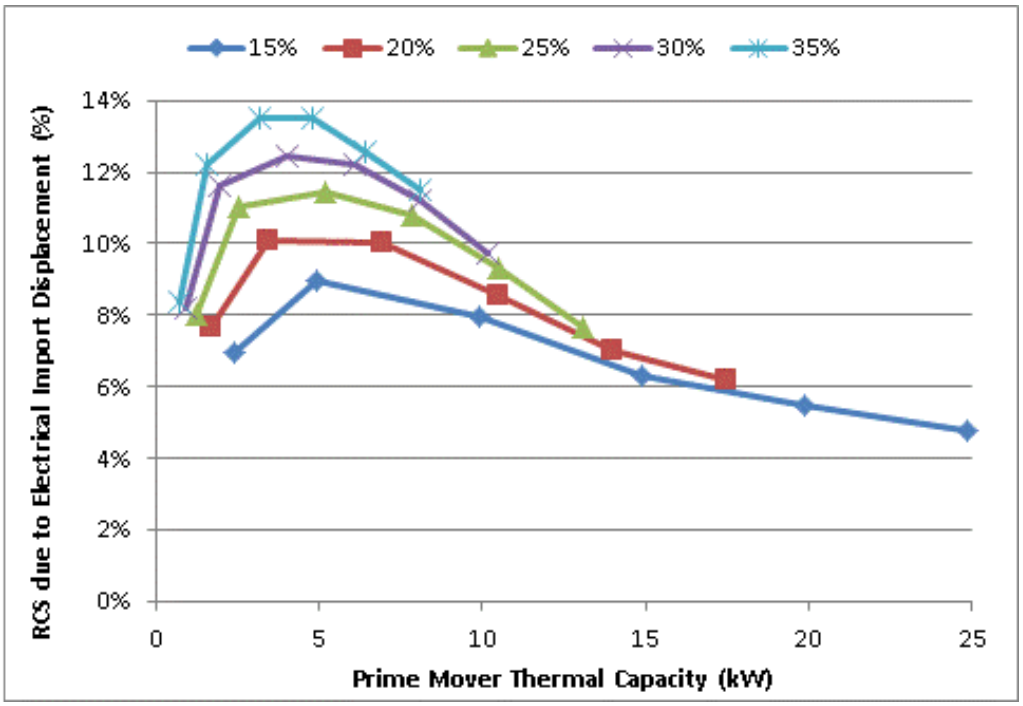

Figure 4.16: RCS due to Electrical Import Displacement (% of base-case CO_2) versus Prime Mover Thermal Capacity (kW_{th}), for each design variant of SE TLF µCHP

Similar to the Relative Carbon Saving due to Thermal Generation Displacement (as discussed in Section 4.3.5), Figure 4.17 illustrates that RCS due to Electrical Import Dispalcement are significant for PTSDRs between 0.5 and 1.5. The operation of prime movers with thermal capacities above approximately $8kW_{th}$ (i.e. ratios above 1.5) is dominated by warm-up (where heat is generated, but not electricity), and part-load modulation (where electrical and thermal output is lower than rated values).

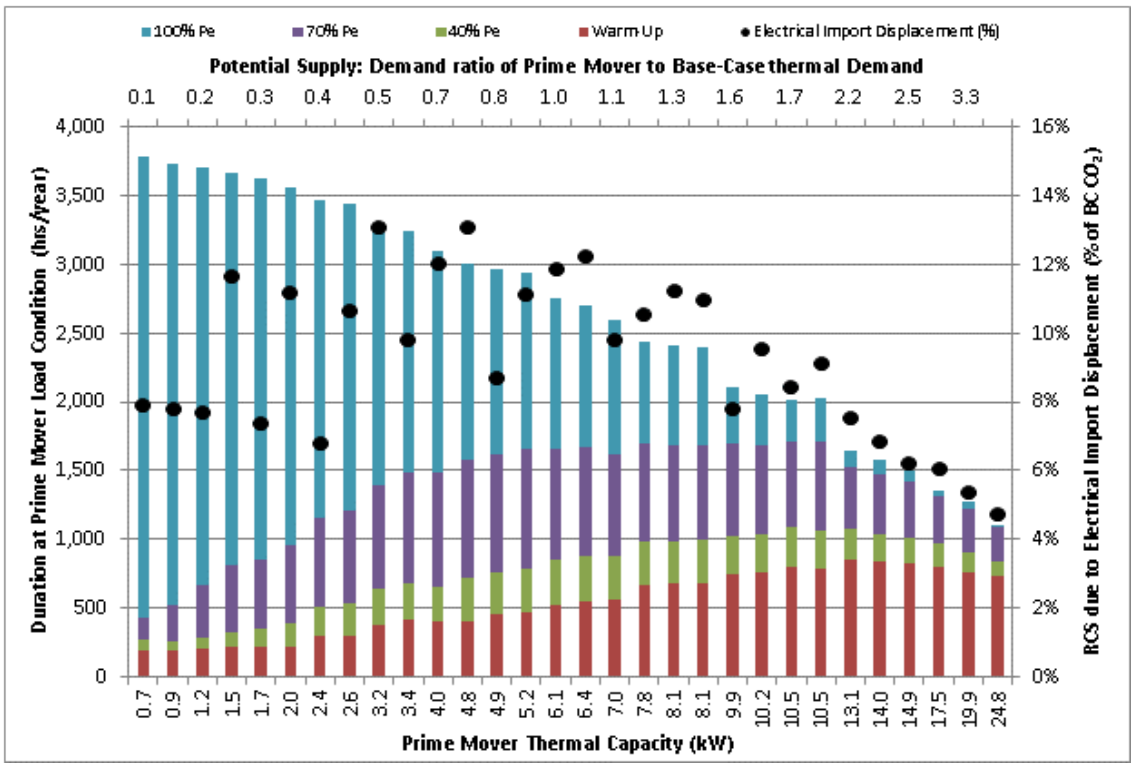

Figure 4.17: Prime Mover duration at load conditions (hours/year) and RCS due to Electrical Import Displacement (% of BC CO_2) vs. Prime Mover Thermal Capacity (kW_{th}) and PTSDR

Figure 4.18 demonstrations that, like Electrical Import Displacement, the design variants with higher η_e consistently displaced more import, regardless of rated electrical output. Unlike, electrical import, however, electrical export increases with prime mover rated electrical output, until eventually tending to a maximum. This is in line with expectations, as increased P_e (with the same net electric and heat recovery efficiencies) results in increased thermal capacity, which will eventually limit run-time of the SE TLF µCHP prime mover.

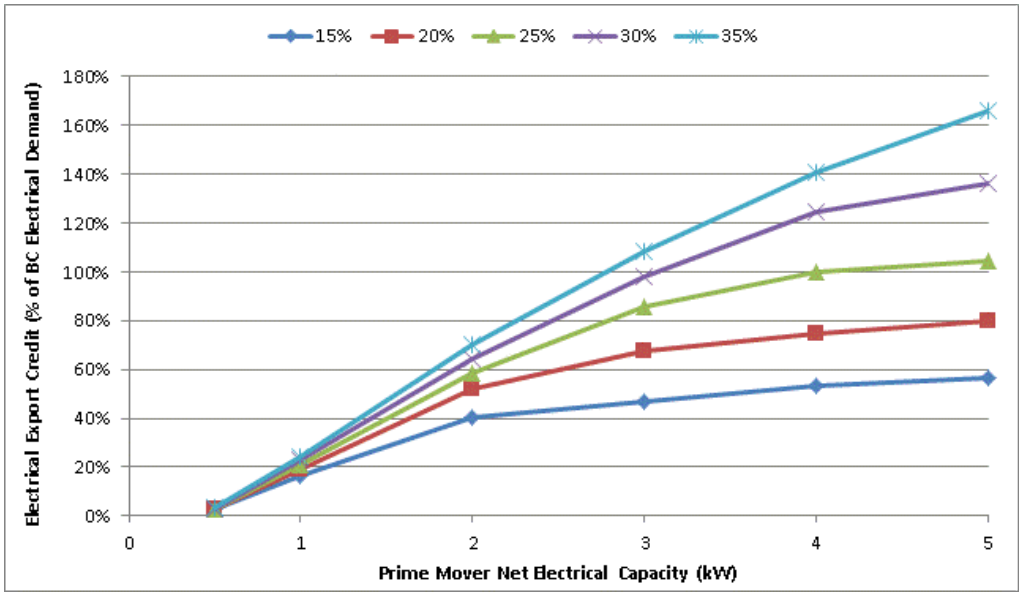

Figure 4.18: Electrical Export from building with thermal load following SE µCHP system, as a percentage of base-case electrical demand

Figure 4.19 shows that as prime mover thermal (and therefore electrical) capacity increases, so does RCS due to electrical export credit, with a steeper slope for higher η_e. However, as discussed in Section 4.3.5, thermal generation displacement will eventually saturate, and provide marginal additional carbon savings to offset the increasing carbon penalty of additional fuel consumption, as illustrated in Figure 4.5.

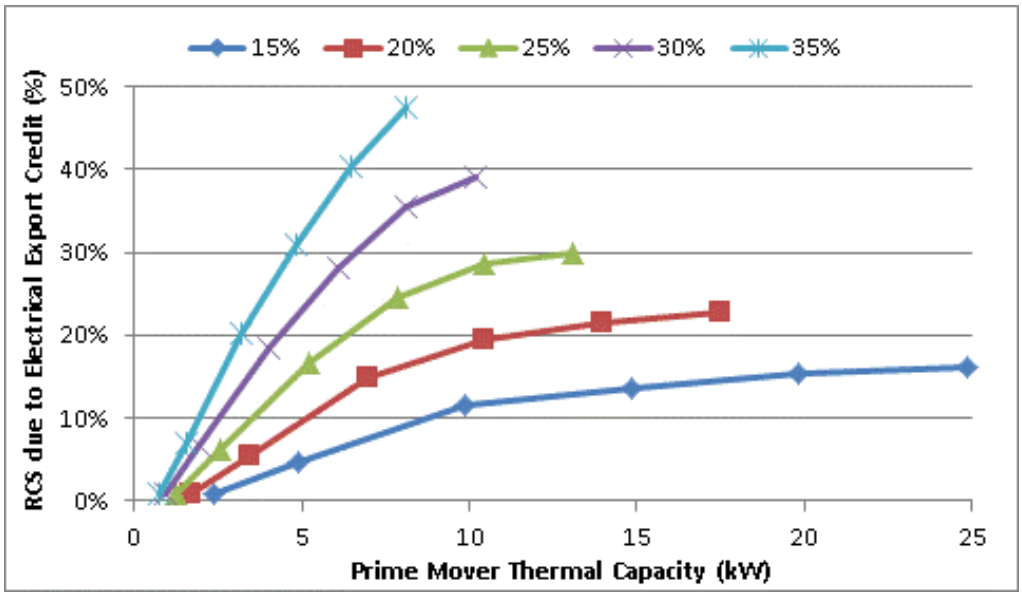

Figure 4.19: RCS due to Electrical Export Credit (% of base-case CO_2) versus Prime Mover Thermal capacity (kW_{th}), for each design variant

In Figure 4.20, the RCS due to both electrical import and export are plotted against the RCS of the µCHP system. It is interesting to note that the RCS for design variants with 35% η_e tends to a maximum, even as the RCS due to electrical generation increases. This is due to the carbon intensity of generated electricity (CI_{gen}, as driven by η_e and CI_{fuel}) exceeding that of the NEG (CI_{grid}). As proven in Section 4.3.5, as thermal generation displacement (as the system-level carbon saving it provides) does not increase indefinitely with prime mover capacity (either thermal or electrical).

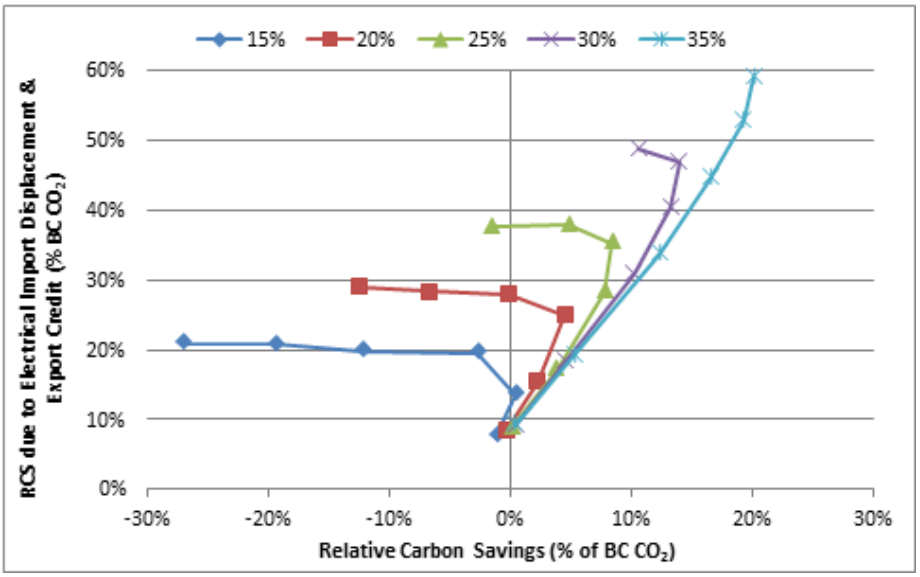

Figure 4.20: Relative Carbon Saving due to Electrical Import Displacement plus Electrical Export Credit (% of base-case CO_2) versus RCS (% of base-case CO_2) for each design variant

Even if the carbon intensity of generated electricity was lower than CI grid, the RCS will be limited, even for high electrical efficiencies, by the run-time restrictions inherent to the thermal load following operating regime. This would suggest that alternative operating regimes could allow high thermal capacity µCHP systems to deliver higher RCS, whenever $CI_{gen} < CI_{grid}$, by allowing the production of excess thermal generation and hence more electricity.

4.3.7 Load Conditions

In the previous sections, the correlation of load conditions with thermal capacity of the design variant has been discussed on an annual basis. Figure 4.12 and Figure 4.13 presents the duration under each load condition and relative carbon saving, for each

design variant on an annual basis. From those graphs, it is apparent that similar levels of relative carbon saving are achievable from prime movers with low thermal capacity (where operation at 100% load dominates), and high thermal capacity (where warm-up and part-load operation dominates).

This concept is explored further in Figure 4.21, looking at estimated annual results, for the 8 design variants with significant (>10%) RCS. As expected, total operating hours decrease with thermal capacity of the prime mover, as understood by considering design variants with different electrical capacities but the same η_e, or with different η_e but the same P_e.

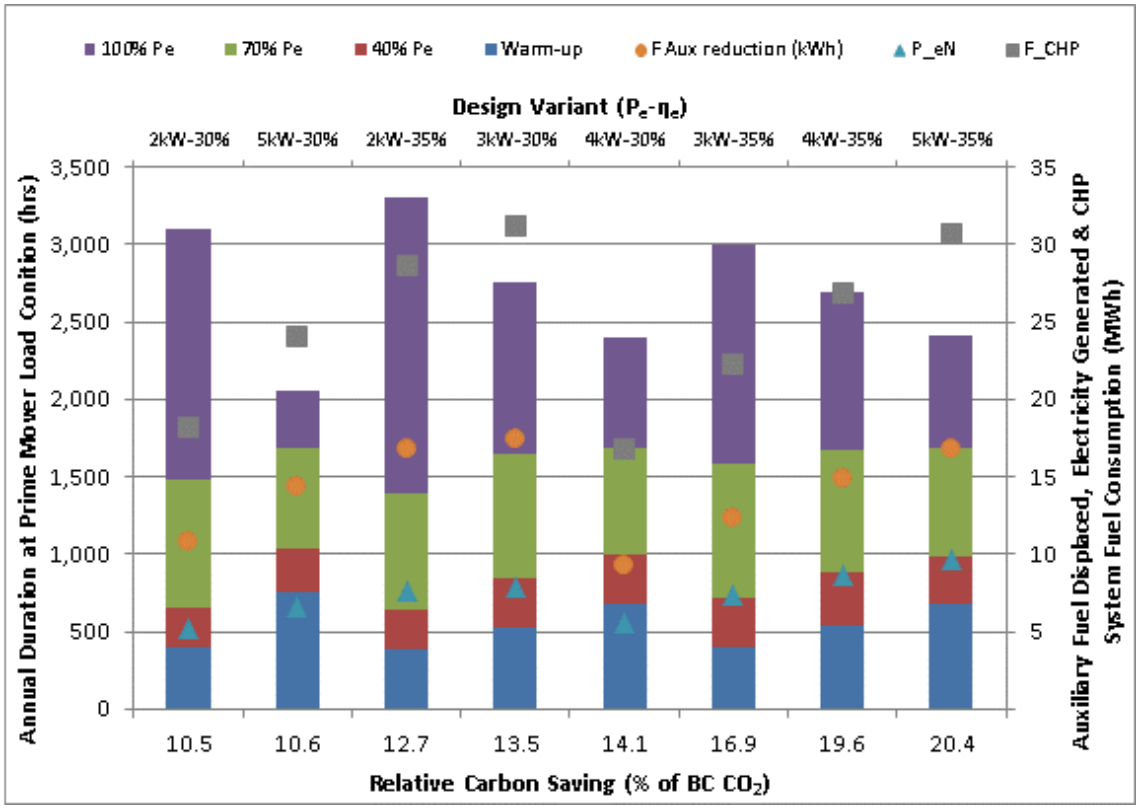

Figure 4.21: Duration of Prime Mover at Load Conditions (hours annually), Auxiliary thermal generation displaced, Generated Electricity, and prime mover fuel consumption vs. RCS for 8 design variants

In order to understand the relationship between load condition and thermal demand, investigation of load conditions for each design variant under every demand scenario was undertaken. It is interesting to note that the spread of PTSDRs over which

significant RCS occur is wider for primary demand scenarios with weekend occupancy patterns (Figure 4.23) than for weekday occupancy patterns (Figure 4.22).

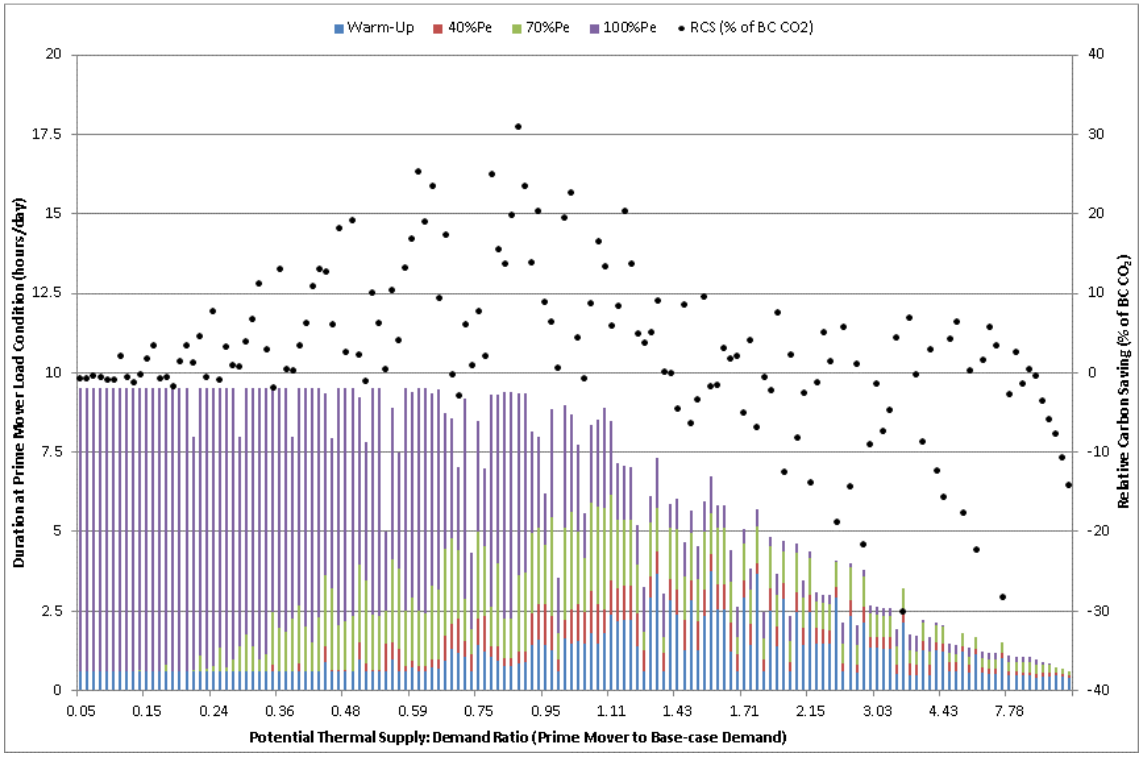

Figure 4.22: Prime Mover Duration at Load Conditions (hours daily) and RCS versus PTSDR (prime mover to base-case thermal demand) for all Weekday PDS and design variants under investigation

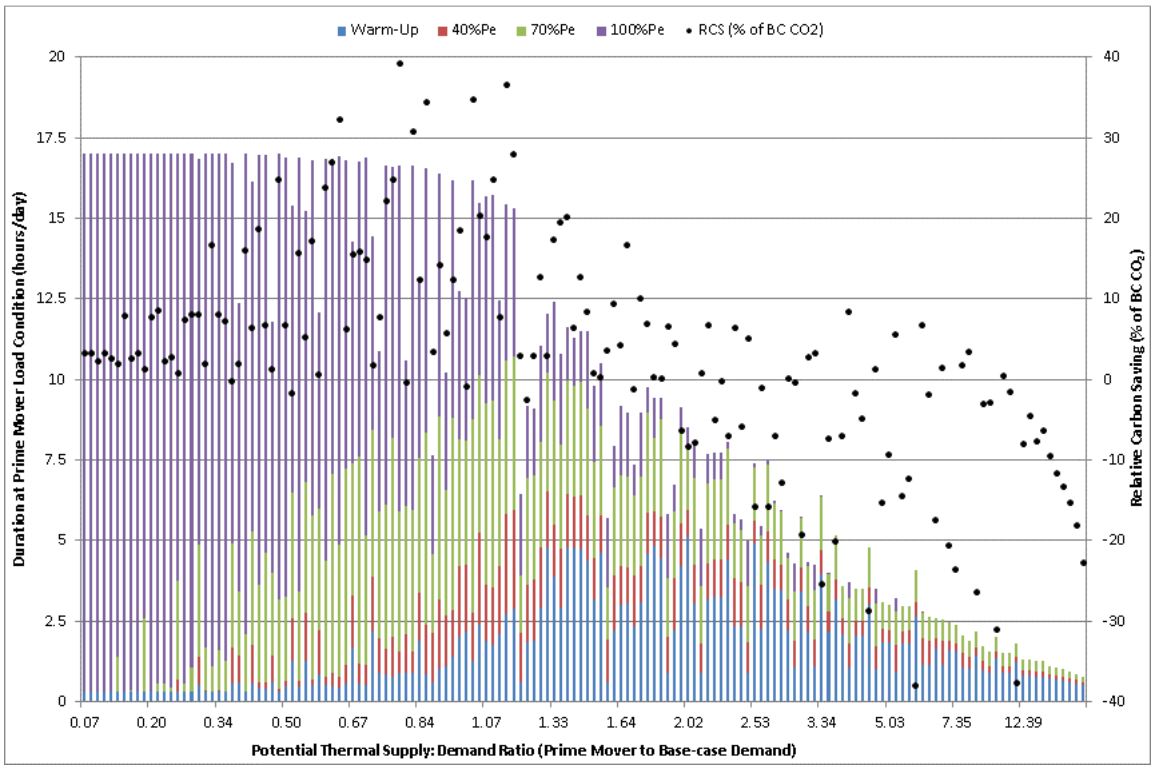

Figure 4.23: Prime Mover Duration at Load Conditions (hours daily) and RCS versus PTSDR (prime mover to base-case thermal demand) for all Weekend PDS and design variants under investigation

To understand the variation of load conditions with thermal demand for a particular design variant, the 5kW$_e$-35% variant was investigated further. Considering the results for the WE-EWin scenario in Figure 4.24, it is apparent that higher thermal demand does not consistently result in increased run-time at 100% output.

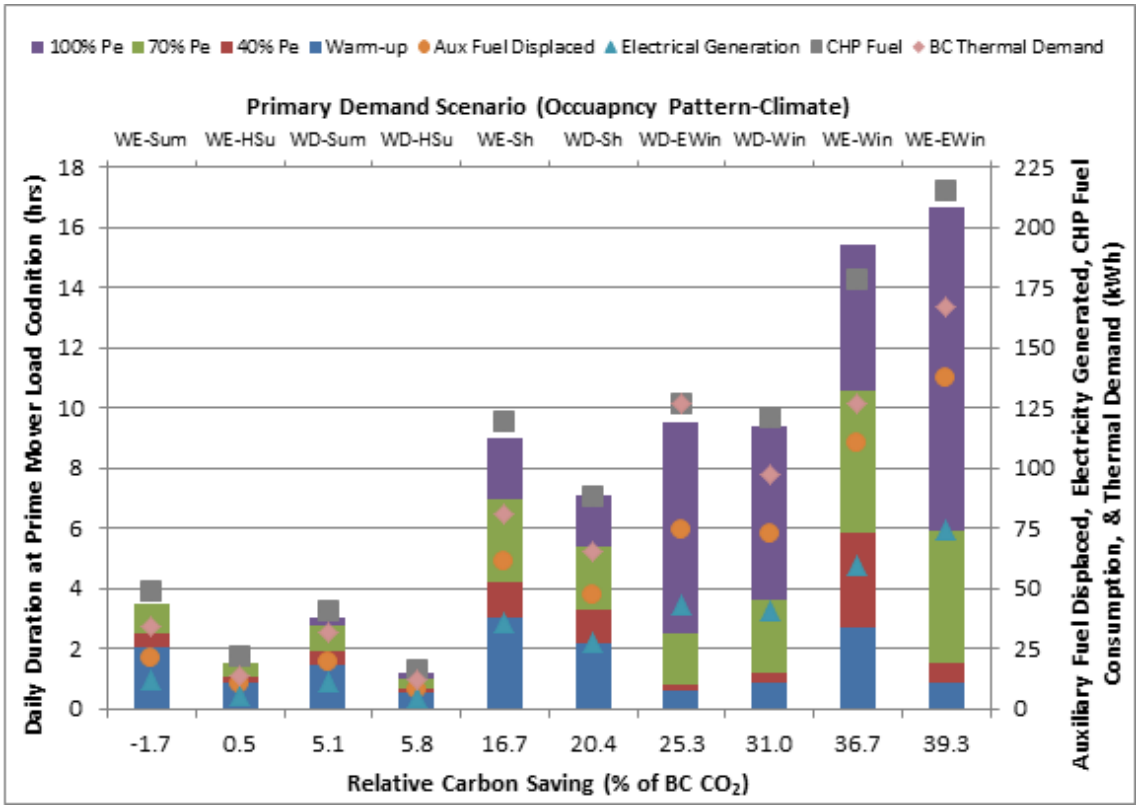

Figure 4.24: Duration of Prime Mover at Load Conditions (hours daily), Auxiliary thermal generation displaced, Generated Electricity, prime mover fuel consumption, and BC Thermal Demand (kWh) versus RCS for 5kW$_e$-35% design variant for each PDS

The relationship between load conditions and Restricted Seasonal Operation (a concept introduced in Section 4.3.3) was investigated. In Figure 4.25 and Figure 4.26, the annual duration at each load condition, and relative carbon saving, was plotted for the 8 design variants with significant RCS (as introduced previously). Additionally, the corresponding results for RSO were plotted as hatched columns. Figure 4.25 compares 12-months of operation with RSO without High Summer primary demand scenarios (RSO-NoHSum), whilst Figure 4.26 compares with RSO without Summer and High Summer primary demand scenarios (RSO-NoSummer).

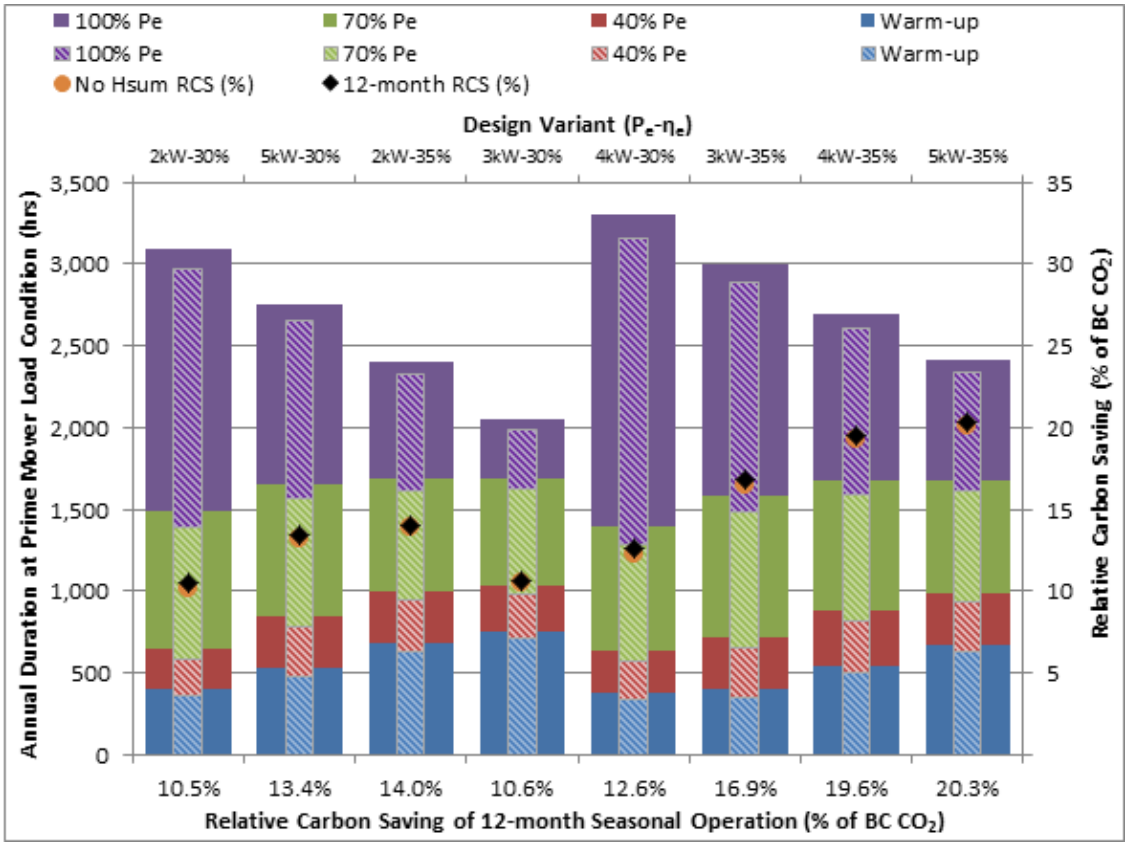

Figure 4.25: Duration of Prime Mover at Load Conditions (hours/year) versus Relative Carbon Saving (% of BC), for 8 design variants (with indicated rated net electrical output and rated η_e), comparing 12-month operation (solid bars) versus RSO-NoHSum (hatched bars)

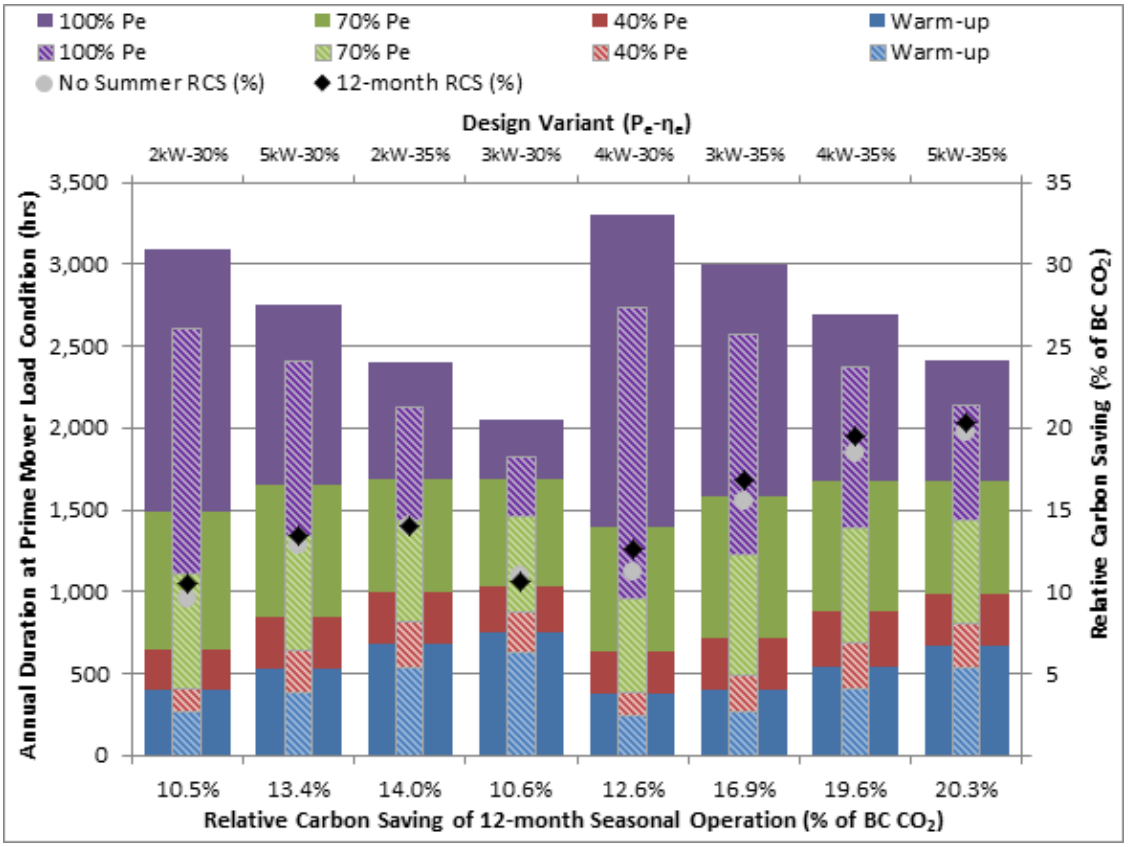

Figure 4.26: Duration of Prime Mover at Load Conditions (hours/year) versus Relative Carbon Saving (% of BC), for 8 design variants (with indicated rated net electrical output and rated η_e), comparing 12-month operation (solid bars) versus RSO-NoSummer (hatched bars)

The results presented in Figure 4.25 suggest that marginal reductions in cumulative prime mover operating duration can be made, whilst marginally decreasing RCS. Of more relevance are the results in Figure 4.26, which show that significant reductions in cumulative prime mover operating duration are possible with minimal corresponding reductions in RCS. This has implications for the operating lifetime of the prime mover and balance-of-plant, which is reasonably expected to be limited by total operating hours, amongst other factors.

4.3.8 Thermal Cycling & Prime Mover Lifetime

As discussed in Section 4.2.2, prime mover and balance-of-plant operating lifetime, that is the time before replacement or major overhaul, is limited by a number of operational factors. The relative impact of these factors will be technology specific, however it is understood that Stirling Engines are sensitive to the number of thermal cycles and cumulative operating duration.

If a target prime mover lifetime of 5 years were to be set, then the 6,000 thermal cycle lifetime limit assumption made in Section 4.2.2 would require that the quantity of thermal cycles does not exceed an average of 3.3 thermal cycles per day. To understand the frequency of daily thermal cycles for thermal load following operation, this was plotted for each design variant, operating for every primary demand scenario, in Figure 4.27. Whilst significant RCS and infrequent thermal cycling (<4 per day) are achievable by design variants operating in certain demand scenarios, a significant proportion of simulation results with significant carbon savings report thermal cycles of between 4-12 per day, in excess of the arbitrary limit discussed previously.

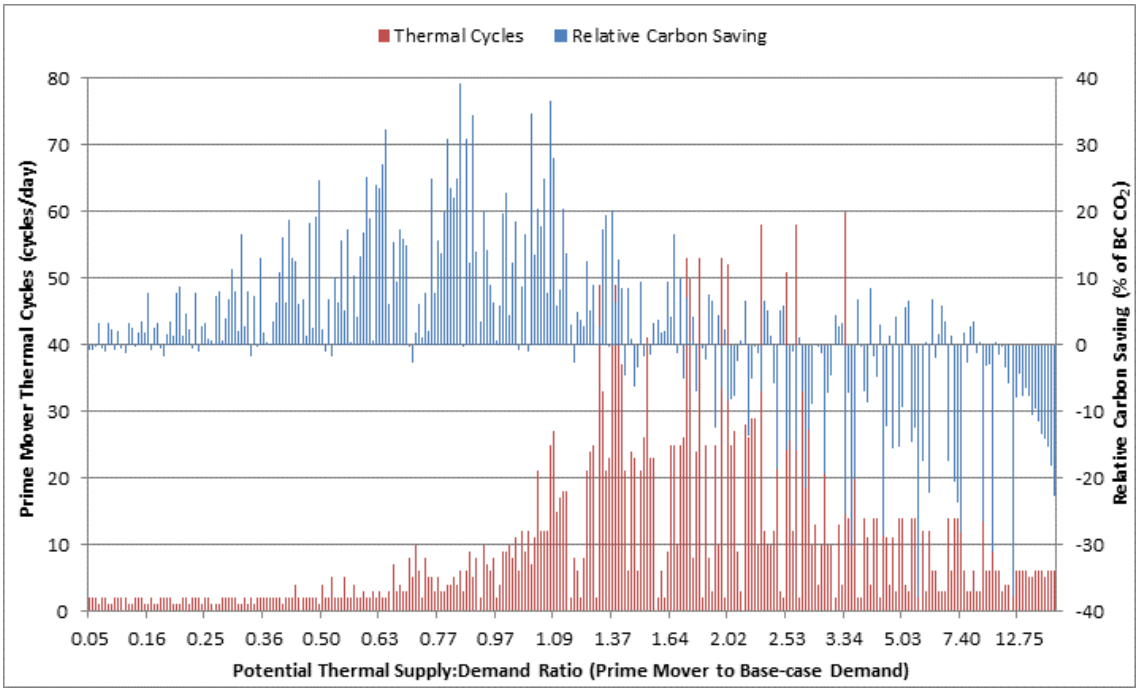

Figure 4.27: Quantity of Thermal Cycles (cycles/day) and Relative Carbon Saving (% of base-case) for each design variant, operating for every primary demand scenario

Thermal cycling, and associated RCS, was then investigated on an annual basis, for each design variant, as presented in Figure 4.28. None of the design variants with significant RCS have accumulated less than 1,200 thermal cycles per annum, which relates to the 5 year lifetime discussed previously. As η_e increases, so does the frequency of thermal cycling, whilst thermal cycling increases with increasing electrical (and hence thermal) rated capacity. As electrical rated outputs (for a particular η_e) increases above that corresponding to maximum RCS, there is a diminishing increase in

frequency of thermal cycling. This diminishing effect does not correspond exactly with the maximum RCS, but appears to correspond to PTSDR values above 1.5.

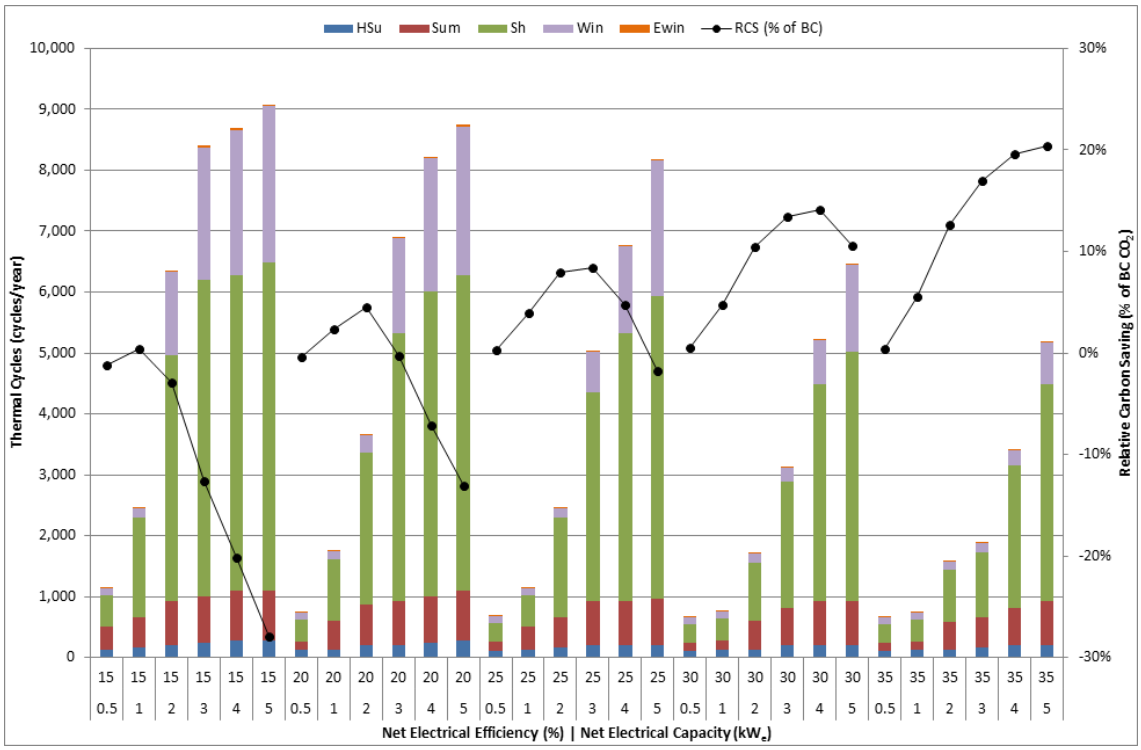

Figure 4.28: Annual Thermal Cycles and annual RCS (% of base-case) for each design variant

The increase on RCS due to RSO has already been investigated in Section 4.3.3, as has the effect of RSO on reduced operating duration in Section 4.3.7. The thermal cycling of the two alternative RSO options, RSO-NoHSum and RSO-NoSummer, were investigated for the 30% η_e (Figure 4.29) and 35% η_e (Figure 4.30) design variants. As Figure 4.30 illustrates, reductions in thermal cycling to between 1,000-1,200 cycles per annum is achievable with the RSO-NoSummer operating restriction, with a minimal decrease in RCS.

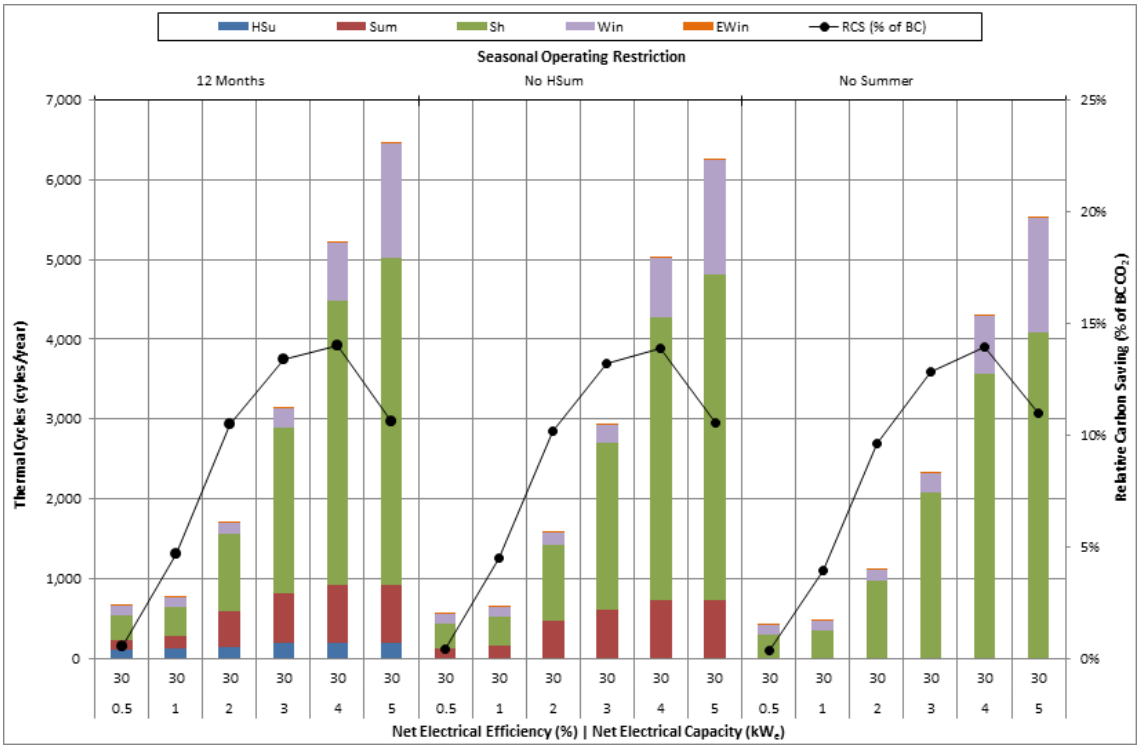

Figure 4.29: Annual Thermal Cycles and annual RCS for 30% η_e design variants without RSO (12 Months), with RSO during High Summer, and with RSO during High Summer and Summer

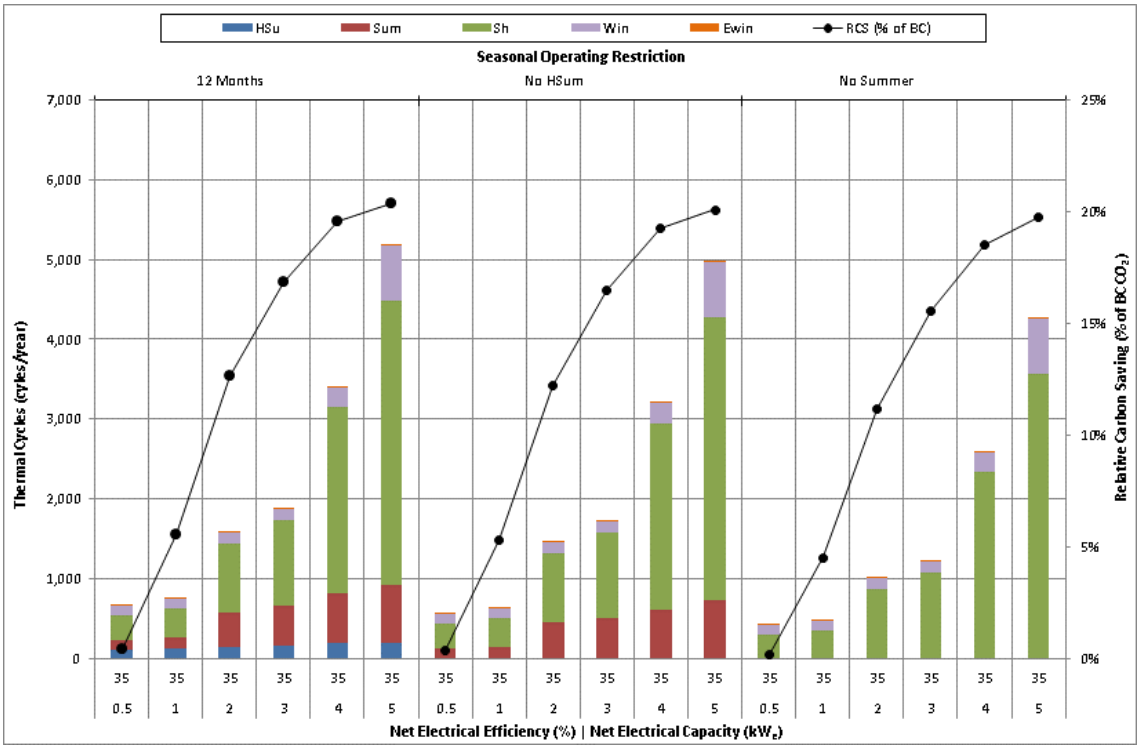

Figure 4.30: Annual Thermal Cycles and annual RCS for 35% η_e design variants without RSO (12 Months), with RSO during High Summer, and with RSO during High Summer and Summer

The effect of RSO on prime mover lifetime and relative carbons savings was analysed for the 8 design variants with significant RCS. Assuming that a SE prime mover is limited to 6,000 thermal cycles, Figure 4.31 shows that restricting all summer operation can provide significant extensions to prime mover lifetime with minimal reduction of relative carbon savings, where the latter can be seen clearly in Figure 4.4.

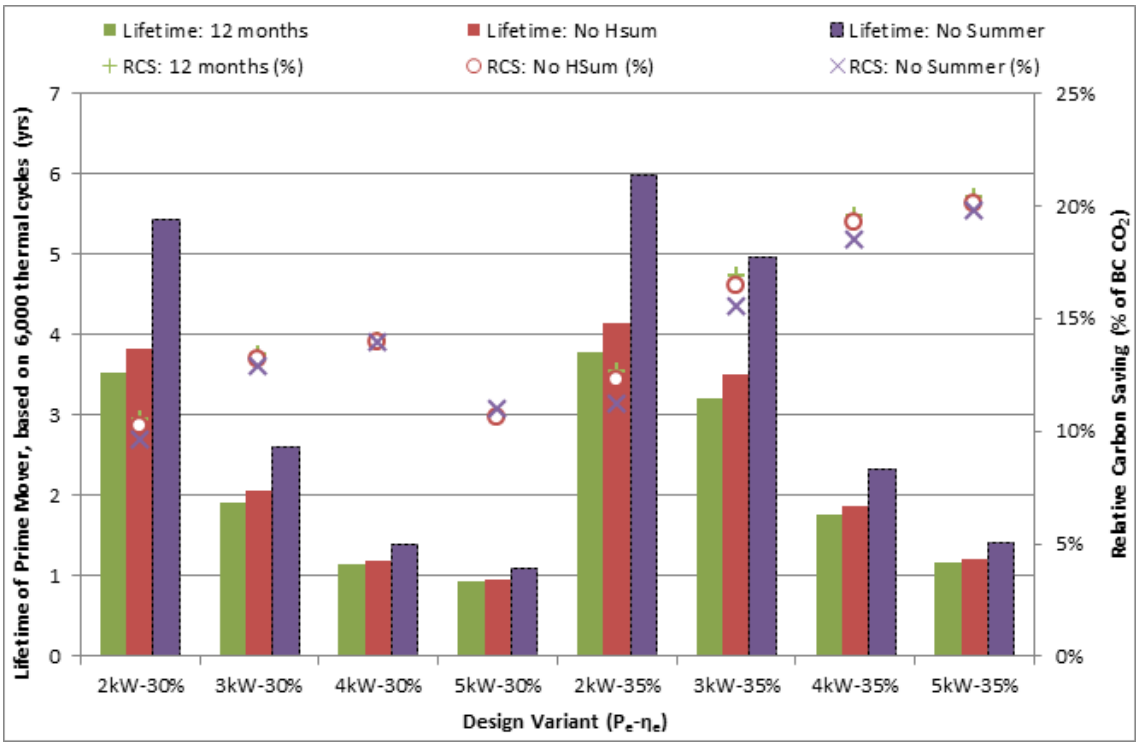

Figure 4.31: Lifetime of SE Prime Mover (years), assuming a limit of 6,000 thermal cycles, and RCS (% of BC CO_2), for each design variant with significant (>10%) RCS

By referring to Figure 4.32, it is easy to visualise the relationship between RSO and frequency of thermal cycling, for systems controlled by each RSO. It confirms that design variants with 30% η_e may achieve significant RCS with thermal cycling frequencies well under 2,000 per annum.

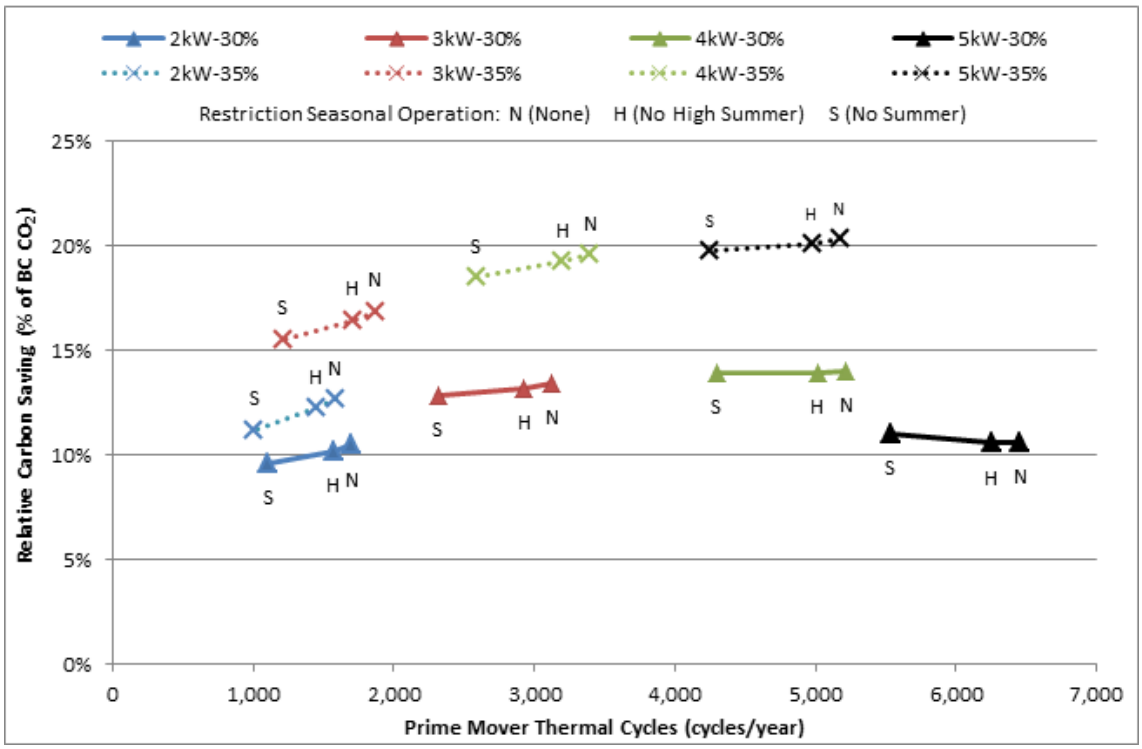

Figure 4.32: RCS (% of BC CO_2) versus annual frequency of thermal cycling, for each design variant with significant (>10%) RCS, compared under all modes of RSO

The concept of thermal cycle and total prime mover operating duration lifetime limitations is combined in Figure 4.33. This draws upon the results of run-time analysis for RSO, as presented in Figure 4.25 and Figure 4.26. The relationship between thermal cycles and operating hours may prove to be important in assessing the operation costs of various prime mover technologies (and associated balance-of-plant).

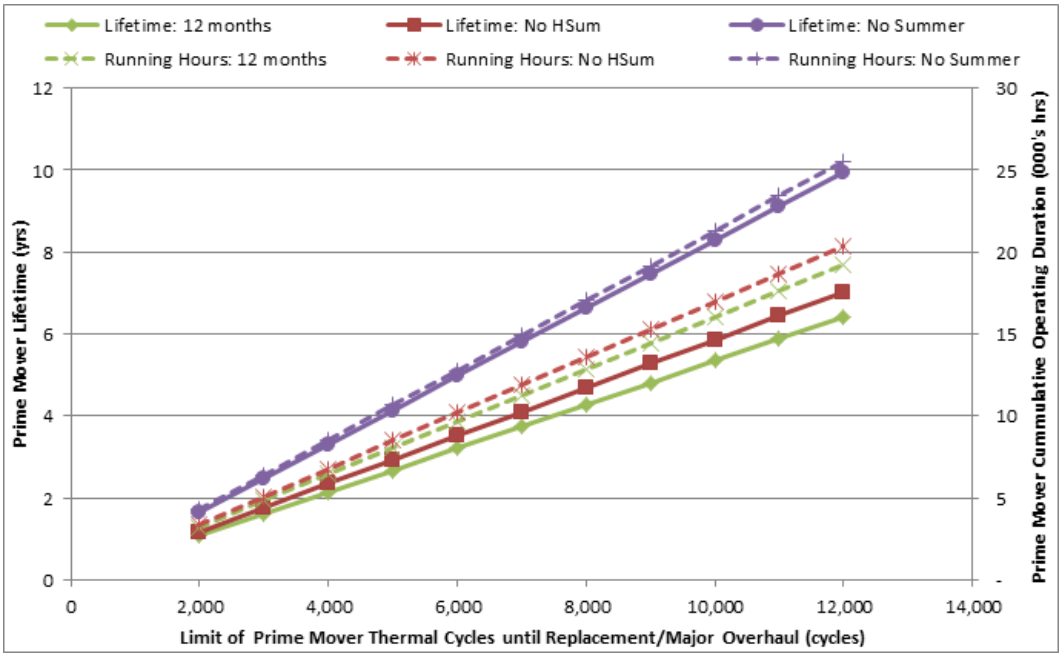

Figure 4.33: Lifetime of SE Prime Mover (years), for a range of thermal cycle lifetime limits, and cumulative operating duration experienced over prime mover lifetime (000's hours), for the 3kW$_e$-35% design variant, under all RSO scenarios: None (12 months), No High Summer Operation (No HSum) and No Summer Operation (No Summer)

4.3.9 Carbon Saving vs. Thermal Demand

Each of the primary demand scenarios used thus far has a unique profile of thermal demand, in terms of daily magnitude and temporal distribution. The same statement can be made of the associated results for carbon saving calculations, for each of the 30 design variants, when considered on a scenario-by-scenario basis. Derivation of guidance information, for interested stakeholders, on appropriate µCHP design decisions is an aim of this project. The panacea in this regard would be a numerical relationship between the relative carbon saving achievable by certain design variations, relative to other design variations, and all relevant system design factors and complex demand descriptors. This, unfortunately, is unrealistic, for several basic reasons: the number of terms in such a relationship would be unwieldy, hence resulting in a large combined error; complex demand descriptors would require retroactive quantitative analysis of detailed demand information, which is typically unavailable for domestic buildings; and finally, these demand descriptors would be far too specific to apply to the dwelling in question at another moment in time, or indeed any other dwelling.

Potential Thermal Supply:Demand Ratio of the prime mover was introduced in Section 4.3.5 as metric to describe matching of prime mover thermal capacity to thermal demand. This metric has been calculated for each design variant, under all primary demand scenarios, operating without RSO. These have been plotted individually for each value of rated η_e, as presented in Figure 4.34, Figure 4.35, Figure 4.36, Figure 4.37, and Figure 4.38. The maximum RCS for each set of design variants (by η_e) increases with thermal demand of the primary demand scenario. The maximum RCS for each PDS corresponds to a value of PTSDR, typically between 0.5 and 1.5, where the RCS maxima occurs at higher PTSDR values for PDSs with higher thermal demand. As η_e increases, the magnitude of the RCS maxima increases, as do other RCS values.

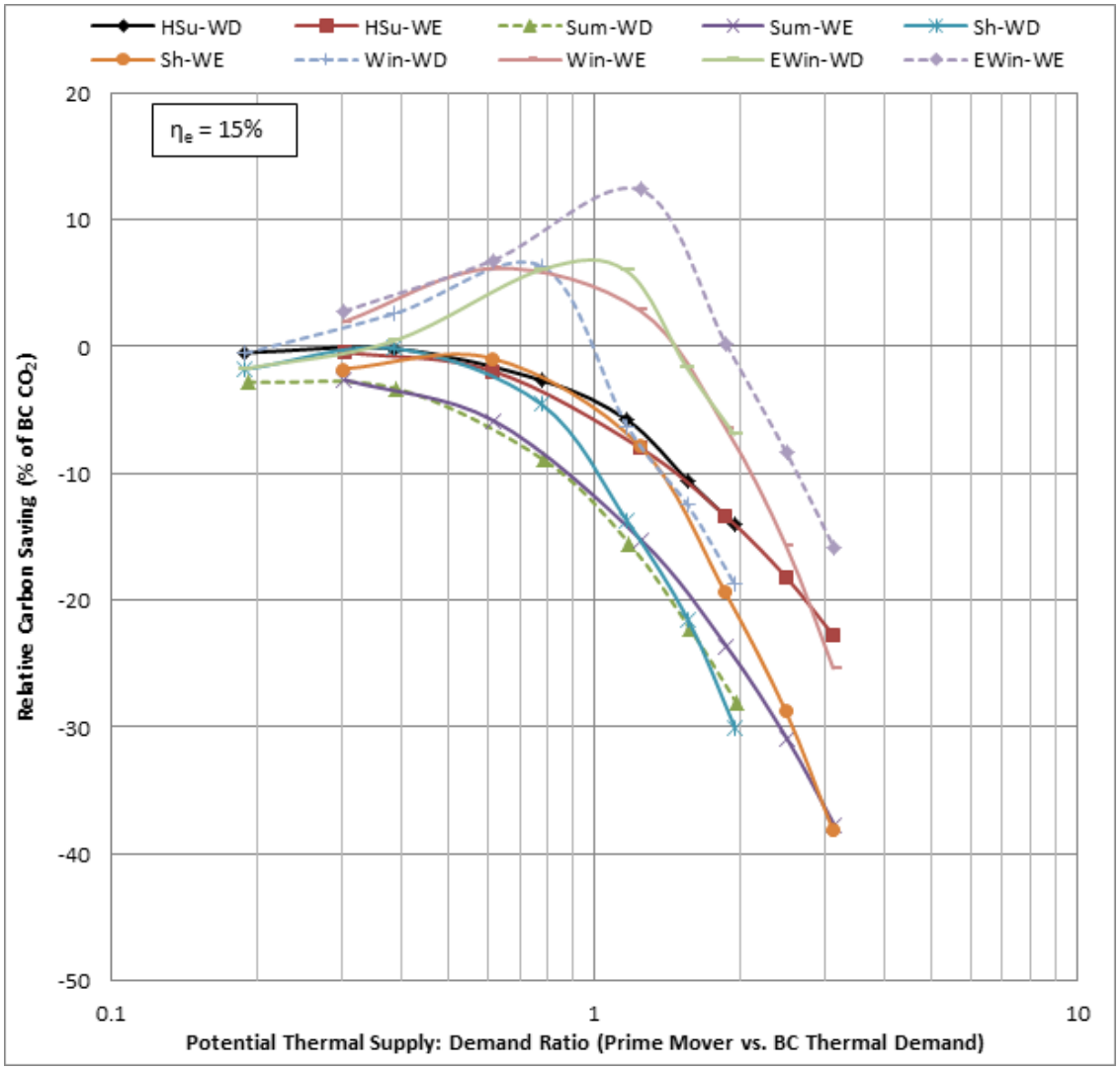

Figure 4.34: RCS vs. PTSDR, for all 15% η_e design variants, disaggregated by PDS, with RSO-NoSummer

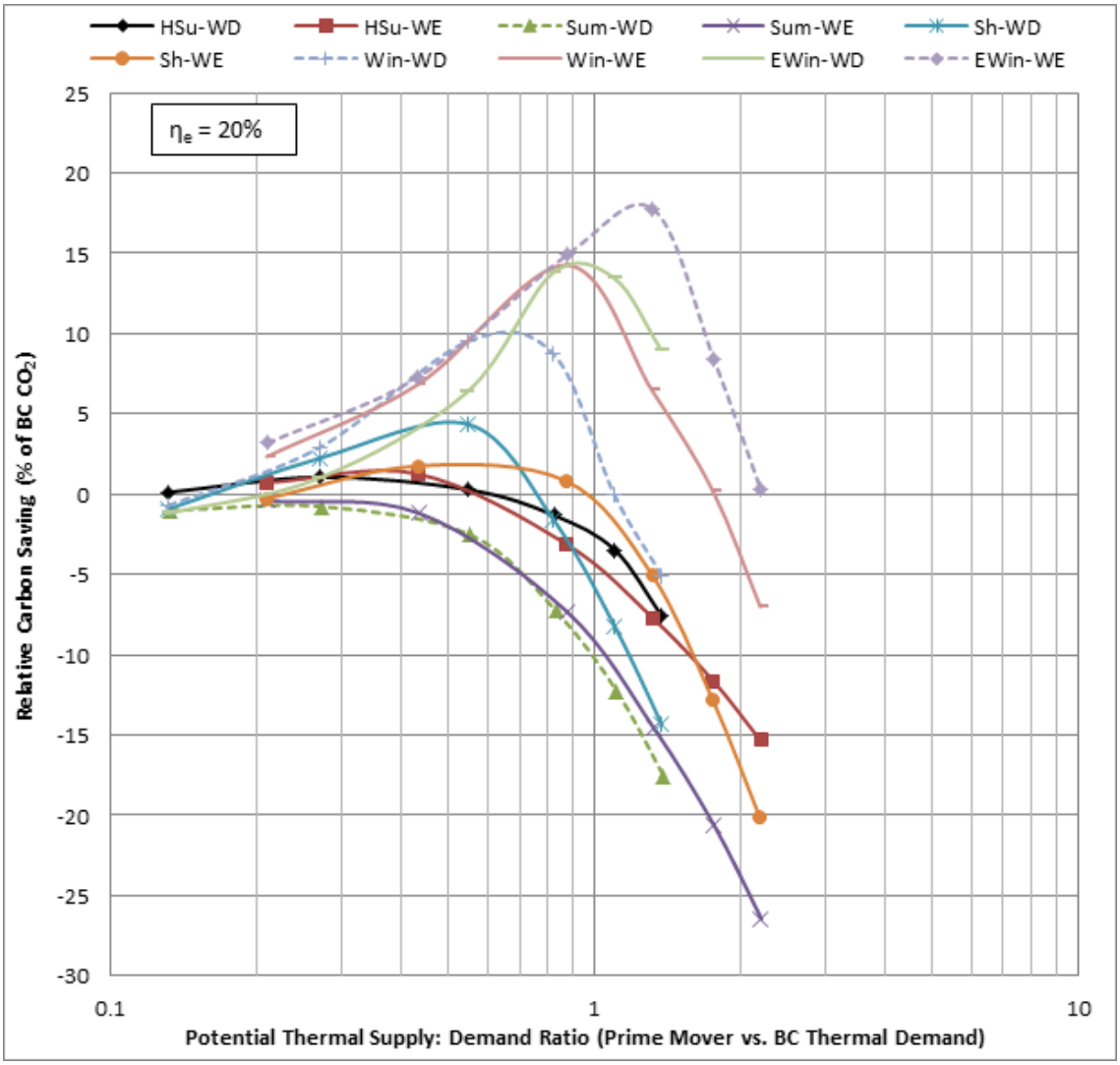

Figure 4.35: RCS vs. PTSDR, for all 20% η_e design variants, disaggregated by PDS, with RSO-NoSummer

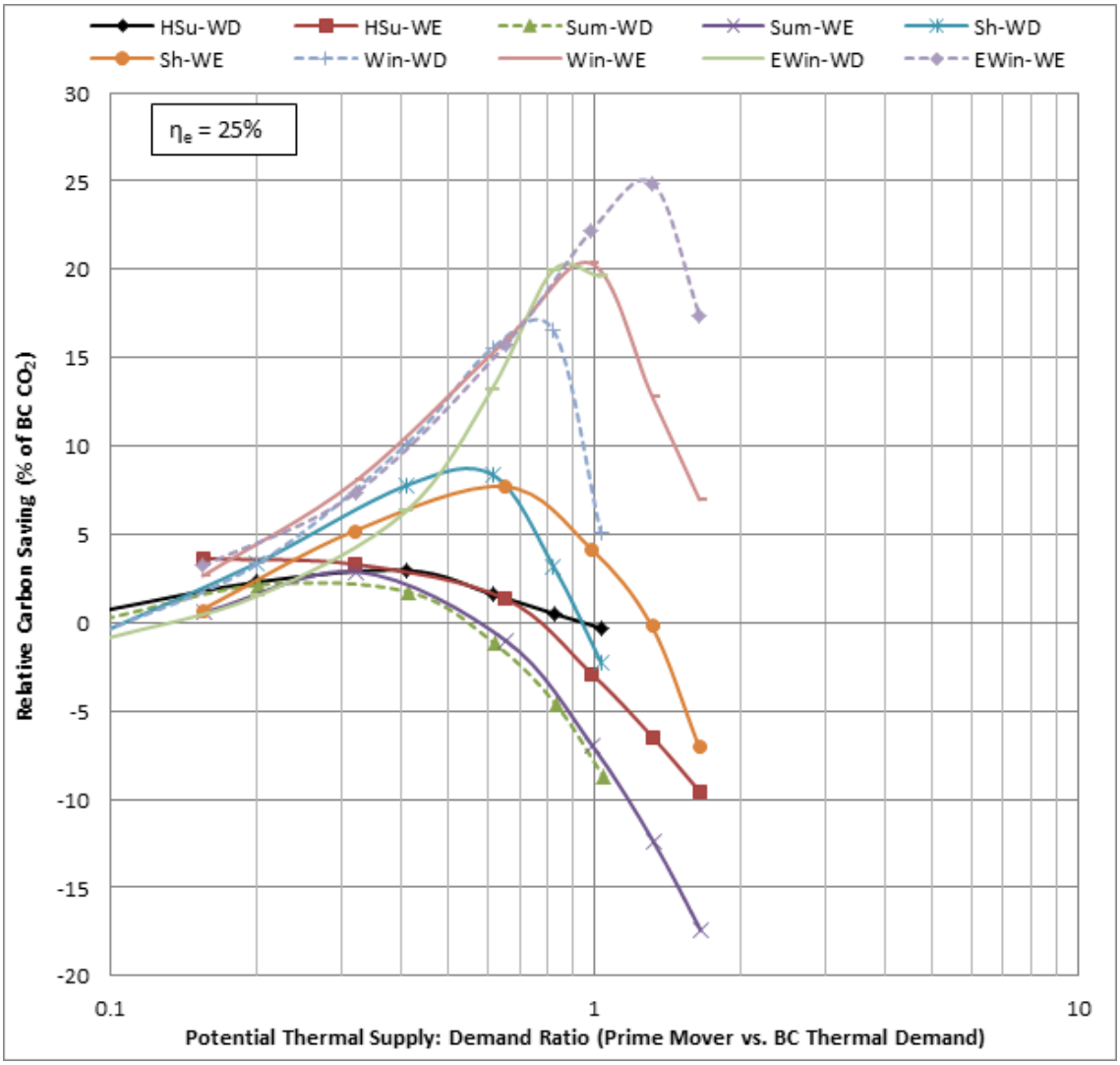

Figure 4.36: RCS vs. PTSDR, for all 25% η_e design variants, disaggregated by PDS, with RSO-NoSummer

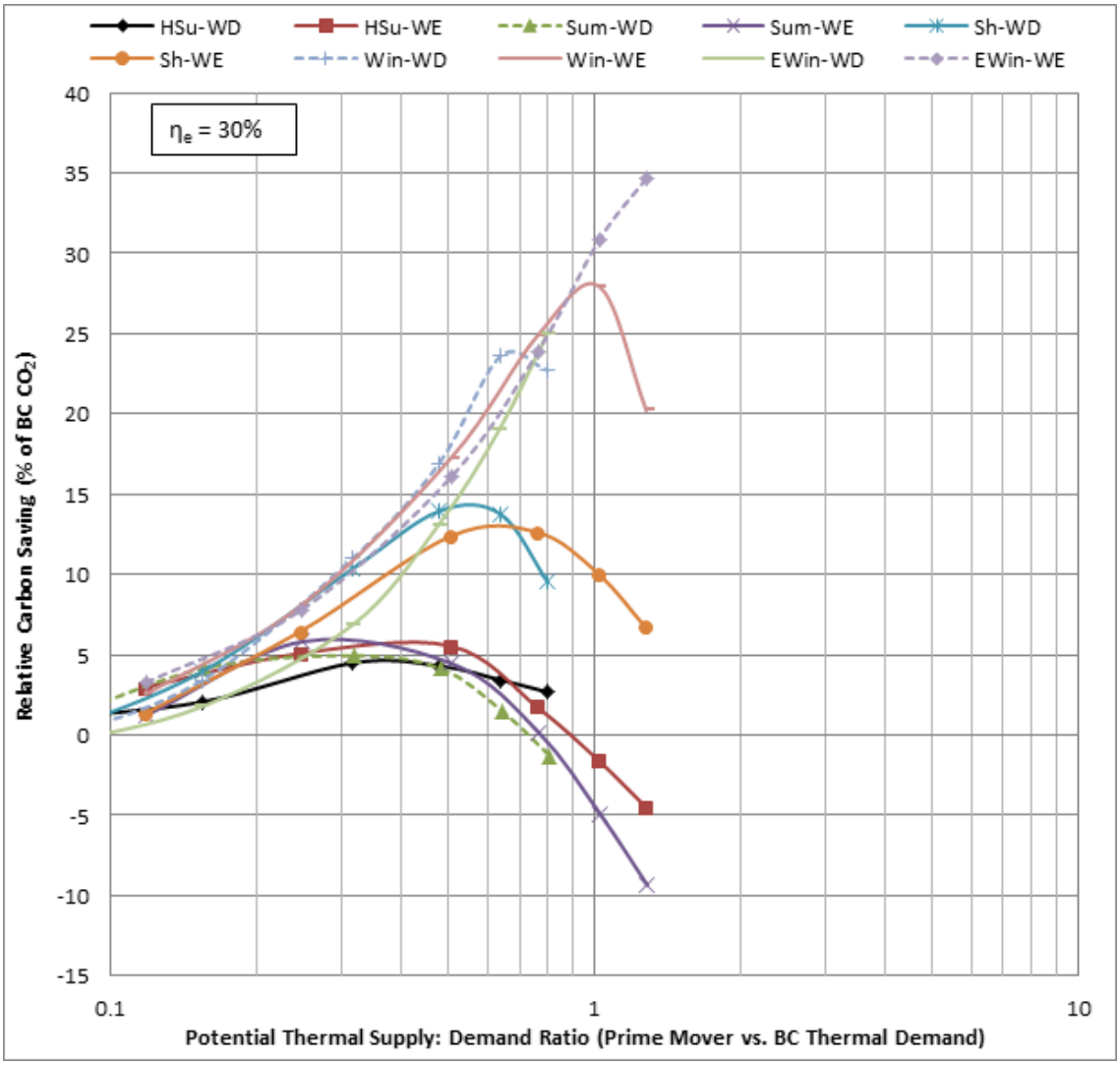

Figure 4.37: RCS vs. PTSDR, for all 30% η_e design variants, disaggregated by PDS, with RSO-NoSummer

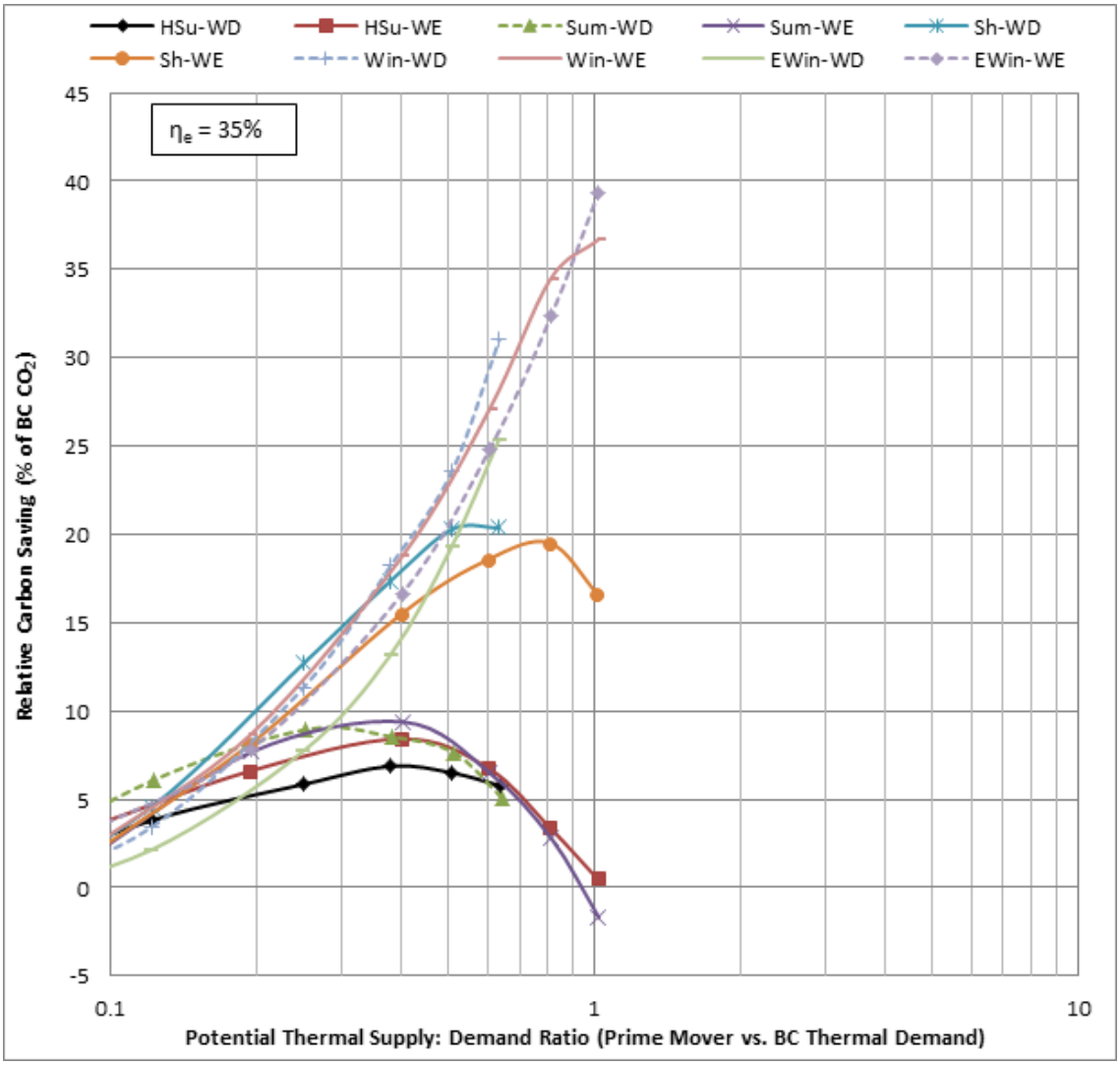

Figure 4.38: RCS vs. PTSDR, for all 35% η_e design variants, disaggregated by PDS, with RSO-NoSummer

It is interesting to examine the relationship between RCS and PTSDR at the level of an individual primary demand scenario. As each PDS has a different thermal demand profile, driven by climate and occupancy pattern, the daily total thermal demand can be used a substitute for considering µCHP performance in dwellings of differing thermal demands. This has been plotted for the weekday and weekend occupancy patterns, for Extreme Winter, Shoulder and Summer climate scenarios, in Figure 4.39, Figure 4.40, Figure 4.41, Figure 4.42, Figure 4.43, and Figure 4.44. The maximum value of RCS for design variants with a common η_e appear to correspond to a particular value of PTSDR that changes between primary demand scenarios. During the extreme Winter PDSs, the value of PTSDR that corresponds to maximum RCS does not appear to have been reached for 30% and 35% η_e families. This suggests that a system with P_e>5kWe

would be required to maximise RCS for 30% and 35% η_e design variants with those PDS. The value of PTSDR that corresponds to the RCS maxima increases as the thermal demand of the PDS decreases. The magnitude of RCS increases with both thermal demand of PDS and η_e for each design variant. It is important to note, however, that many design variants, especially those with lower η_e, result in relative carbon penalties (versus the base-case energy system), even in PDSs with high thermal demand. During the summer months, none of the design variants achieve significant RCS, and indeed many produce carbon penalties during operation. This supports the concept of RSO, as introduced in Section 4.3.3.

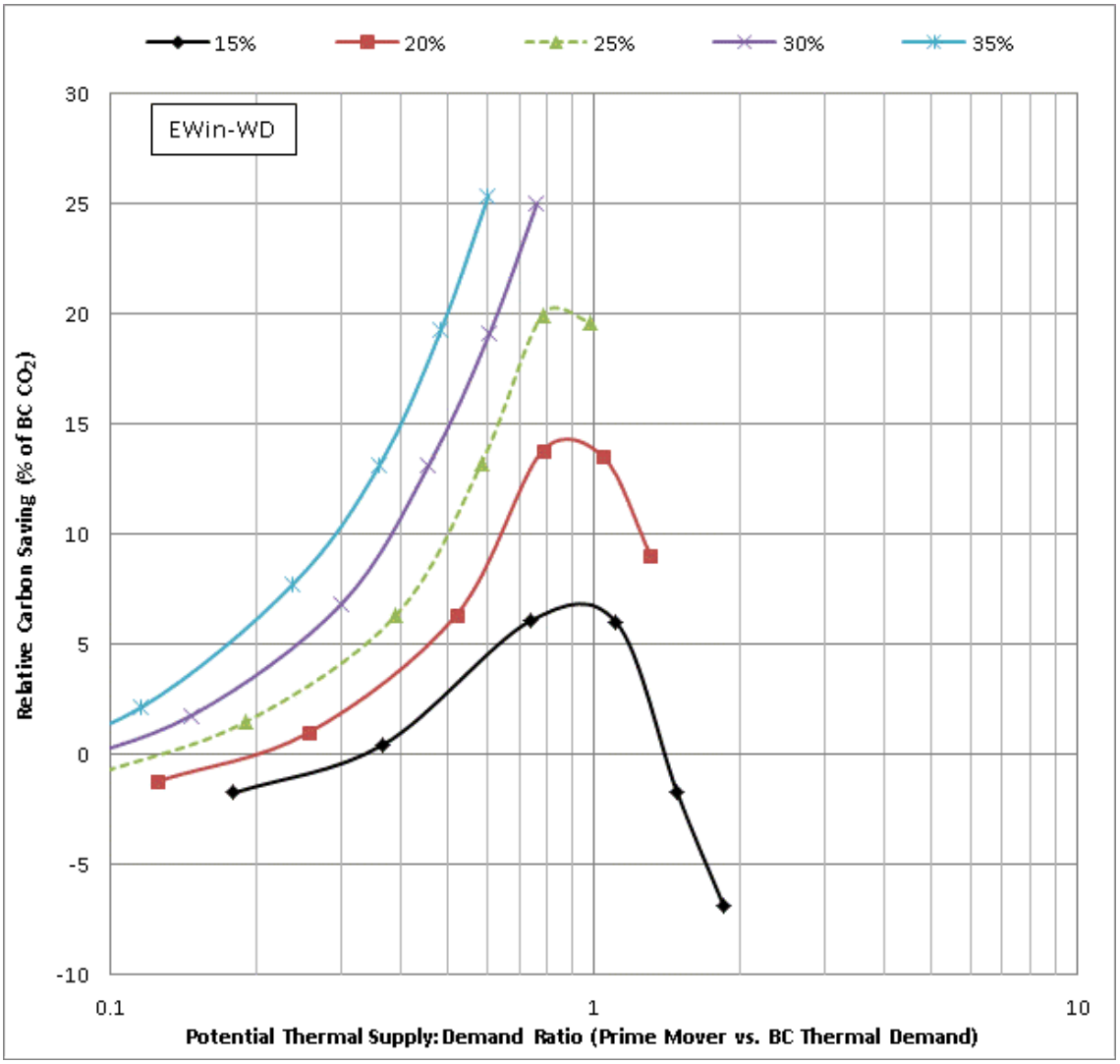

Figure 4.39: RCS versus PTSDR, for the Extreme Winter-Weekday PDS, for all design variants, disaggregated by rated η_e, with RSO-NoSummer

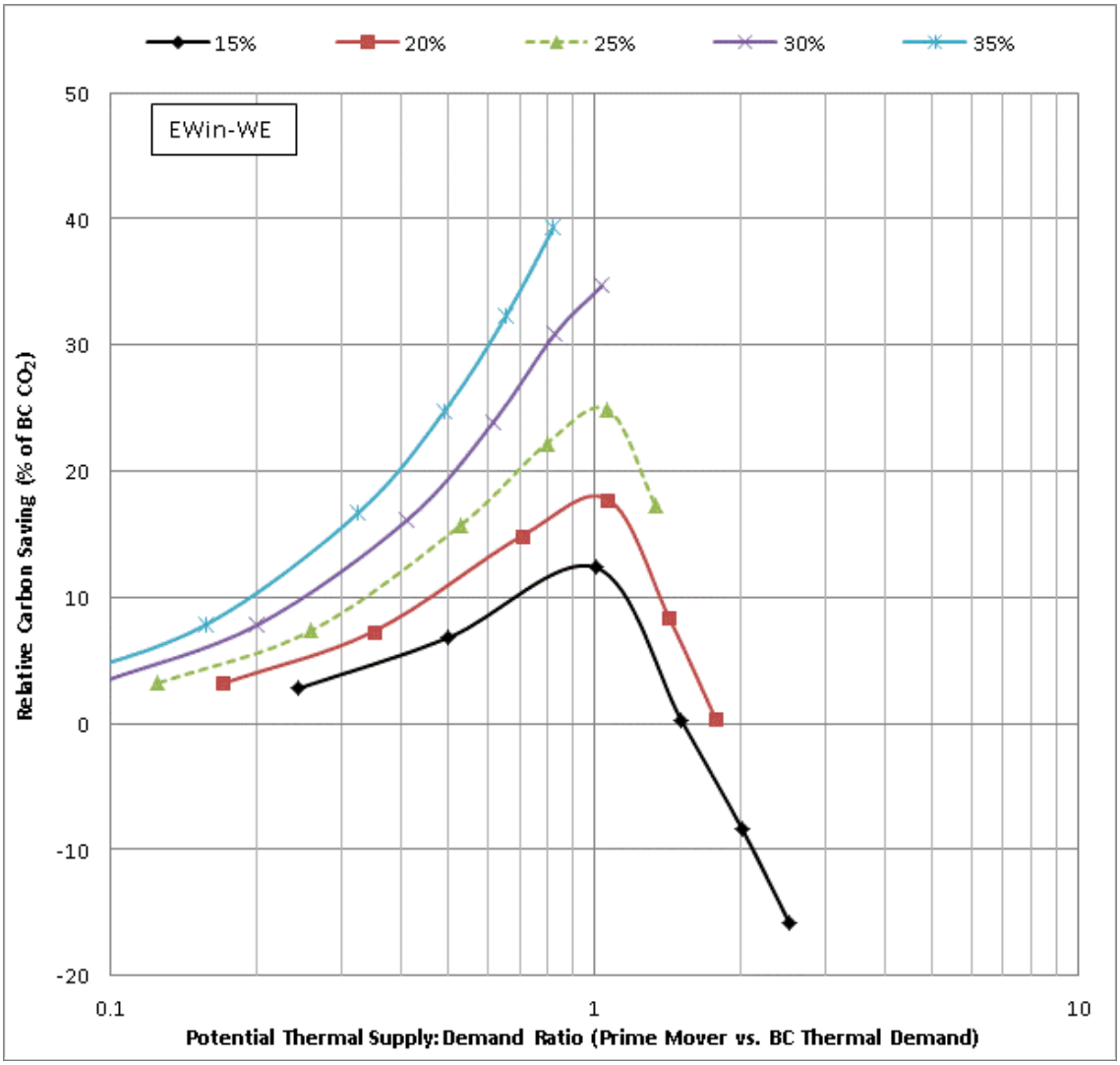

Figure 4.40: RCS versus PTSDR, for the Extreme Winter-Weekend PDS, for all design variants, disaggregated by rated η_e, with RSO-NoSummer

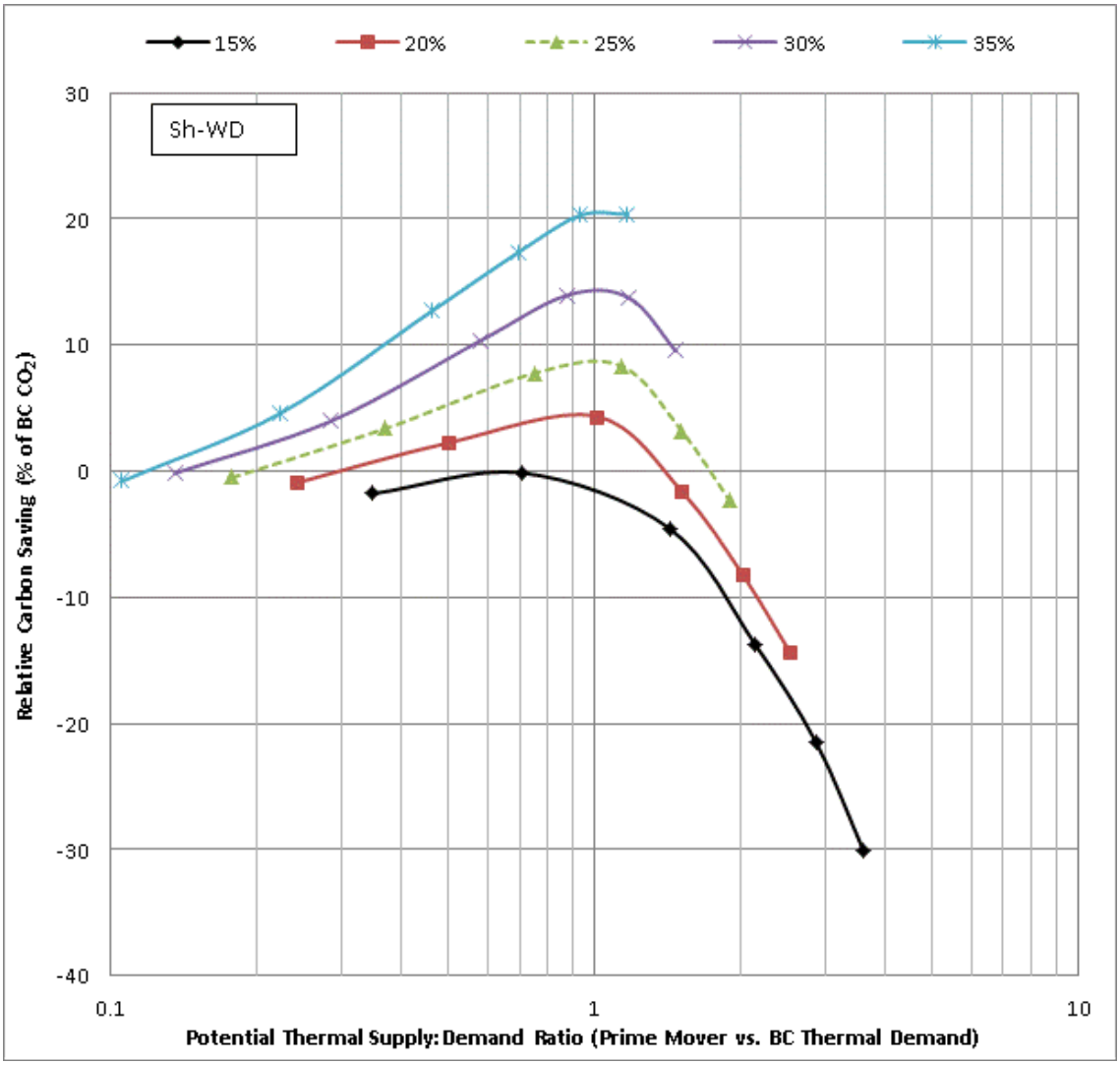

Figure 4.41: RCS versus PTSDR, for the Shoulder-Weekday PDS, for all design variants, disaggregated by rated η_e, with RSO-NoSummer

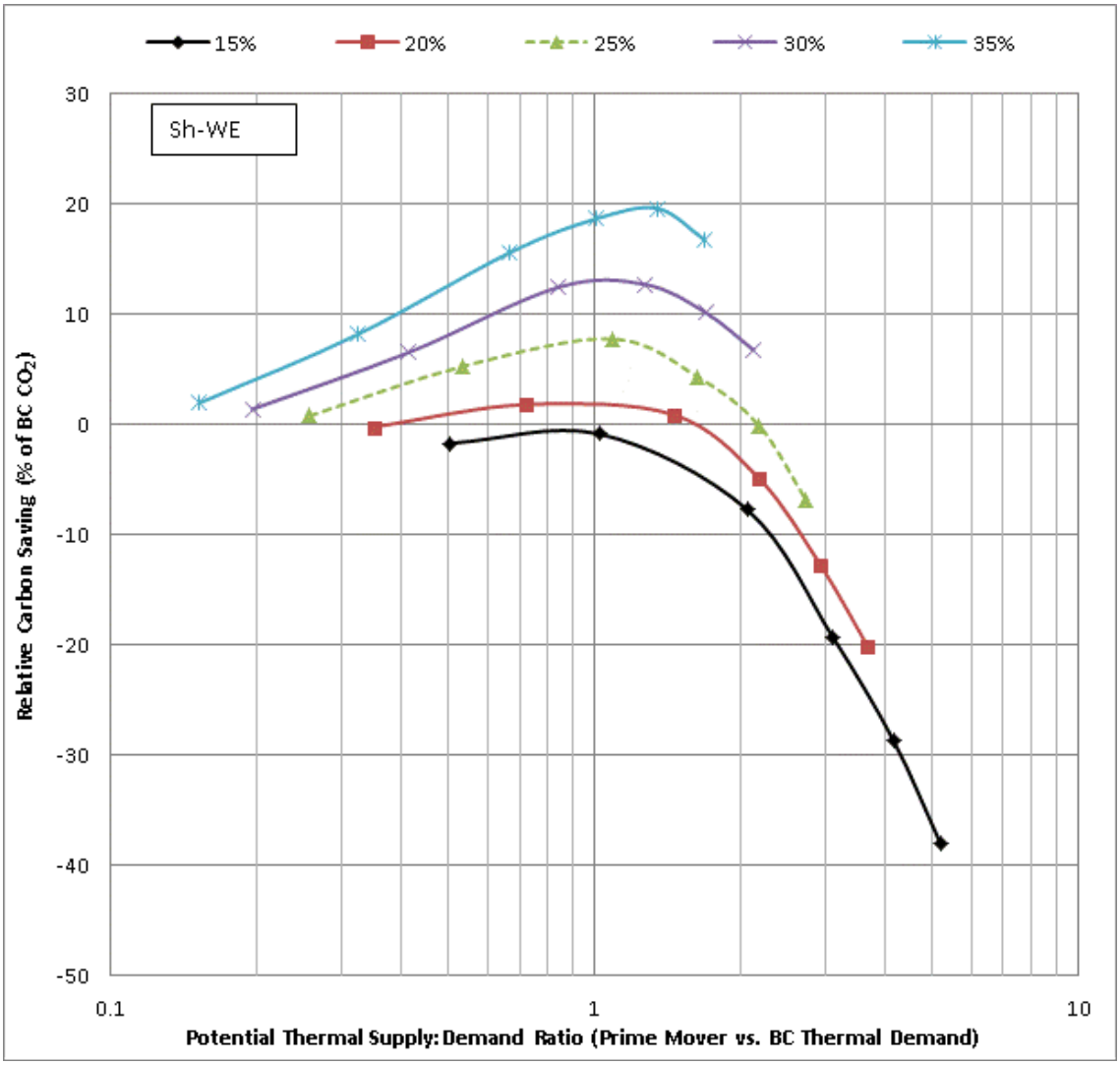

Figure 4.42: RCS versus PTSDR, for the Shoulder-Weekend PDS, for all design variants, disaggregated by rated η_e, with RSO-NoSummer

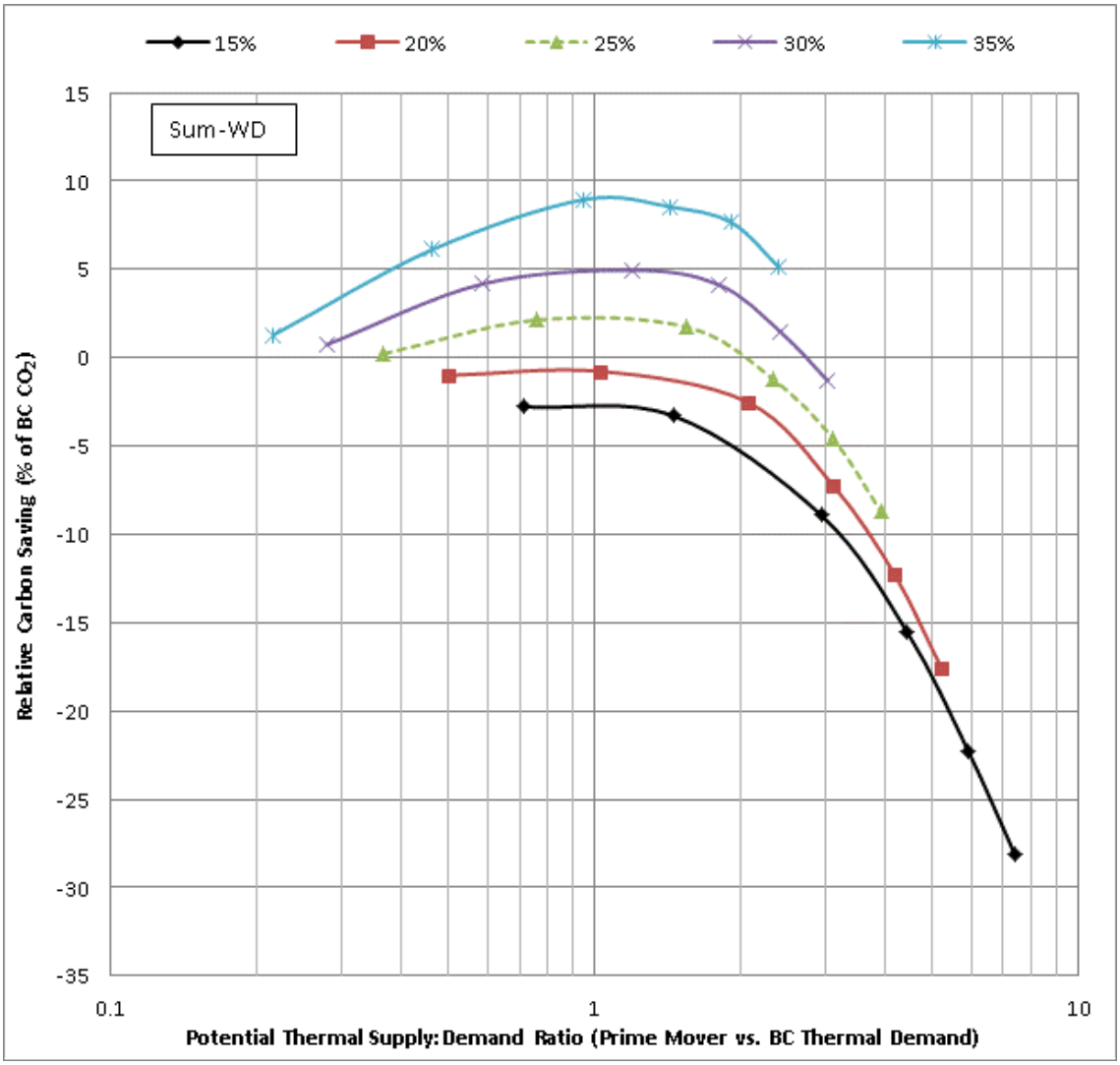

Figure 4.43: RCS versus PTSDR, for the Summer-Weekday PDS, for all design variants, disaggregated by rated η_e, with RSO-NoSummer

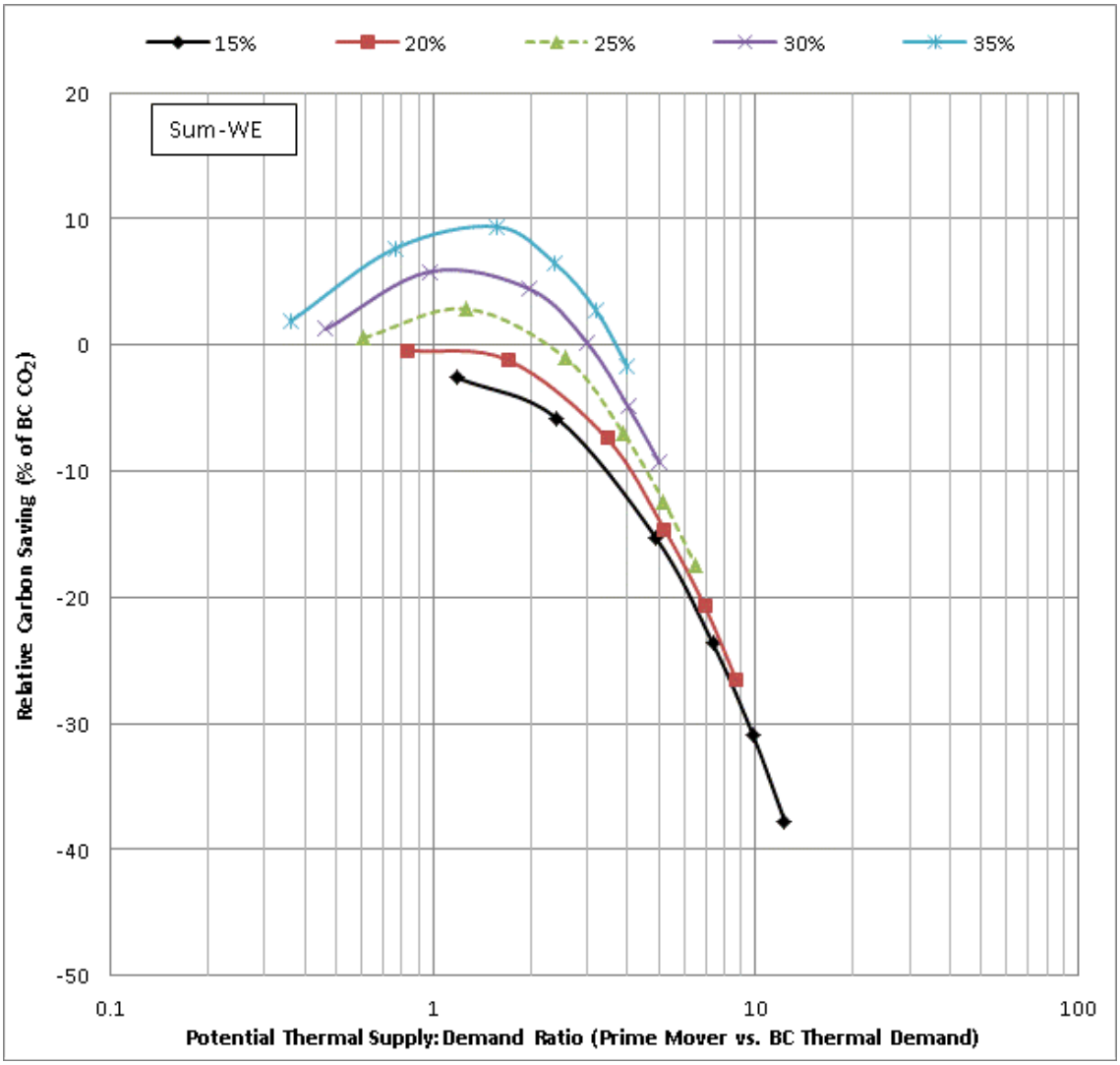

Figure 4.44: RCS versus PTSDR, for the Summer-Weekend PDS, for all design variants, disaggregated by rated η_e, with RSO-NoSummer

The plots of PTSDR versus relative carbon saving is presented for each mode of RSO in Figure 4.45, Figure 4.46, and Figure 4.47. The thermal demand indicated on each graph is the thermal demand present during the seasons that the RSO mode allows prime mover operation, which acts as the maximum auxiliary thermal generation that the prime mover could displace throughout the year.

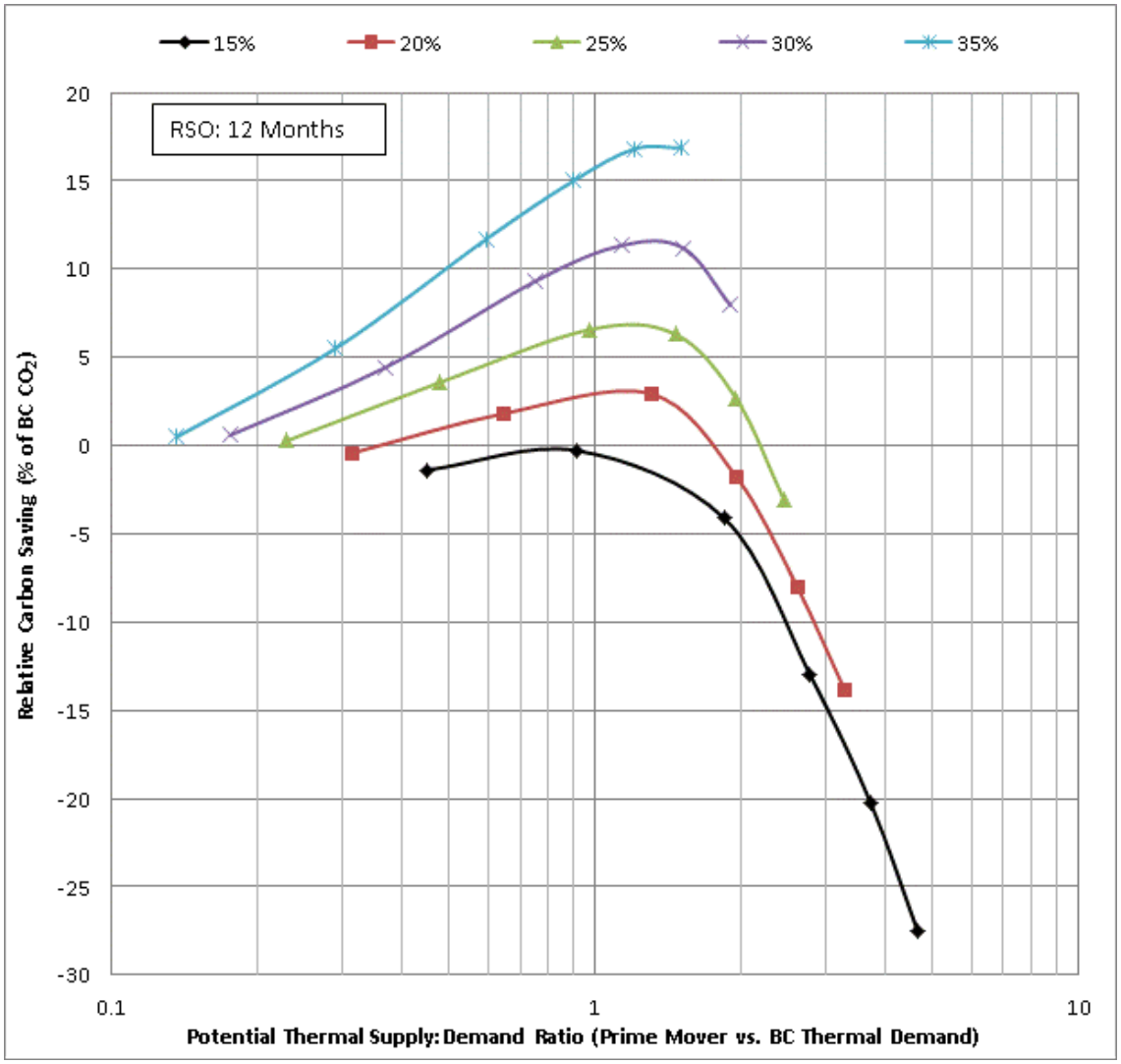

Figure 4.45: RCS (% of base-case CO_2) versus PTSDR for all design variants, disaggregated by rated η_e, with no RSO-NoSummer

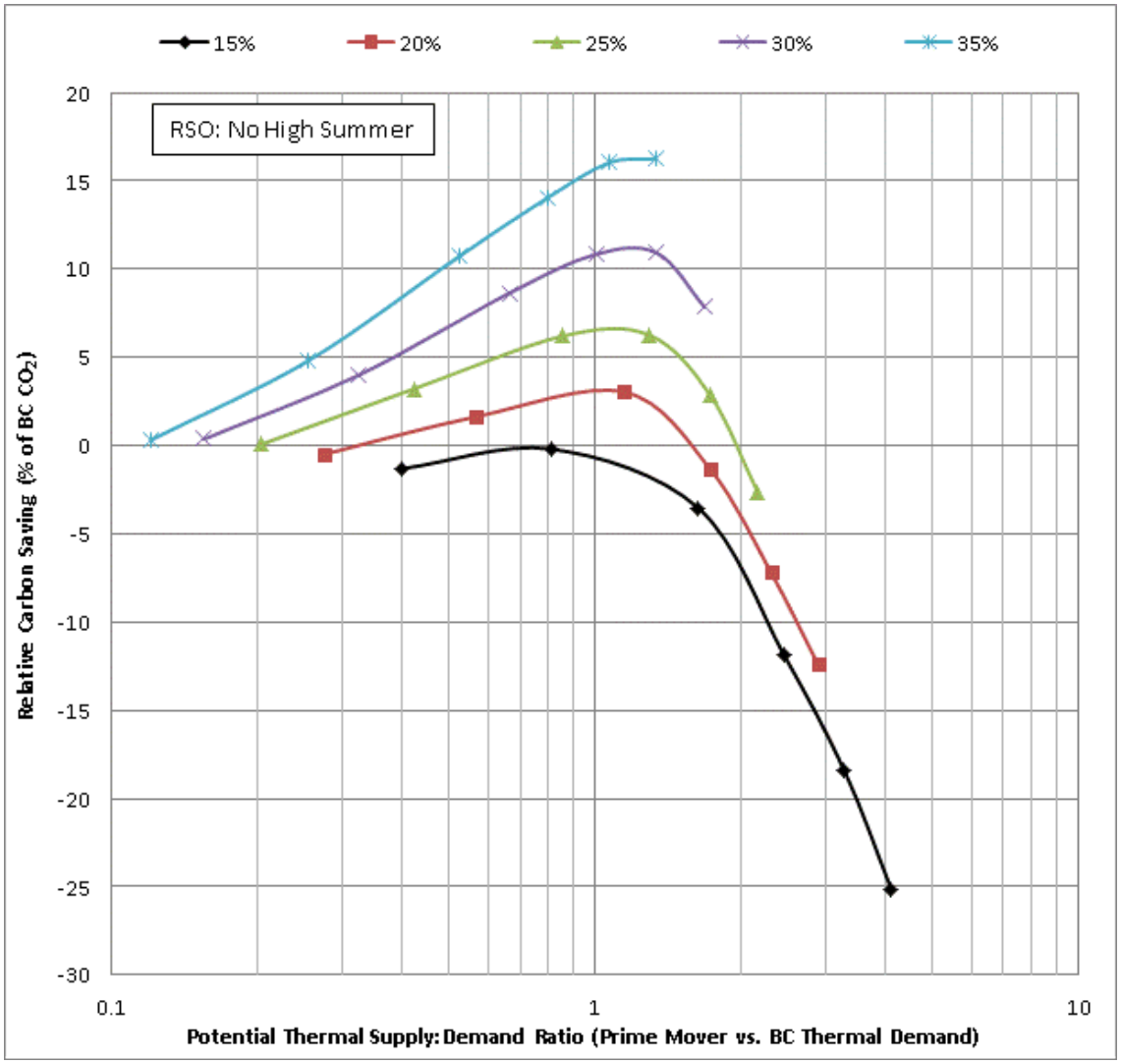

Figure 4.46: RCS (% of base-case CO_2) versus PTSDR for all design variants, disaggregated by rated η_e, with RSO-NoHSum

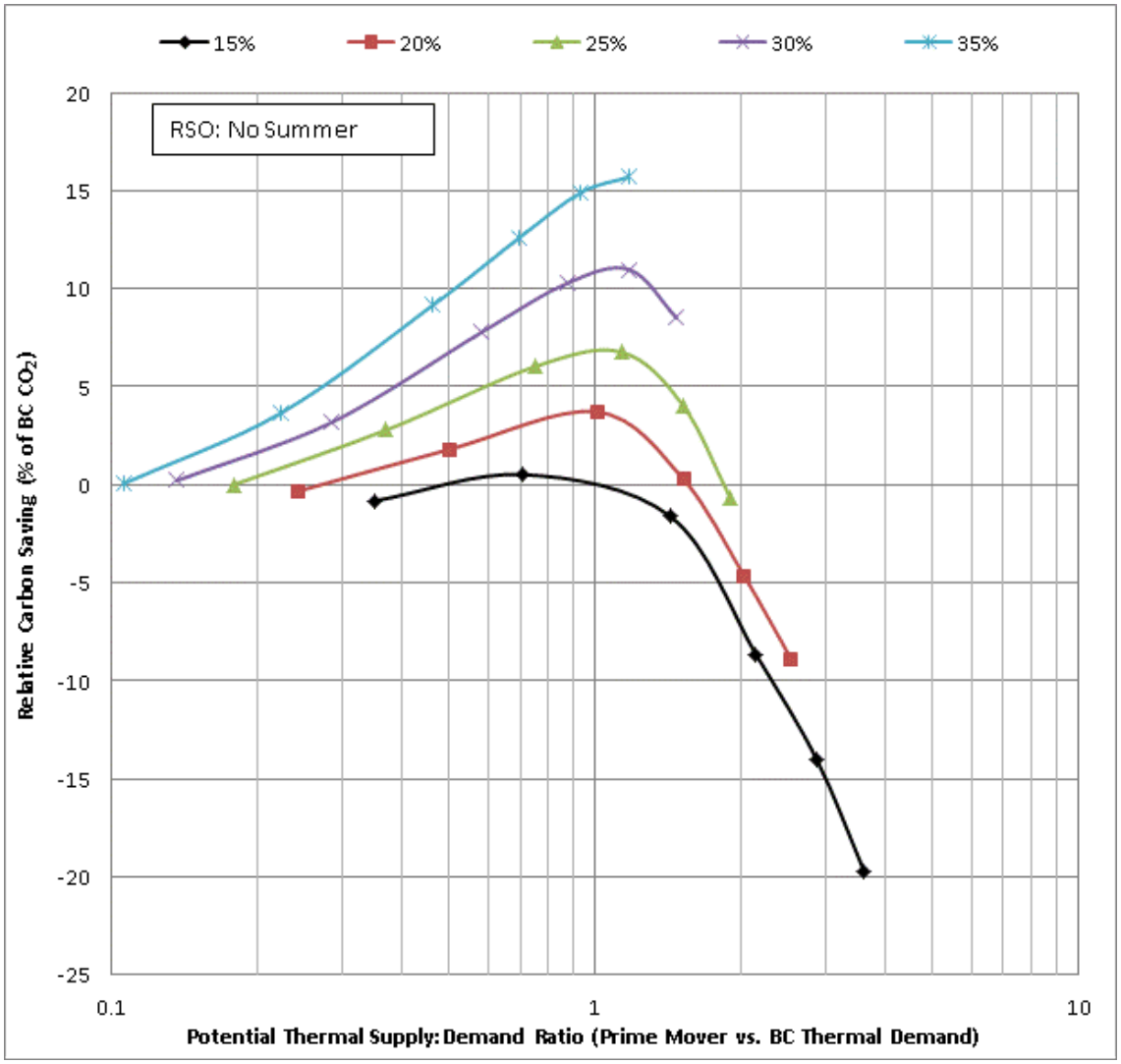

Figure 4.47: RCS (% of base-case CO_2) versus PTSDR for all design variants, disaggregated by rated η_e, with RSO-NoSummer

The RCS for the modes of RSO are compared in Figure 4.48. As seasonal restriction is introduced for High Summer, and subsequently extended to include Summer PDSs, the PTSDR corresponding to the maximum RCS (for design variants of common η_e) shifts towards lower values. For design variants with η_e of 25% or more, RSO reduces peak RCS, whilst peak RCS appears to increase for design variants with η_e below 25%.

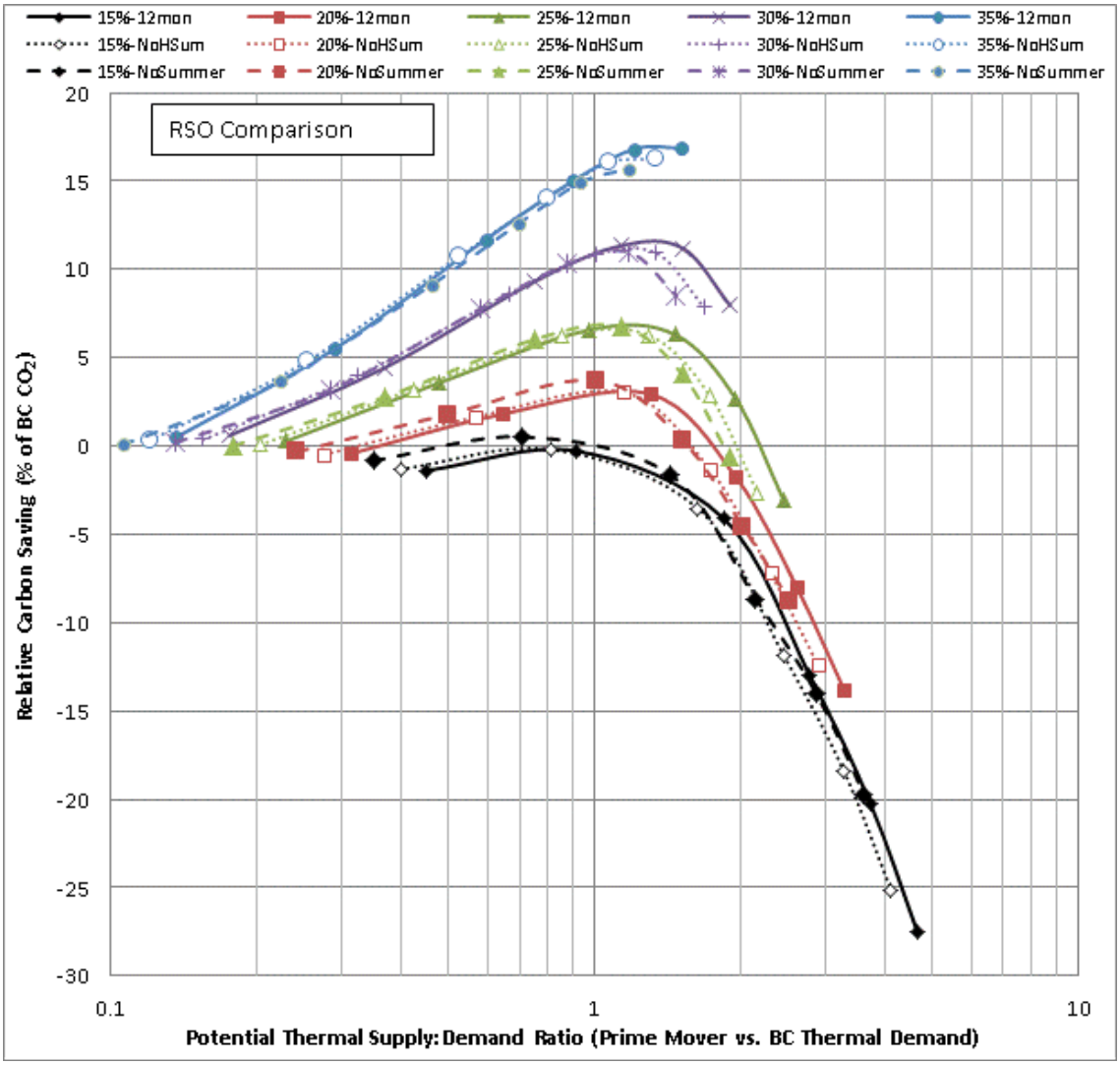

Figure 4.48: RCS (% of base-case CO_2) versus PTSDR for all design variants, disaggregated by rated η_e, comparing RSO: None (12 months), No High Summer Operation (No HSum) and No Summer Operation (No Summer)

4.4 Discussion & Conclusions

In this chapter, simulation results and analysis of the transient operation of thermal load following µCHP systems were presented and discussed. The simulation routines for thermal demand estimation and supply:demand matching were previously discussed in Chapter 2, and the definition methodology for demand scenarios was discussed in Chapter 3. The simulation and analysis methodology for µCHP is discussed in Section 4.2, and the base-case energy system was previously discussed in Section 2.4. The investigation results for thermal load following µCHP are presented and

discussed in Section 4.3, along with the details of several novel performance analysis methodologies for μCHP systems, and a control & operating approach to optimise carbon saving and prime mover lifetime.

Due to the frequency of prime mover thermal cycling observed in the simulation results for a thermal load following μCHP system, it is understood that this operating regime is incompatible with prime movers requiring longer start-up periods, or with greater restrictions in thermal cycles before replacement or major refurbishment. This would preclude the application of the thermal load following operating regime to currently developed FC technologies, as was discussed in Section 4.1.

The relative carbon savings results for each primary demand scenario (PDS), as presented in 4.4.2, revealed that some design variants do not provide relative carbon savings in many of the demand scenarios. Depending on design variant and PDS, RCS of approximately 40% can be achieved, as could maximum carbon penalties of 40%. The main driver of this research is to identify the potential of μCHP to reduce CO_2 emissions. Design variants that exhibit relative carbon penalties are not only unsuitable from an environmental performance perspective, but would increase primary energy consumption, and likely increase household energy costs. Analysis of the scenario-level simulation results indicates that RCS (as a percentage) increases with thermal demand. That is, not only does the absolute value of carbon savings increase between PDS's with increased thermal demand, but the percentage of the PDS's carbon footprint that can be saved increases as the thermal demand of a PDS increases.

Carbon Saving Attribution was introduced in Section 4.3.4 as a novel μCHP performance analysis methodology, with specific investigation of several constituent values:

- Thermal Generation Displacement, whose interaction with design variants and RCS is investigated in Section 4.3.5
- Electrical Import Displacement and Electrical Export Credit, whose interaction with design variants and RCS is investigated in Section 4.4.6

Potential Thermal Supply:Demand Ratio of prime movers was introduced in Section 4.3.5 as metric to describe matching of prime mover thermal capacity to thermal demand. Analysing RCS results with this metric allowed a set of design variants with the top-ranking RCS to be predicted for each demand scenario. These top-ranked design variants consistently have a potential thermal supply:demand ratio between 0.5-1.5, where such ratios are possible due to the particular thermal demands and design variants under investigation. The magnitude of relative carbons savings increases with thermal demand, and the value of PTSDR corresponding to the RCS maxima increases with thermal demand. This has consequences for the optimal sizing of μCHP systems between dwellings with different values of annual thermal demand.

Applying the Carbon Saving Attribution methodology to simulation results provided several significant conclusions:

- RCS results reported are heavily reliant on Electrical Export Credit – without it, none of the design variants would save carbon, as the carbon intensity of the NEG and natural gas fuel used in the investigation is too low for electrical output alone to provide carbon savings. This would be the case even if the operational η_e of the prime mover equals rated η_e (which is technically impossible)
- For the design variants and demand scenarios investigated, the RCS due to Thermal Generation Displacement (i.e. reduced boiler fuel consumption) appear to saturate with increasing thermal capacity, and also with increasing potential thermal supply:demand ratio
- RCS due to Electrical Import Displacement appears to saturate with increasing rated electrical output, and appears to reach maximum values for potential thermal supply:demand ratios between 0.5-1.1
- For the design variants and demand scenarios investigated, the RCS due to Electrical Export Credit appear to saturate with increasing electrical capacities for design variants with lower η_e. It is expected that RCS for design variants with much higher η_e will also saturate with rated electrical output
- In order to increase the point of saturation for Thermal Generation Displacement, either control restrictions (additional to those inherent to the

simulated control regime) need to be applied to the auxiliary boiler, or alternative operating regimes for the prime mover are required to limit thermal cycling and/or shift operation from part-load to full load conditions

- In order to increase the point of saturation for Electrical Import Displacement, or alternative operating regimes for the prime mover are required to limit thermal cycling and/or shift operation from part-load to full load conditions

Restricted Seasonal Operation (RSO) was introduced in Section 4.3.3 as a control approach to optimising carbon saving and prime mover lifetime, where the importance of lifetime is discussed in Section 4.3.8. By applying RSO to μCHP control & operating regimes, prime mover operation is excluded in seasons where carbon penalties occur, whilst decreasing annual operating duration and cumulative annual thermal cycles. The carbon savings benefits are particularly prevalent in systems with limited carbon savings (and even carbon penalties); although the approach increases the already significant RCS for the $4kW_e$-30% & $5kW_e$-30% design variants. Some design variants with high η_e provide RCS in all primary demand scenarios; therefore RSO would reduce carbon savings, however would also decrease annual thermal cycling and operating hours.

The duration at prime mover load conditions, for design variants with significant annual RCS, was presented in Sections 4.3.5 and 4.3.6. In Section 4.3.7, the relationship between total prime mover operating duration (at any load condition) and RCS was investigated, for both daily and annual scenario, incorporating RSO. The results of the daily analysis show a general trend of decreasing run-time with increasing potential thermal supply:demand ratio, and decreasing run-time with decreasing thermal demand. This causes some design variants operating under low demand scenarios to produce run-times much lower than would otherwise be expected from their PTSDR alone.

Thermal cycling of the prime mover was explored in detail in Section 4.3.8, where it becomes clear that thermal cycling can differ dramatically between design variants with very similar RCS. It is believed that the frequency of thermal cycling is a function

of both electrical efficiency and potential thermal supply:demand ratio. Understanding the effect on thermal cycling frequency for design variants which provide marginal increases in RCS will be important in the design ad specification of μCHP systems with low operating costs and high return on investment (both financial and embodied carbon). Based on an assumed limitation of 6,000 thermal cycles before a SE requires replacement or extensive overhaul, prime mover lifetimes of up-to 6 years were achievable (with 11.2% RCS), where the $5kW_e$-35% design variant with maximum RCS (20.4%) had a lifetime of 1.2 years.

The scope for alternative μCHP operating regimes has already been discussed in the context of increasing RCS due to Thermal Generation Displacement and Electrical Import Displacement. Such alternative operating regimes, as introduced in Section 4.2.6, would aim to reduce thermal cycling, hence increasing prime mover lifetime.

Perhaps the most important conclusion of this chapter is that, even after applying restricted seasonal operation, significant (i.e. >10%) RCS are achievable, for the annual demand scenario used in this investigation, for only 8 out of 30 design variants. These μCHP prime mover design variants with a thermal load following operating regime have net electrical rated efficiencies of 30% or 35%, rated electrical capacities between 2-$5kW_e$, and provide RCS of between 10.5-20.4% of base-case CO_2.

After the investigation underpinning this chapter was completed, it was clear that alternative μCHP operating regimes may provide increased RCS, whilst increasing prime mover lifetime by decreasing thermal cycling. These alternative operating regimes are defined and investigated in Chapter 5.

4.5 References

[1] M. Newborough, Demand modulation for micro-CHP systems, EPSRC Final Report GR/J8130, 1997

[2] Roger Dettmer; Home Station; IEE Review January 1998; pp11-13

[3] N.W. Lane and W.T. Beale; A Biomass-fired 1kWe Stirling Engine Generator and its applications in South Africa; Sunpower Inc.; USA; accessed online at http://www.sunpower.com/library/pdf/publications/Doc0076.pdf

[4] A. Baumuller & E. Schmieder; Field-Test and Market Introduction of a 10 kW Stirling Engine as CHP- and Solar- Module; Proceedings of 10th International Stirling Engine Conference 2001 (10th ISEC); 24-26 September 2001; Osnabruck; Germany; pp106-113

[5] Sunpower Inc.; Accessed online March 2012 at http://www.sunpower.com/services/technology/benefits.php

[6] Onovwiona H.I. and Ugursal V.I; Residential cogeneration systems: review of the current technology; Renewable and Sustainable Energy Reviews; 10 (2006) 389-431

[7] Private Conversation at Stirling Engine Conference; 2005; Prof. M. Newborough

[8] T. Kaarsberg; R. Fiskum; A. Deppe; S. Kumar; A. Rosenfeld; J. Romm; 2000; Combined Heat and Power for Saving Energy and Carbon in Residential Buildings; Lawrence Berkeley National Laboratory. Retrieved from: http://www.escholarship.org/uc/item/6kc9t47g

[9] C.M. Dickson, J.E. Dunster, S.Z. Lafferty, L.D. Shorrock; BREDEM: Testing monthly and seasonal versions against measurements and against detailed simulation models; Building Services Engineering Research and Technology; August 1996; 17; 135-140; doi:10.1177/014362449601700306

[10] Michel De Paepe, Peter D'Herdt, David Mertens, Micro-CHP systems for residential applications, Energy Conversion and Management, Volume 47, Issues 18 & 19, November 2006, Pages 3435-3446

[11] A.D. Hawkes, P. Aguiar, B. Croxford, M.A. Leach, C.S. Adjiman, N.P. Brandon, Solid oxide fuel cell micro combined heat and power system operating strategy: Options for provision of residential space and water heating, Journal of Power Sources, Volume 164, Issue 1, 10 January 2007, Pages 260-271

5 Alternative Operating Regimes for Micro-CHP Systems

5.1 Introduction

An investigation into alternative CHP operating regimes, to address the issues outlined in Section 4.4, is presented in this chapter. This investigation includes the seasonal combination of operating regimes to maximise RCS and lifetime of prime movers. The applicability of alternative and combined operating regimes to various prime mover technologies, with a range of electrical efficiencies and associated operational constraints, is discussed.

As discussed in Sections 1.4 and 4.1, fuel cell technology has already been applied to μCHP systems, with resulting net electrical efficiencies greater than the 35% design variants investigated in Chapter 4, potentially exceeding 50%. It was shown in Chapter 4 that RCS increases with η_e for the thermal load following operating regime. However, Apfel et al [1] point out that SOFCs, with a lifetime limitation on thermal cycles of below 100, may require an operating regime which forces the prime mover to operate continuously. Whilst other predictions of FC lifetimes discussed in Section 1.4.3 were not as restrictive regarding cumulative thermal cycling, it is likely to be 1 or 2 orders of magnitude less than the Stirling Engine technology investigated in the previous chapter. Reducing thermal capacity alone does not reduce thermal cycling dramatically, as Section 4.3.8 reported that the 0.5kW$_e$-35% SE design variant exhibited hundreds of thermal cycles per annum.

Aside from lifetime constraints, the performance penalties associated with the long cold-start periods of FCs and fuel-processing sub-systems may necessitate alternative operating regimes. Regardless of prime mover technology, there are technical and economic challenges in the definition of control algorithms that balance environmental performance with factors driving prime mover lifetime. This becomes less of an issue for μCHP systems with electrical generation carbon intensities lower than that of the NEG, as addressed in Section 6.4. Otherwise, the thermal (and hence electrical) capacity of the prime mover must be carefully specified to ensure that sufficient

proportions of its thermal output is used to displace auxiliary boilers, or the relative carbon savings from the μCHP system will be significantly diminished.

5.2 Alternative Operating Regimes

5.2.1 Summary of Alternative Operating Regimes

A number of alternative operating regimes have been considered in this chapter, although many more have been conceived, particularly combining features of the regimes listed below.

- Continuous Operation over Thermal Demand Periods (CsO-TDP)
- Continuous Operation over Daily Demand Periods (CsO-DDP)
- Continuous Operation over 24 hours (CsO-24hr)
- Constant Operation (CtO)

Details of these operating regimes are provided in the corresponding sub-sections that follow. The performance and lifetime of dynamically combining operating regimes on a seasonal basis to devise an annual control regime is considered in Section 5.3.

5.2.2 Carbon Intensity of Generated Electricity

If the μCHP system was only to supply useful electricity, then we would consider the carbon intensity of its net generated electricity, CI_{gen}, using equation (5.1). Selection of the appropriate value of η_e is vital to the prediction of carbon intensity. The rated value of η_e would never be achieved in practice, due to start-up losses and part-load inefficiencies. However, using typical estimates for operational η_e (i.e. replace the design value of η_e with a value reflective of average operation), equation (5.1) allows estimated μCHP-generated electricity CI to be calculated.

$$CI_{gen} = CI_{fuel} / \eta_e \qquad (5.1)$$

However, in most situations, some proportion of a μCHP system's heat output will be useful. This usefulness could be defined as either displacing alternative thermal

generation to satisfy the pre-determined thermal comfort and/or DHW requirements, or providing additional comfort to occupants. In the context of CO_2 emissions reduction, a narrow definition of usefulness would be appropriate, i.e. the displacement of fuel for thermal generation otherwise consumed by the base-case energy system.

There are several approaches to discussing the carbon intensity of a μCHP system. The carbon intensity of the (net) generated electricity could be adjusted to include a 'credit' for the thermal generation displaced. Alternatively, the CI of the displaced thermal generation could be 'credited' with the electrical generation. The suitability of either approach depends upon the context of any subsequent analysis, i.e. if the control regime under assessment is designed to prioritise electrical or thermal generation.

The effective operational carbon intensity, $CI_{en\text{-}eff\text{-}op}$, of net generated electricity from the μCHP system could be estimated using equation (5.2). However, this equation incorporates net electrical energy generated, Q_e, and reduction in auxiliary thermal generation between μCHP and base-case energy system, ΔQ_{aux}. Therefore, it is difficult to calculate effective electrical CI outside the context of simulation results or recorded operational data, unlike equation (5.1).

$$CI_{en\text{-}eff\text{-}op} = (F_{CHP} * CI_{fuel}) / (Q_e + \Delta Q_{aux}) \quad (5.2)$$

The difference between the effective operational CI of generated electricity and the CI of grid electricity (CI_{grid}) is plotted versus RCS in Figure 5.1. The data plotted relates to each design variant of the TLF SE μCHP system reported in Chapter 4, operating under each PDS. As expected, relative carbon savings (as opposed to carbon penalties) occur whenever $CI_{en\text{-}eff\text{-}op} < CI_{grid}$. By normalising the RCS against kWh of electrical generation, as plotted in Figure 5.2, it is apparent that the much of the spread in RCS (at similar values of $CI_{en\text{-}eff\text{-}op}$) is due to the cumulative electrical generation of the μCHP. As discussed in Section 4.3, electrical generation under a TLF operating regime is limited by the thermal demand and the heat-to-power ratio of the system. Equation (5.2) constitutes a simplified approach, as it considers the reduction in output from the

auxiliary thermal generator. In reality, the direct driving factor for carbon emissions is the fuel consumption of the auxiliary generator, which is predicated by the output and average thermal efficiency over the operating period. This explains the simulation results with $CI_{en\text{-}eff\text{-}op} < CI_{grid}$ that exhibit relatively low RCS in Figure 5.1 and Figure 5.2.

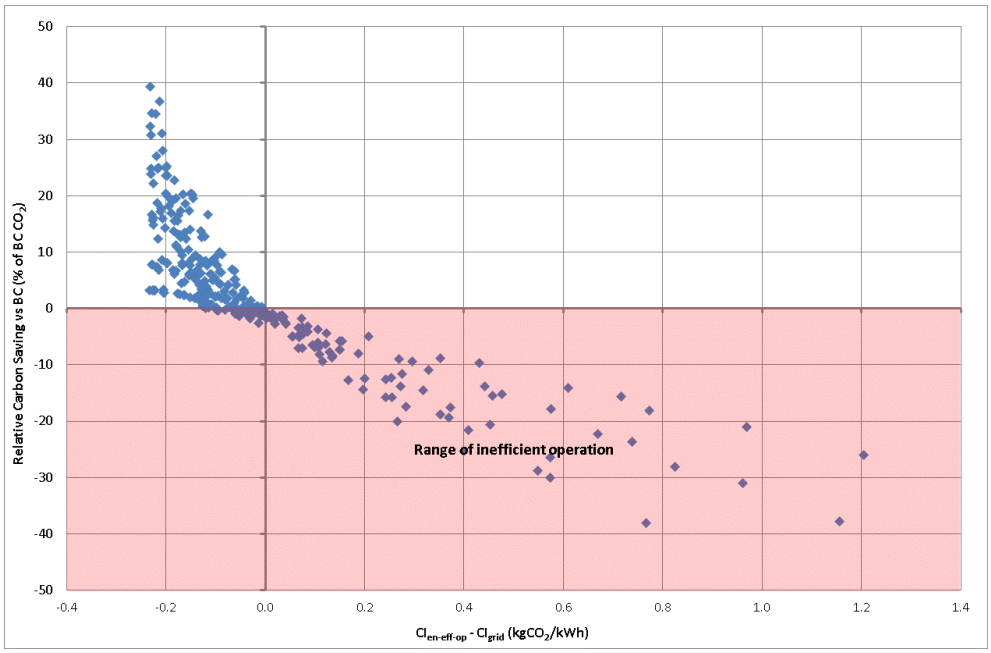

Figure 5.1: Difference between effective operational CI of generated electricity ($CI_{en\text{-}eff\text{-}op}$) and CI_{grid}, vs. RCS, for each SE TLF design variant

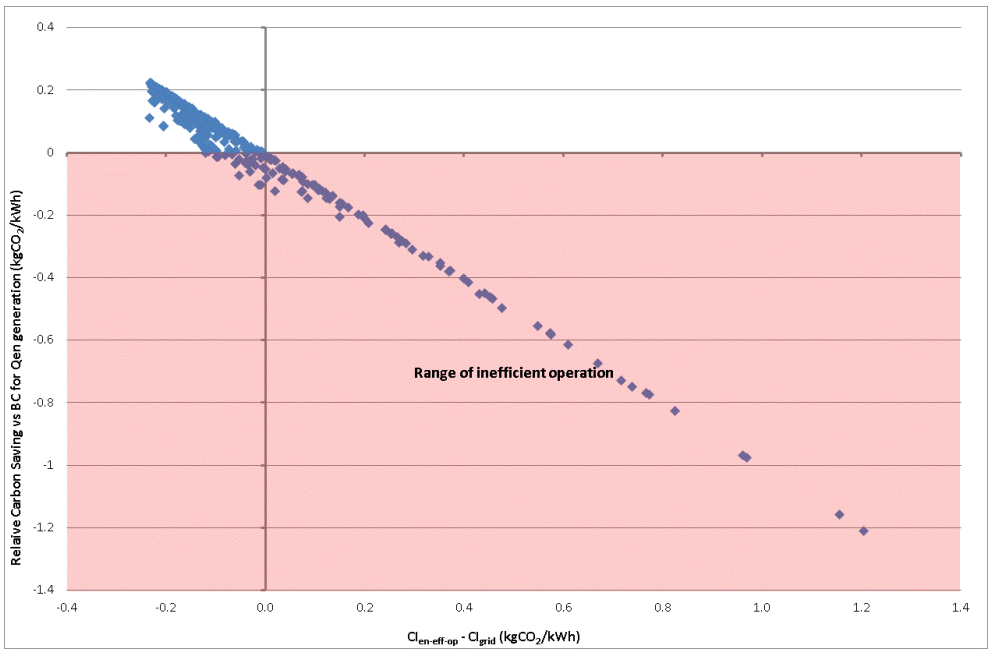

Figure 5.2: Difference between effective operational CI of generated electricity ($CI_{en\text{-}eff\text{-}op}$) and CI_{grid}, vs. RCS normalised by kWh of generated electricity, for each SE TLF design variant

The effective carbon intensity, $CI_{en\text{-}eff}$, of net generated electricity from the μCHP system could be defined in a manner that uses design values to estimate the CI for a μCHP system operating with ideal performance. $CI_{en\text{-}eff}$ is calculated using equation (5.3) on the assumption that 100% of the prime mover's thermal output will displace the same amount of output from auxiliary boiler (unless the demand is smaller than the cumulative daily output from the prime mover). Equation (5.3) assumes that the reduction in auxiliary fuel consumption, ΔF_{aux}, is calculated from ΔQ_{aux} using a pre-determined thermal efficiency of the auxiliary boiler. It also assumes that the prime mover achieves the design value of η_e during operation. As with equation (5.2), the incorporation of Q_e requires some estimate of total operation (i.e. cumulative duration at load conditions) across the calculation period. As discussed later, however, effective CI can be used to assess operational performance versus design performance to understand the ability to predict operational μCHP performance.

$$CI_{en\text{-}eff} = (CI_{fuel} / \eta_e) - [(\Delta F_{aux} * CI_{fuel}) / Q_e] \quad (5.3)$$

If a relationship could be found between rated thermal and/or electrical output of a μCHP system, the typical proportion of auxiliary thermal generation displaced, and the thermal and/or electrical demand that the CHP system is intended to satisfy, perhaps an estimative method could be created to predict the CI of μCHP-generated electricity. This would allow designers and specifiers to understand the minimum operational η_e required from a μCHP system, within a demand scenario defined by the aforementioned relationship, to produce electricity with certain CI. This CI could then be used to decide if and when the μCHP system should run in an electric-led operating regime, i.e. because the value of $CI_{en\text{-}eff}$ is less than grid average or less than the CI of some other grid-connected generator that may otherwise be switched on.

It may, however, not be desirable to operate a μCHP system in an electric-led manner. This could be for economic reasons related to fuel and maintenance costs, i.e. the £/kWh of electricity generated, once transmission and distribution costs are included, exceeds that of alternative grid-connected generators. In this case, consideration of electrical or thermal CI as separate values may be redundant, as carbon savings from

µCHP systems are reliant on both generated electricity and displaced auxiliary thermal generation.

The concept of µCHP system carbon intensity (CI_{system}) could be introduced, where the cumulative CI of the µCHP system (prime mover and auxiliary thermal generator) is divided by the combined electrical and thermal output of the µCHP system (i.e. prime mover and auxiliary). In this case, the carbon footprint would be equal to the combined fuel consumption of the µCHP system minus the net electrical generation of the µCHP system (regardless of whether this is exported to the NEG or displaces import of electricity from the NEG). The calculation for CI_{system} is presented in equation (5.4), but as with equations (5.2) and (5.3), it incorporates variables that would be difficult to estimate prior to operation or simulation.

$$CI_{system} = [(F_{system} * CI_{fuel}) - (Q_e * CI_{grid})] / (Q_e + Q_{th\text{-}system}) \quad (5.4)$$

If we compare the operational effective CI (Figure 5.3) with the effective CI derived from design values (Figure 5.4), we notice several major differences. The effective CI under operation is higher than the CI calculated from design values for all design variants, but CIs are much higher than expected for design variants with rated electrical output above $2kW_e$. After investigating the simulation results, it is understood that the difference between design and operational effective CI is due to thermal demand saturation. As shown in Section 4.3.5, as the PTSDR increases for a set of design variants under a common demand scenario, Thermal Generation Displacement eventually saturates once the PTSDR exceeds 1. As illustrated in Figure 5.5, for several sets of design variants, the reduction in effective CI with increasing rated electrical output is curtailed once PTSDR exceeds 1. Furthermore, as discussed in Section 4.3.5, once PTSDR exceeds approximately 1.5, the RCS begin to decline.

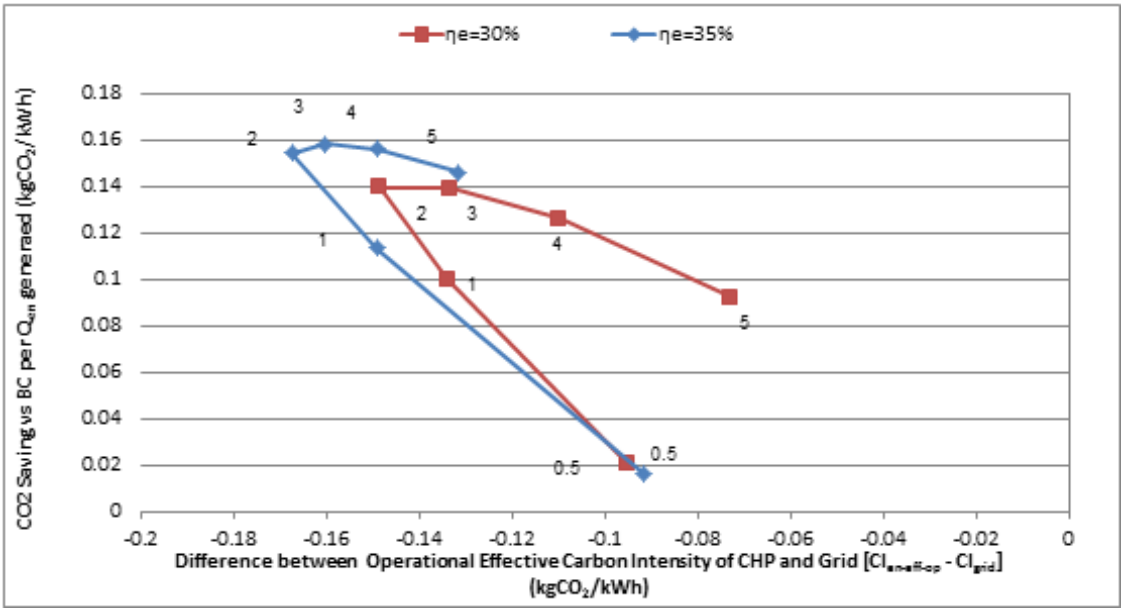

Figure 5.3: Difference between effective operational CI of generated electricity and CI_{grid}, vs. RCS normalised by kWh of generated electricity, for TLF SE µCHP design variants with η_e=30% & 35%

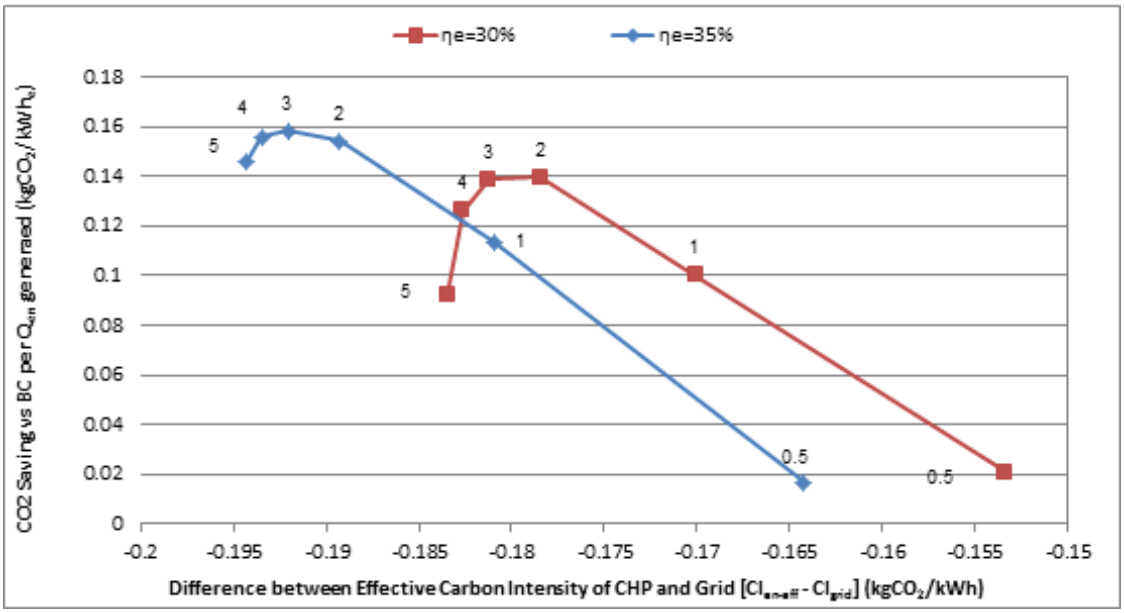

Figure 5.4: Difference between effective CI of generated electricity and CI_{grid}, vs. RCS normalised by kWh of generated electricity, for TLF SE µCHP design variants with η_e=30% & 35%

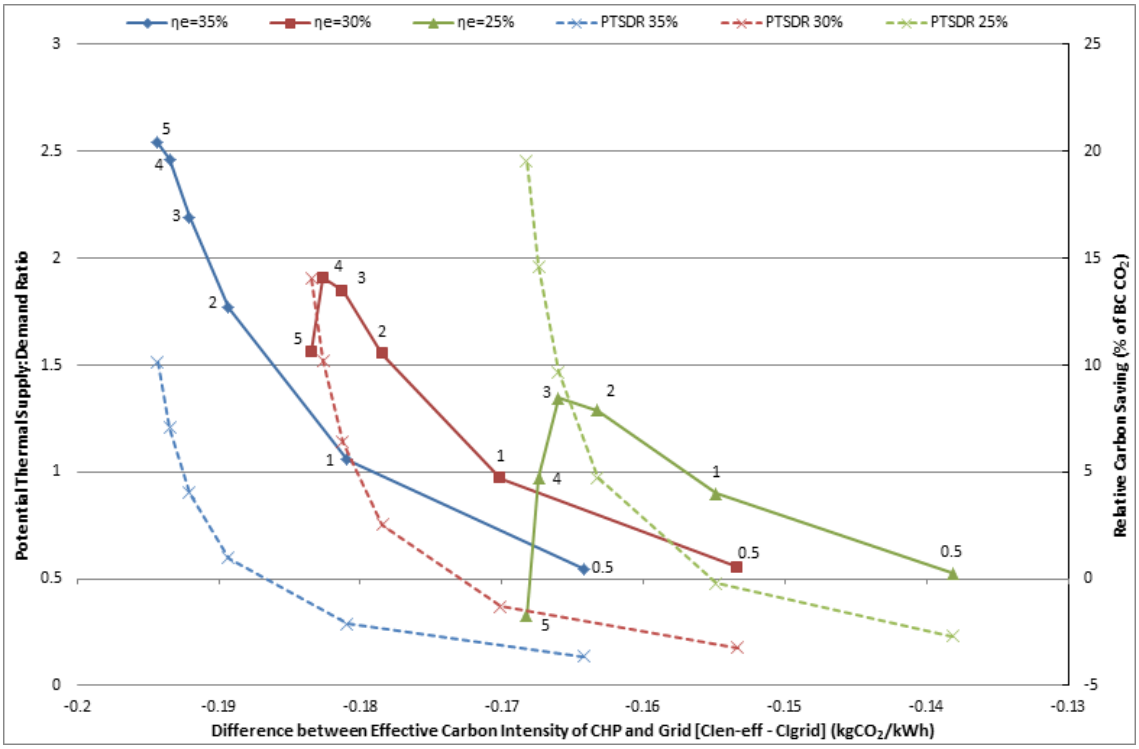

Figure 5.5: PTSDR and RCS vs. the difference between the effective CI of generated electricity and CI_{grid}, for design varaints with η_e= 25%, 30% & 35%

5.2.3 Thermal Dumping with Micro-CHP

The concept of thermal dumping, sometime referred to as thermal surplus, was introduced in Section 1.5 as a control strategy to allow prime movers to continue generation despite satisfying the thermal demand or reaching the limit of thermal storage capacity. As discussed in Section 1.6, many investigations of µCHP performance have elected to restrict thermal dumping, even though it could be achieved by mechanically increasing convection of air across a heat exchanger, and subsequently venting this warm air to the atmosphere, as theoretically implemented by Hawkes & Leach [2].

Thermal dumping has been investigated for both thermal and electrical load following operating regimes [3][4], in order to maximise electrical load following potential or minimise thermal cycling. Peacock & Newborough [4] reported that whilst thermal dumping would reduce the annual thermal cycling frequency of a 1kW$_e$ 15% η_e SE µCHP system from 1,898 to 1,182, RCS would reduce from 10% to -3%.

Thermal dumping would be advantageous once the μCHP system can generate electricity with an effective CI less than CI_{grid}. The trade-off between maximising electrical generation and minimising system efficiency due to increased thermal dumping was discussed in Section 4.1. Considering equation (5.3) for a design variant of a fixed fuel type and η_e, can be rearranged to produce equation (5.5), which must be valid for generated electricity to have CI lower than CI_{grid}.

$$(\Delta F_{aux} / Q_e) > [(1 - \eta_e) - (CI_{grid} / CI_{fuel})] \quad (5.5)$$

Table 5.1 has been populated using the values of CI_{fuel} = 0.19kgCO_2/kWh and CI_{grid} = 0.43kgCO_2/kWh. The carbon intensity of net generated electricity where the thermal output of the prime mover is not used, CI_{ne}, is calculated on the assumption that the prime mover achieves the rated value of η_e. The ratio of required displacement of auxiliary fuel consumption to generated electricity, $\Delta F_{aux}/Q_e$, in order for the effective CI of μCHP-generated electricity to achieve grid parity is shown in Table 5.1. Once the ratio has been adjusted for thermal efficiency of auxiliary generation, $\eta_{th\text{-}aux}$, it translates to the ratio $\Delta Q_{aux}/Q_e$, and eventually prime mover heat-to-power ratio.

η_e	(%)	15%	20%	25%	30%	35%	40%	45%	50%	55%
CI_{ne}	($kgCO_2/kWh_e$)	1.27	0.95	0.76	0.63	0.54	0.48	0.42	0.38	0.35
$\Delta F_{aux} / Q_{en}$	(kWh_{th}/kWh_e)	4.40	2.74	1.74	1.07	0.59	0.24	-0.04	-0.26	-0.44

Table 5.1: Ratio of required displacement of auxiliary fuel consumption to generated electricity, $\Delta F_{aux}/Q_e$, in order for the effective CI of μCHP-generated electricity to achieve grid parity, based on the CI of net generated electricity where the thermal output of the prime mover is unused, CI_{ne}, for rated values of η_e

Analysis of Table 5.1 suggests that a natural gas-fired μCHP system with η_e (during operation) of approximately 44.2% will generate electricity with a carbon intensity equal to CI_{grid}. For such a design variant, it would be advantageous to operate the system for as long as possible, in order to displace as much auxiliary thermal generation as possible (as limited by the transient magnitude of thermal demand and the prime mover's peak thermal output).

5.2.4 Continuous Operation for Thermal Demand Period (CsO-TDP)

The research presented in Chapter 4 identified that TLF SE µCHP systems exhibit a high frequency of thermal cycling, compared with assumed lifetime limit of 6,000 cycles. Thermal cycling of the prime mover was found to introduce electrical and thermal inefficiencies, as fuel is combusted for the sole purpose of raising the SE's hot end to operating temperature. The transient thermal output limitations during start-up limited the proportion of auxiliary thermal generation that was displaced by the prime mover. These issues limited RCS for all design variants.

An operating regime was devised that forces the prime mover to operate continuously during the TDPs, whilst retaining the ability to modulate in response to thermal demand (or more specifically thermal store temperature), where excess thermal energy is dumped to the environment. This operating regime is referred to in subsequent analysis as Continuous Operation for Thermal Demand Period (CsO-TDP).

Thermal cycling is dramatically reduced versus the TLF operating regime, with 2 thermal cycles per weekday, and 1 thermal cycle per day at the weekend. If RSO is not enforced, this would result in 626 cycles per annum, however, as discussed in Chapter 4, some form of RSO would likely be applied in practice. Thermal cycling frequency under No-HSum and NoSummer RSO would drop to 537 and 436 cycles per annum, respectively, resulting in over 10 years of operation within the 6,000 cycles lifetime limit.

Cumulative operating duration will be significantly increased with this operating regime, as the prime mover operates 9.5 hours each weekday, and 17 hours per day at the weekend. This results in cumulative annual operation of 4,250 hours without RSO, or 3,645 hours and 2,891 hours respectively with No-HSum and NoSummer RSO. However, assuming the limit on cumulative operating duration is 20,000-40,000 hours, as discussed in Section 4.2.2, this operating regime should result in lifetimes in excess of 10 years.

This operating regime should be compatible with prime mover technology that can tolerate hundreds of thermal cycles per annum (as opposed to several thousand for TLF). Most prime movers would likely be compatible, with the exception of high temperature FCs such as SOFC. Excessive efficiency penalties due to the time and energy involved in PEM start-up cycles could be avoided by de-coupling reformer operation from the stack, where the reformer starts in advance of the TDP, storing any produced hydrogen awaiting the start-up of the stack itself. As discussed in Section 1.4.3, PEM prime movers have been reported with η_e between 43-48%. If η_e>44.2% is achieved during operation in commercially available systems, there will be no carbon penalty associated with thermal dumping, as the CI of generated electricity is less than CI_{grid} without using the recovered thermal output. The only barrier for non-SE technologies is the requirement for modulation. The RCS results plotted in Figure 5.5 and Figure 5.6 were simulated using the SE-based µCHP system defined in Section 2.4, with fixed electrical modulation steps of 40% and 70% of rated output.

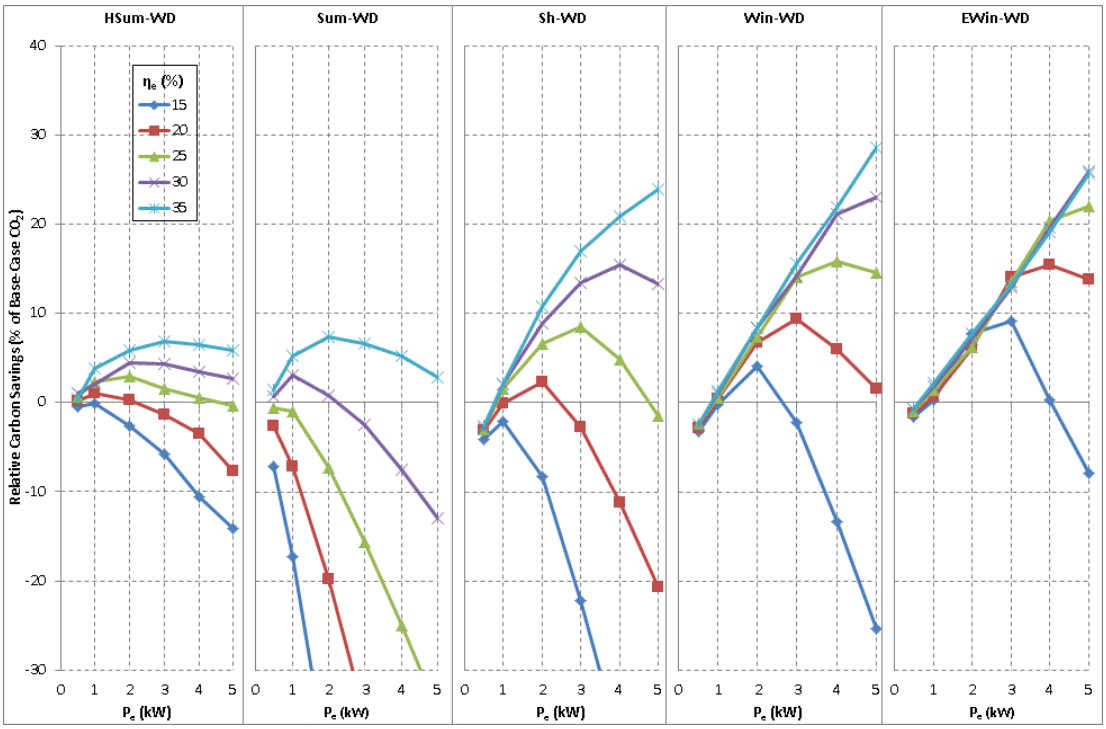

Figure 5.6: RCS for each design variant, during Weekday Primary Demand Scenarios for SE-based µCHP system with CsO-TDP operating regime

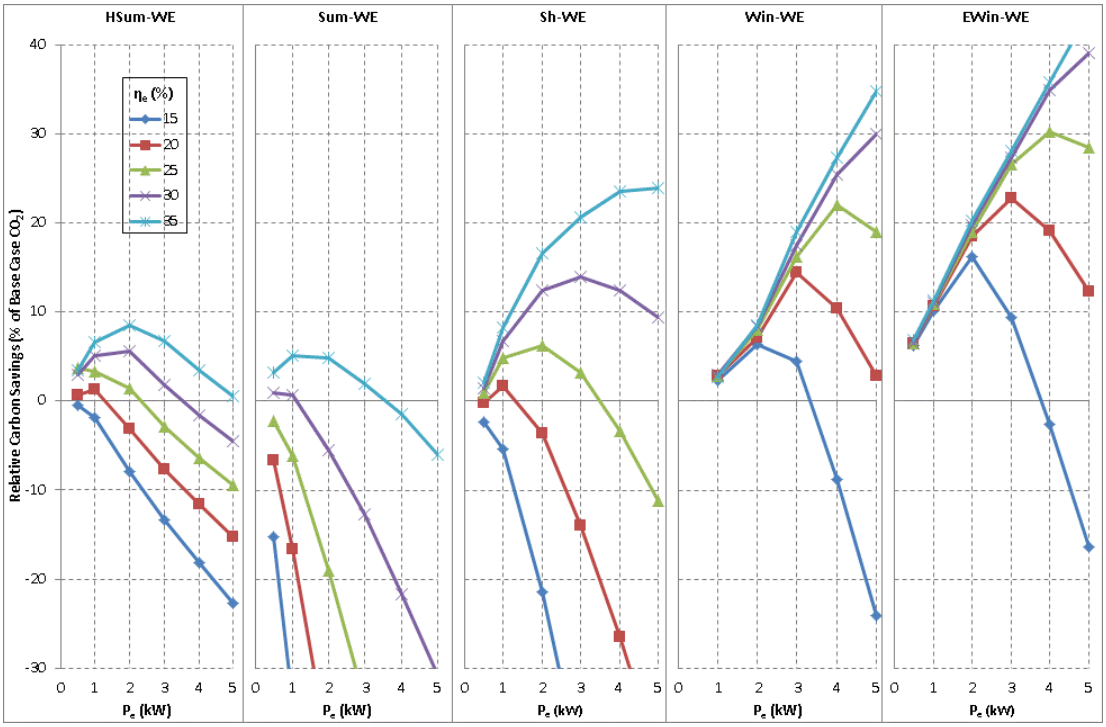

Figure 5.7: RCS for each design variant, during Weekend Primary Demand Scenarios, for SE-based µCHP system with CsO-TDP operating regime

In comparison to the RCS results for the same design variants with TLF operating regime, as presented in Figure 4.1 and Figure 4.2, the RCS have increased for demand scenarios for high thermal demand (from 39.3% under TLF to 43.6% under CsO-TDP for the 35%-5kW$_e$ variant during EWin-WE), and decreased for those with low thermal demand (from 2.2% under TLF to -0.1% under CsO-TDP for the 20%-1kW$_e$ variant during Sh-WD). This is due to thermal dumping during design days with low thermal demand. With reference to Table 5.1, it is clear that to achieve a positive RCS even design variants with 35% η_e need to displace auxiliary fuel consumption (between BC and µCHP scenarios) to the value of 59% of the cumulative electrical generation during the design day.

The RCS for all design variants of the SE µCHP system operating under the CsO-TDP operating regime, without RSO, are presented in Figure 5.8. When compared to the results for the TLF operating regime in Figure 4.3, it is clear that the RCS for 7 of the 8 top-performing design variants have increased, where 2kW$_e$-30% no longer has significant RCS. The RCS for the other design variants have decreased. This is true for all modes of RSO.

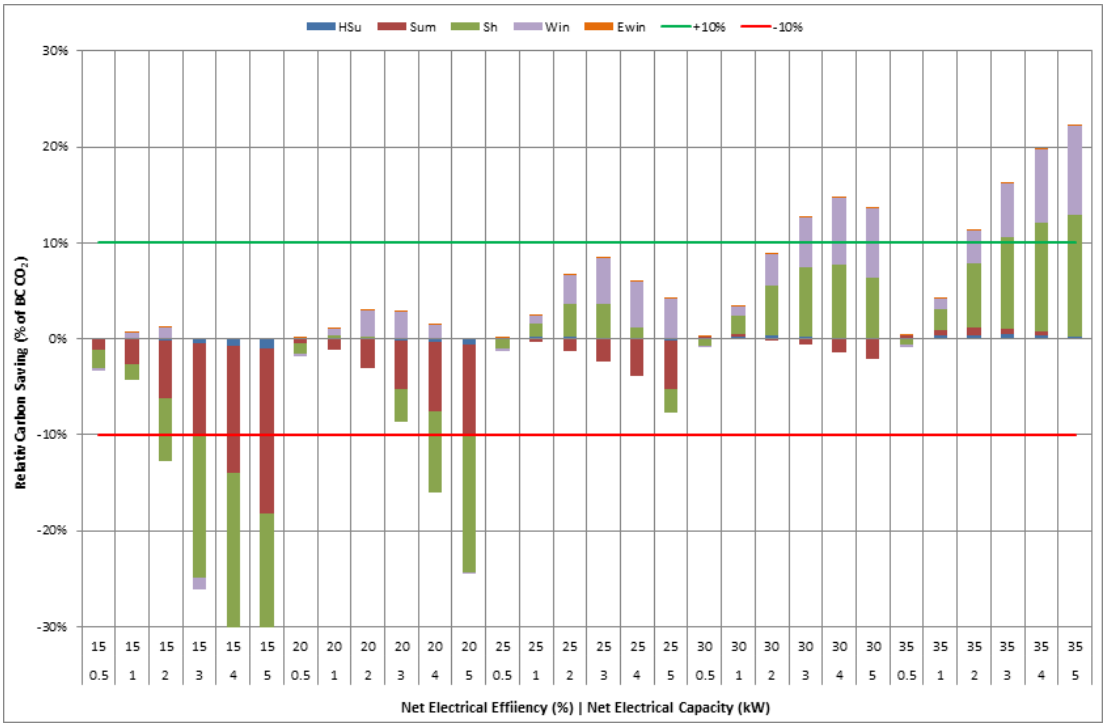

Figure 5.8: RCS for each µCHP design variant operating under 'Continuous Operation for Thermal Demand Period' operating regime without RSO

5.2.5 Continuous Operation for Daily Demand Period (CsO-DDP)

The logical extension to the previous operating regime is to avoid the thermal cycle between morning and afternoon TDPs during weekdays. As before, the prime mover can modulate in response to thermal output, but cannot switch off from the start of the first TDP to the end of the final TDP during a design day. Excess thermal energy that cannot be stored is dumped to the environment. The frequency of thermal cycling is reduced to 365, 313 and 248 per annum, for no RSO, No-HSum RSO and No-Summer RSO respectively. Cumulative operating duration would increase to 6,205 hours, 5,321 hours and 4,220 hours for those RSO options.

As with the CsO-TDP operating regime, this Continuous Operation for Daily Demand Period (CsO-DDP) operating regime is compatible with prime mover technologies that support modulation, and can tolerate hundreds of thermal cycles per annum. However, this operating regime is suited to prime movers with higher η_e, and hence lower heat-to-power ratios, as the increased thermal dumping reduces RCS of SE µCHP versus TLF systems, as illustrated in Figure 5.9 and Figure 5.10.

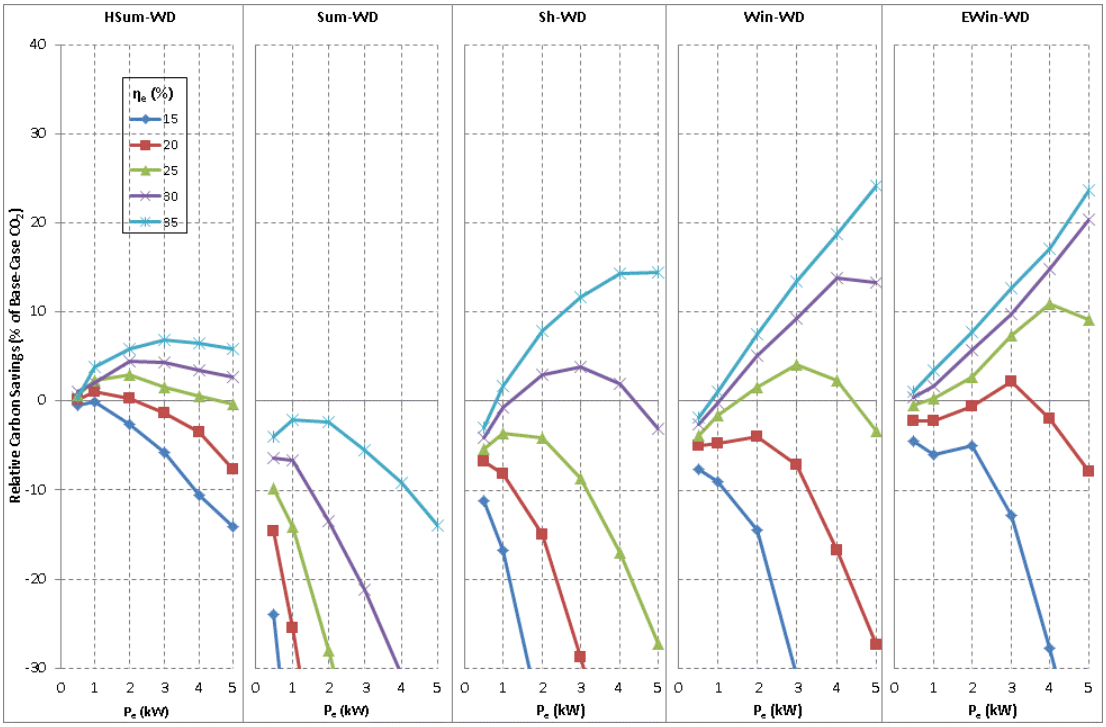

Figure 5.9: RCS for design variant, during Weekday Primary Demand Scenarios, for SE µCHP system with CsO-DDP operating regime

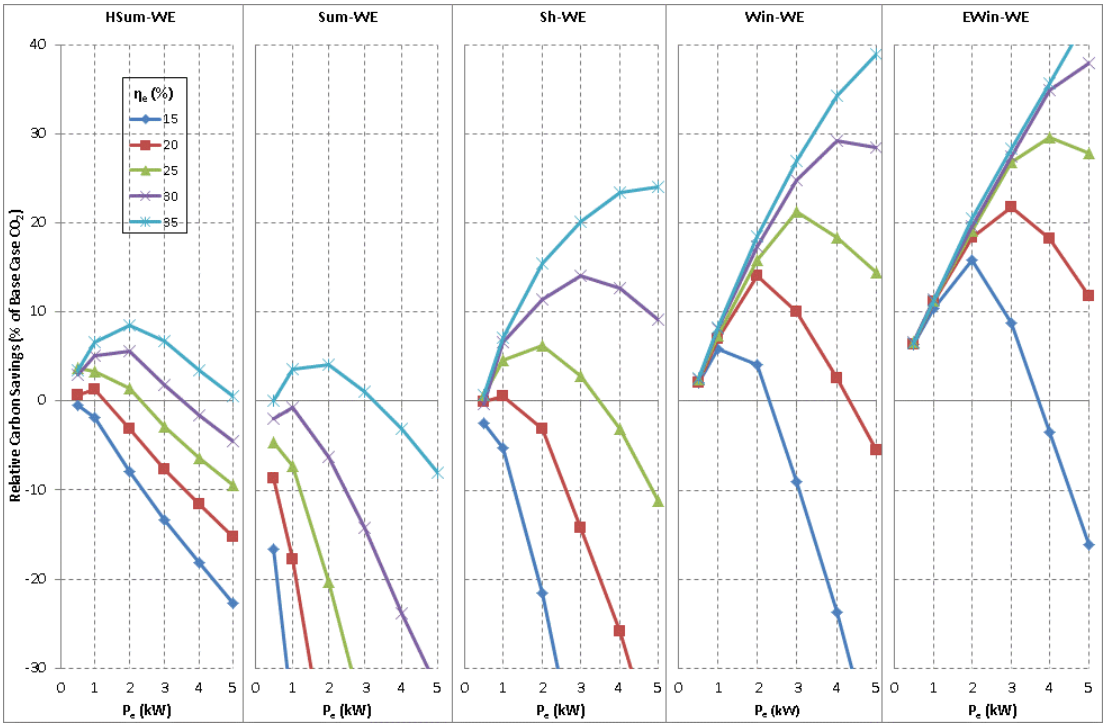

Figure 5.10: RCS for design variant, for Weekend Primary Demand Scenarios, for SE µCHP system with CsO-DDP operating regime

The RCS for all design variants of µCHP system operating under the CsO-DDP operating regime, without RSO, are presented in Figure 5.11. When compared to the results for the TLF operating regime in Figure 4.3, it is clear that the RCS for all design variants have decreased. Using this operating regime, only 3 design variants have significant RCS, compared to 8 with the other operating regimes, as is the case for RSO modes.

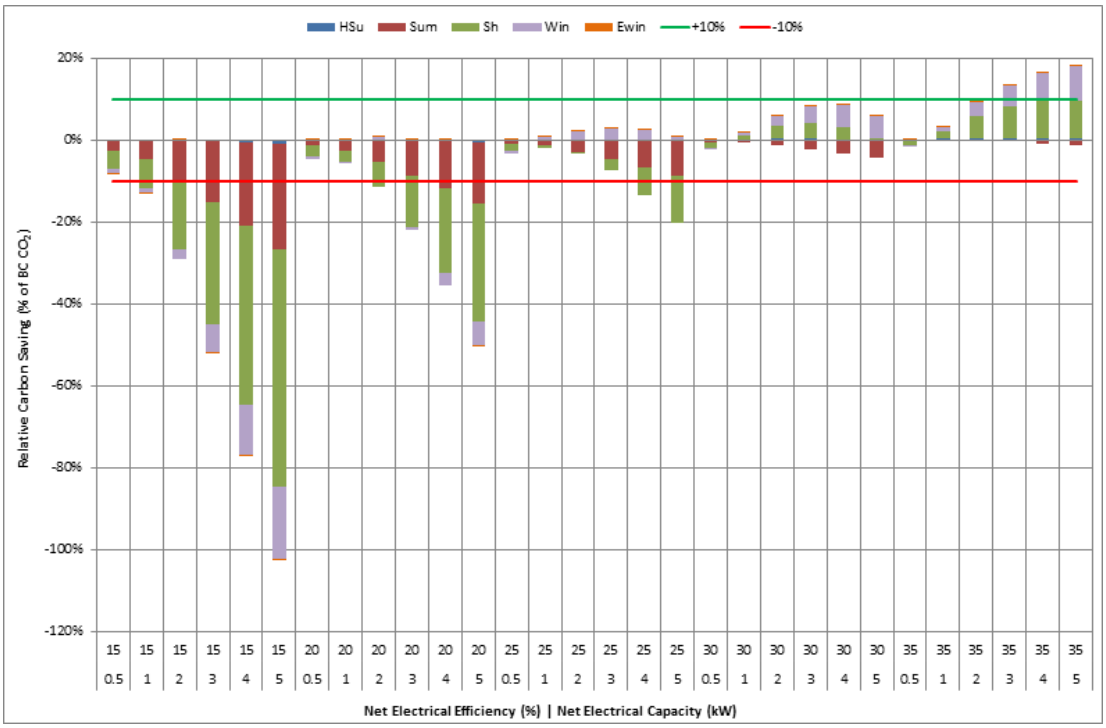

Figure 5.11: RCS for SE µCHP design variants with 30% & 35% η_e with 'Continuous Operation for Daily Demand Period', operating regime without RSO

5.2.6 Continuous Operation over 24 hours (CsO-24hr)

An operating regime was devised to be compatible with prime movers with lifetimes limited to several tens or hundreds of thermal cycles. In the Continuous Operation over 24 hours (CsO-24hr) regime, the prime mover can modulate to follow thermal demand, but cannot switch off throughout its annual operating schedule. This operating schedule is determined by the mode of RSO, the requirements for maintenance, and sustained building vacancies (i.e. holidays) where the user switches the µCHP system off. The resulting frequency of thermal cycling is the order of 1-5 cycles per annum, and with the anticipated RSO of No-Summer, the annual operating duration would be 5,958 hours.

The limited set of simulation results presented in Figure 5.12 and Figure 5.13 prove that such operating regimes are not suitable for prime movers with low η_e, due to high levels of thermal dumping. The auxiliary Thermal Generation Displacement from 35% η_e design variants is sufficient to provide RCSs, so long as the prime mover thermal efficiency is sufficiently high. As shown in Table 2.11, design variants with low P_e have a relatively wide margin between net and gross electrical efficiencies, hence reducing thermal efficiencies (versus design variants with high P_e) significantly.

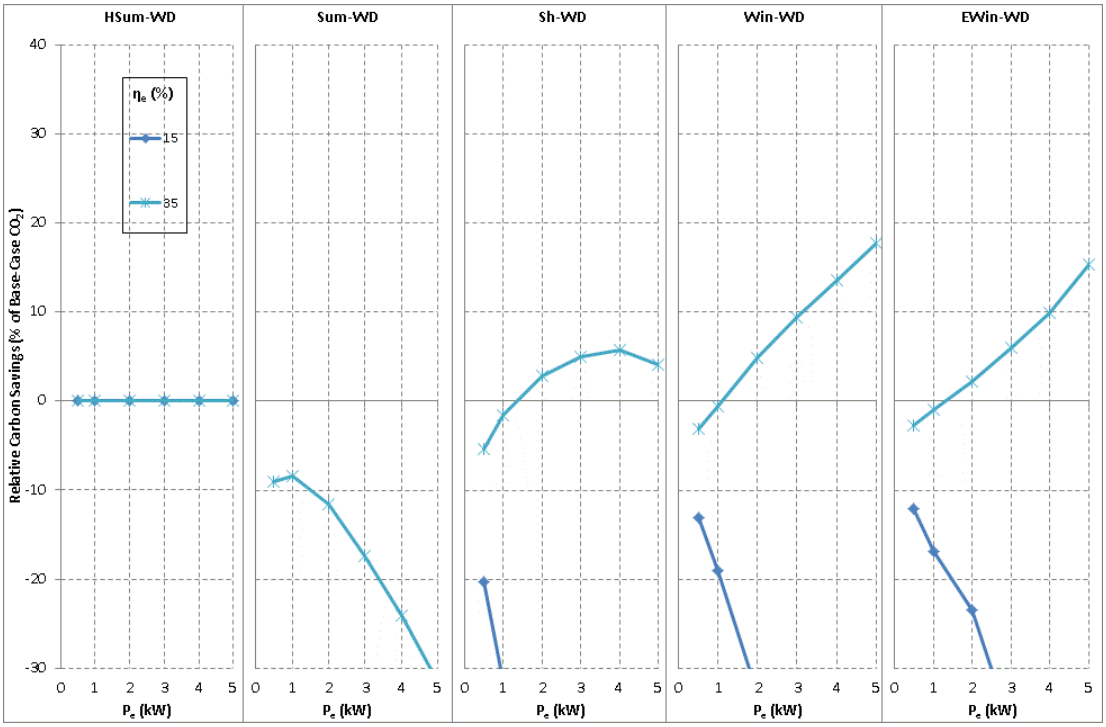

Figure 5.12: RCS or each design variant, during Weekday Primary Demand Scenarios, for SE µCHP system with CsO-24hr operating regime

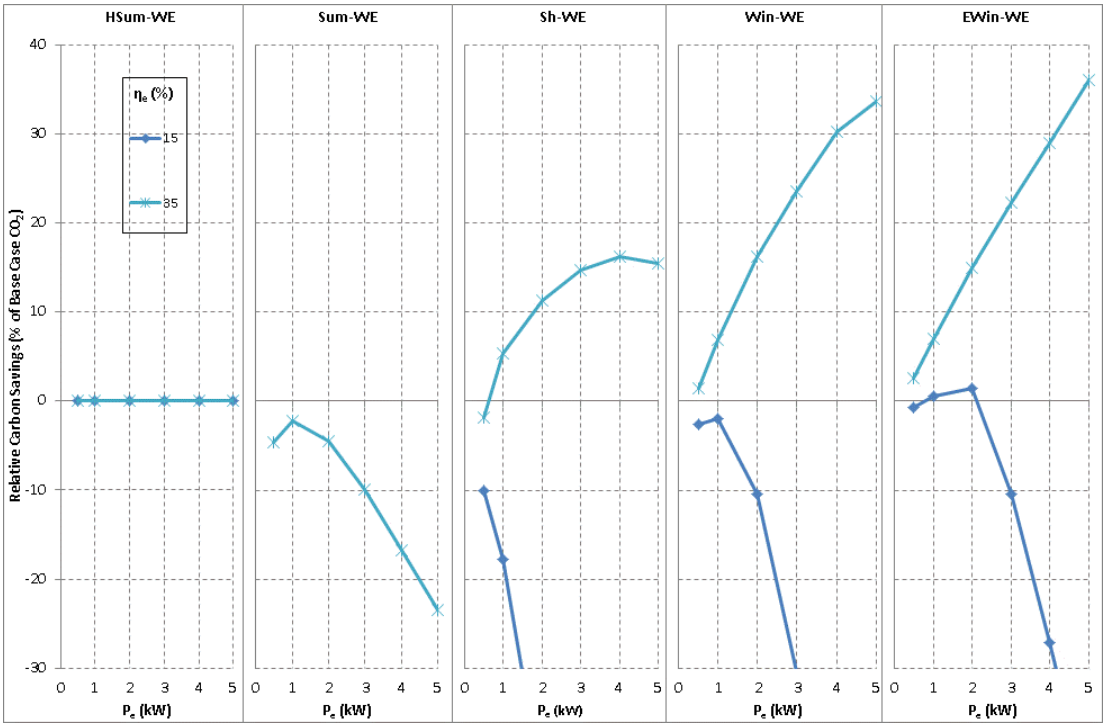

Figure 5.13: RCS or each design variant, during Weekend Primary Demand Scenarios, for SE µCHP system with CsO-24hr operating regime

The RCS for the 35% and 15% η_e design variants of µCHP system operating under the CsO-24hr operating regime, without RSO, are presented in Figure 5.14. When compared to the results for the TLF operating regime in Figure 4.3, it is clear that no design variants of the SE µCHP system have significant RCS. It is only once RSO-NoSummer is applied that significant RCS results are found, for the 4kW_e-35% and 5kW_e-35% design variants.

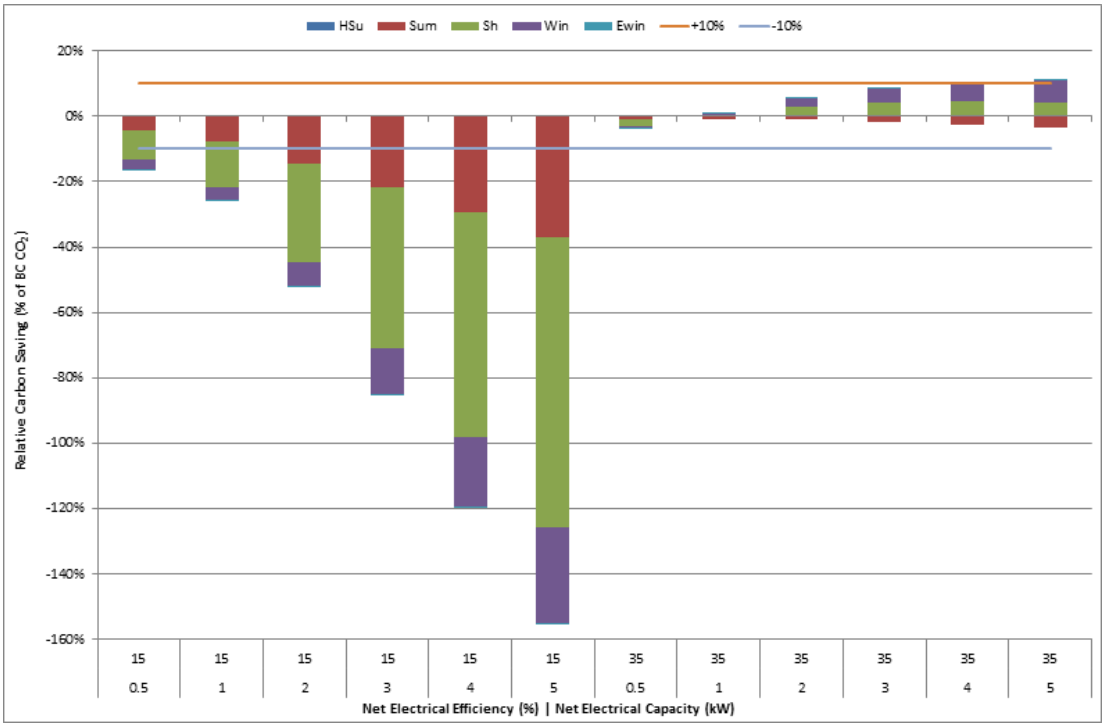

Figure 5.14: RCS for the 15% and 35% η_e SE µCHP design variants, with 'Continuous Operation for Daily Demand Period' operating regime without RSO

5.2.7 Constant Operation (CtO)

The 'Constant Operation' operating regime requires that the prime mover operate at 100% output throughout the year, unless constrained by RSO. However, the poor RCS results presented in Section 5.2.6 for a similar regime (CsO-24hr) wherein the primer move is allowed to modulate indicate that such an operating regime would not provide significant RCS for the scenarios and design variants under investigation. With the η_e and heat-to-power ratios of the design variants investigated in this thesis, even a 0.5kW$_e$ prime mover, which would generate less electricity than daily dwelling demand, would fail to provide RCS.

A significantly different thermal demand may allow such an operating regime to deliver significant RCS, but a suitable thermal storage system would be required to match constant output with varying load. If an alternative low-carbon fuel was used, a concept explored in Section 6.4.1, perhaps such an operating system would be feasible. This links with the concept of effective CI of µCHP-generated electricity, as discussed in Section 5.2.2. Considering the requirements for utilisation of thermal

output in Table 5.1, this operating regime may deliver significant RCS for prime movers with increased η_e, and/or when CI_{grid} is much higher (a concept explored in Section 6.4.2).

5.2.8 Comparing Operating Regimes

Selected µCHP design variants for the alternative operating regimes that reported significant RCS, without RSO, are compared in Figure 5.15. As discussed in Section 5.2.4, RCS have increased for 7 out of the 8 top performing design variants by switching to the 'Continuous Operation for Thermal Demand Period' operating regime.

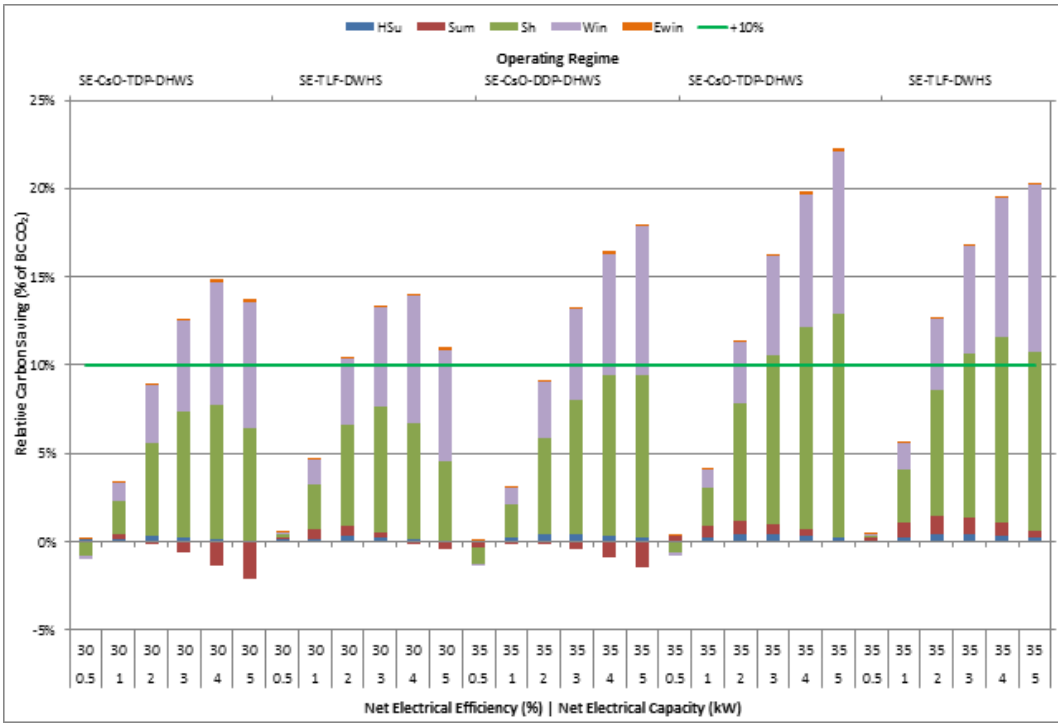

Figure 5.15: Annual RCS for selected SE µCHP design variants, operating under Thermal Load Following (TLF), Continuous Operation during Thermal Demand Periods (CsO-TDP), or Continuous Operation throughout Daily Demand Period (CsO-DDP) operating regimes, where the contribution from each climate is indicated, along with assumed significance limit

As discussed in the relevant sections for each alternative operating regime, the annual frequency of thermal cycling has reduced dramatically for the alternative regimes presented in Figure 5.16.

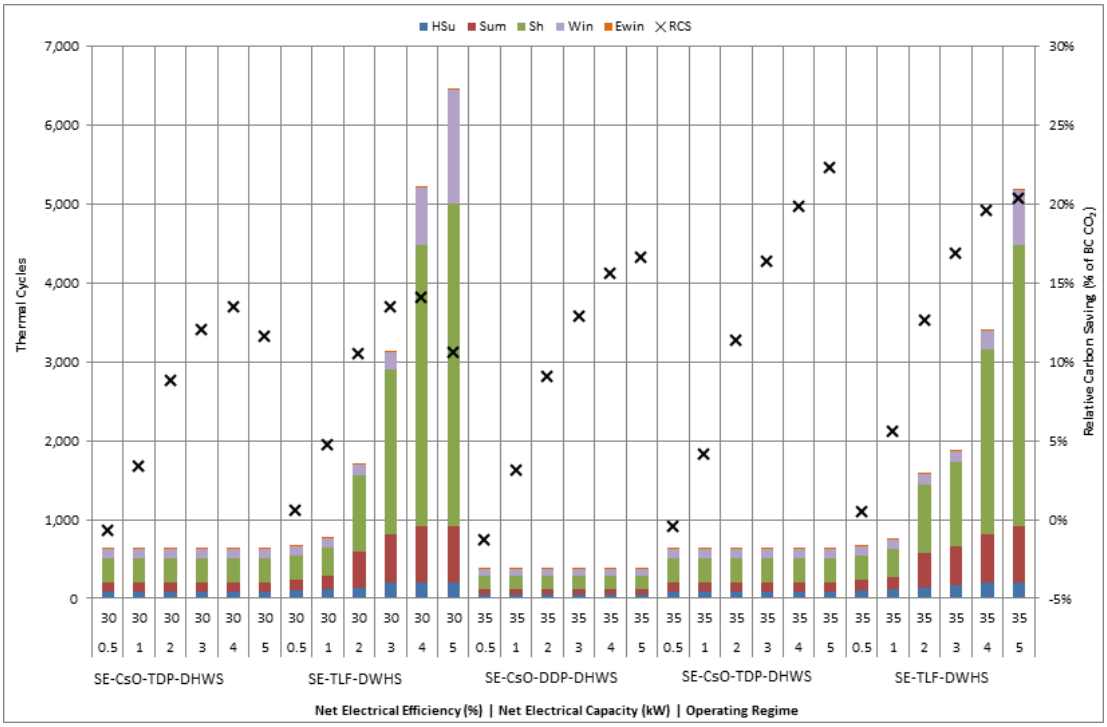

Figure 5.16: Annual Frequency of Thermal Cycling and RCS for selected SE µCHP design variants, operating under Thermal Load Following (TLF), Continuous Operation during Thermal Demand Periods (CsO-TDP), or Continuous Operation throughout Daily Demand Period (CsO-DDP) operating regimes, where the contribution from each climate is indicated, along with assumed significance limit

The impact of operating regimes on thermal cycling is compared in Figure 5.17 with the associated RCS for the 35% η_e design variants with highest RCS. The difference in both thermal cycling and RCS between CsO-24hr and all other operating regimes is readily apparent. The results also suggest that environmental performance of 4kW_e-5kW_e 35% η_e design variants is improved by switching operating regimes from TLF to CsO-TDP, unlike variants with small electrical capacities.

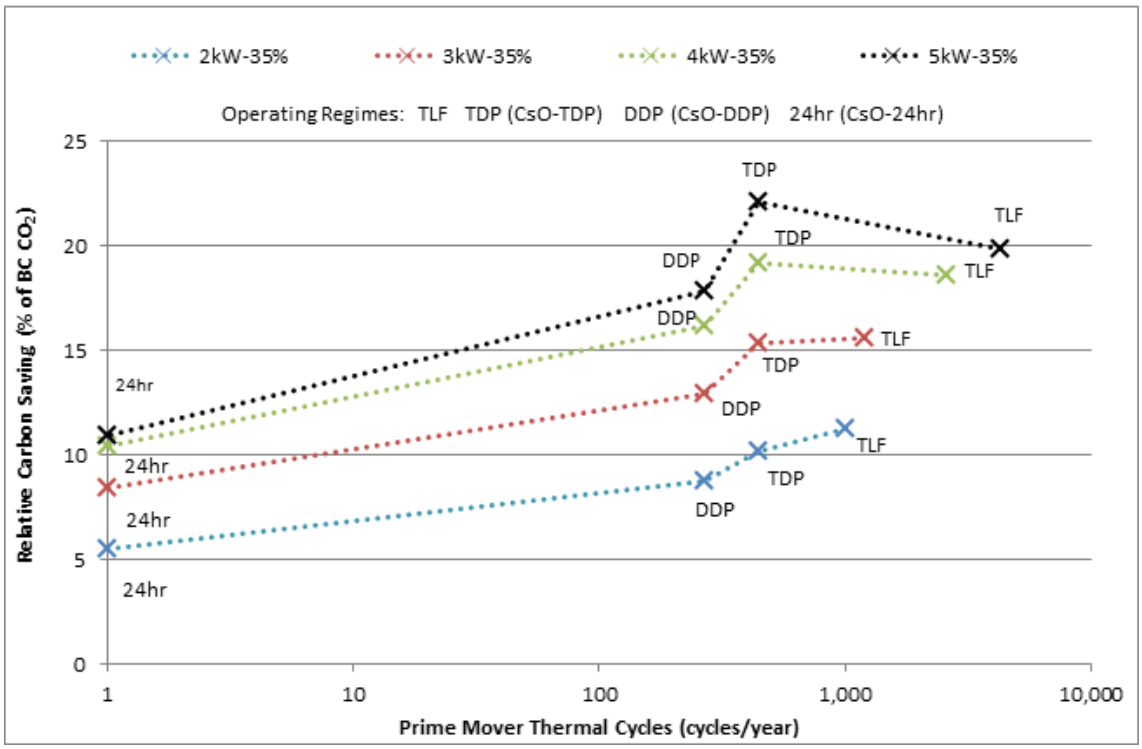

Figure 5.17: RCS vs. annual frequency of thermal cycling, for SE µCHP design varaints with η_e= 35% and P_e=2-5kW_e, comparing between operating regimes

The RCS results for the top performing 35% η_e design variants under TLF, CsO-TDP, CsO-DDP and CsO-24hr operating regimes are plotted in Figure 5.18 versus cumulative annual operating duration. For 2kW_e and 3kW_e design variants, moving from the TLF to CsO-TDP regime, a small decrease in operating duration is achievable with small and marginal RCS penalties, respectively. For the 4kW_e design variant, a marginal decrease in duration and a marginal increase in RCS result from such a change in operating regime. For the 5kW_e design variant, there is a small increase in both operating duration and RCS. For all design variants, applying CsO-DDP and CsO-24hr result in a significant increase in operation duration and decrease in RCS.

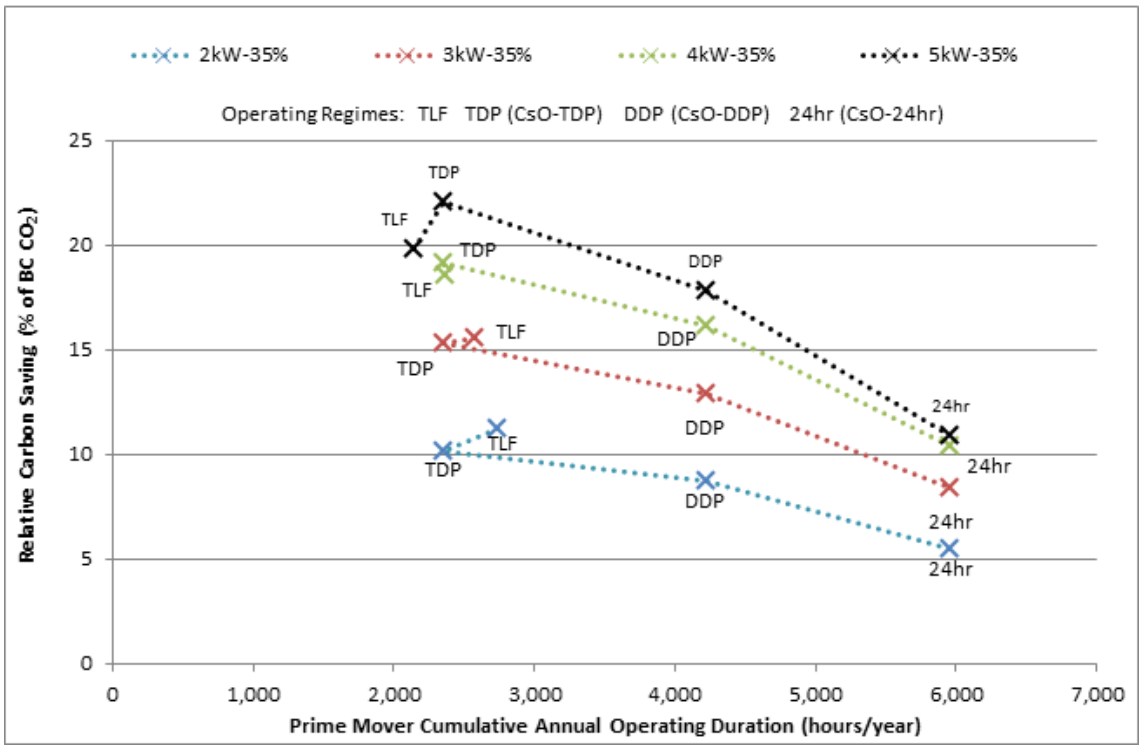

Figure 5.18: RCS vs. cumulative annual operating duration, for SE µCHP design varaints with η_e= 35% and P_e=2-5kW_e, comparing between operating regimes

5.3 Combining Operating Regimes

5.3.1 Seasonal Combination of Operating Regimes

In the investigation of operating regimes presented thus far, the concept of restricted seasonal operation has been explored. It may be feasible to implement an external control signal (such as current or previous day or week's average external air temperature) to select an operating regime for the prime mover. This approach is already widely used, especially in commercial buildings, for space heating and boiler controls such as weather compensation and optimised start controls. In the former, the flow temperature in space heating circuits is reduced in response to higher external air temperatures, in order to reduce cycling of the boiler. Optimised start controls determine when to start the boiler to achieve a set-point temperature by the start of the TDP using the external air temperature are the learned response of the building's internal temperature to heat input.

Such a seasonal combination of operating regimes could be used maximise RCS or lifetime, or achieve a suitable trade-off between these performance metrics, as investigated in the following sub-sections.

5.3.2 Effect on Carbon Savings

RCS, for selected design variants, with several combined operating regimes are presented in Figure 5.19. The operating regime which resulted in maximum RCS was dynamically selected during each climate scenario (i.e. the same regime was applied to weekday and weekend occupancy patterns) for each design variant with η_e >=30%.

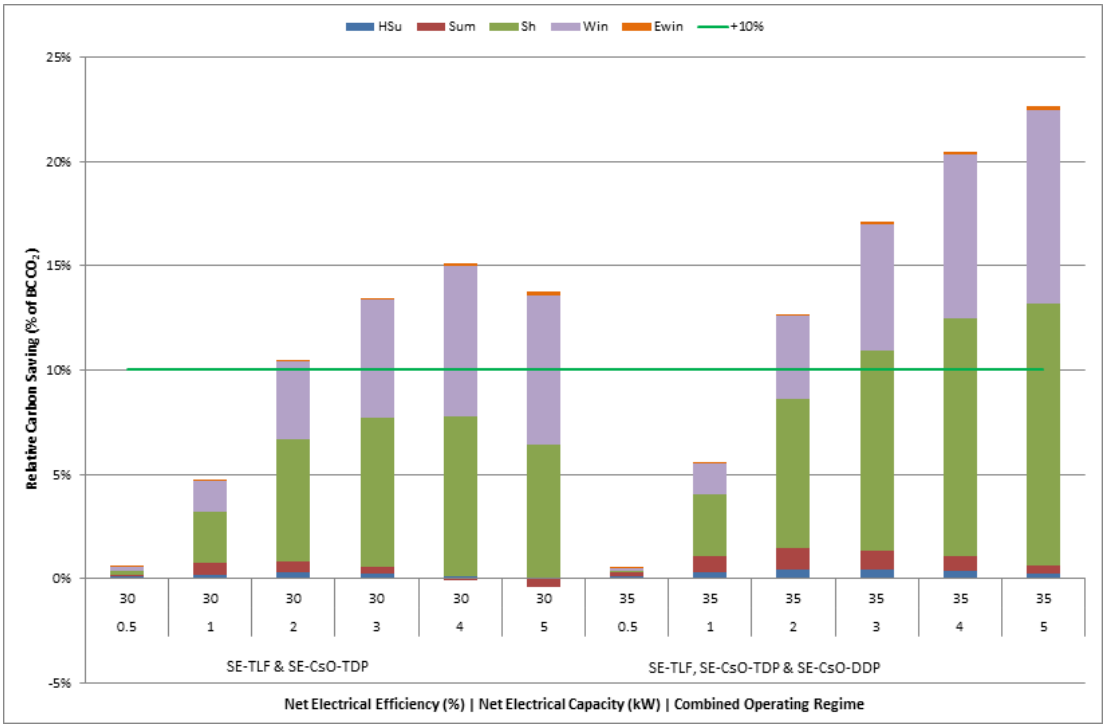

Figure 5.19: RCS results for selected SE µCHP design variants with seasonal combinations of operating regimes incorporating Thermal Load Following (TLF), Continuous Operation during Thermal Demand Periods (CsO-TDP), or Continuous Operation throughout Daily Demand Period (CsO-DDP)

The RCS of 30% η_e design variants under TLF, CsO-TDP and the corresponding combined operating regime are presented in Figure 5.20. The TLF operating regime achieves maximum RCS for design variants with P_e <3kW_e, although the improvements in RCS are very small.

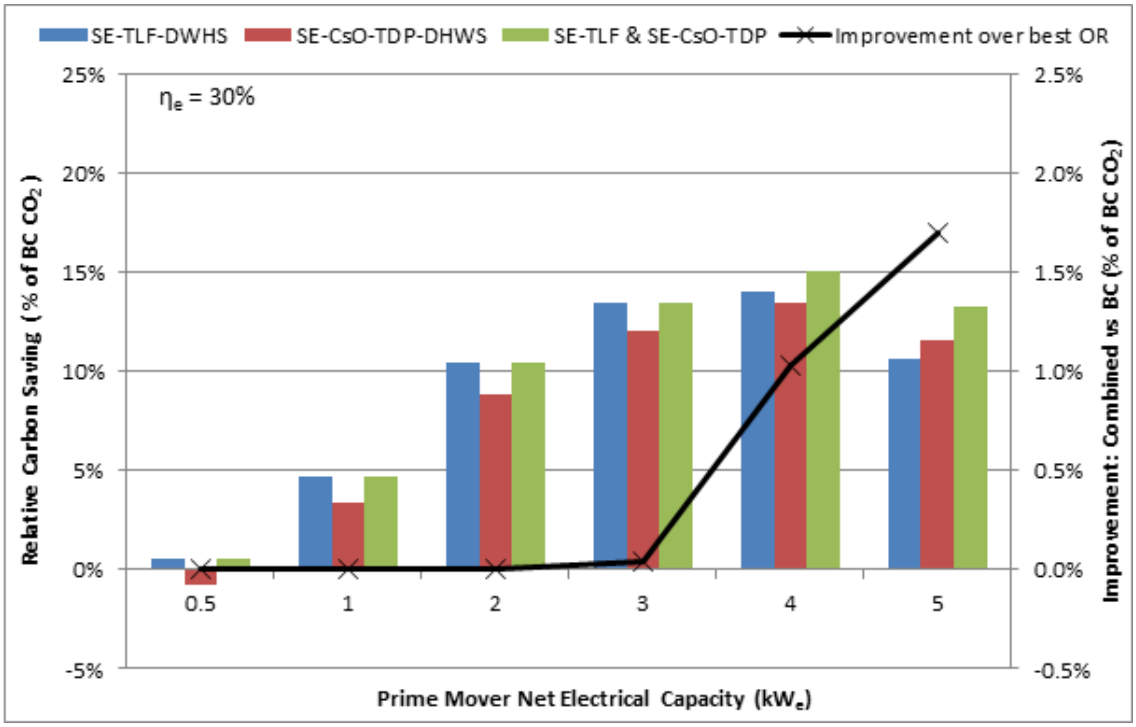

Figure 5.20: RCS, and improvement of combined operating regime over the best performing operating regime for that design variant, vs. prime mover rated P_e, for SE µCHP design variants with η_e=30%, operating under Thermal Load Following (TLF), Continuous Operation during Thermal Demand Periods (CsO-TDP), and combined operating regime

The RCS of 35% η_e design variants under TLF, CsO-TDP, CsO-DDP and the corresponding combined operating regime are presented in Figure 5.21. The TLF operating regime achieves maximum RCS for all design variants, however the improvements are marginal or all variants, especially with P_e <3kW_e.

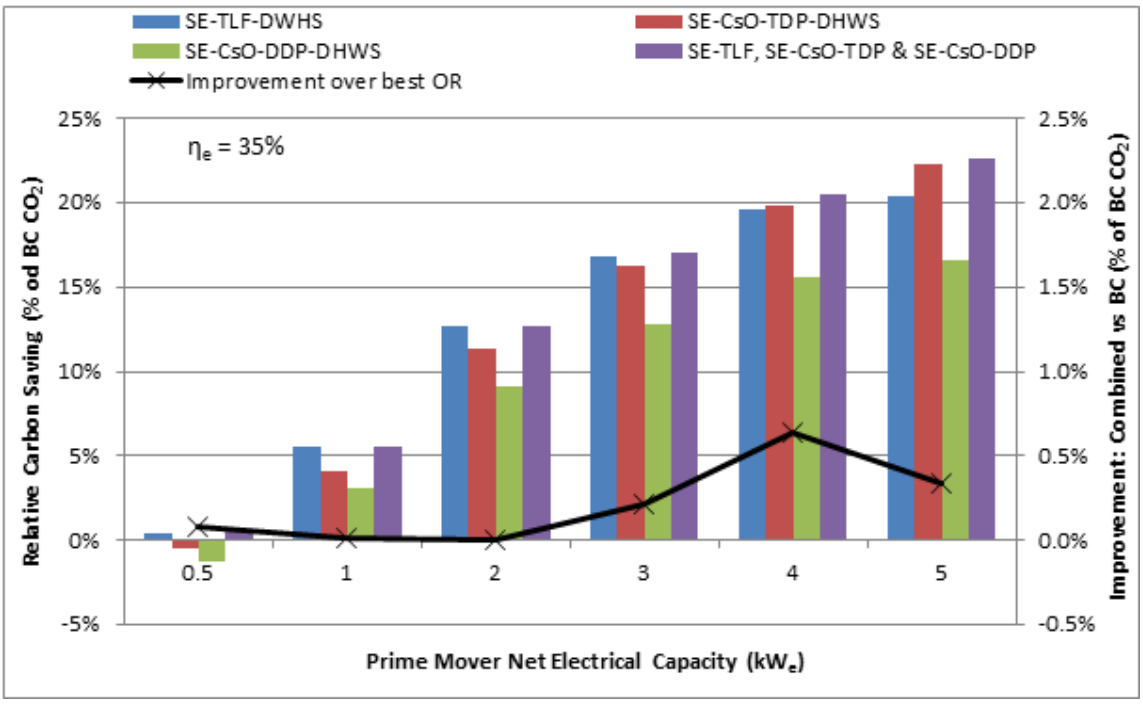

Figure 5.21: RCS, and improvement of combined operating regime over the best performing operating regime for that design variant, vs. prime mover rated P_e, for SE µCHP design variants with η_e=35%, operating under Thermal Load Following (TLF), Continuous Operation during Thermal Demand Periods (CsO-TDP), Continuous Operation throughout Daily Demand Period (CsO-DDP), and combined operating regime

5.3.3 Effect on Thermal Cycles

The annual frequency of thermal cycling, for selected design variants, with several combined operating regimes are presented in Figure 5.22, with the seasonal combination of operating regimes presented in Figure 5.20 and Figure 5.21.

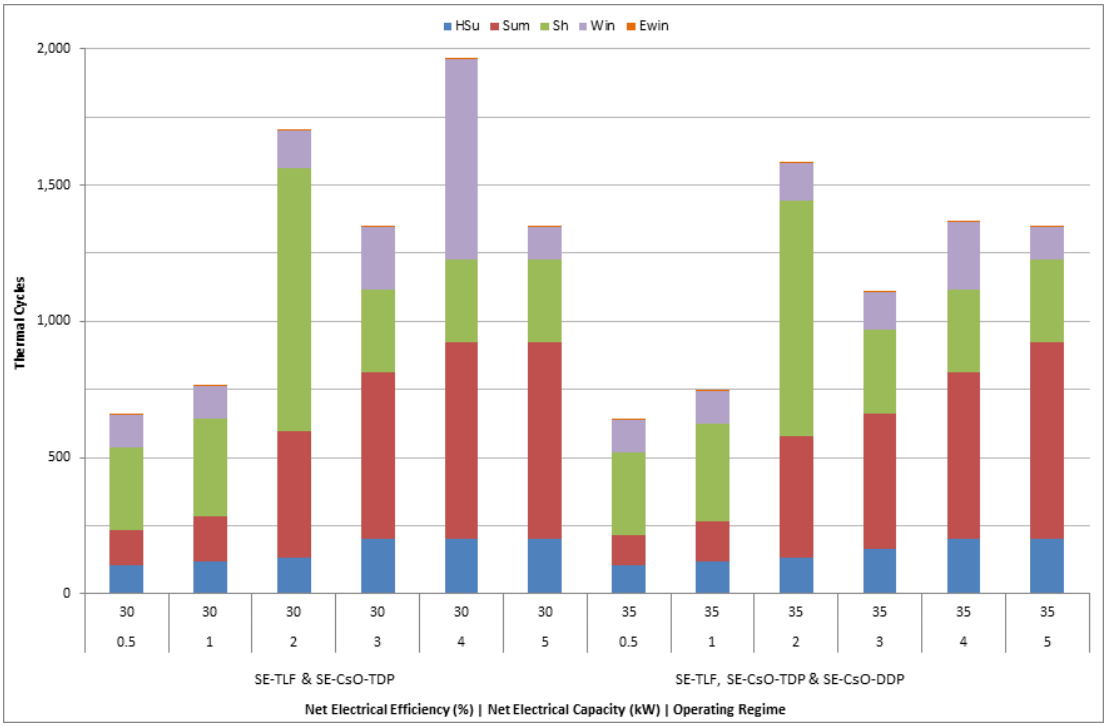

Figure 5.22: Annual frequency of thermal cycling for SE µCHP design variants with η_e=30% & 35%, with combined operating regimes incorporating Thermal Load Following (TLF), Continuous Operation during Thermal Demand Periods (CsO-TDP) and Continuous Operation throughout Daily Demand Period (CsO-DDP)

The optimised seasonal combination presented in Figure 5.23 provides less frequent thermal cycling for a minimal reduction in RCS. However, some attention would need to be paid to the process for defining combined operating regimes, to ensure that an acceptable trade-off between increased carbon saving and reduced thermal cycling is maintained.

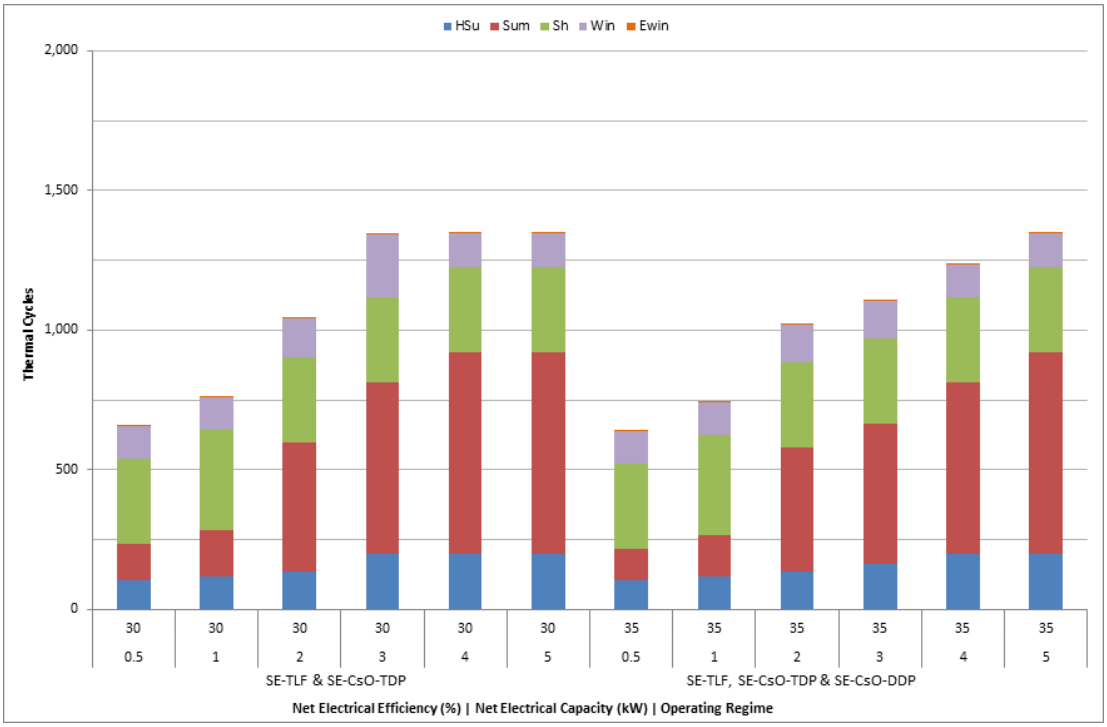

Figure 5.23: Annual frequency of thermal cycling for SE µCHP design variants with η_e=30% & 35%, with optimised (to reduce thermal cycling) combined operating regimes incorporating Thermal Load Following (TLF), Continuous Operation during Thermal Demand Periods (CsO-TDP) and Continuous Operation throughout Daily Demand Period (CsO-DDP)

The annual frequency of thermal cycling of 30% η_e design variants under TLF, CsO-TDP and the corresponding combined operating regime are presented in Figure 5.24, along with RCS for each operating regime. The reduction in thermal cycling frequency for the combined operating regime versus the TLF operating regime, indicated by the line series, is substantial for design variants with P_e>2kW_e. This would increase lifetime of up to a factor of 5. The RCS is marginally increased for those design variants if the combined operating regime is implemented.

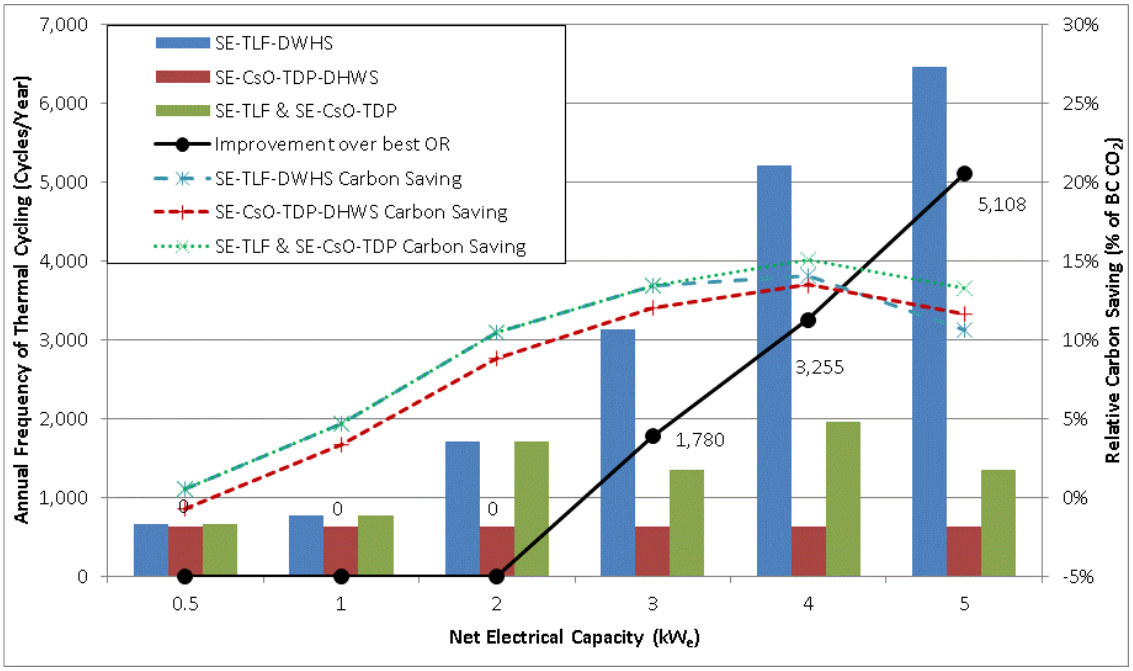

Figure 5.24: Annual frequency of thermal cycling and RCS vs. rated P_e, for SE µCHP design variants with η_e=30%, operating under Thermal Load Following (TLF), Continuous Operation during Thermal Demand Periods (CsO-TDP), and combined operating regime, indicating the reduction in thermal cycling between TLF and combined operating regime

The annual frequency of thermal cycling of 35% η_e design variants under TLF, CsO-TDP, CsO-DDP and the corresponding combined operating regime are presented in Figure 5.25, along with RCS for each operating regime. The reduction in thermal cycling frequency for the combined operating regime versus the TLF operating regime is again substantial for design variants with P_e>2kW_e. This would increase lifetime of up to a factor of 5. The RCS is marginally increased for the 3kW_e and 4kW_e design variants, and significantly increased for the 5kW_e design variant, if the combined operating regime is implemented.

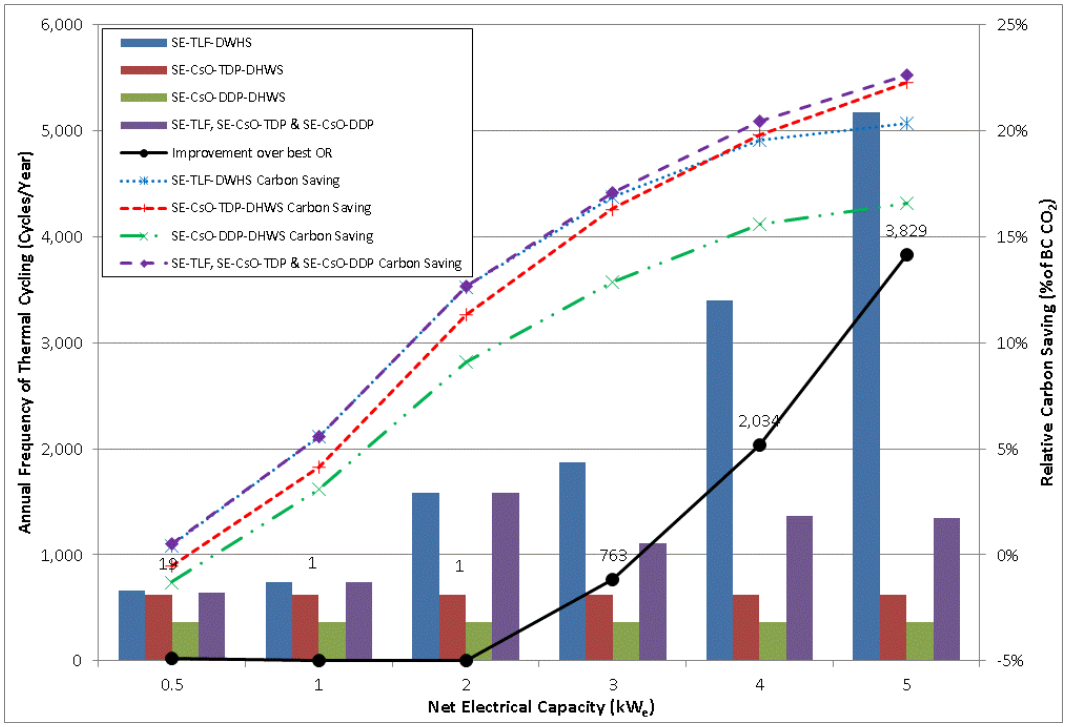

Figure 5.25: Annual frequency of thermal cycling and RCS vs. rated P_e, for SE µCHP design variants with η_e=35%, operating under Thermal Load Following (TLF), Continuous Operation during Thermal Demand Periods (CsO-TDP), Continuous Operation throughout Daily Demand Period (CsO-DDP), and combined operating regime, indicating the reduction in thermal cycling between TLF and combined operating regime

5.3.4 Effect on Load Duration

The annual cumulative operating durations of 30% η_e design variants under TLF, CsO-TDP and the corresponding combined operating regime are presented in Figure 5.25, along with RCS for each operating regime. The dynamically-combined operating regime differentiates from TLF for design variants with P_e>1kW_e, resulting in increasing operating duration (versus TLF) as P_e increases. This would likely decrease operating duration-driven lifetime by a marginal amount for engine-based prime movers.

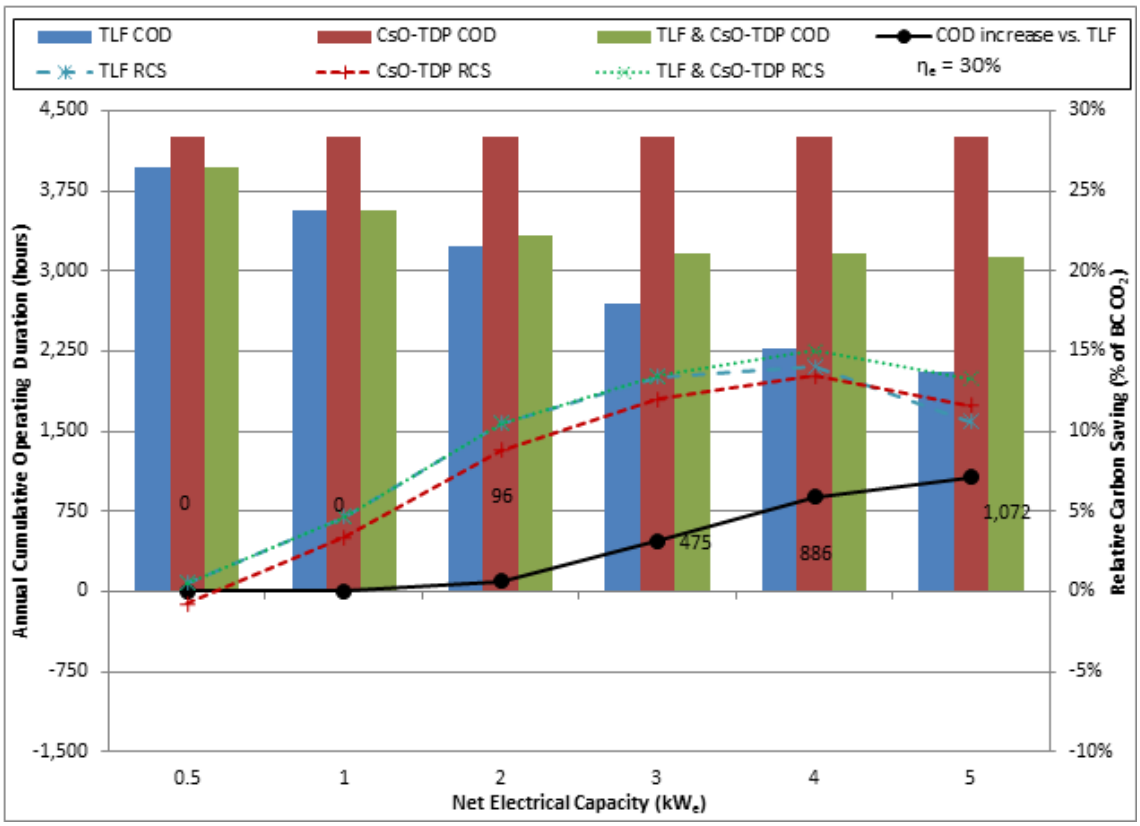

Figure 5.26: Annual cumulative operating duration and RCS vs. rated P_e, for SE µCHP design variants with η_e=30%, operating under Thermal Load Following (TLF), Continuous Operation during Thermal Demand Periods (CsO-TDP) and combined operating regime, indicating the increase in operating duration between TLF and combined operating regime

The annual cumulative operating durations of 35% η_e design variants under TLF, CsO-TDP and the corresponding combined operating regime are presented in Figure 5.27, along with RCS for each operating regime. The dynamically-combined operating regime differentiates from TLF for all design variants, resulting in increasing operating duration (versus TLF) as P_e increases above 1kW_e or when P_e=0.5kW_e. This would likely decrease operating duration-driven lifetime by a marginal amount for engine-based prime movers.

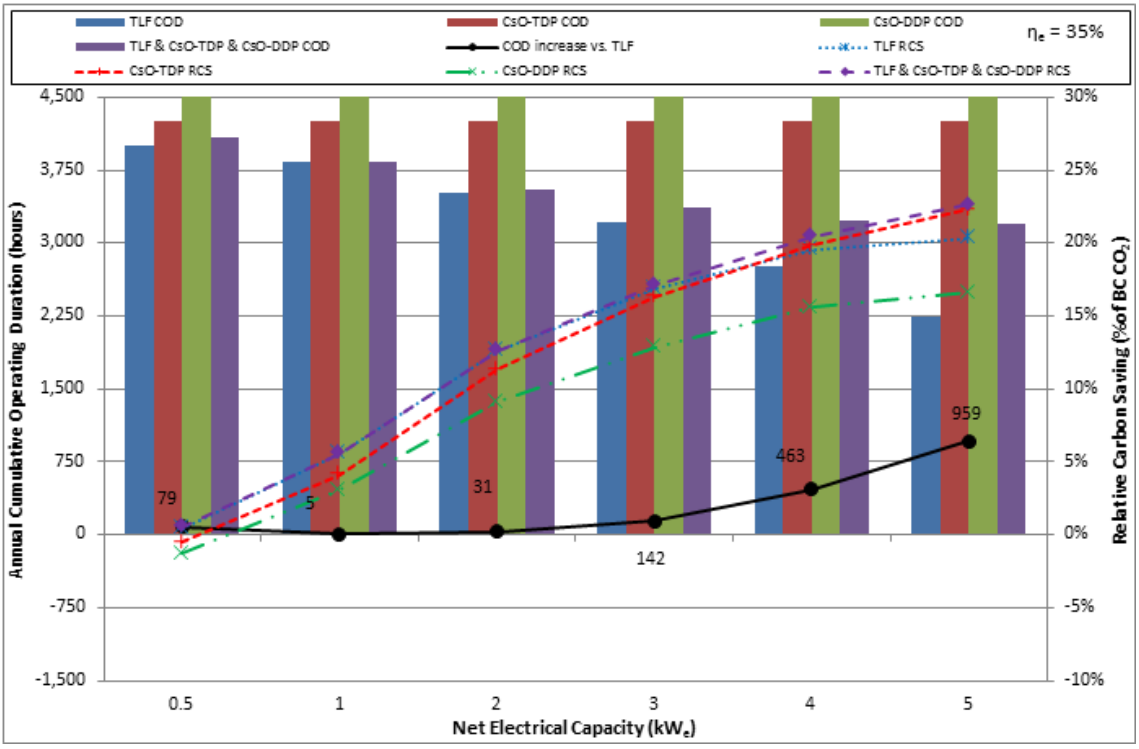

Figure 5.27: Annual cumulative operating duration and RCS vs. rated P_e, for SE µCHP design variants with η_e=35%, operating under Thermal Load Following (TLF), Continuous Operation during Thermal Demand Periods (CsO-TDP), Continuous Operation throughout Daily Demand Period (CsO-DDP) and combined operating regime, indicating the increase in operating duration between TLF and combined operating regime

5.4 Discussion & Conclusions

In this chapter, simulation results and analysis of the transient operation of µCHP systems under various alternative operating regimes were presented and discussed. The concept of carbon intensities of µCHP-generated electricity was discussed in Section 5.2.2, and the consequences of thermal dumping were discussed in Section 5.2.3. Furthermore, the concept of dynamically-combining operating regimes, based on season (i.e. primary demand scenario) was investigated. Whilst initial investigations concluded that these alternative operating regimes would result in reduced relative carbon savings (or increased relative carbon penalties), the effect on thermal cycling frequency and cumulative operating regimes was quantified.

Changing the TLF SE μCHP concept system reported in Chapter 4 to utilise the Continuous Operation for Thermal Demand Period (CsO-TDP) operating regime results in annual increases in RCS for 7 top-performing design variants. All other design variants report decreased RCS. This can be understood with reference to results for each design day, where the RCS have increased for demand scenarios for high thermal demand, and decreased for those with low thermal demand. This is due to thermal dumping during design days with low thermal demand.

With CsO-TDP, the annual frequency of thermal cycling drops to 626, 537 and 436 cycles/annum, respectively, for None, No-HSum and No-Summer RSO conditions. Cumulative annual operation with the CsO-TDP operating regime was 4,250, 3,645 and 2,891 hours, respectively, with None, No-HSum and No-Summer RSO. Whilst this results in increased annual operating durations for the majority of design variants, especially without No-Summer RSO, lifetime due to cumulative operation (based on a limitation of 20,000-40,000 hours), should be similar to that due to thermal cycling.

Annual results for the Continuous Operation for Daily Demand Period (CsO-DDP) operating regime report decreased RCS (versus TLF) for all design variants. Indeed, only 3 top-performing design variants retain significant annual RCS. Annual thermal cycling frequency drops to 365, 313 and 248 cycles/annum, respectively, for None, No-HSum and No-Summer RSO conditions. Cumulative annual operation with the CsO-TDP operating regime increased significantly to 6,205, 5,321 and 4,220 hours, respectively, with None, No-HSum and No-Summer RSO. Prime movers operating under CsO-DDP would likely be lifetime-limited by cumulative operating duration, as opposed to thermal cycling (based on a limitation of 20,000-40,000 hours and 6,000 cycles).

The Continuous Operation over 24 hours (CsO-24hr) operating regime was conceived for prime mover technologies that could tolerate 10’s or hundreds of thermal cycles before replacement. With the anticipated RSO of No-Summer, the annual operating duration would be 5,958 hours, where annual thermal cycling would result from maintenance or sustained building vacancies. The operating regime results in decreased RCS, such that no design variants have significant RCS. Once RSO-

NoSummer is applied, significant RCS results are reported for the 4kWe-35% and 5kWe-35% design variants.

A Constant Operation (CtO) operating regime was defined, with thermal cycling and cumulative operating durations like CsO-24hr, but without the efficiency penalty of part-loading. However, initial calculations identified that even low P_e design variants would result in excessive thermal dumping, due to the ηe and heat-to-power ratios of the design variants investigated. In order to achieve an effective CI of μCHP-generated electricity (as discussed in Section 5.2.2) lower than CI_{grid}, either prime movers with increased η_e or higher CI_{grid} would be required.

Much of the comparative analysis of operating regimes was confined to the design variants with 30% and 35% η_e, as the remaining design variants exhibited insignificant RCS or carbon penalties.

TLF and CsO-TDP operating regimes were combined, on the basis of season, to maximise RCS for design variants with 30% η_e; and with TLF, CsO-TDP and CsO-DDP for the 35% η_e variants. The combined regimes increase RCS for 30% η_e variants with P_e <3kW$_e$, and for all 35% η_e design variants, although the improvements in RCS are marginal.

Combining regimes to minimise thermal cycling delivers substantial reductions for design variants with P_e>2kW$_e$, resulting in marginally increased RCS for those design variants, and indeed significantly increased RCS for the 35%-5kW$_e$ variant. The cumulative operating duration is increased, for the combined operating regimes versus TLF, for all 30% & 35% variants, except for 30%-0.5kW$_e$, 30%-1kW$_e$ and 35%-1kW$_e$.

5.5 References

[1] H. Apfel, M. Rzepka, H. Tu, U. Stimming, Thermal start-up behaviour and thermal management of SOFC's, Journal of Power Sources, Volume 154, Issue 2, 21 March 2006, Pages 370-378

[2] A. Hawkes, M. Leach, Solid oxide fuel cell systems for residential micro-combined heat and power in the UK: Key economic drivers, Journal of Power Sources, Volume 149, 26 September 2005, Pages 72-83

[3] H.I. Onovwiona, V.I. Ugursal, A.S. Fung, Modeling of internal combustion engine based cogeneration systems for residential applications, Applied Thermal Engineering, Volume 27, Issues 5–6, April 2007, Pages 848-861

[4] A.D. Peacock, M. Newborough, Impact of micro-CHP systems on domestic sector CO2 emissions, Applied Thermal Engineering, Volume 25, Issues 17–18, December 2005, Pages 2653-2676

6 Alternative Scenarios: Demand & Carbon Intensities

6.1 Introduction

This chapter focuses on alternative scenarios that are external to the design of the μCHP system, in order to quantify the impact on relative carbon savings and prime mover lifetime. Changes to cumulative annual thermal demand are studied, in order to further the understanding of μCHP system performance under various demand conditions. Whilst the previously presented studies have addressed the matching of μCHP system design variants with thermal demand, it is important to consider the performance of μCHP in a future context. Systems installed now, or in the near future, may be expected to achieve relative carbon savings despite changes to demand as driven by technological or behavioural factors. The impact of changing carbon intensities of fuel (for μCHP and base-case boiler) and electricity from the NEG is assessed in Section 6.4. Understanding the sensitivity of μCHP-derived relative carbon savings to external factors, such as those carbon intensities, would serve to increase confidence in what is likely to be a long-term financial investment in a μCHP system.

The investigation of μCHP systems presented in Chapters 4 & 5 do not incorporate electrical load following operating regimes, hence the prime mover is controlled in relation to thermal demand only. As this research considers the carbon savings due to electrical import displacement and electrical export to be interchangeable, as discussed in Section 4.3.6, changes to the electrical demand profile will not have a direct effect on system performance and associated carbon savings. It should be noted, however, that as electrical load profiles change, the knock-on changes to casual thermal gains from lights and appliances will have a marginal effect on thermal demand, which in turn will have a marginal effect on carbons savings. However, within the restricted time available for this project, evaluation of μCHP performance under changes to the electrical demand profile was not undertaken.

Alternative electrical demand profiles, with the associated casual gains profiles, were prepared using th BIM-G model and subsequently applied in a published investigation into domestic space cooling requirements within the TARBASE project [1]. Examples of

alternative demand scenarios are listed in Table 6.1, with a short description of the impact on electrical and thermal demand.

Scenario	Description
2030 Electrical Demand Decrease	Proliferation of LED lighting by 2030 reduces Electrical Demand, and associated casual gain
2030 Electrical Demand Increase	Electrical Demand decrease from LED's countered by Consumer Electronics increase, and Drinks Fridge introduction
2030 Electrical Profile change with Base-load Decrease	Replacement of Cyclic Refrigeration with Stirling Coolers, and proliferation of LED's lower electrical base-load, whilst consumer electronics increases result in zero net electrical demand decrease
2030 Building Fabric Improvement	TARBASE interventions on building fabric reduces Thermal Demand
2030 Climate Change	Climate files adjusted using UK CIP algorithms exhibit higher temperatures, hence lowering Thermal Demand
Increasing Comfort Temperature	Increase target Internal Air Temperature, and hence Thermal Demand
Electric Showers	Replacement of DHW Shower with Electric Shower, and the subsequent reduction of thermal demand, and increase in electrical demand

Table 6.1: Examples of Alternative Demand Scenarios

Changes to annual thermal demand were investigated, as reported in Section 6.3, by applying alternative annual weighting factors to the simulation results for the Primary Demand Scenario design days. This study explores the effect of increasing and decreasing thermal demand by 10% and 20%, due to fabric improvement of thermal comfort changes, on the carbon savings and thermal cycling of the μCHP system.

It is acknowledged that significant changes in the magnitude and daily distribution of thermal and electrical demand, as could technically be achieved in households [2], would likely have a significant effect on μCHP performance, as reported elsewhere [3][4]. It is recommended that future research consider the full effect of future technological improvements and appliance ownership on demand profiles, and the result effect on μCHP performance.

6.2 Drivers for Thermal Demand Changes

6.2.1 Summary of Thermal Demand Drivers

Demand drivers that effect thermal demand within the dwelling can loosely be categorised as those that significantly alter the shape of the demand profile, i.e. the distribution of demand across the day or year, and those that broadly offer a percentage reduction across the day or year.

Demand Drivers likely to affect the shape of daily demand profiles:

- Change from boiler-supplied showers to electric showers
- Alternative occupants
- Alternative occupancy patterns
- Alternative thermal demand periods

Demand Drivers likely to affect the distribution of annual demand profiles:

- Alternative occupancy patterns
- Climate Change

Demand Drivers likely to affect the magnitude of demand profile, but not necessarily the generic shape or distribution of demand:

- Building Fabric Improvements
- Change in Building Air-tightness
- Changing Space Heating Set-point Temperatures
- Alternative Location (i.e. Climate)

6.2.2 Electric Showers

It is understood that around 50% of UK dwellings have electric showers [5], although the Primary Demand Scenarios investigated in previous chapters use showers supplied by the thermal store. Switching to electric showers would change the shape of thermal and electrical demand profile within the context of a dwelling with a µCHP system. Non-electrically heated showers result in high thermal extraction rates from the thermal store. The PDS assume shower event durations of 5 minutes, once per day,

which is supported by Jordan & Vajen [6], where all 4 occupants shower within an hour or so on weekday mornings. This can rapidly lower the thermal store's water temperature, especially on winter mornings where the store is already taxed to provide energy for the space heating system. The control system, in this investigation, responds to low storage temperatures by activating the auxiliary boiler alongside the prime mover. In milder climates, the shower DHW load on the thermal store provides an opportunity for the prime mover to operate at full or part load for a sustained period. Shifting to electric showers would eliminate this thermal demand, potentially introducing increased thermal cycles of TLF µCHP systems, and introducing more part-load operation of the prime mover within operating regimes that allow it. Future research could address the effect on µCHP performance due to the change from shower showers supplied by the thermal store to electrical showers.

6.3 Impact of Thermal Demand Changes on Micro-CHP Performance

6.3.1 Changes to magnitude of Annual Demand

In order to estimate annual performance of the µCHP and base-case systems, Primary Demand Scenarios were assigned an annual weighting factor, as presented in Table 3.23. To investigate µCHP systems under different annual demand scenarios, these weighting factors were altered to produce scenarios with a 10% and 20% increase, and a 10% and 20% decrease, in thermal demand. The new and existing weighting factors are presented in Table 6.2.

Thermal Demand		High Summer		Summer		Shoulder		Winter		Extreme Winter	
(kWh)	(%)	WD	WE	WD	WE	WD	WE	WD	WE	WD	WE
22,694	0	10.2%	4.1%	12.7%	5.1%	34.8%	13.9%	13.6%	5.4%	0.2%	0.1%
24,963	+10%	9.2%	3.7%	10.1%	4.1%	31.3%	12.5%	19.5%	7.8%	1.4%	0.5%
27,233	+20%	8.1%	3.3%	8.9%	3.5%	25.4%	10.2%	26.2%	10.5%	2.8%	1.1%
20,425	-10%	14.7%	14.9%	30.9%	10.9%	0.1%	5.9%	6.0%	12.4%	4.3%	0.0%
18,155	-20%	19.3%	7.7%	17.4%	6.9%	26.3%	10.5%	8.4%	3.4%	0.0%	0.0%

Table 6.2: Annual weighting factors, as applied to each PDS, for original, increased and decreased thermal demand scenarios

The annual electrical demand will vary slightly (0.5%-2.2%) with thermal demand, due to the thermal-demand-driven electrical load of the SHDS pumps and boiler parasitic load whilst firing, and the climate-dependent lighting profile. The carbon footprint of the base-case energy system operating under each thermal demand scenario is presented in Table 6.3.

Thermal Demand		Gas		Electricity	
(kWh)	(%)	(kWh)	($kgCO_2$)	(kWh)	($kgCO_2$)
22,694	0	25,752	20,344	4,580	1,970
24,963	+10%	28,328	22,379	4,629	1,990
27,233	+20%	30,903	24,413	4,681	2,013
20,425	-10%	23,177	18,310	4,550	1,957
18,155	-20%	20,602	16,275	4,521	1,944

Table 6.3: Annual energy and CO_2 values calculated for the base-case energy system operating in each thermal demand scenario

The impact of changing thermal demand on RSO was evaluated, as will be discussed in the upcoming sections. As each RSO restricts the prime mover's operation within certain seasons, the annual thermal demand that the prime mover could potentially satisfy is also restricted. For reference, the annual thermal demand calculated for the alternative demand scenarios, under each RSO mode, is presented in Table 6.4.

RSO	Thermal Demand for each RSO (kWh)		
	No RSO	No-HSum	No-Summer
(%)	(kWh)	(kWh)	(kWh)
0	22,694	22,045	19,934
10%	24,963	24,250	21,927
20%	27,233	26,454	23,921
-10%	20,425	19,841	17,941
-20%	18,155	17,636	15,947

Table 6.4: Annual thermal demand for each annual scenario under each RSO mode

Thermal demand decreases of 10% and 20% were selected on the basis of research, published by the author and others as part of the TARBASE project, identifying technological interventions to reduce the carbon footprint of buildings. This research identified many building fabric measures that could easily deliver that magnitude of savings. Alternatively, such savings could be due to reduction in set-point temperatures, or a different demand scenario in terms of building, occupants, or

occupant behaviour. Thermal demand increases of 10% and 20% were defined for consistency of comparison when investigating µCHP performance with changing thermal demand.

6.3.2 Relative Carbon Savings for Thermal Load Following Operation

The effect of annual demand changes on µCHP RCS and thermal cycling was investigated for the SE µCHP system with the TLF operating regime, under each RSO mode. Analysis of the results plotted in Figure 6.1, Figure 6.2 and Figure 6.3 show that with or without RSO, the RCS tends to increase with thermal demand.

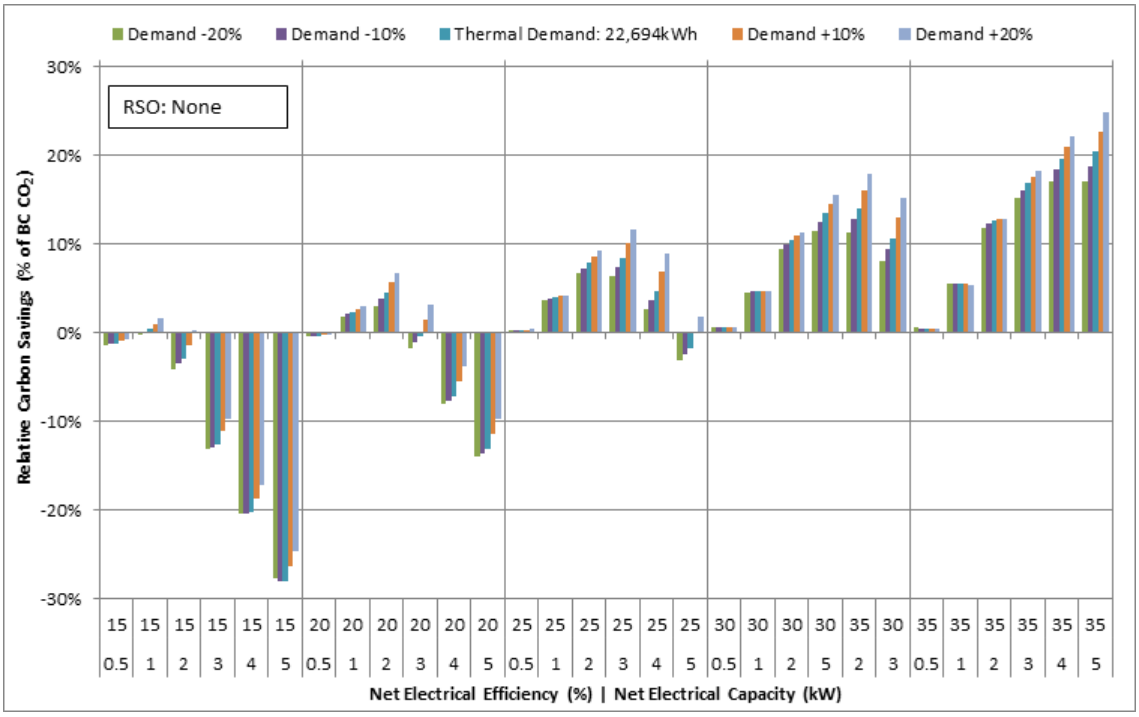

Figure 6.1: RCS for each design variant, operating without RSO, comparing each annual thermal demand scenario

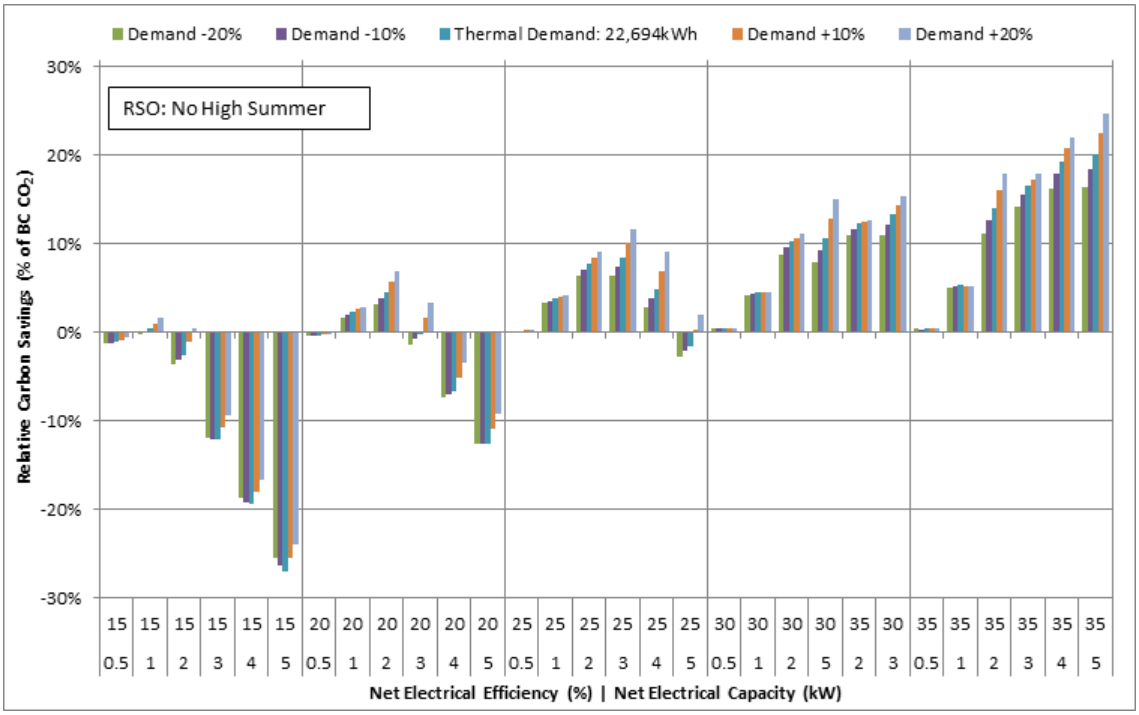

Figure 6.2: RCS for each design variant, operating under RSO-NoHSum, comparing each annual thermal demand scenario

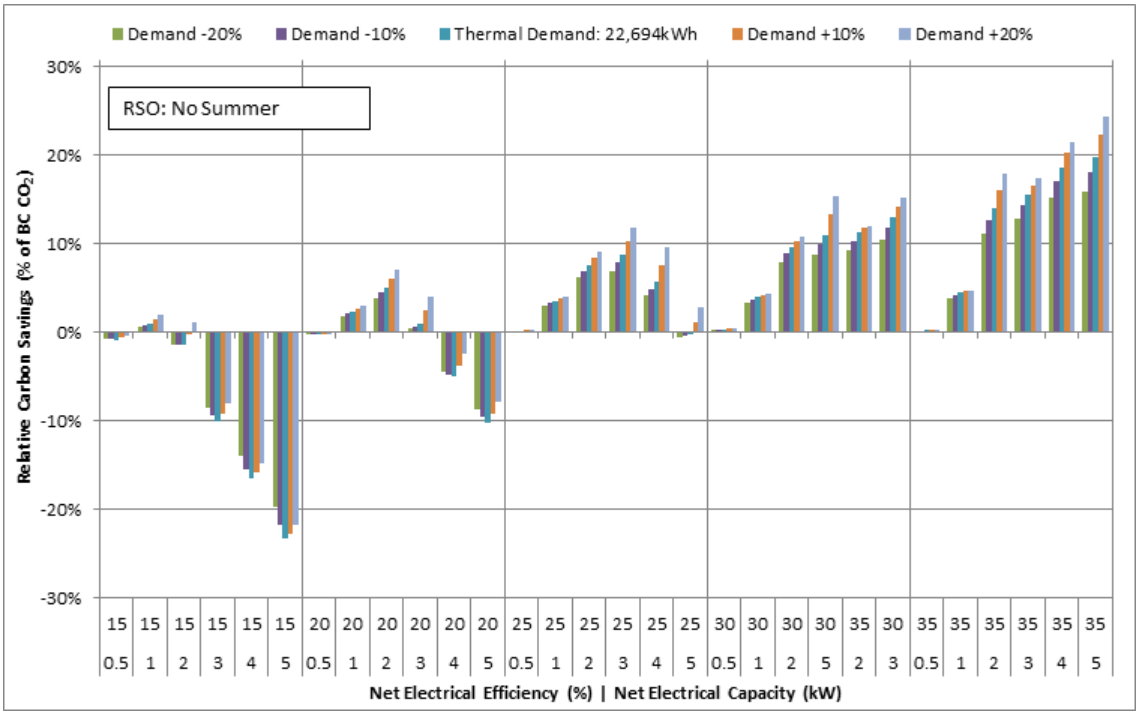

Figure 6.3: RCS for each design variant, operating under RSO-NoSummer, comparing each annual thermal demand scenario

The results in Figure 6.1 to Figure 6.3 suggest that the relationship between annual RCS (from weighted PDS results) and annual thermal demand (from weighted PDS

results) is not linear. To evaluate this relationship, a new performance metric was defined: 'Specific Relative Carbon Savings' (% of BC CO_2/MWh_{th}), calculated as RCS per MWh of Annual Thermal Demand. The metric was calculated for the results plotted in Figure 6.1, as presented in Figure 6.4. The value of the Specific RCS metric increases with absolute annual thermal demand for low η_e (15% and 20%) design variants. For the remaining design variants, Specific RCS either increases or decreases with absolute annual thermal demand. It is postulated that this is a simulation artefact due to the determination of new annual weighting factors for Primary Demand Scenarios. For particular design variants, the simulation results for specific PDS may report a RCS that deviates from the expected correlation with daily thermal demand. As the weighting factors are applied to 10 design days (i.e. the PDS), and small deviations in a single PDS are readily magnified by the annual weighting factors. This should be taken into account when considering the marginal RCS results presented in Section 6.3.3.

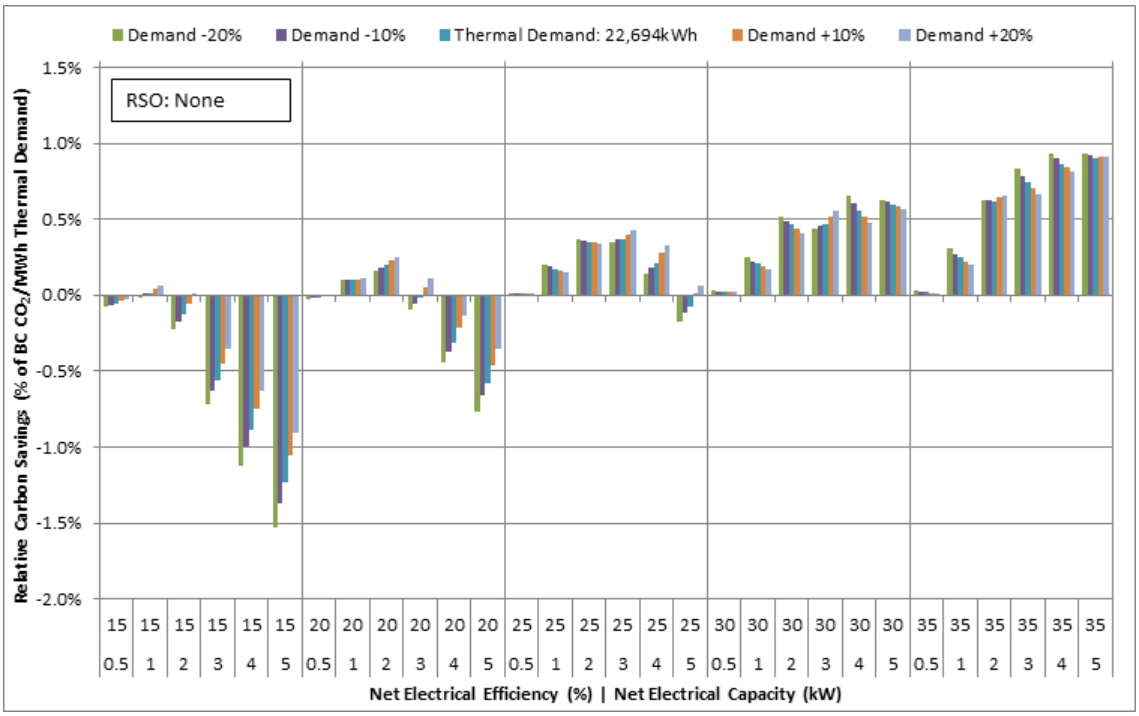

Figure 6.4: Specific RCS (% of BC CO_2/MWh_{th}) for each design variant, operating without RSO, and each annual thermal demand scenario

6.3.3 Marginal effect on Relative Carbon Savings for TLF Operation

The marginal change in relative carbon saving due to changing thermal demand, as a percentage of RCS experienced during the original thermal demand scenario, is plotted

in Figure 6.5. It is interesting to note that a 20% increase in thermal demand can decrease RCS by approximately 4%, in the worst case, and increase RCS by 42%, in the best case. The analysis supports the earlier conclusions drawn in Section 4.3.9, that peak relative carbon saving, as a percentage of base-case carbon footprint, increases with thermal demand. The marginal change in RCS increases with rated electrical (and thermal) output, but decreases with net electrical capacity.

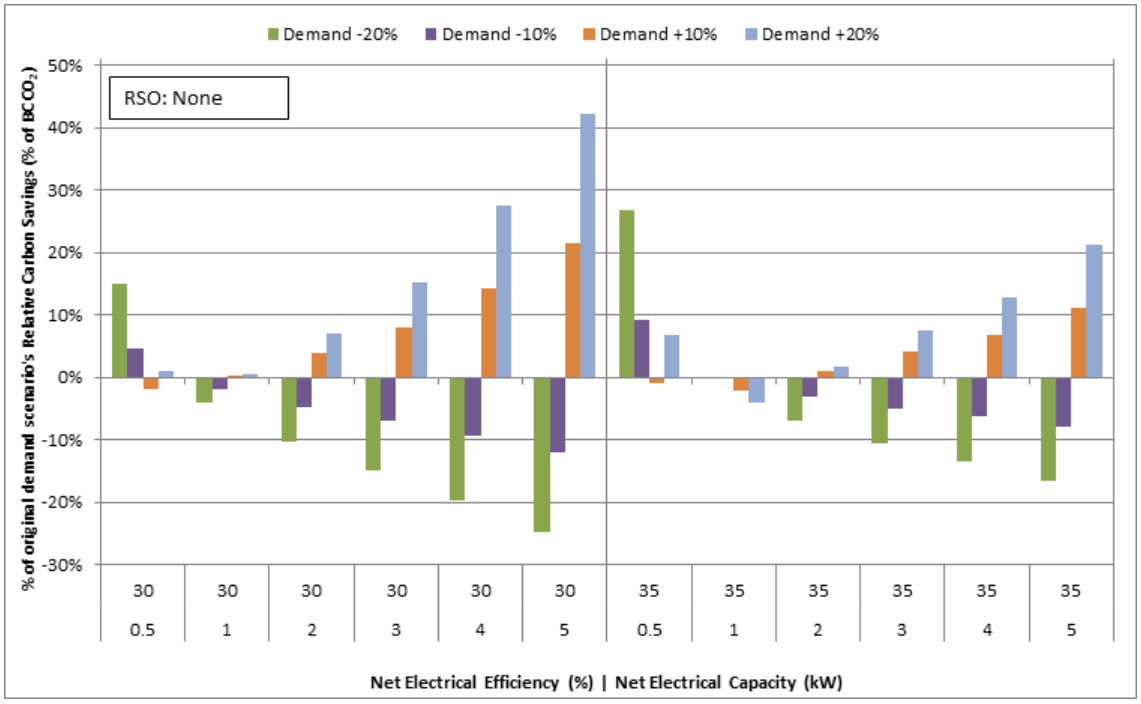

Figure 6.5: Marginal change in RCS (as % of RCS experience during original thermal demand scenario) due to change in annual thermal demand scenario, for 30% and 35% η_e design variants, operating without RSO

Similar analysis was undertaken for system operating under RSO, as presented in Figure 6.6 and Figure 6.7 where the relationships between change in RCS and both P_e and η_e are skewed. In order to understand the observed behaviour further, it was decided to analyse the RCS from the thermal demand scenarios using the potential thermal supply:demand ratio, which is discussed in the next section.

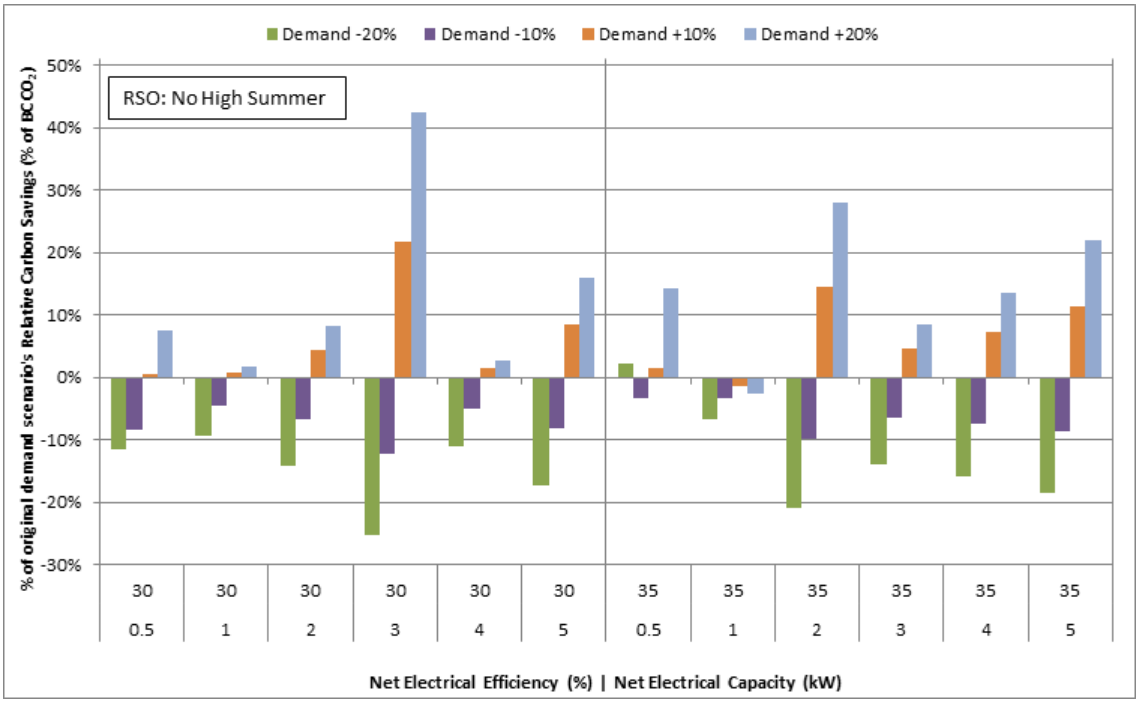

Figure 6.6: Marginal change in RCS (as % of RCS experience during original thermal demand scenario) due to change in annual thermal demand scenario, for 30% and 35% η_e design variants, operating under RSO-NoHSum

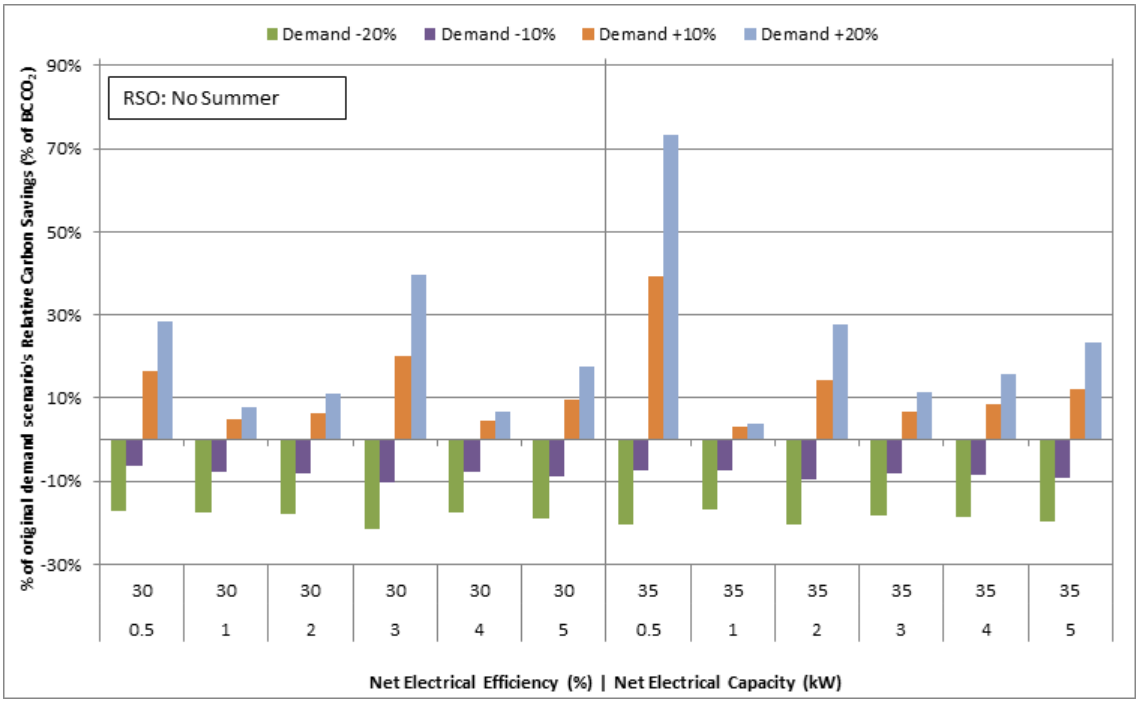

Figure 6.7: Marginal change in RCS (as % of RCS experience during original thermal demand scenario) due to change in annual thermal demand scenario, for 30% and 35% η_e design variants, operating under RSO-NoSummer

6.3.4 Potential Thermal Supply:Demand Ratio and Changing Demand

The analysis presented in Figure 6.8 to Figure 6.12 was undertaken to understand the relationship of the Specific Relative Carbon Saving (% of BC CO_2/MWh_{th}) with Potential Thermal Supply:Demand Ratio for each design variant. As with early analysis discussed in Section 4.3.9, specific RCS peaks at a given value of PTSDR. As thermal demand increases, this maxima shift towards lower values of PTSDR, and vice versa. Counter-intuitive, however, is the observation that the peak specific RCS is smallest for the original demand, i.e. it increases with both increasing and decreasing thermal demand. It is suspected that this is an artefact of the re-weighting process, as discussed in Section 6.3.2, as it is unlikely that the magnitude of thermal demand originally investigated is concurrent with a minima in a notional relationship of specific RCS versus thermal demand.

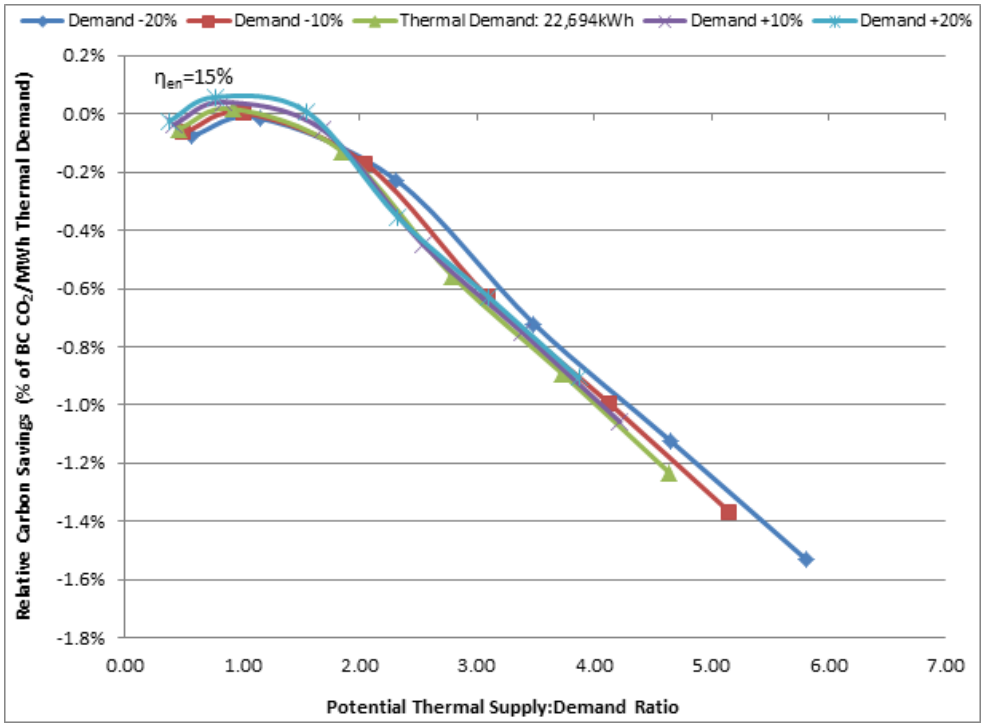

Figure 6.8: Specific RCS (% of BC CO_2/MWh_{th}) versus PTSDR, for each design variant with 15% η_e, comparing each thermal demand scenario

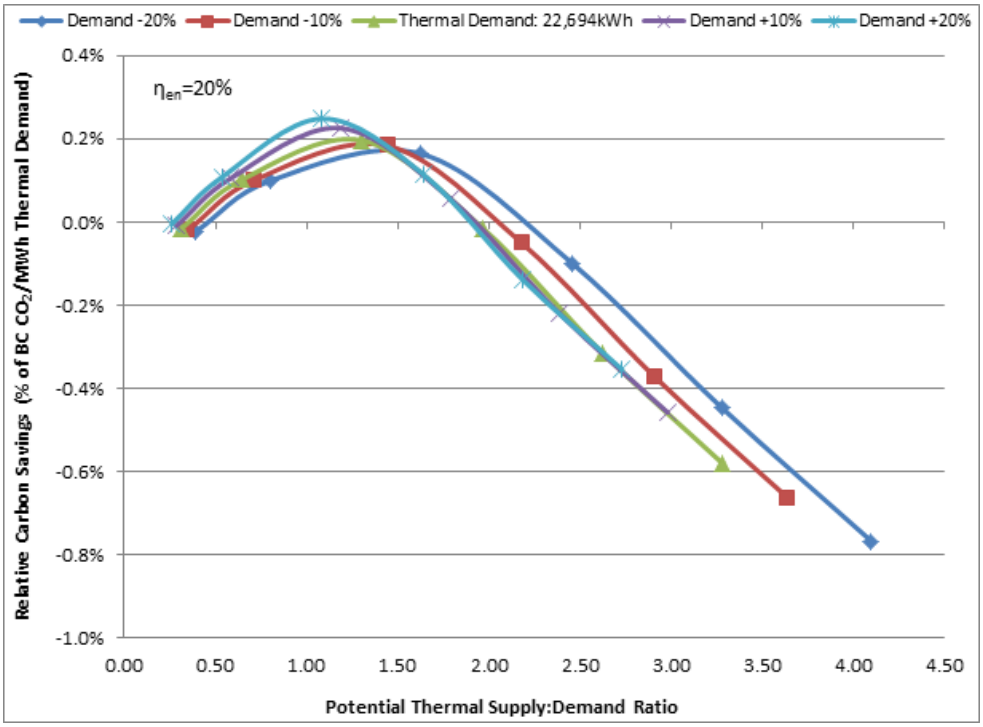

Figure 6.9: Specific RCS (% of BC CO_2/MWh_{th}) versus PTSDR, for each design variant with 20% η_e, comparing each thermal demand scenario

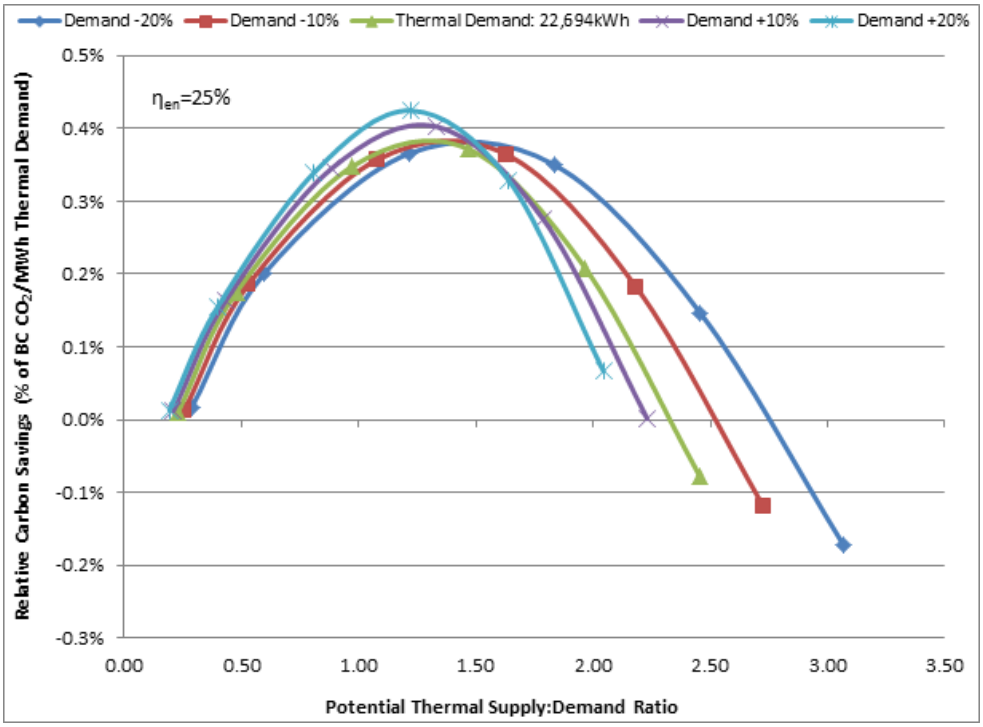

Figure 6.10: Specific RCS (% of BC CO_2/MWh_{th}) versus PTSDR, for each design variant with 25% η_e, comparing each thermal demand scenario

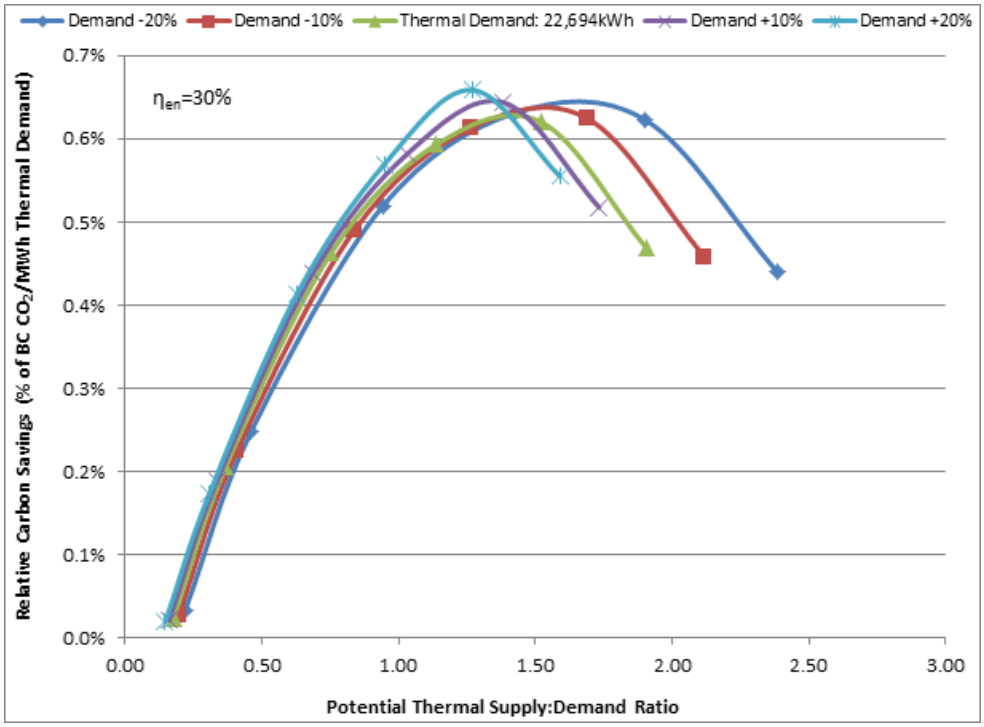

Figure 6.11: Specific RCS (% of BC CO_2/MWh$_{th}$) versus PTSDR, for each design variant with 30% η_e, comparing each thermal demand scenario

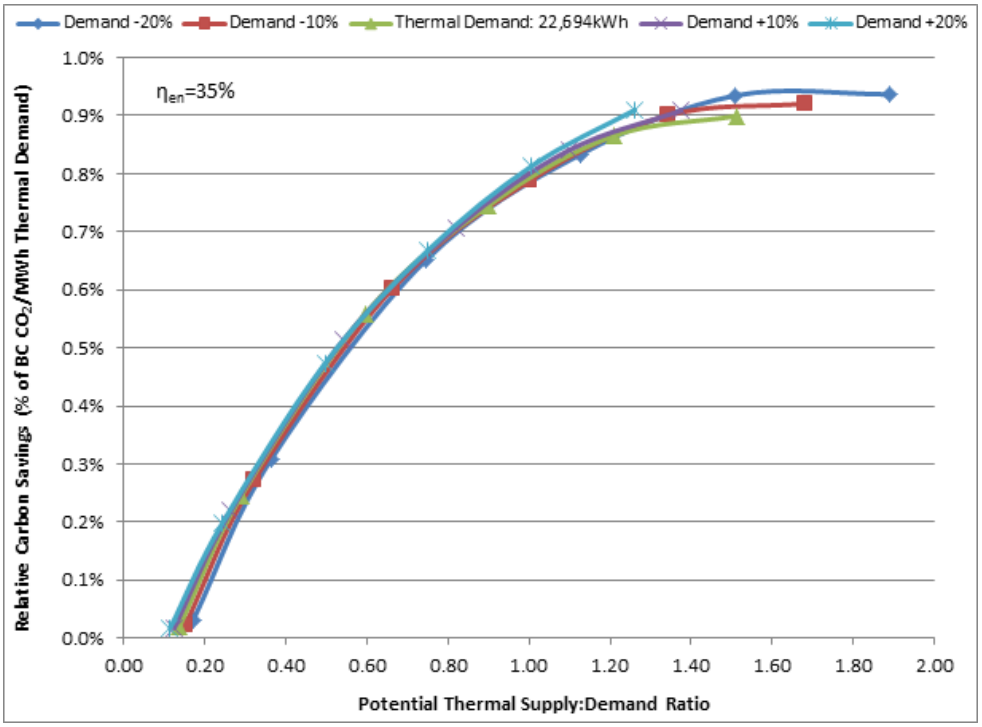

Figure 6.12: Specific RCS (% of BC CO_2/MWh$_{th}$) versus PTSDR, for each design variant with 35% η_e, comparing each thermal demand scenario

6.3.5 Thermal Cycling & Changing Thermal Demand

As discussed in Section 4.3.8, it is important to consider prime mover thermal cycling alongside RCS, due to the impact of thermal cycling on prime mover lifetime, and hence operation and maintenance costs. The effect of changing thermal demand on thermal cycling was assessed for the 8 top-performing TLF SE µCHP design variants, operating under each RSO mode. The effect on the alternative and combined operating regimes investigated in Chapter 5 was not studied, as these regimes are inherently restricted to specific daily frequency of thermal cycling.

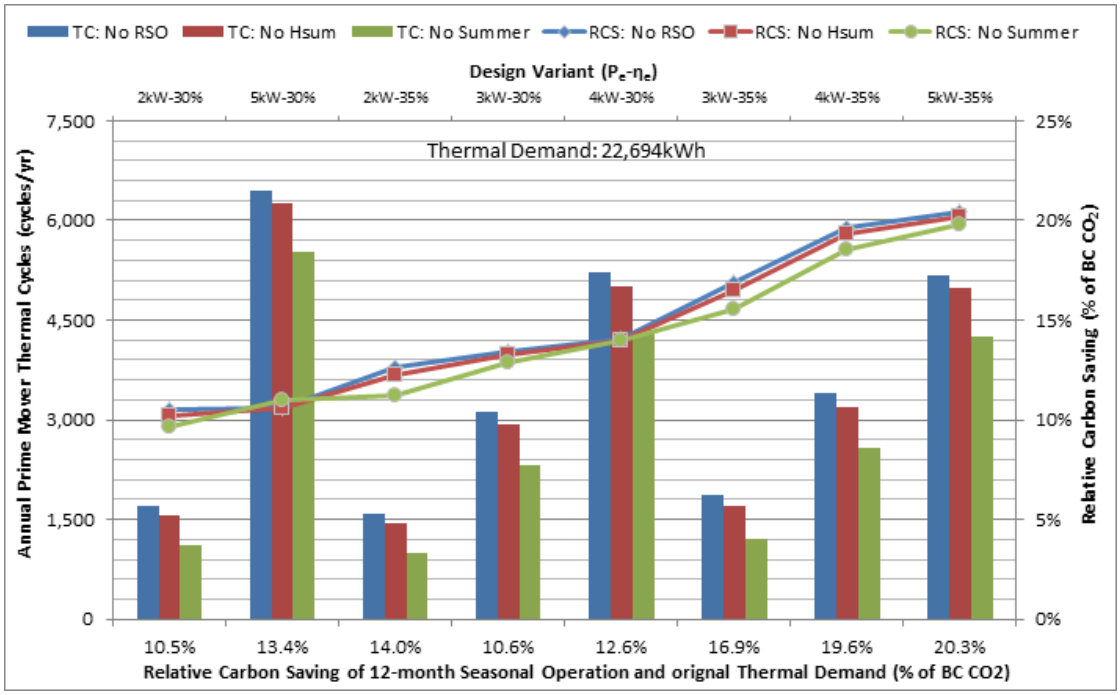

Figure 6.13: Annual Frequency of Thermal Cycles and the RCS, for 8 design variants, operating under each RSO, for the original Thermal Demand Scenario

Comparing the thermal cycling with the original thermal demand (Figure 6.13) with the increased demand scenarios (Figure 6.14 and Figure 6.15), the frequency of thermal cycling appears to decrease with increasing demand for 7 out of 8 design variants. This relationship would be explained by a greater annual contribution of PDSs with low frequency thermal cycling (i.e. winter climate). The 5kW$_e$-30% design variant, whose thermal cycling increased by approximately 1% with a 10% growth in thermal demand, displayed much more frequent thermal cycling during the winter primary demand

scenarios, as shown in Figure 4.28. As the winter climate scenarios have a larger annual weighting factor in the increased demand scenarios, this behaviour is intuitive.

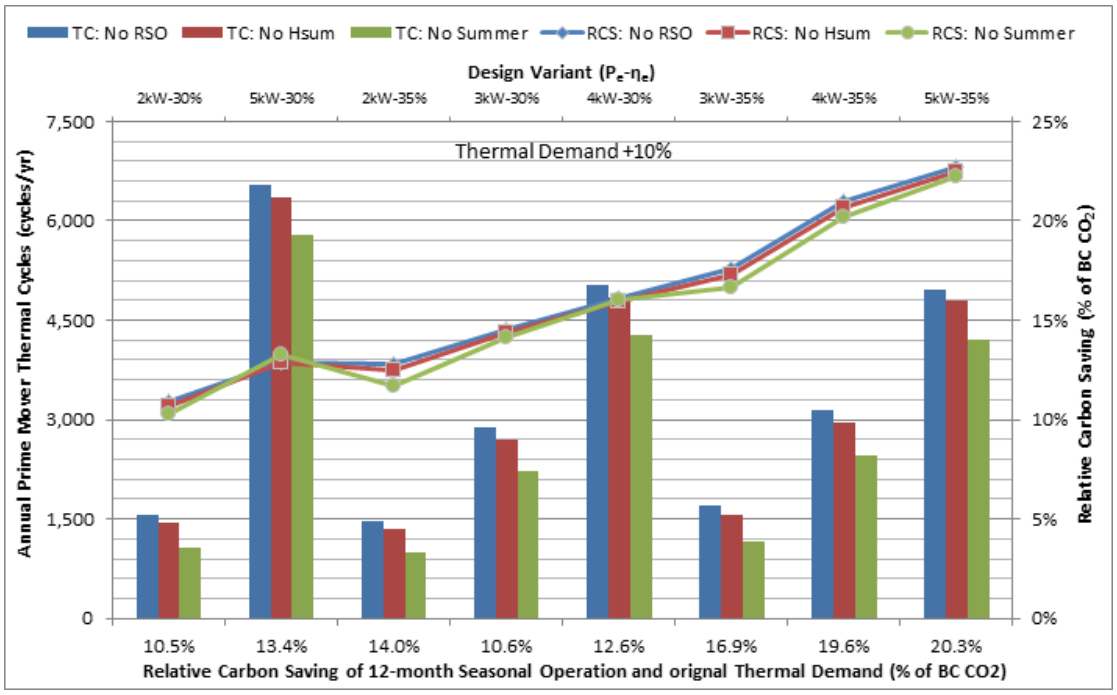

Figure 6.14: Annual Frequency of Thermal Cycles and the RCS, for 8 design variants, operating under each RSO, for the +10% Thermal Demand Scenario

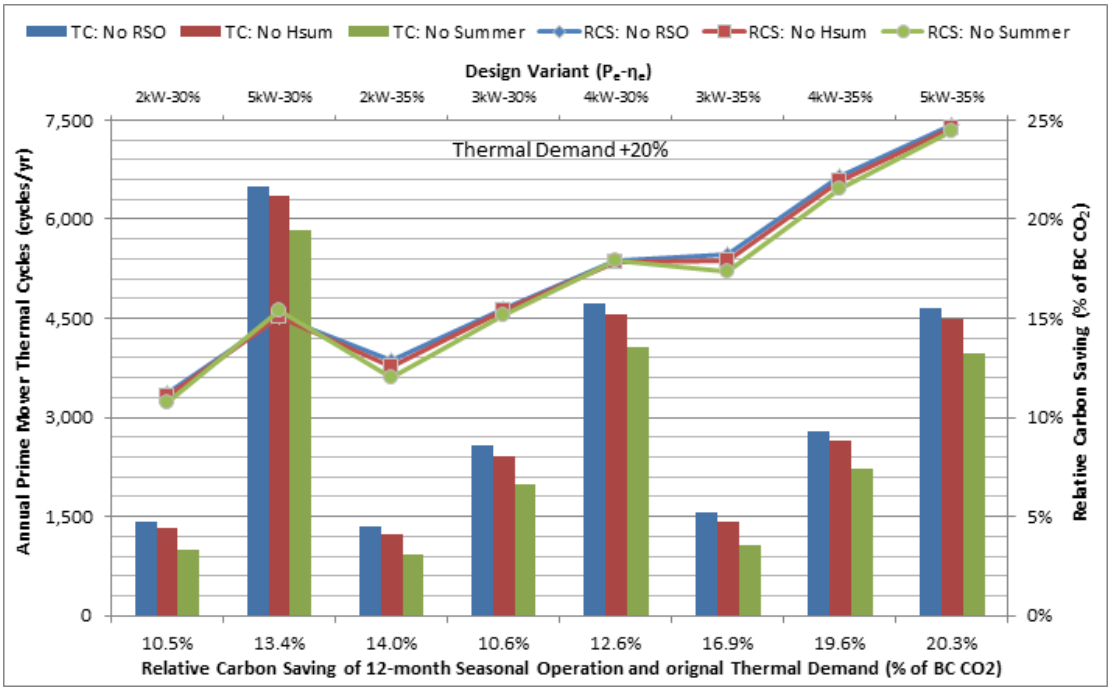

Figure 6.15: Annual Frequency of Thermal Cycles and the RCS, for 8 design variants, operating under each RSO, for the +20% Thermal Demand Scenario

Comparing the thermal cycling with the original thermal demand (Figure 6.13) with the decreased demand scenarios (Figure 6.16 and Figure 6.17), the frequency of thermal cycling increases (by up to 1%) for the 2kW$_e$-30%, 2kW$_e$-35% & 3kW$_e$-35% design variants, and decreases significantly for the remaining design variants. Again this can be explained by reference to Figure 4.28, where the 3 design variants in question have a comparatively low frequency of thermal cycling, and a different distribution of thermal cycling throughout the year.

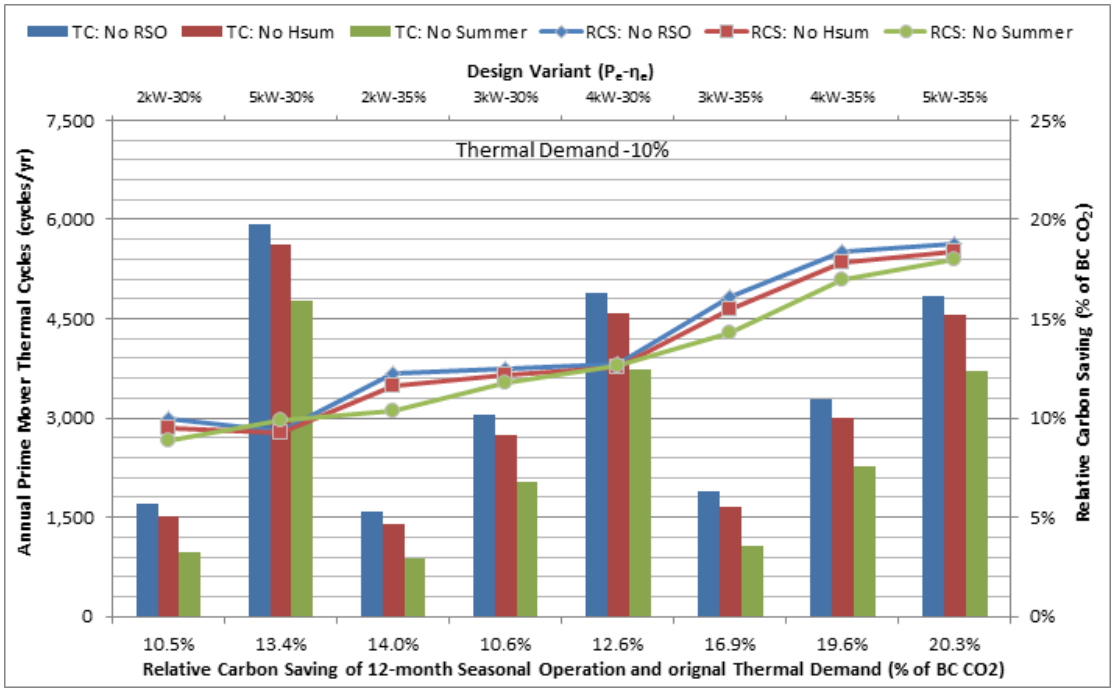

Figure 6.16: Annual Frequency of Thermal Cycles and the RCS, for 8 design variants, operating under each RSO, for the -10% Thermal Demand Scenario

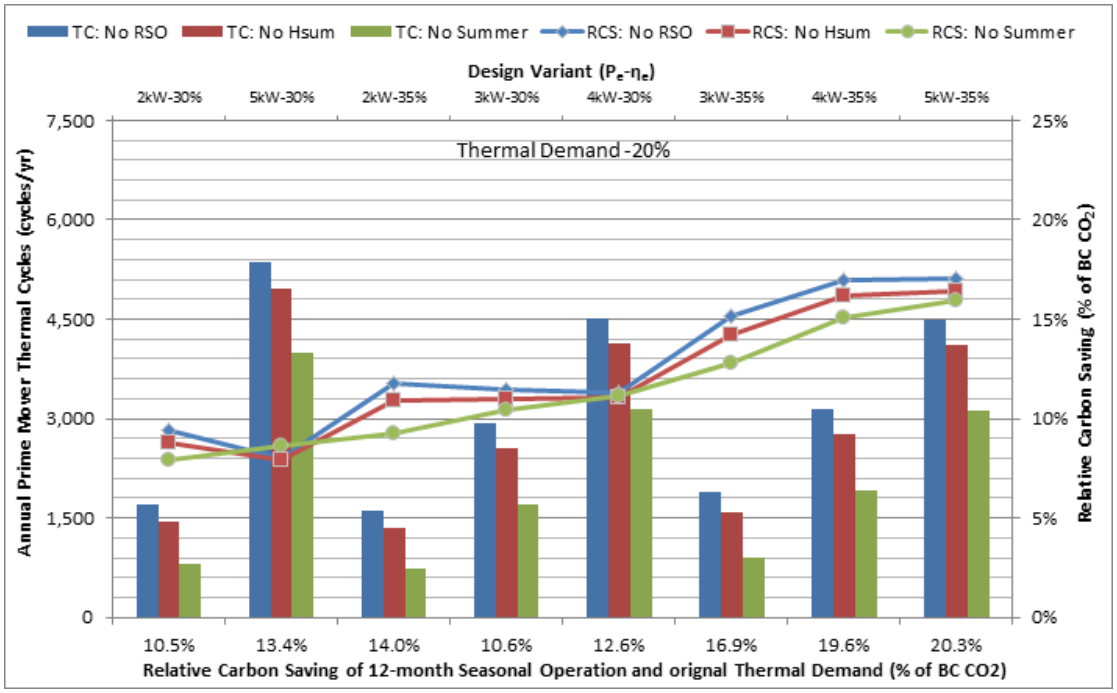

Figure 6.17: Annual Frequency of Thermal Cycles and the RCS, for 8 design variants, operating under each RSO, for the -20% Thermal Demand Scenario

6.4 Changing Carbon Intensities

6.4.1 Low-Carbon Fuel

Investigation thus far has considered natural gas, with a carbon intensity of 0.19kgCO_2/kWh, as the fuel source of both the base-case and µCHP energy systems. If alternative, low-carbon fuels were to be used in place of natural gas, such as biogas or hydrogen-enriched natural gas, this would affect the relative carbon savings presented in this thesis. In the Netherlands, a 3-year field trial of hydrogen mixing within the local natural gas network was undertaken [7]. By the end of the trial, a number of boilers, µCHP systems and cookers were operating on a mixture of 80% natural gas & 20% hydrogen, by volume. Associated lab tests were undertaken with up to 30% hydrogen, however, there are concerns regarding safety and leakage by hydrogen permeation through pipework and joints if applied to existing infrastructure [7]. Harrison [8] claims that research by the UK's natural gas grid operator indicates that up to 18% of the UK's natural gas consumption could be derived from renewable gas, disregarding crop-derived bio-methane.

The relative carbon savings discussed in this thesis are quoted as percentage of base-case carbon footprint (in $kgCO_2$). This footprint includes natural gas consumption for the boiler, and electrical imports from the NEG with CI_{grid} of 0.43 CO_2/kWh.

A brief sensitivity study was undertaken, to understand the effect on RCS due to a switch (of both base-case and μCHP system) to fuels with a range of lower carbon intensities. The results of this study are presented for the 8 top-performing design variants, using TLF operating regime, with RSO-NoSummer RSO. The range of carbon intensities studied ranges from 0$kgCO_2$/kWh (corresponding to hydrogen created using a zero-carbon energy source) to the approximate CI of natural gas, 0.19$kgCO_2$/kWh. To put this in context, the carbon intensities of the 20%, 30% and 41% mixture of hydrogen to natural gas (by volume) discussed previously are 0.176$kgCO_2$/kWh, 0.167$kgCO_2$/kWh and 0.156$kgCO_2$/kWh, respectively. Where technical barriers exist for the widespread provision of high hydrogen content fuel from nationwide infrastructure, or issues with combusting hydrogen-rich fuels for existing heat generators, a local hydrogen generation and storage system could be installed to serve specifically-designed μCHP prime movers, auxiliary boilers and presumably cooking appliances.

The annual carbon footprint of the base-case energy system, split between heating fuel and electrical import, is presented in Table 6.5. As the heating fuel accounts for 71% of the original carbon footprint of the base-case, the overall carbon footprint is very sensitive to changes in heating fuel CI.

Fuel Carbon Intensity	Base-case Gas		Base-case Electricity		Base-case Total	
($kgCO_2$/kWh)	($kgCO_2$)	(%)	($kgCO_2$)	(%)	($kgCO_2$)	(% of Original)
0.19	4,893	71%	1,971	29%	6,864	100%
0.15	3,863	66%	1,971	34%	5,834	85%
0.1	2,575	57%	1,971	43%	4,546	66%
0.05	1,288	40%	1,971	60%	3,258	47%
0	0	0%	1,971	100%	1,971	29%

Table 6.5: Carbon footprint of base-case energy system for a range of heating fuel CIs

The relative carbon savings, versus the base-case carbon footprint as calculated using the corresponding fuel CI, for each of the 8 top-performing design variants is presented in Table 6.6. RCS can increase by approximately a factor of 14. However, it is more relevant to consider the absolute carbon savings, which can increase by a factor of 4 over the original CI_{fuel} scenario.

P_e (kW_e)	η_e (%)	Carbon Intensity of Fuel ($kgCO_2/kWh$)					Carbon Intensity of Fuel ($kgCO_2/kWh$)				
		0.19	0.15	0.1	0.05	0	0.19	0.15	0.1	0.05	0
		Relative Carbon Savings (% of BC CO_2)					Absolute Carbon Savings ($kgCO_2$)				
2	30	10%	16%	27%	47%	93%	663	910	1,220	1,530	1,839
5	30	13%	21%	36%	63%	125%	886	1,217	1,631	2,045	2,459
2	35	14%	23%	41%	73%	146%	961	1,366	1,873	2,379	2,886
3	30	11%	21%	40%	74%	152%	757	1,229	1,820	2,411	3,002
4	30	11%	18%	30%	51%	100%	771	1,025	1,343	1,662	1,980
3	35	16%	24%	40%	69%	136%	1,070	1,410	1,833	2,257	2,681
4	35	19%	29%	48%	83%	164%	1,275	1,686	2,200	2,713	3,227
5	35	20%	32%	54%	93%	185%	1,360	1,840	2,440	3,040	3,640

Table 6.6: Relative Carbon Savings (% of BC CO_2) and Absolute Carbon Savings ($kgCO_2$) for the 8 top-performing TLF SE µCHP design variants, operating with RSO-NoSummer

The novel analysis methodology introduced in Section 4.3.4, Carbon Saving Attribution, allows this increase in absolute carbon savings to be explained. Figure 4.5 illustrates that, using the original value of CI_{fuel} ($0.19kgCO_2/kWh$), the 8 prime mover design variants in question provided RCS despite a carbon penalty of between 45-85% of base-case carbon footprint due to additional fuel consumption of the µCHP system (versus the base-case boiler). This carbon penalty scales linearly with CI_{fuel}, however the RCS due to thermal generation displacement, electrical import displacement and electrical export credit is static. The net result is that additional carbon savings are achieved by using fuel with lower carbon intensity.

The switch to low-carbon fuel could also allow design variants, which did not provide significant carbon savings with natural gas, to produce significant levels of RCS. This includes the $0.5kW_e$ systems, which have between 426 and 629 thermal cycles per annum with RSO-NoSummer. This is dramatically lower than the annual frequency of

thermal cycling (1,005-5,534 cycles per annum) experienced by the 8 design variants discussed in Table 6.6, almost doubling predicted lifetime of the prime mover.

6.4.2 National Electricity Grid

Prior investigations presented in this thesis have assumed that the carbon intensity of electricity imported from the NEG, CI_{grid}, is 0.43kgCO_2/kWh. This was selected as it was used as the emission factor of grid electricity by UK government for calculating emission savings, as discussed in Section 1.1. This is based upon the estimated long-term marginal factor. However, the UK government, and its various quangos[1], have since regularly published new factors for use with government funded consultancy projects, with 0.525kgCO_2/kWh in-use as of February 2012.

The effect of varying CI_{grid} on the 8 top-performing design variants, using thermal load following operating regime with the RSO-NoSummer seasonal restriction was studied. To put the range of assessed grid CIs in context, Harrison [8] claims that the CI of central electricity generation displaced by µCHP is generally taken to be 0.568kgCO_2/kWh. He quotes the 2009 UK average grid electricity CI as 0.51kgCO_2/kWh, with a peak marginal CI of 0.80kgCO_2/kWh.

The annual carbon footprint of the base-case energy system, split between heating fuel and electrical import, is presented in Table 6.7. As electricity accounts for 29% of the original carbon footprint of the base-case, the overall carbon footprint is not as sensitive to changes in CI_{grid} as it is for heating fuel.

Grid CI	Base-case Gas		Base-case Electricity		Base-case Total	
(kgCO_2/kWh)	(kgCO_2)	(%)	(kgCO_2)	(%)	(kgCO_2)	(% of Original)
0.43	4,893	71%	1,971	29%	6,864	100%
0.50	4,893	68%	2,292	32%	7,185	105%
0.55	4,893	66%	2,521	34%	7,414	108%
0.40	4,893	73%	1,833	27%	6,726	98%
0.35	4,893	75%	1,604	25%	6,497	95%
0.30	4,893	78%	1,375	22%	6,268	91%

Table 6.7: Carbon footprint of base-case energy system for a range of grid CIs

[1] DEFRA, DECC, Carbon Trust

The relative carbon savings, versus the base-case carbon footprint as calculated using the corresponding grid carbon intensity, for each of the 8 top-performing design variants is presented in Table 6.8. RCS can increase by a factor of 2 (for CI_{grid} = 0.55kgCO_2/kWh), or decrease by 82% (for CI_{grid} = 0.3kgCO_2/kWh). However, it is more relevant to consider the absolute carbon savings, which can increase by 111% (for CI_{grid}=0.55kgCO_2/kWh), or decrease to the point of carbon penalty (for CI_{grid} = 0.3kgCO_2/kWh).

P_e	η_e (%)	Carbon Intensity of Grid (kgCO_2/kWh)						Carbon Intensity of Grid (kgCO_2/kWh)					
(kW_e)		0.43	0.50	0.55	0.40	0.35	0.30	0.43	0.50	0.55	0.40	0.35	0.30
		Relative Carbon Saving (% of BC CO_2)						Absolute Carbon Saving (kgCO_2)					
2	30	10	13	16	8	5	2	663	962	1,176	535	321	107
5	30	13	18	21	11	7	2	886	1,286	1,572	714	428	142
2	35	14	20	24	11	7	1	961	1,431	1,767	760	424	89
3	30	11	17	22	8	3	-2	757	1,246	1,595	547	198	-151
4	30	11	15	18	9	6	3	771	1,093	1,323	632	402	172
3	35	16	21	25	13	9	4	1,070	1,507	1,819	883	571	260
4	35	19	25	29	16	10	5	1,275	1,800	2,176	1,050	675	300
5	35	20	27	32	16	11	4	1,360	1,952	2,376	1,106	682	259

Table 6.8: Relative Carbon Savings (% of BC CO_2) and Absolute Carbon Savings (kgCO_2) for the 8 top-performing TLF SE µCHP design variants, operating with RSO-NoSummer

The novel analysis methodology introduced in Section 4.3.4, Carbon Saving Attribution, allows this increase in absolute carbon savings to be explained. Figure 4.5 illustrates that, using the original value of CI_{grid} (0.43kgCO_2/kWh), the combined relative carbon saving from electrical import displacement and electrical export credit, for the 8 prime mover design variants in question, was 30-58% of base-case carbon footprint. As the RCS due to thermal generation displacement and additional fuel consumption of the µCHP system remains constant, altering the CI of the grid (which is used to calculate the electrical carbon savings) will alter total RCS.

A decrease in CI_{grid} would reduce the RCS to insignificant levels for those design variants, from the 8 investigated, with lowest annual frequency of thermal cycling. This would negatively impact the lifetime of the prime mover. Increasing CI_{grid} to 0.55kgCO_2/kWh would increase the RCS of the 1kW_e-35% design variant to significant

levels, which makes a prime mover with less than 500 annual thermal cycles feasible from a carbon saving standpoint.

6.5 Discussion & Conclusions

In this chapter, alternative scenarios that are external to the design of the μCHP system are discussed and investigated, specifically changing annual thermal demand and changing carbon intensities of fuel and NEG-derived electricity.

Regardless of RSO, RCS tends to increase with thermal demand. As the relationship between RCS and thermal demand was understood to be non-linear, a performance metric was defined; Specific Relative Carbon Savings (% of BC CO_2/MWh_{th}). Analysis of simulation results with the new metric were inconclusive, as some design variants show increasing Specific RCS with increasing thermal demand, and others decreasing Specific RCS. However, as this relationship does not correspond with the η_e families of design variant, further investigation suggests that this is a modelling artefact derived from the weighting of design days. In general, it can be concluded that μCHP is appropriate for dwellings with large thermal demand, and less so for dwelling with lower thermal demand.

Analysis of Marginal Relative Carbon Savings revealed that a 20% increase in annual thermal demand could result in a 4% to 42% (of RCS in original scenario) increase in RCS. This supported the earlier conclusion that the relationship between RCS and thermal demand was non-linear, hence prompting analysis of Specific RCS versus Potential Thermal Supply:Demand Ratio. As with early analysis discussed in Section 4.3.9, specific RCS peaks at a given value of PTSDR. As thermal demand increases, this maxima shift towards lower values of PTSDR, and vice versa. Counter-intuitive, however, is the observation that the peak specific RCS is smallest for the original demand, i.e. it increases with both increasing and decreasing thermal demand. It is suspected that this is an artefact of the re-weighting process (versus the original annual weighting factors), as discussed in Section 6.3.2, as it is unlikely that the

magnitude of thermal demand originally investigated is concurrent with a minima in a notional relationship of specific RCS versus thermal demand.

The frequency of thermal cycling appears to decrease with increasing demand for 7 out of 8 design variants. As the winter climate scenarios have a larger annual weighting factor in the increased demand scenarios, compared with the original weighting factor, this behaviour is intuitive. As annual thermal demand decreases, the frequency of thermal cycling increases (by up to 1%) for the 2kWe-30%, 2kWe-35% & 3kWe-35% design variants, and decreases significantly for the remaining design variants. Again this can be explained by reference to Figure 4.28, where the 3 design variants in question have a comparatively low frequency of thermal cycling, and a different distribution of thermal cycling throughout the year. The sensitivity of the thermal cycling frequency to thermal demand is relatively low, and hence unlikely to dramatically alter prime mover lifetime due to thermal demand changes over time.

A switch from natural gas to a lower carbon fuel, as assessed in Section 6.4, would allow design variants that did not provide significant carbon savings with natural gas to produce significant levels of RCS. This includes the $0.5kW_e$ systems, which have between 426 and 629 thermal cycles per annum with RSO-NoSummer, which is dramatically lower than the annual frequency of thermal cycling experienced by the 8 design variants discussed in Table 6.6, almost doubling predicted lifetime of the prime mover. The RCS of the design variants that otherwise exhibited significant carbon savings increases linearly with decreasing CI_{fuel}, related to the additional μCHP system fuel consumption (versus base-case).

In a future context, decreased CI of a NG/hydrogen fuel mixture could be due to localised hydrogen production and storage, or centralised (or distributed) production with subsequent injection into the natural gas network. Whilst a modest dilution of natural gas with hydrogen will lower carbon intensity, the quantity of hydrogen required to achieve a substantially lower carbon intensity fuel than natural gas is very high. This would require substantial electrical energy inputs to an electrolyser, which is infeasible due to the limited capacity of renewable generators (e.g. solar PV and micro-

wind) that could be installed on typical dwellings (especially those in an urban context). Large scale hydrogen production would be easier to achieve with larger generators (e.g. marine power or wind farms) than at distributed scale.

The effect of changing CI_{grid} on the RCS was evaluated for the 8 top-performing design variants, as presented in Section 6.4.2. Due to the large contribution of electrical export and electrical import displacement on RCS for those design variants, increasing CI_{grid} results in significantly increasing RCS. The increased values of CI_{grid} investigated are within the range understood to relate to central generation plant that would actually be displaced by μCHP. It is prudent to note that reducing CI_{grid} by just over 20% is sufficient to render all design variants without significant RCS. This is especially relevant when considering the potential for widespread adoption of μCHP as grid carbon intensity either decreases due to increased renewable generation, or increases due to retired nuclear generation or replacement of gas-fired central generation with coal due to security of supply concerns.

6.6 References

[1] A.D. Peacock, D.P. Jenkins, D. Kane, Investigating the potential of overheating in UK dwellings as a consequence of extant climate change, Energy Policy, Volume 38, Issue 7, Pages 3277-3288, July 2010

[2] A.D. Peacock and M. Newborough; Effect of heat-saving measures on the CO2 savings attributable to micro-combined heat and power (mCHP) systems in UK dwellings; Energy; 33; 2008; pp601–612

[3] A.D. Hawkes and M.A. Leach, Comparison of Fuel Cell and Combustion Micro-CHP under Future Residential Energy Demand Scenarios, Centre for Energy Policy and Technology, Imperial College London, June 2007

[4] A.D. Hawkes & M. Leach; Future scenarios for micro-CHP in the UK as residential building insulation improves; eceee 2007 Summer Study Proceedings; 2007

[5] Market Transformation Programme; www.mtprog.com; Jun 2006; Policy Brief: UK Water Consumption of Domestic Showers

[6] Jordan & Vajen; Influence of the DHW Load Profile on the Fractional Energy Savings: A Case Study of a Solar Combi-System with TRNSYS Simulations; Solar Energy; Vol. 59; Nos. 1-6; pp. 197-208; 2000

[7] M.J. Kippers, J.C. De Laat, R.J.M. Hermkens, J.J. Overdiep, A. van der Molen, W.C. van Erp, A. van der Meer; Pilot Project On Hydrogen Injection In Natural Gas On Island Of Ameland In The Netherlands; International Gas Union Research Conference 2011; Seoul; October 2011

[8] J. Harrison; The role of Micro-CHP within a decarbonizing energy system; Cogeneration & On-Site Power Production Magazine; Volume 12; Issue 4; pp33-40; 25th July 2011; Access online at http://www.cospp.com

7 Electrical Storage Sub-Systems and Carbon Security

7.1 Introduction

In this chapter, the opportunities available to increase Carbon Security through integration of on-site electrical storage into μCHP systems are investigated. By application of a transient lead-acid battery performance model [1][2], as developed by the author in collaboration with others, the environmental performance penalties associated with displacing additional electrical import using an electrical storage sub-system are calculated. Furthermore, the concept of storing excess electricity as hydrogen, for later use as μCHP fuel source, by application of electrolysis is explored. With the introduction of energy storage in the form of hydrogen, the concept of daily, weekly and seasonal storage durations is explored. Various operating regimes, seasonal operating restrictions, and control strategies are considered for selected μCHP system design variants from Chapters 4 & 5, to maximise both environmental performance and carbon security.

The interactions of specific μCHP concept systems that include electrical storage with on-site renewable generation are investigated, using solar PV generation profiles created by application of an existing micro-generation model [3]. By combining several forms of micro-generation with on-site storage, the concept of an autonomous home energy system is introduced.

The assumption thus far in this thesis has been that electrical export to the NEG will displace centrally generated electricity of the same carbon intensity as imported electricity. This is the basis of the Electrical Export Credit (EEC) defined in Section 4.3.4, where the relationship between EEC and Relative Carbon Savings (RCS) was explored in Section 4.3.6. However, many publications [4][5][6][7][8]have addressed the issue of marginal generation, i.e. the central generation that may be displaced as micro-generation causes electrical import to buildings to decrease and electricity to be exported to the NEG. The study presented in Section 6.4.2 identified the effect of changing grid carbon intensity on the RCS estimated for SE-based μCHP systems operated in a thermal load following manner. That study could be extended to

consider the time-varying grid carbon intensity, in response to changes in the grid-connected generation mix.

It has been identified that the mass deployment of domestic µCHP systems with high levels of electrical export (or indeed other electrical micro-generation technologies) can lead to other issues. The problematic effect of voltage rise in the low voltage (LV) distribution network, due to up-stream flow from buildings to LV transformers, has been discussed by other studies [9][10]. As the penetration level of distributed micro-generation increases, regulatory action may eventually be required to restrict, or smooth on a temporal basis, electrical export from buildings.

Indeed, from the perspective of the consumer, high levels of electrical export may be economically disadvantageous, due to low export prices paid by their utility. The UK Feed-In Tariff, which subsidised micro-generation systems, guarantees an export rate of 3.1p/kWh in early 2012, which is a fraction of typical import prices for domestic consumers (9-14p/kWh). Whilst there are cost (both capital and maintenance) implications of electrical storage, and energy losses due to the round trip efficiency (RTE) of the storage and reconversion processes, there may be an economic justification to store electrical energy instead of exporting it, should the import price be sufficiently greater than the export price.

Finally, on-site storage of electricity may offer consumers a measure of energy security, in that an appropriately configured system may be capable of operating without availability of the NEG. This may be particularly important for those dwellings in areas with low NEG reliability (e.g. in remote locations, or where there are capacity constraints), or for all grid-connected dwellings if there were fuel issues for central generation plant.

7.2 Battery Storage

7.2.1 Introduction

A model of a lead-acid battery storage system, with 1-minute temporal precision, was developed by the author and others, the basis of which was previously published [1][2]. In summary, the battery model considers the state of charge (SoC) for a defined capacity of battery bank, with limited maximum charge and discharge rates linked to capacity. The RTE is calculated from cumulative charge and discharge, and is driven by the load-dependent charge controller efficiency.

A weekly demand profile was synthesised from 5 weekday and 2 weekend design days, using BIM-G generated electrical demand data for the primary demand scenarios relating to extreme winter and shoulder, averaged to 1-minute intervals (as this was the temporal precision of the previously-developed battery model). Weekly SE µCHP generation profiles were created in the same manner for the $5kW_e$-35% design variant with the thermal load following operating regime and the $2kW_e$-35% design variant operating under CsO-TDP.

A Solar PV generation profile, for a $2.5kW_e$ peak output system, interpolated from 60-minute to 1-minute, was extracted from previously published research using the battery model [1][2]. The Solar PV model was developed by an MSc student [3], and was based upon the angular solar irradiance model created to process climate scenario data for BIM-G. The input climate data was based on the same Edinburgh climate file as used for the primary demand scenarios in BIM-G.

The battery store is designed to absorb as much export (from the µCHP/solar PV Renewable Energy System) as can be accepted by the charge controller, due to state of charge and maximum charge current. The electrical capacity of the batteries is sized to displace all electrical import from the NEG, as discussed in Section 7.2.4.

7.2.2 Supply & Demand Scenarios Investigated

Eight scenarios were defined, combining dwelling energy supply system and primary demand scenarios as presented in Table 7.1. The cumulative, peak and total electrical

demand over each week is compared with the cumulative generation of the available supply technologies in Table 7.1. The peak output of the TLF µCHP design variant exceeds the peak load of all demand profiles, and the cumulative output of both µCHP systems exceeds demand in all scenarios.

Climate	Operating Regime	Design Variant	Solar PV System	Demand			Generation (kWh)	
				Total (kWh)	Peak (kW)	Average (kW)	CHP	PV
Shoulder	TLF	5kW$_e$-35%	2.5kWp	91.2	4.07	0.54	210.1	54.3
Shoulder	TLF	5kW$_e$-35%	None	91.2	4.07	0.54	210.1	0.0
Ex Winter	TLF	5kW$_e$-35%	2.5kWp	101.2	4.56	0.60	365.8	11.4
Ex Winter	TLF	5kW$_e$-35%	None	101.2	4.56	0.60	365.8	0.0
Shoulder	CsO-TDP	2kW$_e$-35%	2.5kWp	96.8	4.02	0.58	135.8	54.3
Shoulder	CsO-TDP	2kW$_e$-35%	None	96.8	4.02	0.58	135.8	0.0
Ex. Winter	CsO-TDP	2kW$_e$-35%	2.5kWp	99.1	4.55	0.59	159.5	11.4
Ex. Winter	CsO-TDP	2kW$_e$-35%	None	99.1	4.55	0.59	159.5	0.0

Table 7.1: Weekly Demand statistics and cumulative generation values for SE µCHP system and Solar PV system, for a selection of primary demand scenarios and a selection of design varaints operating under TLF or CsO-TDP operating regimes

The energy demand satisfied by the dwelling energy system is compared with the NEG import and export in Table 7.2, where no battery storage is specified. In this case, a full electrical export credit would be applied to the relative carbon savings calculation.

Climate	Operating Regime	Design Variant	Solar PV System	Demand (kWh)	Generation (kWh)		Demand Satisfied by (kWh)			Export (kWh)
					CHP	PV	CHP & PV	Battery	Grid Import	
Sh	TLF	5kW$_e$-35%	2.5kWp	91.2	210.1	54.3	56.7	0.0	34.4	207.6
Sh	TLF	5kW$_e$-35%	None	91.2	210.1	0.0	42.8	0.0	48.3	167.2
EWin	TLF	5kW$_e$-35%	2.5kWp	101.2	365.8	11.4	84.8	0.0	16.5	292.4
EWin	TLF	5kW$_e$-35%	None	101.2	365.8	0.0	80.7	0.0	20.6	285.1
Sh	CsO-TDP	2kW$_e$-35%	2.5kWp	96.8	135.8	54.3	69.9	0.0	26.9	120.2
Sh	CsO-TDP	2kW$_e$-35%	None	96.8	135.8	0.0	51.2	0.0	45.5	84.6
EWin	CsO-TDP	2kW$_e$-35%	2.5kWp	99.1	159.5	11.4	72.6	0.0	26.5	98.2
EWin	CsO-TDP	2kW$_e$-35%	None	99.1	159.5	0.0	68.6	0.0	30.5	90.9

Table 7.2: Weekly breakdown of demand as satisfied from SE µCHP system and Solar PV system, battery storage and import from NEG, with indicated export to the NEG, for a selection of PDSs and design varaints with TLF or CsO-TDP operating regimes

7.2.3 Integration of Electrical Storage to Energy System

A battery storage system was then defined for each scenario, by an iterative approach, to achieve grid independence in terms of import. It should be noted, however, that the system exports surplus generation to the grid once the battery store has reached 100% SoC. The losses due to storage and subsequent re-conversion to mains voltage a.c. electricity presented in Table 7.3 represent a reduction in electrical export, with a corresponding reduction in EEC for RCS calculations.

Climate	Operating Regime	Design Variant	Solar PV System	Demand (kWh)	Generation (kWh)		Losses	
					CHP	PV	(kWh)	(%)
Sh	TLF	5kW$_e$-35%	2.5kWp	91.2	210.1	54.3	11.5	25%
Sh	TLF	5kW$_e$-35%	None	91.2	210.1	0.0	13.3	22%
EWin	TLF	5kW$_e$-35%	2.5kWp	101.2	365.8	11.4	4.5	22%
EWin	TLF	5kW$_e$-35%	None	101.2	365.8	0.0	5.2	20%
Sh	CsO-TDP	2kW$_e$-35%	2.5kWp	96.8	135.8	54.3	10.4	28%
Sh	CsO-TDP	2kW$_e$-35%	None	96.8	135.8	0.0	16.5	27%
EWin	CsO-TDP	2kW$_e$-35%	2.5kWp	99.1	159.5	11.4	10.9	29%
EWin	CsO-TDP	2kW$_e$-35%	None	99.1	159.5	0.0	12.2	29%

Table 7.3: Weekly losses from battery storage compared with cumulative genration from SE µCHP system and Solar PV system, and elctrical demand, for a selection of PDSs and design varaints with TLF or CsO-TDP operating regimes

The reductions in relative carbon savings due to battery storage losses for the µCHP-only scenarios are presented in Table 7.4. The high losses experienced by the µCHP system with CsO-TDP operating regime translates into significant reductions in RCS.

Climate	Operating Regime	Design Variant	Losses		RCS (% of BC CO_2)		
			(kWh)	(%)	Without Storage	With Storage	Reduction
Shoulder	TLF	5kWe-35%	13.3	22%	19%	15%	4%
Ex Winter	TLF	5kWe-35%	5.2	20%	30%	29%	1%
Shoulder	CsO-TDP	2kWe-35%	16.5	27%	13%	8%	5%
Ex Winter	CsO-TDP	2kWe-35%	12.2	29%	12%	10%	2%

Table 7.4: Impact of battery storage losses on RCS of selected µCHP design variants

The profiles of electrical demand satisfied by the renewable energy system (RES), battery storage, and grid import are presented in Figure 7.1 to Figure 7.8 for each scenario. The value of electrical import is constantly equal to zero, as expected, but

there are significant levels of export to the NEG in every scenario. This exported energy could not be absorbed by the battery store as the state of charge was at 100%, or the electrical current generated was greater than the maximum charge current of the batteries. When the RES incorporates a solar PV system, there is a substantial quantity of export, and direct contribution to meet demand, during the daytime. The µCHP system selected contributes to export and demand during early morning, evenings and weekends.

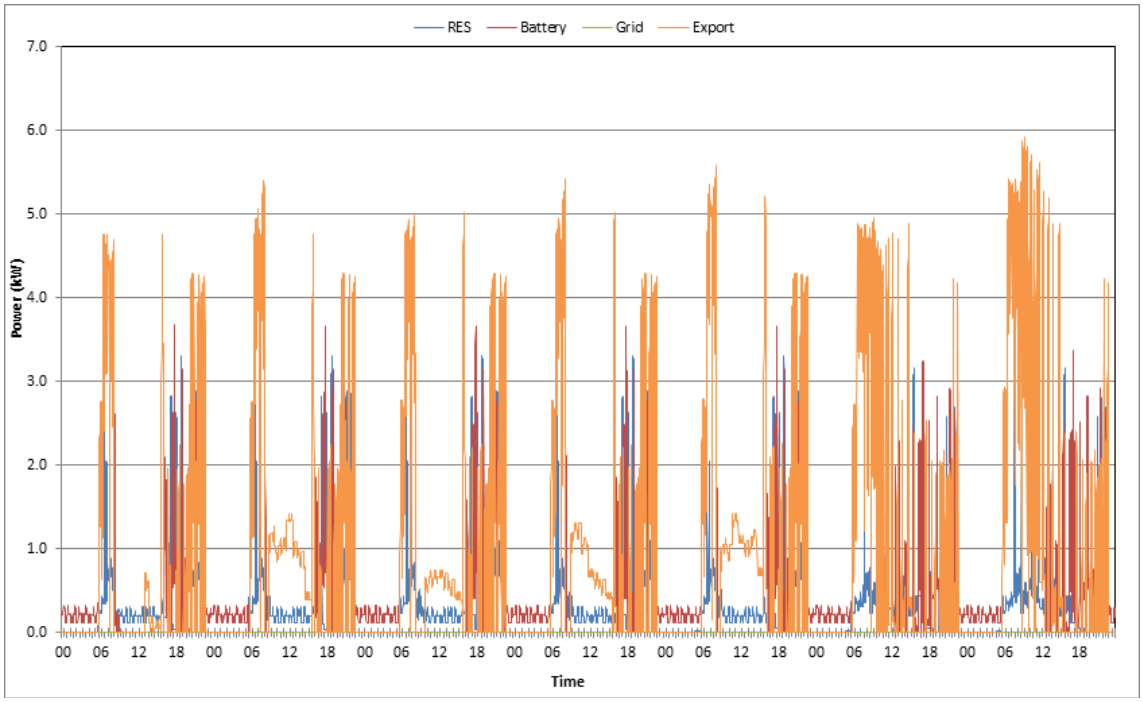

Figure 7.1: Electrical demand satisfied by the renewable energy system (RES), i.e. SE-TLF-5kW$_e$-35% µCHP and solar PV, battery storage and NEG import, and electrical export to NEG, for Week with Shoulder climate

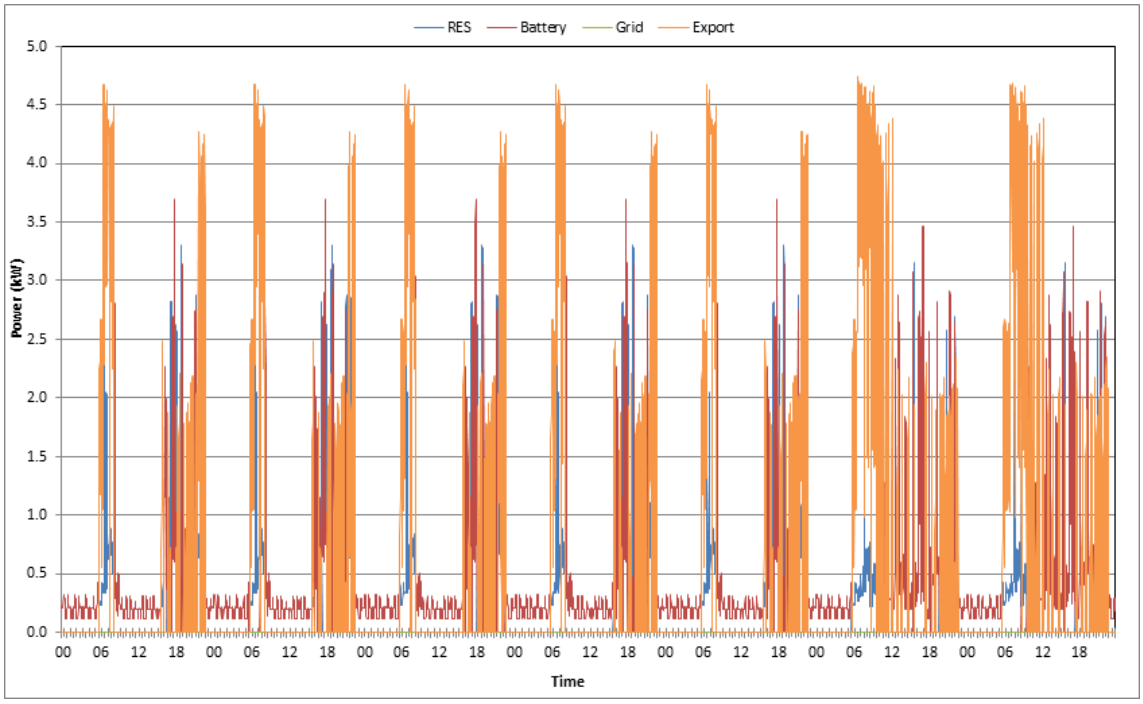

Figure 7.2: Electrical demand satisfied by the RES (SE-TLF-5kW$_e$-35% µCHP), battery storage and NEG import, and electrical export to NEG, for Week with Shoulder climate

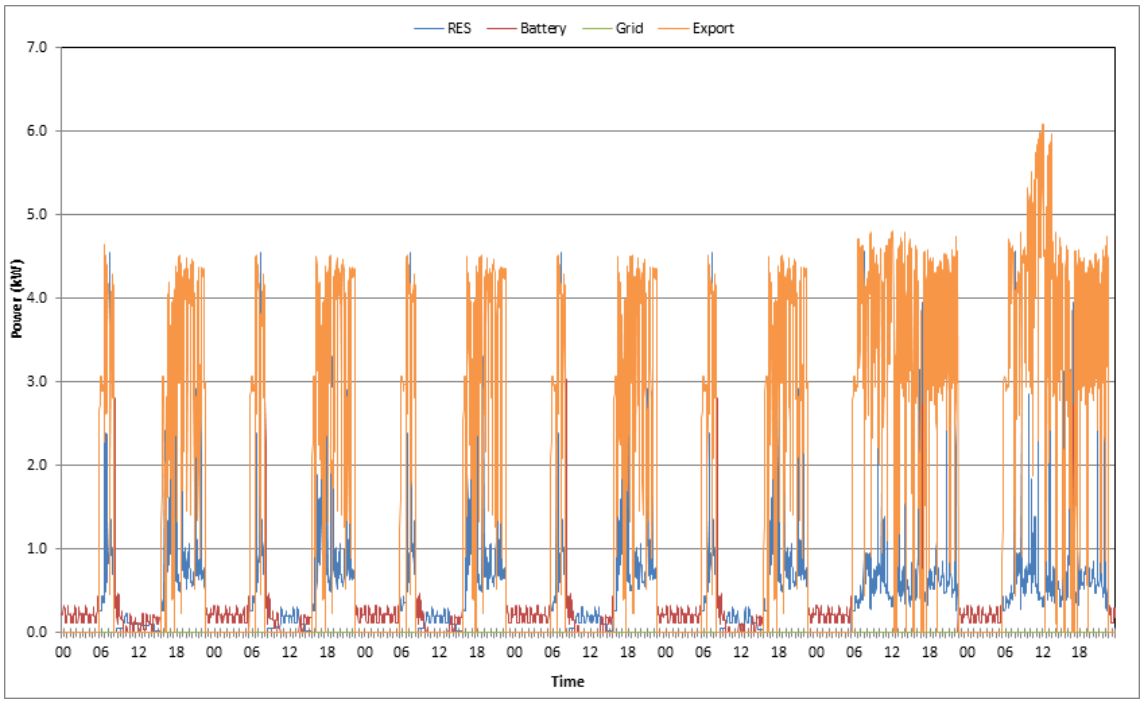

Figure 7.3: Electrical demand satisfied by the RES (SE-TLF-5kW$_e$-35% µCHP and solar PV), battery storage and NEG import, and electrical export to NEG, for Week with Extreme Winter climate

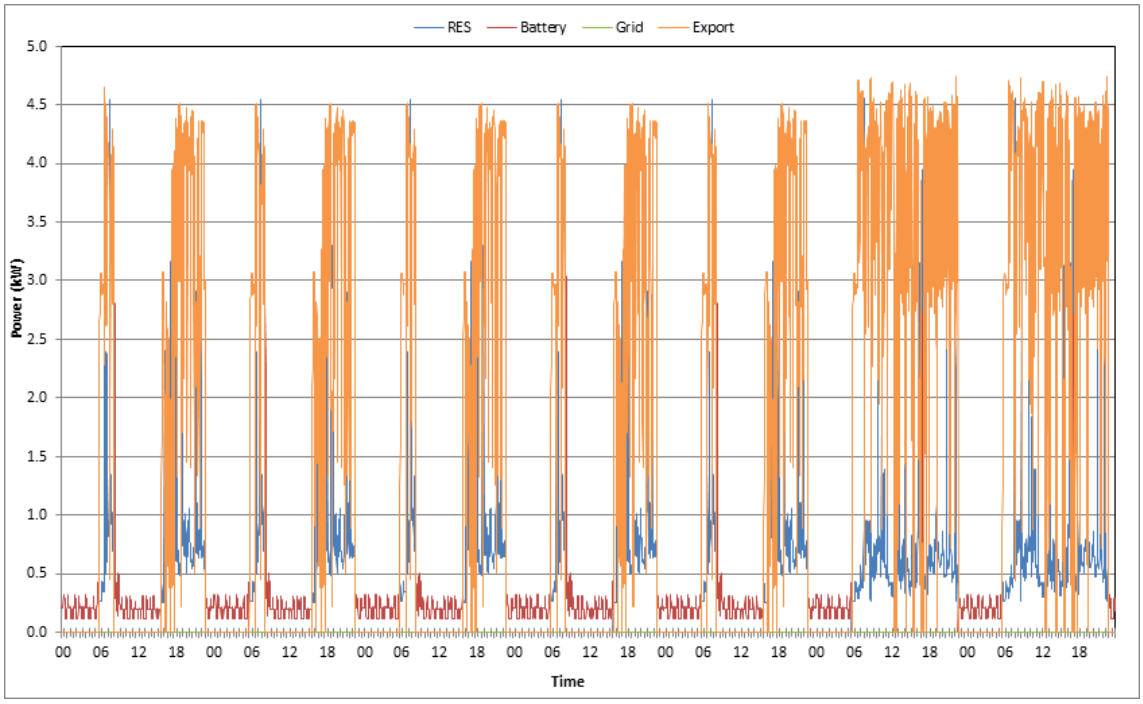

Figure 7.4: Electrical demand satisfied by the RES (SE-TLF-5kW$_e$-35% µCHP), battery storage and NEG import, and electrical export to NEG, for Week with Extreme Winter climate

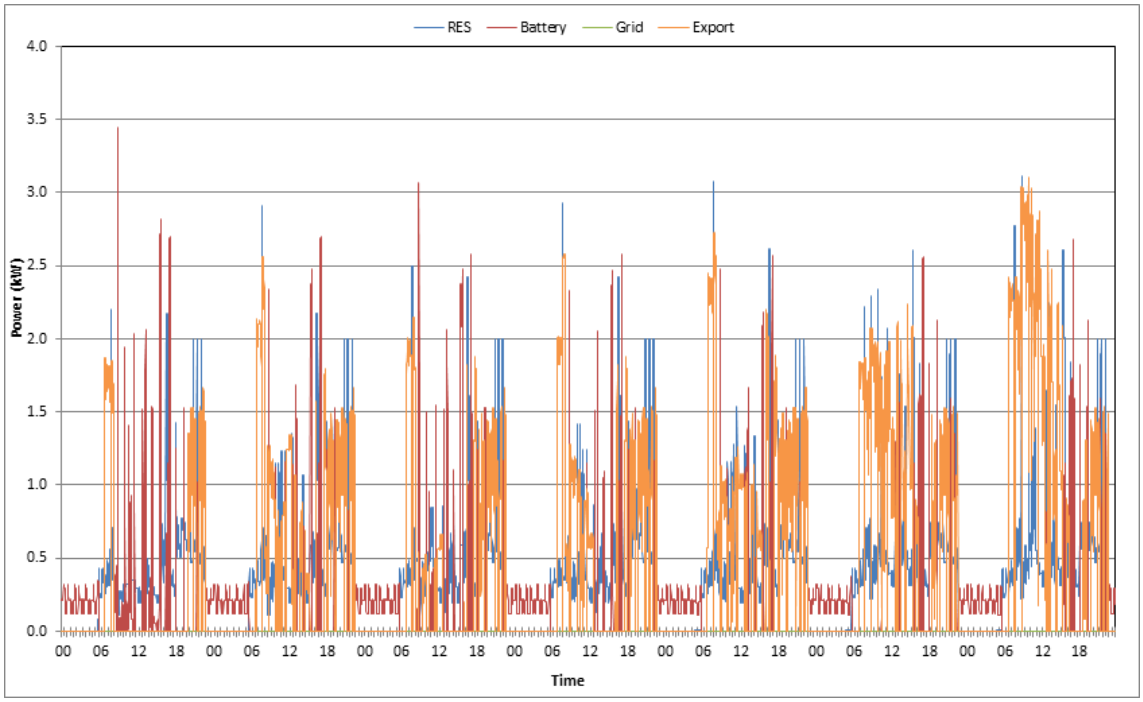

Figure 7.5: Electrical demand satisfied by the RES (SE-CsO-TDP-2kW$_e$-35% µCHP and solar PV), battery storage and NEG import, and electrical export to NEG, for Week with Shoulder climate

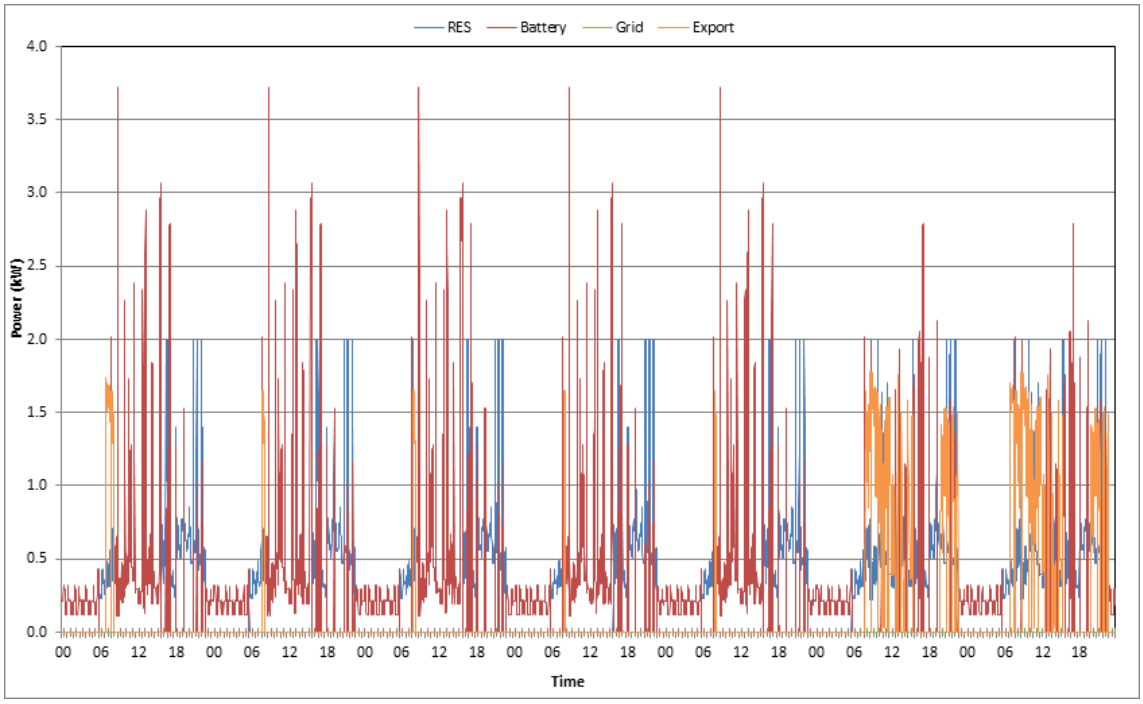

Figure 7.6: Electrical demand satisfied by the RES (SE-CsO-TDP-2kW$_e$-35% µCHP), battery storage and NEG import, and electrical export to NEG, for Week with Shoulder climate

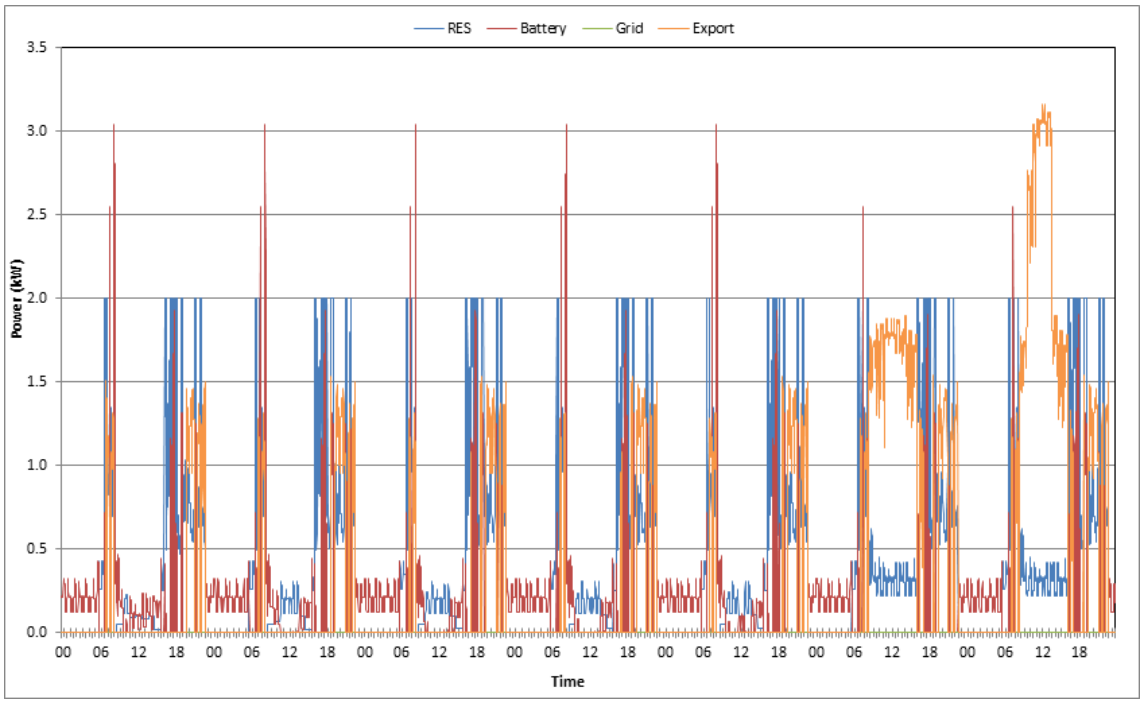

Figure 7.7: Electrical demand satisfied by the RES (SE-CsO-TDP-2kW$_e$-35% µCHP and solar PV), battery storage and NEG import, and electrical export to NEG, for Week with Extreme Winter climate

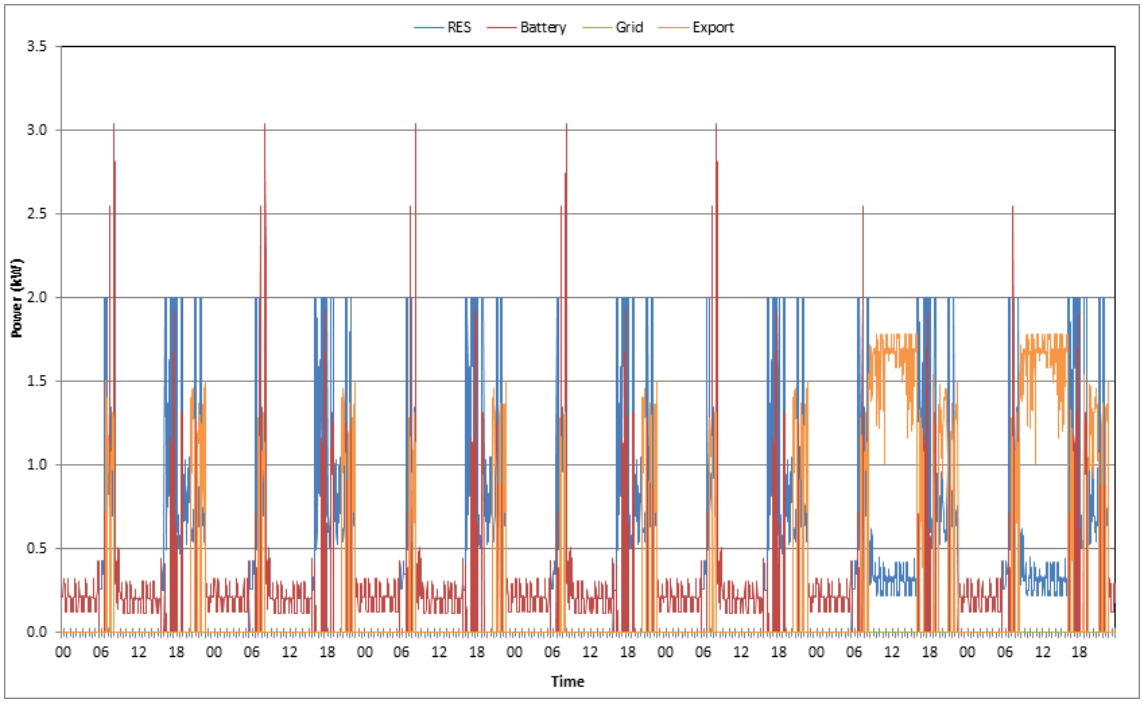

Figure 7.8: Electrical demand satisfied by the RES (SE-CsO-TDP-2kW$_e$-35% µCHP), battery storage and NEG import, and electrical export to NEG, for Week with Extreme Winter climate

The supply and export load profiles for a concurrent weekday and weekend demand scenario are presented in Figure 7.9 to Figure 7.16 for each generation/storage scenario defined in Table 7.1. It is interesting to compare the export profile between systems with and without solar PV, as the electrical export during the day on the weekday increases significantly. Without solar PV, the µCHP system operating under the TLF and CsO-TDP regimes will rely upon battery storage for the majority of the 7.5 hours that elapses between thermal demand periods.

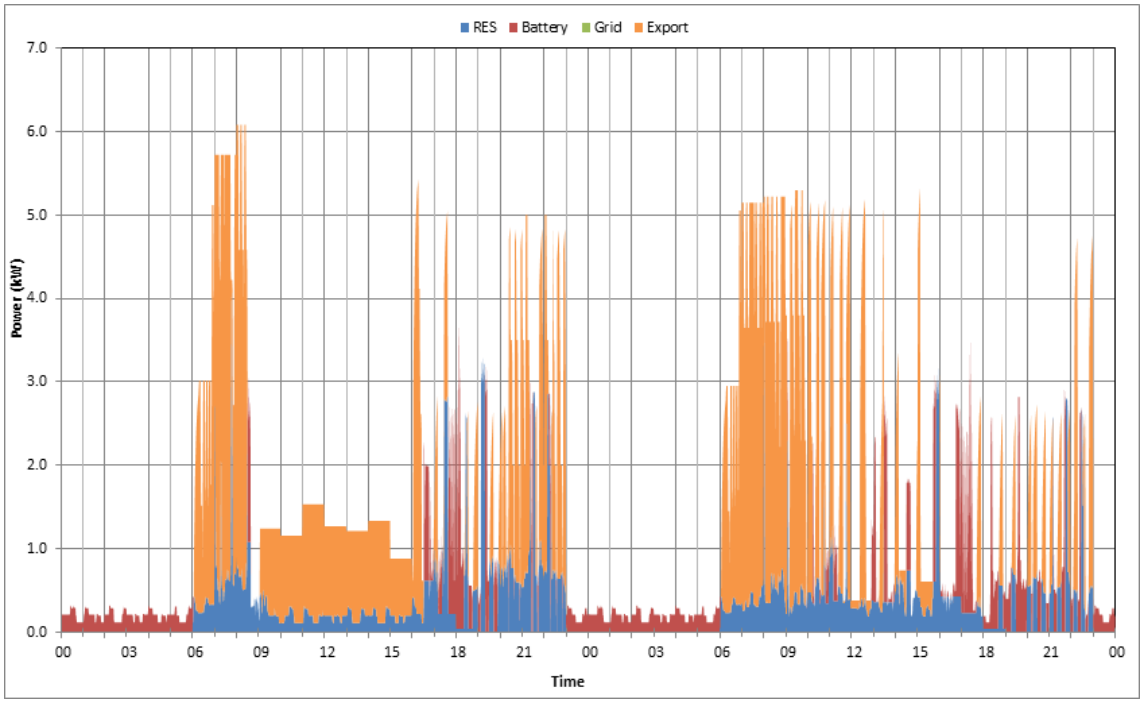

Figure 7.9: Electrical demand satisfied by the RES (SE-TLF-5kWe-35% µCHP and solar PV), battery storage and NEG import, and electrical export to NEG, for Weekday and Weekend day with Shoulder climate

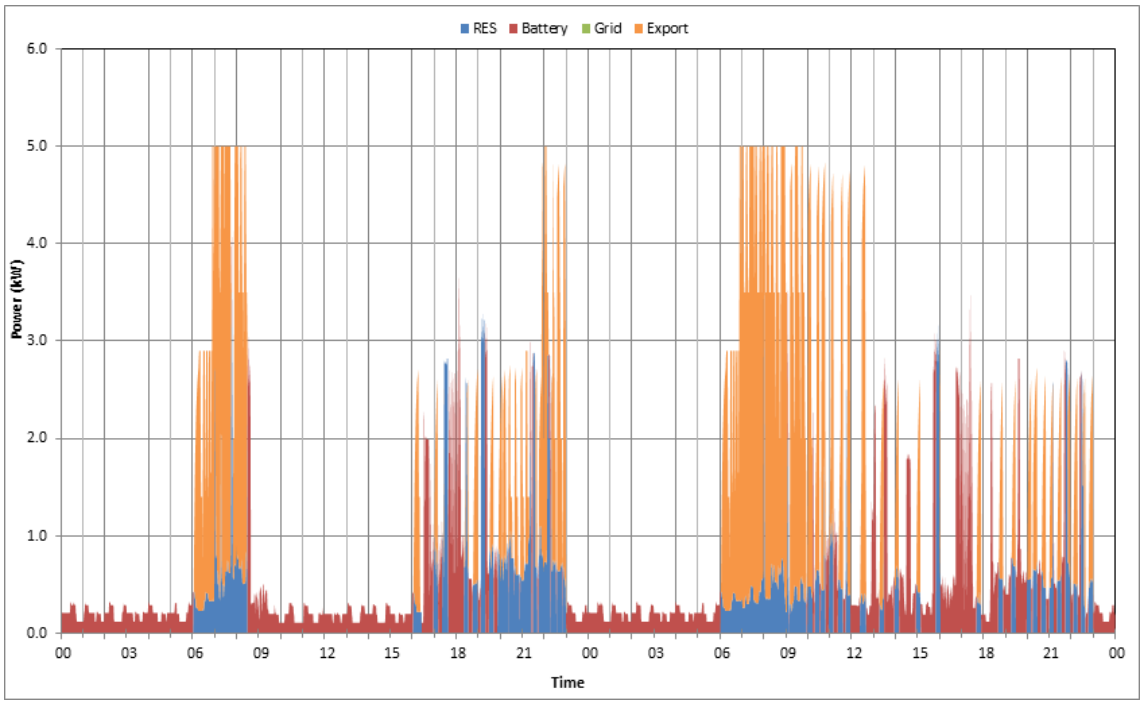

Figure 7.10: Electrical demand satisfied by the RES (SE-TLF-5kWe-35% µCHP), battery storage and NEG import, and electrical export to NEG, for Weekday and Weekend day with Shoulder climate

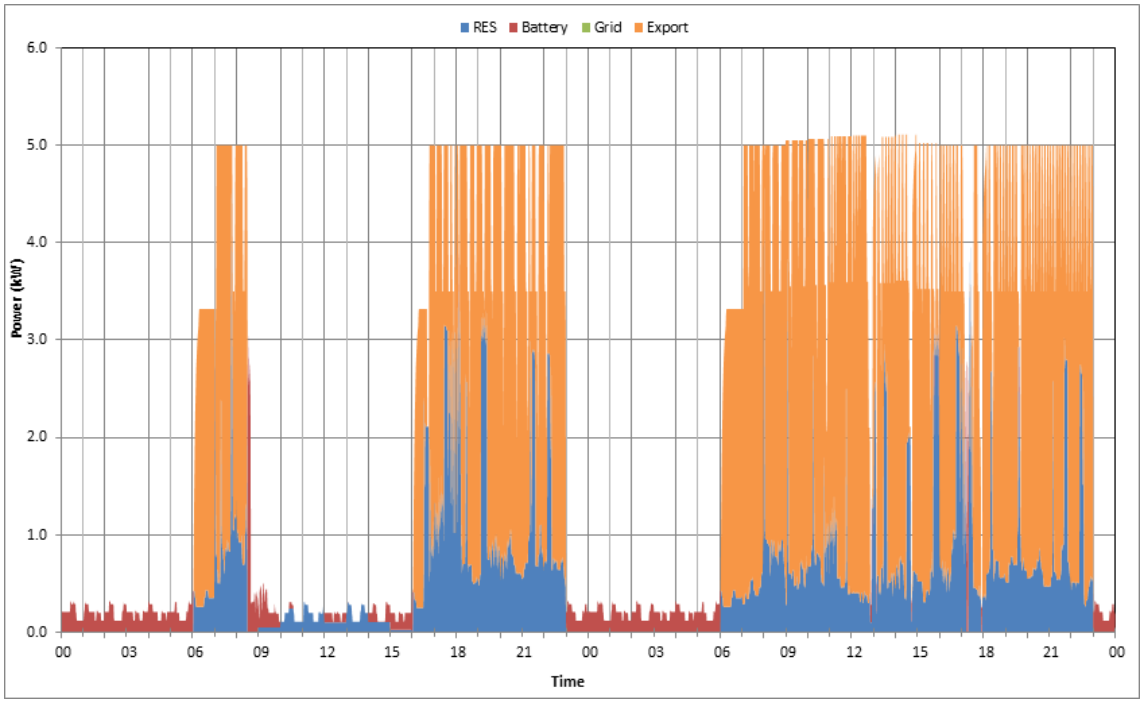

Figure 7.11: Electrical demand satisfied by the RES (SE-TLF-5kWe-35% µCHP and solar PV), battery storage and NEG import, and electrical export to NEG, for Weekday and Weekend day with Extreme Winter climate

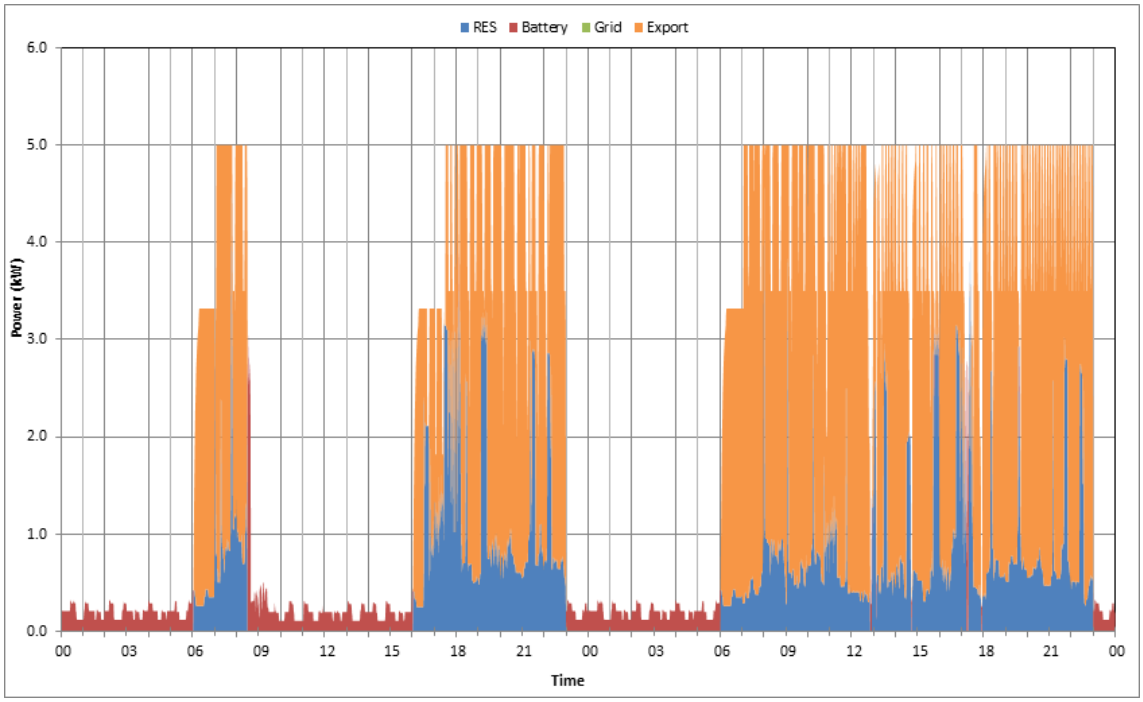

Figure 7.12: Electrical demand satisfied by the RES (SE-TLF-5kWe-35% µCHP), battery storage and NEG import, and electrical export to NEG, for Weekday and Weekend day with Extreme Winter climate

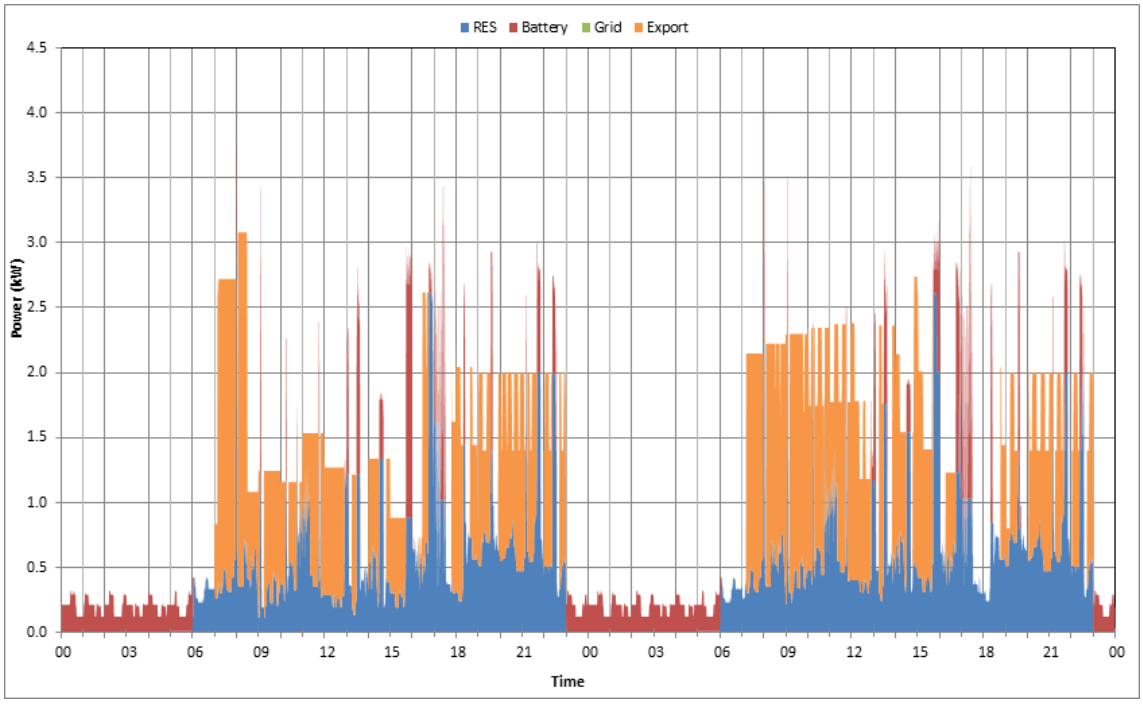

Figure 7.13: Electrical demand satisfied by the RES (SE-CsO-TDP-2kWe-35% µCHP and solar PV), battery storage and NEG import, and electrical export to NEG, for Weekday and Weekend day with Shoulder climate

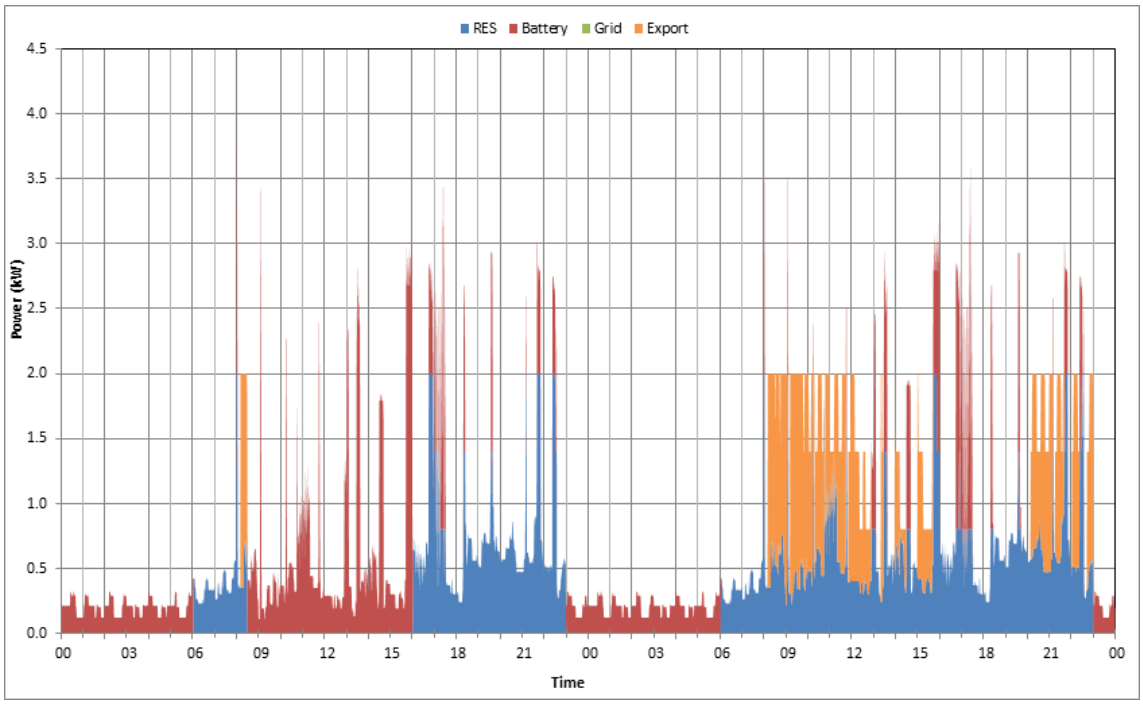

Figure 7.14: Electrical demand satisfied by the RES (SE-CsO-TDP-2kWe-35% µCHP), battery storage and NEG import, and electrical export to NEG, for Weekday and Weekend day with Shoulder climate

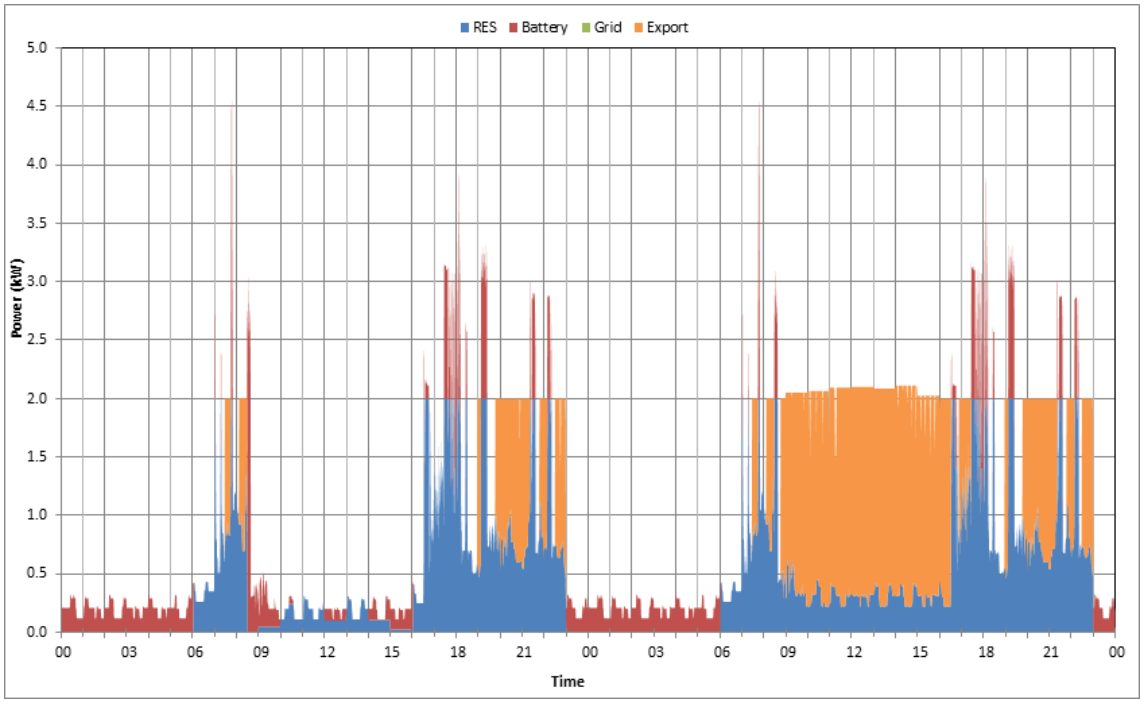

Figure 7.15: Electrical demand satisfied by the RES (SE-CsO-TDP-2kWe-35% µCHP and solar PV), battery storage and NEG import, and electrical export to NEG, for Weekday and Weekend day with Extreme Winter climate

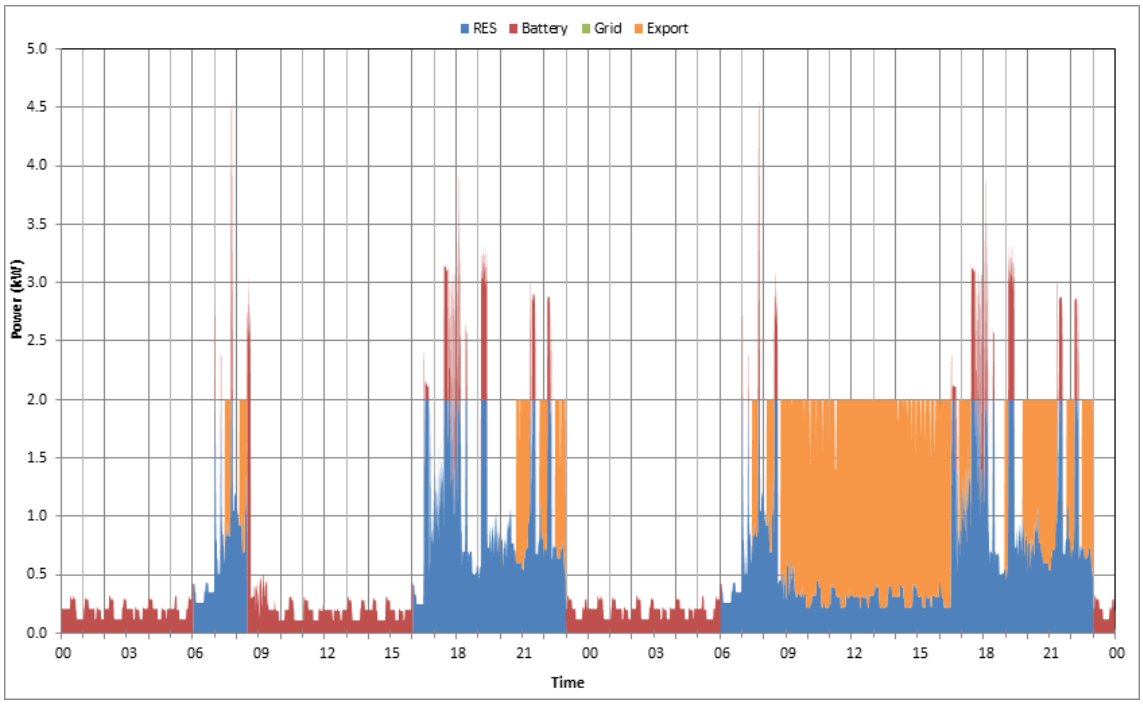

Figure 7.16: Electrical demand satisfied by the RES (SE-CsO-TDP-2kWe-35% µCHP), battery storage and NEG import, and electrical export to NEG, for Weekday and Weekend day with Extreme Winter climate

7.2.4 Discussion of Battery Sizing & Lifetime

Appropriate sizing of the battery system, in terms of both batteries and charge controller, is important to maximise RTE and minimise cost [2]. The maximum charge and rate is limited by charge capacity in the model to ensure reasonably high charge efficiencies. It is not strictly necessary to capture peak output from on-site generation, so long as electrical import is completely displaced. Indeed, capturing more energy than is required (after accounting for storage and re-conversion losses) would serve to decrease RTE, due to standing losses in SoC. The SoC is maintained above 20% to prevent damage due to deep discharge, hence maintaining battery lifetime. Indeed, SoC seldom falls much below 89% during the scenarios assessed. Lead acid batteries, as used in this simulation exercise, whilst relatively cheap, offer relatively low volumetric energy densities. The required storage volume would have to be considered before battery storage could be implemented in a domestic environment.

The characteristics of the battery stores sized for each scenario are presented in Table 7.5. Interestingly, the maximum charge power is significantly less than the total rated power of the dwelling energy system in all but one case (CsO-TDP µCHP without solar PV during Shoulder climate). Whilst the maximum discharge power quoted in Table 7.5 is less than peak demand, the demand peaks occur when the µCHP system is generating electricity, hence no import is required. It should be noted that the battery model used 1-minute profiles for demand and generation. In reality, for the storage system to avoid grid imports, very fast-response capacitive storage would need to be integrated within the charge controller.

Climate	Operating Regime	Design Variant	Solar PV System	Max Battery Capacity (Wh)	Max Charge Power (kW)	Max Discharge Power (kW)	Average Battery SOC (%)
Sh	TLF	5kW$_e$-35%	2.5kWp	500	2.1	4.2	98%
Sh	TLF	5kW$_e$-35%	None	500	2.1	4.2	94%
EWin	TLF	5kW$_e$-35%	2.5kWp	400	1.68	3.36	97%
EWin	TLF	5kW$_e$-35%	None	400	1.68	3.36	96%
Sh	CsO-TDP	2kW$_e$-35%	2.5kWp	450	1.89	3.78	98%
Sh	CsO-TDP	2kW$_e$-35%	None	500	2.1	4.2	91%
EWin	CsO-TDP	2kW$_e$-35%	2.5kWp	400	1.68	3.36	97%
EWin	CsO-TDP	2kW$_e$-35%	None	400	1.68	3.36	95%

Table 7.5: Battery characteristics as selected to completely displace grid imports with average State of Charge (SoC), for a selection of primary demand scenarios and a selection of SE µCHP design varaints operating under TLF or CsO-TDP operating regimes, with and without a Solar PV system

7.3 Hydrogen Storage

7.3.1 Introduction

The concept of storing electricity, as generated on-site by a micro-generation system, has been explored in previous studies [11][12][13][14]. Best & Riffat [11] investigated a µCHP concept incorporating an ORC engine supplied with heat from a solar thermal collector. Excess electricity was then converted to hydrogen and oxygen by electrolysis, which is stored for later recombination in a fuel cell to provide electricity when the solar collector output is low. They discussed the addition of a wind turbine to generate additional electricity, and a gas burner to provide additional heat for the ORC engine. This concept could be adapted for a prime mover primarily or solely fuelled by natural gas, and the wind turbine replaced with other micro-generation technologies, such as solar PV.

Energy storage as hydrogen is a flexible option, as it can be utilised as a prime mover fuel (either by combustion or within a fuel cell), or combusted as a heating or cooking fuel. As discussed in Section 6.4, hydrogen could be co-combusted with natural gas (NG), although there may be limitations with existing combustion appliances and gas

distribution infrastructure. In addition, hydrogen could be stored for transfer into a hydrogen or bi-fuel vehicle.

Converting surplus electricity to hydrogen by electrolysis of water has an inherent efficiency dependent on the full load, part load and transient performance characteristics of the electrolyser, as well as any parasitic loads relating to the storage of hydrogen. Unless the hydrogen is to be immediately mixed into a fuel stream, it is usually compressed for storage, due to the low volumetric energy density of gaseous hydrogen. In this study, a constant electrolyser and storage efficiency of 70% has been considered, although more detailed analysis would require the transient and part load performance characteristics to be defined.

Hydrogen storage was investigated on a weekly and seasonal basis. In the weekly study, the weekly 1-minute export profiles for the SE μCHP, as defined in the previous section, were considered alongside the μCHP system fuel consumption profile. Each timestep, surplus electricity, otherwise exported, is assumed to be converted to hydrogen by a 70% efficient electrolyser. The storage capacity was not fixed, but store extraction (to supply the μCHP system) was fixed based on a maximum hydrogen content of a H_2-NG mixture. Any surplus hydrogen that remains in storage at the end of each week is carried forward into seasonal analysis.

The hydrogen content, by energy, was varied between 18%, 12% and 7%, where the values correspond to 40%, 30% and 20% mixture by volume. Pure hydrogen can be directly utilised by PEM prime movers, improving electrical efficiency as the reformer is not required. As an external combustion engine, Stirling Engines are capable of combusting pure hydrogen, with an appropriate burner design. However, it was outside the scope of this investigation to determine whether a single burner (for the SE) could accommodate a wide range of fuel mixtures from 100% NG to 100% H_2. It is assumed, therefore, that the SE μCHP system and auxiliary boiler would be limited to the 18%, 12% and 7% H_2 mixtures.

A μCHP system incorporating two prime movers could be defined, where the hydrogen fuel supplies a low output, high efficiency PEM-based μCHP system designed to satisfy electrical base-load. To fuel such a system, hydrogen could also be generated from natural gas using a reformer, as typically incorporated in a NG-fired PEM-based μCHP system. The thermal energy required for reformation of NG is typically provided by combustion of off-gas from the PEM stack. However, if thermal energy at a suitable temperature was recovered from a high temperature fuel-cell or engine, then a proportion of the H_2 content in the off-gas could be recovered, increasing electrical efficiency. If this recovered thermal energy was otherwise surplus from the main (as opposed to base-load) prime mover that was controlled by an operating regime that required thermal dumping. The hydrogen storage would de-couple the PEM stack from the reformer, reducing transient performance constraints, increasing load response and part load electrical efficiencies.

The seasonal H_2 storage investigation quantified the capacity of store required to buffer surplus H_2 from shoulder profiles to winter and to summer.

The relative carbon savings (% of base-case CO_2) were quantified with hydrogen storage for each of the SE μCHP scenarios defined in the previous section. This is compared with the reduction in RCS versus the non-storage (export) scenarios. It is expected that due to the difference in carbon intensity between grid electricity (which forms the basis of the EEC) and the fuel displaced by generated hydrogen (i.e. natural gas), that the RCS would be decreased significantly. This reduction in RCS will be further exacerbated by the electrolyser efficiency, which introduces a reduction in stored hydrogen versus electricity available for export or electrolysis.

7.3.2 Weekly Results

The stored energy content of hydrogen for the three fuel mixtures discussed in Section 7.3.1 is compared for each weekly scenario in Figure 7.17 to Figure 7.20. Regardless of scenario, the high H_2 fuel mixture results in negligible storage carried forward to the next week, suggesting that surplus H_2 would not be available for storage and

subsequent use in later seasons. The low H_2 fuel mixture results in significant volumes of H2 carried forward to the next week, regardless of season.

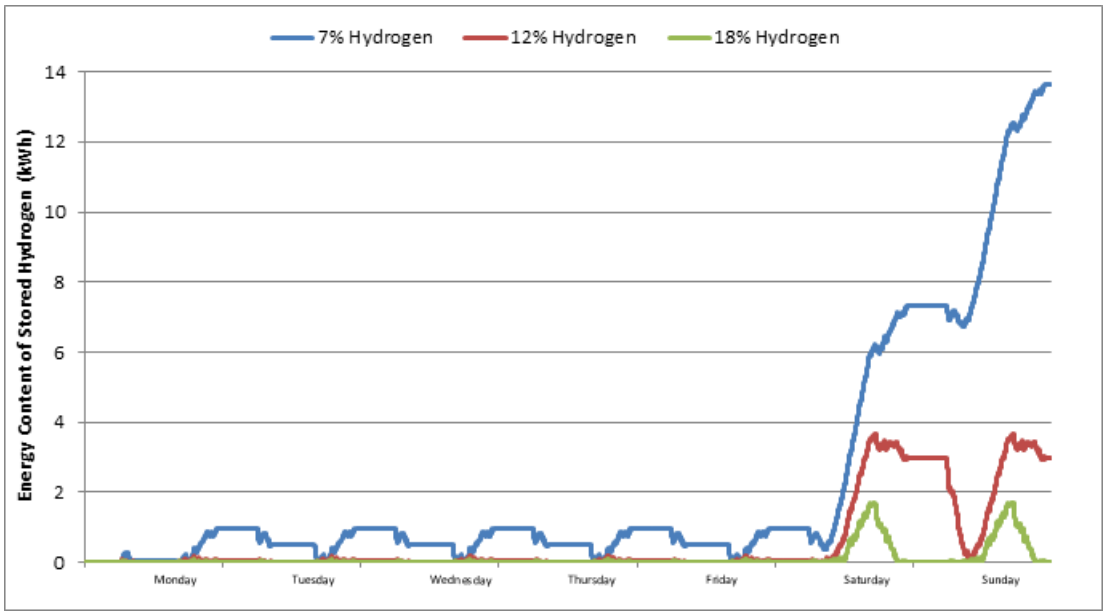

Figure 7.17: Energy Content of Stored Hydrogen (kWh) during Extreme Winter week for 2kW$_e$-35% SE µCHP with CsO-TDP operating regime, comparing limit of hydrogen content (% by energy) within µCHP fuel mixture

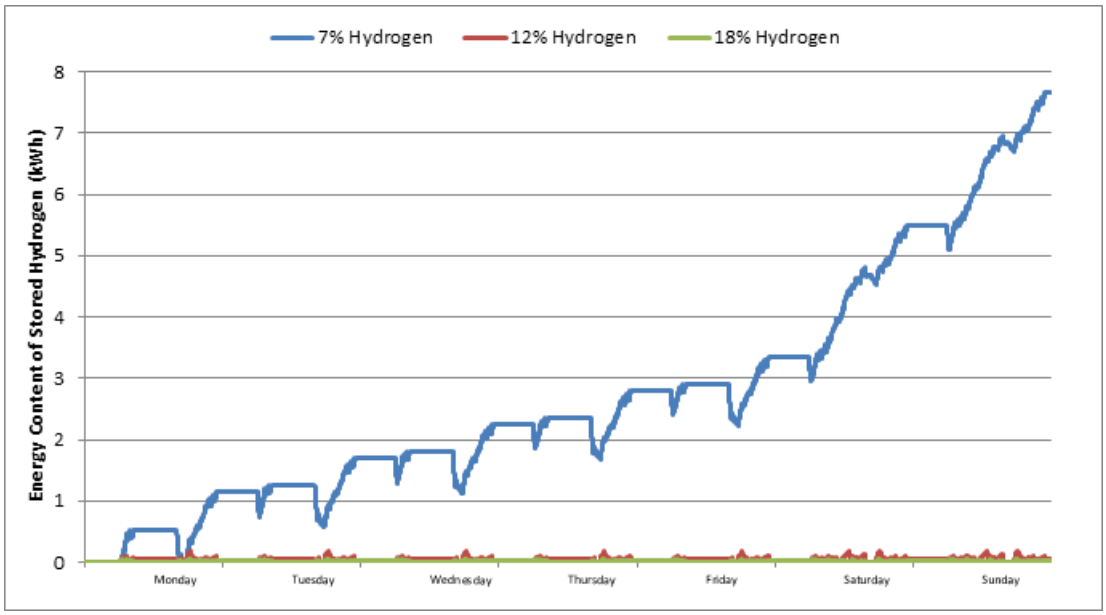

Figure 7.18: Energy Content of Stored Hydrogen (kWh) during Shoulder week for 2kW$_e$-35% SE µCHP with CsO-TDP operating regime, comparing limit of hydrogen content (% by energy) within µCHP fuel mixture

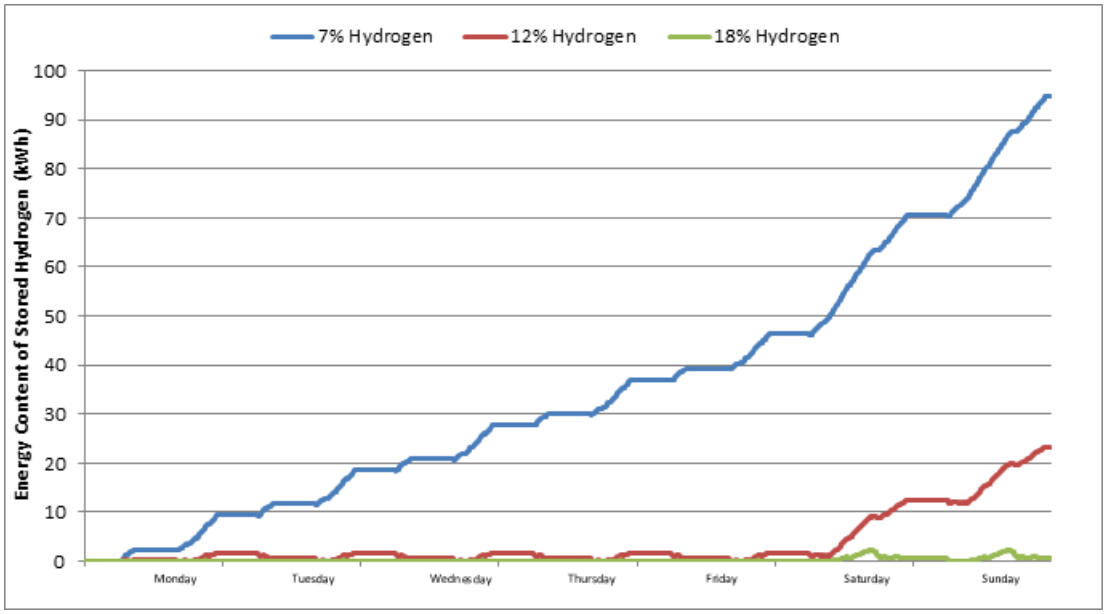

Figure 7.19: Energy Content of Stored Hydrogen (kWh) during Extreme Winter week for 5kW$_e$-35% SE µCHP with TLF operating regime, comparing limit of hydrogen content (% by energy) within µCHP fuel mixture

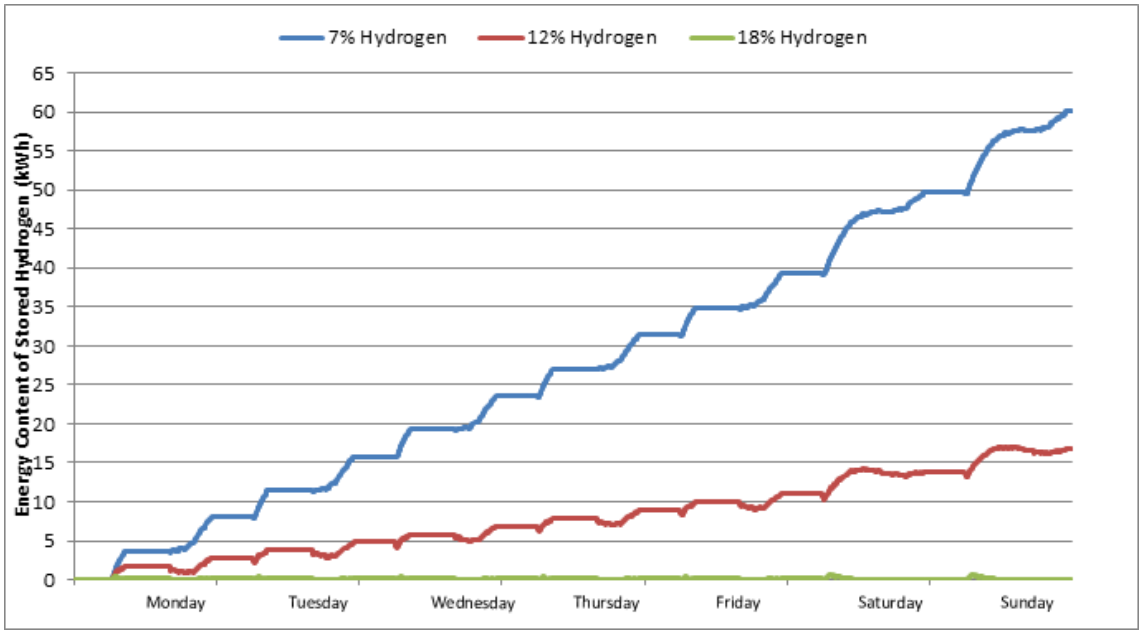

Figure 7.20: Energy Content of Stored Hydrogen (kWh) during Shoulder week for 5kW$_e$-35% SE µCHP with TLF operating regime, comparing limit of hydrogen content (% by energy) within µCHP fuel mixture

The relative carbon savings for the scenarios are compared in Table 7.6 between hydrogen storage and the original case where electrical surplus is exported and EEC is

assigned to the dwelling's carbon footprint. Due to the high reliance of RCS on EEC, as discussed in Sections 4.3.4 and 4.3.6, for the design variants investigated, the RCS is heavily penalised with hydrogen storage. Indeed, in all but one scenario, significant carbon savings are diminished to carbon penalties.

Climate	Operating Regime	Design Variant	RCS with EEC	RCS with H_2 Storage	RCS Difference
Shoulder	TLF	5kW-35%	35%	-16%	-50%
Ex Winter	TLF	5kW-35%	45%	-4%	-49%
Shoulder	CsO-TDP	2kW-35%	21%	-5%	-25%
Ex Winter	CsO-TDP	2kW-35%	17%	1%	-16%

Table 7.6: RCS for selected weekly scenarios compared with and without hydrogen storage

7.3.3 Seasonal Results

As discussed in Section 7.3.2, there is a significant difference in the energy content of hydrogen, at the end of each weekly scenario, depending on the limit on hydrogen content imposed on the µCHP fuel mixture. As seen in Table 7.7, when compared with the µCHP fuel consumption for each weekly scenario, the energy content stored for the 7% and 12% mixtures is almost insignificant. Increasing the mixture of H_2 allowed in the fuel will eventually result in the exhaustion of the hydrogen store by the end of the week, as seen for most scenarios in Table 7.7.

Climate	Operating Regime	Design Variant	Energy Content of Store at End of Week (kWh)			
			7% Hydrogen	12% Hydrogen	18% Hydrogen	µCHP Fuel (kWh)
Shoulder	TLF	5kW-35%	60.1	16.7	0.1	877
Ex Winter	TLF	5kW-35%	94.7	23.4	0.8	1,523
Shoulder	CsO-TDP	2kW-35%	13.6	3.0	0.0	745
Ex Winter	CsO-TDP	2kW-35%	13.6	3.0	0.0	1,300

Table 7.7: Energy content of stored hydrogen at end of each weekly scenario and µCHP system fuel consumption during each weekly scenario

The concept of seasonal storage was studied, where the stored hydrogen from a shoulder season (i.e. autumn) is carried over into winter, or stored hydrogen in winter carried over into spring. The results presented in Table 7.8 show that less than 10% of fuel consumption for the following season would be carried forward from the season

before. The stored energy content of hydrogen would be increased if another micro-generation system, such as the solar PV system studied in Section 7.2, were incorporated in a dwelling energy system.

Climate	Operating Regime	Design Variant	Season Length (Weeks)	Energy Content of Store at End of Season (kWh)			
				7% Hydrogen	12% Hydrogen	18% Hydrogen	µCHP Fuel (kWh)
Shoulder	TLF	5kW-35%	13	781	217	1	11,401
Ex Winter	TLF	5kW-35%	10	947	234	8	15,226
Shoulder	CsO-TDP	2kW-35%	13	177	39	0	9,690
Ex Winter	CsO-TDP	2kW-35%	10	136	30	0	12,997

Table 7.8: Energy content of stored hydrogen at end of each season, based on weekly scenario results, and associated µCHP system fuel consumption during each season

7.4 Discussion & Conclusions

Battery storage was investigated for two µCHP design variants, of different rated electrical output and operating regime, operating under 2 weeks comprising Extreme Winter or Shoulder primary demand scenarios. Home energy system scenarios were investigated where a solar PV system is included, and the batteries were sized to reduce electrical import to zero (although it is assumed capacitive storage would satisfy large peak loads shorter than 5 seconds).

The round-trip electrical losses from the battery system resulted in 20-29% losses (of the energy sent to storage), reducing RCS by 1-5% (of BC CO_2). However, this may be acceptable in situations where electrical export is technically undesirable or financially disadvantageous versus a reduction in electrical import.

The concept of hydrogen storage was explored in Section 7.3, where export electricity was converted to hydrogen by electrolysis. This hydrogen was mixed with natural gas, within 3 potential limits of mixture by volume, to create low-carbon fuel mixtures. This fuel is then used to fuel the prime mover and auxiliary boiler. Under each mixture limit, the energy content of storage hydrogen was simulated for two µCHP design variants operating during the weekly demand scenarios discussed above. Where the

µCHP system can tolerate an 18% mixture of hydrogen content (by energy), negligible hydrogen energy is carried forward at the end of the weekly scenarios. Where hydrogen content is restricted to 7% (by energy), which corresponds with 20% mixture by volume, significant amounts of energy remains in storage at the end of the week.

This energy could be transferred between seasons, i.e. shoulder season into winter or winter into spring, is quantified. However, the results presented in Table 7.8 show that less than 10% of fuel consumption for the following season would be carried forward from the season before. In order to utilise this hydrogen on-site, however, the restriction of maximum H_2 in the fuel mixture would have to be relaxed at some point in time. An alternative would be to inject the excess hydrogen into the national gas network, which could conceivably be preferable (to national grid operators) to electrical export in certain situations. From the perspective of net carbon footprint, however, this would likely be an unattractive option due to the high carbon intensity of grid electricity compared with natural gas. However, as the paradigm of electrical export credit relies upon the assumption that electrical generation, of assumed carbon intensity, will be displaced by this export, export of hydrogen may be appropriate if the exported electricity does not displace central fossil fuel generation.

7.5 References

[1] Jenkins D, Fletcher J and Kane D, A model for evaluating the impact of battery storage on microgeneration systems in dwellings, Energy Conversion and Management 49, 2413-2424, 2008

[2] Jenkins D.P., Fletcher J. and Kane D., Lifetime prediction and sizing of lead-acid batteries for microgeneration and storage applications, IET Renewable Power Generation, 49, 2413-2424, 2008

[3] Z. Kontoutsikos; The Use of Small-scale Photovoltaic Technologies for Satisfying Domestic Electrical Demands; MSc Dissertation; School of Engineering and Physical Sciences, Heriot-Watt University, Edinburgh; September 2007

[4] A.D. Hawkes; Estimating marginal CO2 emissions rates for national electricity systems; Energy Policy; 38; 2010; pp5977–5987

[5] A.D. Peacock, M. Newborough, Controlling micro-CHP systems to modulate electrical load profiles, Energy, Volume 32, Issue 7, July 2007, Pages 1093-1103

[6] C. Pout, R. Hitchin, Apportioning carbon emissions from CHP systems, Energy Conversion and Management, Vol. 46, Issues 18–19, Nov. 2005, pp 2980-2995

[7] Hitchin, E & Pout C; 2002; The carbon intensity of electricity: how many kgC per kWhe?'; Building Services Engineering Research & Technology; 23; 4; pp. 215-222

[8] J. Harrison; The role of Micro-CHP within a decarbonizing energy system; Cogeneration & On-Site Power Production Magazine; Volume 12; Issue 4; pp33-40; 25th July 2011; Access online at http://www.cospp.com

[9] Mott MacDonald, DGCG & DTI; System integration of additional micro-generation (SIAM); September 2004

[10] Ingram S, et al. The impact of small scale embedded generation on the operating parameters of distribution networks, DTI. Report No K/EL/00303/04/01, 2003

[11] F.G. Best, S.B. Riffat, Miniature combined heat and power system, Renewable Energy, Volume 6, Issue 1, February 1995, Pages 49-51

[12] R.G.M. Crockett, M. Newborough, D.J. Highgate, S.D. Probert, Electrolyser-based electricity management, Applied Energy, Volume 51, Issue 3, 1995, pp 249-263

[13] R.G.M Crockett, M Newborough, D.J Highgate, Electrolyser-based energy management: a means for optimising the exploitation of variable renewable-energy resources in stand-alone applications, Solar Energy, Volume 61, Issue 5, November 1997, Pages 293-302

[14] M. Newborough, A.D. Peacock, Micro-generation systems and electrolysers for refuelling private bi-fuel cars at home, International Journal of Hydrogen Energy, Volume 34, Issue 10, May 2009, Pages 4438-4451

8 Conclusions

8.1 Introduction

In this chapter, major conclusions of the research project are summarised, and future research themes are introduced.

8.2 Conclusions

The BIM-G model was developed to investigate the supply:demand matching between µCHP output and thermal and electrical dwelling demand, with 5-second temporal precision, incorporating energy storage devices and adaptable controls. The BIM-G model generates demand profiles using 1-D thermal simulation using finite difference analysis, and bottom-up synthesis of electrical load and casual gains from appliances, lighting & occupants linked to scripts of occupant events.

Carbon Saving Attribution was introduced in Section 4.3.4 as a novel µCHP performance analysis methodology, with specific investigation of several constituent values:

- Thermal Generation Displacement, whose interaction with design variants and relative carbon savings is investigated in Section 4.3.5
- Electrical Import Displacement and Electrical Export Credit, whose interaction with design variants and relative carbon savings is investigated in Section 4.3.6
- Additional Fuel Consumption of prime mover versus base-case energy system (which is a carbon penalty)

Potential Thermal Supply:Demand Ratio of prime movers was introduced in Section 4.3.5 as a metric to describe the matching of prime mover thermal capacity to thermal demand. The relationship between PTSDR and relative carbon savings, and the attribution of RCS, suggests that PTSDR would be useful in the specification and design of a µCHP for a known annual thermal demand. The largest values of RCS, within a set of prime mover design variants, occurs when the value of PTSDR is between 0.5-1.5.

The RCS (as both an absolute and specific value) increases as thermal demand increases. However, even with increased thermal demand, it is important to match the thermal output of the prime mover with the demand to maximise RCS. In Chapter 5, the concept of effective carbon intensity of μCHP-generated electricity was introduced as a means of understanding the impact of thermal dumping on RCS. The study concluded that, for the μCHP design variants investigated, auxiliary fuel consumption needs to be displaced by a minimum of 59% of the net electrical energy generated in order to achieve a positive RCS. However, if net electrical efficiency was increased above 44.2%, thermal output need not be used for the μCHP to provide relative carbon savings.

In order to improve μCHP annual RCS and prime mover lifetime, several control approaches were studied. Restricted Seasonal Operation, which restricts prime mover operation during non-heating season (High Summer climate scenario), or during all low thermal demand days (High Summer and Summer climate scenarios), was applied to avoid operation of the prime mover when relative carbon savings are negative or when the frequency of thermal cycling is high (with limited benefit to CO_2 savings). Restricted operation had the added benefit of reducing annual operating duration, which would increase lifetime, and potentially reduce maintenance requirements.

Options to store excess electrical energy, otherwise exported to the NEG, were investigated in Chapter 7, including lead acid batteries and production of hydrogen by electrolysis for later use as a fuel. However, the penalties involved in storage had a significant impact on RCS for the investigated design variants. This was expected, as the top-performing design variants were found to rely heavily on the assumption that export electricity displaces centrally-generated electricity with the same carbon intensity.

Alternative Operating Regimes were defined and investigated for SE-based μCHP systems in Chapter 5, namely:

- Continuous Operation over Thermal Demand Periods (CsO-TDP)

- Continuous Operation over Daily Demand Periods (CsO-DDP)
- Continuous Operation over 24 hours (CsO-24hr)
- Constant Output (CtO)

The impact of these operating regimes on RCS is varied across the design variants, however CsO-TDP is the only regime where increased RCS are reported for any design variant. As with the Thermal Load Following operating regime, maximum RCS corresponds with a range of PTSDR values approximately between 0.5-1.5. All operating regimes provide a significant reduction in thermal cycling, which would increase prime mover lifetime despite the significant increase in cumulative annual operating duration.

The effect of combining operating regimes on a seasonal basis was investigated for selected design variants. Marginal increases in RCS and marginal reductions in thermal cycling frequency were reported for some (but not all) design variants, suggesting that such control methodologies are sensitive to the matching of design variants to thermal demand.

The effective carbon intensity study suggests that a high η_e prime mover using the Constant Output operating regime, coupled with sufficient thermal storage, could provide relative carbon savings. In contrast to other operating regimes, the lack of modulation and frequent thermal cycling avoids performance and lifetime penalties that were identified with certain fuel cell technologies.

The various studies presented in this thesis attest that both relative carbon savings from μCHP systems, and prime mover lifetimes, are sensitive to the matching of supply and demand. Changing operating regimes or control approaches alters the relationship between potential thermal supply and thermal demand, where matching thermal energy is essential under the paradigm of full carbon credit for electrical export. The results suggest that designs of Stirling Engine-based μCHP systems need to achieve a rated η_e of almost 30% before they will achieve significant (>10%) relative carbon savings. Indeed, μCHP systems with lower η_e, or a rated thermal output that is poorly

matched to thermal demand, are likely to achieve very modest or negative savings. Advocating μCHP systems of such designs is likely to increase the carbon footprint of the dwelling (despite any financial savings that can be made), and therefore future legislative or regulatory measures that prohibit such installations should be enforced.

Encouragingly, this investigation suggests that relative carbon savings over 23% could be achieved by a SE prime mover of 35% rated net electrical efficiency, after selecting the appropriate rated electrical output and applying a combined operating regime. In order to achieve substantial relative carbon savings, a Stirling Engine prime mover with exceptionally high (in the context of SE technology) net electrical efficiency would be required.

8.3 Future Research

A number of research themes have been identified, during the execution of this doctoral project, which would merit investigation in the future.

The BIM-G model could be applied to the investigation of other micro-generation technologies in conjunction with storage technologies, including:

- Hydrogen as a means of storing excess electrical generation from on-site renewables (e.g. solar PV and micro-wind) that would otherwise be exported, where the hydrogen is used to decarbonise the boiler and cooking fuel source
- Integration of on-site renewable electricity generation with electrical heat pump, and potentially battery storage, as a means of utilising electrical export to satisfy thermal demand

The investigation of alternative prime movers, utilising technologies such as fuel cells, with the associated improvements in electrical efficiencies, and challenges related to start-up profiles and thermal cycle limitations. It is suggested that the following themes be investigated in the future:

- Investigate other prime movers in detail, especially with regards to start & stop profiles for fuel cells

- Investigate fuel cell prime movers with de-coupled operation of fuel cell and reformer, i.e. incorporating a hydrogen buffer vessel
- Investigate the 'Constant Operation' operating regime for prime movers with higher electrical efficiencies than those studied in this project, identifying the magnitude of thermal dumping for various prime mover electrical capacities, and its effect on effective carbon intensity of generated electricity
- Investigate dual prime movers within a μCHP system, of similar or different technologies, where a low P_e prime mover is controlled to meet the base-load, and another responds to periods of increased demand

Control changes, and especially control flexibility throughout the seasons, may present a major opportunity to increase carbon savings from μCHP systems, as they already do for traditional thermal generation technologies. Among the control changes for future investigation are:

- Investigate control system techniques to optimise performance during restricted operation regimes
- Investigate optimised start controller, to optimise start time of space heating to minimise auxiliary boiler operation
- Investigate whether compensation control techniques for space heating, where space heating flow temperature is adjusted to optimise efficiency of operation
- Investigate thermal store control techniques, perhaps incorporating weather compensation for storage temperature

The impact of temporal precision (of the modelling and simulation technique) on the reported relative carbon savings and frequency of prime mover thermal cycling could be investigated in subsequent research. If temporal precision cold be relaxed (versus the 5 seconds used by the BIM-G model), this would reduce the challenges with synthesising or recording demand data when analysing a range of demand scenarios.

Thermal storage is essential in order to maximise prime mover run-time or useful recovery of thermal output for space heating and DHW purposes. Some topics to

consider for future research on the improved carbon savings due to alternative thermal storage are listed below:

- Investigate multiple thermal storage vessels, to provide flexible storage capacity across the seasons, minimising standing losses
- Investigate alternative thermal storage options, such as phase change materials
- Investigate reformer and hydrogen storage as a means of utilising excess thermal output to generate carbon-free fuel for prime mover from natural gas, as either for direct use with fuel cell, or mix with natural gas for combustion

The effect of thermal demand on µCHP performance and lifetime has been discussed at length in this thesis. However, future research could consider the following:

- Investigate the performance and lifetime of prime movers on the basis of altered shape of thermal demand profiles, due to factors such as:
    - Alternative occupants
    - Alternative occupancy patterns
    - Alternative thermal demand periods
    - Switch of shower DHW supply from thermal store to electric showers
- Investigate effect of thermal demand on alternative operating regimes and prime movers
- Investigate the potential for prime movers to displace auxiliary thermal generation under different thermal demand scenarios, expanding on the relationship between PTSDR and "% of thermal generation displacement" explored in Section 4.3.5

In the wider context of financial viability of µCHP operation, and potential effects on NEG due to export power flows, the potential to reduce electrical export from µCHP without significantly reducing CO_2 savings or lifetime should be studied. This could entail to investigation of operating regimes and control techniques that respond to both thermal and electrical demand.

Appendix A Household Definition Study

A.1 Appendix Overview

This appendix is a reformatted version of the internal report produced by the student for the TARBASE project. This report was titled “Vector Classification of Households - Analysis of the UK General Household Survey”, and was originally distributed in April 2005.

A.2 Report Abstract

This report details the work undertaken to classify the households described in the UK Government’s General Household Survey 2002-2003. The purpose of these classifications is identified in the context of the overall goal of Occupancy Classifications. The final vector classification system created in this exercise was used to produce a list of the 18 most prevalent household classifications, which jointly cover 90.31% of UK households.

A.3 Background

The General Household Survey (GHS) is a yearly survey commissioned by the Office of National Statistics (ONS). The remit of the work is to survey households (and their members) who cumulatively cover a spectrum of racial, economic, social and geographical locations. Although the GHS covers England, Scotland and Wales, the Scottish Executive commissions a similar survey for the confines of Scotland – the Scottish Household Survey (SHS).

A.4 Survey Details

The GHS data, which is available for download from the “UK Data Archive” (www.data-archive.ac.uk), is available as a Tab Delaminated file, which can be opened and manipulated with Excel. The dataset contains four files, two of which are not of interest, as they cover views on local authorities and details on sport and leisure activities. The two files which were analysed are detailed in Table A.1.

File Name	Description	No. of Records	No. of Fields	Key Field(s)
ghs02clienthhld	Household records, with details of Household Reference Person (HPR)	8620	203	HSerial
ghs02client	Individual records, detailing each person in every household described in file above	20149	1460	HSerial PersNo

Table A.1: General household Survey data files analysed, with key field names, and indicated quantity of records and fields

The "Household Serial Number" (HSerial) is common to both files, and therefore used to identify the records in "ghs02client" that corresponded to a record in "ghs02clienthhld".

The survey results are weighted, so that each record represents a proportion of the population, as estimated from the national census information. It is the weighted results (in the "Weight02" field) which are of interest to this report.

A.5 Data Analysis Goals

The objective of this exercise was to classify households – by size, composition and occupancy. In order to swiftly and accurately analyse the GHS data, a loose plan was drawn up. Further research into analysis methods necessitated an overhaul of this plan – in order to improve on accuracy – and it is the revised method which is detailed in this report.

Through data analysis, we sought to achieve the following goals:

1. Summarize the Number of HH's in "ghs02client" which match every available combination of Number of Adults and Number of Adults, producing 'Full HH Size & Composition Categories'.
2. Reduce 'Full HH Size & Composition Categories' to 'Selected HH Size & Composition Categories'.
3. Filter the data in "ghs02client" to include only those who are 'Out of HH'.
4. Produce results for all occupancy ratios of all 'Selected HH Size & Composition Categories'.
5. Reduce results to 'Final HH Size & Composition Categories'.

6. Produce "Vector System of HH Occupancy Classification" and summarize Number of HH's in each Vector category.

A.6 Data Analysis & Results

A.6.1 Analysis Step 1

As the "ghs02client" data file had too many fields for either MS Access or MS Excel to import, it was necessary to select which fields were imported. A total of 33 fields were imported, although many of these are intended for future use. Table A.2 details the fields analysed at this time:

Field Name	Description
Hserial	Household Serial Number
PersNo	Person Number within HH
NumAdult	Number of Adults in HH
NumChild	Number of Children in HH
Weight02	Weighting of Person's response towards national total
EcstILO	Harmonised Economic Status (Inland Revenue Office definitions)

Table A.2: Fields analysed from "ghs02client" data file during investigation

A query in MS Access produced the sum totals of "Weight02" of every combination of "NumAdult" & "NumChild" – producing 'Full HH Size & Composition Categories', shown in Table A.3. The "HH Weight" is calculated using equation (A.1).

$$\text{HH Weight} = \text{Weight02} / (\text{NumAdult} + \text{NumChild}) \quad \text{(A.1)}$$

Full HH Category	NumAdult	NumChild	No. of People	No. of HH's	% of National HH Total
a	1	0	7,535,771	7,535,771	30.72%
b	1	1	1,551,569	775,784	3.16%
c	1	2	1,366,591	455,530	1.86%
d	1	3	578,024	144,506	0.59%
e	1	4	239,140	47,828	0.19%
f	1	5	31,372	5,229	0.02%
g	1	6	19,758	2,823	0.01%
h	2	0	15,585,655	7,792,828	31.77%
i	2	1	5,162,932	1,720,977	7.02%
j	2	2	7,051,225	1,762,806	7.19%
k	2	3	2,374,853	474,971	1.94%
l	2	4	613,740	102,290	0.42%
m	2	5	212,636	30,377	0.12%
n	2	6	53,432	6,679	0.03%
o	2	7	19,295	2,144	0.01%
p	3	0	5,061,247	1,687,082	6.88%

q	3	1	2,183,589	545,897	2.23%
r	3	2	1,056,972	211,394	0.86%
s	3	3	331,772	55,295	0.23%
t	3	4	61,627	8,804	0.04%
u	3	5	78,931	9,866	0.04%
v	3	6	56,342	6,260	0.03%
w	3	7	19,435	1,944	0.01%
x	4	0	2,673,875	668,469	2.73%
y	4	1	776,336	155,267	0.63%
z	4	2	301,309	50,218	0.20%
aa	4	3	149,196	21,314	0.09%
ab	4	4	25,485	3,186	0.01%
ac	5	0	704,179	140,836	0.57%
ad	5	1	185,078	30,846	0.13%
ae	5	2	73,931	10,562	0.04%
af	5	3	20,624	2,578	0.01%
ag	6	0	155,404	25,901	0.11%
ah	6	1	64,583	9,226	0.04%
ai	7	0	47,217	6,745	0.03%
aj	7	1	28,170	3,521	0.01%
ak	7	3	57,884	5,788	0.02%
al	8	0	32,298	4,037	0.02%
am	8	1	28,918	3,213	0.01%
		Totals	56,570,394	24,528,793	100.00%

Table A.3: HH Size & Composition Categories, indicated by quantity of resident adults and children, using weighting factors to calculate the quantity of people and households within each category, with percentage of national total of households within each category

A.6.2 Analysis Step 2

By elimination of marginal categories, a table of 'Selected HH Size & Composition Categories' was produced, as shown in Table A.4.

Category	NumAdult	NumChild	% of HH's	No. of HH's
A	1	0	30.72%	7,535,771
B	1	1	3.16%	775,784
C	1	2	1.86%	455,530
D	2	0	31.77%	7,792,828
E	2	1	7.02%	1,720,977
F	2	2	7.19%	1,762,806
G	2	3	1.94%	474,971
H	3	0	6.88%	1,687,082
I	3	1	2.23%	545,897
J	3	2	0.86%	211,394
K	4	0	2.73%	668,469
L	4	1	0.63%	155,267
		Totals	**96.97%**	**23,786,778**

Table A.4: Household Size & Composition Categories selected for further investigation

A.6.3 Analysis Step 3

The "ghs02client" file was filtered in MS Access, to include only those persons who could reasonably be assumed to be vacant from the home for regular periods on weekdays. The variables defined in the "EcstILO" field that were selected by the filter are presented In Table A.5.

Variable Code	Description
1	Working (including Unpaid)
2	Government School with Employment
3	Government School at College
9	Student

Table A.5: Variables selected from "EcstILO" field in "ghs02client" file to represent people reasonable expected to be absent from the home for regular periods on weekdays

A.6.4 Analysis Step 4

The filtered data was then split by NumAdult and exported to MS Excel, where logic routines were added to separate HH's with different ratios of vacant-to-present adults. The weighting was sub-totalled for each ratio, and the results used to produce the following tables of 'Selected HH Size & Composition Categories':

Cat.	Num Adult	Num Child	No. HH's	0 Present	1 Present	2 Present	3 Present	4 Present
A	1	0	7,535,771	3,282,233	4,253,538			
B	1	1	775,784	480,620	295,165			
C	1	2	455,530	260,435	195,095			
D	2	0	7,792,828	3,476,519	1,517,516	2,798,792		
E	2	1	1,720,977	1,106,503	499,860	114,614		
F	2	2	1,762,806	1,208,395	477,067	77,345		
G	2	3	474,971	257,703	183,280	33,988		
H	3	0	1,687,082	828,658	415,233	306,104	137,087	
I	3	1	545,897	319,999	167,883	50,854	7,161	
J	3	2	211,394	90,701	80,639	33,374	6,681	
K	4	0	668,469	367,935	131,432	116,148	29,258	23,696
L	4	1	155,267	64,521	44,421	31,401	11,877	3,047
		Totals	23,786,77	11,744,22	8,261,129	3,562,619	192,063	26,743

Table A.6: Selected HH Size & Composition Categories, with quantities of resident adults and children, and number of UK households which each day-time occupancy level relates to for each household Size & Composition category

Cat.	Num Adul	Num Child	No. HH's	0 Present	1 Present	2 Present	3 Present	4 Present
A	1	0	30.72%	13.38%	17.34%			
B	1	1	3.16%	1.96%	1.20%			
C	1	2	1.86%	1.06%	0.80%			
D	2	0	31.77%	14.17%	6.19%	11.41%		
E	2	1	7.02%	4.51%	2.04%	0.47%		
F	2	2	7.19%	4.93%	1.94%	0.32%		
G	2	3	1.94%	1.05%	0.75%	0.14%		
H	3	0	6.88%	3.38%	1.69%	1.25%	0.56%	
I	3	1	2.23%	1.30%	0.68%	0.21%	0.03%	
J	3	2	0.86%	0.37%	0.33%	0.14%	0.03%	
K	4	0	2.73%	1.50%	0.54%	0.47%	0.12%	0.10%
L	4	1	0.63%	0.26%	0.18%	0.13%	0.05%	0.01%
		Totals	96.97%	47.88%	33.68%	14.52%	0.78%	0.11%

Table A.7: Selected HH Size & Composition Categories, with quantities of resident adults and children, and percentage of total UK households which each day-time occupancy level relates to for each household Size & Composition category

A.6.5 Analysis Step 5

Those cells in Table A.7 that are darkened out were disregarded in the creation of the 'Final HH Size & Composition Categories'. **The percentage of households covered by the final categories is 90.31%.**

A.6.6 Analysis Step 6

A vector system to classify each category was designed, based upon three variables: x, y and z, combining to produce a vector (x,y,z). Details of these variables are given in Table A.8.

Variable	Description	Values
X	Number of Adults vacant from home for regular intervals on weekdays. Duration, Start & Stop Times will fall randomly with predetermined ranges.	0, 1, 2, 3 or 4
y	Number of Adults present in home continually on weekdays. Short vacancies from the home, of random duration, will fall at random.	0, 1 or 2
z	Number of Children vacant from home for regular intervals on weekdays. Duration, Start & Stop Times will fall randomly with predetermined ranges. Any model will account for term time variation by emulating behaviour of the 'y' Variable.	0, 1, 2 or 3

Table A.8: Description of each variable within the vector for classifying households, as design during this investigation and discussed in this section

Table A.9 lists all the permutations taken forward by the "Vector System of HH Occupancy Classification".

Vector (x,y,z)	% HH's
(1,0,0)	13.38%
(2,0,0)	14.17%
(3,0,0)	3.38%
(4,0,0)	1.50%
(0,1,0)	17.34%
(0,2,0)	11.41%
(1,1,0)	6.19%
(1,2,0)	1.25%
(2,1,0)	1.69%
(1,0,1)	1.96%
(1,0,2)	1.06%
(2,0,1)	4.51%
(2,0,2)	4.93%
(2,0,3)	1.05%
(3,0,1)	1.30%
(0,1,1)	1.20%
(1,1,1)	2.04%
(1,1,2)	1.94%
Totals	**90.31%**

Table A.9: All permutations of households identified in this investigation, defined by vector classification (a concept discussed in the previous section), that were subsequently considered for bottom-up domestic demand research as art of the TARBASE project

A.7 Conclusions

The objective of this exercise was to produce a classification system (and list of most common classifications) for UK household size, composition and occupancy. The source data was the UK General Household Survey, as published by the Office of National Statistics.

A vector classification system has been produced, which is based upon three predefined variables; x, y & z. Using this vector system, 18 classification "Vectors" have been identified, which cover 90.31% of UK households (according to GHS weighting).

A.8 Further Work

There are two suggestions at present for future work that would expand upon this exercise.

- Examine the Scottish Household Survey and the location parameters of the General Household Survey (UK Wide), in order to examine regional variations in HH size, composition & occupancy
- Examine projections on the GHS, to predict HH size, composition & occupancy through to 2030 – the reach of the Carbon Vision projects

A.9 References

General Household Survey 2002 -2003: Datafiles, Data Dictionaries & User Guide

Appendix B Demand Profile Event Scripting Assumptions

B.1 Appendix Overview

In this appendix, a selection of the assumptions underpinning the event scripting for demand profile synthesis are presented.

B.2 Common to all Demand Profiles

B.2.1 Weekday Occupancy

Sig ID	Type	Weekday - Occupant			
		1	2	3	4
Sleeping	*Start*	23:00:00	23:00:00	23:00:00	22:00:00
	Stop	07:00:00	07:00:00	07:00:00	07:30:00
	Duration	08:00:00	08:00:00	08:00:00	09:30:00
Vacant	*Start*	08:15:00	08:30:00	07:30:00	08:30:00
	Stop	17:45:00	16:30:00	17:15:00	16:30:00
	Duration	09:30:00	08:00:00	09:45:00	08:00:00
Active (1)	*Start*	07:44:00	08:16:00	07:16:00	~
	Stop	07:54:00	08:26:00	07:26:00	~
	Duration	00:10:00	00:10:00	00:10:00	~
Active (2)	*Start*	21:17:00	16:30:00	~	~
	Stop	21:22:00	18:15:00	~	~
	Duration	00:05:00	01:45:00	~	~
Active (3)	*Start*	~	~	~	~
	Stop	~	~	~	~
	Duration	~	~	~	~

B.2.2 Weekend Occupancy

Sig ID	Type	Weekend - Occupant			
		1	2	3	4
Sleeping	*Start*	23:00:00	23:00:00	23:00:00	22:30:00
	Stop	07:00:00	07:30:00	08:00:00	08:00:00
	Duration	08:00:00	08:30:00	09:00:00	09:30:00
Vacant	*Start*	10:00:00	13:30:00	18:30:00	13:30:00
	Stop	11:30:00	15:30:00	21:30:00	15:30:00
	Duration	01:30:00	02:00:00	03:00:00	02:00:00
Active (1)	*Start*	07:59:00	13:20:00	15:30:00	~
	Stop	08:09:00	13:30:00	15:40:00	~
	Duration	00:10:00	00:10:00	00:10:00	~
Active (2)	*Start*	12:30:00	16:40:00	21:30:00	~
	Stop	13:30:00	17:40:00	21:40:00	~
	Duration	01:00:00	01:00:00	00:10:00	~
Active (3)	*Start*	14:25:00	10:40:00	~	~
	Stop	14:45:00	11:25:00	~	~
	Duration	00:20:00	00:45:00	~	~

B.2.3 DHW Event Scripting

Bathroom Hand Washing Draw-Offs				
Event	**Weekday** t_{Event_Start}	**Weekday** t_{Event_Stop}	**Weekend** t_{Event_Start}	**Weekend** t_{Event_Stop}
1	07:01:00	07:02:00	07:24:00	07:25:00
2	07:16:00	07:17:00	07:54:00	07:55:00
3	07:27:00	07:28:00	08:49:00	08:50:00
4	07:55:00	07:56:00	09:24:00	09:25:00
5	16:49:00	16:50:00	10:56:00	10:57:00
6	18:57:00	18:58:00	12:27:00	12:28:00
7	19:43:00	19:44:00	13:11:00	13:12:00
8	20:28:00	20:29:00	14:37:00	14:38:00
9	22:58:00	22:59:00	16:51:00	16:52:00
10	22:49:00	22:50:00	18:34:00	18:35:00
11	21:56:00	21:57:00	20:18:00	20:19:00
12	~	~	21:56:00	21:57:00
13	~	~	22:49:00	22:50:00
14	~	~	22:58:00	22:59:00
15	~	~	08:22:00	08:23:00
16	~	~	20:34:00	20:35:00

Kitchen Hand Washing Draw-Offs				
Event	**Weekday** t_{Event_Start}	**Weekday** t_{Event_Stop}	**Weekend** t_{Event_Start}	**Weekend** t_{Event_Stop}
1	07:26:00	07:27:00	08:01:00	08:02:00
2	07:45:00	07:46:00	08:11:00	08:12:00
3	07:51:00	07:52:00	09:05:00	09:06:00
4	07:57:00	07:58:00	09:16:00	09:17:00
5	08:03:00	08:04:00	09:18:00	09:19:00
6	17:20:00	17:21:00	12:30:00	12:31:00
7	17:40:00	17:41:00	16:40:00	16:41:00
8	18:48:00	18:49:00	17:02:00	17:03:00
9	18:51:00	18:52:00	21:36:00	21:37:00
10	18:59:00	19:00:00	11:31:00	11:32:00
11	21:20:00	21:21:00	18:06:00	18:07:00
12	~	~	17:54:00	17:55:00
13	~	~	10:57:00	10:58:00
14	~	~	15:19:00	15:20:00

Kitchen Dishes/Food Prep Draw-Offs				
Event	**Weekday** t_{Event_Start}	**Weekday** t_{Event_Stop}	**Weekend** t_{Event_Start}	**Weekend** t_{Event_Stop}
1	17:31:00	17:32:00	12:31:00	12:32:00
2	18:01:00	18:02:00	12:51:00	12:52:00
3	21:49:00	21:50:00	16:53:00	16:54:00
4	~	~	21:37:00	21:38:00

B.2.4 Appliance Event Scripting (Weekday only)

Steady Loads with Standby									
Sig ID	**WD Qty Apps**	**WE Qty Apps**	**WD n_{Events}**	**WE n_{Events}**	**Weekday t_{Event_Start}**				**Notes**
					1	**2**	**3**	**4**	
GC1A			1	2	16:33:00	~	~	~	bedroom
	1	1			17:32:55	~	~	~	
MT1A			1	1	23:00:00	23:00:00	23:00:00	23:00:00	
	4	4			07:00:00	07:00:00	07:00:00	07:00:00	
PA1A			1	1	07:02:00	19:57:00	18:51:00	~	lounge
					08:01:55	20:56:55	19:50:55	~	bedroom
PA1B			1	1	17:31:00	19:24:00	17:17:00	~	
	3	3			18:00:55	19:53:55	17:46:55	~	
TV1A			2	2	07:29:00	17:25:00	~	~	lounge
	1	1			08:28:55	22:54:55	~	~	
TV2A			1	1	16:32:00	20:28:00	~	~	bedroom
	2	2			19:01:55	22:57:55	~	~	

Event Signature Only				
	Weekday t_{Event_Start}			
Sig ID	**1**	**2**	**3**	**4**
DW1A	21:21:00	~	~	~
EI1A	16:49:00	~	~	~
EK1A	07:45:00	18:26:00	~	~
EK1B	07:01:00	16:32:00	21:22:00	~
EO1A	17:27:00	~	~	~
ES1A	07:04:00	07:17:00	07:28:00	07:56:00
ET1A	07:17:00	07:46:00	~	~
GH1A	17:45:00	~	~	~
HC1A	08:00:00	08:13:00	~	~
HC2A	07:35:00	08:03:00	~	~
MV1A	18:05:00			
TD1A	19:05:00	~	~	~
VC1A	16:35:00	~	~	~
WM1A	08:26:00			

B.2.5 Lighting Event Scripting (Weekday only)

Lighting												
Sig ID	WD Qty Apps	WE Qty Apps	WD n_{Events}	WE n_{Events}	Weekday t_{Event_Start}							
					1	2	3	4	5	6	7	8
LBA1	1	1	4	4	07:04:05	07:15:05	07:26:05	07:54:05	~	~	~	~
					07:13:00	07:24:00	07:35:00	08:03:00	~	~	~	~
LBA2	1	1	8	14	22:57:00	22:48:00	21:55:00	22:53:00	16:48:00	18:56:00	19:42:00	21:17:00
					23:00:00	22:51:00	21:58:00	22:56:00	16:51:00	18:59:00	19:45:00	21:20:00
LHA	1	1	4	5	07:00:05	17:00:05	21:30:05	22:30:05	~	~	~	~
					08:30:00	18:30:00	22:00:00	23:00:00	~	~	~	~
LLA	1	1	4	5	07:00:05	17:00:05	21:30:05	22:30:05	~	~	~	~
					08:30:00	18:00:00	22:00:00	23:00:00	~	~	~	~
LDI	1	1	1	1	18:00:05	~	~	~	~	~	~	~
					19:00:00	~	~	~	~	~	~	~
LKI	1	1	7	5	07:00:05	07:16:05	07:44:05	08:23:05	17:00:05	21:17:05	21:48:05	~
					07:07:00	07:26:00	08:01:00	08:28:00	18:16:00	21:27:00	21:53:00	~
LLO	1	1	2	2	07:28:05	19:00:05	~	~	~	~	~	~
					08:29:00	22:53:00	~	~	~	~	~	~
LBE1	1	1	4	5	07:00:05	07:24:05	16:31:05	22:50:05	~	~	~	~
					07:15:00	08:15:00	16:32:00	23:00:00	~	~	~	~
LBE2	1	1	4	4	07:00:05	07:09:05	20:20:05	22:55:05	~	~	~	~
					07:02:00	07:16:00	20:30:00	23:00:00	~	~	~	~
LBE3	1	1	4	4	07:30:05	08:03:05	19:23:05	21:48:05	~	~	~	~
					07:33:00	08:29:00	20:59:00	22:00:00	~	~	~	~

B.2.6 Ventilation Event Scripting

	Weekday t_{Event_Start}				Weekend t_{Event_Start}			
Sig ID	1	2	3	4	1	2	3	4
EF1A	07:04:00	07:17:00	07:28:00	07:56:00	07:04:00	07:17:00	07:28:00	07:56:00
Starts with Shower	07:13:55	07:26:55	07:37:55	08:05:55	07:13:55	07:26:55	07:37:55	08:05:55
EF2A	17:27:00	~	~	~	17:27:00	~	~	~
	18:26:55	~	~	~	18:26:55	~	~	~

Appendix C Demand Profile Summary Data

C.1 Appendix Overview

In this appendix, summaries of the electrical and DHW demand profiles, and casual gains profiles are presented for the Winter climate scenario.

C.2 Winter Weekday Summary Tables

Weekday Total Electrical Demand Summary					
Period	**Total (kWh)**	**Average (kW)**	**Peak (kW)**	**Minimum (kW)**	**Load Factor**
Daily	*12.4486*	*0.5187*	*6.3911*	*0.0937*	*8%*
Sleeping	1.5447	0.1932	0.3830	0.1081	*50%*
Vacant	1.9096	0.2387	6.2198	0.0937	*4%*
Actively Occupied	8.9943	1.1247	6.3911	0.0961	*18%*
Weekday Lighting ONLY Electrical Demand Summary					
Period	**Total (kWh)**	**Average (kW)**	**Peak (kW)**	**Minimum (kW)**	**Load Factor**
Daily	*1.6403*	*0.0683*	*0.6265*	*0.0000*	*11%*
Sleeping	0.0003	0.0000	0.1822	0.0000	*0%*
Vacant	0.0001	0.0000	0.0436	0.0000	*0%*
Actively Occupied	1.6399	0.2051	0.6265	0.0000	*33%*
Weekday Total Thermal Gains Summary					
Period	**Total (kWh)**	**Average (kW)**	**Peak (kW)**	**Minimum (kW)**	**Load Factor**
Daily	*16.2899*	*0.6787*	*7.4140*	*0.1772*	*9%*
Sleeping	3.1102	0.3889	0.5756	0.3887	*68%*
Vacant	1.4421	0.1803	0.2772	0.1772	*65%*
Actively Occupied	11.7376	1.4677	7.4140	0.1772	*20%*
Weekday Appliances & Lighting ONLY Thermal Gains Summary					
Period	**Total (kWh)**	**Average (kW)**	**Peak (kW)**	**Minimum (kW)**	**Load Factor**
Daily	*12.8366*	*0.5349*	*7.1441*	*0.1772*	*7%*
Sleeping	1.5142	0.1893	0.3761	0.1892	*50%*
Vacant	1.4421	0.1803	0.2772	0.1772	*65%*
Actively Occupied	9.8804	1.2355	7.1441	0.1772	*17%*
Weekday Metabolic ONLY Thermal Gains Summary					
Period	**Total (kWh)**	**Average (kW)**	**Peak (kW)**	**Minimum (kW)**	**Load Factor**
Daily	*3.4533*	*0.1439*	*0.2819*	*0.0000*	*51%*
Sleeping	1.5960	0.1996	0.1995	0.1995	*100%*
Vacant	0.0000	0.0000	0.0000	0.0000	*0%*
Actively Occupied	1.8573	0.2322	0.2819	0.0000	*82%*
Weekday DHW Summary					
Period	**Total (l)**	**Average (l)**	**Peak (l)**	**Minimum (l)**	**Load Factor**
Daily	*3.3333*	*0.1389*	*9.0000*	*0.0000*	*2%*
Sleeping	0.0000	0.0000	0.0000	0.0000	*0%*
Vacant	0.0000	0.0000	0.0000	0.0000	*0%*
Actively Occupied	3.3333	0.4168	9.0000	0.0000	*5%*

C.3 Winter Weekend Summary Tables

Weekend Total Electrical Demand Summary					
Period	**Total (kWh)**	**Average (kW)**	**Peak (kW)**	**Minimum (kW)**	**Load Factor**
Daily	*13.5955*	*0.5665*	*6.3526*	*0.0961*	*9%*
Sleeping	1.5455	0.1933	0.3961	0.1081	*49%*
Vacant	~	~	~	~	~
Actively Occupied	12.0500	0.7532	6.3526	0.0961	*12%*
Weekend Lighting ONLY Electrical Demand Summary					
Period	**Total (kWh)**	**Average (kW)**	**Peak (kW)**	**Minimum (kW)**	**Load Factor**
Daily	*2.2000*	*0.0917*	*0.6727*	*0.0000*	*14%*
Sleeping	0.0002	0.0000	0.1360	0.0000	*0%*
Vacant	~	~	~	~	~
Actively Occupied	2.1998	0.1375	0.6727	0.0000	*20%*
Weekend Total Thermal Gains Summary					
Period	**Total (kWh)**	**Average (kW)**	**Peak (kW)**	**Minimum (kW)**	**Load Factor**
Daily	*20.1472*	*0.8395*	*6.6081*	*0.3435*	*13%*
Sleeping	3.4361	0.3895	0.5532	0.3887	*70%*
Vacant	~	~	~	~	~
Actively Occupied	17.0327	1.0646	6.6081	0.3435	*16%*
Weekend Appliances & Lighting ONLY Thermal Gains Summary					
Period	**Total (kWh)**	**Average (kW)**	**Peak (kW)**	**Minimum (kW)**	**Load Factor**
Daily	*14.9484*	*0.6229*	*6.3262*	*0.1772*	*10%*
Sleeping	2.4268	0.1899	0.3537	0.1892	*54%*
Vacant	~	~	~	~	~
Actively Occupied	13.4298	0.8394	6.3262	0.1772	*13%*
Weekend Metabolic ONLY Thermal Gains Summary					
Period	**Total (kWh)**	**Average (kW)**	**Peak (kW)**	**Minimum (kW)**	**Load Factor**
Daily	*5.1988*	*0.2166*	*0.3030*	*0.1428*	*71%*
Sleeping	2.3087	0.1996	0.1995	0.1995	*100%*
Vacant	~	~	~	~	~
Actively Occupied	3.6028	0.2252	0.3030	0.1428	*74%*
Weekend DHW Summary					
Period	**Total (l)**	**Average (l)**	**Peak (l)**	**Minimum (l)**	**Load Factor**
Daily	*3.5667*	*0.1486*	*8.0000*	*0.0000*	*2%*
Sleeping	0.0000	0.0000	0.0000	0.0000	*0%*
Vacant	~	~	~	~	~
Actively Occupied	3.5667	0.2229	8.0000	0.0000	*3%*

C.4 Winter Summary Charts

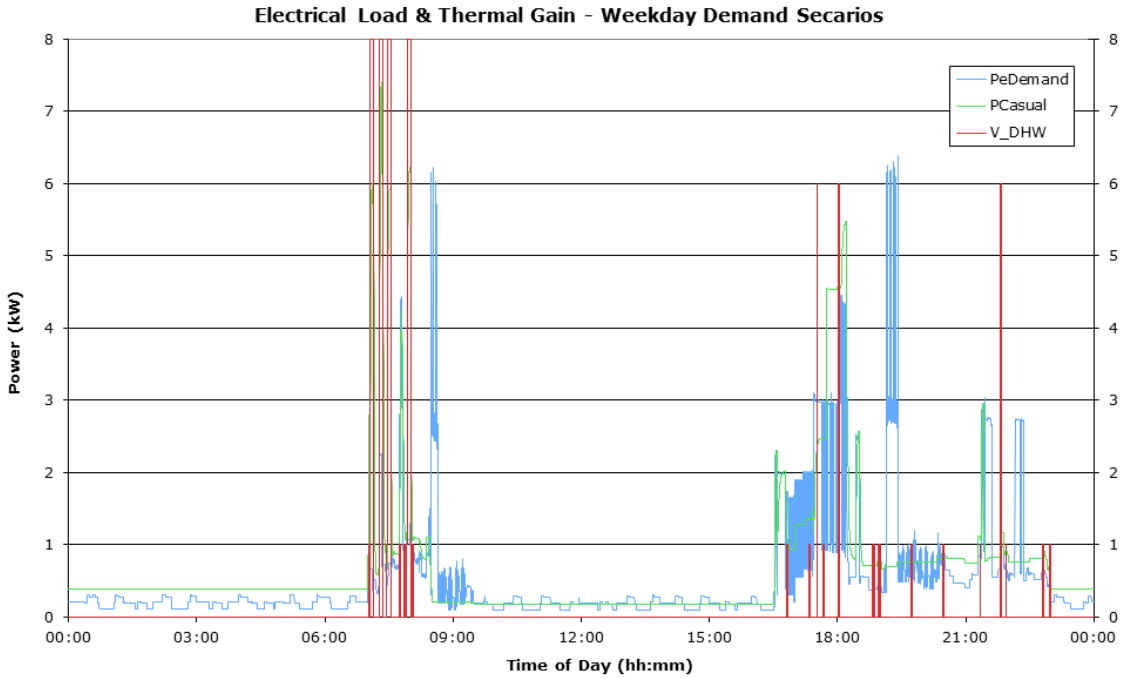

Figure C.1: Electrical demand profile (except for heating system loads), thermal gains profile, and DHW extraction profile for primary demand scenarios using weekday occupancy pattern and winter or extreme winter climate scenarios

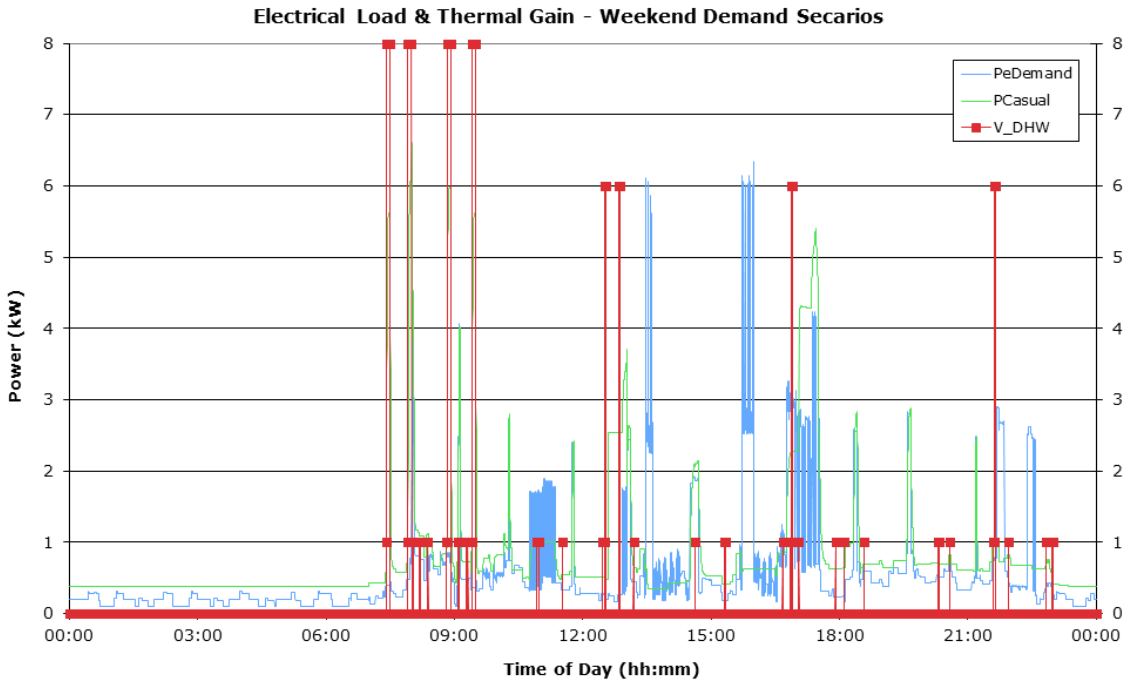

Figure C.2: Electrical demand profile (except for heating system loads), thermal gains profile, and DHW extraction profile for primary demand scenarios using weekday occupancy pattern and winter or extreme winter climate scenarios

Appendix D Appliance Data Acquisition Exercise

D.1 Appendix Overview

In this appendix, details are presented of the appliance data acquisition exercise to measure electric load profiles and estimate casual thermal gain profiles.

D.2 Summary of Experimental Method

To perform electrical load measurements, a current transformer (CT) was clamped around the live conductor of a modified mains extension cable. The CT was connected to the voltage input channel of an OWL data logger. Voltage measurements were achieved using a plug-in energy monitor, where instantaneous voltage readings were recorded at the beginning and end of each load measurement. Power was calculated retrospectively from the 5-second current readings and average of the two instantaneous voltage readings in a spreadsheet.

To record temperature, T-type thermocouples were bonded inside a light-weight plastic hemisphere to minimise radiative heat transfer to the surface of the thermocouple. The thermocouple was attached at the centre point, pointing toward the centre of a notional sphere, where the tip of the thermocouple would reach the centre the notional sphere. A number of holes were drilled in the hemisphere to allow free air circulation. The exterior of the hemisphere was coated with reflective foil to minimise radiative heat transfer to the sphere. The sphere was temporarily bonded to the measurement surface (on the appliance) so as to avoid introducing additional thermal mass around the tip of the thermocouple. The thermocouple was attached to a thermocouple-specific port on a multi-channel Squirrel 800 data logger (S/N: K80602001) that was configured to measure the voltage across the thermocouple. The data logger software converted the 5-second voltage readings to °C automatically.

D.3 Summary of Appliances under Investigation

The appliances that were measured during the electrical load monitoring exercise are listed in Table D.1, where those that were included in the temperature monitoring exercise are indicated by a shaded row.

Signature ID	Date	Signature Description	App. Category	Manufacturer & Model	Logger S/N
WM1A	31/08/05	Prog. 4 - Rapid Wash, 40°C - "Quick Wash" Option	Washing Machine	Beko WMA 15105 (Eco Case)	28364
WM1B	31/08/05	Immediately after previous identical cycle - Prog 4 - Rapid Wash, 40°C - "Quick Wash" Option	Washing Machine	Beko WMA 15105 (Eco Case)	28364
WM1C	01/09/05	Prog 6 - 60°C - "Quick Wash" Option	Washing Machine	Beko WMA 15105 (Eco Case)	28367
WM1D	01/09/05	Immediately after previous identical cycle - Prog 6 - 60°C - "Quick Wash" Option	Washing Machine	Beko WMA 15105 (Eco Case)	28367
RF1A	31/08/05	24 hours of normal operation - no additional loading - normal withdrawal only	Fridge Freezer	Beko Fridge Freezer	28364
EK1A/B	01/09/05	1.5l (2hrs since lasts) & 0.75l (30mins last use)	Electric Kettle	Kenwood 2 litre Kettle	28367
DD1A	11/02/05	Continuous Operating Load (Average)	Digital Decoder	Hauppauge DEC 1000	28367
TV1A/B	11/02/05	Standby / Continuous Operation with Variable Volume Level	Television	Philips Matchline Classic (26" LCD)	28364
VR1A	11/02/05	Standby Load	Video Recorder	Philips VR 757	28536
DP1A	11/02/05	Standby Load	DVD Player	Samsung DVD-709	28364
PC1A	08/09/05	Printer Standby, Laptop On & Broadband Connected	PC System	Apple iBook G4 14" (On charger & On), HP PSC1215 Multifunction & Netgear DG834G Wireless Broadband Router	28364
HC1A	23/09/05	Standard Straightening Event	Hair Care	Remington Hair Straighteners	28536
GC1A/B	27/09/05	Standby / Active & Playing Game	Games Console	Sony PlayStation 2	28537
PA1A	27/09/05	Standby Load	Powered Audio	Kenwood Hi-Fi Component System NV-301	28367
PA1B	27/09/05	Playing CD - Constant Volume	Powered Audio	Kenwood Hi-Fi Component System NV-301	28367
PA1C	27/09/05	FM Tuner - Constant Volume	Powered Audio	Kenwood Hi-Fi Component System NV-301	28367
-	27/09/05	Failed Measurement	Tumble Dryer	Linda's Tumble Dryer	28536
EI1A	27/09/05	Full power	Electric Iron	Morphy Ricahrds Breeze 40311	28536
PT1A	27/09/05	Made about 15mins of calls	Powered Telephony	BT Synergy Cordless Phone	28537
MP1A	27/09/05	Did Not Work!!!! - Phone On	Mobile Phone	Nokia 3310 Charger	28536
TV1A/B	02/06/06	Standby & Continuous Operation	Television	Bush (20" CRT)	28364
TD1A	13/02/06	Full Load	Tumble Dryer	Hotpoint	K80602001
ES1A	02/09/06	Mid-range temp & maximum flow rate	Electric Shower	Mira Sport 8kW	K80602001
DW1A	14/02/06	Std Wash (55°C)	Dishwasher	Hoover - AAA Total Dry Whisper DT999	K80602001
MV1A/B	02/11/06	Full power	Microwave oven	Panasonic Dimension 4 Genius (850W)	K80602001
RF2A	04/02/06	24 hours	Freezer	Phillips VR 757	28537
ET1A	04/09/06	2 Slices @Medium	Electric Toaster	Kenwood 2 slice	28536

Table D.1: Details of logged appliance measuremens (as opposed to instantaneous monitoring, including appliance make & model, and logger serial number

Appendix E Tabulated Simulation Results

E.1 Relative Carbon Saving Results for SE-TLF

P_e-η_e	HSum-WD	Sum-WD	Sh-WD	Win-WD	EWin-WD
0.5kW-15%	-0.5%	-2.8%	-1.8%	-0.5%	-1.7%
1kW-15%	-0.2%	-3.3%	-0.1%	2.6%	0.4%
2kW-15%	-2.7%	-8.9%	-4.5%	6.4%	6.1%
3kW-15%	-5.8%	-15.5%	-13.8%	-6.3%	6.0%
4kW-15%	-10.6%	-22.3%	-21.5%	-12.5%	-1.7%
5kW-15%	-14.1%	-28.2%	-30.1%	-18.8%	-6.9%
0.5kW-20%	0.1%	-1.0%	-0.9%	-0.7%	-1.2%
1kW-20%	1.1%	-0.8%	2.2%	2.9%	1.0%
2kW-20%	0.3%	-2.5%	4.4%	9.5%	6.3%
3kW-20%	-1.3%	-7.3%	-1.6%	8.7%	13.8%
4kW-20%	-3.5%	-12.3%	-8.2%	0.0%	13.5%
5kW-20%	-7.6%	-17.6%	-14.3%	-5.0%	9.0%
0.5kW-25%	0.7%	0.2%	-0.5%	-0.5%	-0.9%
1kW-25%	2.3%	2.1%	3.4%	3.3%	1.5%
2kW-25%	3.0%	1.7%	7.8%	10.1%	6.3%
3kW-25%	1.6%	-1.2%	8.4%	15.6%	13.2%
4kW-25%	0.5%	-4.6%	3.2%	16.5%	19.9%
5kW-25%	-0.3%	-8.7%	-2.2%	5.1%	19.6%
0.5kW-30%	1.0%	0.7%	-0.1%	-0.5%	-0.7%
1kW-30%	2.1%	4.2%	4.0%	3.4%	1.8%
2kW-30%	4.5%	4.9%	10.4%	11.0%	6.8%
3kW-30%	4.3%	4.1%	14.0%	16.9%	13.1%
4kW-30%	3.4%	1.5%	13.8%	23.6%	19.1%
5kW-30%	2.7%	-1.3%	9.5%	22.7%	24.9%
0.5kW-35%	0.4%	1.3%	-0.8%	-0.4%	-0.7%
1kW-35%	3.8%	6.1%	4.6%	3.4%	2.1%
2kW-35%	5.9%	8.9%	12.7%	11.3%	7.7%
3kW-35%	6.9%	8.5%	17.4%	18.2%	13.1%
4kW-35%	6.5%	7.6%	20.3%	23.5%	19.2%
5kW-35%	5.8%	5.1%	20.4%	31.0%	25.3%

Table E.1: Data plotted in Figure 4.1 - Relative Carbon Saving vs. Base-case energy system (%) for each design variant, for each Weekday PDS, for SE-TLF concept system

P_e-η_e	HSum-WE	Sum-WE	Sh-WE	Win-WE	EWin-WE
0.5kW-15%	-0.4%	-2.6%	-1.7%	2.0%	2.8%
1kW-15%	-1.9%	-5.8%	-0.9%	6.2%	6.8%
2kW-15%	-7.9%	-15.2%	-7.8%	2.9%	12.4%
3kW-15%	-13.3%	-23.6%	-19.3%	-6.4%	0.2%
4kW-15%	-18.1%	-31.0%	-28.7%	-15.7%	-8.4%
5kW-15%	-22.7%	-37.7%	-38.1%	-25.4%	-15.8%
0.5kW-20%	0.7%	-0.4%	-0.3%	2.3%	3.2%
1kW-20%	1.3%	-1.2%	1.8%	6.8%	7.3%
2kW-20%	-3.1%	-7.3%	0.8%	14.3%	14.9%
3kW-20%	-7.6%	-14.5%	-5.0%	6.4%	17.8%
4kW-20%	-11.6%	-20.6%	-12.7%	0.2%	8.5%
5kW-20%	-15.3%	-26.4%	-20.1%	-7.0%	0.3%
0.5kW-25%	3.6%	0.6%	0.7%	2.6%	3.2%
1kW-25%	3.3%	2.9%	5.2%	8.0%	7.4%
2kW-25%	1.4%	-1.0%	7.7%	15.9%	15.7%
3kW-25%	-2.8%	-7.0%	4.2%	20.3%	22.2%
4kW-25%	-6.4%	-12.4%	-0.2%	12.8%	24.9%
5kW-25%	-9.5%	-17.4%	-7.0%	7.0%	17.3%
0.5kW-30%	3.0%	1.2%	1.3%	2.5%	3.3%
1kW-30%	5.1%	5.8%	6.4%	8.1%	7.8%
2kW-30%	5.6%	4.5%	12.4%	17.3%	16.1%
3kW-30%	1.8%	0.2%	12.6%	24.9%	23.9%
4kW-30%	-1.6%	-4.9%	10.1%	27.9%	30.8%
5kW-30%	-4.5%	-9.3%	6.7%	20.2%	34.7%
0.5kW-35%	3.5%	1.9%	1.9%	2.3%	3.3%
1kW-35%	6.6%	7.7%	8.1%	8.7%	7.8%
2kW-35%	8.4%	9.4%	15.5%	18.7%	16.7%
3kW-35%	6.8%	6.5%	18.6%	27.0%	24.8%
4kW-35%	3.4%	2.8%	19.5%	34.5%	32.3%
5kW-35%	0.5%	-1.7%	16.7%	36.7%	39.3%

Table E.2: Data plotted in Figure 4.2 - Relative Carbon Saving vs. Base-case energy system (%) for each design variant, for each Weekend PDS, for SE-TLF concept system

P_e-η_e	12 Months	RSO-NoHSum	RSO-NoSummer
0.5kW-15%	-1.2%	-1.2%	-1.0%
1kW-15%	0.3%	0.5%	1.1%
2kW-15%	-3.1%	-2.8%	-1.7%
3kW-15%	-12.8%	-12.9%	-12.2%
4kW-15%	-20.4%	-20.7%	-20.1%
5kW-15%	-28.2%	-28.7%	-28.4%
0.5kW-20%	-0.4%	-0.4%	-0.3%
1kW-20%	2.2%	2.4%	2.8%
2kW-20%	4.3%	4.8%	6.0%
3kW-20%	-0.5%	-0.1%	1.2%
4kW-20%	-7.3%	-7.2%	-6.1%
5kW-20%	-13.3%	-13.3%	-12.4%
0.5kW-25%	0.2%	0.2%	0.1%
1kW-25%	3.9%	4.1%	4.3%
2kW-25%	7.8%	8.2%	9.3%
3kW-25%	8.3%	9.0%	10.6%
4kW-25%	4.6%	5.1%	6.8%
5kW-25%	-1.9%	-1.7%	-0.3%
0.5kW-30%	0.5%	0.5%	0.4%
1kW-30%	4.7%	4.8%	4.8%
2kW-30%	10.4%	10.9%	11.7%
3kW-30%	13.3%	14.1%	15.7%
4kW-30%	13.9%	14.9%	17.0%
5kW-30%	10.5%	11.3%	13.4%
0.5kW-35%	0.4%	0.4%	0.2%
1kW-35%	5.6%	5.6%	5.5%
2kW-35%	12.7%	13.1%	13.6%
3kW-35%	16.9%	17.6%	18.9%
4kW-35%	19.5%	20.5%	22.6%
5kW-35%	20.3%	21.5%	24.1%

Table E.3: Data plotted in Figure 4.4 - Relative Carbon Saving vs. Base-case energy system (%) for each design variant, as calculated for annual operation with Restricted Seasonal Operation (RSO) modes: None (12 Months), No High Summer (RSO-NoHSum) and No Summer (RSO-NoSummer)

E.2 Comparing Operating Regimes

Operating Regime	Thermal Cycling Frequency (cycles/year)	2kW-35%	3kW-35%	4kW-35%	5kW-35%
TLF	1,005	11.2%			
TDP	447	10.2%			
DDP	269	8.8%			
24hr	1	5.5%			
TLF	1,208		15.6%		
TDP	447		15.3%		
DDP	269		12.9%		
24hr	1		8.4%		
TLF	2,589			18.6%	
TDP	447			19.2%	
DDP	269			16.2%	
24hr	1			10.4%	
TLF	4,255				19.8%
TDP	447				22.1%
DDP	269				17.8%
24hr	1				10.9%

Table E.4: Data plotted in Figure 5.17 - RCS vs. annual frequency of thermal cycling, for SE µCHP design varaints with η_e= 35% and P_e=2-5kW_e, comparing between operating regimes

Operating Regime	Thermal Cycling Frequency (cycles/year)	2kW-35%	3kW-35%	4kW-35%	5kW-35%
TLF	1,005	11.2%			
TDP	447	10.2%			
DDP	269	8.8%			
24hr	1	5.5%			
TLF	1,208		15.6%		
TDP	447		15.3%		
DDP	269		12.9%		
24hr	1		8.4%		
TLF	2,589			18.6%	
TDP	447			19.2%	
DDP	269			16.2%	
24hr	1			10.4%	
TLF	4,255				19.8%
TDP	447				22.1%
DDP	269				17.8%
24hr	1				10.9%

Table E.5: Data plotted in Figure 5.18 - RCS vs. cumulative annual operating duration, for SE µCHP design varaints with ηe= 35% and Pe=2-5kWe, comparing between operating regimes